Arthritis & Rheumatology

An Official Journal of the American College of Rheumatology
www.arthritisrheum.org and wileyonlinelibrary.com

Cover design: Todd Machen

This journal is printed on acid-free paper.

Arthritis & Rheumatology

An Official Journal of the American College of Rheumatology
www.arthritisrheum.org and wileyonlinelibrary.com

VOLUME 72 • July 2020 • NO. 7

Cover image: The figure on the cover, created at the Centers for Disease Control and Prevention, depicts ultrastructural morphology exhibited by coronaviruses. Note the spikes that adorn the outer surface of the virus, which impart the look of a corona surrounding the virion, when viewed under an electron microscope. This issue of *Arthritis & Rheumatology* includes two articles related to COVID-19 and rheumatology, with many more anticipated as the world faces the pandemic that has so indelibly impacted us all.

In this Issue

Highlights from this issue of *A&R* | By Lara C. Pullen, PhD

Cartilage Microbial DNA Signatures Associated with Osteoarthritis

A growing body of literature has identified constituent microbial DNA signatures in human tissues previously believed to be sterile. Moreover, alterations of the gut microbiota have been implicated in many forms of arthritis. For example, a study of adults within the Dutch Rotterdam and LifeLines-DEEP cohorts identified 4 bacterial clades associated with knee pain as measured by the Western Ontario and McMaster Universities Osteoarthritis Index score. Until now, however, researchers had not examined cartilage microbial patterns.

p. 1111

In this issue, Dunn et al (p. 1111) report the results of their characterization of the microbial DNA profile of articular cartilage. The investigators present the first evidence of a microbial DNA signature in human and mouse cartilage, and describe how alteration in this signature occurs during the development and progression of human osteoarthritis (OA). They document increases in gram-negative constituents and strain-specific signatures in both mouse and human cartilage, and call for further study to establish a potential pathogenic role for these DNA signatures.

In the study, researchers documented a reduction in alpha diversity, or microbiome diversity within a single sample, in human OA versus control samples and in hip versus knee samples. This difference between human OA and control samples could be seen in numerous clades, as well as when the researchers compared OA-susceptible B6 mice to OA-resistant MRL mice. Upon performing a functional analysis, researchers found OA to be associated with an increase in lipopolysaccharide production, phosphatidylinositol signaling, and nitrogen metabolism, as well as decreases in sphingolipid metabolism.

Brain Hyperactivation in Fibromyalgia May Result From Aberrant Salience

Extensive brain research on fibromyalgia (FM) has indicated that FM patients are hyperresponsive to painful stimuli. Some of this research has also suggested that the increased pain-related brain activity observed in FM studies may be the result of stronger responses to salient aspects of the stimulation rather than, or in addition to, the stimulation's painfulness. In this issue, Hubbard et al (p. 1203) report the results of their investigation of the hypothesis that FM patients demonstrate elevated brain responses to both pain onset and offset. They chose onset pain (the event signaling the beginning of pain) and offset pain (the termination of pain) to represent 2 salient sensory events of opposing valences. The investigators found that the increased sensitivity exhibited by FM patients in response to painful stimuli may reflect a more generalized hypersensitivity to salient sensory events. If true, then these findings suggest that brain hyperactivation may be involved in the generalized hypervigilance to salient stimuli in FM.

p. 1203

The researchers measured response to a moderately painful pressure stimulus to the leg during blood oxygen level–dependent (BOLD) functional magnetic resonance imaging. When they compared FM patients to healthy controls, they found a higher BOLD signal response during pain onset in the dorsolateral and ventrolateral prefrontal cortices, orbitofrontal cortex, frontal pole cortex, and precentral gyrus. During pain offset, FM patients had higher and more widespread BOLD signal response in frontal regions significantly hyperactivated in response to onset. In the case of FM patients, some of these responses were positively correlated with pain unpleasantness ratings, pain catastrophizing scores, or negatively correlated with stimulus intensity.

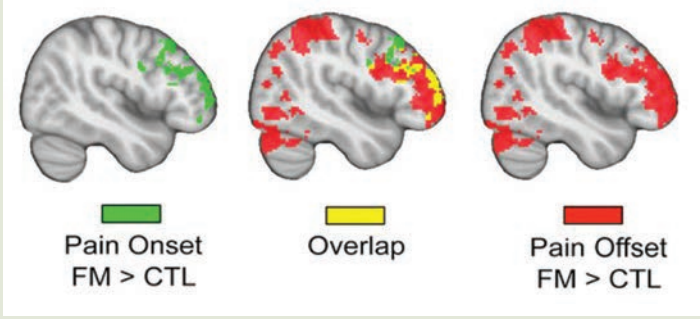

Figure 1. Statistical maps showing group differences in brain responses for fibromyalgia (FM) patients compared to healthy controls (CTL) during pain onset, pain offset and overlapping regions common to both groups.

Physicians With High Opioid Prescribing Rates Have Patients With Long-term Opioid Use

In this issue, Lee et al (p. 1082) report that the rates of opioid prescription for patients with rheumatoid arthritis (RA) vary widely. Moreover, after controlling for patient characteristics, baseline prescribing rates are a strong predictor of whether a patient will become a long-term opioid user. The investigators analyzed a large, population-based cohort of individuals with RA and assessed rates of opioid use among physicians' practices. During the 12-month follow-up period, physicians with a very low prescribing rate reported long-term opioid use by 7.0% of patients, physicians with a moderate prescribing rate reported long-term opioid use by 12.5% of patients, and physicians with a high prescribing rate reported long-term opioid use by 12.7% of patients. The odds ratio for long-term opioid use after the baseline period was 1.16 for patients of low-intensity prescribing physicians, 1.89 for patients of moderate-intensity prescribing physicians, and 2.01 for patients of high-intensity prescribing physicians, compared to very low-intensity prescribing physicians.

p. 1082

RA Remission With Treat-to-Target Strategies

In this issue, Norvang et al (p. 1072) report that 2 early rheumatoid arthritis cohorts were able to achieve study-specific treatment targets in most patients. For their study, the researchers compared a tight control treat-to-target (TTT) strategy targeting remission according to a Disease Activity Score (DAS) of <1.6 plus 0 swollen joints on a 44-joint count in a randomized control trial setting (the Aiming for Remission in Rheumatoid Arthritis: a randomised trial examining the benefit of ultrasound in a Clinical Tight Control regimen [ARCTIC] trial) to a TTT approach targeting remission according to the DAS28 in an observational setting (the Norwegian Very Early Arthritis Clinic [NOR-VEAC] study). The comparison included 189 patients from the ARCTIC trial and 330 patients from the NOR-VEAC study.

p. 1072

The investigators found that, at 6 months, the study-specific treatment targets were achieved in more than half of the patients in each cohort. This increased to >60% at 12 months and 24 months. They researchers noted, however, that more patients in the ARCTIC trial cohort than in the NOR-VEAC study group were able to achieve the American College of Rheumatology (ACR)/European League Against Rheumatism (EULAR) Boolean remission during follow-up. The odds ratios of achieving ACR/EULAR Boolean remission during follow-up at 3 months, 12 months, and 24 months were 1.73, 1.97, and 1.82, respectively. The authors concluded from this that targeting a more stringent definition of remission provides further potential for favorable outcomes of a TTT strategy.

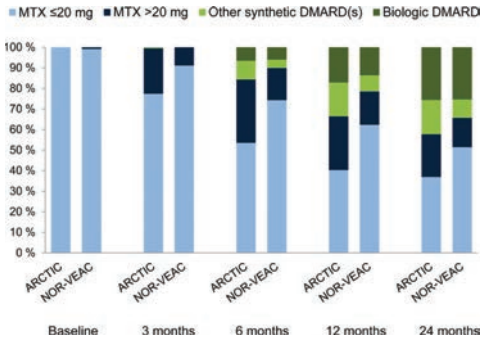

Figure 1. Percentage of patients receiving methotrexate (MTX) ≤20 mg/week, MTX >20 mg/week, other synthetic disease-modifying antirheumatic drugs (DMARDs), and biologic DMARDs at baseline and during follow-up in the Aiming for Remission in Rheumatoid Arthritis: a randomised trial examining the benefit of ultrasound in a Clinical Tight Control regimen (ARCTIC) trial versus the Norwegian Very Early Arthritis Clinic (NOR-VEAC) study.

Organ-Specific Lupus Flares Vary Over Space and Time

Researchers use cluster detection in spatial epidemiology and disease surveillance to identify spatial units associated with distinctive patterns of data of interest relative to background variation. In this issue, Stojan et al (p. 1134) describe the results of their efforts to use spatiotemporal cluster analysis to identify clusters of systemic lupus erythematosus organ-specific flares and characterize the relationship of these clusters to fine particulate matter pollution, temperature, ozone concentration, result wind, relative humidity, and barometric pressure. Theirs is the first report of spatiotemporal clusters of lupus organ-specific disease activity.

p. 1134

The investigators performed a spatiotemporal cluster analysis of the Hopkins Lupus Cohort and identified seasonal, as well as multiyear, cluster patterns that differed in extent and location for the various organ-specific flare types. They found significant clusters for joint flares, rash flares, hematologic flares, neurologic flares, renal flares, serositis, and pulmonary flares. The researchers then used generalized estimating equation–based regression analysis to quantify the effects of individual, county, and environmental variables on the odds of flare outcomes. Adjusting for these environmental variables, they found that most of the clusters changed in significance, temporal extent, or spatial extent, which suggests that these variables in part drive the formation, location, or temporal extent of the identified clusters. The authors call for further research focused on each individual lupus organ-specific activity to better understand the driving forces behind the observed changes.

Clinical Connections

Positive Effects of a Young Systemic Environment and High Growth Differentiation Factor 11 Levels on Chondrocyte Proliferation and Cartilage Matrix Synthesis in Old Mice

Li et al, *Arthritis Rheumatol* 2020;78:1103–1110

CORRESPONDENCE
Lei Wei, MD, PHD: lei_wei@brown.edu
Xiaochun Wei, MD, PHD: sdeygksys@163.com

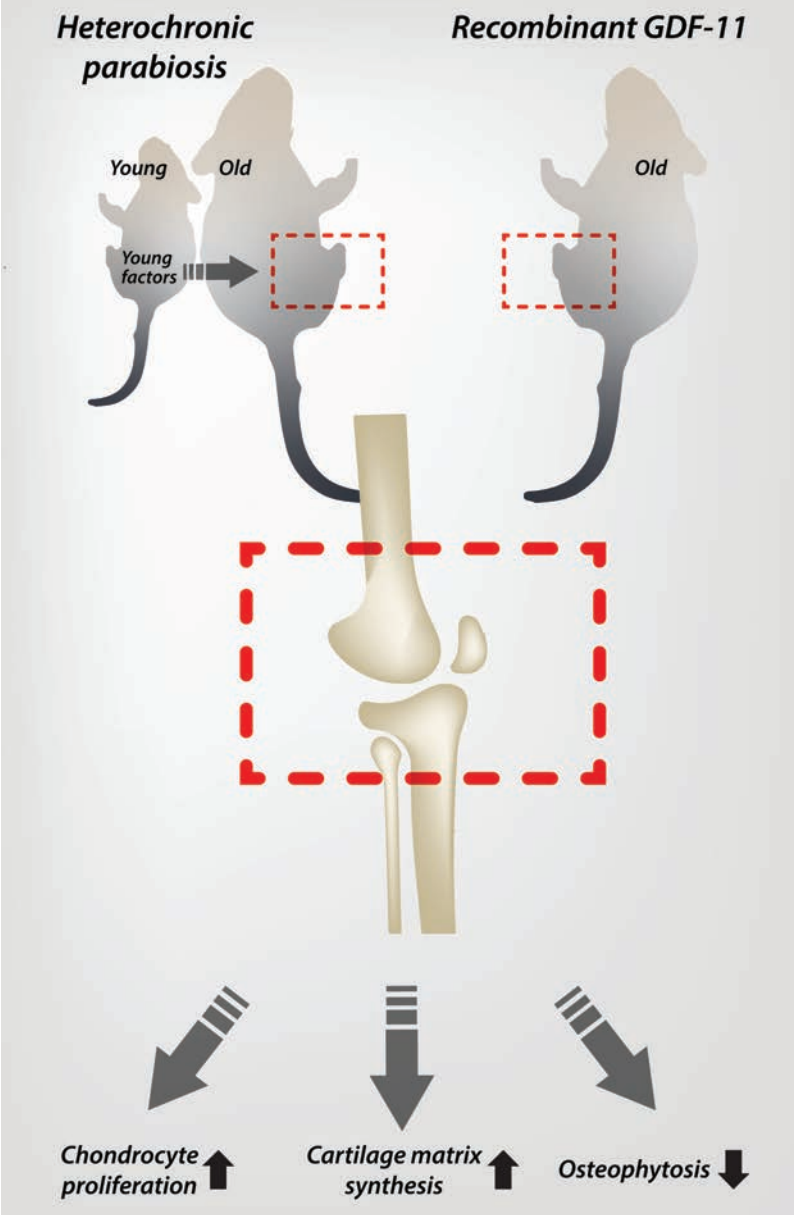

SUMMARY

Heterochronic parabiosis, in which a young mouse is surgically joined to an aged partner, can improve tissue function in the old partner. Osteoarthritis is characterized by progressive degeneration of the cartilage at the ends of bones and by reduced numbers of cells in the cartilage. Li et al demonstrated that a young systemic environment in heterochronic parabiosis can improve knee function in aged mice by enhancing chondrocyte proliferation, increasing cartilage matrix synthesis, and decreasing bone spurs. The protein growth differentiation factor 11 (GDF-11), one of the "young factors" in the blood that appears important in the aging process, was shown to promote chondrocyte proliferation, increase cartilage matrix synthesis, and reduce bone spurs. These data demonstrate a novel link between GDF-11 and cartilage aging in mice.

KEY POINTS

- The young systemic environment in heterochronic parabiosis can delay cartilage degeneration in old mice.
- GDF-11, a circulating "young" factor, can delay knee degeneration in older mice.

Association of a Type 2–Polarized T Cell Phenotype With Methotrexate Nonresponse in Patients With Rheumatoid Arthritis

Slauenwhite et al, *Arthritis Rheumatol* 2020;78:1091–1102

CORRESPONDENCE
Thomas B. Issekutz, MD: Thomas.Issekutz@dal.ca
John G. Hanly, MD: John.Hanly@nshealth.ca

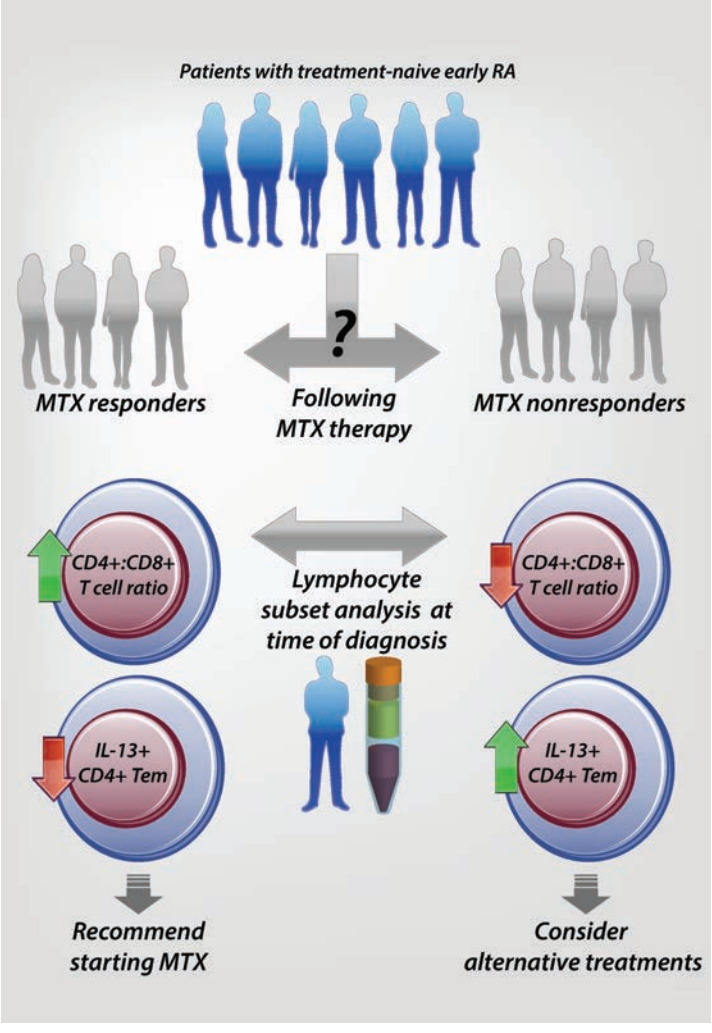

SUMMARY

Early control of inflammation in rheumatoid arthritis (RA) leads to better long-term outcomes, emphasizing the importance of timely initiation of effective therapies. Achieving a better understanding of how disease mechanisms differ between patients is important for applying effective therapies, such as in the common circumstance of methotrexate (MTX)–responsive and MTX-nonresponsive RA. Slauenwhite et al implemented a simple immunophenotyping approach using blood from patients with treatment-naive early RA. With this approach, differences in immune parameters were identified as discriminators of MTX nonresponsiveness, including a lower CD4:CD8 T cell ratio and a higher interleukin-13–positive (IL-13+) CD4+ T effector memory (Tem) cell frequency compared to MTX responders. These features, prior to treatment initiation, outperformed demographic, clinical, or routine laboratory variables as predictors of MTX efficacy. This provides support for the use of immunophenotyping as a potentially convenient, noninvasive strategy for identification of RA patients who are unlikely to have meaningful responses to MTX-based therapy. Furthermore, MTX-nonresponsive RA patients may form a distinct group, identifiable through a skewed CD4:CD8 T cell ratio and elevated IL-13+CD4+ Tem frequencies, with an increased type 2–polarized immune response.

KEY POINTS

- Immunologic phenotypes as prognostic tests for MTX effectiveness following diagnosis may outperform traditional clinical and laboratory variables in RA patients.
- Distinct baseline immune profiles in MTX-nonresponsive RA include lower CD4:CD8 T cell ratio and higher IL-13+CD4+ Tem cell frequency.
- Targeting the IL-13+CD4+ T cell pathway could be a new therapeutic strategy in MTX-resistant RA patients.

Arthritis & Rheumatology
Vol. 72, No. 7, July 2020, pp 1045
DOI 10.1002/art.41282

American College of Rheumatology
Empowering Rheumatology Professionals

Introducing the New Editor of *Arthritis & Rheumatology*, Daniel H. Solomon, MD, MPH

On July 1, 2020, Daniel H. Solomon, MD, MPH became Editor-in-Chief of *Arthritis & Rheumatology*. He is the thirteenth Editor of the journal, succeeding Dr. Richard J. Bucala for a 5-year term.

Dr. Solomon is Professor of Medicine at Harvard Medical School and Chief of the Section of Clinical Sciences in the Division of Rheumatology, Inflammation and Immunity at Brigham and Women's Hospital. He earned his undergraduate degree and MD from Yale University and an MPH in Clinical Effectiveness from Harvard University. In 1998, after completing his residency in internal medicine and fellowship in rheumatology at Brigham and Women's Hospital and fellowship in medicine at Harvard Medical School, he joined the faculty at Harvard Medical School, as an Instructor and subsequently Assistant Professor, Associate Professor, and since 2012, Professor.

Dr. Solomon has received numerous service and professional awards, including the Henry Kunkel Young Investigator Award from the American College of Rheumatology, the Kenneth L. Baughman Faculty Mentoring Award from the Brigham and Women's Hospital Department of Medicine, and, shared with several other colleagues in rheumatology, the Program Award for a Culture of Excellence in Mentoring from Harvard Medical School. He holds the Matthew H. Liang Distinguished Chair in Arthritis and Population Health at Brigham and Women's Hospital.

At Brigham and Women's Hospital, Dr. Solomon serves on the Scientific Advisory Boards of the Brigham Rheumatoid Arthritis Sequential Study (BRASS) and the Brigham and Women's Hospital/National Institute of Arthritis and Musculoskeletal and Skin Diseases Joint Biology Consortium. He is Principal Investigator of the National Institutes of Health–supported VERITY P30 Clinical Research Core at Brigham and Women's Hospital, which aims to improve clinical research in rheumatology. He additionally has served in several prominent professional roles at the national level and is currently Chair of the Food and Drug Administration Arthritis Advisory Committee and a member of the Arthritis Foundation National Scientific Advisory Board.

Dr. Solomon's early work focused on the cardiovascular safety of nonsteroidal antiinflammatory drugs and selective cyclooxygenase 2 inhibitors, and he continues to study analgesics. His current research focuses on cardiovascular disease in rheumatoid arthritis, and he is co–principal investigator on the National Institutes of Health–funded TARGET trial testing the effect of disease-modifying antirheumatic drugs on cardiovascular disease. He has been instrumental in advancing the collaborative clinical Cardiovascular in Rheumatology Medicine practice at Brigham and Women's Hospital. He has several ongoing projects focused on improving implementation of treat-to-target in rheumatoid arthritis.

Daniel H. Solomon, MD, MPH

At the American College of Rheumatology, Dr. Solomon has served in multiple volunteer roles, including membership on the Blue Ribbon Task Force on Nonsteroidal Antiinflammatory Drugs and Coxibs, the Quality Leadership Council, and the Quality of Care Committee, which he chaired. He currently chairs the Health Services Abstract Review Committee.

The author of more than 400 published original research articles and reviews and 60 editorials and book chapters, Dr. Solomon also has extensive experience in the journal editorial arena. At *Arthritis & Rheumatology*, he is a past Co-Editor, and he has just completed a 5-year term as Deputy Editor.

The editorial team working with Dr. Solomon consists of well-known and respected experts in clinical, translational, and basic research spanning all aspects of rheumatology and related disciplines, including Deputy Editors Richard Bucala, MD, PhD, Mariana Kaplan, MD, and Peter Nigrovic, MD and Co-Editors Karen Costenbader, MD, MPH, David Felson, MD, MPH, and Richard Loeser, MD, along with an international team of 20 prominent Associate Editors.

The ACR is excited and honored to have Dr. Solomon as the next Editor-in-Chief of *A&R*. We look forward to the innovation he will bring and the tradition of excellence he will continue to uphold.

Ellen M. Gravallese, MD
President, American College of Rheumatology

American College of Rheumatology
Empowering Rheumatology Professionals

Arthritis & Rheumatology
Vol. 72, No. 7, July 2020, pp 1046–1048
DOI 10.1002/art.41280

EDITORIAL

An Opportunity Missed: Biosimilars in the United States

Guro L. Goll and Tore K. Kvien

For the past 7 years, the European and North American experiences with biosimilars have diverged. While the implementation and clinical experience with biosimilars have developed rapidly in many European countries, the US has stalled. In this issue of *Arthritis & Rheumatology*, Baker and colleagues discuss how this disparity came about and also how it may be corrected (1).

A biosimilar is a reproduction of an originator therapeutic molecule, with the same amino acid sequence but with some subtle differences that are by definition deemed to be of no clinical significance. In the context of rheumatology, a biosimilar is a large, complex molecule rather than a smaller first-generation biosimilar such as filgrastim. All approved biosimilars go through a careful approval process by the European Medicines Agency (EMA) and/or the Food and Drug Administration (FDA), where the emphasis is to demonstrate molecular similarity to the originator through a comprehensive comparability exercise. The approval of the first second-generation biosimilar, infliximab CT-P13, by the EMA in 2013 and the FDA in 2016 was based on this preclinical comparability exercise, but also on data derived from 2 randomized controlled trials conducted using patients with ankylosing spondylitis (AS) (Programme Evaluating the Autoimmune Disease Investigational Drug CT-P13 in AS Patients, a phase I study) and patients with rheumatoid arthritis (RA) (Programme Evaluating the Autoimmune Disease Investigational Drug CT-P13 in RA Patients, a phase III study) (2,3). Approval was extended not only for AS and RA but also for inflammatory bowel disease, psoriatic arthritis, and psoriasis.

Biosimilars are approved based on so-called "extension of indication," meaning that clinical studies are required only in one of the relevant diseases in order to gain regulatory approval for all the indications of the originator. This reduced need for clinical trials results in lower costs for biosimilars. A biosimilar is neither better nor worse than its reference product in terms of efficacy and safety. Hence, the only reason to choose a biosimilar agent rather than the originator is to save costs (4–6).

Despite many biosimilars being approved in the US, they have struggled to gain significant market shares: of 13 approved biosimilars relevant to rheumatology, only 3 have actually been launched (7). Baker et al performed a cross-sectional study of uptake in the ordering of biosimilars at 2 medical centers in the same geographical region in the US. One of these was an academic medical center, the other a Veterans Affairs Medical Center (VAMC). The average sales price has been lower for biosimilar infliximab than for the originator since 2017, indicating an attractive opportunity to save medication costs. Assessing the impact of biosimilars at the 2 institutions between May 1, 2015 and July 31, 2019, the authors found that the biosimilar infliximab was used in 38% of infusions at the VAMC, with a cost per vial 81% lower for biosimilar infliximab compared to the originator. In comparison, the academic medical center, while administering far more infliximab infusions, used the originator in 99% of patients. The authors argue that current reimbursement rules outside the VA system explain the slow uptake of biosimilars, with the estimated institutional incentive being the same or even larger for originator infliximab compared to the biosimilar. The inferred conclusion is that with stronger cost-saving initiatives from US institutions and health authorities, significant savings on drug prices can be made.

The importance of government and institutional incentives is made clear when looking at how biosimilars have been implemented in Europe. Biosimilars now enjoy a substantial market share in most European countries (8). The biosimilar experience in Scandinavia has been particularly successful. Norway and Denmark have annual national tender systems for biologic medicines within rheumatology, gastroenterology, and dermatology, covering either the whole country or large regions, where biosimilars compete alongside originator products. The perception among regulators as well as clinicians is that biosimilars are equivalent to the originator regarding efficacy, safety, and immunogenicity, based on several studies, including switch/transition studies (9–11). The winner of the tender becomes the preferred drug for patients

Guro L. Goll, MD, PhD, Tore K. Kvien, MD, PhD: Diakonhjemmet Hospital, Oslo, Norway.

Dr. Goll has received consulting fees, speaking fees, and/or honoraria from AbbVie, Biogen Idec, Boehringer Ingelheim, Orion Pharma, Eli Lilly, Novartis, Pfizer, MSD, Roche, and UCB Pharma (less than $10,000 each). Dr. Kvien has received consulting fees, speaking fees, and/or honoraria from AbbVie, Amgen, Biogen, Bristol Myers Squibb, Celltrion, Egis, Eli Lilly, Evapharma, Ewopharma, Janssen, MSD, Mylan, Oktal Pharma, Orion Pharma, Pfizer, Roche, Sandoz, Sanofi, and UCB Pharma (less than $10,000 each).

Address correspondence to Tore K. Kvien, MD, PhD, Diakonhjemmet Hospital, Department of Rheumatology, Box 23 Vinderen, Oslo, Norway N-0319. E-mail: t.k.kvien@medisin.uio.no.

Submitted for publication March 5, 2020; accepted in revised form March 31, 2020.

starting a new biologic treatment during the tender period. A different choice of drug is possible at the discretion of the treating physician, provided the reasons for doing so are documented in the patient records.

In Norway, this national tender system has seen prices fall dramatically. In 2014, the offered price for infliximab CT-P13 (Remsima) was 39% lower than the price for the originator infliximab (Remicade). The price reduction the following year was 69%. Because of confidential pricing of pharmaceutical products in the following years, we cannot provide details about price reductions, but official government estimates of cost savings in 2019 were $50–60 million. This constitutes a 25% reduction in cost from 2018 to 2019 for biologic drugs within rheumatology, gastroenterology, and dermatology. Notably, lower costs were mainly caused by a major price reduction for Humira in competition with several biosimilar adalimumab products. While actual production costs make such huge year-on-year savings impossible, it is clear that competition has caused dramatically lower prices both for biosimilars and the originator drugs competing with them.

A viable market share for biosimilars requires that not only new patients receive a biosimilar; a truly competitive environment mandates that patients already receiving an originator biologic drug are also switched to a corresponding biosimilar. In Denmark, the government mandated such a switch for infliximab in May 2015. Etanercept and adalimumab have followed, with no adverse results reported on a group level (12–14). Following publication of results from the NOR-SWITCH study (11,15), patients in Norway have also been widely switched from their originator drug to a corresponding biosimilar. The reductions in cost have also led to a higher uptake of biologic drugs in Norway, even though this uptake was high before the entry of biosimilars. Biologics were on average prescribed to RA patients showing moderate disease activity (16). For example, prescriptions of Humira increased 2.5-fold in 2019 after winning the national tender. The use of etanercept increased by 40% from 2016 to 2019 (about 85% of the prescribed etanercept was a biosimilar by the end of 2019). Also, there has been a >3-fold increase in the use of infliximab since 2015, with very few patients still using the originator Remicade. Thus, in Norway, competition, national tenders, and availability of biosimilars have led to better access to therapy for more people in need of biologic drugs, while at the same time showing a total cost reduction for biologics for use in rheumatology, gastroenterology, and dermatology.

According to the Organization for Economic Cooperation and Development (OECD), US health care is the most expensive in the world at $10,000 per capita versus $5,300 per capita on average for other wealthy OECD countries (17). This high-cost health care is not necessarily reflected in better outcomes for American patients: the US now has the lowest life expectancy and the highest infant mortality rate among high-income countries (18,19). High price of medication has been a particular concern as a contributor to high costs without improved patient benefits, as shown in academic papers and in public debate (20,21). The slow implementation of biosimilars across the US falls neatly in line with this high cost profile. Unless there is a real zeal to reform, the experience with biosimilars in rheumatology does not augur well for other fields such as oncology. As Americans seem to lose out on the cost-cutting potential of biosimilars, this missed opportunity is set to get even more expensive.

AUTHOR CONTRIBUTIONS

Drs. Goll and Kvien drafted the article, revised it critically for important intellectual content, and approved the final version to be published.

REFERENCES

1. Baker JF, Leonard CE, Lo Re V III, Weisman MH, George MD, Kay J. Biosimilar uptake in academic and Veterans Health Administration settings: influence of institutional incentives. Arthritis Rheumatol 2020;72:1067–71.
2. Park W, Hrycaj P, Jeka S, Kovalenko V, Lysenko G, Miranda P, et al. A randomised, double-blind, multicentre, parallel-group, prospective study comparing the pharmacokinetics, safety, and efficacy of CT-P13 and innovator infliximab in patients with ankylosing spondylitis: the PLANETAS study. Ann Rheum Dis 2013;72:1605–12.
3. Yoo DH, Hrycaj P, Miranda P, Ramiterre E, Piotrowski M, Shevchuk S, et al. A randomised, double-blind, parallel-group study to demonstrate equivalence in efficacy and safety of CT-P13 compared with innovator infliximab when coadministered with methotrexate in patients with active rheumatoid arthritis: the PLANETRA study. Ann Rheum Dis 2013;72:1613–20.
4. Uhlig T, Goll GL. Reviewing the evidence for biosimilars: key insights, lessons learned and future horizons. Rheumatology (Oxford) 2017;56:iv49–62.
5. Kay J, Schoels MM, Dörner T, Emery P, Kvien TK, Smolen JS, et al. Consensus-based recommendations for the use of biosimilars to treat rheumatological diseases. Ann Rheum Dis 2018;77:165–74.
6. Schneider CK. Biosimilars in rheumatology: the wind of change [editorial]. Ann Rheum Dis 2013;72:315–8.
7. US Food and Drug Administration. Center for Drug Evaluation and Research. List of licensed biological products with (1) reference product exclusivity and (2) biosimilarity or interchangeability evaluations to date. 2020. URL: https://www.fda.gov/media/89589/download.
8. Quintiles IMS. The impact of biosimilar competition in Europe. URL: https://www.medicinesforeurope.com/wp-content/uploads/2017/05/IMS-Biosimilar-2017_V9.pdf.
9. Yoo DH, Prodanovic N, Jaworski J, Miranda P, Ramiterre E, Lanzon A, et al. Efficacy and safety of CT-P13 (biosimilar infliximab) in patients with rheumatoid arthritis: comparison between switching from reference infliximab to CT-P13 and continuing CT-P13 in the PLANETRA extension study. Ann Rheum Dis 2017;76:355–63.
10. Park W, Yoo DH, Miranda P, Brzosko M, Wiland P, Gutierrez-Urena S, et al. Efficacy and safety of switching from reference infliximab to CT-P13 compared with maintenance of CT-P13 in ankylosing spondylitis: 102-week data from the PLANETAS extension study. Ann Rheum Dis 2017;76:346–54.
11. Jorgensen KK, Olsen IC, Goll GL, Lorentzen M, Bolstad N, Haavardsholm EA, et al. Switching from originator infliximab to biosimilar CT-P13 compared with maintained treatment with originator infliximab (NOR-SWITCH): a 52-week, randomised, double-blind, non-inferiority trial. Lancet 2017;389:2304–16.
12. Glintborg B, Sorensen IJ, Loft AG, Lindegaard H, Linauskas A, Hendricks O, et al. A nationwide non-medical switch from originator

infliximab to biosimilar CT-P13 in 802 patients with inflammatory arthritis: 1-year clinical outcomes from the DANBIO registry. Ann Rheum Dis 2017;76:1426–31.

13. Glintborg B, Ibsen R, Bilbo RE, Lund Hetland M, Kjellberg J. Does a mandatory non-medical switch from originator to biosimilar etanercept lead to increase in healthcare use and costs? A Danish register-based study of patients with inflammatory arthritis. RMD Open 2019;5:e001016.
14. Glintborg B, Loft AG, Omerovic E, Hendricks O, Linauskas A, Espesen J, et al. To switch or not to switch: results of a nationwide guideline of mandatory switching from originator to biosimilar etanercept. One-year treatment outcomes in 2061 patients with inflammatory arthritis from the DANBIO registry. Ann Rheum Dis 2019;78:192–200.
15. Goll GL, Jorgensen KK, Sexton J, Olsen IC, Bolstad N, Haavardsholm EA, et al. Long-term efficacy and safety of biosimilar infliximab (CT-P13) after switching from originator infliximab: open-label extension of the NOR-SWITCH trial. J Intern Med 2019;285:653–69.
16. Aga AB, Lie E, Uhlig T, Olsen IC, Wierod A, Kalstad S, et al. Time trends in disease activity, response and remission rates in rheumatoid arthritis during the past decade: results from the NOR-DMARD study 2000-2010. Ann Rheum Dis 2015;74:381–8.
17. OECDiLibrary. Health resources. Health spending. 2020. URL: https://www.oecd-ilibrary.org/social-issues-migration-health/health-spending/indicator/english_8643de7e-en.
18. OECDiLibrary. Health status. Life expectancy at birth. 2020. URL: https://www.oecd-ilibrary.org/social-issues-migration-health/life-expectancy-at-birth/indicator/english_27e0fc9d-en.
19. OECDiLibrary. Health status. Infant mortality rates. 2020. URL: https://www.oecd-ilibrary.org/social-issues-migration-health/infant-mortality-rates/indicator/english_83dea506-en.
20. Papanicolas I, Woskie LR, Jha AK. Health care spending in the United States and other high-income countries. JAMA 2018;319:1024–39.
21. Yazdany J. Failure to launch: biosimilar sales continue to fall flat in the United States. Arthritis Rheumatol 2020;72:870–3.

Arthritis & Rheumatology
Vol. 72, No. 7, July 2020, pp 1049–1058
DOI 10.1002/art.41246

American College of Rheumatology
Empowering Rheumatology Professionals

EMERGING TREATMENT MODELS IN RHEUMATOLOGY

Current and Future Outlook on Disease Modification and Defining Low Disease Activity in Systemic Sclerosis

Vivek Nagaraja,[1] Marco Matucci-Cerinic,[2] Daniel E. Furst,[3] Masataka Kuwana,[4] Yannick Allanore,[5] Christopher P. Denton,[6] Ganesh Raghu,[7] Vallerie Mclaughlin,[1] Panduranga S. Rao,[1] James R. Seibold,[8] John D. Pauling,[9] Michael L. Whitfield,[10] and Dinesh Khanna[1]

Systemic sclerosis (SSc) is an autoimmune rheumatic disease with heterogeneous clinical manifestations and a variable course in which the severity of the pathology dictates the disease prognosis and course. Among autoimmune rheumatic diseases, SSc has the highest mortality rate among all rheumatic diseases, though there are exciting new therapeutic targets that appear to halt the progression of SSc manifestations such as skin or lung fibrosis. In selected patients, high-intensity regimens with autologous stem cell transplantation can favorably modify the course. In what was once thought to be an untreatable disease, targeted therapies have now changed the outlook of SSc to a treatable disorder. Herein, we discuss the targeted therapies modifying the outlook on selected organ involvement and creating opportunities for future treatment. We also present a framework for defining low disease activity in SSc.

INTRODUCTION

Systemic sclerosis (SSc) is a rare disease characterized by vasculopathy and fibrosis in the skin and internal organs (1). The proposed pathophysiology is a triad of vascular damage with endothelial dysfunction, dysregulation of innate and adaptive immunity, and widespread fibrosis in multiple organs (2,3). The mortality rate in SSc is higher than in any other rheumatic disease (4,5).

In contrast to rheumatoid arthritis (RA), the concept and use of disease-modifying therapies that attenuate or reverse pathology and clinical impact are not currently applied to SSc. The notion of disease modification in SSc has now advanced to reality based on data from recent clinical trials. Autologous hematopo-

Drs. Furst and Raghu's work was supported by the NIH. Dr. Khanna's work was supported by the National Institute of Arthritis and Musculoskeletal and Skin Diseases, NIH (grants K24-AR-063120 and R01-AR-07047) and the National Institute of Allergy and Infectious Disease, NIH.

[1]Vivek Nagaraja, MD, Vallerie Mclaughlin, MD, Panduranga S. Rao, MD, Dinesh Khanna, MD, MSc: University of Michigan, Ann Arbor; [2]Marco-Matucci Cerinic, MD, PhD: University of Florence, Florence, Italy; [3]Daniel E. Furst, MD: University of California, Los Angeles, University of Washington, Seattle, and University of Florence, Florence, Italy; [4]Masataka Kuwana, MD, PhD: Nippon Medical School, Tokyo, Japan; [5]Yannick Allanore, MD, PhD: Paris Descartes University, INSERM U116, Université Sorbonne Paris Cité, and Cochin Hospital, Paris, France; [6]Christopher P. Denton, MD: University College London and Royal Free Hospital, London, UK; [7]Ganesh Raghu, MD: University of Washington, Seattle; [8]James R. Seibold, MD: Scleroderma Research Consultants, LLC, Aiken, South Carolina; [9]John D. Pauling, BMedSci, BMBS, PhD, FRCP: Royal National Hospital for Rheumatic Diseases, Royal United Hospitals, Bath, UK; [10]Michael L. Whitfield, PhD: Geisel School of Medicine at Dartmouth, Hanover, New Hampshire.

Dr. Nagaraja has received honoraria from Eicos Sciences. Dr. Cerinic has received consulting fees from Bristol-Myers Squibb, Pfizer, ChemomAb, Actelion, Janssen, and Eli Lilly (less than $10,000 each). Dr. Furst has received consulting fees from Amgen, Bristol-Myers Squibb, Corbus, Galapagos, Novartis, Pfizer, Roche/Genentech, Talaris, CSL Behring, and Boehringer Ingelheim (less than $10,000 each) and research support from Bristol-Myers Squibb, Corbus, Galapagos, GlaxoSmithKline, Pfizer, Sanofi, Talaris, and CSL Behring. Dr. Kuwana has received consulting fees from Actelion, Roche/Chugai, Bayer, Boehringer Ingelheim, Corbus, and GlaxoSmithKline (less than $10,000 each) and speaking fees from Roche/Chugai and Actelion (less than $10,000 each). Dr. Allanore has received consulting fees from Actelion, Bayer, Bristol-Myers Squibb, Curzion, Boehringer Ingelheim, Inventiva, Roche, and Sanofi (less than $10,000 each). Dr. Denton has received consulting fees, speaking fees, and/or honoraria from Roche/Genentech, Actelion, GlaxoSmithKline, Sanofi/Aventis, Acceleron, Inventiva, CSL Behring, Boehringer Ingelheim, and Bayer (less than $10,000 each). Dr. Raghu has received consulting fees from Avalyn, Acceleron, Biogen, Blade Therapeutics, Bridge Biotherapeutics, Bristol-Meyers Squibb, Bellerophon, FibroGen, Gilead Sciences, IQVIA, Promedior, Nitto, Respivant, Roche/Genentech, Sanofi/Aventis, Veracyte, Zambon, and Boehringer Ingelheim (less than $10,000 each). Dr. Mclaughlin has received consulting fees from Actelion, Acceleron, Arena, Bayer, Caremark, Gilead, SoniVie, and United Therapeutics (less than $10,000 each). Dr. Seibold has received consulting fees from Atlantic, Blade, Eicos, Eiger, Indalo, Mitsubishi, Bayer, Boehringer Ingelheim, Camurus, Corbus, EMD Serono, DRG, and Guidepoint (less than $10,000 each) and owns stock or stock options in BriaCell and Pacific Therapeutics. Dr. Pauling has received consulting fees from Actelion, Boehringer Ingelheim, and Sojournix (less than $10,000 each) and research support from Actelion. Dr. Whitfield has received consulting fees from Bristol-Myers Squibb and Celdara Medical (less than $10,000 each). Dr. Khanna has received consulting fees from Actelion, AstraZeneca, Bayer, Bristol-Myers Squibb, Boehringer Ingelheim, ChemomAb, Corbus, CSL Behring, Cytori, GlaxoSmithKline, Horizon, Pfizer, Regeneron, Roche/Genentech, Sanofi/Aventis, and UCB Pharma (less than $10,000 each) and owns stock or stock options in Eicos Sciences. No other disclosures relevant to this article were reported.

Address correspondence to Dinesh Khanna, MD, MSc, University of Michigan, Division of Rheumatology, Department of Internal Medicine, Suite 7C27, 300 North Ingalls Street, SPC 5422, Ann Arbor, MI 48109. E-mail: khannad@med.umich.edu.

Submitted for publication April 12, 2019; accepted in revised form February 27, 2020.

ietic stem cell transplantation (HSCT) trials in diffuse cutaneous SSc (dcSSc) have demonstrated survival benefit, including meaningful improvements in skin, lung fibrosis, and health-related quality of life (HRQoL) (6–9).

In this report, we discuss specific treatments that have modified the course of organ-specific manifestations in SSc and have started the conversation on defining low disease activity in SSc.

What is disease-modifying therapy?

We borrow the concept of "disease-modifying therapy" from the use of disease-modifying antirheumatic drugs (DMARDs) and biologic response modifiers in RA. In the past 3 decades, RA treatment has evolved from symptom management to the implementation of DMARDs and/or biologic response modifiers. The early institution of DMARDs or biologic response modifiers in RA induces clinical remission, reduces the frequency of relapse, abrogates joint damage, preserves physical function, improves HRQoL, and prevents long-term disability (10). Similarly, we can conceptualize disease-modifying therapy in SSc as therapies or medication regimens that positively impact the disease course by stabilizing and potentially improving organ function. This, in turn, improves HRQoL and reduces morbidity and mortality (11).

Natural history of the disease

Understanding the natural history of the SSc disease process is vital to the concept of disease-modifying therapy in the context of timing and patient selection. Early clinical features include Raynaud's phenomenon (RP) and gastroesophageal reflux disease (12). Skin fibrosis is a pathologic hallmark of the disease and is frequently preceded by puffy and swollen fingers. Patients with puffy fingers, definite RP, typical nailfold capillary changes, and the presence of SSc-specific antibodies can be considered to have very-early-diagnosed SSc (13,14). Thereafter, patients may progress to 1 of 3 clinical disease subsets based on the extent of skin involvement.

Patients with skin involvement restricted to the limbs distal to the elbows or knees, with or without face involvement, are classified as having limited cutaneous SSc (lcSSc). Patients with distal as well as proximal involvement (including the torso) are classified as having dcSSc. A small subset of patients without skin involvement but who have scleroderma-specific antibodies and internal organ involvement are considered to have SSc without scleroderma (15–17). This differentiation is important as dcSSc is associated with higher morbidity and mortality, mainly due to more severe and/or progressive internal organ involvement (18). However, this differentiation of the clinical phenotypes is an oversimplification of the disease process.

The biology of SSc is complex, heterogeneous, and dynamic, with sequentially overlapping features of inflammation, autoimmunity, tissue injury, and fibrosis. Skin thickness is generally progressive within the first 3 years after the start of RP in dcSSc, but there is individual variability (15,16). The extent and severity of skin involvement in dcSSc generally level off by years 4 and 5, and then clinically appear to improve both via de-remodeling and atrophy (19). Only a minority of patients have a new emergence of progressive cutaneous involvement beyond 5 years after disease onset. There is an increased risk for the development of internal organ involvement during the progressive skin phase. For example, in dcSSc, most internal organ involvement (lung, renal, cardiac, and gastrointestinal) occurs in the first 3–5 years after disease onset (Figure 1) (16). In the early phase of dcSSc, internal organ involvement—although clinically silent—may evolve at the same time as progressive skin disease. There are, however, exceptions. For example, pulmonary arterial hypertension (PAH) is generally a late complication that is more common in lcSSc (20). Lung fibrosis can also develop separately from or in conjunction with pulmonary hypertension. Fibrosis can advance in a self-perpetuating manner and may not be driven solely by an immune-mediated process (21).

We believe SSc can be conceptualized as a family of similar diseases—an idea supported by the identification of molecular subsets by whole-genome gene expression profiling, with distinct clinical and serologic features and recognized phases within some subtypes (22). The delayed emergence of new organ involvement and gradual progression of the disease provide clinicians with a realistic opportunity to impede disease progression and change disease course.

Why is disease-modifying therapy a challenge in SSc?

Many challenges exist in demonstrating disease-modifying effects in SSc patients. First, the disease is heterogeneous with different patterns of evolution among the clinical subsets, as previously outlined (5,23–25). Patients usually present with predominantly vasculopathic complications (such as RP, digital

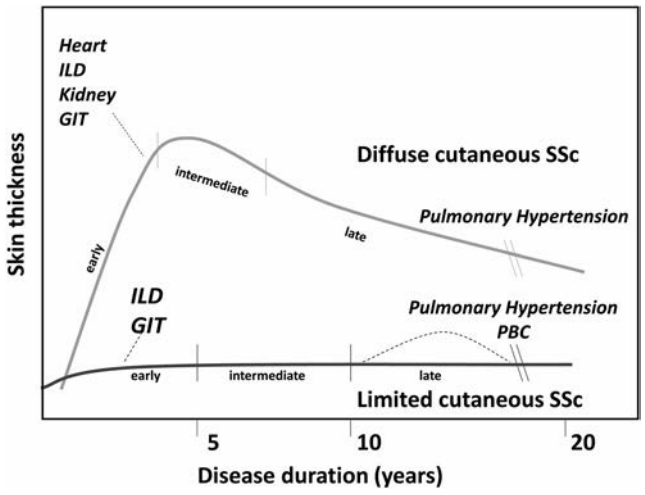

Figure 1. The usual timing of organ-specific manifestations in systemic sclerosis (SSc). ILD = interstitial lung disease; GIT = gastrointestinal tract; PBC = primary biliary cirrhosis. Adapted, with permission, from Steen V, Medsger TA. Systemic sclerosis. Lippincott Williams & Wilkins; 1996.

ulcers, PAH, scleroderma renal crisis [SRC], and gastrointestinal involvement), predominately fibrotic complications (such as skin fibrosis, joint involvement, lung fibrosis, and cardiac fibrosis), or a combination of these features. Within each cutaneous subgroup, there is heterogeneity in internal organ involvement (18). Second, there are molecular differences in the skin gene expression data in patients with a similar phenotype. One such formulation identified 4 subsets based on skin gene expression data: normal-like, inflammatory, fibroproliferative, and limited (22,26). These subsets help identify patients at risk for internal organ involvement, such as interstitial lung disease (ILD), as well as their response to current therapies (26,27). Measuring gene expression subsets in clinical trials, and possibly even in routine clinical care, may clearly distinguish and clarify patient heterogeneity in the near future and provide a window through which to understand and predict patient response to therapy. Third, the predictors of disease status at a specific time point (incidence or severity of organ-based complications, which is largely influenced by autoantibodies) may differ from predictors of disease progression (28,29).

Unlike the Disease Activity Score in 28 joints (30), Clinical Disease Activity Index (31), or other disease activity measures in RA, we lack reliable tools with which we can define the achievement of remission in SSc. In dcSSc, the modified Rodnan skin score (MRSS) (32), and recently, a combined responder index in dcSSc (American College of Rheumatology Combined Response Index in diffuse cutaneous Systemic Sclerosis [ACR CRISS] [33]—a composite end point that captures cardiopulmonary-renal involvement and change in MRSS, Health Assessment Questionnaire disability index [HAQ DI] [34], patient global assessment of disease activity, physician global assessment of disease activity, and forced vital capacity percent predicted [FVC%]) are used as outcome measures to assess the efficacy of drugs. These measures have not been validated in lcSSc, and some of these may not perform well (35). Further, clinical heterogeneity of the disease does not allow for precise definition of global disease activity. Composite scores such as the revised European Scleroderma Research Group Activity Index (28) have been proposed but not widely accepted in the evaluation of disease activity. Novel approaches for assessing disease activity in SSc are currently under development (36).

Are there currently disease-modifying therapies for SSc?

Despite the limitations in disease activity measurement in SSc, treatment approaches directed toward specific biologic targets appear to be positively influencing outcomes in SSc (Supplementary Table 1, available on the *Arthritis & Rheumatology* web site at http://onlinelibrary.wiley.com/doi/10.1002/art.41246/abstract). This concept can be approached by categorizing SSc manifestations into vasculopathic, immunologic, or inflammatory involvement as well as tissue fibrosis.

Vasculopathy

The predominant vascular complications in SSc are RP, PAH, SRC, and digital ulcers. Morbidity and mortality are high in patients with PAH and SRC. RP and digital ulcers are chronic complications that can limit hand function, increase morbidity and disability (37), and impact HRQoL. Pathophysiologic mechanisms in SSc vasculopathy are characterized by initial vascular endothelial injury and dysfunction followed by vessel wall remodeling with intimal and medial thickening, leading to luminal narrowing, vascular stiffness, and tissue hypoxia (38).

Pulmonary arterial hypertension. One of the relevant vasculopathic manifestations, which is associated with significant mortality and morbidity in SSc patients, is PAH. The prevalence of PAH measured by right-sided heart catheterization in large cohorts of SSc patients ranges from 5% to 12% (39,40). SSc-PAH is associated with a worse outcome compared to idiopathic PAH because there are non–PAH-related factors in SSc like coexistent ILD-associated pulmonary hypertension, pulmonary venoocclusive disease, SSc-related myocardial disease, and later age at disease onset (41,42). Greater emphasis has been put on early screening and detection of SSc-PAH with the use of composite algorithms, allowing for the earlier institution of PAH-specific therapy (43–45). There is a growing body of evidence that this approach may improve morbidity outcomes, although the effect on long-term mortality is unclear (46). The lower incidence of SSc-PAH in patients treated with dihydropyridine calcium antagonists offers a tantalizing glimpse into the potential disease-modifying actions of fairly modest vasodilator therapy on long-term outcomes in SSc (47).

There are multiple approved therapies for PAH management that target 1 of the 3 pathogenic pathways: 1) endothelin antagonists, 2) nitric oxide (NO)/soluble guanylate cyclase (GC) agonists/stimulators, and 3) prostacyclin analogs (48). High-quality randomized controlled trials (RCTs) have shown that upfront or sequential combination therapies delay time to clinical worsening in PAH patients. Similar approaches with combination therapies have suggested efficacy in treating SSc-PAH. In a recent meta-analysis, combination therapy targeting PAH was demonstrated to have greater therapeutic efficacy than monotherapy in patients with SSc-PAH. There was a 27% reduction in clinical worsening (pooled relative risk 0.73 [95% confidence interval 0.60–0.89]) (P = 0.002) and probable improvement of exercise capacity in these patients (49). A recent trial of rituximab (RTX) in SSc-PAH showed trends of benefit on functional status (6-munute walk test) and pulmonary vascular resistance versus placebo (ClinicalTrials.gov identifier: NCT01086540), and there is also an ongoing trial of tocilizumab in the background of currently approved therapies (ClinicalTrials.gov identifier: NCT02676947) (50,51).

Raynaud's phenomenon and digital ulcers. In SSc, common and burdensome vascular manifestations include RP and digital ulcers. RP can be an early sign preceding the diagnosis of SSc, usually emerging prior to tissue fibrosis (52). RP is a manifestation of abnormal cutaneous vessel function involved in thermal regulation of blood flow (53). The presence of RP and the loss of normal regulation of cutaneous vascular tone are often predictors of SSc development—although they are not specific to SSc, cannot be used alone as predictors, and may be long-delayed symptoms (52,54).

Digital ulcers are a significant cause of morbidity, with ~50% of SSc patients developing digital ulcers during their disease course (18). Digital ulcers can be a sporadic phenomenon, but for some patients, they are recurrent, continuous, and/or refractory (55). Digital ulcers can lead to significant disability in the form of impaired hand function and increased pain, loss of employment, and medical complications like gangrene, cellulitis, osteomyelitis, and digital amputation. Progress has been made in secondary prevention, although with mixed results. Phosphodiesterase 5 (PDE5) inhibitors, especially sildenafil, can reduce the frequency of RP episodes in SSc (56). A recent RCT comparing the use of oral sildenafil (20 mg/3 times a day) to placebo favored sildenafil in significantly decreasing the number of digital ulcers at week 12, but did not meet the primary end point of time to healing (57). In SSc patients with refractory and recurrent digital ulcers, it has been shown that 62.5 mg of bosentan (an endothelin 1 receptor antagonist) 2 times a day over a 4-week-period, followed by 125 mg of bosentan 2 times a day can reduce the number of new digital ulcers in those with >4 previous digital ulcers, without any effect on healing digital ulcers that already present (58,59). Intravenous (IV) prostanoid therapy improves digital ulcer healing and reduces the number of new digital ulcers. In 2 multicenter, double-blind, randomized trials, IV prostanoid therapy (iloprost 0.5–2.0 ng/kg/minute over 6 hours for 5 consecutive days) was associated with significant improvement in the frequency of RP episodes and greater improvement in digital ulcer healing (60,61).

Scleroderma renal crisis. A major, life-threatening vasculopathic manifestation of SSc is SRC (62). SRC is a rare complication that affects 2–15% of patients with SSc (11% of dcSSc patients and 4% of lcSSc patients) (40). SRC typically presents in patients with early, rapidly progressive dcSSc, often with the presence of anti-RNA polymerase III antibodies (63). The prognosis of SRC substantially improved in the 1980s with the introduction of angiotensin-converting enzyme (ACE) inhibitors for rapid blood pressure control and with additional antihypertensive agents as required (62). In a prospective analysis of 108 patients with SRC in a single center, patients who received ACE inhibitors (captopril [n = 47] and enalapril [n = 8]) had a significantly better survival rate at 1 year (76%) and 5 years (66%) compared to patients who did not receive ACE inhibitors (1 year [15%] and 5 years [10%]) (62). In another prospective trial, 145 patients with SRC treated with ACE inhibitors demonstrated survival rates of 90% and 85% at 5 and 8 years, respectively, after onset of SRC (64). Furthermore, treatment with ACE inhibitors decreased the need for permanent dialysis (16). Overall, current patient survival is 70–82% at 1 year, but decreases to 50–60% at 5 years despite dialysis support.

In summary, there are therapies available for vasculopathy that have disease-modifying effects, including improved HRQoL, morbidity, and survival. These effects are well-demonstrated for SRC and PAH with unequivocal benefits in clinical trials.

Immunoinflammatory involvement

The concept of ablating an autoreactive immune system followed by its replacement with a self-tolerant one (also called HSCT) has been successfully explored in SSc (7,8). Oral or pulse IV cyclophosphamide (CYC) therapy in individuals with symptomatic, established SSc-ILD has a significant, though modest, beneficial effect on lung function, thickening of the skin, dyspnea, and HRQoL (65,66) and has no impact on long-term survival (67,68).

Three major prospective trials were initiated to examine the role of HSCT in SSc treatment—the Autologous Stem Cell Transplantation International Scleroderma (ASTIS) trial (7), the American Scleroderma Stem Cell versus Immune Suppression trial (ASSIST) (8), and the Scleroderma: Cyclophosphamide Or Transplantation (SCOT) trial (6). These studies compared autologous HSCT (with and without radiation) to various IV CYC treatment regimens. All studies included patients with early dcSSc who had moderate-to-severe skin thickness and internal organ involvement (lung involvement largely accounted for the vast majority of patients). Study patients were those who were predicted to have disease activity that would rapidly progress. Although there were substantial differences in the study design among these trials, the results of the 3 studies allowed for valid conclusions to be drawn with regard to the effect of HSCT in patients with early SSc who have progressive skin and/or lung involvement. The notable observations of outcomes among patients who underwent HSCT were as follows: 1) clinically meaningful improvement in skin thickness, 2) overall stabilization of lung function, 3) clinically meaningful improvement in HRQoL, 4) overall survival benefit (although higher short-term serious adverse events in the ASTIS and SCOT trials and a higher mortality rate during the first year after transplantation in patients who underwent HSCT in the ASTIS trial were recorded), and 5) the observation that SSc heart disease (myocardial involvement and PAH) appears to be the main driver of transplantation-related death (6–8,69).

In summary, HSCT trials provide clear evidence of immune-mediated pathogenesis in SSc and document long-term, clinically important disease modification in early aggressive disease.

Tissue fibrosis

Three important manifestations of tissue fibrosis include skin fibrosis, ILD, and myocardial fibrosis.

Skin involvement. Skin fibrosis is a cardinal manifestation and is observed in most SSc patients, although a small minority have no skin involvement (SSc without scleroderma) (17,70). Skin fibrosis is associated with significant morbidity due to pruritis, digital ulcers, skin tightness, and skin ulcers at other sites as well as markedly decreased function. A rapidly progressive phenotype of skin fibrosis is associated with a higher mortality rate due to progressive internal organ involvement (71). Recently, immunosuppressive therapies such as CYC, mycophenolate mofetil (MMF), and biologic response modifiers (such as abatacept and tocilizumab) have been evaluated for their effects on skin thickening in dcSSc. Based on the data from Scleroderma Lung Studies I and II (SLS I and II), treatment of patients with dcSSc with CYC or MMF resulted in clinically meaningful improvement in the MRSS as compared to those receiving placebo (72). In a recent RCT, abatacept treatment (versus placebo) resulted in clinically meaningful change in ACR CRISS scores despite no significant change in MRSS. Decline in MRSS over 12 months was clinically and significantly higher in the abatacept group versus the placebo group for the inflammatory and normal-like skin gene expression subsets (73). In another RCT, subcutaneous tocilizumab trended to improve MRSS but also highlighted a marked heterogeneity in individual response (74).

Interstitial lung disease in SSc. ILD is present in 70–80% of patients with SSc, with ~20–25% developing symptomatic ILD (75,76). ILD is the leading cause of death in SSc and accounts for over one-third of SSc-related deaths (25). Immunosuppressive therapies have been consistently explored for the treatment of SSc-ILD, with differing results.

In SLS I, patients with SSc-ILD received oral CYC or matching placebo for 12 months and were followed up in a double-blind trial for an additional 12 months (65). After 12 months, significant (though modest) treatment effects of CYC versus placebo were observed on FVC and total lung capacity (TLC), but not on diffusing capacity for carbon monoxide (DL_{CO}). The effect on FVC persisted at 18 months in the CYC group (although CYC was no longer being given), but was no longer present at 24 months. Additionally, CYC improved dyspnea, HRQoL, and functional ability. CYC treatment did not change long-term survival, a finding that was not unexpected, given that the treatment was administered for only 1 year (68). In SLS II, patients with SSc-ILD were randomized to receive either 3 grams of oral MMF each day for 24 months or oral CYC each day for 12 months (followed by placebo for 12 months) (77). No significant differences were observed in the long-term survival or organ failure for patients who randomly received CYC versus MMF.

In a recent long-term follow-up of patients in SLS I and II, the majority of patients died of complications related to SSc, with respiratory failure from end-stage lung disease as one of the leading causes of death (68). Data from a phase III clinical trial suggested that interleukin-6 inhibition in early SSc with elevated C-reactive protein levels led to stabilization of FVC% in the tocilizumab group versus a clinically meaningful decline in the placebo group over 48 weeks (treatment difference of 4.2%; $P = 0.0002$) (74). The mean ± SD FVC% was 82.1 ± 14.8 at baseline, which highlights the benefit of treating patients with subclinical ILD who have high-risk features (early dcSSc and elevated C-reactive protein levels). RTX therapy in SSc has shown promising effects on both ILD and skin thickening. In a recent open-label, randomized, controlled trial of RTX treatment (administered in 2 doses of 1,000 mg each) versus monthly pulse CYC therapy, a population of 60 treatment-naive, anti–Scl-70 positive patients with early dcSSc and ILD were analyzed (78). FVC% was improved in the RTX group at the end of 6 months (+5.8% in the RTX group versus –1.2% in the CYC group). The data, overall, suggest that targeted biologic therapies may have disease-modifying effect in ILD with regard to preservation of lung function (74,79).

A recent 52-week, placebo-controlled RCT, treatment with nintedanib, a tyrosine kinase inhibitor, slowed the progression of FVC decline in SSc-ILD, which led to approval by the Food and Drug Administration (80). The adjusted annual rate of decline in FVC was lower in the nintedanib-treated group than in the placebo-treated group (difference 41.0 ml per year; $P = 0.04$), although no clinical benefits for other manifestations of SSc, dyspnea, or function were observed. Overall, ~50% of the patients were receiving MMF at baseline. Among these patients who had received prior MMF treatment, those who were given placebo experienced a smaller decline in the FVC, and in the nintedanib group, the magnitude of the nintedanib treatment effect on the FVC was lower. The rate of gastrointestinal adverse events was higher in the nintedanib group versus the placebo group. Currently, there is an ongoing double-blind RCT (SLS III) comparing the combination of MMF with pirfenidone (an antifibrotic agent approved for treating idiopathic pulmonary fibrosis) versus MMF alone in the treatment of SSc-ILD (ClinicalTrials.gov identifier: NCT03221257) (80).

Cardiac involvement. Cardiac involvement is marked by myocardial fibrosis and has been reported in >50% of autopsies (81). It is frequently encountered in SSc patients, is often asymptomatic, and is associated with higher mortality rate (23,40,63). Alteration in heart rhythm with hemodynamically significant arrhythmias, including ventricular tachycardia, is associated with high mortality. Apart from medical therapy for systolic heart failure, other supportive measures such as implantable cardioverter defibrillators, dual-chamber pacing, or cardiac transplantation may be necessary.

In summary, with regard to fibrosis, data suggest that improvement in skin involvement may not be an achievable end

point in trials at present due to measurement tools that lack sensitivity, difficulty in defining sufficiently uniform entry criteria for trials, and individual heterogeneity in clinical manifestations. However, fibrosis in other organs, particularly in the lungs, may be amenable to treatment with biologic agents, and recently, a tyrosine kinase inhibitor.

Other unmet needs

There are other disabling manifestations in SSc wherein the pathogenesis is poorly understood and/or does not have validated outcome measures. The gastrointestinal tract is involved in up to 95% of patients with SSc and is a presenting feature in ~10% of patients (82). Gastrointestinal involvement causes substantial morbidity and is responsible for 6–12% of deaths in SSc patients. Calcinosis, characterized by the deposition of insoluble calcium salts in the skin and subcutaneous tissue, is observed in ~25% of patients with SSc (83). In SSc, arthritis and joint contractures of the small and large joints are commonly seen in about one-third of patients, with the presence of large joint contractures being predictive of mortality (84,85). Telangiectasias, while themselves harmless in the skin, can be a major source of body image dissatisfaction in addition to a predecessor of pulmonary vascular disease, which would make them valuable markers of disease progression. They may also be a source of gastrointestinal bleeding, leading to potential increased morbidity (86). These manifestations are often unaccounted for as a disease outcome in pharmacologic trials and need to be included in future trials with consistent ways to measure the treatment outcome.

What should modification of disease course look like today, and how should it be measured?

Ideal disease-modifying therapy should halt the progression of the disease and hopefully induce remission, and preferably also reverse some major organ complications, as seen in the recent HSCT trials on fibrotic complications (Figure 2). It is reasonable to expect disease-modifying therapy to stabilize organ function without any further worsening of other domains.

Reliable, valid, and responsive outcome measures are needed to assess the effect of disease-modifying therapy. Based on the RCTs conducted for key clinical manifestations in SSc (shown in Supplementary Table 1, available on the *Arthritis & Rheumatology* web site at http://onlinelibrary.wiley.com/doi/10.1002/art.41246/abstract), lessons have been learned about outcome measures. MRSS (a measure of skin thickness) has shown natural regression, despite enrichment for early disease and/or elevated acute reactants at baseline (73,74,87). Combined measures of response, analogous to such measures used in RA, may be a way forward.

In the RCTs of abatacept and tocilizumab in dcSSc, MRSS was not able to distinguish the efficacy of active therapies compared to placebo, but there were statistically significant and clinically meaningful improvements in the ACR CRISS, a combined measure designed to capture the global or holistic evaluation in early SSc. In the tocilizumab trial, the ACR CRISS was driven by improvement in and stabilization of FVC%, whereas results from the HAQ DI and physician global assessments of disease activity were statistically significant in the abatacept trial. ACR CRISS core set of outcome measures should be included in forthcoming clinical trials.

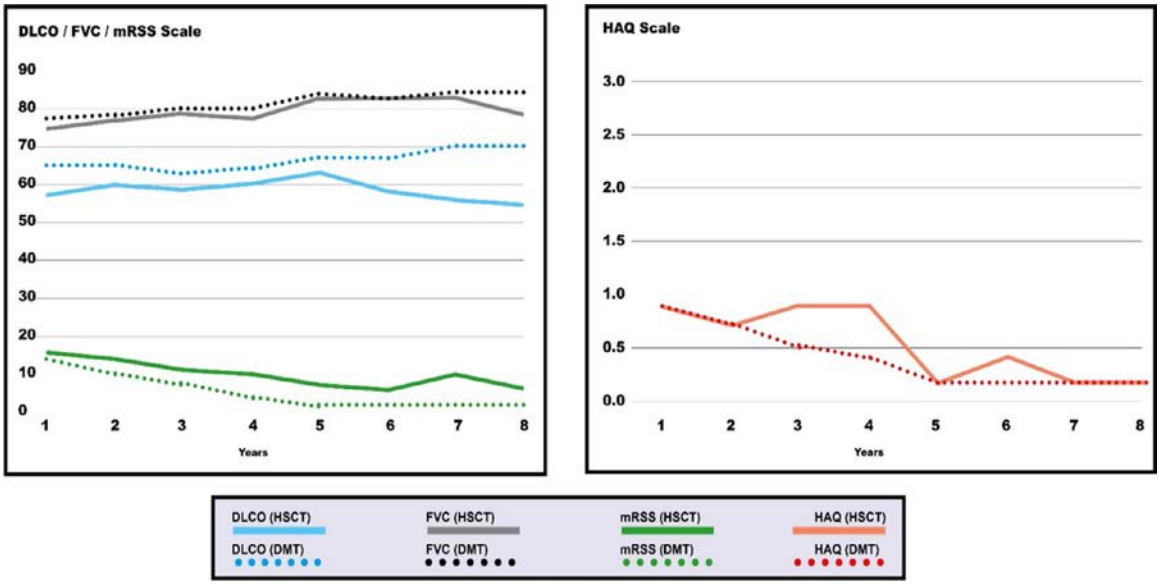

Figure 2. The long-term impact of ideal disease-modifying therapy (DMT), in comparison to hematopoietic stem cell therapy (HSCT), on outcomes in systemic sclerosis (SSc) with a predominantly fribotic phenotype. DLco = diffusing capacity for carbon monoxide; FVC = forced vital capacity; MRSS = modified Rodnan skin score; HAQ = Health Assessment Questionnaire.

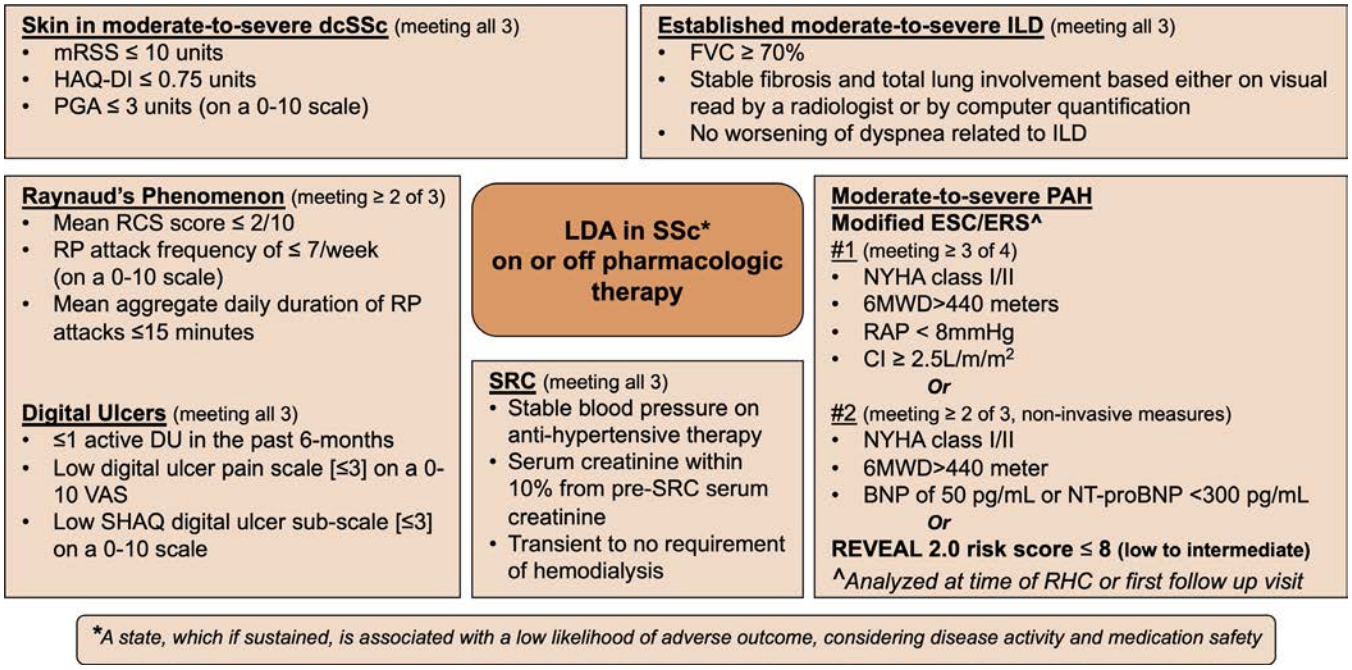

Figure 3. Suggested parameters for low disease activity state (LDA) in systemic sclerosis (SSc). These are author-driven preliminary proposals, influenced by data from randomized control trials and observational studies, which will need further testing and validation in future investigations. dcSSc = diffuse cutaneous SSc; MRSS = modified Rodnan skin score; HAQ DI = Health Assessment Questionnaire disability index; PGA = patient global assessment of disease activity; ILD = interstitial lung disease; FVC = forced vital capacity (percent predicted); RCS = Raynaud's Condition Score; RP = Raynaud's phenomenon; DU = digital ulcer; VAS = visual analog scale; SHAQ = Scleroderma Health Assessment Questionnaire; SRC = scleroderma renal crisis; PAH = pulmonary arterial hypertension; PAP = pulmonary arterial pressure; ESC/ERS = European Society of Cardiology and European Respiratory Society; NYHA = New York Heart Association; 6MWD = 6-minute walking distance; RAP = right atrial pressure; CI = cardiac index; BNP = B-type natriuretic peptide; NT-ProBNP = N-terminal proBNP; REVEAL = Registry to Evaluate Early and Long-Term PAH Disease Management; RHC = right heart catheterization.

Another example is the global rank composite score used in the SCOT trial, which utilized a hierarchical combined measure of response. In SSc-ILD, a combination of objective measures (FVC, DL_{CO}, and lung imaging scores of fibrosis) and a patient-reported measure of dyspnea demonstrated responses and, in combination, could be utilized to increase sensitivity and discrimination. At this point, FVC currently appears to be a valid end point that could be used in these types of clinical trials if given regulatory approval (65,66). In PAH, recent successes have been achieved with clinically meaningful end points such as time to clinical worsening, which is a combined end point influenced by morbidity (such as worsening performance on 6-minute walk distance, worsening of New York Heart Association functional classification, requirement of additional PAH therapy, and hospitalizations due to PAH) or all-cause mortality as a valid end point in PAH (88).

How should we define remission and low disease activity in SSc?

Based on our current understanding and constraints with testing, disease remission, which we define as the absence of disease activity, may not be achievable in the setting of SSc due to the heterogeneity of the disease and the few positive trials that have been conducted to this effect. Buoyed by the outcomes in PAH and HSCT trials, it is time to start creating a framework for the conceptual definition for low disease activity in SSc.

First, low disease activity in SSc should be an individual disease state (on or off therapy). Second, low disease activity (when sustained over a period of time) should be associated with better outcomes and positive effects on HRQoL (89). Future studies should define the time period of low disease activity that demonstrates a favorable impact on outcomes and HRQoL, although this will differ based on organ involvement. Third, the distinction between what represents disease activity and what represents damage is a challenge that is currently an area of investigation (36). Activity is defined as the component of disease severity that is largely reversible and may result in little or no damage in the future. Damage is the component of severity that is largely irreversible. In Figure 3, we lay out a preliminary proposal to define low disease activity for the different manifestations in SSc (65,66,80,90–93). This is an author-driven preliminary proposal, influenced by data obtained from RCTs and observational studies. This proposal will need rigorous testing and validation using a consensus methodology in future studies.

Conclusions

Using data and outcome measures from recent clinical trials in SSc, we propose a conceptual framework on how to define low disease activity for different organ-specific manifestations in SSc. Disease-modifying therapies (such as HSCT in dcSSc, for example) and their effect on SSc should be considered in future investigations.

ACKNOWLEDGMENT

We would like to acknowledge Thomas A. Medsger, Jr., MD (Division of Rheumatology, University of Pittsburgh Medical Center, Pittsburgh) for his thoughtful input on a previous version of the submitted manuscript.

AUTHOR CONTRIBUTIONS

All authors drafted the article, revised it critically for important intellectual content, and approved the final version to be published.

REFERENCES

1. Denton CP, Khanna D. Systemic sclerosis. Lancet 2017;390: 1685–99.
2. Allanore Y, Simms R, Distler O, Trojanowska M, Pope J, Denton CP, et al. Systemic sclerosis. Nat Rev Dis Primers 2015;1:15002.
3. Varga J, Trojanowska M, Kuwana M. Pathogenesis of systemic sclerosis: recent insights of molecular and cellular mechanisms and therapeutic opportunities. J Scleroderma Relat Disord 2017;2: 137–52.
4. Nihtyanova SI, Tang EC, Coghlan JG, Wells AU, Black CM, Denton CP. Improved survival in systemic sclerosis is associated with better ascertainment of internal organ disease: a retrospective cohort study. QJM 2010;103:109–15.
5. Elhai M, Meune C, Boubaya M, Avouac J, Hachulla E, Balbir-Gurman A, et al. Mapping and predicting mortality from systemic sclerosis. Ann Rheum Dis 2017;76:1897–905.
6. Sullivan KM, Goldmuntz EA, Keyes-Elstein L, McSweeney PA, Pinckney A, Welch B, et al. Myeloablative autologous stem-cell transplantation for severe scleroderma. N Engl J Med 2018;378: 35–47.
7. Van Laar JM, Farge D, Sont JK, Naraghi K, Marjanovic Z, Larghero J, et al. Autologous hematopoietic stem cell transplantation vs intravenous pulse cyclophosphamide in diffuse cutaneous systemic sclerosis: a randomized clinical trial. JAMA 2014;311:2490–8.
8. Burt RK, Shah SJ, Dill K, Grant T, Gheorghiade M, Schroeder J, et al. Autologous non-myeloablative haemopoietic stem-cell transplantation compared with pulse cyclophosphamide once per month for systemic sclerosis (ASSIST): an open-label, randomised phase 2 trial. Lancet 2011;378:498–506.
9. Nash RA, McSweeney PA, Crofford LJ, Abidi M, Chen CS, Godwin JD, et al. High-dose immunosuppressive therapy and autologous hematopoietic cell transplantation for severe systemic sclerosis: long-term follow-up of the US multicenter pilot study. Blood 2007;110:1388–96.
10. Smolen JS, Aletaha D, McInnes IB. Rheumatoid arthritis. Lancet 2016;388:2023–38.
11. St. Clair EW, van der Heijde DM, Smolen JS, Maini RN, Bathon JM, Emery P, et al. Combination of infliximab and methotrexate therapy for early rheumatoid arthritis: a randomized, controlled trial. Arthritis Rheum 2004;50:3432–43.
12. Van den Hombergh WM, Carreira PE, Knaapen-Hans HK, van den Hoogen FH, Fransen J, Vonk MC. An easy prediction rule for diffuse cutaneous systemic sclerosis using only the timing and type of first symptoms and auto-antibodies: derivation and validation. Rheumatology (Oxford) 2016;55:2023–32.
13. Van den Hoogen F, Khanna D, Fransen J, Johnson SR, Baron M, Tyndall A, et al. 2013 classification criteria for systemic sclerosis: an American College of Rheumatology/European League against Rheumatism collaborative initiative. Arthritis Rheum 2013;65:2737–47.
14. Minier T, Guiducci S, Bellando-Randone S, Bruni C, Lepri G, Czirják L, et al. Preliminary analysis of the very early diagnosis of systemic sclerosis (VEDOSS) EUSTAR multicentre study: evidence for puffy fingers as a pivotal sign for suspicion of systemic sclerosis. Ann Rheum Dis 2014;73:2087–93.
15. Wirz EG, Jaeger VK, Allanore Y, Riemekasten G, Hachulla E, Distler O, et al. Incidence and predictors of cutaneous manifestations during the early course of systemic sclerosis: a 10-year longitudinal study from the EUSTAR database. Ann Rheum Dis 2016;75:1285–92.
16. Steen VD, Medsger TA Jr. Severe organ involvement in systemic sclerosis with diffuse scleroderma. Arthritis Rheum 2000;43:2437–44.
17. LeRoy EC, Black C, Fleischmajer R, Jablonska S, Krieg T, Medsger TA, et al. Scleroderma (systemic sclerosis): classification, subsets and pathogenesis. J Rheumatol 1988;15:202–5.
18. Walker UA, Tyndall A, Czirjak L, Denton C, Farge-Bancel D, Kowal-Bielecka O, et al. Clinical risk assessment of organ manifestations in systemic sclerosis: a report from the EULAR Scleroderma Trials And Research group database. Ann Rheum Dis 2007;66: 754–63.
19. Merkel PA, Silliman NP, Clements PJ, Denton CP, Furst DE, Mayes MD, et al. Patterns and predictors of change in outcome measures in clinical trials in scleroderma: an individual patient meta-analysis of 629 subjects with diffuse cutaneous systemic sclerosis. Arthritis Rheum 2012;64:3420–9.
20. Hachulla E, Launay D, Mouthon L, Sitbon O, Berezne A, Guillevin L, et al. Is pulmonary arterial hypertension really a late complication of systemic sclerosis? Chest 2009;136:1211–9.
21. Bhattacharyya S, Midwood KS, Yin H, Varga J. Toll-like receptor-4 signaling drives persistent fibroblast activation and prevents fibrosis resolution in scleroderma. Adv Wound Care (New Rochelle) 2017;6:356–69.
22. Milano A, Pendergrass SA, Sargent JL, George LK, McCalmont TH, Connolly MK, et al. Molecular subsets in the gene expression signatures of scleroderma skin. PLoS One 2008;3:e2696.
23. Tyndall AJ, Bannert B, Vonk M, Airo P, Cozzi F, Carreira PE, et al. Causes and risk factors for death in systemic sclerosis: a study from the EULAR Scleroderma Trials and Research (EUSTAR) database. Ann Rheum Dis 2010;69:1809–15.
24. Steen VD, Medsger TA. Changes in causes of death in systemic sclerosis, 1972-2002. Ann Rheum Dis 2007;66:940–4.
25. Elhai M, Meune C, Avouac J, Kahan A, Allanore Y. Trends in mortality in patients with systemic sclerosis over 40 years: a systematic review and meta-analysis of cohort studies [review]. Rheumatology (Oxford) 2012;51:1017–26.
26. Hinchcliff M, Huang CC, Wood TA, Mahoney JM, Martyanov V, Bhattacharyya S, et al. Molecular signatures in skin associated with clinical improvement during mycophenolate treatment in systemic sclerosis. J Invest Dermatol 2013;133:1979–89.
27. Martyanov V, Whitfield ML. Molecular stratification and precision medicine in systemic sclerosis from genomic and proteomic data [review]. Curr Opin Rheumatol 2016;28:83–8.
28. Nevskaya T, Baron M, Pope JE. Canadian Scleroderma Research Group. Predictive value of European Scleroderma Group Activity Index in an early scleroderma cohort. Rheumatology (Oxford) 2017;56:111–22.

29. Nihtyanova SI, Sari A, Harvey JC, Leslie A, Derrett-Smith EC, Fonseca C, et al. Using autoantibodies and cutaneous subset to develop outcome-based disease classification in systemic sclerosis. Arthritis Rheumatol 2020;72:465–76.
30. Prevoo ML, van 't Hof MA, Kuper HH, van Leeuwen MA, van de Putte LB, van Riel PL. Modified disease activity scores that include twenty-eight–joint counts: development and validation in a prospective longitudinal study of patients with rheumatoid arthritis. Arthritis Rheum 1995;38:44–8.
31. Aletaha D, Nell VP, Stamm T, Uffmann M, Pflugbeil S, Machold K, et al. Acute phase reactants add little to composite disease activity indices for rheumatoid arthritis: validation of a clinical activity score. Arthritis Res Ther 2005;7:R796–806.
32. Clements P, Lachenbruch P, Seibold J, White B, Weiner S, Martin R, et al. Inter and intraobserver variability of total skin thickness score (modified Rodnan TSS) in systemic sclerosis. J Rheumatol 1995;22:1281–5.
33. Khanna D, Berrocal VJ, Giannini EH, Seibold JR, Merkel PA, Mayes MD, et al. The American College of Rheumatology Provisional Composite Response Index for clinical trials in early diffuse cutaneous systemic sclerosis. Arthritis Rheumatol 2016;68:299–311.
34. Fries JF, Spitz P, Kraines RG, Holman HR. Measurement of patient outcome in arthritis. Arthritis Rheum 1980;23:137–45.
35. Allanore Y. Limited cutaneous systemic sclerosis: the unfairly neglected subset [editorial]. J Scleroderma Relat Disord 2016;1:241–6.
36. Baron M, Kahaleh B, Bernstein EJ, Chung L, Clements PJ, Denton C, et al. An interim report of the scleroderma clinical trials consortium working groups. J Scleroderma Relat Disord 2019;4:17–27.
37. Mihai C, Landewe R, van der Heijde D, Walker UA, Constantin PI, Gherghe AM, et al. Digital ulcers predict a worse disease course in patients with systemic sclerosis. Ann Rheum Dis 2016;75:681–6.
38. Matucci-Cerinic M, Kahaleh B, Wigley FM. Evidence that systemic sclerosis is a vascular disease [review]. Arthritis Rheum 2013;65:1953–62.
39. Avouac J, Airo P, Meune C, Beretta L, Dieude P, Caramaschi P, et al. Prevalence of pulmonary hypertension in systemic sclerosis in European Caucasians and metaanalysis of 5 studies [review]. J Rheumatol 2010;37:2290–8.
40. Nihtyanova SI, Schreiber BE, Ong VH, Rosenberg D, Moinzadeh P, Coghlan JG, et al. Prediction of pulmonary complications and long-term survival in systemic sclerosis. Arthritis Rheumatol 2014;66:1625–35.
41. Lefevre G, Dauchet L, Hachulla E, Montani D, Sobanski V, Lambert M, et al. Survival and prognostic factors in systemic sclerosis-associated pulmonary hypertension: a systematic review and meta-analysis. Arthritis Rheum 2013;65:2412–23.
42. Sobanski V, Giovannelli J, Lynch BM, Schreiber BE, Nihtyanova SI, Harvey J, et al. Characteristics and survival of anti-U1 RNP antibody-positive patients with connective tissue disease-associated pulmonary arterial hypertension. Arthritis Rheumatol 2016;68:484–93.
43. Coghlan JG, Denton CP, Grunig E, Bonderman D, Distler O, Khanna D, et al. Evidence-based detection of pulmonary arterial hypertension in systemic sclerosis: the DETECT study. Ann Rheum Dis 2014;73:1340–9.
44. Khanna D, McLaughlin V. Screening and early detection of pulmonary arterial hypertension in connective tissue diseases: it is time to institute it! Am J Respir Crit Care Med 2015;192:1032–3.
45. Young A, Nagaraja V, Basilious M, Habib M, Townsend W, Gladue H, et al. Update of screening and diagnostic modalities for connective tissue disease-associated pulmonary arterial hypertension. Semin Arthritis Rheum 2019;48:1059–67.
46. Mihai C, Antic M, Dobrota R, Bonderman D, Chadha-Boreham H, Coghlan JG, et al. Factors associated with disease progression in early-diagnosed pulmonary arterial hypertension associated with systemic sclerosis: longitudinal data from the DETECT cohort. Ann Rheum Dis 2018;77:128–32.
47. Steen V, Medsger TA Jr. Predictors of isolated pulmonary hypertension in patients with systemic sclerosis and limited cutaneous involvement. Arthritis Rheum 2003;48:516–22.
48. Klinger JR, Elliott G, Levine DJ, Bossone E, Duvall L, Fagan K, et al. Therapy for pulmonary arterial hypertension in adults 2018: update of the CHEST guideline and expert panel report. Chest 2019;155:565–86.
49. Pan J, Lei L, Zhao C. Comparison between the efficacy of combination therapy and monotherapy in connective tissue disease associated pulmonary arterial hypertension: a systematic review and meta-analysis. Clin Exp Rheumatol 2018;36:1095–102.
50. Nicolls M, Badesch D, Chung L, Domsic R, Medsger T, Pinckney A, et al. Safety and efficacy of B-cell depletion with rituximab for the treatment of systemic sclerosis-associated pulmonary arterial hypertension in a multi-center NIH clinical trial [abstract]. Arthritis Rheumatol 2019; 71 Suppl 10. URL: https://acrabstracts.org/abstract/safety-and-efficacy-of-b-cell-depletion-with-rituximab-for-the-treatment-of-systemic-sclerosis-associated-pulmonary-arterial-hypertension-in-a-multi-center-nih-clinical-trial/.
51. Zamanian R, Badesch D, Chung L, Domsic R, Medsger T, Pinckney A, et al, on behalf of the Asco1 Investigators. Safety and efficacy of B-cell depletion with rituximab for the treatment of systemic sclerosis-associated pulmonary arterial hypertension. Eur R J 2019;54 Suppl 63. URL: https://erj.ersjournals.com/content/54/suppl_63/RCT1884.
52. Avouac J, Fransen J, Walker UA, Riccieri V, Smith V, Muller C, et al. Preliminary criteria for the very early diagnosis of systemic sclerosis: results of a Delphi Consensus Study from EULAR Scleroderma Trials and Research Group. Ann Rheum Dis 2011;70:476–81.
53. Flavahan NA. A vascular mechanistic approach to understanding Raynaud phenomenon [review]. Nat Rev Rheumatol 2015;11:146–58.
54. Koenig M, Joyal F, Fritzler MJ, Roussin A, Abrahamowicz M, Boire G, et al. Autoantibodies and microvascular damage are independent predictive factors for the progression of Raynaud's phenomenon to systemic sclerosis: a twenty-year prospective study of 586 patients, with validation of proposed criteria for early systemic sclerosis. Arthritis Rheum 2008;58:3902–12.
55. Matucci-Cerinic M, Krieg T, Guillevin L, Schwierin B, Rosenberg D, Cornelisse P, et al. Elucidating the burden of recurrent and chronic digital ulcers in systemic sclerosis: long-term results from the DUO Registry. Ann Rheum Dis 2016;75:1770–6.
56. Herrick AL, van den Hoogen F, Gabrielli A, Tamimi N, Reid C, O'Connell D, et al. Modified-release sildenafil reduces Raynaud's phenomenon attack frequency in limited cutaneous systemic sclerosis. Arthritis Rheum 2011;63:775–82.
57. Hachulla E, Hatron PY, Carpentier P, Agard C, Chatelus E, Jego P, et al. Efficacy of sildenafil on ischaemic digital ulcer healing in systemic sclerosis: the placebo-controlled SEDUCE study. Ann Rheum Dis 2016;75:1009–15.
58. Korn JH, Mayes M, Matucci Cerinic M, Rainisio M, Pope J, Hachulla E, et al. Digital ulcers in systemic sclerosis: prevention by treatment with bosentan, an oral endothelin receptor antagonist. Arthritis Rheum 2004;50:3985–93.
59. Matucci-Cerinic M, Denton CP, Furst DE, Mayes MD, Hsu VM, Carpentier P, et al. Bosentan treatment of digital ulcers related to systemic sclerosis: results from the RAPIDS-2 randomised, double-blind, placebo-controlled trial. Ann Rheum Dis 2011;70:32–8.
60. Wigley FM, Seibold JR, Wise RA, McCloskey DA, Dole WP. Intravenous iloprost treatment of Raynaud's phenomenon and ischemic ulcers secondary to systemic sclerosis. J Rheumatol 1992;19:1407–14.
61. Wigley FM, Wise RA, Seibold JR, McCloskey DA, Kujala G, Medsger TA Jr, et al. Intravenous iloprost infusion in patients with Raynaud phenomenon secondary to systemic sclerosis: a

multicenter, placebo-controlled, double-blind study. Ann Intern Med 1994;120:199–206.

62. Steen VD, Costantino JP, Shapiro AP, Medsger TA Jr. Outcome of renal crisis in systemic sclerosis: relation to availability of angiotensin converting enzyme (ACE) inhibitors. Ann Intern Med 1990;113:352–7.
63. Jaeger VK, Wirz EG, Allanore Y, Rossbach P, Riemekasten G, Hachulla E, et al. Incidences and risk factors of organ manifestations in the early course of systemic sclerosis: a longitudinal EUSTAR study. PLoS One 2016;11:e0163894.
64. Steen VD, Medsger TA Jr. Long-term outcomes of scleroderma renal crisis. Ann Intern Med 2000;133:600–3.
65. Tashkin DP, Elashoff R, Clements PJ, Goldin J, Roth MD, Furst DE, et al. Cyclophosphamide versus placebo in scleroderma lung disease. N Engl J Med 2006;354:2655–66.
66. Tashkin DP, Roth MD, Clements PJ, Furst DE, Khanna D, Kleerup EC, et al. Mycophenolate mofetil versus oral cyclophosphamide in scleroderma-related interstitial lung disease (SLS II): a randomised controlled, double-blind, parallel group trial. Lancet Respir Med 2016;4:708–19.
67. Volkmann ER, Tashkin DP, Li N, Roth MD, Khanna D, Hoffmann-Vold AM, et al. Mycophenolate mofetil versus placebo for systemic sclerosis-related interstitial lung disease: an analysis of scleroderma lung studies I and II. Arthritis Rheumatol 2017;69:1451–60.
68. Volkmann ER, Tashkin DP, Sim M, Li N, Goldmuntz E, Keyes-Elstein L, et al. Short-term progression of interstitial lung disease in systemic sclerosis predicts long-term survival in two independent clinical trial cohorts. Ann Rheum Dis 2019;78:122–30.
69. Sullivan K, Pinckney A, Goldmuntz E, Welch B, Khanna D, Simms RW, et al. Myeloablative autologous hematopoietic stem cell transplantation for severe scleroderma: long-term outcomes 6-11 years after entry on a randomized study comparing transplantation and cyclophosphamide [abstract]. Arthritis Rheumatol 2018;70 Suppl 9. URL: https://acrabstracts.org/abstract/myeloablative-autologous-hematopoietic-stem-cell-transplantation-for-severe-scleroderma-long-term-outcomes-6-11-years-after-entry-on-a-randomized-study-comparing-transplantation-and-cyclophosphamide/.
70. Poormoghim H, Lucas M, Fertig N, Medsger TA. Systemic sclerosis sine scleroderma: demographic, clinical, and serologic features and survival in forty-eight patients. Arthritis Rheum 2000;43:444–51.
71. Shand L, Lunt M, Nihtyanova S, Hoseini M, Silman A, Black CM, et al. Relationship between change in skin score and disease outcome in diffuse cutaneous systemic sclerosis: application of a latent linear trajectory model. Arthritis Rheum 2007;56:2422–31.
72. Namas R, Tashkin DP, Furst DE, Wilhalme H, Tseng CH, Roth MD, et al. Efficacy of mycophenolate mofetil and oral cyclophosphamide on skin thickness: post-hoc analyses from two randomized placebo-controlled trials. Arthritis Care Res (Hoboken) 2018;70439–44.
73. Khanna D, Spino C, Johnson S, Chung L, Whitfield M, Denton CP, et al. Abatacept in early diffuse cutaneous systemic sclerosis: results of a phase 2 investigator-initiated, multicenter, double-blind randomized placebo-controlled trial. Arthritis Rheumatol 2020;72125–36.
74. Khanna D, Lin CJ, Kuwana M, Allanore Y, Batalov A, Butrimiene I, et al. Efficacy and safety of tocilizumab for the treatment of systemic sclerosis: results from a phase 3 randomized controlled trial [abstract]. Arthritis Rheumatol 2018;70 Supple 10. URL: https://acrabstracts.org/abstract/efficacy-and-safety-of-tocilizumab-for-the-treatment-of-systemic-sclerosis-results-from-a-phase-3-randomized-controlled-trial/.
75. Launay D, Remy-Jardin M, Michon-Pasturel U, Mastora I, Hachulla E, Lambert M, et al. High resolution computed tomography in fibrosing alveolitis associated with systemic sclerosis. J Rheumatol 2006;33:1789–801.
76. Hoa S, Bernatsky S, Steele RJ, Baron M, Hudson M. Association between immunosuppressive therapy and course of mild interstitial lung disease in systemic sclerosis. Rheumatology (Oxford) 2019. E-pub ahead of print.
77. Tashkin DP, Roth MD, Clements PJ, Furst DE, Khanna D, Kleerup EC, et al. Mycophenolate mofetil versus oral cyclophosphamide in scleroderma-related interstitial lung disease (SLS II): a randomised controlled, double-blind, parallel group trial. Lancet Respir Med 2016;4:708–19.
78. Sircar G, Goswami RP, Sircar D, Ghosh A, Ghosh P. Intravenous cyclophosphamide vs rituximab for the treatment of early diffuse scleroderma lung disease: open label, randomized, controlled trial. Rheumatology (Oxford) 2018;57:2106–13.
79. Khanna D, Denton CP, Jahreis A, van Laar JM, Frech TM, Anderson ME, et al. Safety and efficacy of subcutaneous tocilizumab in adults with systemic sclerosis (faSScinate): a phase 2, randomised, controlled trial. Lancet 2016;387:2630–40.
80. Distler O, Highland KB, Gahlemann M, Azuma A, Fischer A, Mayes MD, et al. Nintedanib for systemic sclerosis-associated interstitial lung disease. N Engl J Med 2019;380:2518–28.
81. Kahan A, Allanore Y. Primary myocardial involvement in systemic sclerosis. Rheumatology (Oxford) 2006;45 Suppl 4:iv14–7.
82. Forbes A, Marie I. Gastrointestinal complications: the most frequent internal complications of systemic sclerosis. Rheumatology (Oxford) 2009;48 Suppl 3:iii36–9.
83. Herrick AL, Gallas A. Systemic sclerosis-related calcinosis. J Scleroderma Relat Disord 2016;1:194–203.
84. Avouac J, Walker U, Tyndall A, Kahan A, Matucci-Cerinic M, Allanore Y, et al. Characteristics of joint involvement and relationships with systemic inflammation in systemic sclerosis: results from the EULAR Scleroderma Trial and Research Group (EUSTAR) database. J Rheumatol 2010;37:1488–501.
85. Clements PJ, Wong WK, Hurwitz EL, Furst DE, Mayes M, White B, et al. The Disability Index of the Health Assessment Questionnaire is a predictor and correlate of outcome in the high-dose versus low-dose penicillamine in systemic sclerosis trial. Arthritis Rheum 2001;44:653–61.
86. Ghrénassia E, Avouac J, Khanna D, Derk CT, Distler O, Suliman YA, et al. Prevalence, correlates and outcomes of gastric antral vascular ectasia in systemic sclerosis: a EUSTAR case-control study. J Rheumatol 2014;41:99–105.
87. Distler O, Allanore Y, Denton C, Kuwana M, Matucci-Cerinic M, Pope J, et al. OP0183 Efficacy and safety of riociguat in patients with early diffuse cutaneous systemic sclerosis and interstitial lung disease (SSc-ILD): results from the Phase IIb RISE-SSc Study. Ann Rheum Dis 2019;78:167.
88. Sitbon O, Gomberg-Maitland M, Granton J, Lewis MI, Mathai SC, Rainisio M, et al. Clinical trial design and new therapies for pulmonary arterial hypertension. Eur Respir J 2019;53:1801908.
89. Van Vollenhoven R, Voskuyl A, Bertsias G, Aranow C, Aringer M, Arnaud L, et al. A framework for remission in SLE: consensus findings from a large international task force on definitions of remission in SLE (DORIS). Ann Rheum Dis 2017;76:554–61.
90. Khanna PP, Maranian P, Gregory J, Khanna D. The minimally important difference and patient acceptable symptom state for the Raynaud's condition score in patients with Raynaud's phenomenon in a large randomised controlled clinical trial. Ann Rheum Dis 2010;69:588–91.
91. Pauling JD, Reilly E, Smith T, Frech TM. Factors influencing Raynaud's condition score diary outcomes in systemic sclerosis. J Rheumatol 2019;46:1326–34.
92. Steen VD, Medsger TA Jr. The value of the Health Assessment Questionnaire and special patient-generated scales to demonstrate change in systemic sclerosis patients over time. Arthritis Rheum 1997;40:1984–91.
93. Benza RL, Gomberg-Maitland M, Elliott CG, Farber HW, Foreman AJ, Frost AE, et al. Predicting survival in patients with pulmonary arterial hypertension: the REVEAL risk score calculator 2.0 and comparison with ESC/ERS-based risk assessment strategies. Chest 2019;156:323–37.

Arthritis & Rheumatology
Vol. 72, No. 7, July 2020, pp 1059–1063
DOI 10.1002/art.41285

American College of Rheumatology
Empowering Rheumatology Professionals

NOTES FROM THE FIELD

On the Alert for Cytokine Storm: Immunopathology in COVID-19

Lauren A. Henderson,[1] Scott W. Canna,[2] Grant S. Schulert,[3] Stefano Volpi,[4] Pui Y. Lee,[1] Kate F. Kernan,[2] Roberto Caricchio,[5] Shawn Mahmud,[6] Melissa M. Hazen,[1] Olha Halyabar,[1] Kacie J. Hoyt,[1] Joseph Han,[7] Alexei A. Grom,[3] Marco Gattorno,[4] Angelo Ravelli,[8] Fabrizio De Benedetti,[9] Edward M. Behrens,[10] Randy Q. Cron,[11] and Peter A. Nigrovic[12]

Poor outcomes in COVID-19 correlate with clinical and laboratory features of cytokine storm syndrome. Broad screening for cytokine storm and early, targeted antiinflammatory therapy may prevent immunopathology and could help conserve limited health care resources. While studies are ongoing, extrapolating from clinical experience in cytokine storm syndromes may benefit the multidisciplinary teams caring for patients with severe COVID-19.

COVID-19 (coronavirus disease 2019) is sweeping across the globe. Most patients have mild-to-moderate symptoms, but a subgroup will become severely ill. Sepsis, respiratory failure, and acute respiratory distress syndrome (ARDS) are common complications of the disease (1). Factors associated with admission to the intensive care unit and death include older age, comorbid conditions, elevated body mass index, lymphopenia, and elevated blood levels of transaminases, lactate dehydrogenase (LDH), D-dimer, ferritin, and soluble interleukin-2 receptor (sIL-2R) (1–4).

This constellation of features is reminiscent of a family of syndromes broadly gathered under the umbrella of cytokine

Dr. Henderson's work was supported by the National Institute of Arthritis and Musculoskeletal and Skin Diseases, NIH (grants K08-AR-073339 and P30-AR-070253) and the Investigator Award of the Rheumatology Research Foundation. Dr. Canna's work was supported by the National Institute of Child Health and Human Development, NIH (grant R01-HD-098428), the National Institute of General Medical Sciences, NIH (grant 2R01-GM-108618), and the RK Mellon Institute for Pediatric Research. Dr. Caricchio's work was supported in part by a grant from the Lupus Research Alliance. Dr. Mahmud's work was supported in part by a University of Minnesota Medical School Academic Investment Education Program grant. Dr. Nigrovic's work was supported by the National Institute of Arthritis and Musculoskeletal and Skin Diseases, NIH (awards 2R01-AR-065538, R01-AR-075906, R01-AR-073201, P30-AR-070253, and R21-AR-076630), the National Heart, Lung, and Blood Institute, NIH (award R21-HL-150575), the Fundación Bechara, and the Arbuckle Family Fund for Arthritis Research.

[1]Lauren A. Henderson, MD, MMSc, Pui Y. Lee, MD, PhD, Melissa M. Hazen, MD, Olha Halyabar, MD, Kacie J. Hoyt, MS: Boston Children's Hospital and Harvard Medical School, Boston, Massachusetts; [2]Scott W. Canna, MD, Kate F. Kernan, MD: UPMC Children's Hospital of Pittsburgh and University of Pittsburgh, Pittsburgh, Pennsylvania; [3]Grant S. Schulert, MD, PhD, Alexei A. Grom, MD: Cincinnati Children's Hospital Medical Center and University of Cincinnati College of Medicine, Cincinnati, Ohio; [4]Stefano Volpi, MD, PhD, Marco Gattorno, MD: Center for Autoinflammatory Diseases and Immunodeficiency, IRCCS Istituto Giannina Gaslini, and Università degli Studi di Genova, Genoa, Italy; [5]Roberto Caricchio, MD: Temple University Hospital and Lewis Katz School of Medicine, Philadelphia, Pennsylvania; [6]Shawn Mahmud, MD, PhD: University of Minnesota Medical Center and University of Minnesota School of Medicine, Minneapolis; [7]Joseph Han, BS: Icahn School of Medicine at Mount Sinai, New York, New York; [8]Angelo Ravelli, MD: Clinica Pediatrica e Reumatologia, IRCCS Istituto Giannina Gaslini, and Università degli Studi di Genova, Genoa, Italy; [9]Fabrizio De Benedetti, MD: Ospedale Pediatrico Bambino Gesù, Rome, Italy; [10]Edward M. Behrens, MD: Children's Hospital of Philadelphia and the University of Pennsylvania Perelman School of Medicine; [11]Randy Q. Cron, MD, PhD: Children's of Alabama, University of Alabama at Birmingham; [12]Peter A. Nigrovic, MD: Boston Children's Hospital, Brigham and Women's Hospital, and Harvard Medical School, Boston, Massachusetts.

Drs. Henderson and Canna contributed equally to this work.

Dr. Henderson has received salary support from the Childhood Arthritis and Rheumatology Alliance and consulting fees from Sobi (less than $10,000). Dr. Canna has received research support from AB2 Bio related to a clinical trial. Dr. Schulert has received consulting fees from Sobi and Novartis (less than $10,000 each). Dr. Caricchio has received consulting fees from GlaxoSmithKline, Aurinia Pharmaceuticals, and Janssen (less than $10,000 each) and investigator-initiated research support from Janssen. Dr. Grom has received consulting fees from Novartis, AB2 Bio, and Sobi (less than $10,000 each) and research support from those companies. Dr. Gattorno has received consulting fees, speaking fees, and/or honoraria from Novartis and Sobi (less than $10,000 each) and research support from the Eurofever Project. Dr. Ravelli has received consulting fees, speaking fees, and/or honoraria from AbbVie, Bristol-Myers Squibb, Pfizer, Hoffmann-LaRoche, Novartis, Centocor, Angelini Holding, and Reckitt Benckiser (less than $10,000 each). Dr. De Benedetti has received research support paid to his institution from AbbVie, Hoffmann-La Roche, Pfizer, NovImmune, Novartis, Sobi, and Sanofi. Dr. Behrens has received research support from AB2 Bio to run a clinical trial. Dr. Cron has received consulting fees from Sobi, Novartis, and Pfizer (less than $10,000 each) and is a co–Principal Investigator of an investigator-initiated clinical trial to study anakinra in secondary hemophagocytic lymphohistiocytosis funded by Sobi. Dr. Nigrovic has received salary support from the Childhood Arthritis and Rheumatology Research Alliance, consulting fees from Sobi, Pfizer, Quench Bio, XBiotech, and Bristol-Myers Squibb (less than $10,000 each) and from Simcere and Miach Orthopedics (more than $10,000 each), royalties from UpToDate Inc. and the American Academy of Pediatrics, and research support from Novartis, Sobi, Pfizer, and Bristol-Myers Squibb. No other disclosures relevant to this article were reported.

Address correspondence to Lauren A. Henderson, MD, MMSc, 1 Blackfan Circle, Karp Family Research Building, Tenth Floor, Boston, MA 02115. E-mail: Lauren.Henderson@childrens.harvard.edu.

Submitted for publication March 31, 2020; accepted in revised form April 7, 2020.

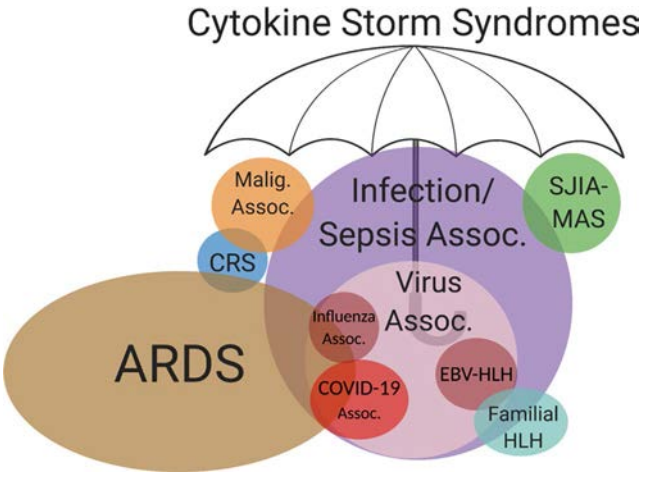

Figure 1. The family of conditions characterized by cytokine storm. Malig. = malignancy; Assoc. = associations; SJIA = systemic juvenile idiopathic arthritis; MAS = macrophage activation syndrome; CRS = cytokine release syndrome; ARDS = acute respiratory distress syndrome; EBV = Epstein-Barr virus; HLH = hemophagocytic lymphohistiocytosis.

storm syndrome, in which hyperinflammation and multiorgan disease arise through excessive cytokine release from uncontrolled immune activation (Figure 1). Rheumatologists face this foe regularly in systemic juvenile idiopathic arthritis (JIA), adult-onset Still's disease, and systemic lupus erythematosus, among other diseases. Macrophage activation syndrome (MAS), one form of cytokine storm syndrome, develops in at least 10% of patients with systemic JIA. Compared to systemic JIA patients without MAS, those with this complication are more likely to carry heterozygous variants in genes mediating the release of cytotoxic granules from natural killer (NK) cells and CD8+ T cells; biallelic mutations of these genes cause an inherited form of cytokine storm syndrome termed familial hemophagocytic lymphohistiocytosis (HLH). Reduced cytotoxicity impairs clearance of infected cells and elimination of activated macrophages, leading to massive release of proinflammatory mediators. One of these mediators, IL-6, further impairs NK cell function. Patients present with rapid onset of fever, cytopenias, coagulopathy, elevated transaminase levels, hyperferritinemia, and multiorgan

Table 1. Biomarkers of cytokine storm syndrome (CSS)*

Biomarker	Biology	Status in hyperinflammation	Status in COVID-19	Test availability
CRP	Hepatic release in response to IL-6	Nonspecific, useful for monitoring, blunted by IL-6 blockade	Associated with severity, ARDS	A
Complete blood cell count	Multifactorial cytopenias	May be indicative of CSS (especially thrombocytopenia)	Associated with severity, ARDS	A
↑ D-dimer, ↓ fibrinogen	Fibrin degradation product, reflective of DIC	May be indicative of active CSS	Associated with severity, ARDS	A
LDH, AST, ALT	Tissue injury, hepatitis	May be indicative of active CSS	Associated with severity, ARDS	A
Ferritin	Macrophage/hepatocyte activation	Integral part of CSS diagnosis, predictive of sepsis mortality	Associated with severity, ARDS	A
Ferritin:ESR ratio	ESR falls with fibrinogen consumption	Higher specificity than ferritin alone	Not assessed	A
Procalcitonin	Adipokine	Nonspecific, useful for monitoring	Variably associated with severity, ARDS	A, S
IL-2Ra (CD25)	Cleaved from T cells by inflammatory proteases	Part of HLH diagnostic criteria, useful for monitoring	Associated with severity	S
IL-6	Pleiotropic inflammatory cytokine	Elevated, nonspecific	Associated with severity	S
Neopterin	Metabolite of GTP induced by IFNγ	Elevated in blood and CSF	Not assessed	S
IFNγ	Classic type 1/Th1 cytokine	Elevated, but poor dynamic range	Elevated compared with healthy control	S, R
CXCL9	Chemokine induced by IFNγ	Elevated in most CSS, useful for monitoring	Not assessed	S
IL-1β	Inflammasome-activated	Elevated, but poor dynamic range	Variably elevated with severity	S, R
IL-18	Inflammasome-activated, IFNγ inducing	Very high levels may indicate MAS, not useful for monitoring	Not assessed	S
ADA-2	Released by IFNγ-activated monocytes	Elevated in most CSS, useful for monitoring	Not assessed	S, R
S100 proteins	Neutrophil/monocyte activation	Elevated in active systemic JIA and MAS, and in some ARDS	Not assessed	S, R
CD163	Cleaved from tissue macrophages	Elevated in active systemic JIA and MAS, and in ARDS	Not assessed	S, R

* Relevant citations are provided in Supplementary Table 1 (available on the *Arthritis & Rheumatology* web site at http://onlinelibrary.wiley.com/doi/10.1002/art.41285/abstract). COVID-19 = coronavirus disease 2019; CRP = C-reactive protein; IL-6 = interleukin-6; ARDS = acute respiratory distress syndrome; A = widely available; DIC = disseminated intravascular coagulation; LDH = lactate dehydrogenase; AST = aspartate aminotransferase; ALT = alanine aminotransferase; ESR = erythrocyte sedimentation rate; S = typically send-out; IL-2Ra = IL-2 receptor antagonist; HLH = hemophagocytic lymphohistiocytosis; IFNγ = interferon-γ; CSF = cerebrospinal fluid; R = may be available only on a research basis; MAS = macrophage activation syndrome; ADA-2 = adenosine deaminase 2; JIA = juvenile idiopathic arthritis.

dysfunction. Historically, the cornerstones of treatment were glucocorticoids, intravenous immunoglobulin (IVIG), and cyclosporine. Despite these interventions, mortality was as high as 20%. Identification of key mediators driving MAS—including IL-1β, IL-6, IL-18, and interferon-γ (IFNγ)—have inaugurated a new era of cytokine neutralization, potentially enabling a marked reduction in mortality (5,6).

Herpes family viruses (e.g., Epstein-Barr virus) and influenza are major triggers of cytokine storm, both in systemic JIA and in patients without a preexisting immunologic diagnosis. As in systemic JIA–related MAS, the inflammatory cytokines IFNγ and IL-18 are key mediators of hyperinflammation in a murine model of repeated Toll-like receptor 9 stimulation, which mimics severe viral infection (6). In one study of patients without underlying rheumatic disease who died of H1N1 influenza, 81% displayed features of cytokine storm, and 36% carried pathologic variants in the cytolytic pathway (7). Treatments effective in systemic JIA–related MAS can benefit patients with cytokine storm triggered by infections (8,9). Post hoc analysis of a phase III randomized controlled trial of anakinra (recombinant IL-1 receptor antagonist) in sepsis showed that patients with coagulopathy and elevated transaminase levels exhibited better survival with IL-1 blockade than with standard of care (65% versus 35%; hazard ratio for death 0.28, $P = 0.007$) (10). Similarly, IL-6 blockade is effective in treating the related cytokine release syndrome from chimeric antigen receptor T cell (CAR-T) therapy (11).

Hyperinflammation in COVID-19 is not MAS, and it may even be distinct from other forms of viral-induced cytokine storm, in that ferritin elevation is modest and severe end-organ disease is focused on the lung. Some patients with

Table 2. Treatments for cytokine storm syndrome of potential utility in severe COVID-19*

Intervention	Biology	Experience in hyperinflammation	Experience in COVID-19	Potential likelihood of impairing viral suppression/clearance†	Concerns
Glucocorticoids (<2 mg/kg/day)‡	Transcriptional regulation via glucocorticoid receptor	Mainstay of treatment	May improve outcomes in ARDS (ChiCTR2000029386)§	++	Hypertension, immunosuppression, metabolic changes, mood alterations
Glucocorticoids (>250 mg/day)‡	Transcriptional regulation via glucocorticoid receptor	Commonly used during initiation	May improve outcomes in ARDS (ChiCTR2000029386)§	++	Hypertension, immunosuppression, metabolic changes, mood alterations
Cyclosporine, tacrolimus	Inhibit calcineurin-mediated lymphocyte activation	Case reports/small series in MAS, part of HLH treatment protocol	Theoretical	++	Hypertension, renal failure, immunosuppression
Anakinra	Block IL-1 signaling	Re-analysis of sepsis trials, large series in MAS and HLH (NCT02780583)	NCT04324021	+	Rare transaminitis, neutropenia, eosinophilia
Sarilumab, tocilizumab	Block IL-6 signaling	CAR-T cytokine release syndrome, case reports, ongoing clinical trials¶	NCT04322773, NCT04317092, NCT04320615, NCT04306705, NCT04324073, NCT04315298	+	Cytopenias, immunosuppression
Emapalumab	Neutralize IFNγ	Refractory familial HLH, other case reports, ongoing trials¶	NCT04324021	+	Immunosuppression
JAK inhibitors	Inhibit JAK/STAT pathway cytokines	Case reports, ongoing clinical trials	NCT04320277, NCT04321993	+++	Cytopenias, immunosuppression
Cytokine adsorption	Remove from circulation	Case reports	NCT04324528	Minimal	Central line access
IVIG	Unclear mechanism	Case reports	Theoretical	Minimal	Hypertension, hemolysis
Therapeutic plasma exchange	Remove cytokines/chemokines/DAMPs, replace factors	Case reports	Theoretical	Minimal	Central line access

* Relevant citations are provided in Supplementary Table 2 (available on the *Arthritis & Rheumatology* web site at http://onlinelibrary.wiley.com/doi/10.1002/art.41285/abstract). COVID-19 = coronavirus disease 2019; ARDS = acute respiratory distress syndrome; MAS = macrophage activation syndrome; HLH = hemophagocytic lymphohistiocytosis; IL-1 = interleukin-1; CAR-T = chimeric antigen receptor T cell therapy; IFNγ = interferon-γ; IVIG = intravenous immunoglobulin; DAMPs = damage-associated molecular patterns.
† +, ++, and +++ indicate low, moderate, and high likelihood of impairment.
‡ In methylprednisolone equivalent doses.
§ Dosage unclear.
¶ Approved by the US Food and Drug Administration.

COVID-19 may simply have "garden-variety" ARDS associated with the tropism of the virus for the lung. However, critically ill patients with COVID-19 often demonstrate features suggestive of cytokine storm, including fever, characteristic changes in laboratory study findings, and ARDS. Lung tissue from patients with severe acute respiratory syndrome (SARS), the etiology of which has been attributed to a related coronavirus, showed hemophagocytosis—a central pathologic feature of cytokine storm—in 2 of 6 patients who succumbed to the disease (12). Patients with SARS also exhibited high levels of IFNγ and IL-18, which are particularly important in cytokine storm syndrome (13). Thus, the host's immune response and development of tissue-focused inflammation in the lung likely plays an important role in COVID-19.

These considerations suggest that, beyond antiviral therapy and supportive care, it will be important to monitor hospitalized patients with COVID-19 for evidence of cytokine storm. Impending hyperinflammation can manifest as cytopenias (thrombocytopenia and lymphopenia), coagulopathy (low platelet and fibrinogen levels, and elevated D-dimer levels), tissue damage/hepatitis (elevated LDH, aspartate aminotransferase, and alanine aminotransferase levels), and macrophage/hepatocyte activation (elevated ferritin levels) (Table 1 and Supplementary Table 1, available on the *Arthritis & Rheumatology* web site at http://onlinelibrary.wiley.com/doi/10.1002/art.41285/abstract). Cytokine measurement is a theoretically appealing approach, but IFNγ and IL-1β are not easily assessed in the peripheral blood and IL-6 levels have not yet been proven consistently predictive of poor outcomes. CXCL9, a stable chemokine, is a useful surrogate for IFNγ activity in MAS, as is adenosine deaminase 2 (ADA-2); however, real-time measurement of CXCL9 is not commonly available and ADA-2 testing remains available largely on a research basis. Experience suggests that trends in laboratory test findings, rather than threshold values, will be most informative. In a patient with COVID-19 who develops lymphopenia, worsening coagulopathy, hepatitis, and rising ferritin levels, it may make sense to target immune hyperactivity before end-organ manifestations, such as ARDS, ensue.

The US Centers for Disease Control and Prevention provided an unqualified recommendation against the use of glucocorticoids for the treatment of COVID-19, based on prior experience with influenza, SARS, and coronavirus-induced Middle East respiratory syndrome (MERS) (14). However, a Cochrane review of glucocorticoids as adjunctive therapy in influenza found that the evidence was of low quality, largely because of confounding by indication (15). The literature with regard to glucocorticoids in patients with MERS and SARS has reported similar findings, although some data suggest that glucocorticoids could delay viral clearance (16). Importantly, these data reflect treatment of "all comers" with influenza, MERS, or SARS, rather than therapy targeted to patients with evidence of hyperinflammation. Of note, in one COVID-19 case series, the mortality rate was lower in patients with ARDS who were treated with methylprednisolone compared with those who did not receive glucocorticoids (46% versus 62%; hazard ratio for death 0.38, $P = 0.003$), although, again, the possibility of confounding by indication is difficult to exclude (2).

Experience from hyperinflammation in HLH, MAS, and cytokine release syndrome suggests that early intervention is essential to avoiding life-threatening tissue damage. In patients with COVID-19 who exhibit evidence of cytokine storm, treatment with glucocorticoids, IVIG, and/or anticytokine therapies should be considered, with the aim of reverting hyperinflammation before ARDS occurs (Table 2 and Supplementary Table 2, available on the *Arthritis & Rheumatology* web site at http://onlinelibrary.wiley.com/doi/10.1002/art.41285/abstract) (8,17). Glucocorticoids remain a key first-line option, and clinical trials are urgently needed to test their efficacy and to identify optimal dosing, especially given the clear advantage of glucocorticoids in worldwide availability and cost. IL-1 blockade has shown particular promise as a treatment for cytokine storm syndrome, and high-dose regimens are safe even in the context of overt sepsis (5,10). Tocilizumab (anti–IL-6 receptor) is effective in cytokine release syndrome associated with CAR-T therapy, a syndrome notably reminiscent of COVID-19 in that many patients develop ARDS (11). Emapalumab (anti-IFNγ) is approved by the US Food and Drug Administration for the treatment of HLH and may be effective in MAS. JAK inhibition appears promising; however, the safety of these medications in severe viral infection remains unknown.

Clinical trials are currently enrolling patients with COVID-19 to study the safety and efficacy of glucocorticoids and cytokine blockade strategies utilizing neutralization of IL-1, IL-6, and IFNγ (Table 2). Absent the opportunity to enroll patients in one of these studies, we would consider immunosuppression in patients with COVID-19 who have incipient cytokine storm. Ideally, treatment decisions will be undertaken with the help of a multidisciplinary team familiar with the triggers, manifestations, and treatments of cytokine storm (17). Glucocorticoids will likely be useful. Cytokine blockers may play an important role as well, while we must remain cognizant of the ongoing need for these medications in patients with chronic rheumatologic conditions. Unfortunately, many patients with COVID-19 will become critically ill before high-quality evidence of treatment efficacy is available, leaving us to extrapolate as best we can from the available evidence and from current clinical experience in cytokine storm syndromes.

AUTHOR CONTRIBUTIONS

All authors drafted the article, revised it critically for important intellectual content, and approved the final version to be published.

REFERENCES

1. Zhou F, Yu T, Du R, Fan G, Liu Y, Liu Z, et al. Clinical course and risk factors for mortality of adult inpatients with COVID-19 in Wuhan, China: a retrospective cohort study. Lancet 2020;395:1054–62.
2. Wu C, Chen X, Cai Y, Xia J, Zhou X, Xu S, et al. Risk factors associated with acute respiratory distress syndrome and death in patients with coronavirus disease 2019 pneumonia in Wuhan, China. JAMA Intern Med 2020. E-pub ahead of print.
3. Chen G, Wu D, Guo W, Cao Y, Huang D, Wang H, et al. Clinical and immunologic features in severe and moderate coronavirus disease 2019. J Clin Invest 2020;130:2620–9.
4. Huang C, Wang Y, Li X, Ren L, Zhao J, Hu Y, et al. Clinical features of patients infected with 2019 novel coronavirus in Wuhan, China. Lancet 2020;395:497–506.
5. Eloseily EM, Weiser P, Crayne CB, Haines H, Mannion ML, Stoll ML, et al. Benefit of anakinra in treating pediatric secondary hemophagocytic lymphohistiocytosis. Arthritis Rheumatol 2020;72:326–34.
6. Weiss ES, Girard-Guyonvarc'h C, Holzinger D, de Jesus AA, Tariq Z, Picarsic J, et al. Interleukin-18 diagnostically distinguishes and pathogenically promotes human and murine macrophage activation syndrome. Blood 2018;131:1442–55.
7. Schulert GS, Zhang M, Fall N, Husami A, Kissell D, Hanosh A, et al. Whole-exome sequencing reveals mutations in genes linked to hemophagocytic lymphohistiocytosis and macrophage activation syndrome in fatal cases of H1N1 influenza. J Infect Dis 2016;213:1180–8.
8. Kumar B, Aleem S, Saleh H, Petts J, Ballas ZK. A personalized diagnostic and treatment approach for macrophage activation syndrome and secondary hemophagocytic lymphohistiocytosis in adults. J Clin Immunol 2017;37:638–43.
9. Carcillo JA, Simon DW, Podd BS. How we manage hyperferritinemic sepsis-related multiple organ dysfunction syndrome/macrophage activation syndrome/secondary hemophagocytic lymphohistiocytosis histiocytosis. Pediatr Crit Care Med 2015;16:598–600.
10. Shakoory B, Carcillo JA, Chatham WW, Amdur RL, Zhao H, Dinarello CA, et al. Interleukin-1 receptor blockade is associated with reduced mortality in sepsis patients with features of macrophage activation syndrome: reanalysis of a prior phase III trial. Crit Care Med 2016;44:275–81.
11. Maude SL, Frey N, Shaw PA, Aplenc R, Barrett DM, Bunin NJ, et al. Chimeric antigen receptor T cells for sustained remissions in leukemia. N Engl J Med 2014;371:1507–17.
12. Nicholls JM, Poon LL, Lee KC, Ng WF, Lai ST, Leung CY, et al. Lung pathology of fatal severe acute respiratory syndrome. Lancet 2003;361:1773–8.
13. Huang KJ, Su IJ, Theron M, Wu YC, Lai SK, Liu CC, et al. An interferon-γ-related cytokine storm in SARS patients. J Med Virol 2005;75:185–94.
14. Centers for Disease Control and Prevention. Coronavirus disease (2019). Interim clinical guidance for management of patients with confirmed coronavirus disease (COVID-19). March 2020. URL: https://www.cdc.gov/coronavirus/2019-ncov/hcp/clinical-guidance-management-patients.html#clinical-management-treatment%3C.
15. Lansbury LE, Rodrigo C, Leonardi-Bee J, Nguyen-Van-Tam J, Lim WS. Corticosteroids as adjunctive therapy in the treatment of influenza: an updated Cochrane systematic review and meta-analysis. Crit Care Med 2020;48:e98–106.
16. Lee N, Allen Chan KC, Hui DS, Ng EK, Wu A, Chiu RW, et al. Effects of early corticosteroid treatment on plasma SARS-associated coronavirus RNA concentrations in adult patients. J Clin Virol 2004;31:304–9.
17. Halyabar O, Chang MH, Schoettler ML, Schwartz MA, Baris EH, Benson LA, et al. Calm in the midst of cytokine storm: a collaborative approach to the diagnosis and treatment of hemophagocytic lymphohistiocytosis and macrophage activation syndrome. Pediatr Rheumatol Online J 2019;17:7.

American College of Rheumatology
Empowering Rheumatology Professionals

Arthritis & Rheumatology
Vol. 72, No. 7, July 2020, pp 1064–1066
DOI 10.1002/art.41278

NOTES FROM THE FIELD

Stand Together and Deliver: Challenges and Opportunities for Rheumatology Education During the COVID-19 Pandemic

Fotios Koumpouras[1] and Simon Helfgott[2]

In a matter of weeks, the COVID-19 crisis has totally upended clinical medicine and the practice of rheumatology. Our old ways of seeing patients in person, precepting fellows in clinic or on the consult service, and leading in-person interactive teaching rounds are gone for now and possibly for good. But how can we replace these critical teaching and training elements? Despite the mounting challenges of managing a growing population of COVID-19–infected patients and caregivers, we must find innovative ways to foster our trainees' professional development. The challenge is how to pursue our educational mission safely and effectively during these critical times, when isolation and social distancing have become the new rules of disengagement.

Recent health and environmental crises have provided limited evidence on their disruptive effect on medical training in the US (1). The experience of a Canadian training program during the 2003 SARS epidemic demonstrated that there was fear and anxiety surrounding the potential risk of trainees acquiring SARS (2,3). Residents reported that their scheduled rotations during the epidemic were severely affected, while other educational endeavors were canceled.

More recently, the response to the 2014 Ebola virus disease outbreak raised the question of whether trainees should be allowed to care for infected patients. The Accreditation Council for Graduate Medical Education (ACGME) published guidelines stating that all trainees should gain familiarity with the basic signs and symptoms of Ebola infection, receive training on proper safety protocols for all care settings, and only provide care for patients under direct supervision of attending physicians trained in treatment and infection control (4). Some have argued that residents should be expected to participate in disaster responses: "completely removing trainees from these situations can be detrimental to their overall experience and education" (1,5). As others have noted, "if we avoided all situations that we couldn't understand in advance and that posed any risk, we would spend our lives in a state of paralysis" (6). The key is to strike a balance between the inherent risks associated with serving on the front lines of care during a pandemic and creating sufficient safety measures for our trainees as they move beyond the normal scope of the practice of rheumatology.

We must remember that our fellows are specialists *in training*. They still need our mentoring and guidance to help them navigate through the COVID-19 crisis. They need to proceed along their learning curves, acquiring the knowledge required of a practicing rheumatologist. For this to happen, medical pedagogy must change, and it already has. For example, unprecedented use of videoconferencing during the COVID-19 pandemic is occurring at many levels, particularly to facilitate education and patient care in times of social distancing. "Zoom" has replaced "Google" as our favorite verb. Leveraging video platforms by including trainees from other programs in videoconferences affords an innovative way to expand both the educator and learner pools, thus increasing the value of team-based learning exercises.

We implore program personnel to initiate or maintain and expand telecommunications opportunities in patient care, training evaluation, and education. For example, rheumatology program directors could engage in larger collectives or in smaller groups to promote virtual teaching and training seminars. One of us (SH) recently organized a multiprogram virtual journal club to review the published data and discuss the quality of evidence regarding the use of hydroxychloroquine and chloroquine as treatments for COVID-19 infection. This exercise was attended by 3 times as many participants as a typical journal club (~70 participants) and included rheumatologists from other cities. Such events could serve as a springboard for new virtual education curriculums that could expand well beyond the current urgent needs.

Other potential virtual learning opportunities come to mind. Our role as experts in inflammation might be used to teach the concepts of hyperinflammation and cytokine storm in COVID-19

[1]Fotios Koumpouras, MD: Yale School of Medicine, New Haven, Connecticut; [2]Simon Helfgott, MD: Brigham and Women's Hospital, Boston, Massachusetts.

No potential conflicts of interest relevant to this article were reported.

Address correspondence to Fotios Koumpouras, MD, Yale School of Medicine, 300 Cedar Street, The Anlyan Center for Medical Research Room S525b, New Haven, CT 06520. E-mail: fotios.koumpouras@yale.edu.

Submitted for publication March 29, 2020; accepted in revised form March 31, 2020.

infection to an ever-widening audience of our peers and even patients. Telemedicine will allow rheumatologists to interact with colleagues working in areas that are more severely impacted by COVID-19, so that we can quickly disseminate our collective experience. As our own patients become infected, it will be critical that we disseminate the information to our colleagues across the globe; we are all in this together.

Remote learning has its drawbacks, particularly for the assessment of skill acquisition and development. Also, it may restrict our ability to assess a trainees' personal development. Lost are the spontaneous interactions that occur in the "fellows' room" or in the hallway, and the nearly imperceptible whispers during Grand Rounds. One of us (FK) noticed that during video meetings, the chat sections are often very active with thoughtful insights, quips, and sharing of concerns and fears among fellows. It is highly reassuring that *esprit de corps* remains alive and well among our fellows and that the instinctual impetus to gather and share collective experiences remains very powerful. It might be worth making fellows-only chat rooms available in videoconference meetings.

Programs must create protocols for managing both inpatient consults and outpatient care. With the relaxation of many telemedicine-related regulations, telephone and video visits can easily be established as the primary means of maintaining contact with patients to provide guidance through these critical times. Our early experience precepting fellows in telemedicine has been highly successful, and it may become one of the most positive features to emerge from this pandemic. Videoconferencing applications allow for the creation of separate virtual rooms in which the preceptor could be present, and that the fellow could enter when needed.

Inpatient consults require new approaches too, since hospitals are quickly filling up with infected patients. For example, many consultations could occur via video without the need to see the patient in person, with most of the history gathering occurring via telephone or video with the primary team members. The role of the fellow would be to assemble the patient's history, review the data, write the note, discuss the case with the preceptor, formulate a differential diagnosis, and recommend a treatment plan. It is important that the educational value of this activity is demonstrated. Written communication is key. For consult service patients who are infected with COVID-19, there will be opportunities to hold virtual visits using newly developed video programs on Microsoft and other platforms. The key element for all these activities is the practice of safe social distancing. Last, many subspecialty sections are being reorganized into command treatment teams to address the anticipated surge in hospitalized patients. For trainees who are excluded from performing face-to-face encounters, we suggest reorganizing consult teams to allow at least one member (preferably faculty) to participate in face-to-face encounters while fellows gather data and facilitate communication.

During these times of crisis, it is important to remember some key words to guide our thinking about rheumatology training and education. The first is *flexibility*. Flexibility must occur at all levels, including the ACGME, the National Board of Medical Examiners, the American Board of Internal Medicine, the American College of Rheumatology, our sponsoring institutions, our faculty, and all learners. The ACGME granted flexibility for training requirements by enacting a national Pandemic Emergency Status executed under its Extraordinary Circumstances policy. This allows all residents and fellows to care for all patients, while loosening many regulatory requirements. Though supervision requirements and work hour limits remain in effect, all other Common Program Requirements and specialty-specific Program Requirements have been suspended. This allows for subspecialty fellows who are board-certified or -eligible and meet criteria for medical staff appointments to function within their core specialty for up to 20% of the academic year. Recognizing the need and opportunity for medical education to continue and for trainees to remain involved, the ACGME has proven so far to be highly flexible and understanding (7,8).

The second word is *innovation*. As noted above, this includes the deployment of virtual medicine to provide clinical care and rheumatology education. We will need to be able to evaluate competency milestones pertaining to virtual patient visits by our fellows (9). Programs may need to consider using some newly developed tools for virtual-space medicine, including virtual musculoskeletal ultrasound and the use of virtual reality simulators to teach palpation skills (10). Much of radiology is already in the virtual space and should be readily incorporated into rheumatologists' virtual care visits in the near future.

The third key word to guide us is *safety*. Our fellows are young, generally healthy people who represent the future of rheumatology. Program directors will have to carefully weigh requests from their hospitals to deploy trainees to other critical tasks during the pandemic. How do we weigh the risk of acquiring infection when a fellow is the parent of a newborn or is pregnant, postpartum, or has increased personal risk of infection due to underlying medical conditions? These issues have generated considerable anxiety and are not easily answered. Integrated stress management resources that are specialized for medical crisis work must be available to our trainees.

We have entered uncharted waters. The Herculean effort underway to prepare our medical centers for the times ahead requires us to prepare our trainees for these changes, keeping them well informed. It is our duty to ensure their preparedness as trainees remain on the front lines. During this time of crisis, let us reiterate that our trainees embody what is good in medicine. Their education must continue, and we must stand shoulder to shoulder with them and deliver.

ACKNOWLEDGMENT

We thank Dr. Rick Bucala for his comments.

AUTHOR CONTRIBUTIONS

Drs. Koumpouras and Helfgott drafted the article, revised it critically for important intellectual content, and approved the final version to be published.

1. Pepe D, Martinello RA, Juthani-Mehta M. Involving physicians-in-training in the care of patients during epidemics. J Grad Med Educ 2019;11:632–4.
2. Rambaldini G, Wilson K, Rath D, Lin Y, Gold WL, Kapral MK, et al. The impact of severe acute respiratory syndrome on medical house staff: a qualitative study. J Gen Intern Med 2005;20:381–5.
3. Straus SE, Wilson K, Rambaldini G, Rath D, Lin Y, Gold WL, et al. Severe acute respiratory syndrome and its impact on professionalism: qualitative study of physicians' behaviour during an emerging healthcare crisis. BMJ 2004;329:83.
4. Accreditation Council for Graduate Medical Education. ACGME guidance statement on Ebola virus infection and resident/fellow training in the United States. October 2014. URL: https://www.acgme.org/Portals/0/PDFs/Nasca-Community/ACGME-GME-Ebola-Final1.pdf.
5. Bernstein SL, Shayne P. Ebola, physicians in training, and the duty to treat. Acad Emerg Med 2015;22:88–90.
6. Rosenbaum L. License to serve—US trainees and the Ebola epidemic. N Engl J Med 2015;372:504–6.
7. Accreditation Council for Graduate Medical Education. ACGME response to COVID-19: clarification regarding telemedicine and ACGME surveys. March 2020. URL: https://www.acgme.org/Newsroom/Blog/Details/ArticleID/10125/ACGME-Response-to-COVID-19-Clarification-regarding-Telemedicine-and-ACGME-Surveys.
8. Accreditation Council for Graduate Medical Education. ACGME response to pandemic crisis. URL: https://www.acgme.org/covid-19.
9. Isaza-Restrepo A, Gómez MT, Cifuentes G, Argüello A. The virtual patient as a learning tool: a mixed quantitative qualitative study. BMC Med Educ 2018;18:297.
10. Zhang Y, Phillips R, Ward J, Pisharody S. A survey of simulators for palpation training. Stud Health Technol Inform 2009;142:444–6.

Arthritis & Rheumatology
Vol. 72, No. 7, July 2020, pp 1067–1071
DOI 10.1002/art.41277

American College of Rheumatology
Empowering Rheumatology Professionals

BRIEF REPORT

Biosimilar Uptake in Academic and Veterans Health Administration Settings: Influence of Institutional Incentives

Joshua F. Baker,[1] Charles E. Leonard,[2] Vincent Lo Re III,[2] Michael H. Weisman,[3] Michael D. George,[2] and Jonathan Kay[4]

Objective. To compare uptake in the ordering of biosimilars at a Veterans Affairs Medical Center (VAMC) to that at an academic medical center, where institutional incentives for infused medications differ.

Methods. We performed a cross-sectional study of medical record data and estimated institutional financial incentives at 2 medical centers in Philadelphia: 1) the University of Pennsylvania Health System (UPHS), and 2) the local VAMC. All ordering events for filgrastim or infliximab products were quantified over time and stratified according to product (biosimilar versus reference product) and center. Financial incentives to the institutions over time were determined based on actual drug costs for the VAMC and average sales prices (ASPs) and Medicare Part B reimbursement rates for UPHS.

Results. There were 15,761 infusions of infliximab at UPHS, of which 99% were for the reference product. There was a sharper decline in the use of reference products at the VAMC; 62% of the 446 infliximab infusions ordered at the VAMC were for the reference product. ASPs were consistently lower for biosimilar infliximab products, but the estimated institutional financial incentives remained similar over time for biosimilar and reference infliximab at UPHS. At the VAMC, the costs for 100-mg vials of reference infliximab and infliximab-abda were $623.48 and $115.58, respectively: a $507.90 (81%) savings per vial.

Conclusion. The uptake of infliximab biosimilars has been slow at an academic medical center compared to a nearby VAMC, where financial savings are realized by the institution from its use. Slow adoption of biosimilar medications may impact the rates of decline in costs.

INTRODUCTION

More than 20 biosimilars have been approved for marketing in the US, and >50 have been approved in Europe (1). Nonmedical mandatory switching and required use of a biosimilar for patients newly initiating treatment have resulted in the rapid uptake of biosimilars in some Scandinavian countries (2). However, in the US, changes in biosimilar prescribing patterns have occurred gradually in the absence of similar large-scale mandates from health care institutions or payers (3).

Few studies have investigated the uptake of biosimilars in the US. One study of US Medicare Part B prescription claims for

The opinions or assertions presented herein are the private views and opinions of the authors and do not represent the views of the Department of Veterans Affairs.

Dr. Baker's work was supported by a Veterans Affairs Clinical Science Research and Development Career Development Award (IK2-CX-000955), a Veterans Affairs Merit Award (I01-CX-001703), and a Veterans Affairs SPiRE Award. Dr. Leonard's work was supported by the NIH (grants R01-AG-060975, R01-AG-025152, R01-DA-048001, and R01-AG-064589) and the American Diabetes Association (1-18-ICTS-097). Dr. Lo Re's work was supported by the NIH (grants R01-CA-20646, R01-AI-136626, and R01-AR-076392).

[1]Joshua F. Baker, MD, MSCE: Corporal Michael J. Crescenz VA Medical Center and University of Pennsylvania Perelman School of Medicine, Philadelphia; [2]Charles E. Leonard, PharmD, MSCE, Vincent Lo Re III, MD, MSCE, Michael D. George, MD, MSCE: University of Pennsylvania Perelman School of Medicine, Philadelphia; [3]Michael H. Weisman, MD: Cedars-Sinai Medical Center, Los Angeles, California; [4]Jonathan Kay, MD: University of Massachusetts Medical School and UMass Memorial Medical Center, Worcester.

Dr. Baker has received consulting fees from Bristol-Myers Squibb and Gilead (less than $10,000 each) and research support from the VA. Dr. Leonard has received consulting fees, speaking fees, and/or honoraria from Pfizer, Sanofi, and the American College of Clinical Pharmacy Research Institute (less than $10,000 each). Dr. Kay has received consulting fees from AbbVie, Alvotech, Boehringer Ingelheim, Celltrion Healthcare, Merck Sharp & Dohme, Pfizer, Samsung Bioepis, Sandoz, and UCB (less than $10,000 each) and research support from Pfizer and UCB. No other disclosures relevant to this article were reported.

Address correspondence to Joshua F. Baker, MD, MSCE, University of Pennsylvania, 5th Floor White Building, 3400 Spruce Street, Philadelphia, PA 19104. E-mail: joshua.baker@pennmedicine.upenn.edu.

Submitted for publication November 26, 2019; accepted in revised form March 27, 2020.

filgrastim products found biosimilar filgrastim-sndz to account for 32% of all filgrastim prescriptions by 21 months after its approval by the US Food and Drug Administration (4). The uptake of infliximab biosimilars is likely to differ since incentives and financial drivers at the institutional level are different for infused therapies.

Currently in the US, Medicare (one of the largest payers for infused therapies) is not permitted to negotiate drug prices. Infused therapies are reimbursed based on the average selling price (ASP) over the prior quarter. Biosimilar therapies that are priced lower than their reference products (lower ASP) will have lower reimbursement rates and may have less room to negotiate with institutions for a lower purchase price compared to the reference product. Since the financial incentive to use a product depends on the difference between the reimbursement rate and the purchase price, there will not necessarily be an incentive for an institution to use the lower-priced product. This may result in slow adoption of biosimilars and negatively impact the ability of these products to effectively stem increasing health care costs.

The uptake of biosimilar products has not been evaluated in the Veterans Affairs (VA) medical system, which uses centralized negotiation and contract management to establish a national formulary (5). To save costs and promote the use of less expensive therapies, the VA has designated biosimilar options for preferred use and has mandated switching patients to these therapies, including biosimilar infliximab and filgrastim products, unless there are special clinical circumstances. In such instances, physicians are required to submit non-formulary requests if they wish to use the nonpreferred therapy. Thus, a comparison of biosimilar ordering at a VA Medical Center (VAMC) to that at a nearby academic medical center provides a natural experiment to assess how tendering and national policy mandating use of biosimilars can affect uptake of these therapies and impact health care costs (6).

We hypothesized that the rate of uptake of biosimilar infliximab therapies at an academic medical center would be less than that at a nearby VAMC, where lower acquisition costs had been negotiated for infliximab biosimilars. We further hypothesized that institutional incentives at the academic medical center, based on Medicare reimbursement policies for infused therapies, would not favor a switch to the biosimilar therapies despite their lower ASP.

METHODS

We compared the frequency of prescribing of biosimilars at a VAMC to that at a nearby academic medical center between January 1, 2015 and May 31, 2019. We leveraged data from a prior analysis of pharmacy data from the University of Pennsylvania Health System (UPHS) electronic medical record and the Corporal Michael J. Crescenz VAMC pharmacy databases (7). These institutions are geographically adjacent (<0.5 miles) and share health care providers who work at both facilities.

We focused on 3 medications for which biosimilars have been marketed over the past 3–5 years: infliximab, filgrastim, and pegfilgrastim. Filgrastim and pegfilgrastim were examined in order to assess patterns of use of non-infusion therapies at UPHS and the VAMC. We included the reference products and all approved biosimilars. We summarized the frequency of ordering of infliximab, filgrastim, and pegfilgrastim reference and biosimilar or alternative products after the approval date for the first biosimilar or alternative product of each.

Medicare was the predominant payer, with approximately 35% of infusions covered by Medicare or Medicare Advantage, 21% of infusions covered by Medicaid, and 44% of infusions covered by commercial insurance. We therefore estimated institutional reimbursement for infliximab reference product and biosimilars at UPHS based on the Medicare Part B reimbursement policy: infusions are reimbursed at the quarterly Medicare Part B ASP for the reference product or biosimilar plus 4.3% of the ASP for the reference product (8). The ASP reflects the actual average price for medications, considering all negotiated discounts and rebates. Competition and price negotiations between payers, pharmacy benefits managers (PBMs), and institutions are expected to result in reductions in ASP over time. We used the published ASP from 2 quarters in the future in order to estimate the acquisition cost to an institution for each medication during the current quarter (9). We defined the difference in reimbursement and estimated acquisition cost as the financial incentive to the institution to utilize that therapy. We then compared these estimated incentives for UPHS to the VA institutional incentives, which were based on actual purchasing costs to the VA for each individual therapy (10).

RESULTS

Between July 1, 2015 and May 31, 2019, there were 15,761 infusions of infliximab at UPHS and 446 at the VAMC. At UPHS, 99% of infliximab infusions were for the reference product Remicade (Janssen Pharmaceuticals), compared to 62% at the VAMC over the same time period. The initial shift to the use of biosimilar infliximab-dyyb (Inflectra; Pfizer) at the VAMC occurred in December 2017, with an abrupt change in ordering around this date (11) (Figure 1). Use of biosimilar infliximab was similar across the divisions of gastroenterology (39% of all infliximab orders) and rheumatology (31% of all infliximab orders).

Since July 2017, after initially having a higher ASP, ASPs for biosimilar infliximab products have been consistently lower than those for the reference product (Figure 2). However, estimated institutional incentives based on Medicare Part B reimbursement and estimated acquisition costs for both reference and biosimilar infliximab have been similar since 2018. In fact, in 2019, the estimated institutional incentive favored the reference product (Remicade) by $49–64 per 100-mg vial.

At the VAMC, the situation is very different: the costs of 100-mg vials of reference infliximab (Remicade) and infliximab-abda (Renflexis; Merck & Company) are $623.48 and $115.58 each, respectively, yielding a $507.90 (81%) savings per 100-mg vial

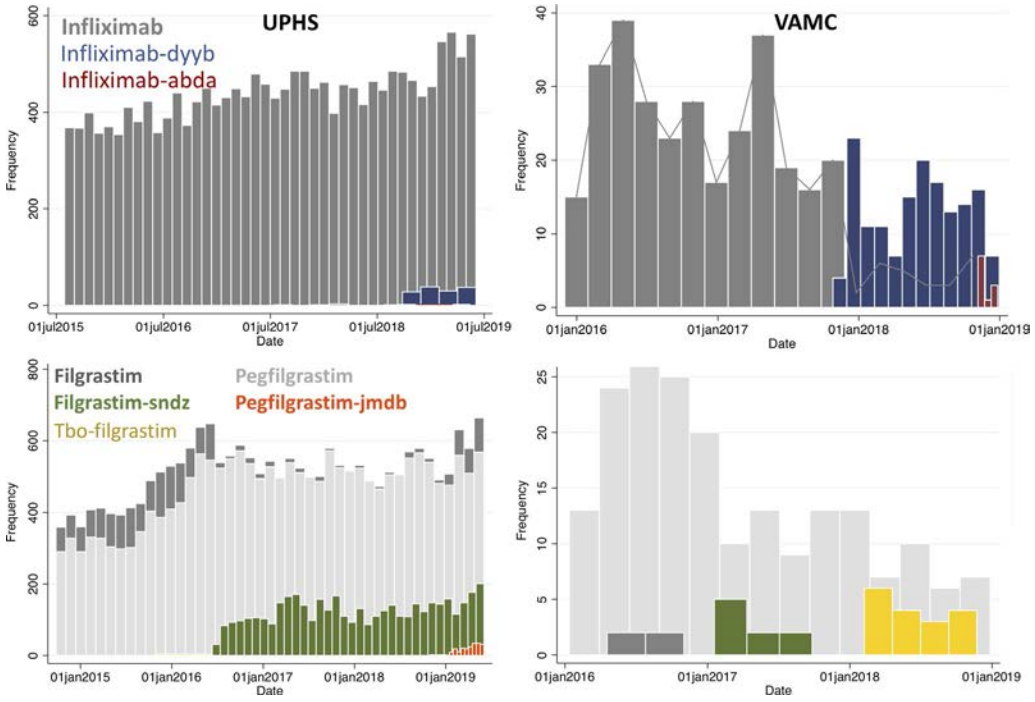

Figure 1. Frequency of orders for reference and biosimilar infliximab and filgrastim/pegfilgrastim at a Veterans Affairs Medical Center (VAMC) compared to a nearby academic medical center, the University of Pennsylvania Health System (UPHS).

for the biosimilar. The current cost to the VA for infliximab-abda is 79% lower than the Medicare ASP for the same therapy ($116 versus $546).

Between January 1, 2015 and May 31, 2019, there were 46,683 orders for filgrastim or pegfilgrastim at UPHS, of which 90% were for either reference product (Neupogen or Neulasta; Amgen) (Figure 1). There was modest use of filgrastim-sndz at UPHS, beginning in 2016. At the VAMC, 88% of prescriptions were for one of the reference products but with a sharper decline in use of the reference product and a sharper increase in the use of biosimilar products after September 2016, when biosimilars were designated as the preferred product.

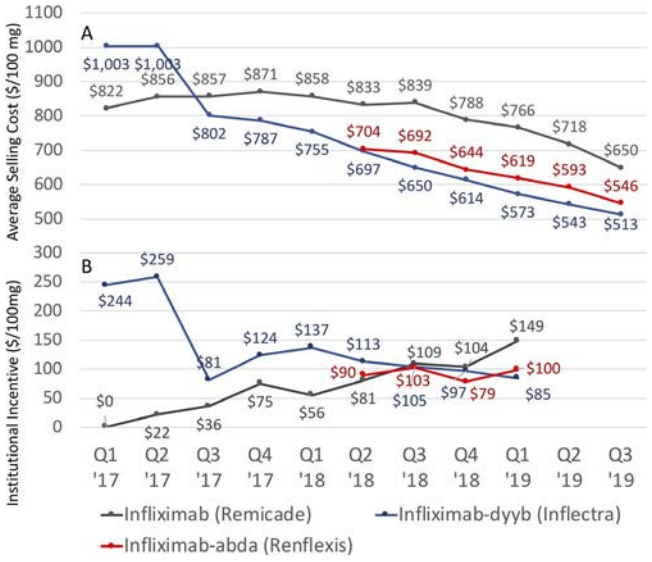

Figure 2. **A**, Average sales prices (ASPs) for reference infliximab and biosimilar products infliximab-dyyb (Inflectra) and infliximab-abda (Renflexis) by quarter. **B**, Estimated financial incentive to an institution per 100-mg vial for use of each product, based on Medicare Part B reimbursement policy and subsequent ASP.

DISCUSSION

Compared to a nearby academic medical center hospital, the uptake of biosimilars, particularly infliximab products, has been dramatically faster at the VAMC, where tendering and a nationwide policy change mandating preferred use of the biosimilar have resulted in clear financial savings for the institution. These data suggest that, with the current Medicare Part B reimbursement policy, the absence of financial incentives to encourage use of infliximab biosimilars has resulted in slower uptake of biosimilar use at institutions outside of the VA system. The implications of this are a slower reduction in costs to the health care system, since decreases in ASP over time are predicated on negotiations at the institutional level, which have been gradual and stepwise.

The use of biosimilars has been widely accepted in Europe, especially where tender processes and changes in policy at a national level have mandated their use (12). The lesser discounting of biosimilars in the US and the observed slow adoption have delayed realization of the potential economic benefits of biosimilars on health care spending. This analysis demonstrates that, even

when the ASP of an infusible biosimilar is lower than that of its reference product, current Medicare Part B reimbursement policy does not necessarily provide an institution with a financial incentive to transition to use of the biosimilar.

Because an institution is now reimbursed for a Medicare Part B medication at 104.3% of its ASP, use of a medication with a lower ASP will yield lower reimbursement. In this context, the incentive for an institution to use an individual therapy depends primarily on the negotiated purchase price relative to the reimbursement rate. Our analysis reveals that, because more expensive therapies have more room to negotiate, a similar relative reduction in price for a more expensive therapy can result in a greater incentive for the institution to use that therapy. These observations are in spite of the reimbursement for an infused biosimilar being its ASP plus an additional 4.3% of the ASP of the more expensive reference product.

In addition, while a gradual reduction of the ASPs of reference infliximab and both infliximab biosimilars has occurred with ongoing negotiations between institutions and manufacturers, the rate of decline in ASP has been slow, and substantially less than that which has been observed at the VA, where costs have already been reduced by 80% compared to the ASP of reference infliximab. This may be, in part, because major reductions in pricing on behalf of the manufacturer are expected to result in only short-term incentives for use of the product.

As observed, despite lower ASPs, providers at the academic medical center have not incorporated biosimilar infliximab substantially into their practice. In addition to the lack of clear financial incentives, other economic or market factors and uncertainty and misperceptions about biosimilars among health care providers, pharmacists, and patients may also slow the transition to their acceptance and use (13,14). This study suggests that institutional mandates for the use of specific products, such as that observed in the VA medical system for biosimilar infliximab, can surmount these barriers that are observed at the level of individual providers. In The Netherlands, structured educational programs have increased patient acceptance of transitioning from a reference product to its biosimilar (15). Thus, any institutional mandate to use biosimilars should be accompanied by education of health care providers, pharmacists, and patients about the efficacy, safety, and utility of biosimilars.

Although ASPs reflect prices, after discounts and rebates, averaged throughout the US for drugs reimbursed by Medicare Part B, we were not able to ascertain actual acquisition costs to the UPHS. The actual financial incentives to an institution depend upon price negotiations with individual manufacturers. However, our estimate of acquisition costs using ASPs can be generalized nationally. Although some of our results may not be applicable to other geographical regions of the US, the comparison of 2 affiliated institutions in geographical proximity and with shared health care providers is a strength. Our findings should be replicated using national VAMC data or data from other health care systems.

Our observations may not be applicable to medications that are not administered by infusion and thus are not covered by Medicare Part B. However, because PBMs often receive rebates that are calculated as a percentage of the manufacturer's list price, they may receive a larger rebate for a more expensive drug. Thus, while not studied directly here, PBMs may receive incentives that continue to promote the use of reference products that have higher manufacturer's list prices, which will likely limit the uptake of both infused and injectable biosimilar therapies over time. This hypothesis is supported by our data, which demonstrate that the use of biosimilar filgrastim-sndz remains low relative to its reference product at UPHS, in comparison to the relative use of the biosimilar at the VAMC, despite the ASP of biosimilar filgrastim being approximately 40% lower than that of its reference product (9). This finding has important implications for when non-infused biosimilars (e.g., etanercept and adalimumab) are eventually introduced to the US market.

In conclusion, we observed slower uptake of an infused biosimilar at an academic medical center compared to that at a neighboring VAMC, where preferred use of biosimilar infliximab is mandated and clear financial savings are realized by its use. These observations demonstrate how complexities of financial incentives for the use of biosimilar medications may delay their adoption. A slower incorporation of the use of a biosimilar is expected to result in delays in the reductions in pricing and costs to Medicare, particularly compared to the reduction in costs observed for the VA. The incentivization of policy changes at the institutional level, as observed in the VA, may be the most effective way to increase use of biosimilars in the US and to realize savings to the health care system.

AUTHOR CONTRIBUTIONS

All authors were involved in drafting the article or revising it critically for important intellectual content, and all authors approved the final version to be published. Dr. Baker had full access to all of the data in the study and takes responsibility for the integrity of the data and the accuracy of the data analysis.

Study conception and design. Baker, Leonard, Kay.

Acquisition of data. Baker.

Analysis and interpretation of data. Baker, Leonard, Lo Re, Weisman, George, Kay.

REFERENCES

1. US Food and Drug Administration. Biosimilar product information. February 2020. URL: https://www.fda.gov/drugs/biosimilars/biosimilar-product-information.
2. Mack A. Norway biosimilars in different funding systems: what works? GaBi J 2015;4:90–2.
3. Sarpatwari A, Barenie R, Curfman G, Darrow JJ, Kesselheim AS. The US biosimilar market: stunted growth and possible reforms. Clin Pharmacol Ther 2019;105:92–100.
4. Kozlowski S, Birger N, Brereton S, McKean SJ, Wernecke M, Christl L, et al. Uptake of the biologic filgrastim and its biosimilar

product among the medicare population [letter]. JAMA 2018;320: 929–31.

5. Maniadakis N, Holtorf AP, Otavio Correa J, Gialama F, Wijaya K. Shaping pharmaceutical tenders for effectiveness and sustainability in countries with expanding healthcare coverage. Appl Health Econ Health Policy 2018;16:591–607.
6. Mulcahy AW, Hlavka JP, Case SR. Biosimilar cost savings in the United States: initial experience and future potential. Rand Health Q 2018;7:3.
7. Sentinel. Investigation of nonproprietary name suffix use for biologics and biosimilars. April 2019. URL: https://www.sentinelinitiative.org/sentinel/methods/investigation-nonproprietary-name-suffix-use-biologics-and-biosimilars.
8. Code of federal regulation. October 2018. URL: https://www.govinfo.gov/content/pkg/CFR-2018-title42-vol3/xml/CFR-2018-title42-vol3-sec414-904.xml.
9. CMS.gov. Medicare Part B drug average sales price. November 2019. URL: https://www.cms.gov/Medicare/Medicare-Fee-for-Service-Part-B-Drugs/McrPartBDrugAvgSalesPrice/index.html.
10. US Department of Veterans Affairs. National acquisition center. Pharmaceutical catalog search. 2019. URL: https://www.vendorportal.ecms.va.gov/NAC/Pharma/List.
11. US Department of Veterans Affairs. Pharmacy benefits management services. 2019. URL: https://www.pbm.va.gov/apps/VANational Formulary/.
12. Dranitsaris G, Jacobs I, Kirchhoff C, Popovian R, Shane LG. Drug tendering: drug supply and shortage implications for the uptake of biosimilars. Clinicoecon Outcomes Res 2017;9:573–84.
13. Cohen H, Beydoun D, Chien D, Lessor T, McCabe D, Muenzberg M, et al. Awareness, knowledge, and perceptions of biosimilars among specialty physicians. Adv Ther 2017;33:2160–72.
14. Leonard E, Wascovich M, Oskouei S, Gurz P, Carpenter D. Factors affecting health care provider knowledge and acceptance of biosimilar medicines: a systematic review. J Manag Care Spec Pharm 2019;25:102–12.
15. Tweehuysen L, Huiskes VJ, van den Bemt BJ, Vriezekolk JE, Teerenstra S, van den Hoogen FH, et al. Open-label, non-mandatory transitioning from originator etanercept to biosimilar sb4: six-month results from a controlled cohort study. Arthritis Rheumatol 2018;70:1408–18.

Arthritis & Rheumatology
Vol. 72, No. 7, July 2020, pp 1072–1081
DOI 10.1002/art.41232

American College of Rheumatology
Empowering Rheumatology Professionals

Achievement of Remission in Two Early Rheumatoid Arthritis Cohorts Implementing Different Treat-to-Target Strategies

Vibeke Norvang,[1] Gina H. Brinkmann,[2] Kazuki Yoshida,[3] Siri Lillegraven,[4] Anna-Birgitte Aga,[4] Joseph Sexton,[4] Sara K. Tedeschi,[3] Houchen Lyu,[5] Ellen S. Norli,[6] Till Uhlig,[1] Tore K. Kvien,[1] Maria D. Mjaavatten,[4] Daniel H. Solomon,[3] and Espen A. Haavardsholm,[4] the ARCTIC Trial Group and the NOR-VEAC Study Group

Objective. The objective of this study was to compare achievement of remission in 2 early rheumatoid arthritis (RA) treat-to-target (TTT) cohorts, a tight control cohort with a target of stringent remission in a randomized controlled trial and an observational cohort targeting a looser definition of remission in clinical practice.

Methods. We analyzed data from the Aiming for Remission in Rheumatoid Arthritis: a randomised trial examining the benefit of ultrasound in a Clinical Tight Control regimen (ARCTIC) trial and the Norwegian Very Early Arthritis Clinic (NOR-VEAC) observational study. Both were Norwegian multicenter studies that included disease-modifying antirheumatic drug (DMARD)–naive RA patients and implemented TTT. The target in the ARCTIC trial was remission defined as a Disease Activity Score (DAS) of <1.6 plus 0 swollen joints on a 44-joint count, while the target in the NOR-VEAC study was the less stringent remission target of a DAS28 of <2.6. We assessed achievement of the study-specific targets and compared the odds of achieving the American College of Rheumatology(ACR)/European League Against Rheumatism (EULAR) Boolean remission during 2 years of follow-up.

Results. We included 189 patients from the ARCTIC trial and 330 patients from the NOR-VEAC study. The study-specific target had been achieved in more than half of the patients in each cohort at 6 months, increasing to >60% at 12 and 24 months. The odds of achieving ACR/EULAR Boolean remission during follow-up were higher in the ARCTIC trial than in the NOR-VEAC study, with significant differences at 3 months (odds ratio 1.73 [95% confidence interval 1.03–2.89]), 12 months (odds ratio 1.97 [95% confidence interval 1.21–3.20]), and 24 months (odds ratio 1.82 [95% confidence interval 1.05–3.16]).

Conclusion. A majority of patients in both cohorts reached the study-specific treatment targets. More patients in the ARCTIC trial than in the NOR-VEAC study achieved ACR/EULAR Boolean remission during follow-up, suggesting that targeting a more stringent definition of remission provides further potential for favorable outcomes of a TTT strategy.

INTRODUCTION

Treat-to-target (TTT) strategies have become a cornerstone in the care of patients with rheumatoid arthritis (RA) (1,2). Key elements of a TTT strategy include defining a treatment target when initiating a new drug therapy, close monitoring of treatment response, and intensification of treatment if the target is not reached (1). A TTT approach has consistently shown favorable outcomes compared to conventional care (3,4) and is included in current treatment recommendations from the American College

The Aiming for Remission in Rheumatoid Arthritis: a randomised trial examining the benefit of ultrasound in a Clinical Tight Control regimen (ARCTIC) trial was supported by the Norwegian Research Council, the South-East Health Region in Norway, the Norwegian Rheumatism Association, the Norwegian Women's Public Health Association, and unrestricted grants from AbbVie, Pfizer, MSD, Roche, and UCB. The Norwegian Very Early Arthritis Clinic (NOR-VEAC) study was funded by the Norwegian Foundation for Health and Rehabilitation and the South-Eastern Norway Regional Health Authority. Dr. Norvang's work was supported by an Inger Helene Høver legacy grant paid to the Diakonhjemmet Hospital Department of Rheumatology.

Presented in part at the 2018 American College of Rheumatology/Association of Rheumatology Health Professionals Annual Meeting, Chicago, IL, October 2018; and at the 2019 American College of Rheumatology/Association of Rheumatology Professionals Annual Meeting, Atlanta, GA, November 2019.

[1]Vibeke Norvang, MD, Till Uhlig, MD, PhD, Tore K. Kvien, MD, PhD: Diakonhjemmet Hospital and University of Oslo, Oslo, Norway; [2]Gina H. Brinkmann, MD, PhD: Østfold Hospital, Grålum, Norway; [3]Kazuki Yoshida, MD, ScD, Sara K. Tedeschi, MD, Daniel H. Solomon, MD, MPH: Brigham and Women's Hospital and Harvard Medical School, Boston, Massachusetts; [4]Siri Lillegraven, MD, PhD, MPH, Anna-Birgitte Aga, MD, PhD, Joseph Sexton, PhD, Maria D. Mjaavatten, MD, PhD, Espen A. Haavardsholm, MD, PhD: Diakonhjemmet Hospital, Oslo, Norway; [5]Houchen Lyu, MD, PhD: Brigham and Women´s Hospital, Boston, Massachusetts; [6]Ellen S. Norli, MD, PhD: Martina Hansens Hospital, Sandvika, Norway.

Drs. Solomon and Haavardsholm contributed equally to this work.

of Rheumatology (ACR) (5) and the European League Against Rheumatism (EULAR) (6). However, despite the known benefits and recommendations, TTT strategies are still inadequately implemented in clinical practice for a variety of reasons (7–9), and many patients continue to have moderate or high disease activity despite treatment with disease-modifying antirheumatic drugs (DMARDs) (10,11). Identifying successful strategies for incorporating TTT into routine care is crucial for improving RA outcomes.

The evidence base for TTT in RA mainly consists of randomized controlled trials (RCTs) comparing a TTT strategy with conventional care or studies comparing the outcomes of TTT implemented in RCTs or observational cohorts with conventional care in clinical practice (3,4). No previous study has made a head-to-head comparison of a TTT strategy in an RCT versus a TTT strategy in an observational cohort. This analytic approach may lead to a better understanding of what factors are important for achieving the treatment target and how to improve the incorporation of TTT in clinical practice.

The preferred treatment target in a TTT strategy in RA is a state of sustained clinical remission (1). Different composite disease activity indices or criteria may be used to define remission, and the frequency of patients reaching remission depends on the definition used (12,13). Current TTT recommendations suggest defining remission using the ACR/EULAR Boolean criteria, the Clinical Disease Activity Index (CDAI), or the Simplified Disease Activity Index (1,14). Remission according to these definitions allows for limited remaining disease activity and is associated with the prevention of joint destruction, improved functional outcomes, and a reduced risk of comorbidities (13,15). While several studies have compared the outcomes of having achieved different disease activity states or remission according to different criteria (13,16–18), limited data exist on the impacts of targeting different definitions of remission in a TTT strategy (19).

The objective of the present study was to compare the achievement of remission during 2 years of follow-up in 2 early RA cohorts implementing different TTT strategies. For this purpose, we used data from 2 Norwegian multicenter TTT studies of DMARD–naive RA patients: the Aiming for Remission in Rheumatoid Arthritis: a randomised trial examining the benefit of ultrasound in a Clinical Tight Control regimen (ARCTIC) trial (20) and the Norwegian Very Early Arthritis Clinic (NOR-VEAC) observational study (21). We assessed achievement of the study-specific remission target in each cohort and examined whether the tight control TTT strategy with a target of stringent remission in the ARCTIC trial led to achievement of the ACR/EULAR Boolean remission in more patients compared to the TTT approach targeting a less stringent definition of remission in the NOR-VEAC study.

PATIENTS AND METHODS

Study design. A list of the ARCTIC trial and NOR-VEAC study investigators is shown in Appendix A. The ARCTIC trial (20) (ClinicalTrials.gov identifier: NCT01205854) compared the outcomes of an ultrasound TTT strategy with a conventional TTT strategy in patients with early RA. The target in both arms was stringent remission, defined as a Disease Activity Score (DAS) (22,23) of <1.6 plus 0 swollen joints on a 44-joint count, with the additional requirement of no power Doppler ultrasound activity in the ultrasound group. A total of 230 DMARD-naive RA patients were included at 11 rheumatology centers across Norway between 2010 and 2013. The main inclusion criteria were age 18–75 years, fulfillment of the 2010 ACR/EULAR classification criteria for RA (24), <2 years since the first patient-reported swollen joint, and indication for start of DMARD therapy without prior DMARD use. All patients provided written informed consent, and the trial was conducted in compliance with the Declaration of Helsinki. Patients were followed up for 2 years, with visits at baseline and after 1, 2, 3, 4, 6, 8, 10, 12, 14, 16, 20, and 24 months. Treatment for all patients followed a predefined protocol, starting with methotrexate (MTX) monotherapy in combination with tapering doses of prednisolone. Subsequent escalation in patients who had poor improvement in disease activity and had not reached the target included optimizing the dosage of MTX to 25–30 mg/week, synthetic DMARD triple therapy, and biologic therapy. Treatment for patients with high disease activity and risk factors for progressive joint destruction (anti–cyclic citrullinated peptide [anti-CCP] or rheumatoid factor [RF] positivity, and either erosions on computed radiography or baseline RA magnetic resonance imaging bone marrow edema score of >2) could be escalated directly to biologic therapy if initial therapy with MTX failed. Overviews of the treatment algorithm and the decision rules for escalation of therapy in the ARCTIC trial are found in Supplementary Tables 1 and 2 (available on the *Arthritis & Rheumatology* web site at http://onlinelibrary.wiley.com/doi/10.1002/art.41232/abstract).

The NOR-VEAC study (21) was a multicenter prospective observational study implementing a TTT approach in patients with early RA initiating DMARD therapy. The target was remission defined as a DAS28 of <2.6 (23,25). A total of 429 patients with early RA were included at 6 rheumatology centers in southeastern Norway between 2010 and 2016. The main inclusion criteria for patients starting follow-up according to TTT principles

Dr. Kvien has received consulting fees, speaking fees, and/or honoraria from Biogen, Egis, Eli Lilly, Hikma, Mylan, Novartis/Sandoz, Oktal, Hospira/Pfizer, Sanofi, and UCB (less than $10,000 each). Dr. Solomon has received research support from AbbVie, Amgen, Corrona, Genentech, Janssen, and Pfizer. Dr. Haavardsholm has received research support from AbbVie, MSD, Pfizer, Roche, and UCB (for the ARCTIC trial). No other disclosures relevant to this article were reported.

Address correspondence to Vibeke Norvang, MD, Diakonhjemmet Hospital, PO Box 23 Vinderen, 0319 Oslo, Norway. E-mail: v.norvang@gmail.com.

Submitted for publication November 8, 2019; accepted in revised form February 6, 2020.

were ages 18–75 years, <12 months since the first patient-reported swollen joint, a clinical diagnosis of RA, and indication for DMARD therapy without prior DMARD use. All patients provided written informed consent, and the study was conducted in compliance with the Declaration of Helsinki. Patients initiating DMARD therapy were scheduled to have monthly follow-up visits until the target of DAS28 remission had been reached. Further follow-up was scheduled every 3 months up to 24 months and, if still at target, every 6 months up to a total of 5 years. The study protocol did not include a specific treatment algorithm; however, participating centers committed to treat patients according to current EULAR recommendations for the management of RA, following TTT principles (26–28). The EULAR recommendations suggested initiating MTX as the first-line DMARD and rapidly increasing the dosage to 20–30 mg/week. Further escalation of therapy to either another synthetic DMARD regimen or to a biologic DMARD was to be guided by the presence or absence of poor prognostic factors, such as RF or anti-CCP positivity, high levels of disease activity, or early erosions. Short-term glucocorticoid treatment was recommended as part of the initial therapy.

For inclusion of patients from the ARCTIC trial and the NOR-VEAC study into the current analyses, we applied a set of common eligibility criteria: RA patients ages 18–75 years who fulfilled the 2010 ACR/EULAR classification criteria for RA (24), who were DMARD-naive, and who had started MTX monotherapy within 31 days of a study visit and had at least one follow-up visit (see Supplementary Figure 1, available on the *Arthritis & Rheumatology* web site at http://onlinelibrary.wiley.com/doi/10.1002/art.41232/abstract). Although the inclusion criteria for the NOR-VEAC study allowed for a maximum of 12 months since the first patient-reported swollen joint at the time of study enrollment, some patients were followed up for a period of time before initiating DMARD therapy. For inclusion into the current analyses, we allowed for a maximum of 13 months from the first patient-reported swollen joint to the time the first DMARD therapy was initiated.

Ethics approval. The ARCTIC trial and the NOR-VEAC study were approved by an independent ethics committee (the Regional Committee for Medical and Health Research Ethics South East; reference no. 2010/744 and reference no. 2010/719, respectively).

Standardization of study visits. The visits scheduled according to the study protocols were fairly similar in the 2 cohorts. However, the implemented study visits were more frequent in the ARCTIC trial than in the NOR-VEAC study. Further, visits in the NOR-VEAC study occurred with highly varying frequency, both within patients and between patients. In order to compare outcomes, we standardized the follow-up schedules by specifying certain time points of interest (3, 6, 12, and 24 months) and allowing the inclusion of observations within a time window of 2 months before or after the ideal visit date. For the 3-month time point only, we used observations within 1 month before or after the ideal time point. If a patient had >1 observation within the time window for a visit of interest, the observation closest to the ideal time point was selected for analyses.

Outcome assessments. The main outcomes were 1) achievement of the study-specific treatment targets, and 2) achievement of remission as defined by the ACR/EULAR Boolean criteria (14). Both outcome measures were assessed after 3, 6, 12, and 24 months.

Study-specific targets were defined as 1) DAS <1.6 (22,23) plus 0 swollen joints on a 44-joint count in the ARCTIC trial, and 2) DAS28 <2.6 (25) in the NOR-VEAC study. ACR/EULAR Boolean remission was defined as a score of ≤1 for the following: swollen joint count (SJC), tender joint count (TJC), C-reactive protein (CRP) level (mg/dl), and patient global assessment of disease (14). For the calculation of ACR/EULAR Boolean remission, we used a 28-joint count, which was calculated in both cohorts.

In additional analyses, we assessed disease activity during follow-up according to the CDAI, defining remission as CDAI ≤2.8, low disease activity as CDAI >2.8 and ≤10, moderate disease activity as CDAI >10 and ≤22, and high disease activity as CDAI >22 (29,30).

Statistical analysis. To balance the 2 cohorts on baseline covariates, we used inverse probability of treatment weights using the propensity scores (31). The propensity score is defined as the probability of being assigned to a specific group or treatment conditional on the observed covariates (32). The propensity scores were calculated by fitting a multivariable logistic regression model, including variables considered to be potential confounders in the estimation of the main outcome (see Supplementary Text, available on the *Arthritis & Rheumatology* web site at http://onlinelibrary.wiley.com/doi/10.1002/art.41232/abstract). Inverse probability of treatment weights using the propensity score assigns a weight to each subject based on the inverse propensity score and creates a weighted cohort (pseudo-population) in which observed confounders have been balanced between the 2 treatment groups (31). The weighted sample was used for further analyses of the outcome. We assessed the adequacy of the specification of the model by examining the degree of balancing of baseline covariates between the 2 cohorts, comparing means and prevalence, and comparing the distribution of continuous variables (31) (Table 1 and Supplementary Figures 2 and 3, available on the *Arthritis & Rheumatology* web site at http://onlinelibrary.wiley.com/doi/10.1002/art.41232/abstract).

We used descriptive statistics to evaluate the proportion of patients reaching the study-specific remission targets as well as the disease activity states according to the CDAI during follow-up. To compare achievement of the ACR/EULAR Boolean remission in longitudinal analyses, we combined baseline balancing using

Table 1. Baseline characteristics before and after propensity score weighting using inverse probability of treatment weights*

Characteristic	Observed cohorts		Propensity score–weighted cohorts		
	ARCTIC trial (n = 189)	NOR-VEAC study (n = 330)	ARCTIC trial (n = 183)	NOR-VEAC study (n = 277)	Standardized mean difference†
Age, years	51.1 ± 13.9	53.8 ± 13.7	52.5 ± 13.3	53.1 ±14.2	−0.046
Female, %	61.4	66.1	65.2	62.8	0.049
Anti-CCP positivity, %	82.0	75.5	78.9	79.1	−0.008
Rheumatoid factor positivity, %	71.4	63.3	66.8	67.4	−0.014
Time since first patient-reported swollen joint, months	5.5 ± 3.5	4.5 ± 2.8	4.8 ± 3.3	4.8 ± 3.0	−0.001
Presence of ≥1 comorbidity, %	52.9	51.8	52.8	54.9	−0.043
Body mass index, kg/m^2	25.5 ± 4.4	25.8 ± 4.5	25.6 ± 4.4	25.6 ± 4.3	0.008
Current smoker, %	21.7	24.2	23.1	22.1	0.023
University/college degree, %	41.8	49.7	49.8	49.8	0.001
Full-time employment, %	35.4	35.5	36.0	37.6	−0.034
CRP level, mg/liter	16.2 ± 22.3	19.5 ± 25.8	17.4 ± 23.9	18.0 ± 24.3	−0.025
ESR, mm Hg	25.2 ± 19.1	27.9 ± 20.5	26.6 ± 20.0	26.4 ± 19.6	0.012
SJC28	7.2 ± 5.6	6.3 ± 5.2	6.8 ± 5.5	6.8 ± 5.4	−0.003
TJC28	7.1 ± 5.0	6.7 ± 5.6	6.8 ± 5.0	6.9 ± 5.6	−0.025
Physician global assessment (0–100 mm VAS)	41.5 ± 20.6	41.1 ± 19.6	41.6 ± 21.1	41.8 ± 20.1	−0.008
Patient global assessment (0–100 mm VAS)	50.5 ± 23.8	49.4 ± 24.8	50.2 ± 24.4	49.7 ± 23.9	0.022
SDAI	25.2 ± 12.8	24.1 ± 13.3	24.5 ± 12.9	24.6 ± 13.7	−0.002
DAS28	4.8 ± 1.3	4.7 ± 1.3	4.8 ± 1.3	4.8 ± 1.3	−0.003
EQ-5D	0.51 ± 0.29	0.49 ± 0.31	0.49 ± 0.30	0.50 ± 0.30	−0.027
RAID	4.55 ± 2.09	4.52 ± 2.21	4.54 ± 2.15	4.49 ± 2.17	0.025

* Except where indicated otherwise, values are the mean ± SD. ARCTIC = Aiming for Remission in Rheumatoid Arthritis: a randomised trial examining the benefit of ultrasound in a Clinical Tight Control regimen; NOR-VEAC = Norwegian Very Early Arthritis Clinic; anti-CCP = anti–cyclic citrullinated peptide; CRP = C-reactive protein; ESR = erythrocyte sedimentation rate; SJC28 = swollen joint count in 28 joints; TJC28 = tender joint count in 28 joints; VAS = visual analog scale; SDAI = Simplified Disease Activity Index; DAS28 = Disease Activity Score in 28 joints; EQ-5D = EuroQol-5 dimensions; RAID = Rheumatoid Arthritis Impact of Disease.
† After propensity score weighting.

inverse probability of treatment weights with methods to account for imbalances in missing data between the 2 cohorts during follow-up. Missing data in the ARCTIC trial were almost exclusively a result of missing visits due to dropout. The dropout rate in the ARCTIC trial was 6.9% at 12 months and 10.6% at 24 months. Missing data in the NOR-VEAC study were a result of missing variables at existing visits, missing visits in patients with subsequent follow-up visits (i.e., intermittent missing visits), or missing visits due to dropout. The overall amount of missing outcome data in the NOR-VEAC study was 21.2% at 12 months and 35.6% at 24 months.

We applied a combination of methods to account for missing data, assuming a missing at random mechanism (33). First, we used multiple imputation by chained equations to impute missing variables at existing visits in the NOR-VEAC study (34,35). We used the full data set (n = 330) to impute the following covariates if missing: CRP, erythrocyte sedimentation rate (ESR), patient global assessment of disease, SJC28, and TJC28. Second, we used a strict censoring approach to account for intermittent missing visits by censoring each patient at the first missing visit as recommended by Robins et al (36). Finally, we used inverse probability of censoring weighting (IPCW) to account for missing data due to dropout in both studies (37). This method assigns weights to individuals with complete follow-up data corresponding to the inverse of their estimated probability of having complete data. The IPCW model was specified with regard to the probability of missing data due to study dropout and included the following covariates: cohort affiliation, age, sex, symptom duration, CRP, ESR, patient global assessment of disease, SJC28, and TJC28. The final outcome model was a logistic regression model combining the baseline balancing with inverse probability of treatment weights, with the IPCW accounting for missing data due to dropout.

RESULTS

Patients and baseline characteristics. A total of 189 patients from the ARCTIC trial and 330 patients from the NOR-VEAC study fulfilled the common eligibility criteria (see Supplementary Figure 1, available on the *Arthritis & Rheumatology* web site at http://onlinelibrary.wiley.com/doi/10.1002/art.41232/abstract). After balancing the cohorts using inverse probability of treatment weights, the distributions of baseline covariates were similar with standardized mean differences of <10%, which is considered negligible (Table 1) (31). Fifty-three patients (16.1%) included from the NOR-VEAC study and 6 patients (3.2%) included from the ARCTIC trial were missing ≥1 covariates for calculation of the propensity score at baseline, and these patients were excluded from comparative analyses using inverse probability

Table 2. Methotrexate dosage among patients receiving methotrexate monotherapy from baseline to 24 months in the ARCTIC trial and the NOR-VEAC study*

	ARCTIC trial	NOR-VEAC study	*P*
Baseline	16.0 ± 2.8	15.5 ± 2.8	0.05
3 months	20.7 ± 3.0	17.8 ± 4.0	<0.001
6 months	21.4 ± 3.7	18.4 ± 4.5	<0.001
12 months	21.3 ± 3.7	18.4 ± 4.6	<0.001
24 months	20.8 ± 4.3	18.0 ± 4.9	<0.001

* Values are the mean ± SD mg/week. ARCTIC = Aiming for Remission in Rheumatoid Arthritis: a randomised trial examining the benefit of ultrasound in a Clinical Tight Control regimen; NOR-VEAC = Norwegian Very Early Arthritis Clinic.

of treatment weights. No substantial differences in baseline characteristics or follow-up data were observed when comparing patients with complete data and those without complete data for calculation of the propensity score at baseline. The median classification score in patients who met the 2010 ACR/EULAR classification criteria for RA was similar in the 2 cohorts (median 7 [interquartile range 7–8] in ARCTIC and 7 [interquartile range 6–9] in NOR-VEAC; $P = 0.31$). Of the original 429 patients included in the NOR-VEAC study who were clinically diagnosed as having RA, 46 patients (10.7%) did not fulfill the 2010 ACR/EULAR classification criteria for RA and were excluded from the present study. Compared to patients who met the criteria, a significantly greater number of excluded patients were seronegative (43.5% versus 19.0%; $P < 0.001$), and mean disease activity was lower in both seropositive and seronegative patients (see Supplementary Table 3, available on the *Arthritis & Rheumatology* web site at http://onlinelibrary.wiley.com/doi/10.1002/art.41232/abstract).

Drug therapy and adverse events. Patients in both cohorts started MTX monotherapy, at a mean dosage of 16.0 mg/week in the ARCTIC trial and 15.5 mg/week in the NOR-VEAC study (Table 2). During follow-up, more patients in the NOR-VEAC study continued receiving the initial MTX monotherapy, while more patients in the ARCTIC trial switched to synthetic DMARD triple therapy (Figure 1). Therapy was escalated to a biologic DMARD regimen in a similar proportion of patients in the 2 cohorts (6.5% in the ARCTIC trial versus 6.0% in the NOR-VEAC study at 6 months, 17.1% versus 13.6% at 12 months, and 25.6% versus 25.4% at 24 months) (Figure 1).

During follow-up, mean dosages of MTX were higher in the ARCTIC trial than in the NOR-VEAC study (Table 2), which was mainly a result of the dosage of MTX being escalated to >20 mg/week in more patients in the ARCTIC trial (Figure 1). At baseline, more patients in the ARCTIC trial than in the NOR-VEAC study started co-medication with oral prednisolone (93.1% versus 56.7%; Table 3). At follow-up visits during the first year, more patients in the NOR-VEAC study were treated with prednisolone, while a similar proportion of patients in the 2 studies were treated with prednisolone at 24 months (Table 3). The mean ± SD dosage of prednisolone was higher in the ARCTIC trial than in the NOR-VEAC study at baseline (13.6 ± 3.4 mg versus 11.8 ± 4.3 mg; $P < 0.001$), but similar during follow-up.

In the ARCTIC trial, 529 treatment-emergent adverse events were observed compared to 379 in the NOR-VEAC study; however, a similar proportion of patients in the 2 cohorts switched treatment due to adverse events (see Supplementary Table 4, available on the *Arthritis & Rheumatology* web site at

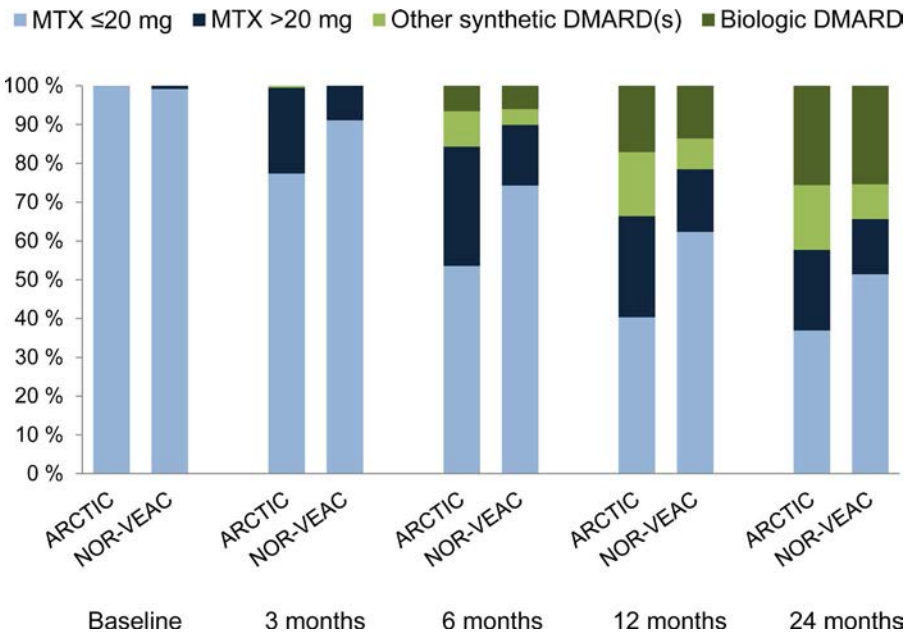

Figure 1. Percentage of patients receiving methotrexate (MTX) ≤20 mg/week, MTX >20 mg/week, other synthetic disease-modifying antirheumatic drugs (DMARDs), and biologic DMARDs at baseline and during follow-up in the Aiming for Remission in Rheumatoid Arthritis: a randomised trial examining the benefit of ultrasound in a Clinical Tight Control regimen (ARCTIC) trial versus the Norwegian Very Early Arthritis Clinic (NOR-VEAC) study.

Table 3. Co-medication with prednisolone from baseline to 24 months in the ARCTIC trial and the NOR-VEAC study*

	ARCTIC trial	NOR-VEAC study	*P*
Baseline	93.1	56.7	<0.001
3 months	17.4	38.2	<0.001
6 months	11.9	30.5	<0.001
12 months	12.9	25.4	0.001
24 months	11.8	13.2	0.7

* Values are the percent of patients. ARCTIC = Aiming for Remission in Rheumatoid Arthritis: a randomised trial examining the benefit of ultrasound in a Clinical Tight Control regimen; NOR-VEAC = Norwegian Very Early Arthritis Clinic.

http://onlinelibrary.wiley.com/doi/10.1002/art.41232/abstract). Of the 189 patients included in the ARCTIC trial, 5 patients experienced a serious adverse event, and of the 330 patients included in the NOR-VEAC study, 2 patients experienced a serious adverse event (Supplementary Table 4, http://onlinelibrary.wiley.com/doi/10.1002/art.41232/abstract).

Visit frequency during follow-up. The median number of follow-up visits in the ARCTIC trial corresponded to the 13 protocoled study visits over 2 years of follow-up. In the NOR-VEAC study, a median of 8 visits per patients was observed during 2 years of follow-up. The median time between visits during the first 12 months was 1.5 months (interquartile range 1.3–1.5) in the ARCTIC trial and 2.4 months (interquartile range 1.7–3.0) in the NOR-VEAC study. During the second year of follow-up, the median time between visits was 3.0 months (interquartile range 2.4–3.0) in the ARCTIC trial and 4.0 months (interquartile range 4.0–6.0) in the NOR-VEAC study.

Achievement of study-specific remission targets and ACR/EULAR Boolean remission. In the ARCTIC trial, the study-specific target of a DAS of <1.6 plus 0 swollen joints on a 44-joint count had been achieved in 37.4% of patients at 3 months, increasing to 53.5% of patients at 6 months, 69.8% of patients at 12 months, and 66.3% of patients at 24 months (Table 4). In the NOR-VEAC study, the less stringent target of DAS28 remission was achieved in 45.5% of patients at 3 months, 50.9% of patients at 6 months, 61.0% of patients at 12 months, and 65.1% of patients at 24 months (Table 4).

When comparing the observed achievement of ACR/EULAR Boolean remission in the 2 cohorts during follow-up, the remission rates were considerably higher in the ARCTIC trial (Table 4). Also, after balancing the 2 cohorts at baseline using propensity score weights and accounting for missing data with a combination of multiple imputation by chained equations and IPCW, the odds of reaching ACR/EULAR Boolean remission were significantly higher in the ARCTIC trial than in the NOR-VEAC study at 3, 12, and 24 months (Table 5).

At all follow-up visits, a majority of patients in both cohorts reached CDAI remission or low disease activity (see Supplementary Table 5, available on the *Arthritis & Rheumatology* web site at http://onlinelibrary.wiley.com/doi/10.1002/art.41232/abstract). Remission according to the CDAI was achieved in more patients in the ARCTIC trial than in the NOR-VEAC study (37.9% versus 26.0% at 3 months, and increasing to 62.5% versus 44.0% at 24 months), while more patients in the NOR-VEAC study than in the ARCTIC trial had moderate or high disease activity (28.6% versus 24.8% at 3 months, and decreasing to 16.4% versus 7.9% at 12 months and 16.6% versus 12.5% at 24 months).

DISCUSSION

In this study, we compared achievement of remission in 2 early RA cohorts, examining whether a tight control TTT strategy targeting DAS remission plus 0 swollen joints on a 44-joint count in an RCT setting (the ARCTIC trial) led to superior disease activity outcomes compared to a TTT approach targeting DAS28 remission in an observational setting (the NOR-VEAC study). We found

Table 4. Percentage of patients in whom study-specific remission targets and ACR/EULAR Boolean remission were achieved during the follow-up period

	Study-specific remission target*		ACR/EULAR Boolean remission†	
	ARCTIC trial (n = 189)	NOR-VEAC study (n = 330)	ARCTIC trial (n = 183)	NOR-VEAC study (n = 277)
3 months	37.4	45.5	28.0	19.4
6 months	53.5	50.9	32.4	25.7
12 months	69.8	61.0	45.4	30.1
24 months	66.3	65.1	51.5	34.7

* The study-specific remission targets were a Disease Activity Score of <1.6 and 0 swollen joints on a 44-joint count in the Aiming for Remission in Rheumatoid Arthritis: a randomised trial examining the benefit of ultrasound in a Clinical Tight Control regimen (ARCTIC) trial and a Disease Activity Score in 28 joints of <2.6 in the Norwegian Very Early Arthritis Clinic (NOR-VEAC) study.
† American College of Rheumatology/European League Against Rheumatism (ACR/EULAR) Boolean remission was assessed in patients with recorded data for calculation of propensity scores at baseline and was defined as a C-reactive protein level of ≤1 mg/dl, a swollen joint count in 28 joints of ≤1, a tender joint count in 28 joints of ≤1, and patient global assessment of ≤1 on a 0–10 scale.

Table 5. Odds of achieving ACR/EULAR Boolean remission in the ARCTIC trial versus the NOR-VEAC observational study during follow-up*

Study visit	OR (95% CI)†	*P*‡
3 months	1.73 (1.03–2.89)	0.04
6 months	1.44 (0.88–2.38)	0.15
12 months	1.97 (1.21–3.20)	0.01
24 months	1.82 (1.05–3.16)	0.03

* The 2 cohorts were balanced on baseline covariates using inverse probability of treatment weights using the propensity score. Multiple imputation by chained equations was used to impute missing variables at existing visits in the Norwegian Very Early Arthritis Clinic (NOR-VEAC) study. ARCTIC = Aiming for Remission in Rheumatoid Arthritis: a randomised trial examining the benefit of ultrasound in a Clinical Tight Control regimen; OR = odds ratio; 95% CI = 95% confidence interval.
† American College of Rheumatology/European League Against Rheumatism (ACR/EULAR) Boolean remission was assessed in patients with recorded data for calculation of propensity scores at baseline and was defined as a C-reactive protein level of ≤1 mg/dl, a swollen joint count in 28 joints of ≤1, a tender joint count in 28 joints of ≤1, and patient global assessment of ≤1 on a 0–10 scale.
‡ *P* values were obtained using logistic regression with inverse probability of censoring weights to account for imbalanced missing data.

that more than half of the patients in each cohort had reached the study-specific remission targets at 6 months, and this number increased to more than 60% in each cohort at 12 and 24 months. However, ACR/EULAR Boolean remission was achieved in significantly more patients in the ARCTIC trial than in the NOR-VEAC study at 12 and 24 months, suggesting that tight control and targeting a more stringent definition of remission improves the disease activity outcomes of a TTT strategy.

The results demonstrate that a TTT approach is feasible in clinical practice and may lead to achievement of remission in a majority of patients. The proportion of patients reaching the treatment target of DAS28 remission in the NOR-VEAC observational study was similar to achievement of DAS28 remission in the Dutch Rheumatoid Arthritis Monitoring (DREAM) remission induction cohort (38). Further, achievement of remission according to both the DAS28 and ACR/EULAR Boolean criteria in the NOR-VEAC study during follow-up was more prevalent than previously described in conventional care cohorts (12,39,40). In both the ARCTIC trial and NOR-VEAC study, >80% of patients had reached remission or low disease activity according to the CDAI at 12 and 24 months, confirming the successful results of applying a TTT strategy in both an RCT setting and in clinical practice.

Different factors may explain why ACR/EULAR Boolean remission was achieved in more patients in the ARCTIC trial than in the NOR-VEAC study during follow-up. Therapy was escalated by increasing the dosage of MTX or by switching to synthetic DMARD triple therapy in more patients in the ARCTIC trial than in the NOR-VEAC study, which may have contributed to a lower degree of inflammation (41). Targeting a more stringent definition of remission in the ARCTIC trial is likely to have influenced therapy decisions during follow-up, leading to more therapy escalations. Furthermore, using a 44-joint count in the ARCTIC trial may have detected disease activity in joints not included in the DAS28 score used in the NOR-VEAC study (42), leading to better overall disease control in the ARCTIC trial. Another explanation may be that more frequent study visits in the ARCTIC trial led to earlier therapy escalations as a result of tight monitoring of disease activity, contributing to earlier disease control in the ARCTIC trial than in the NOR-VEAC study. Previous studies have suggested that the level of disease activity improvement during the first few months of therapy predicts subsequent disease activity levels (43–45). More frequent study visits in the ARCTIC trial may also have positively influenced patients' adherence to drug therapy by providing more opportunities for dialog between patient and provider about side effects, disease activity level, and the importance of reaching the desired target (46).

Considerably more treatment-emergent adverse events were recorded in the ARCTIC trial compared to the NOR-VEAC study, including more serious adverse events. This could suggest that the more aggressive treatment strategy leading to favorable disease activity outcomes in the ARCTIC trial also may increase the risk of harm to the patients. However, it is likely that frequent visits and close monitoring in the ARCTIC trial led to better recording of adverse events than in the NOR-VEAC study, which makes clear-cut conclusions challenging.

Limited data exist on comparing the outcomes of aiming for different definitions of remission in a TTT strategy. One previous study assessed 5-year outcomes when aiming for DAS remission compared to DAS low disease activity in 2 different early RA RCT cohorts (47). Targeting remission or targeting low disease activity led to similar functional and radiographic outcomes over time. However, similar to the present study, remission was achieved in a higher proportion of patients in the cohort aiming for the more stringent target (DAS remission). Another study compared routine care with TTT strategies aiming for either DAS28 remission or a target of no swollen joints in patients with established RA (19). The investigators found no significant differences in disease activity outcomes between the 2 TTT strategies during 18 months of follow-up.

Strengths of this study include the ability to compare patients across 2 Norwegian cohorts of DMARD-naive patients with early RA followed up during similar periods of time (2010–2013 and 2010–2016). The treatment algorithm in the ARCTIC trial was similar to the EULAR recommendations (26,27) that guided therapy in the NOR-VEAC study, enabling comparison of outcomes of TTT strategies with different targets and disease-monitoring approaches.

Methodologic challenges arising from the comparison of outcomes in patients from 2 different cohorts were addressed by applying common eligibility criteria and using propensity score weighting on baseline covariates, which enabled comparison of different strategies in similar patients. Further, we used a combi-

nation of methods to adjust for differences in follow-up patterns, with more frequent visits in the ARCTIC trial and more missing data in the NOR-VEAC study. The present study highlights the challenges of analyzing observational data, but also demonstrates how state-of-the-art statistical methods, considering subtle forms of selection bias, facilitate comparison of RCT data with observational data.

The main limitation of this study was comparing outcomes of treatment strategies in 2 different cohorts with different study designs, which presented a risk for biased estimates. In the ARCTIC trial, patients and rheumatologists agreed to adhere to the treatment plan and visits specified in the protocol. During the conduct of the study, investigators entered clinical and ultrasound assessments into a data program that provided a recommendation of whether or not to escalate therapy (20). This is likely to have positively influenced adherence to the TTT strategy (48,49). In the NOR-VEAC study, current EULAR recommendations guided therapy decisions, which might have given the individual preferences of patients and provider, as well as available time and resources at the study centers, a larger influence over treatment decisions and follow-up (48,49). If commitment to the TTT strategy by patients and rheumatologists was better in the ARCTIC trial than in the NOR-VEAC study, this may in part explain the favorable disease activity outcomes in the ARCTIC trial.

Another limitation of the present study was that the eligibility criteria applied may limit the generalizability of results to a broader population. In both the ARCTIC trial and the NOR-VEAC study, inclusion was restricted to patients age 18–75 years. Excluding older patients may have led to less comorbidity, fewer adverse events, and better treatment response (50). Furthermore, patients in the NOR-VEAC study who were excluded from the present study due to not fulfilling the 2010 ACR/EULAR classification criteria for RA had lower disease activity than patients who fulfilled the criteria, and more were seronegative. These patients, likely to be observed in clinical practice, may have required less intensive therapy to reach the treatment target.

Finally, comparison of radiographic data may have contributed to a more clear-cut clinical conclusion and the lack of such data in the NOR-VEAC study represented another limitation of this study.

In conclusion, we found that TTT implemented in an observational cohort resulted in high remission rates according to the study-specific target, similar to a TTT clinical trial. This confirms that TTT is feasible in clinical practice and should encourage wider implementation of TTT principles. However, significantly more patients in the ARCTIC trial reached ACR/EULAR Boolean remission during follow-up, indicating that targeting a more stringent definition of remission and implementing more frequent visits provide further potential for favorable outcomes of a TTT strategy. Both the ARCTIC trial and the NOR-VEAC study employed protocols for TTT, demonstrating the value of algorithms to improve rheumatologic care.

ACKNOWLEDGMENTS

The authors would like to thank the patients for their participation and the local rheumatology staffs at all participating centers of the ARCTIC trial and the NOR-VEAC study for data collection.

AUTHOR CONTRIBUTIONS

All authors were involved in drafting the article or revising it critically for important intellectual contact, and all authors approved the final version to be published. Dr. Norvang had full access to all of the data in the study and takes responsibility for the integrity of the data and the accuracy of the data analysis.

Study conception and design. Norvang, Brinkmann, Yoshida, Lillegraven, Aga, Sexton, Tedeschi, Uhlig, Kvien, Mjaavatten, Solomon, Haavardsholm.

Acquisition of data. Brinkmann, Aga, Norli, Uhlig, Mjaavatten, Haavardsholm.

Analysis and interpretation of data. Norvang, Yoshida, Lillegraven, Aga, Sexton, Tedeschi, Lyo, Uhlig, Kvien, Mjaavatten, Solomon, Haavardsholm.

REFERENCES

1. Smolen JS, Breedveld FC, Burmester GR, Bykerk V, Dougados M, Emery P, et al. Treating rheumatoid arthritis to target: 2014 update of the recommendations of an international task force. Ann Rheum Dis 2016;75:3–15.
2. Burmester GR, Pope JE. Novel treatment strategies in rheumatoid arthritis. Lancet 2017;389:2338–48.
3. Stoffer MA, Schoels MM, Smolen JS, Aletaha D, Breedveld FC, Burmester G, et al. Evidence for treating rheumatoid arthritis to target: results of a systematic literature search update [review]. Ann Rheum Dis 2016;75:16–22.
4. Schoels M, Knevel R, Aletaha D, Bijlsma JW, Breedveld FC, Boumpas DT, et al. Evidence for treating rheumatoid arthritis to target: results of a systematic literature search. Ann Rheum Dis 2010;69:638–43.
5. Singh JA, Saag KG, Bridges SL Jr, Akl EA, Bannuru RR, Sullivan MC, et al. 2015 American College of Rheumatology guideline for the treatment of rheumatoid arthritis. Arthritis Rheumatol 2016;68:1–26.
6. Smolen JS, Landewe R, Bijlsma J, Burmester G, Chatzidionysiou K, Dougados M, et al. EULAR recommendations for the management of rheumatoid arthritis with synthetic and biological disease-modifying antirheumatic drugs: 2016 update. Ann Rheum Dis 2017;76:960–77.
7. Sepriano A, Ramiro S, FitzGerald O, Østergaard M, Homik J, van der Heijde D, et al. Adherence to treat-to-target management in rheumatoid arthritis and associated factors: data from the international RA BIODAM cohort. J Rheumatol 2019. https://doi.org/10.3899/jrheum.190303. E-pub ahead of print.
8. Tymms K, Zochling J, Scott J, Bird P, Burnet S, de Jager J, et al. Barriers to optimal disease control for rheumatoid arthritis patients with moderate and high disease activity. Arthritis Care Res (Hoboken) 2014;66:190–6.
9. Zak A, Corrigan C, Yu Z, Bitton A, Fraenkel L, Harrold L, et al. Barriers to treatment adjustment within a treat to target strategy in rheumatoid arthritis: a secondary analysis of the TRACTION trial. Rheumatology (Oxford) 2018;57:1933–7.
10. Reed GW, Collier DH, Koenig AS, Saunders KC, Pappas DA, Litman HJ, et al. Clinical and demographic factors associated with change and maintenance of disease severity in a large registry of patients with rheumatoid arthritis. Arthritis Res Ther 2017;19:81.
11. Yun H, Chen L, Xie F, Patel H, Boytsov N, Zhang X, et al. Do patients with moderate or high disease activity escalate RA therapy accord-

ing to treat-to-target principles? Results from the Rheumatology Informatics System for Effectiveness Registry of the American College of Rheumatology. Arthritis Care Res (Hoboken) 2020;72:166–75.

12. Einarsson JT, Willim M, Ernestam S, Saxne T, Geborek P, Kapetanovic MC. Prevalence of sustained remission in rheumatoid arthritis: impact of criteria sets and disease duration, a nationwide study in Sweden. Rheumatology (Oxford) 2019;58:227–36.
13. Klarenbeek NB, Koevoets R, van der Heijde DM, Gerards AH, Ten Wolde S, Kerstens PJ, et al. Association with joint damage and physical functioning of nine composite indices and the 2011 ACR/EULAR remission criteria in rheumatoid arthritis. Ann Rheum Dis 2011;70:1815–21.
14. Felson DT, Smolen JS, Wells G, Zhang B, van Tuyl LH, Funovits J, et al. American College of Rheumatology/European League Against Rheumatism provisional definition of remission in rheumatoid arthritis for clinical trials. Arthritis Rheum 2011;63:573–86.
15. Sakellariou G, Scirè CA, Verstappen SM, Montecucco C, Caporali R. In patients with early rheumatoid arthritis, the new ACR/EULAR definition of remission identifies patients with persistent absence of functional disability and suppression of ultrasonographic synovitis. Ann Rheum Dis 2013;72:245–9.
16. Ruyssen-Witrand A, Guernec G, Nigon D, Tobon G, Jamard B, Rat AC, et al. Aiming for SDAI remission versus low disease activity at 1 year after inclusion in ESPOIR cohort is associated with better 3-year structural outcomes. Ann Rheum Dis 2015;74:1676–83.
17. Smolen JS, Han C, van der Heijde DM, Emery P, Bathon JM, Keystone E, et al. Radiographic changes in rheumatoid arthritis patients attaining different disease activity states with methotrexate monotherapy and infliximab plus methotrexate: the impacts of remission and tumour necrosis factor blockade. Ann Rheum Dis 2009;68:823–7.
18. Combe B, Logeart I, Belkacemi MC, Dadoun S, Schaeverbeke T, Daurès JP, et al. Comparison of the long-term outcome for patients with rheumatoid arthritis with persistent moderate disease activity or disease remission during the first year after diagnosis: data from the ESPOIR cohort. Ann Rheum Dis 2015;74:724–9.
19. Pope JE, Haraoui B, Rampakakis E, Psaradellis E, Thorne C, Sampalis JS. Treating to a target in established active rheumatoid arthritis patients receiving a tumor necrosis factor inhibitor: results from a real-world cluster-randomized adalimumab trial. Arthritis Care Res (Hoboken) 2013;65:1401–9.
20. Haavardsholm EA, Aga AB, Olsen IC, Lillegraven S, Hammer HB, Uhlig T, et al. Ultrasound in management of rheumatoid arthritis: ARCTIC randomised controlled strategy trial. BMJ 2016;354:i4205.
21. Brinkmann GH, Norvang V, Norli ES, Grøvle L, Haugen AJ, Lexberg AS, et al. Treat to target strategy in early rheumatoid arthritis versus routine care: a comparative clinical practice study. Semin Arthritis Rheum 2019;48:808–14.
22. Van der Heijde DM, van 't Hof M, van Riel PL, van de Putte LB. Development of a disease activity score based on judgment in clinical practice by rheumatologists. J Rheumatol 1993;20:579–81.
23. Van Riel PL, van Gestel AM. Clinical outcome measures in rheumatoid arthritis. Ann Rheum Dis 2000;59 Suppl 1:i28–31.
24. Aletaha D, Neogi T, Silman AJ, Funovits J, Felson DT, Bingham CO III, et al. 2010 rheumatoid arthritis classification criteria: an American College of Rheumatology/European League Against Rheumatism collaborative initiative. Arthritis Rheum 2010;62:2569–81.
25. Prevoo ML, van 't Hof MA, Kuper HH, van Leeuwen MA, van de Putte LB, van Riel PL. Modified disease activity scores that include twenty-eight–joint counts: development and validation in a prospective longitudinal study of patients with rheumatoid arthritis. Arthritis Rheum 1995;38:44–8.
26. Smolen JS, Landewé R, Breedveld FC, Dougados M, Emery P, Gaujoux-Viala C, et al. EULAR recommendations for the management of rheumatoid arthritis with synthetic and biological disease-modifying antirheumatic drugs. Ann Rheum Dis 2010;69:964–75.
27. Smolen JS, Landewé R, Breedveld FC, Buch M, Burmester G, Dougados M, et al. EULAR recommendations for the management of rheumatoid arthritis with synthetic and biological disease-modifying antirheumatic drugs: 2013 update. Ann Rheum Dis 2014;73:492–509.
28. Smolen JS, Aletaha D, Bijlsma JW, Breedveld FC, Boumpas D, Burmester G, et al. Treating rheumatoid arthritis to target: recommendations of an international task force. Ann Rheum Dis 2010;69:631–7.
29. Aletaha D, Nell VP, Stamm T, Uffmann M, Pflugbeil S, Machold K, et al. Acute phase reactants add little to composite disease activity indices for rheumatoid arthritis: validation of a clinical activity score. Arthritis Res Ther 2005;7:R796–806.
30. Aletaha D, Ward MM, Machold KP, Nell VP, Stamm T, Smolen JS. Remission and active disease in rheumatoid arthritis: defining criteria for disease activity states. Arthritis Rheum 2005;52:2625–36.
31. Austin PC, Stuart EA. Moving towards best practice when using inverse probability of treatment weighting (IPTW) using the propensity score to estimate causal treatment effects in observational studies. Stat Med 2015;34:3661–79.
32. Rosenbaum PR, Rubin DB. The central role of propensity score in observational studies for causal effects. Biometrika 1983;70:41–55.
33. Rubin DB. Inference and missing data. Biometrika 1976;63:581–92.
34. White IR, Royston P, Wood AM. Multiple imputation using chained equations: issues and guidance for practice. Stat Med 2011;30:377–99.
35. Van Buuren S. Multiple imputation of discrete and continuous data by fully conditional specification. Stat Methods Med Res 2007;16:219–42.
36. Robins JM, Rotnitzky A, Zhao LP. Analyses of semiparametric regression models for repeated outcomes in the presence of missing data. J Am Stat Assoc 1995;90:106–21.
37. Seaman SR, White IR. Review of inverse probability weighting for dealing with missing data. Stat Methods Med Res 2013;22:278–95.
38. Vermeer M, Kuper HH, Moens HJ, Drossaers-Bakker KW, van der Bijl AE, van Riel PL, et al. Sustained beneficial effects of a protocolized treat-to-target strategy in very early rheumatoid arthritis: three-year results of the Dutch Rheumatoid Arthritis Monitoring remission induction cohort. Arthritis Care Res (Hoboken) 2013;65:1219–26.
39. Britsemmer K, van Schaardenburg D, Boers M, de Cock D, Verschueren P, Radner H, et al. Prevalence and validity of ACR/EULAR remission in four European early rheumatoid arthritis cohorts. Clin Exp Rheumatol 2018;36:362–70.
40. Conigliaro P, Chimenti MS, Triggianese P, Ballanti E, Sunzini F, Duca I, et al. Remission and low disease activity in a cohort of real-life patients with rheumatoid arthritis treated with first-line antitumour necrosis factor. J Int Med Res 2016;44:90–4.
41. Visser K, van der Heijde D. Optimal dosage and route of administration of methotrexate in rheumatoid arthritis: a systematic review of the literature. Ann Rheum Dis 2009;68:1094–9.
42. Landewé R, van der Heijde D, van der Linden S, Boers M. Twenty-eight-joint counts invalidate the DAS28 remission definition owing to the omission of the lower extremity joints: a comparison with the original DAS remission. Ann Rheum Dis 2006;65:637–41.
43. Aletaha D, Funovits J, Keystone EC, Smolen JS. Disease activity early in the course of treatment predicts response to therapy after one year in rheumatoid arthritis patients. Arthritis Rheum 2007;56:3226–35.

44. Schipper LG, Fransen J, den Broeder AA, van Riel PL. Time to achieve remission determines time to be in remission. Arthritis Res Ther 2010;12:R97.
45. Kuriya B, Xiong J, Boire G, Haraoui B, Hitchon C, Pope J, et al. Earlier time to remission predicts sustained clinical remission in early rheumatoid arthritis: results from the Canadian Early Arthritis Cohort (CATCH). J Rheumatol 2014;41:2161–6.
46. Hope HF, Hyrich KL, Anderson J, Bluett J, Sergeant JC, Barton A, et al. The predictors of and reasons for non-adherence in an observational cohort of patients with rheumatoid arthritis commencing methotrexate. Rheumatology (Oxford) 2020;59:213–23.
47. Akdemir G, Markusse IM, Bergstra SA, Goekoop RJ, Molenaar ET, van Groenendael J, et al. Comparison between low disease activity or DAS remission as treatment target in patients with early active rheumatoid arthritis. RMD Open 2018;4:e000649.
48. Weiss NS. Generalizing from the results of randomized studies of treatment: can non-randomized studies be of help? Eur J Epidemiol 2019;34:715–8.
49. Beaulieu-Jones BK, Finlayson SG, Yuan W, Altman RB, Kohane IS, Prasad V, et al. Examining the use of real-world evidence in the regulatory process. Clin Pharmacol Ther 2020;107:843–52.
50. Soubrier M, Tatar Z, Couderc M, Mathieu S, Dubost JJ. Rheumatoid arthritis in the elderly in the era of tight control. Drugs Aging 2013;30:863–9.

APPENDIX A: THE ARCTIC TRIAL GROUP AND THE NOR-VEAC STUDY GROUP INVESTIGATORS

The ARCTIC trial group investigators are as follows: Hallvard Fremstad, Tor Magne Madland, Åse Stavland Lexberg, Hilde Haukeland, Erik Rødevand, Christian Høili, Hilde Stray, Anne Noraas Bendvold, Inger Johanne Widding-Hansen, Gunnstein Bakland.

The NOR-VEAC study group investigators are as follows: Åse Stavland Lexberg, Cathrine Thunem, Inger Johanne Widding-Hansen, Heidi Kverneggen Øvreås.

American College of Rheumatology
Empowering Rheumatology Professionals

Arthritis & Rheumatology
Vol. 72, No. 7, July 2020, pp 1082–1090
DOI 10.1002/art.41240

Physician Prescribing Patterns and Risk of Future Long-Term Opioid Use Among Patients With Rheumatoid Arthritis: A Prospective Observational Cohort Study

Yvonne C. Lee,[1] Bing Lu,[2] Hongshu Guan,[2] Jeffrey D. Greenberg,[3] Joel Kremer,[4] and Daniel H. Solomon[2]

Objective. To identify the extent to which opioid prescribing rates for patients with rheumatoid arthritis (RA) vary in the US and to determine the implications of baseline opioid prescribing rates on the probability of future long-term opioid use.

Methods. We identified patients with RA from physicians who contributed ≥10 patients within the first 12 months of participation in the Corrona RA Registry. The baseline opioid prescribing rate was calculated by dividing the number of patients with RA reporting opioid use during the first 12 months by the number of patients with RA providing data that year. To estimate odds ratios (ORs) for long-term opioid use, we used generalized linear mixed models.

Results. During the follow-up period, long-term opioid use was reported by 7.0% (163 of 2,322) of patients of physicians with a very low rate of opioid prescribing (referent) compared to 6.8% (153 of 2,254) of patients of physicians with a low prescribing rate, 12.5% (294 of 2,352) of patients of physicians with a moderate prescribing rate, and 12.7% (307 of 2,409) of patients of physicians with a high prescribing rate. The OR for long-term opioid use after the baseline period was 1.16 (95% confidence interval [95% CI] 0.79–1.70) for patients of low-intensity prescribing physicians, 1.89 (95% CI 1.27–2.82) for patients of moderate-intensity prescribing physicians, and 2.01 (95% CI 1.43–2.83) for patients of high-intensity prescribing physicians, compared to very low-intensity prescribing physicians.

Conclusion. Rates of opioid prescriptions vary widely. Our findings indicate that baseline opioid prescribing rates are a strong predictor of whether a patient will become a long-term opioid user in the future, after controlling for patient characteristics.

INTRODUCTION

Pain is the most common presenting complaint in primary care and rheumatology practices (1,2). Even with the availability of many targeted treatments in rheumatic diseases, most patients experience persistent pain (3,4). While analgesics such as acetaminophen and nonsteroidal antiinflammatory drugs provide relief for many patients with chronic pain, they cause a wide range of side effects (5–7). Thus, opioids present an important option for short-term pain relief. However, controversy exists regarding the appropriateness of opioids for long-term, noncancer pain, and there is a notable lack of data on the use of opioids in specific patient subgroups.

To our knowledge, the only published recommendations for the long-term use of opioids in patients with inflammatory arthritis was put forth by the 3e (Evidence, Expertise, Exchange)

The Corrona Rheumatoid Arthritis registry has been supported by AbbVie, Amgen, AstraZeneca, Bristol-Myers Squibb, Crescendo, Eli Lilly, Genentech, GlaxoSmithKline, Horizon Pharma, Janssen, Momenta Pharmaceuticals, Novartis, Pfizer, Roche, and UCB through contracted subscriptions. Dr. Lee's work was supported by the NIH (grant P30-AR-072579), and Mr. Guan and Dr. Solomon's work was supported by the NIH (grant P30-AR-072577), both from the National Institute of Arthritis and Musculoskeletal and Skin Diseases.

[1]Yvonne C. Lee, MD, MMSc: Northwestern University Feinberg School of Medicine, Chicago, Illinois, and Brigham and Women's Hospital, Boston, Massachusetts; [2]Bing Lu, MD, DrPH, Hongshu Guan, MS, Daniel H. Solomon, MD, MPH: Brigham and Women's Hospital, Boston, Massachusetts; [3]Jeffrey D. Greenberg, MD: Corrona, LLC, Waltham, Massachusetts, and New York University, New York, New York; [4]Joel Kremer, MD: Corrona, LLC, Waltham, Massachusetts, and Albany Medical College, Albany, New York.

Dr. Lee has received consulting fees, speaking fees, and/or honoraria from Eli Lilly (less than $10,000 each) and research support from Pfizer, and owns stock or stock options in Cigna. Dr. Greenberg has received consulting fees from Genentech, Janssen, Novartis, Pfizer, and Eli Lilly (less than $10,000 each) and owns stock or stock options in Corrona, LLC. Dr. Kremer has received consulting fees, speaking fees, and/or honoraria from AbbVie, Gilead, Eli Lilly, and Pfizer (less than $10,000 each), research support from AbbVie, Eli Lilly, Novartis, and Pfizer, and owns stock or stock options in Corrona, LLC. Dr. Solomon has received consulting fees, speaking fees, and/or honoraria from AbbVie, Amgen, Genentech, Janssen, and Pfizer (less than $10,000 each). No other disclosures relevant to this article were reported.

Address correspondence to Yvonne C. Lee, MD, MMSc, Division of Rheumatology, 633 North St. Clair Street, 18-093, Chicago, IL 60611. E-mail: yvonne.lee@northwestern.edu.

Submitted for publication June 11, 2019; accepted in revised form February 20, 2020.

Initiative (8). The 3e Initiative could not find any studies supporting the efficacy of long-term opioid use in patients with inflammatory arthritis at a population level, but they acknowledged that there was some mechanism-based rationale for prolonged use of opioids. Ultimately, they concluded that long-term opioid use may be considered in certain individuals, though caution was strongly advised.

Despite the concern surrounding long-term opioid use, data demonstrate that between 4% and 40% of patients with RA use opioids persistently (9–13). This practice appears to be associated with patient-related characteristics, particularly comorbidities (e.g., back pain, fibromyalgia, depression, and anxiety) and measures of RA severity (e.g., pain intensity, high inflammatory disease activity, and disability) (10,11). In addition, studies from other settings suggest that factors not related to patient characteristics may also correlate with the long-term use of opioids. For example, one study found that the prescribing rate of emergency physicians was significantly associated with rates of long-term opioid use among patients who had not previously received opioids (14). In light of this literature, we examined the potential role of a physician's previous opioid prescribing practices in future long-term prescribing for RA, testing the hypothesis that a clinician's baseline opioid prescribing rate predicts future long-term opioid use by his or her patients, independent of patient factors.

PATIENTS AND METHODS

Study cohort. We examined data from the Corrona RA Registry. Since 2001, Corrona has enrolled >42,000 individuals with RA through 650 academic and community rheumatologists across 40 states in the US (15). The analyses in the present study included data from registry inception in 2001 through December 31, 2016. Patients and rheumatologists provided data at the time of routine clinical visits, as often as once every 3 months. For the analyses described in this article, physicians were included if they contributed ≥10 patients with RA within the first 12 months of participation in the registry. The rationale for this inclusion criterion was that 1) ≥10 patients were required to provide a stable estimate of each physician's opioid prescribing rate (defined as <10% change if 1 patient were switched from being prescribed an opioid to not being prescribed an opioid), and 2) 12 months optimized the balance between having enough time to enroll patients to allow accurate calculation of baseline opioid prescribing rates, while also maximizing the number of patients and follow-up time for prediction analyses. Patients of these physicians were included if they had: 1) RA diagnosed by a physician, 2) ≥12 months of follow-up, 3) no cancer diagnosis at study entry, 4) no prevalent opioid use at study entry, and 5) no missing data on opioid use. All subjects provided written informed consent, and the study protocol was approved by the appropriate institutional review boards.

Study design. Data from Corrona were divided into a baseline period and a follow-up period (Figure 1). The baseline period included data from patients enrolled within the first 12 months of physician enrollment in the Corrona RA Registry. These data were used to calculate each physician's baseline opioid prescribing rate. The follow-up period included data from patients enrolled after the first 12 months of physician enrollment in Corrona and was used to examine associations between opioid prescribing rates and subsequent development of long-term opioid use. Patients included in the follow-up period were distinct from those included in the baseline period.

Exposure. The exposure of interest was each physician's opioid prescribing rate during the baseline period. To determine the baseline opioid prescribing rate, we used data on opioid use from questionnaires completed by patients at routine clinical visits, as previously described (10). For each physician, we calculated the

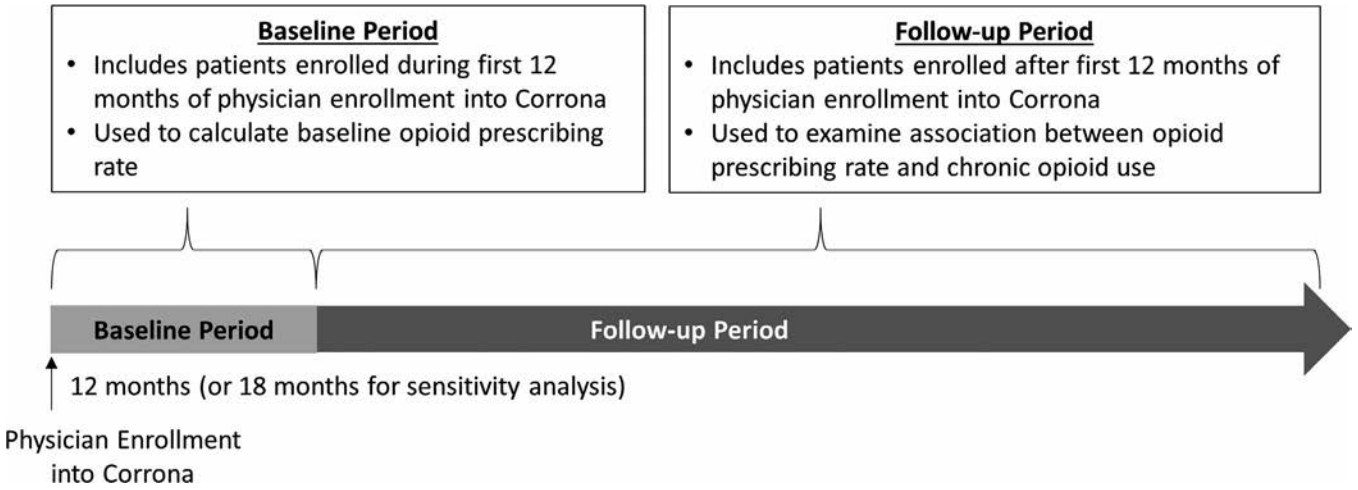

Figure 1. Study design. Data from the Corrona Rheumatoid Arthritis Registry were divided into a baseline period, from which opioid prescribing rates were calculated, and a follow-up period, which was used to examine the association between opioid prescribing rate and long-term opioid use.

proportion of their patients with RA who reported opioid use during the baseline period. In other words, the number of their patients with RA reporting opioid use during the baseline period was divided by the total number of patients with RA providing data during the same period. We then grouped physicians into quartiles of baseline opioid prescribing rates. Physicians in the lowest quartile were designated as the referent group. Physicians in the upper three quartiles were classified as low-, moderate-, or high-intensity prescribers.

Outcome measures. The primary outcome measure was long-term opioid use during the follow-up period. Long-term opioid use was defined as any opioid use reported during ≥2 consecutive study visits. We chose this definition because the median time between follow-up visits was 156 days (interquartile range [IQR] 113–209 days), and previous studies have used intervals from 90 to 180 days as the threshold for long-term opioid use (14,16–18).

Practice-level and physician-level covariates. Data on geographic region and practice setting (e.g., urban/rural status) were collected at the time each physician joined the Corrona RA Registry. Data on physician characteristics (e.g., sex, academic/private affiliation) were also collected at the time of physician study entry.

Patient covariates. Demographic information (e.g., age, sex, and race or ethnic group), insurance status, and RA disease duration were collected at the time of study enrollment. RA disease activity was assessed using the Clinical Disease Activity Index (CDAI), which is a composite measure including tender and swollen joint counts, patient global assessment of arthritis activity, and physician global assessment of disease activity (19). The Health Assessment Questionnaire (HAQ) was used to measure disability (20,21). Patients rated their pain intensity on a scale of 0–100 in response to the question, "How much pain have you had because of your arthritis in the past week?" Data on disease-modifying antirheumatic drug (DMARD) and glucocorticoid use were obtained from physicians. Data on antidepressant use were obtained from patient self-report.

Statistical analysis. Descriptive statistics (mean ± SD, median and IQR, and number and frequency) were calculated. To handle missing data on CDAI, HAQ, pain intensity, and insurance status for individuals <65 years old, a multiple imputation procedure that creates multiple imputed data sets for incomplete multivariate data was used. For insurance categories for individuals ≥65 years old, missing data were set to "Medicare." For medication data, we set all missing data to 0 (e.g., not taking that particular medication). Missing data on categorical practice-level and physician-level characteristics (e.g., practice setting, sex, and academic affiliation) were included in the analyses as their own separate category.

To estimate odds ratios (ORs) and 95% confidence intervals (95% CIs) between baseline opioid prescribing rate and long-term opioid use, we constructed unadjusted and multivariable adjusted generalized linear mixed models for binary outcomes adjusting for potential confounding factors and

Table 1. Baseline characteristics of the RA patients in the overall cohort and stratified by baseline physician opioid prescribing rate*

Characteristic	Overall cohort (n = 9,337)	Referent (n = 2,322)	Low (n = 2,254)	Moderate (n = 2,352)	High (n = 2,409)
Age, years	57.3 ± 13.5	57.2 ± 13.8	57.9 ± 13.6	57.3 ± 13.2	56.7 ± 13.6
Female, no. (%)	7,023 (75)	1,791 (77)	1,696 (75)	1,720 (73)	1,816 (75)
Race, no. (%)					
White	7,769 (83)	1,828 (79)	1,835 (81)	2,031 (86)	2,075 (86)
Hispanic	672 (7)	163 (7)	217 (10)	147 (6)	145 (6)
African American	563 (6)	230 (10)	103 (5)	116 (5)	114 (5)
Asian	178 (2)	61 (3)	63 (3)	16 (1)	38 (2)
Other	155 (2)	40 (2)	36 (2)	42 (2)	37 (2)
Insurance, no. (%)					
Private	6,069 (65)	1,554 (67)	1,370 (61)	1,529 (65)	1,616 (67)
Medicare	2,523 (27)	616 (27)	661 (29)	632 (27)	614 (25)
Medicaid	299 (3)	45 (2)	87 (4)	79 (3)	88 (4)
Both Medicaid and Medicare	176 (2)	46 (2)	43 (2)	47 (2)	40 (2)
None	270 (3)	61 (3)	93 (4)	65 (3)	51 (2)
RA duration, years	7.6 ± 9.0	8.1 ± 8.9	7.4 ± 9.1	7.8 ± 9.2	7.0 ± 8.9
CDAI	12.3 ± 11.9	10.4 ± 10.6	11.6 ± 11.3	14.1 ± 13.4	13.2 ± 11.6
HAQ DI	0.3 ± 0.4	0.3 ± 0.4	0.3 ± 0.4	0.3 ± 0.4	0.3 ± 0.4
Pain intensity	29.2 ± 25.8	27.0 ± 25.6	29.1 ± 25.5	29.9 ± 25.4	30.6 ± 25.4
Number of previous DMARDs	1.9 ± 1.4	2.1 ± 1.4	1.9 ± 1.4	1.8 ± 1.5	1.8 ± 1.4
Nonbiologic DMARDs, no. (%)	5,135 (55)	1,207 (52)	1,272 (56)	1,275 (54)	1,381 (57)
Biologic DMARDs, no. (%)	3,445 (37)	971 (42)	847 (38)	803 (34)	824 (34)
Glucocorticoids, no. (%)	2,549 (27)	561 (24)	724 (32)	566 (24)	698 (29)
Antidepressants, no. (%)	1,357 (15)	320 (14)	300 (13)	352 (15)	385 (16)

* Except where indicated otherwise, values are the mean ± SD. RA = rheumatoid arthritis; CDAI = Clinical Disease Activity Index; HAQ DI = Health Assessment Questionnaire disability index; DMARDs = disease-modifying antirheumatic drugs.

intracluster correlation within sites. Covariates included practice-level factors (geographic region, urban/rural status), physician-level factors (sex, academic/private affiliation), and all baseline patient-level variables that were previously reported to be associated with long-term opioid use in unadjusted analyses, with $P < 0.1$. The latter included age, sex, race, insurance status, RA duration, CDAI, HAQ, pain severity, number of historical DMARDs, biologic DMARD use, glucocorticoid use, and antidepressant use (22).

To test the sensitivity of our results to design assumptions, 2 sensitivity analyses were performed. The first examined the implications of using a more stringent definition of long-term opioid use, requiring ≥3 consecutive documentations of opioid use. The second examined the implication of defining baseline opioid prescribing rate using data from the first 18 months of physician enrollment in the Corrona RA Registry, as opposed to the first 12 months. Subgroup analyses were also performed, stratifying by: 1) disease activity (CDAI ≤10 versus >10), 2) pain severity (≤40, >40–60, or >60 on a scale of 0–100), and 3) antidepressant use (yes/no). All analyses were performed using SAS 9.4. To explore the possibility of changes in associations between physician prescribing habits and long-term opioid use over time, we also stratified the analyses by calendar year, including those enrolled before and during 2009 versus those enrolled after 2009.

Patient and public involvement. No patients were involved in developing the research question and outcome measures or designing the study. They were not asked to assess the time required to participate in the research. Patients were not involved in choosing the methods and agreeing on plans for dissemination of the study results to participants and wider relevant communities.

RESULTS

Study participants. Between October 1, 2001 and December 31, 2016, 33,739 patients with RA and data on opioid use from ≥2 visits were enrolled in the Corrona RA registry. Of these patients, 16,209 met all inclusion criteria, with 6,872 patients included in the baseline period (used to determine physician opioid prescribing rates) and 9,337 included in the follow-up period (used in the prediction analyses) (Table 1 and Figure 2). Total follow-up time was 41,389 person-years, with a mean ± SD follow-up time of 4.43 ± 2.94 years.

Physician opioid prescribing rates. Physician characteristics are summarized in Supplementary Table 1, available on the *Arthritis & Rheumatology* web site at http://onlinelibrary.wiley.com/doi/10.1002/art.41240/abstract. During the baseline period, physician opioid prescribing rates varied from 0% to 70%. Physicians in the highest quartile had more than double the proportion of their patients reporting at least 1 instance of opioid use than those in the lowest quartile (Figure 3).

Patient characteristics according to physician opioid prescribing rates. Of the 9,337 participants seen by physicians during the follow-up period, 2,322 were treated by physicians with a very low rate of opioid prescribing (≤18% of patients taking an opioid), 2,254 were treated by physicians with a low rate of

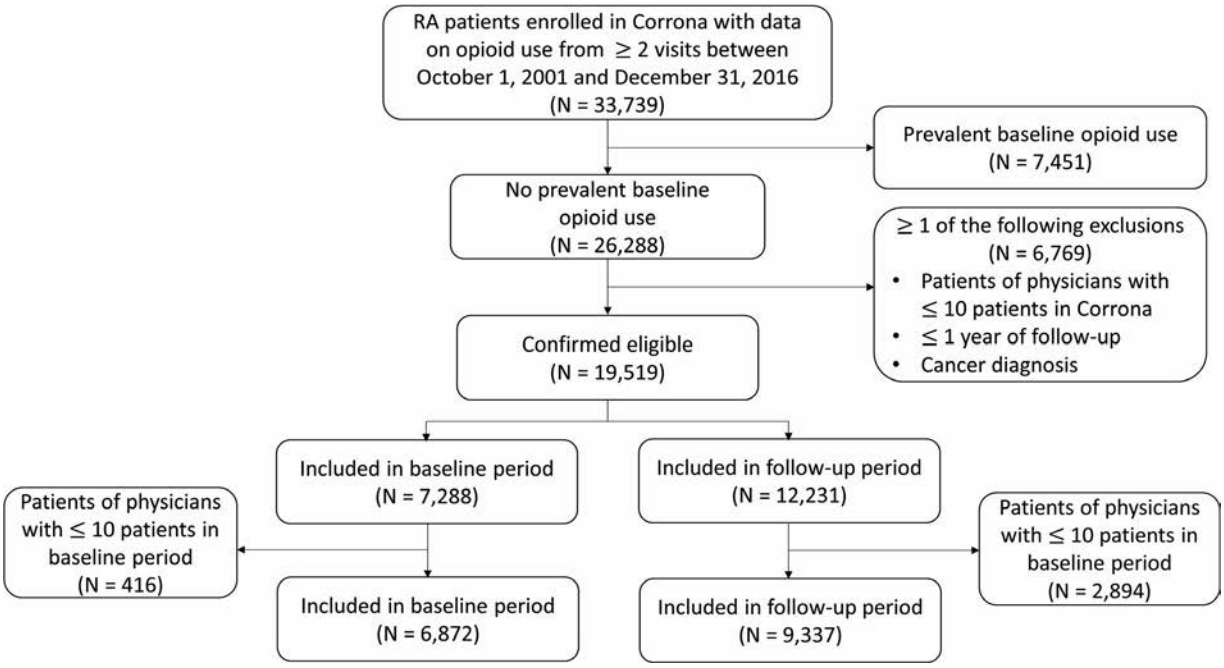

Figure 2. Flow chart showing the construction of the study cohort of patients with rheumatoid arthritis (RA) with data on opioid use for ≥2 visits in the Corrona RA Registry.

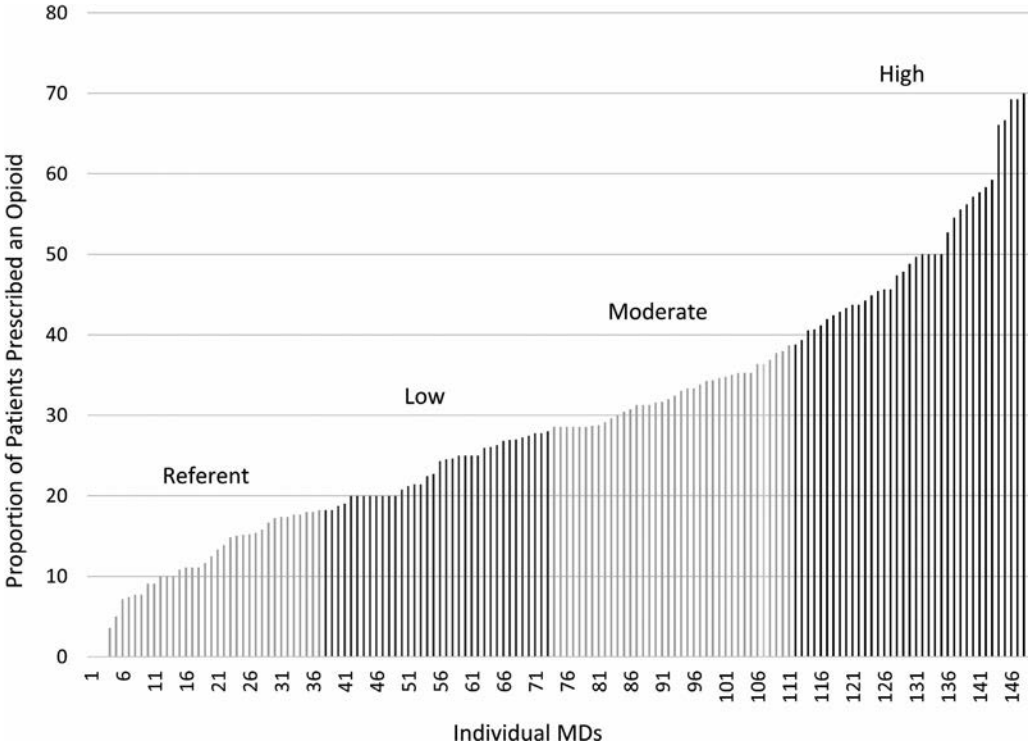

Figure 3. Proportion of patients with rheumatoid arthritis (RA) who were prescribed an opioid during the baseline period. For each physician, the number of his or her patients with RA who reported opioid use during the baseline period was divided by the total number of patients with RA who provided data during the same period.

opioid prescribing (>18–28% of patients taking an opioid), 2,352 were treated by physicians with a moderate rate of opioid prescribing (>28–38% of patients taking an opioid), and 2,409 were treated by physicians with a high rate of opioid prescribing (>38% of patients taking an opioid). Patients of physicians with moderate or high opioid prescribing rates had higher disease activity scores but lower rates of biologic DMARD use. Otherwise, patient characteristics, including average pain intensity, were similar across groups (Table 1). There was a small amount of missing data for CDAI (5.25%), HAQ (3.82%), pain intensity (4.43%), and insurance status (1.87%).

Physician opioid prescribing rates and patient long-term opioid use. During the follow-up period, the percentage of long-term opioid use was higher among patients of physicians with moderate or high baseline opioid prescribing rates (12.5% and 12.7%, respectively), compared to patients of physicians in the referent group (7.0%) (Table 2). Differences in long-term opioid use between patients treated by physicians in each quartile of opioid prescribing were similar across subgroups stratified by disease activity, pain intensity, and antidepressant use (Supplementary Table 2, available on the *Arthritis & Rheumatology* web site at http://onlinelibrary.wiley.com/doi/10.1002/

Table 2. Frequency and ORs of association between physician rate of opioid prescribing and patient long-term opioid use*

	Referent (n = 2,322)†	Low (n = 2,254)	Moderate (n = 2,352)	High (n = 2,409)
No. (%) of patients reporting long-term opioid use	163 (7.0)	153 (6.8)	294 (12.5)	307 (12.7)
Primary analysis, OR (95% CI)‡	1.00	1.16 (0.79–1.70)	1.89 (1.27–2.82)	2.01 (1.43–2.83)
Sensitivity analyses, OR (95% CI)‡				
Long-term opioid use defined as ≥3 consecutive documentations	1.00	1.30 (0.79–2.15)	2.04 (1.22–3.40)	2.33 (1.49–3.65)
Cutoff between baseline and follow-up period at 18 months	1.00	1.69 (1.14–2.52)	2.06 (1.33–3.20)	2.21 (1.50–3.25)

* ORs = odds ratios; 95% CI = 95% confidence interval.
† Patients of physicians with a very low rate of opioid prescribing.
‡ Multivariable analyses were adjusted for practice-level factors (geographic region and urban/rural status), physician-level factors (sex and academic/private affiliation), and baseline patient-level factors (age, sex, race, insurance status, duration of rheumatoid arthritis, Clinical Disease Activity Index, Health Assessment Questionnaire disability index, pain intensity, number of previous disease-modifying antirheumatic drugs [DMARDs], biologic DMARD use, glucocorticoid use, and antidepressant use).

art.41240/abstract). Across categories of baseline physician opioid prescribing rates, long-term opioid use during follow-up was more frequent among those with higher disease activity and higher pain intensity, as well as among those who took antidepressants.

The unadjusted OR for the association between physician opioid prescribing rates and subsequent patient long-term opioid use was 1.15 (95% CI 0.82–1.63) for patients of low-intensity prescribing physicians, 1.94 (95% CI 1.36–2.77) for patients of moderate-intensity prescribing physicians, and 2.16 (95% CI 1.58–2.95) for patients of high-intensity prescribing physicians, compared to patients in the referent group. After adjustment, there was minimal change in these results (for low-intensity prescribers, OR 1.16 [95% CI 0.79–1.70]; for moderate-intensity prescribers, OR 1.89 [95% CI 1.27–2.82]; and for high-intensity prescribers, OR 2.01 [95% CI 1.43–2.83]) (Table 2). The association between baseline opioid prescribing rate and long-term opioid use during follow-up did not differ in a sensitivity analysis in which the definition of long-term opioid use was more stringent (≥3 consecutive documentations of opioid use) (Supplementary Table 3, available on the *Arthritis & Rheumatology* web site at http://onlinelibrary.wiley.com/doi/10.1002/art.41240/abstract) or in a sensitivity analysis in which the cutoff between the baseline and follow-up period was changed from 12 months to 18 months (Supplementary Table 4, available on the *Arthritis & Rheumatology* web site at http://onlinelibrary.wiley.com/doi/10.1002/art.41240/abstract). In addition, similar associations were observed in subgroup analyses stratified by disease activity, pain intensity, and antidepressant use (Figure 4).

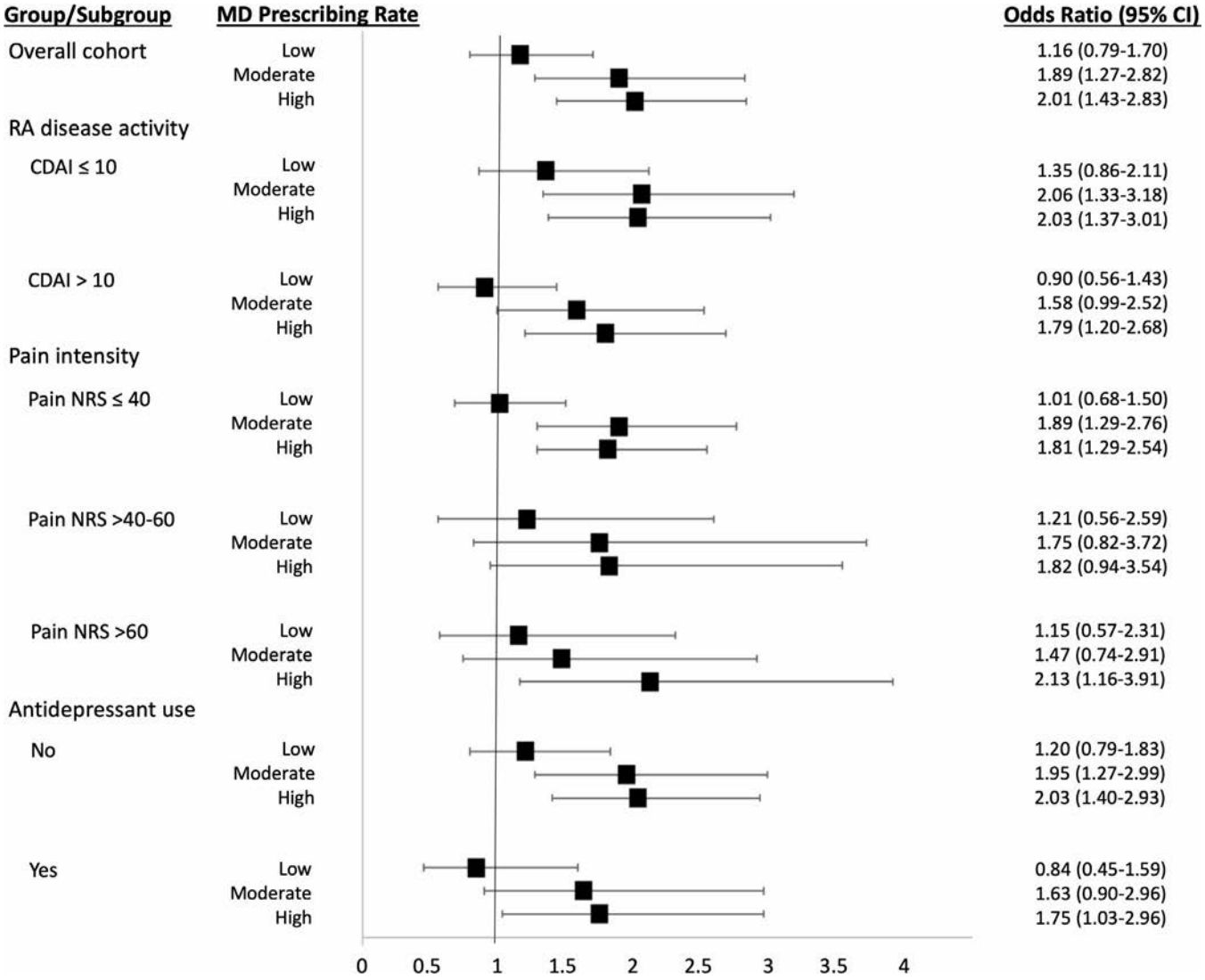

Figure 4. Adjusted odds ratios (ORs) for long-term opioid use by patients with rheumatoid arthritis (RA) who were seen by physicians with low, moderate, or high opioid prescribing rates. Results are presented for the overall cohort and for subgroups stratified by disease activity according to the Clinical Disease Activity Index (CDAI), pain intensity (scored on a numerical rating scale [NRS] of 0–100), and antidepressant use. Values are the OR and 95% confidence interval (95% CI).

In exploratory analyses stratified by calendar year as before and during 2009 versus after 2009, the associations between physician opioid prescribing rates and subsequent patient long-term opioid use were higher among those enrolled before or during 2009 compared to those enrolled after 2009. Among those enrolled before or during 2009, the ORs for the associations between physician opioid prescribing rate and subsequent opioid use were 1.25 (95% CI 0.49–3.18) for patients of low-intensity prescribing physicians, 4.11 (95% CI 1.60–10.53) for patients of moderate-intensity prescribing physicians, and 3.45 (95% CI 1.54–7.73) for patients of high-intensity prescribing physicians, compared to patients in the referent group. Among those enrolled after 2009, the ORs for the associations between physician opioid prescribing rates and subsequent patient long-term opioid use were 0.94 (95% CI 0.58–1.53) for patients of low-intensity prescribing physicians, 1.39 (95% CI 0.85–2.28) for patients of moderate-intensity prescribing physicians, and 1.37 (95% CI 0.89–2.13) for patients of high-intensity prescribing physicians, compared to patients in the referent group.

DISCUSSION

In this large, population-based cohort of individuals with RA, we found large variation in the rates of opioid use among physicians' practices. Moreover, baseline opioid prescribing rates predicted future long-term opioid use by different patients of these same clinicians. These results were robust in a sensitivity analysis with a more stringent definition of long-term opioid use and a sensitivity analysis that increased the duration of the baseline period used to define opioid prescribing rates.

Our investigation contributes important information regarding opioid prescribing rates and their relationship to long-term opioid use in a patient population with a high frequency of chronic, nonmalignant pain. Prescription opioids have contributed to the "opioid crisis" gripping the US. Some data support the possibility that deaths from opioids are starting to wane (23), but continued efforts to battle the epidemic are critical. The decision to initiate treatment with opioids for chronic painful conditions, like RA, appears to be discretionary, with evidence demonstrating variable rates across settings (11,24–26). A recent study reported that, although overall rates of initiating opioid treatment have decreased in recent years, a subgroup of physicians continue to prescribe opioids at high rates (27). While a broad range of prescribing of long-term opioids may stem from heterogeneous patient populations, our results suggest that some variation also originates with clinicians. Some providers prescribe long-term opioids more than others, even after controlling for patient factors.

This is not the first example of distinct clinician prescribing profiles. A study of >1 million patients with acute respiratory infections showed variation in prescribing at the provider level (28). Antibiotics were prescribed at ≥95% of visits to providers in the highest 10% of antibiotic prescribing, whereas antibiotics were prescribed at ≤50% of visits to providers in the lowest 10% of antibiotic prescribing. Studies examining the prescription of other medication categories have demonstrated similar results. For example, an analysis of 192 primary care physicians showed that newer physicians (in practice <20 years) more commonly prescribed nonsteroidal antiinflammatory drugs for pain relief than more experienced physicians (in practice ≥20 years) (68.8% versus 52.1% for sciatica; 80.2% versus 67.7% for osteoarthritis) (29).

Variation in opioid prescribing patterns has been reported across geographic regions and within different clinical settings and medical/surgical specialties. The Centers for Disease Control and Prevention reported that opioid prescribing rates were 2.7 times higher in Alabama, the state with the highest opioid prescribing rate, than in Hawaii, the state with the lowest opioid prescribing rate (30). A similar result was observed in a study of 19,615 ophthalmologists with Medicare Part D prescribing data (31). While 88.8% of ophthalmologists wrote ≤10 prescriptions per year, ~1% wrote >100 prescriptions per year. States with the highest number of opioid prescriptions per physician included Alabama and other southern states, such as Georgia, Arkansas, Tennessee, and Oklahoma. In a retrospective analysis of Medicare beneficiaries who received care in the emergency department, average rates of opioid prescribing varied from 7.3% among low-intensity prescribers to 24.1% among high-intensity prescribers (14).

In our primary analysis, the ORs for the association between baseline opioid prescribing rates and future long-term opioid use were in the range of 1.16 (95% CI 0.79–1.70) for patients of low-intensity prescribers to 2.01 (95% CI 1.43–2.83) for patients of high-intensity prescribers. While the clinical meaning of ORs is difficult to assess, the magnitude of these values is similar to, if not larger than, the ORs reported in a highly cited article on opioid prescribing patterns of emergency physicians and risk of long-term opioid use in patients seen by those physicians (14). In the latter study, ORs ranged from 1.10 (95% CI 1.04–1.16) for low-intensity prescribers up to 1.30 (95% CI 1.23–1.37) for high-intensity prescribers.

In exploratory analyses, we observed a possible secular trend in the association between physician opioid prescribing rates and subsequent patient long-term opioid use. The association was stronger among those enrolled before 2009 compared to those enrolled after 2009, suggesting that the influence of physician prescribing patterns has decreased over time, possibly due to greater public awareness of the risks of long-term opioid use. It is important to note, however, that this was a post hoc analysis, and the study was not powered to formally test for statistically significant differences between these 2 time periods. Future studies are needed to confirm this finding.

The heterogeneity in opioid prescribing rates presents interesting opportunities for research and practice. First, if society has determined that long-term opioid use is risky, the heterogeneity suggests that it is feasible to limit long-term opioid use to a select and small group of patients, i.e., those unable to tolerate other

analgesics and/or disease-specific treatments, or only able to function while using opioids. These prescribing restrictions could be monitored through state-level controlled substance programs, targeting prescribers with higher rates of long-term opioid use. Second, variable prescribing rates across clinicians can be harnessed as a natural experiment. The results of this study and others demonstrate clinician preferences beyond patient characteristics in prescribing. This preference can be opportunistically used by comparative effectiveness researchers as an instrumental variable, a factor that correlates with receipt of a given intervention but has no direct relationship with outcomes (32). Such instrumental variables have been used to turn typical practice into a natural laboratory (33,34). Finally, heterogeneity in prescribing may serve as a marker for areas that require more head-to-head comparative effectiveness studies. This could be used by funders to target scarce research resources.

Strengths of this analysis include the large RA cohort, representing typical rheumatology practices across all regions of the US (35). In addition, detailed information was available on both physician-related and patient-related characteristics, including a comprehensive set of data regarding RA-related characteristics, such as pain intensity, disease activity, and medication use. Incorporating these data enabled us to account for a variety of potential confounding factors. We also performed sensitivity analyses and analyses stratified by important patient characteristics, underscoring the consistency of the results across different subgroups.

The analyses have a few important limitations. First, subjects may have received opioid prescriptions from physicians other than those registered in the Corrona database (e.g., primary care physicians). We were not able to distinguish whether the prescriber was the rheumatologist or another physician. Second, long-term opioid use was determined based on patient self-report, which may be unreliable. We did not have data available from medication reconciliation by the provider or from state prescription drug monitoring programs. Future studies incorporating data from urine opioid tests are needed to provide information regarding the accuracy of self-reported data compared to data from provider medication reconciliation and state prescription drug monitoring programs. Third, long-term opioid use was determined by self-report of opioid use at ≥2 sequential visits. This typically represents a period of ~5 months but could be longer. Thus, we may have underestimated the true event rate if participants used opioids for at least 3 months but stopped prior to their next study visit. Alternatively, it is possible that patients used 2 short courses around each visit, and we misinterpreted 2 short courses to be long-term use. We tested this assumption in sensitivity analyses that required ≥3 sequential visits with opioid reports, and similar results were observed. In addition, questions regarding opioid use changed over calendar time as different opioids became more or less widespread in their use, i.e., increased use of tramadol and restrictions on hydrocodone. These changes in the patient questionnaire may have affected reporting. Finally, we did not include data on important comorbidities, such as fibromyalgia and depression, due to a large amount of missing data in these variables. To address the latter issue, we included antidepressant use as a proxy for the diagnosis of depression.

While it may not be surprising that clinicians demonstrate heterogeneous prescribing patterns, we should examine why this is the case. The evidence base for deciding on long-term opioid use versus other analgesics is weak for patients with RA, and there are no long-term head-to-head studies comparing benefits and risks of different interventions for pain. Future studies are needed to: 1) design and implement effective interventions to decrease opioid prescribing rates, 2) identify subgroups of physicians who would be the most appropriate targets for intervention, and 3) identify trends in use of opioid alternatives (e.g., cannabinoids) and their impact on opioid use.

In conclusion, rates of opioid prescriptions varied widely. Baseline opioid prescribing rates within a physician's practice were a strong predictor of whether a patient would become a long-term opioid user, after controlling for patient characteristics. The association between baseline opioid prescribing rates and long-term opioid use did not differ in subgroups stratified by disease activity, pain intensity, and antidepressant use. Our results suggest that, in addition to targeting patients, interventions directed toward high-intensity prescribers may be helpful to decrease long-term opioid use.

AUTHOR CONTRIBUTIONS

All authors were involved in drafting the article or revising it critically for important intellectual content, and all authors approved the final version to be published. Dr. Lee had full access to all of the data in the study and takes responsibility for the integrity of the data and the accuracy of the data analysis.

Study conception and design. Lee, Solomon.
Acquisition of data. Greenberg, Kremer.
Analysis and interpretation of data. Lee, Lu, Guan, Solomon.

REFERENCES

1. Gureje O, von Korff M, Simon GE, Gater R. Persistent pain and well-being: a World Health Organization study in primary care. JAMA 1998;280:147–51.
2. Chua JR, Castrejon I, Pincus T. Assessment of pain and other patient symptoms in routine clinical care as quantitative, standardised, "scientific" data. Clin Exp Rheumatol 2017;35 Suppl 107:13–20.
3. Altawil R, Saevarsdottir S, Wedren S, Alfredsson L, Klareskog L, Lampa J. Remaining pain in early rheumatoid arthritis patients treated with methotrexate. Arthritis Care Res (Hoboken) 2016;68:1061–8.
4. McWilliams DF, Walsh DA. Factors predicting pain and early discontinuation of tumour necrosis factor-α-inhibitors in people with rheumatoid arthritis: results from the British society for rheumatology biologics register. BMC Musculoskelet Disord 2016;17:337.
5. Radner H, Ramiro S, Buchbinder R, Landewe RB, van der Heijde D, Aletaha D. Pain management for inflammatory arthritis (rheumatoid arthritis, psoriatic arthritis, ankylosing spondylitis and other spondylarthritis) and gastrointestinal or liver comorbidity [review]. Cochrane Database Syst Rev 2012;1:CD008951.

6. Zingler G, Hermann B, Fischer T, Herdegen T. Cardiovascular adverse events by non-steroidal anti-inflammatory drugs: when the benefits outweigh the risks [review]. Expert Rev Clin Pharmacol 2016;9:1479–92.
7. Evans PJ, Halliwell B. Side-effects of drugs used in the treatment of rheumatoid arthritis. Biochem Soc Symp 1995;61:195–207.
8. Whittle SL, Colebatch AN, Buchbinder R, Edwards CJ, Adams K, Englbrecht M, et al. Multinational evidence-based recommendations for pain management by pharmacotherapy in inflammatory arthritis: integrating systematic literature research and expert opinion of a broad panel of rheumatologists in the 3e Initiative. Rheumatology (Oxford) 2012;51:1416–25.
9. Solomon DH, Avorn J, Wang PS, Vaillant G, Cabral D, Mogun H, et al. Prescription opioid use among older adults with arthritis or low back pain. Arthritis Rheum 2006;55:35–41.
10. Lee YC, Kremer J, Guan H, Greenberg J, Solomon DH. Chronic opioid use in rheumatoid arthritis: prevalence and predictors. Arthritis Rheumatol 2019;71:670–7.
11. Curtis JR, Xie F, Smith C, Saag KG, Chen L, Beukelman T, et al. Changing trends in opioid use among patients with rheumatoid arthritis in the United States. Arthritis Rheumatol 2017;69:1733–40.
12. Zamora-Legoff JA, Achenbach SJ, Crowson CS, Krause ML, Davis JM III, Matteson EL. Opioid use in patients with rheumatoid arthritis 2005-2014: a population-based comparative study. Clin Rheumatol 2016;35:1137–44.
13. Herrinton LJ, Harrold L, Salman C, Liu L, Goldfien R, Asgari M, et al. Population variations in rheumatoid arthritis treatment and outcomes, northern California, 1998-2009. Perm J 2016;20:4–12.
14. Barnett ML, Olenski AR, Jena AB. Opioid-prescribing patterns of emergency physicians and risk of long-term use. N Engl J Med 2017;376:663–73.
15. Kremer JM. The Corrona US registry of rheumatic and autoimmune diseases. Clin Exp Rheumatol 2016;34 Suppl 101:S96–9.
16. Jena AB, Goldman D, Karaca-Mandic P. Hospital prescribing of opioids to Medicare beneficiaries. JAMA Intern Med 2016;176:990–7.
17. Dunn KM, Saunders KW, Rutter CM, et al. Opioid prescriptions for chronic pain and overdose: a cohort study. Ann Intern Med 2010;152:85–92.
18. Braden JB, Russo J, Fan MY, Edlund MJ, Martin BC, DeVries A, et al. Emergency department visits among recipients of chronic opioid therapy. Arch Intern Med 2010;170:1425–32.
19. Aletaha D, Nell VP, Stamm T, Uffmann M, Pflugbeil S, Machold K, et al. Acute phase reactants add little to composite disease activity indices for rheumatoid arthritis: validation of a clinical activity score. Arthritis Res Ther 2005;7:R796–806.
20. Fries JF, Spitz P, Kraines RG, Holman HR. Measurement of patient outcome in arthritis. Arthritis Rheum 1980;23:137–45.
21. Bruce B, Fries JF. The Health Assessment Questionnaire (HAQ). Clin Exp Rheumatol 2005;23 Suppl 39:S14–8.
22. D'Agnelli S, Arendt-Nielsen L, Gerra MC, Zatorri K, Boggiani L, Baciarello M, et al. Fibromyalgia: genetics and epigenetics insights may provide the basis for the development of diagnostic biomarkers. Mol Pain 2019;15:1744806918819944.
23. Dart RC, Surratt HL, Cicero TJ, Parrino MW, Severtson SG, Bucher-Bartelson B, et al. Trends in opioid analgesic abuse and mortality in the United States. N Engl J Med 2015;372:241–8.
24. Kuo YF, Raji MA, Chen NW, Hasan H, Goodwin JS. Trends in opioid prescriptions among Part D Medicare recipients from 2007 to 2012. Am J Med 2016;129:e221–30.
25. Paulozzi LJ, Strickler GK, Kreiner PW, Koris CM, Centers for Disease Control and Prevention (CDC). Controlled substance prescribing patterns—prescription behavior surveillance system, eight states, 2013. MMWR Surveill Summ 2015;64:1–14.
26. Axeen S. Trends in opioid use and prescribing in Medicare, 2006-2012. Health Serv Res 2018;53:3309–28.
27. Zhu W, Chernew ME, Sherry TB, Maestas N. Initial opioid prescriptions among U.S. commercially insured patients, 2012-2017. N Engl J Med 2019;380:1043–52.
28. Jones BE, Sauer B, Jones MM, Campo J, Damal K, He T, et al. Variation in outpatient antibiotic prescribing for acute respiratory infections in the veteran population: a cross-sectional study. Ann Intern Med 2015;163:73–80.
29. Maserejian NN, Fischer MA, Trachtenberg FL, Yu J, Marceau LD, McKinlay JB, et al. Variations among primary care physicians in exercise advice, imaging, and analgesics for musculoskeletal pain: results from a factorial experiment. Arthritis Care Res (Hoboken) 2014;66:147–56.
30. Paulozzi LJ, Mack KA, Hockenberry JM. Variation among states in prescribing of opioid pain relievers and benzodiazepines—United States, 2012. J Safety Res 2014;51:125–9.
31. Patel S, Sternberg P Jr. Association between opioid prescribing patterns and abuse in ophthalmology. JAMA Ophthalmol 2017;135:1216–20.
32. Brookhart MA, Wang PS, Solomon DH, Schneeweiss S. Instrumental variable analysis of secondary pharmacoepidemiologic data. Epidemiology 2006;17:373–4.
33. Brookhart MA, Wang PS, Solomon DH, Schneeweiss S. Evaluating short-term drug effects using a physician-specific prescribing preference as an instrumental variable. Epidemiology 2006;17:268–75.
34. Schneeweiss S, Solomon DH, Wang PS, Rassen J, Brookhart MA. Simultaneous assessment of short-term gastrointestinal benefits and cardiovascular risks of selective cyclooxygenase 2 inhibitors and nonselective nonsteroidal antiinflammatory drugs: an instrumental variable analysis. Arthritis Rheum 2006;54:3390–8.
35. Curtis JR, Chen L, Bharat A, Delzell E, Greenberg JD, Harrold L, et al. Linkage of a de-identified United States rheumatoid arthritis registry with administrative data to facilitate comparative effectiveness research. Arthritis Care Res (Hoboken) 2014;66:1790–8.

Arthritis & Rheumatology
Vol. 72, No. 7, July 2020, pp 1091–1102
DOI 10.1002/art.41223

American College of Rheumatology
Empowering Rheumatology Professionals

Association of a Type 2–Polarized T Cell Phenotype With Methotrexate Nonresponse in Patients With Rheumatoid Arthritis

Drew Slauenwhite,[1] Sarah M. McAlpine,[1] John G. Hanly,[2] Anikó Malik,[1] Ian D. Haidl,[3] Jean S. Marshall,[3] and Thomas B. Issekutz[1]

Objective. Rheumatoid arthritis (RA) is a chronic inflammatory disease mediated through complex immunologic pathways. Among RA patients receiving low-dose methotrexate (MTX) monotherapy, approximately one-half exhibit a meaningful clinical response within the first 6 months of starting treatment. Whether baseline immune phenotypes differ between subsequent MTX responders and nonresponders is unknown. This study utilized comprehensive T cell immunophenotyping to identify specific immunologic pathways associated with MTX-nonresponsive joint inflammation in patients with RA.

Methods. In total, 32 patients with recent-onset RA were treated with MTX therapy. After 6 months, 15 patients were categorized as responders and 17 as nonresponders. Comprehensive blood T cell immunophenotyping, using multiparameter immunofluorescence flow cytometry analyses, was performed at baseline and following 6 months of treatment.

Results. Baseline measures of disease activity (Disease Activity Score in 28 joints [DAS28], C-reactive protein level, and erythrocyte sedimentation rate) did not differ between MTX responders and nonresponders following MTX treatment. Frequencies of CD4+ and CD8+ T cells were skewed to favor higher CD4:CD8 T cell ratios in MTX responders compared to nonresponders ($P < 0.05$). The proportion of inducible costimulator–expressing Treg cells was significantly greater among MTX nonresponders. Interleukin-13 (IL-13)–producing, but not interferon-γ– or IL-17–producing, CD4+ effector memory T (Tem) cells were significantly more frequent in MTX nonresponders ($P < 0.05$). The ratio of IL-13+:IL-17+ Tem cells among CD4+ Tem cells was 1.9-fold higher in MTX nonresponders compared to responders ($P < 0.05$). Both the CD4:CD8 T cell ratio and the frequency of IL-13+CD4+ Tem cells correlated with changes in the DAS28 score following MTX treatment, whereas T cell expression of immune checkpoint inhibitor markers (CTLA-4, programmed death 1, and T cell immunoglobulin and mucin domain–containing protein 3) did not differ between MTX responders and nonresponders.

Conclusion. We observed a bias toward type 2–polarized T cell inflammatory responses in the peripheral blood of MTX-nonresponsive RA patients. Targeting the IL-13+CD4+ T cell pathway could be a new therapeutic strategy in RA patients whose disease remains resistant to MTX.

INTRODUCTION

Rheumatoid arthritis (RA) is a complex autoimmune disease with a spectrum of clinical phenotypes, ranging from patients with severe inflammation and early joint destruction to those with milder disease. Adding to the complexity, patients with similar clinical presentations may have very different underlying immunologic, genetic, and molecular pathways exhibiting dysregulation. The heterogeneity of this disease is supported by the unpredictable responses and mixed clinical outcomes following standard treatment

Supported by the Canadian Institutes of Health Research (grant THC 135230). Dr. Slauenwhite's work was supported by the IWK Health Centre. Dr. Malik's work was supported by the IWK Health Centre and Nova Scotia Health Research Foundation.

[1]Drew Slauenwhite, PhD, Sarah M. McAlpine, PhD, Anikó Malik, MD, Thomas B. Issekutz, MD: IWK Health Centre and Dalhousie University, Halifax, Nova Scotia, Canada; [2]John G. Hanly, MD: QEII Health Sciences Centre, Halifax, Nova Scotia, Canada; [3]Ian D. Haidl, PhD, Jean S. Marshall, PhD: Dalhousie University, Halifax, Nova Scotia, Canada.

No potential conflicts of interest relevant to this article were reported.

Address correspondence to Thomas B. Issekutz, MD, IWK Health Centre, Division of Immunology, Department of Pediatrics, 5850 University Avenue, Halifax, Nova Scotia B3K 6R8, Canada (e-mail: Thomas.Issekutz@dal.ca); or to John G. Hanly, MD, QEII-Nova Scotia Rehabilitation and Arthritis Centre, Division of Rheumatology, Suite 245 NS Rehab Building, 1341 Summer Street, Halifax, Nova Scotia B3K 6R8, Canada (e-mail: John.Hanly@nshealth.ca).

Submitted for publication July 18, 2019; accepted in revised form January 24, 2020.

strategies. Guidelines from the American College of Rheumatology (ACR) and European League Against Rheumatism (EULAR) recommend methotrexate (MTX) as the preferred initial disease-modifying antirheumatic drug (DMARD) for RA (1,2). However, ~46% of RA patients started on MTX therapy discontinue treatment by 3 years, due to treatment intolerance and a lack of efficacy (3). It is important to initiate effective therapy as soon as possible after diagnosis, since early control of inflammation is associated with better long-term outcomes (4). However, accurate prediction of outcomes in individual patients is challenging, in part because the disease mechanisms targeted by MTX are not fully understood.

In RA synovium, infiltrating T cells are mostly activated memory cells (5). These contribute to cytokine-dependent and cell–cell contact–dependent activation of synovial cells, including tissue-destructive fibroblast-like synoviocytes, macrophages, and osteoclasts (6–8). CD4+CD25+FoxP3+ Treg cells are also enriched in the joints of patients with RA (9,10). However, high levels of proinflammatory cytokines (e.g., interferon-γ [IFNγ], tumor necrosis factor [TNF], interleukin-6 [IL-6], and IL-17) and the enhanced proliferative capacity of effector T cells counteract the suppressive functions of Treg cells (9,10). MTX, at the doses used for treatment of RA, is thought to have an antiinflammatory effect through release of excess ATP, ADP, and AMP into the extracellular space, all of which are then converted to adenosine by the cell surface enzymes CD39 and CD73 (11). Adenosine binding to its receptors, particularly the A_{2A} receptor, induces antiinflammatory effects in multiple immune cells, including CD4+ T cells, reducing immune cell proliferation and the production of proinflammatory cytokines (12).

Improved understanding of how disease mechanisms differ between MTX-responsive and MTX-resistant RA is needed. In this study, we addressed the hypothesis that unique blood T cell and Treg cell immune phenotypes, indicating specifically activated immunologic pathways, are associated with the occurrence of or lack of clinical response to MTX in RA. We found circulating CD4+ and CD8+ T cell frequencies to be significantly skewed and the proportion of inducible costimulator (ICOS)–expressing Treg cells and frequency of IL-13–producing CD4+ effector memory T (Tem) cells to be significantly lower in MTX responders compared to nonresponders at baseline. Stronger Th2 responses among T cells may constitute a disease mechanism that is less sensitive to MTX-induced antiinflammatory effects, and therefore this phenotype should be further evaluated for its potential to distinguish MTX responders from nonresponders among patients with RA.

PATIENTS AND METHODS

Subjects. Patients with recent-onset, untreated RA (mean disease duration <12 months) fulfilling the 2010 ACR/EULAR classification criteria (13) were recruited from the Rheumatology Clinic at The Arthritis Centre of Nova Scotia, Queen Elizabeth II Health Sciences Centre in Canada. Only patients with moderate-to-high disease activity (defined as a Disease Activity Score in 28 joints using the erythrocyte sedimentation rate [DAS28-ESR] of >3.3 [14]) and no previous exposure to glucocorticoids or DMARDs were included in this study. Healthy volunteers with no infections or autoimmune disease were included as controls. Studies were approved by the Nova Scotia Health Authority Research Ethics Board. All participants provided written informed consent.

Clinical and laboratory evaluation. Patients were evaluated for disease activity using the DAS28-ESR score. In addition, information on demographics, disease duration, plasma C-reactive protein (CRP) level, ESR, and seropositivity for anti–citrullinated protein antibodies (ACPAs) and rheumatoid factor (RF) was collected at study entry. All patients were treated with MTX for 6 months. Eight patients (4 MTX responders and 4 nonresponders) started treatment with hydroxychloroquine at 3 months, and thereafter were continued on double DMARD (MTX and hydroxychloroquine) therapy. After 6 months, patients with low or no disease activity (defined as a DAS28-ESR score of ≤3.2) were considered MTX responders.

Isolation of peripheral blood mononuclear cells (PBMCs) and immunophenotyping. Heparinized blood was collected from all patients at study entry and after 6 months of MTX treatment. PBMCs were isolated using Ficoll-Paque PLUS (GE Healthcare) and stored in liquid nitrogen. Blood samples were also collected in EDTA and centrifuged at 400*g* for 10 minutes at 20°C, and plasma was centrifuged at 2,400*g* for 20 minutes to remove platelets. The samples were then stored at –80°C until analyzed.

For the multicolor flow cytometry analyses carried out for T cell phenotyping and intracellular cytokine staining, 1×10^6 PBMCs were incubated in RPMI 1640 medium (Gibco Life Technologies) with 10% fetal bovine serum (Gibco) at 37°C in an atmosphere of 5% CO_2 for 3 hours, together with 50 ng/ml phorbol myristate acetate (PMA; Sigma-Aldrich), 1 μ*M* ionomycin (Sigma), and 3 μg/ml brefeldin A (eBioscience). Immunophenotyping of T cells was performed using fluorochrome-conjugated monoclonal antibodies. Fixation/permeabilization of the cells and intracellular staining (eBioscience) were performed in accordance with the manufacturer's instructions. Treg cell phenotyping was performed without in vitro activation. Cells were permeabilized and stained using a human Th17/Treg cell phenotyping kit (eBioscience), in accordance with the manufacturer's instructions. Acquisitions were performed on an LSR Fortessa SORP flow cytometer (BD Biosciences), and data were analyzed using FlowJo software (version 10; TreeStar). Further details are available from the corresponding author upon request.

Plasma cytokine measurement. Plasma samples were thawed on ice, followed by centrifugation at 10,000*g* for 5 minutes at 4°C to remove particulates. Cytokines were measured using a Human ProcartaPlex assay (ThermoFisher) in accordance with the manufacturer's instructions, on a Bio-Plex 200 System (Bio-Rad). Data analysis was performed using Bio-Plex Manager software (version 6.0; Bio-Rad).

Statistical analysis. To assess normality of the data, the distributional form of the data and the D'Agostino-Pearson normality test were used. Statistical analyses for comparisons between 3 or more groups were performed using either one-way analysis of variance with Bonferroni's post hoc correction for multiple comparisons or Kruskal-Wallis test with Dunn's post hoc correction. Statistically significant differences between the baseline and 6-month blood samples from patients in the responder and nonresponder groups and between immune cell phenotypes with or without in vitro activation of T cells with PMA/ionomycin were calculated using parametric Student's two-tailed paired *t*-tests or nonparametric Wilcoxon's paired signed rank tests. Linear correlation coefficients were calculated using Pearson's or Spearman's correlation tests. To evaluate diagnostic accuracy, areas under the curve (AUC) in receiver operating characteristic (ROC) curves were constructed. Cutoff values for the optimal frequency of IL-13+CD4+ Tem cells and optimal CD4:CD8 T cell ratio that would maximize sensitivity and specificity of the AUCs were determined based on the maximal Youden's index. Statistical analyses were performed with Prism version 8 (GraphPad Software). Results are presented as the mean ± SEM. *P* values less than 0.05 were considered statistically significant.

RESULTS

Characteristics of the study subjects and outcomes of MTX treatment. The study included 32 DMARD-naive patients with recent-onset RA. After 6 months of MTX treatment, 15 patients (46.9%) were in remission or had low disease activity (DAS28-ESR score of ≤3.2) (MTX responders), while in 17 patients (53.1%), moderate-to-high disease activity (a DAS28-ESR score of >3.2) persisted (nonresponders). The mean age and distribution of sex were similar between the 2 groups, and no significant differences were observed in the baseline disease activity level (DAS28-ESR score), CRP level, ESR, ACPA/RF serostatus, or symptom duration prior to the initiation of DMARD therapy (Table 1). After 6 months of MTX treatment, responder RA patients had significantly reduced DAS28-ESR scores (mean ± SEM DAS28-ESR 5.4 ± 0.3 at baseline and 2.1 ± 0.2 after 6 months; $P < 0.05$ versus baseline) and significantly reduced levels of inflammation markers ($P < 0.05$ versus baseline), and 12 of 15 responders had no swollen joints. In nonresponders, there were no significant reductions in disease activity levels (DAS-28-ESR score 5.9 ± 0.3 at baseline and 4.8 ± 0.3 after 6 months), in the levels of inflammation markers, or in the number of swollen joints from baseline to 6 months of MTX treatment.

Distinct CD4+ T cell, CD8+ T cell, and CD4+ Treg cell immunophenotypes associated with RA. PBMCs from all patients at baseline and at 6 months of MTX treatment (n = 32) and from all healthy participants (n = 18) were enumerated by flow cytometry. Table 2 shows the differences between the groups in the frequencies of selected populations of CD4+ T cells, CD8+ T cells, and CD4+ Treg cells, along with the proportions of cells expressing effector molecules associated with immune cell function. Compared to healthy donors, RA patients had a higher frequency of CD4+ T cells and lower frequency of CD8+ T cells.

CD4+ and CD8+ T cells were further subdivided into subsets of naive T cells and memory-activated T cells (combination of central memory [CM], effector memory [EM], EM re-expressing CD45RA [TEMRA], and effector T cells) on the basis of expression of CD45RA and CCR7. There were no significant differences in the circulating frequencies of memory-activated CD4+ T cells expressing inflammatory cytokines (IFNγ, IL-13, or IL-17), immune checkpoint molecules (programmed death 1 [PD-1], T cell immunoglobulin and mucin domain–containing protein 3 [TIM-3]), or CTLA-4), or HLA–DR. In contrast, among memory-activated CD8+ T cells, the frequency of IFNγ+ cells was lower in RA patients compared to healthy controls, and the frequency of IL-13+ cells was more than twice as high in RA patients compared to healthy controls (each $P < 0.05$ versus controls). The proportions of naive and memory CD4+ Treg cells that were single positive for CD39, ICOS, or lymphocyte activation gene

Table 1. Characteristics of the participants at study entry*

	Healthy controls (n = 18)	RA MTX responders (n = 15)	RA MTX nonresponders (n = 17)
Age, mean ± SD years	47.8 ± 12.7	56.1 ± 12.7	56.8 ± 11.8
Sex, no. female/male	10/8	10/5	11/6
CRP, median (IQR) mg/liter	–	8.6 (5.0–19.2)	13.0 (3.0–25.8)
ESR, median (IQR) mm/hour	–	24.0 (10.5–35.5)	38.0 (12.0–46.0)
DAS28-ESR, median (IQR)	–	5.3 (4.8–6.2)	5.8 (5.1–6.6)
ACPA, no. positive/negative	–	10/5	11/6
RF, no. positive/negative	–	9/6	10/7
Symptom duration, median (IQR) months	–	3.5 (2.5–13.0)	5.5 (4.0–16.0)

* RA = rheumatoid arthritis; MTX = methotrexate; CRP = C-reactive protein; IQR = interquartile range; ESR = erythrocyte sedimentation rate; DAS28-ESR = Disease Activity Score in 28 joints using the ESR; ACPA = anti–citrullinated protein antibody; RF = rheumatoid factor.

Table 2. Frequencies of the CD4+ T cell, CD8+ T cell, and CD4+ Treg cell subsets in the peripheral blood of healthy controls and RA patients at baseline and after 6 months of MTX treatment*

	Healthy controls (n = 18)	Patients with RA	
		At baseline	After 6 months of MTX
CD4	64.2 ± 3.1	73.8 ± 2.0†	74.5 ± 2.2†
Naive	36.4 ± 3.0	30.6 ± 2.5	33.2 ± 2.7
Memory-activated	49.3 ± 3.1	54.1 ± 3.2	52.7 ± 3.4
Th1 (IFNγ)	28.0 ± 2.3	28.6 ± 1.8	27.5 ± 1.5
Th2 (IL-13)	3.9 ± 0.3	5.0 ± 0.4	4.5 ± 0.3
Th17 (IL-17)	2.3 ± 0.2	2.0 ± 0.2	2.1 ± 0.2
CTLA-4	35.9 ± 2.3	32.0 ± 2.1	30.5 ± 2.5
PD-1	44.6 ± 1.9	44.5 ± 1.8	42.8 ± 1.8
TIM-3	1.1 ± 0.1	1.7 ± 0.2	1.6 ± 0.2
HLA–DR	6.5 ± 0.9	6.3 ± 0.7	3.3 ± 0.5†‡
CD8	27.0 ± 2.6	20.2 ± 1.8†	19.4 ± 1.8†
Naive	32.7 ± 5.3	19.8 ± 3.1	22.2 ± 3.1
Memory-activated	56.3 ± 5.7	64.2 ± 3.4	62.7 ± 3.4
Tc1 (IFNγ)	72.8 ± 3.4	60.4 ± 3.5†	58.0 ± 3.3†
Tc2 (IL-13)	3.6 ± 1.0	7.6 ± 1.1†	7.8 ± 1.1†
Tc17 (IL-17)	0.4 ± 0.1	0.4 ± 0.1	0.4 ± 0.1
CTLA-4	5.9 ± 1.1	6.7 ± 0.9	5.1 ± 0.7
PD-1	48.1 ± 3.2	41.6 ± 2.8	38.4 ± 3.2
TIM-3	1.0 ± 0.2	1.5 ± 0.3	1.4 ± 0.3
HLA–DR	4.3 ± 0.5	4.9 ± 0.6	2.4 ± 0.4†‡
CD4 Treg	4.4 ± 0.3	4.8 ± 0.3	4.3 ± 0.2
Naive	27.7 ± 2.1	27.0 ± 2.1	34.6 ± 2.3‡
CD39	7.6 ± 1.6	14.5 ± 2.0†	13.6 ± 1.8†
CD73	9.7 ± 1.3	10.1 ± 1.1	10.2 ± 1.1
Helios	88.7 ± 1.4	85.6 ± 1.1	85.6 ± 1.1
ICOS	0.9 ± 0.1	1.6 ± 0.2†	1.2 ± 0.1
LAG-3	0.5 ± 0.1	0.8 ± 0.1†	0.7 ± 0.1
CCR4	15.7 ± 1.6	22.6 ± 2.0	20.9 ± 1.9
Memory	65.6 ± 2.4	65.6 ± 2.3	56.7 ± 2.5†‡
CD39	47.6 ± 5.6	62.9 ± 3.4†	58.0 ± 3.4
CD73	6.5 ± 0.9	5.4 ± 0.6	6.5 ± 0.6
Helios	82.5 ± 0.9	82.8 ± 1.0	81.2 ± 1.1
ICOS	8.0 ± 0.6	11.6 ± 1.0†	10.2 ± 0.8
LAG-3	1.0 ± 0.1	1.8 ± 0.2†	1.6 ± 0.2
CCR4	92.4 ± 1.2	92.8 ± 0.9	90.4 ± 0.7

* Values are the mean ± SEM. MTX = methotrexate; IFNγ = interferon-γ; IL-13 = interleukin-13; PD-1 = programmed death 1; TIM-3 = T cell immunoglobulin and mucin domain–containing protein 3; ICOS = inducible costimulator; LAG-3 = lymphocyte activation gene 3 protein.
† $P < 0.05$ versus healthy controls.
‡ $P < 0.05$ versus rheumatoid arthritis (RA) patients at baseline.

3 protein (LAG-3) were significantly higher in RA patients compared to healthy controls. Following 6 months of MTX therapy, RA patients exhibited higher frequencies of naive CD4+ Treg cells and lower frequencies of memory CD4+ Treg cells, and also exhibited lower frequency of HLA–DR expression among memory CD4+ and CD8+ T cells.

Distinguishing MTX responders from nonresponders on the basis of skewed ratios of CD4+ to CD8+ T cells. We next examined whether the frequencies of T cell subsets at baseline and at 6 months of MTX treatment in patients with RA could help distinguish MTX responders from nonresponders. No differences in the frequency of CD3+ T cells, either at baseline or at 6 months, were observed between MTX responders and nonresponders (Figure 1A). However, MTX responders had an increased frequency of CD4+ T cells and decreased frequency of CD8+ T cells at both baseline and 6 months, as compared to nonresponders (Figure 1B).

Skewed frequencies of CD4+ and CD8+ T cells translated to a pronounced shift in the CD4:CD8 T cell ratio in MTX responders compared to nonresponders at baseline and at 6 months (Figure 1C). Indeed, the baseline CD4:CD8 T cell ratio in MTX responders was significantly higher than that in nonresponders (mean ± SEM 5.5 ± 0.5 versus 3.7 ± 0.5), with the ratio in nonresponders being similar to that observed in healthy donors (3.0 ± 0.4). Across all RA patients, the CD4:CD8 T cell ratios at baseline correlated positively with the absolute change in disease activity (ΔDAS28-ESR) following MTX treatment (Figure 1D).

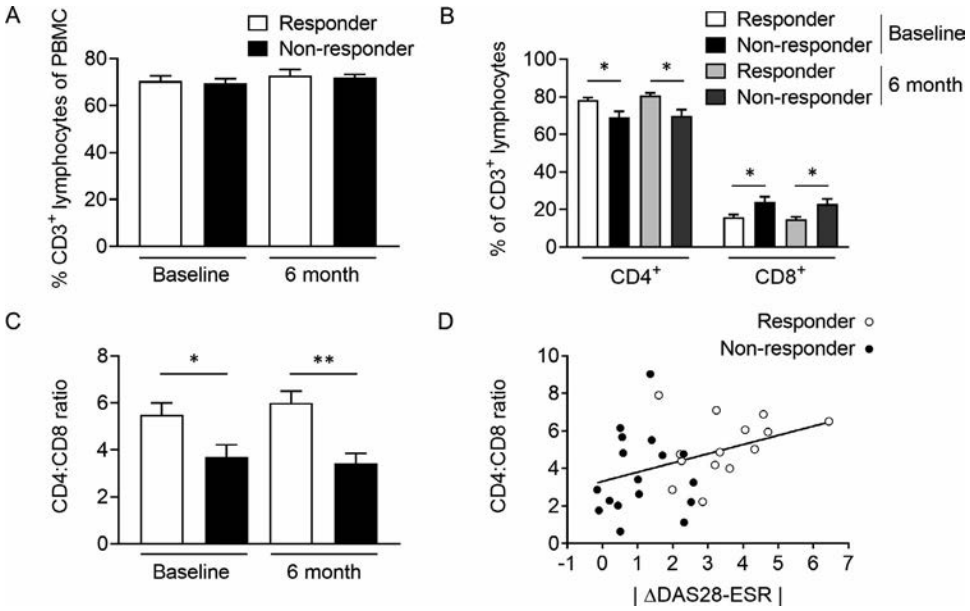

Figure 1. Increased CD4+ and CD8+ T cell frequencies and skewed CD4+:CD8+ T cell ratios in rheumatoid arthritis (RA) patients classified as methotrexate (MTX) responders. **A–C**, Frequency of CD3+ lymphocytes among peripheral blood mononuclear cells (PBMCs) (**A**), frequency of CD4+ and CD8+ cells among CD3+ lymphocytes (**B**), and the CD4:CD8 T cell ratio (**C**) in the blood of MTX responder and nonresponder RA patients at baseline and after 6 months of MTX treatment. Data are the mean ± SEM of 15–17 individuals per group. **D**, Pearson's correlation and linear regression analyses to assess correlations between the CD4:CD8 T cell ratio measured at baseline and the absolute change in disease activity according to absolute change in the Disease Activity Score in 28 joints using the erythrocyte sedimentation rate (ΔDAS28-ESR) from baseline to 6 months following initiation of MTX therapy in RA patients (r = 0.3856; $P = 0.0322$). * = $P < 0.05$; ** = $P < 0.01$ by one-way analysis of variance with Bonferroni's post hoc correction for multiple comparisons.

Higher ICOS+ Treg cell frequencies in MTX nonresponder RA patients. Having identified an increased CD4+ T cell frequency in MTX-responsive RA patients, the characteristics of the CD4+ T cell subpopulations were determined, focusing first on total Treg cells, identified as CD3+CD4+CD25+CD127–FoxP3+ cells (Figure 2A). MTX responders and nonresponders had similar frequencies of Treg cells at baseline and post–MTX therapy (Figure 2B), closely matching those observed in healthy controls (Table 2).

Increased levels of intracellular and extracellular adenosine, which is dependent on the presence of CD39+ and CD73+ cells, represents a potential mechanism of action of MTX in RA (11). No significant differences in the frequencies of CD39+ or CD73+ cells were observed between MTX responders and nonresponders (Figures 2C and D). However, compared to baseline, the 6-month samples from RA patients exhibited decreased frequencies of CD39+ cells and increased frequencies of CD73+ cells.

The frequencies of CD4+ Treg cells expressing the immune checkpoint inhibitor LAG-3 were low and not significantly different between the responder and nonresponder patient groups (Figure 2E). In contrast, the proportion of Treg cells expressing the costimulatory receptor ICOS was significantly greater in MTX nonresponders compared to responders, both at baseline and at 6 months (Figure 2F). In addition, both groups showed a significant decline in the proportion of ICOS+ Treg cells following MTX treatment.

Frequencies of Helios+ and CCR4+ Treg cells were not significantly different between MTX responders and nonresponders. However, CCR4+ cell frequencies were significantly reduced at 6 months compared to baseline (Figures 2G and H).

Similar proportions of T cells expressing immune checkpoint inhibitors and activation markers in MTX responders and nonresponders. T cell activation through T cell receptor–dependent signaling and the resulting proliferative and cytokine responses important for disease pathogenesis can be regulated by ligation of immune checkpoint inhibitors such as CTLA-4, PD-1, and TIM-3 (15). We therefore performed in vitro activation of PBMCs using PMA/ionomycin to assess T cell intracellular cytokine profiles and also to monitor immune checkpoint phenotypes in the presence or absence of T cell activation. Although the frequencies of PD-1+ and HLA–DR+ cells decreased and frequencies of TIM-3+ and CTLA-4+ cells increased after activation of total PBMCs from RA patients, importantly, no differences in the frequencies of cells expressing CTLA-4, PD-1, TIM-3, or HLA–DR at baseline, in the absence of stimulation, were observed between MTX responders and nonresponders (details available from the corresponding author upon request).

We next assessed whether T cell subsets from MTX responders and nonresponders differed in the proportions of cells expressing CTLA-4, PD-1, TIM-3, or HLA–DR pre- or post-MTX. PBMCs were activated in vitro, and CD4+ and CD8+ T cells were identified

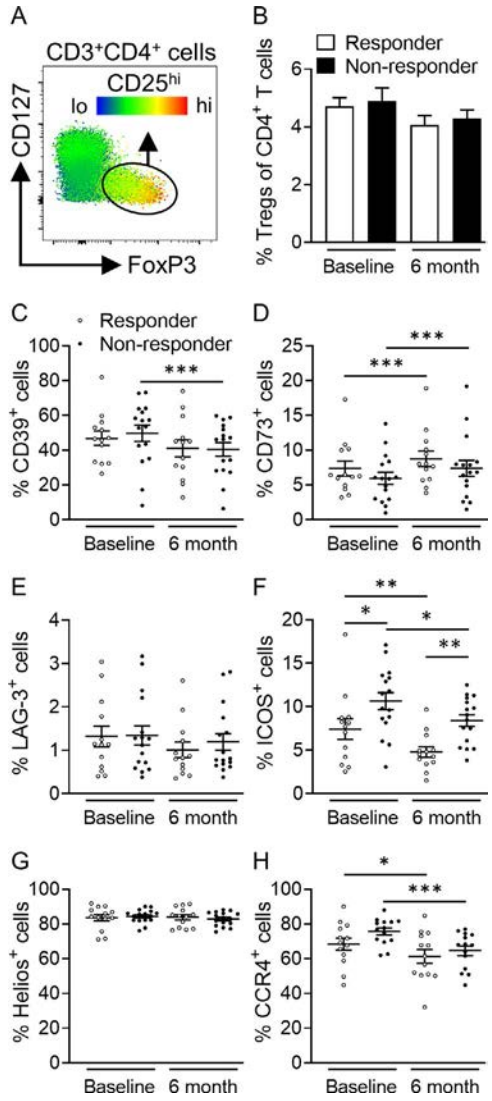

Figure 2. Increased frequency of activated inducible costimulator–positive (ICOS+) CD4+ Treg cells in the blood of MTX nonresponder RA patients. **A**, Representative flow cytometry plots showing expression of CD127 and FoxP3 on gated CD3+CD4+ lymphocytes. Subsequent gating of $CD25^{high}$ cells identified $CD4+CD25^{high}CD127–$ FoxP3+ Treg cells. **B**, Frequency of Treg cells among blood CD4+ T cells from responder and nonresponder patients at baseline and after 6 months of MTX treatment. Data are the mean ± SEM of 13–16 individuals per group. **C–H**, Frequencies of blood Treg cells expressing CD39 (**C**), CD73 (**D**), lymphocyte activation gene 3 protein (LAG-3) (**E**), ICOS (**F**), Helios (**G**), and CCR4 (**H**) in MTX responder and nonresponder RA patients at baseline and after 6 months of MTX treatment. Symbols represent individual subjects; horizontal lines with bars show the mean ± SEM (n = 13–16 individuals per group). * = $P < 0.05$; ** = $P < 0.01$; *** = $P < 0.001$. For responders versus nonresponders, data were compared by one-way analysis of variance with Bonferroni's post hoc correction for multiple comparisons in **C**, **G**, and **H** or by Kruskal-Wallis test with Dunn's post hoc correction in **B**, **D**, **E**, and **F**. For baseline versus 6 months, data were compared by paired *t*-test in **C**, **G**, and **H** or by Wilcoxon's paired signed rank test in **B**, **D**, **E**, and **F**. See Figure 1 for other definitions.

as being either effector, EM, CM, TEMRA, or CXCR5+ T follicular helper or cytotoxic T cells for further analysis. MTX responders and nonresponders did not differ in the frequencies of CTLA-4+, PD-1+, TIM-3+, or HLA–DR+ T cells (Figures 3A–D). Moreover, following 6 months of MTX treatment, reduced HLA–DR+ T cell frequencies, as compared to baseline, were observed across all cell subsets, both in responders and in nonresponders.

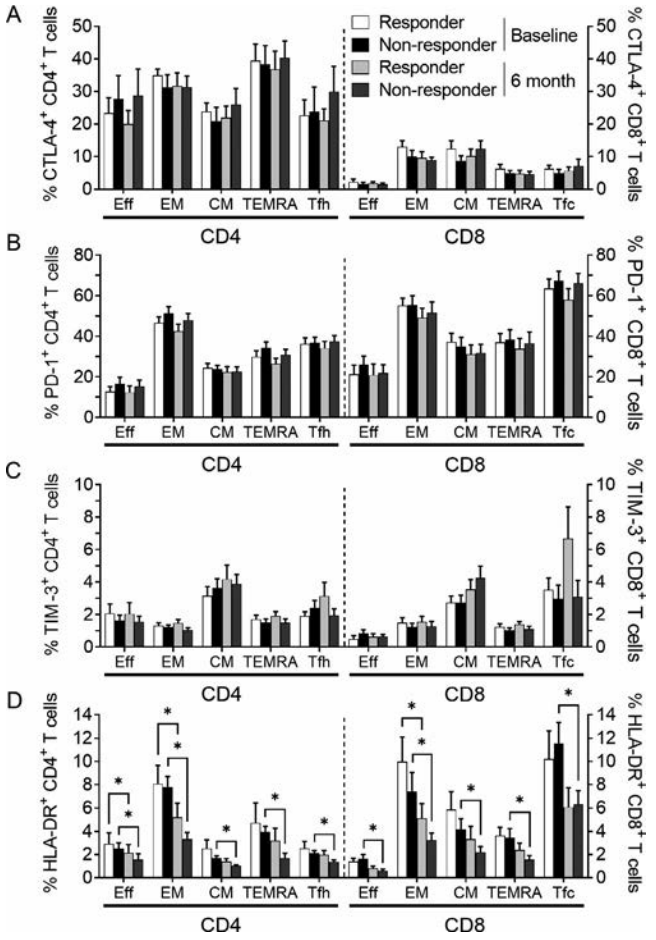

Figure 3. Lack of difference in the levels of inhibitory checkpoint molecules and HLA–DR between MTX responder and nonresponder RA patients. The frequency of cells positive for CTLA-4 (**A**), programmed death 1 (PD-1) (**B**), T cell immunoglobulin and mucin domain–containing protein 3 (TIM-3) (**C**), and HLA–DR (**D**) among blood CD4+ (left) and CD8+ (right) T cell subsets differentiated on the basis of CD45RA and CCR7 expression, comprising the subsets of effector (Eff) cells (CD45RA+CCR7–), effector memory (EM) cells (CD45RA–CCR7–), central memory (CM) cells (CD45RA–CCR7+), effector memory T cells re-expressing CD45RA (TEMRA) ($CD45RA^{low}CCR7–$), or CXCR5+ T follicular helper/cytotoxic (Tfh/Tfc) cells, was determined in MTX responder and nonresponder RA patients at baseline and after 6 months of MTX treatment. Data are the mean ± SEM of 14–15 individuals per group. * = $P < 0.05$ by Kruskal-Wallis test with Dunn's post hoc correction for multiple comparisons for responders versus nonresponders, and by Wilcoxon's paired signed rank test for baseline versus 6 months. See Figure 1 for other definitions.

Increased Th2-polarized T cell frequencies in MTX nonresponder RA patients. IFNγ, IL-13, and IL-17 cytokines are related to Th1-, Th2-, and Th17-type responses, respectively, and each cytokine induces proinflammatory effects through unique mechanisms. Among total CD3+ T lymphocytes, EM cells (CD45RA–CCR7–) and naive cells (CD45RA+CCR7+) constitute the major subsets, with minor proportions of TEMRA, CM, and effector cell subsets (Figure 4A). However, the majority of T cells that produce IFNγ, IL-13, and IL-17 are within the EM subset, and therefore we focused on the frequencies of cytokine-producing Tem cells. MTX responders and healthy control subjects exhibited similar baseline levels of IL-13+CD4+ Tem cells (mean ± SEM

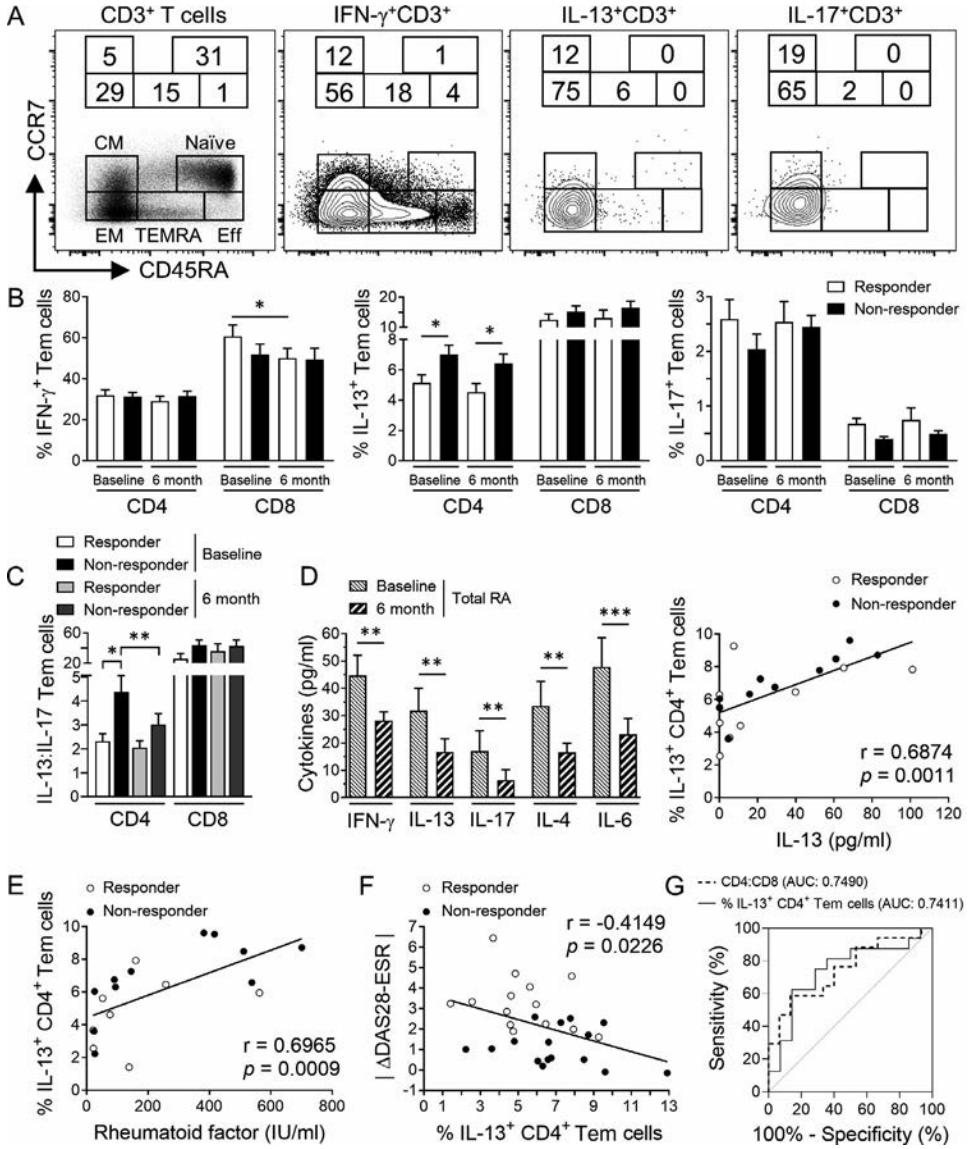

Figure 4. Increased frequency of Th2-polarized interleukin-13–positive (IL-13+) CD4+ effector memory T (Tem) cells in MTX nonresponders and its association with plasma rheumatoid factor (RF) titers and change in the DAS28-ESR. **A**, Representative flow cytometry plots showing the distribution of CCR7 and CD45RA within total gated CD3+ cells as well as interferon-γ–positive (IFNγ+), IL-13+, and IL-17+ gated CD3+ cells. Minor proportions of cell subsets included central memory (CM), effector memory (EM), EM T cells re-expressing CD45RA (TEMRA), and effector (eff) cells. Values represent the percentage of cells within each region. **B** and **C,** Frequencies of IFNγ+, IL-13+, and IL-17+ Tem cells (**B**) and the IL-13+:IL-17+ Tem cell ratio (**C**) among CD4+ and CD8+ Tem cells in MTX responders and nonresponders at baseline and after 6 months of MTX treatment. **D**, Plasma cytokine levels in RA patients at baseline and after 6 months of MTX treatment (left), and Pearson's correlation and linear regression analyses of baseline IL-13+CD4+ Tem cell frequency and plasma IL-13 levels (right). **E**, Spearman's correlation between baseline frequency of IL-13+CD4+ Tem cells and plasma RF levels among RA patients with measurable RF. **F**, Pearson's correlation between baseline frequency of IL-13+CD4+ Tem cells and change in the DAS28-ESR following MTX therapy. **G**, Receiver operating characteristic (ROC) curves showing area under the ROC curve (AUC) for baseline CD4:CD8 T cell ratio and IL-13+CD4+ Tem cell frequency applied to distinguish MTX responders from nonresponders. Data in **B–D** are the mean ± SEM of 14–16 samples per group. * = $P < 0.05$; ** = $P < 0.01$; *** = $P < 0.001$. For responders versus nonresponders, data were compared by one-way analysis of variance with Bonferroni's post hoc correction for multiple comparisons. For baseline versus 6 months, data were compared by paired *t*-test in **B** and **C** or by Wilcoxon's paired signed rank test in **D**. See Figure 1 for other definitions.

5.1 ± 0.5% and 5.1 ± 0.4%, respectively), but nonresponders had significantly higher levels of IL-13+CD4+ Tem cells compared to responders both at baseline (7.0 ± 0.6%) and at 6 months ($P < 0.05$) (Figure 4B). In relation to the proportion of IL-17+CD4+ Tem cells, this translated to a significant difference of 1.9-fold in the ratio of IL-13+:IL-17+ CD4+ Tem cells at baseline in RA patients who were subsequent MTX responders compared to those who were nonresponders ($P < 0.05$) (Figure 4C).

Plasma cytokine levels of IFNγ, IL-13, IL-17, IL-4, and IL-6 were significantly reduced after 6 months of MTX treatment in RA patients (Figure 4D). These declines in cytokine levels were apparent in both MTX responders and nonresponders (data not shown). Despite these reductions, plasma cytokine levels measured at 6 months after MTX therapy in nonresponders (e.g., for IL-13, mean ± SEM 37.3 ± 10.8 pg/ml at baseline and 25.7 ± 8.8 pg/ml after 6 months; $P < 0.05$) were often as high as those measured at baseline in MTX responders (for IL-13, 26.3 ± 9.4 pg/ml at baseline and 12.2 ± 5.1 pg/ml after 6 months; $P < 0.05$). Although the plasma levels of IL-13 were not significantly different between MTX responders and nonresponders, they were positively correlated with the frequency of IL-13+CD4+ Tem cells (Figure 4D). No correlation was observed between the frequencies of IFNγ- or IL-17–producing T cells and plasma levels of these cytokines (data not shown).

Furthermore, the frequencies of IL-13+CD4+ Tem cells at baseline positively correlated with the plasma levels of RF in patients with detectable RF at baseline (Figure 4E) and were negatively correlated with the absolute change in disease activity (ΔDAS28-ESR) following MTX treatment (Figure 4F).

To assess the discriminative power of the baseline measures of IL-13+CD4+ Tem cell frequency and CD4:CD8 T cell ratio for distinguishing MTX responders from nonresponders, we examined the AUC in ROC curves. The frequency of IL-13+CD4+ Tem cells and the CD4:CD8 T cell ratio had AUCs of 0.7411 ($P = 0.0248$) and 0.7490 ($P = 0.0165$), respectively (Figure 4G). Based on the coordinates of the ROC curves, we determined optimal cutoffs for these values in distinguishing MTX responders from nonresponders. The optimal cutoff value for the IL-13+CD4+ Tem cell frequency was determined to be 5.95%, and the optimal cutoff value for the CD4:CD8 T cell ratio was determined to be 3.70. These cutoff values for the IL-13+CD4+ Tem cell frequency and CD4:CD8 T cell ratio were associated with good sensitivity (0.750 and 0.588, respectively) and good positive predictive values (0.750 and 0.833, respectively), while the specificities of these measures were 0.714 and 0.867, respectively, and the negative predictive values were 0.714 and 0.650, respectively.

DISCUSSION

The diversity of patient responses to conventional DMARDs (e.g., MTX) and to highly targeted biologic agents suggests that RA has a heterogeneous pathogenesis with a common clinical presentation (16). Various factors, including indicators of disease activity/inflammation (DAS28, CRP level, and ESR), autoantibody serostatus (RF and ACPA seropositivity), and disease duration, have been evaluated as potential predictors of response to MTX (17). Beyond these, genetic and gene expression studies have revealed a number of associations with responsiveness to MTX (3,18,19). However, despite recognition of some promising correlates, to date, most prognostic factors lack consistency as predictors of MTX responsiveness. We observed no significant associations with MTX response or nonresponse for any of the demographic, clinical, or routine laboratory variables assessed (as listed in Table 1). While this may be partly attributable to the small sample size in our study, clinical and routine laboratory features are poorly predictive of MTX efficacy (20).

Early effective therapy prevents long-term joint damage and disability in RA (4), emphasizing the importance of reliably identifying patients unlikely to respond to MTX who should be offered alternative therapies. The current study examined whether blood T cell phenotyping could uncover immunologic dysregulation in DMARD-naive RA patients and identify unique immune profiles associated with MTX responders and nonresponders. Our significant findings of a higher IL-13+CD4+ Tem cell frequency, lower CD4:CD8 T cell ratio, and higher ICOS+ Treg cell frequency highlight the distinct immunologic phenotypes associated with MTX nonresponse in RA patients. The baseline CD4:CD8 T cell ratio and IL-13+CD4+ Tem cell frequency were each associated with the change in disease activity resulting from MTX therapy. The discriminative power of these novel individual biomarker features, as determined on the basis of ROC AUCs, were fair-to-good as predictors of MTX responsiveness.

Among the observed immunologic perturbations associated with MTX response, the elevated CD4:CD8 T cell ratio among MTX responders was intriguing, particularly because of its ease of adoption as a prognostic test. To the best of our knowledge, this study is the first to show that the phenotype of subsequent MTX responders was characterized by an elevated CD4:CD8 T cell ratio at baseline. The high CD4:CD8 T cell ratio in the blood of RA patients relative to healthy controls (Table 2) is consistent with published findings from some studies (21), but not others (22,23). It is possible that CD4+ and CD8+ T cells may play distinct roles in MTX responders as compared to nonresponders. Alternatively, a lower CD4:CD8 T cell ratio may be an indirect measure of differential recruitment of CD4+ and CD8+ T cells to the inflamed joints in nonresponders. In RA patients, CD4+ T cells are retained in the synovium, while CD8+ T cells accumulate in the synovial fluid (24). Notably, in RA patients who receive lymphodepletion as treatment, disease remission was associated with a high baseline presence and subsequent reduction in the proportion of synovial CD4+ T cells, whereas relapse correlated with the return of CD4+ T cells, but not CD8+ T cells, B cells, or macrophages, to the synovium (25). Determination of the CD4:CD8 T cell ratio could be easily

adopted as a routine prognostic test if validated in a larger study group.

Quantitative and/or qualitative deficiencies of Treg cells in the peripheral blood of RA patients have been suggested as partial explanations for the pathogenesis in RA. Some studies have shown that patients have significantly reduced blood levels of Treg cells (22,23), whereas our results, and those from another study (26), show no difference in the circulating frequency of Treg cells in RA patients compared to healthy controls. Reports on functional capacity among circulating or joint-derived Treg cells are similarly controversial (27). Evidence suggests that mechanisms of MTX activity, MTX resistance, and Treg cell function in RA may be linked (28). Failure of MTX treatment in RA has been associated with low surface expression of CD39, impaired adenosine production, and reduced suppressive activity of Treg cells in MTX nonresponders compared to responders and healthy controls (29). In contrast, we observed significantly higher frequencies of CD39+ naive and memory Treg cells in RA patients. Moreover, similar to the findings in a study by Peres et al (29), we found no differences in Treg cell frequency or baseline frequency of CD39+ or CD73+ Treg cells between MTX responders and nonresponders. Consistent with the recent findings from a study by Wang et al (30), we observed significantly higher frequencies of ICOS+ Treg cells in RA patients compared to healthy controls. The frequency of ICOS+ Treg cells was higher in MTX nonresponders compared to responders, which may have biologic relevance to the outcome of MTX therapy in RA patients. Indeed, ICOS+ Treg cells from RA patients with inactive disease were characterized by their expression of antiinflammatory cytokines, such as IL-10, whereas in patients with active RA, ICOS+ Treg cells expressed more IL-17 (30). Taken together with our results, these findings suggest that ICOS+ Treg cells may have variable roles in the pathogenesis of RA depending on the level of disease activity, and thus further investigation is warranted.

Total CD4+ and CD8+ T cells are often the populations of interest for phenotypic and functional studies. While we and other investigators (26,31) observed no significant differences in the proportions of circulating naive and memory CD4+ and CD8+ T cell subsets, a trend toward fewer naive T cells and increased proportions of memory T cell subsets was observed in RA patients relative to healthy controls. Since naive T cells express very low levels of immune checkpoint inhibitors and cytokines, we focused our analyses on memory and effector cell subsets to avoid potential overlap of differences in subset frequencies and cell phenotypes. Inhibitory receptor pathways, including those mediated by CTLA-4, PD-1, and TIM-3, which negatively regulate T cell activation and function, contribute to favorable long-term outcomes and protect against relapse in multiple autoimmune diseases (32). We found no differences in the frequencies of inhibitory receptor–expressing CD4+ or CD8+ T cell subsets in MTX responders compared to nonresponders. PD-1+ T cells from RA patients appear resistant to PD-1–mediated inhibition (33,34), raising an interesting possibility that, despite similar frequencies of inhibitory receptor–positive cells, T cells from MTX responders and nonresponders may differ in their sensitivity to inhibitory receptor ligation.

RA joint–derived T cell cytokine profiling reveals the presence of CD4+ T cells skewed toward Th1 and Th17 cell lineages (7,35,36). Production of IL-4 and IL-13 and Th2-polarized T cells are not increased in the synovium compared to the blood of RA patients (35). However, activation of blood T cells reveals higher levels of IL-4 and lower levels of IFNγ in RA patients, and when naive CD4+ T cells are cultured under Th2-polarizing conditions, an increased propensity of the T cells to polarize toward Th2 phenotypes has been observed in RA patients compared to healthy controls (37,38). We show that the increased IL-13+ T cell population in the blood of RA patients was attributable to the MTX nonresponder group. Whether the increase in this T cell population results from an expansion of cells or represents a functionally distinct subset in the context of MTX-nonresponsive RA remains to be determined.

In vitro inhibition of T cell cytokine production by MTX has been demonstrated for a range of cytokines, including IFNγ, IL-4, IL-13, and IL-17 (39,40), possibly through an inhibitory effect on NF-κB signaling (41). However, the in vivo effects of MTX are less clear. Generally, plasma cytokine levels were reduced in our RA patients following MTX treatment. On a cellular level, except for a reduction of IFNγ-producing CD8+ T cells in MTX responders, we observed no effect of MTX on the proportions of cytokine-producing T cell subsets irrespective of treatment outcome (Figure 4B). Consistent with our observations, others have shown that MTX-induced changes in disease activity are not reflected in reductions in inflammatory cytokine production by circulating T cells (42,43). Nevertheless, earlier studies demonstrated significant reductions in the frequencies of IL-17+, but not IFNγ+, CD4+ T cells following MTX therapy as compared to baseline (44,45). The reasons for the different observations are not readily apparent. Furthermore, evidence is lacking on the specific mechanisms through which MTX may modify T cell cytokine networks in RA. Our present study is the only study to examine MTX responder and nonresponder cytokine responses specifically in potent cytokine-producing Tem cells, thereby eliminating potentially confounding contributions by fluctuating proportions of naive and memory T cell subsets over the course of treatment.

Herein we show that plasma levels of IL-13 were positively correlated with the frequency of IL-13+CD4+ Tem cells, suggesting that T cells are a major source of circulating IL-13 in RA. CD4+ T cell help to B cells represents an important axis of autoimmunity in ACPA/RF seropositive patients. Interestingly, RF-positive patients, regardless of ACPA status, have significantly higher baseline disease activity compared with RF-negative patients (46). Consistent with this, RF and ACPAs have an additive effect on bone erosion (both the number and size of the erosions), with the RF titer positively influencing erosion size in ACPA-positive patients (47). Human blood Th2 cells have been shown to

support B cell differentiation and immunoglobulin secretion (48). Therefore, the positive association of IL-13+CD4+ Tem cells with plasma RF levels, and negative association with change in disease activity post-MTX, suggests that the frequency of blood IL-13+CD4+ T cells may be indicative of a bias toward more erosive, MTX-resistant RA. Indeed, stratifying patients with early RA by baseline disease activity revealed significantly higher IL-13 serum concentrations in patients with more active disease compared to those with less active disease (49). Taken together, the data from our study and others suggest that Th2 pathways are important in RA. Furthermore, patients who are nonresponsive to MTX may form a distinct subset with an increased type 2–polarized immune response and perhaps a different disease mechanism.

Understanding how these differences in blood immune cell phenotypes translate to changes in the RA synovium presents a greater challenge. Recently, profiling paired synovial biopsy samples from patients with early RA before and after 6 months of combination therapy (MTX with sulfasalazine and hydroxychloroquine) by total RNA sequencing revealed that only a small fraction of the genes whose expression was initially increased in early RA were down-regulated by this therapy (146 of 2,398 genes), even in patients who achieved low disease activity (50). Interestingly, those genes that were down-regulated by the combination treatment and that were associated with clinical response included many genes known to be involved in T cell activation (*ZAP70*/*LCK*/*PRKCQ*) and polarization toward Th2 (*GATA3*), but not Th1 (*TBX21*) or Th17 (*RORC*). More studies are warranted to better understand the association between, and elucidate the mechanisms underlying, type 2 immune pathways and MTX nonresponsiveness in RA patients.

The limitations of this study include that the study assessed only a small sample of treatment-naive patients with early-inception RA. Moreover, we studied PBMCs without paired synovial fluid samples, as synovial fluid is not frequently available in this population. This was an exploratory study designed to test both general and some specific hypotheses, and therefore adjustments for multiple comparisons were employed based on the hypothesis being tested. A larger study is required to replicate these findings and to determine the potential added value of combining T cell subset data with clinical and routine laboratory variables of disease for predicting MTX responsiveness. Furthermore, combining data from PBMCs and data from paired synovial fluid samples may provide interesting insights that could help to resolve the immune-mediated mechanisms of MTX nonresponse.

In our study, elevated frequencies of blood IL-13+CD4+ Tem cells and a lower CD4:CD8 T cell ratio are among the distinct immunologic phenotypes associated with MTX nonresponse in RA patients. Immunologic phenotypes are convenient, noninvasive tests that could be utilized to potentially identify RA patients who are unlikely to have substantial responses to MTX-based therapy. However, validation of these findings in larger cohorts is necessary to support their clinical utility. In our study, these features each individually outperformed traditional clinical and laboratory variables as baseline predictors of MTX responsiveness. The present study advances our understanding of the immune dysregulation in RA and provides support for an immunologic approach to identify RA patients with a high risk of nonresponse to MTX therapy. Additionally, targeting the IL-13+CD4+ T cell pathway could be a new therapeutic strategy in MTX-resistant RA patients.

ACKNOWLEDGMENTS

We gratefully acknowledge the following staff rheumatologists for their support in recruiting patients to the study: Dr. Souad Shatshat, Dr. Elana Murphy, Dr. Trudy Taylor, Dr. Volodko Bakowsky, Dr. Jill Wong, Dr. Emily Shaw, Dr. Evelyn Sutton, Dr. Juris Lazovskis, and Dr. Janet Roberts. We also thank participating patients from the Rheumatology Clinic at the Queen Elizabeth II Health Sciences Centre and healthy control volunteers for donating samples, and Tatjana Brauer-Chapin and Maria Vaci for their excellent technical assistance.

AUTHOR CONTRIBUTIONS

All authors were involved in drafting the article or revising it critically for important intellectual content, and all authors approved the final version to be published. Drs. Hanly and Issekutz had full access to all of the data in the study and take responsibility for the integrity of the data and the accuracy of the data analysis.

Study conception and design. Slauenwhite, McAlpine, Hanly, Haidl, Marshall, Issekutz.

Acquisition of data. Slauenwhite, McAlpine, Hanly, Malik, Haidl, Marshall, Issekutz.

Analysis and interpretation of data. Slauenwhite, McAlpine, Hanly, Malik, Issekutz.

REFERENCES

1. Singh JA, Saag KG, Bridges SL Jr, Akl EA, Bannuru RR, Sullivan MC, et al. 2015 American College of Rheumatology guideline for the treatment of rheumatoid arthritis. Arthritis Rheumatol 2016;68:1–26.
2. Smolen JS, Landewé R, Bijlsma J, Burmester G, Chatzidionysiou K, Dougados M, et al. EULAR recommendations for the management of rheumatoid arthritis with synthetic and biological disease-modifying antirheumatic drugs: 2016 update. Ann Rheum Dis 2017;76:960–77.
3. Plant D, Maciejewski M, Smith S, Nair N, the Maximising Therapeutic Utility in Rheumatoid Arthritis Consortium, the RAMS Study Group, et al. Profiling of gene expression biomarkers as a classifier of methotrexate nonresponse in patients with rheumatoid arthritis. Arthritis Rheumatol 2019;71:678–84.
4. Farragher TM, Lunt M, Fu B, Bunn D, Symmons DP. Early treatment with, and time receiving, first disease-modifying antirheumatic drug predicts long-term function in patients with inflammatory polyarthritis. Ann Rheum Dis 2010;69:689–95.
5. Brennan FM, Smith NM, Owen S, Li C, Amjadi P, Green P, et al. Resting CD4+ effector memory T cells are precursors of bystander-activated effectors: a surrogate model of rheumatoid arthritis synovial T-cell function. Arthritis Res Ther 2008;10:R36.
6. Klimiuk PA, Yang H, Goronzy JJ, Weyand CM. Production of cytokines and metalloproteinases in rheumatoid synovitis is T cell dependent. Clin Immunol 1999;90:65–78.

7. Van Hamburg JP, Asmawidjaja PS, Davelaar N, Mus AM, Colin EM, Hazes JM, et al. Th17 cells, but not Th1 cells, from patients with early rheumatoid arthritis are potent inducers of matrix metalloproteinases and proinflammatory cytokines upon synovial fibroblast interaction, including autocrine interleukin-17A production. Arthritis Rheum 2011;63:73–83.
8. Tran CN, Lundy SK, White PT, Endres JL, Motyl CD, Gupta R, et al. Molecular interactions between T cells and fibroblast-like synoviocytes: role of membrane tumor necrosis factor-α on cytokine-activated T cells. Am J Pathol 2007;171:1588–98.
9. Herrath J, Müller M, Amoudruz P, Janson P, Michaëlsson J, Larsson PT, et al. The inflammatory milieu in the rheumatic joint reduces regulatory T-cell function. Eur J Immunol 2011;41:2279–90.
10. Wehrens EJ, Mijnheer G, Duurland CL, Klein M, Meerding J, van Loosdregt J, et al. Functional human regulatory T cells fail to control autoimmune inflammation due to PKB/c-akt hyperactivation in effector cells. Blood 2011;118:3538–48.
11. Yu MB, Firek A, Langridge WH. Predicting methotrexate resistance in rheumatoid arthritis patients [review]. Inflammopharmacology 2018;26:699–708.
12. Haskó G, Linden J, Cronstein B, Pacher P. Adenosine receptors: therapeutic aspects for inflammatory and immune diseases [review]. Nat Rev Drug Discov 2008;7:759–70.
13. Aletaha D, Neogi T, Silman AJ, Funovits J, Felson DT, Bingham CO, et al. 2010 rheumatoid arthritis classification criteria: an American College of Rheumatology/European League Against Rheumatism collaborative initiative. Arthritis Rheum 2010;62:2569–81.
14. Felson DT, Smolen JS, Wells G, Zhang B, van Tuyl LH, Funovits J, et al. American College of Rheumatology/European League Against Rheumatism provisional definition of remission in rheumatoid arthritis for clinical trials. Arthritis Rheum 2011;63:573–86.
15. Cox MA, Nechanitzky R, Mak TW. Check point inhibitors as therapies for infectious diseases [review]. Curr Opin Immunol 2017;48:61–7.
16. Ouboussad L, Burska AN, Melville A, Buch MH. Synovial tissue heterogeneity in rheumatoid arthritis and changes with biologic and targeted synthetic therapies to inform stratified therapy [review]. Front Med (Lausanne) 2019;6:45.
17. Romão VC, Canhão H, Fonseca JE. Old drugs, old problems: where do we stand in prediction of rheumatoid arthritis responsiveness to methotrexate and other synthetic DMARDs? [review]. BMC Med 2013;11:17.
18. Plant D, Wilson AG, Barton A. Genetic and epigenetic predictors of responsiveness to treatment in RA [review]. Nat Rev Rheumatol 2014;10:329–37.
19. Smith SL, Plant D, Eyre S, Barton A. The potential use of expression profiling: implications for predicting treatment response in rheumatoid arthritis [review]. Ann Rheum Dis 2013;72:1118–24.
20. Hider SL, Silman AJ, Thomson W, Lunt M, Bunn D, Symmons DP. Can clinical factors at presentation be used to predict outcome of treatment with methotrexate in patients with early inflammatory polyarthritis? Ann Rheum Dis 2009;68:57–62.
21. Hussein MR, Fathi NA, El-Din AM, Hassan HI, Abdullah F, Al-Hakeem E, et al. Alterations of the $CD4^+$, $CD8^+$ T cell subsets, interleukins-1β, IL-10, IL-17, tumor necrosis factor-α and soluble intercellular adhesion molecule-1 in rheumatoid arthritis and osteoarthritis: preliminary observations. Pathol Oncol Res 2008;14:321–8.
22. Zare HR, Habibagahi M, Vahdati A, Habibagahi Z. Patients with active rheumatoid arthritis have lower frequency of nTregs in peripheral blood. Iran J Immunol 2015;12:166–75.
23. Dulic S, Vásárhelyi Z, Sava F, Berta L, Szalay B, Toldi G, et al. T-cell subsets in rheumatoid arthritis patients on long-term anti-TNF or IL-6 receptor blocker therapy. Mediators Inflamm 2017;2017:6894374.
24. Haworth O, Hardie DL, Burman A, Rainger GE, Eksteen B, Adams DH, et al. A role for the integrin α6β1 in the differential distribution of CD4 and CD8 T-cell subsets within the rheumatoid synovium. Rheumatology (Oxford) 2008;47:1329–34.
25. Verburg RJ, Flierman R, Sont JK, Ponchel F, van Dreunen L, Levarht EW, et al. Outcome of intensive immunosuppression and autologous stem cell transplantation in patients with severe rheumatoid arthritis is associated with the composition of synovial T cell infiltration. Ann Rheum Dis 2005;64:1397–405.
26. Pandya JM, Lundell AC, Hallström M, Andersson K, Nordström I, Rudin A. Circulating T helper and T regulatory subsets in untreated early rheumatoid arthritis and healthy control subjects. J Leukoc Biol 2016;100:823–33.
27. Ponchel F, Vital E, Kingsbury SR, El-Sherbiny YM. $CD4^+$ T-cell subsets in rheumatoid arthritis. Int J Clin Rheumtol 2012;7:37–53.
28. Cribbs AP, Kennedy A, Penn H, Amjadi P, Green P, Read JE, et al. Methotrexate restores regulatory T cell function through demethylation of the FoxP3 upstream enhancer in patients with rheumatoid arthritis. Arthritis Rheumatol 2015;67:1182–92.
29. Peres RS, Liew FY, Talbot J, Carregaro V, Oliveira RD, Almeida SL, et al. Low expression of CD39 on regulatory T cells as a biomarker for resistance to methotrexate therapy in rheumatoid arthritis. Proc Natl Acad Sci U S A 2015;112:2509–14.
30. Wang HX, Kang X, Chu S, Li H, Li X, Yin X, et al. Dysregulated $ICOS^+$ proinflammatory and suppressive regulatory T cells in patients with rheumatoid arthritis. Exp Ther Med 2018;16:3728–34.
31. Fekete A, Soos L, Szekanecz Z, Szabo Z, Szodoray P, Barath S, et al. Disturbances in B- and T-cell homeostasis in rheumatoid arthritis: suggested relationships with antigen-driven immune responses. J Autoimmun 2007;29:154–63.
32. McKinney EF, Lee JC, Jayne DR, Lyons PA, Smith KG. T-cell exhaustion, co-stimulation and clinical outcome in autoimmunity and infection. Nature 2015;523:612–6.
33. Bommarito D, Hall C, Taams LS, Corrigall VM. Inflammatory cytokines compromise programmed cell death-1 (PD-1)-mediated T cell suppression in inflammatory arthritis through up-regulation of soluble PD-1. Clin Exp Immunol 2017;188:455–66.
34. Onofrio LI, Zacca ER, Ferrero P, Acosta C, Mussano E, Onetti L, et al. Inhibitory receptor expression on T cells as a marker of disease activity and target to regulate effector cellular responses in rheumatoid arthritis. Arthritis Rheumatol 2018;70:1429–39.
35. Morita Y, Yamamura M, Kawashima M, Harada S, Tsuji K, Shibuya K, et al. Flow cytometric single-cell analysis of cytokine production by CD4+ T cells in synovial tissue and peripheral blood from patients with rheumatoid arthritis. Arthritis Rheum 1998;41:1669–76.
36. Janson PC, Linton LB, Bergman EA, Marits P, Eberhardson M, Piehl F, et al. Profiling of CD4+ T cells with epigenetic immune lineage analysis. J Immunol 2011;186:92–102.
37. Haddad A, Bienvenu J, Miossec P. Increased production of a Th2 cytokine profile by activated whole blood cells from rheumatoid arthritis patients. J Clin Immunol 1998;18:399–403.
38. Van Roon JA, Glaudemans CA, Bijlsma JW, Lafeber FP. Differentiation of naive CD4+ T cells towards T helper 2 cells is not impaired in rheumatoid arthritis patients. Arthritis Res Ther 2003;5:R269–76.
39. Gerards AH, de Lathouder S, de Groot ER, Dijkmans BA, Aarden LA. Inhibition of cytokine production by methotrexate: studies in healthy volunteers and patients with rheumatoid arthritis. Rheumatology (Oxford) 2003;42:1189–96.
40. Guggino G, Giardina A, Ferrante A, Giardina G, Schinocca C, Sireci G, et al. The in vitro addition of methotrexate and/or methylprednisolone determines peripheral reduction in Th17 and expansion of conventional Treg and of IL-10 producing Th17

lymphocytes in patients with early rheumatoid arthritis. Rheumatol Int 2015;35:171–5.

41. Spurlock CF III, Gass HM IV, Bryant CJ, Wells BC, Olsen NJ, Aune TM. Methotrexate-mediated inhibition of nuclear factor κB activation by distinct pathways in T cells and fibroblast-like synoviocytes. Rheumatology (Oxford) 2015;54:178–87.
42. Buondonno I, Rovera G, Sassi F, Rigoni MM, Lomater C, Parisi S, et al. Vitamin D and immunomodulation in early rheumatoid arthritis: a randomized double-blind placebo-controlled study. PLoS One 2017;12:e0178463.
43. Sandhu A, Ahmad S, Kaur P, Bhatnagar A, Dhawan V, Dhir V. Methotrexate preferentially affects Tc1 and Tc17 subset of CD8 T lymphocytes. Clin Rheumatol 2019;38:37–44.
44. Kotake S, Nanke Y, Yago T, Kawamoto M, Kobashigawa T, Yamanaka H. Elevated ratio of Th17 cell-derived Th1 cells ($CD161^{+}$Th1 cells) to $CD161^{+}$Th17 cells in peripheral blood of early-onset rheumatoid arthritis patients. Biomed Res Int 2016;2016:4186027.
45. Kosmaczewska A, Swierkot J, Ciszak L, Szteblich A, Chrobak A, Karabon L, et al. Patients with the most advanced rheumatoid arthritis remain with Th1 systemic defects after TNF inhibitors treatment despite clinical improvement. Rheumatol Int 2014;34:243–53.
46. Aletaha D, Alasti F, Smolen JS. Rheumatoid factor, not antibodies against citrullinated proteins, is associated with baseline disease activity in rheumatoid arthritis clinical trials. Arthritis Res Ther 2015; 17:229.
47. Hecht C, Englbrecht M, Rech J, Schmidt S, Araujo E, Engelke K, et al. Additive effect of anti-citrullinated protein antibodies and rheumatoid factor on bone erosions in patients with RA. Ann Rheum Dis 2015;74:2151–6.
48. Morita R, Schmitt N, Bentebibel SE, Ranganathan R, Bourdery L, Zurawski G, et al. Human blood CXCR5+CD4+ T cells are counterparts of T follicular cells and contain specific subsets that differentially support antibody secretion. Immunity 2011;34: 108–21.
49. Siloşi I, Boldeanu MV, Cojocaru M, Biciuşcă V, Pădureanu V, Bogdan M, et al. The relationship of cytokines IL-13 and IL-17 with autoantibodies profile in early rheumatoid arthritis. J Immunol Res 2016;2016:3109135.
50. Walsh AM, Wechalekar MD, Guo Y, Yin X, Weedon H, Proudman SM, et al. Triple DMARD treatment in early rheumatoid arthritis modulates synovial T cell activation and plasmablast/plasma cell differentiation pathways. PLoS One 2017;12:e0183928.

Arthritis & Rheumatology
Vol. 72, No. 7, July 2020, pp 1103–1110
DOI 10.1002/art.41222

American College of Rheumatology
Empowering Rheumatology Professionals

Association of Visceral Adiposity With Pain but Not Structural Osteoarthritis

Shanshan Li,[1] Ann V. Schwartz,[2] Michael P. LaValley,[1] Na Wang,[1] Nancy Desai,[1] Xianbang Sun,[1] Tuhina Neogi,[1] Michael Nevitt,[2] Cora E. Lewis,[3] Ali Guermazi,[1] Frank Roemer,[1] Neil Segal[4] and David Felson,[5] for the Multicenter Osteoarthritis Study Group

Objective. Osteoarthritis (OA) and pain are both made more severe by low-grade inflammation. This study was undertaken to examine whether visceral fat, a major source of inflammatory cytokines and adipokines, is associated with an increased risk of knee OA or musculoskeletal pain.

Methods. Subjects in the Multicenter Osteoarthritis Study cohort, who were age 50–79 years and had or were at high risk of knee OA, underwent whole-body dual x-ray absorptiometry (DXA) at baseline. At baseline, 30 months, and 60 months radiographs and magnetic resonance images (MRIs) of the knees were obtained, and patients were asked to score the severity of their knee pain and to identify sites of joint pain using a body homunculus. Baseline DXA scans were used to measure total body fat and visceral and subcutaneous fat in the torso. The association of fat depot size with structural outcomes (incident radiographic OA and cartilage loss and synovitis on MRI) and with pain outcomes (worsening knee pain, number of painful joints, and widespread pain) was assessed. Regression analyses were adjusted for age, sex, race, education level, smoking status, physical activity, body mass index (BMI), and depressive symptoms.

Results. Of the 2,961 participants at baseline, 60.7% were women. The mean age was 62.5 years and mean BMI was 30.5 kg/m^2. After adjustment for covariates, no fat measures were associated with any structural outcomes. However, total and visceral, but not subcutaneous, fat were positively associated with worsening knee pain (P = 0.0005 for total fat and P = 0.007 for visceral fat) and widespread pain (P = 0.001 for total fat and P = 0.02 for visceral fat), and the amount of visceral fat was associated with the number of painful joints (P = 0.07).

Conclusion. Our findings indicate that visceral fat is associated with an increased risk of musculoskeletal and widespread pain.

INTRODUCTION

When fat tissue in the body is overwhelmed by positive energy balance and becomes dysfunctional, ectopic fat depots form. Among these is visceral fat, whose accumulation is accompanied by low-grade systemic inflammation and abnormal production of adipokines (1). The accumulation of visceral fat increases the risk of diabetes mellitus, dyslipidemia, insulin resistance, and adverse cardiovascular outcomes (2). The unique pathogenic properties of visceral fat, beyond its contributions to overall adiposity, may be due to its role as an endocrine organ secreting adipokines and serving as a home for circulating inflammatory macrophages (3). Further, visceral fat has a more proinflammatory cytokine profile than subcutaneous fat, characterized by higher circulating levels of C-reactive protein (CRP) and other proinflammatory molecules (4).

Increasingly recognized as a disease with an inflammatory component (5), osteoarthritis (OA) is the most common form of arthritis and a leading cause of disability (6). Given the paucity of

Supported by the NIH (grant AR-P30-072571 and a supplement to grant U01-AG-18820). The Multicenter Osteoarthritis Study was supported by the NIH (grants U01-AG-19069, U01-AG-18947, U01-AG-18820, and U01-AG-18832 to Drs. Nevitt, Lewis, and Felson, respectively, and grant U01-AG-18832). Dr. Felson's work was supported by the NIHR (Manchester Musculoskeletal NIHR Biomedical Research Centre Grant).

[1]Shanshan Li, ScD, Michael P. LaValley, PhD, Na Wang, MS, Nancy Desai, MD, Xianbang Sun, MS, Tuhina Neogi, MD, PhD, Ali Guermazi, MD, Frank Roemer, MD: Boston University, Boston, Massachusetts; [2]Ann V. Schwartz, PhD, Michael Nevitt, PhD, MPH: University of California, San Francisco; [3]Cora E. Lewis, MD, MSPH: University of Alabama at Birmingham; [4]Neil Segal, MD: University of Kansas Medical Center, Kansas City; [5]David Felson, MD, MPH: Boston University, Boston, Massachusetts, and University of Manchester, NIHR Manchester Biomedical Research Centre, and Manchester University NHS Trust, Manchester, UK.

Dr. Roemer owns stock or stock options in Boston Imaging Core Lab. Dr. Segal has received consulting fees, speaking fees, and/or honoraria from Springer (less than $10,000) and research support from Flexion Therapeutics, Pacira CryoHealth, Zimmer Biomet, and Tenex Health. No other disclosures relevant to this article were reported.

Address correspondence to David Felson, MD, MPH, Boston University School of Medicine, 650 Albany Street, Suite 200, Boston, MA 02118. E-mail: dfelson@bu.edu.

Submitted for publication November 8, 2019; accepted in revised form February 4, 2020.

effective methods of treatment and prevention and its burgeoning prevalence, there is a desperate need for new insights into OA that may offer opportunities for prevention or treatment. There are two weakly related components of OA, structural damage to the joint and joint pain, each of which may be affected by inflammation. While evidence (predominantly from animal models of posttraumatic OA) has indicated a prominent role of inflammation in causing structural damage including cartilage loss, it has been extremely challenging to find evidence of the contribution of systemic inflammation to chronic knee OA in humans (7–10). For example, in studies showing an association of metabolic syndrome with knee OA, the association vanishes when analyses are adjusted for body mass index (BMI), suggesting that the increased load conferred by obesity accounts for most of this association (8,9). Other studies examining measures of systemic inflammation and knee OA showed no association with disease when analyses were adjusted for BMI (11–14). Identifying a source of inflammation associated with knee OA in humans independent of body weight will provide clues as to what elements of inflammation may induce or contribute to disease and may point to treatment opportunities.

While an association of systemic inflammation with structural features of OA such as cartilage loss has been difficult to identify, another line of inquiry has demonstrated an association of inflammation with localized and generalized pain (15–19), the other component of OA. CRP has been linked more strongly to painful OA than to structural disease (7). Further, in animal models of OA, inflammatory cytokines provoke central pain sensitization (19–21). Chronic low-grade systemic inflammation might contribute to central pain augmentation in the joint (22). Many persons with painful knee OA have pain in many joints, and systemic inflammation may contribute to generalized pain (23).

We are unaware of any previous studies of the relationship of visceral adiposity to the risk of knee OA and its related symptoms. To investigate a potential association of visceral adiposity with structural features of OA, and with pain, we leveraged a unique study—the Multicenter Osteoarthritis Study (MOST), a large prospective cohort study of older adults with or at high risk of knee OA (24). To our knowledge, MOST is the only large-scale cohort study of OA that includes a measure of visceral adiposity. As in studies that have addressed the role of visceral adiposity in cardiometabolic diseases, we included an evaluation of subcutaneous fat depots to examine whether the relationship of fat depots to OA differed depending on the type of fat depot.

PATIENTS AND METHODS

Study sample and design. MOST is a large, longitudinal observational study funded by the National Institutes of Health that is focused on symptomatic and radiographic knee OA in a cohort of community-dwelling older adults with or at high risk of knee OA (24). The study enrolled 3,026 participants age 50–79 years from 2003 to 2006 at 2 clinical sites (Iowa City, Iowa and Birmingham, Alabama). Demographic, medical, and lifestyle data were collected, and imaging was performed, at baseline. Participants were followed up with repeated examinations at 30 and 60 months.

Weight-bearing, semiflexed posteroanterior and lateral views of the knees were obtained at baseline and each examination according to the MOST radiography protocol (25). Two readers interpreted and graded all radiographs according to the Kellgren/Lawrence (K/L) scale (26). In the case of disagreement between the 2 readers, readings were adjudicated by a panel of 3 readers (26). Magnetic resonance images (MRIs) of the knee were acquired at each visit using a 1.0T magnet (OrthOne; ONI) and a circumferential extremity coil. All images were acquired without contrast. As in a previous study (27), we read 1 randomly selected knee MRI per person. This procedure was followed for budgetary reasons and because of the high rate of symmetry in knee MRIs. The MRIs were graded by 2 experienced musculoskeletal radiologists (AG and FR) using the Whole-Organ MRI Score (WORMS) (28). Synovitis and cartilage morphology on MRI were scored at baseline, 30 months, and 60 months. There was good interobserver agreement for each of the features reported (29).

At each examination, participants completed the Western Ontario and McMaster Universities Osteoarthritis Index (WOMAC) questionnaire (30), reporting on the amount of pain experienced in each knee during activity. In addition, participants were presented with a homunculus on which they noted the joint sites that were painful on most days of the month (Supplementary Figure 1, available on the *Arthritis & Rheumatology* web site at http://onlinelibrary.wiley.com/doi/10.1002/art.41222/abstract).

Institutional review board approval was obtained from the University of California, San Francisco (UCSF), Boston University, the University of Alabama at Birmingham, and The University of Iowa. Written informed consent was obtained from all participants.

Measurement of BMI. Weight was measured to the nearest 0.1 kg on a standard medical balance beam scale, and height was measured on full inspiration to the nearest 1 mm with a wall-mounted Harpenden stadiometer by certified MOST personnel following a written protocol. BMI was calculated as weight in kilograms divided by height in meters squared.

Assessment of abdominal visceral adipose tissue and subcutaneous adipose tissue on dual x-ray absorptiometry (DXA) scans. In the MOST study, a whole-body DXA scan was obtained at baseline using Hologic scanners and standard positioning. (A QDR 4500 system was used at the Birmingham, Alabama study site and a Discovery system was used at the Iowa City, Iowa study site.)

Scans were analyzed locally, with central quality control, including certification of local DXA operators, review of selected participant scans, and monitoring of scanner quality control, provided by UCSF. Standard whole-body DXA outcome measures

included total fat mass, total mass, and percent total fat, calculated as (total fat mass/total mass) × 100%. After our study began, Hologic developed software that allows measurement of the visceral fat depot. In 2017, the baseline whole-body scans were re-analyzed centrally at UCSF using Hologic software 13.5 (Apex version 3.5) to obtain estimates of visceral adipose tissue and subcutaneous adipose tissue in an abdominal region of interest (31). Initial placement of the regions of interest was determined by an automated algorithm. Each scan was then reviewed, and regions of interest were adjusted manually as needed. Hologic visceral adipose tissue area results are calibrated to, and highly correlated with, visceral adipose tissue area results provided by a computed tomography slice at the L4–L5 level. Visceral adipose tissue measurement on DXA scan has been shown to have excellent validity compared with visceral adipose tissue measurement on CT scan (r = 0.89 to 0.93) (31–33).

Assessment of OA structure and pain symptoms. We defined 3 structural knee outcome measures: incident radiographic OA, cartilage loss assessed on MRI, and synovitis assessed on MRI. The first structural outcome measure was incident radiographic knee OA up to 5 years after baseline among the subset of participants who had no radiographic OA in either knee (K/L grade <2 for both knees) at baseline. Those who had developed radiographic knee OA (K/L grade ≥2) and those who had undergone arthroplasty in either knee by follow-up were defined as having incident radiographic knee OA.

Based on MRI readings (28), we assessed cartilage loss and change in synovitis. Within each of 14 subregions in each knee, cartilage morphology was graded on a scale of 0–6 according to the WORMS scale. A subregion was characterized as having cartilage loss if the score increased by ≥1 point. Subregions with baseline scores of 6 were excluded. We next examined change in synovitis. Each region (infrapatellar, intercondylar, and suprapatellar) was scored on a scale of 0–3 based on volume at each time point, and the score was then summed (for a possible total of 0–9). We defined worsening synovitis as an increase in the score of ≥1 point. Knees with baseline synovitis scores of 9 were excluded (34).

We assessed 1 knee pain outcome measure (change in the WOMAC pain subscale score) and 2 broader musculoskeletal pain outcome measures (the presence of widespread pain and the number of painful joints). We calculated changes in pain in each knee as the difference in WOMAC pain score from baseline to the end of follow-up (35).

Using a homunculus, we counted the number of painful joint sites identified by participants at each examination. First, we used the homunculus to define whether a participant had widespread pain (defined as present when the participant identified painful joint sites above and below the waist on both sides of the body and in the axial spine). We previously found that those with widespread pain almost always had pain at multiple sites on examination before they met the threshold for widespread pain (36), suggesting that we could not reasonably examine incidence. We therefore focused on the proportion of the 3 examinations that participants met criteria for widespread pain. To gauge the effect of visceral adiposity on the number of painful sites, we examined the number of painful sites at baseline, 30 months, and 60 months and tested whether visceral adiposity led to an increase in the number of painful joints from baseline.

Potential confounders. For our main analyses, we adjusted for participants' demographic characteristics, lifestyle, and medical history reported on the baseline questionnaire, including age, sex (men versus women), education level (college or above [yes versus no]), physical activity (Physical Activity Scale for the Elderly [continuous]) (37), smoking status (never, past, or current), and BMI (kg/m^2 [continuous]). We used an indicator variable to adjust for race (white versus nonwhite). For all knee outcome measures, we included mechanical alignment (varus, neutral, or valgus), history of knee injury or surgery, and K/L grade for the contralateral knee as covariates. For all pain outcome measures, we included depressive symptom score as a covariate (Center for Epidemiologic Studies Depression Scale score ≥16 [yes versus no]) (38).

Statistical analysis. Our analytic sample consisted of 2,961 MOST participants (1,797 women and 1,164 men) with baseline DXA measurements who were followed up from baseline through at least 30 months. Analyses of radiographic OA and MRI findings and of WOMAC pain score were at the level of the knee, or knee subregion for cartilage loss. To adjust for the correlation

Table 1. Baseline characteristics of the 2,961 MOST participants included in the study*

Age, years	62.5 ± 8.08
BMI	30.5 ± 5.65
Modified Charlson comorbidity index	0.52 ± 0.96
CES-D score	7.59 ± 7.80
PASE score	174.6 ± 88.0
Smoking status, no. (%)	
Never smoker	1,646 (55.6)
Current smoker	194 (6.5)
Former smoker	1,121 (37.9)
White, no. (%)	2,481 (83.8)
Some college education or higher, no. (%)	1,306 (44.1)
WOMAC pain subscale score (range 0–20)	3.38 ± 3.75
Widespread pain, no. (%)†	1,486 (50.7)
Number of painful sites	5.95 ± 4.58
Participants from Iowa study site, no. (%)	1,506 (50.9)
Total body fat, %	34.4 ± 8.53
Abdominal visceral adipose tissue, cm^2	165.7 ± 72.0
Abdominal subcutaneous adipose tissue, cm^2	373.2 ± 135.1

* Except where indicated otherwise, values are the mean ± SD. MOST = Multicenter Osteoarthritis Study; BMI = body mass index; CES-D = Center for Epidemiologic Studies Depression Scale; PASE = Physical Activity Scale for the Elderly; WOMAC = Western Ontario and McMaster Universities Osteoarthritis Index.

† Data were not available for all subjects.

between knees (or subregions of knees), we used generalized estimating equations (GEEs). Analyses of body-wide pain outcomes were conducted at the person level. We modeled each adiposity measure in quintiles and estimated the relative risk using quintile 1 (the lowest quintile) as the reference group. For the GEE model, we specified a log-binomial distribution for binary outcomes and a negative binomial for count data. Results of sex-specific analyses were similar to the sex-adjusted results presented here, and we found no statistically significant interactions by sex. For WOMAC pain score and body-wide pain outcomes, we used the score at each follow-up time point as our outcome, adjusting for baseline score in each model. We adjusted the correlation between outcomes at different times using GEEs.

Mechanical forces play a large role in knee OA, and excess body weight is a well-known risk factor. To identify the independent effect of fat depots and their products on OA and pain outcomes, our primary analyses were adjusted for BMI. We carried out secondary analyses substituting weight for BMI and found no difference in results. In addition, we created visceral fat residuals of BMI (in which we used the residuals of the equation of visceral adipose tissue predicting BMI) and substituted this residual and BMI in equations and found no difference in results.

RESULTS

At baseline, the mean age of the patients was 62.5 years, and their mean BMI was 30.5 kg/m^2. Among 3,026 subjects at baseline, 65 (2.2%) had no DXA scans or had scans that were of insufficient quality to measure fat depots and were excluded from the study. A total of 2,961 MOST participants were therefore included in the study. Follow-up examinations included a clinic visit at which radiographs were obtained, but for those subjects who did not attend the visit, we obtained WOMAC and pain data over the phone. While 247 subjects (8.3%) did not undergo radiography during follow-up, all but 3 subjects (0.1%) had WOMAC pain score assessed at at least 1 follow-up visit. Half of the study participants (51%) reported widespread pain at baseline, with a mean number of painful sites of 6 (Table 1).

While fat depot was associated with structural outcomes in knee OA when analyses were not adjusted for BMI, these associations became null when we further adjusted for BMI (Supplementary Table 1, available on the *Arthritis & Rheumatology* web site at http://onlinelibrary.wiley.com/doi/10.1002/art.41222/abstract). For example, incident radiographic OA was present in 584 of 3,032 knees (19.3%) at either the 30-month or 60-month follow-up, and we found no relationship between the size of any

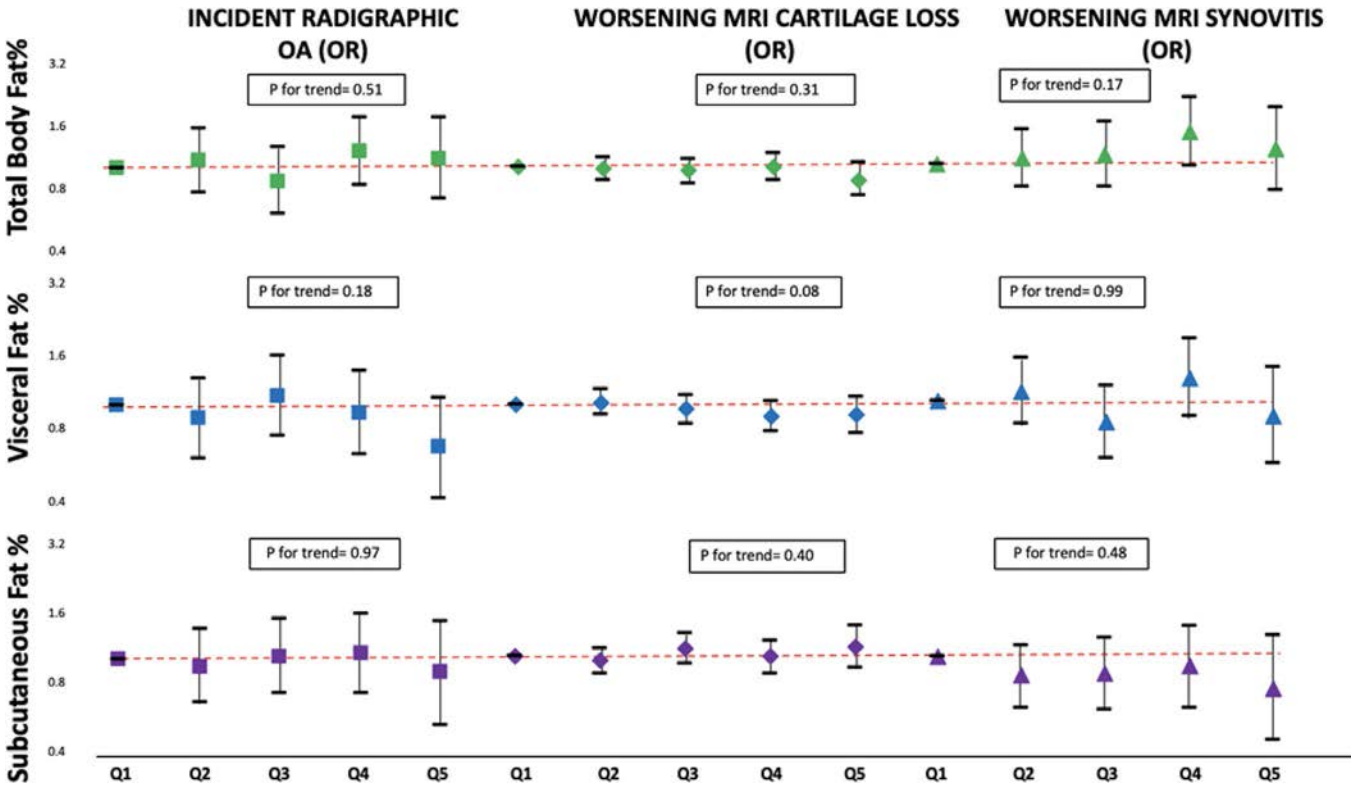

Figure 1. Association of total body fat, the visceral fat depot, and the subcutaneous fat depot with incident radiographic osteoarthritis (OA), worsening cartilage loss on magnetic resonance imaging (MRI), and worsening synovitis on MRI in subjects in the Multicenter Osteoarthritis Study. Analyses were adjusted for age, sex, race (white versus nonwhite), education level (college or above [yes versus no]), smoking status (current, past, or never), physical activity (Physical Activity Scale for the Elderly score [continuous]), alignment (varus, neutral, or valgus), history of knee injury or surgery, Kellgren/Lawrence grade in the contralateral knee, and body mass index (kg/m^2 [continuous]). Values are the odds ratio (OR) and 95% confidence interval. Q1 = lowest quintile (reference group).

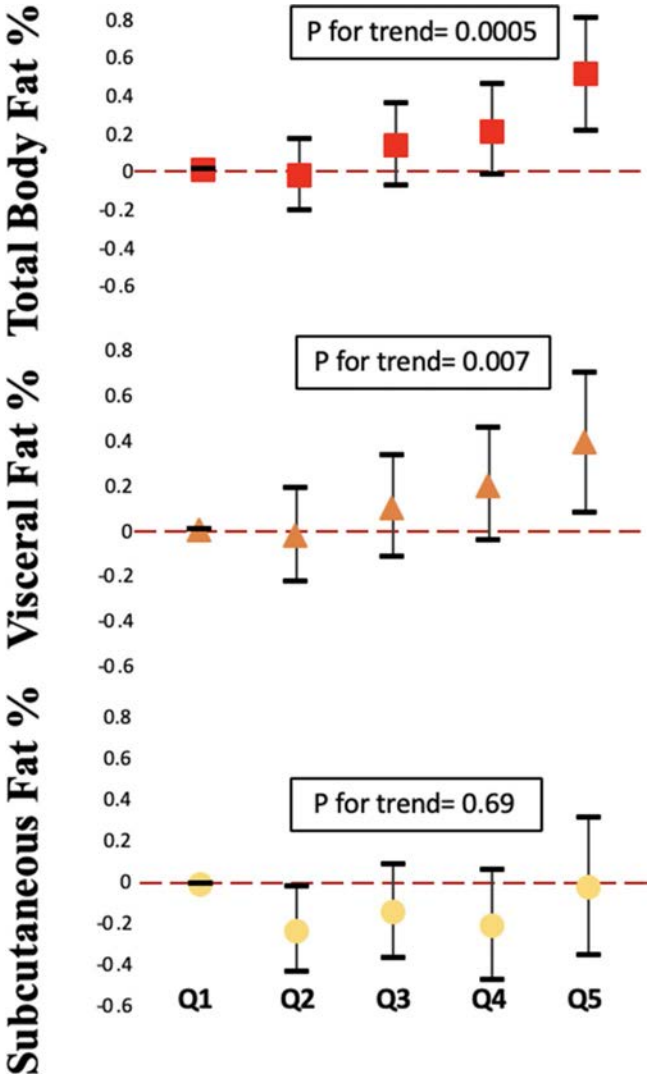

Figure 2. Association of total body fat, the visceral fat depot, and the subcutaneous fat depot with worsening knee pain, as assessed by the Western Ontario and McMaster Universities Osteoarthritis Index (WOMAC) pain subscale (score range 0–20) in subjects in the Multicenter Osteoarthritis Study. Analyses were adjusted for age, sex, race (white versus nonwhite), education level (college or above [yes versus no]), smoking status (current, past, or never), physical activity (Physical Activity Scale for the Elderly score [continuous]), depressive symptoms, alignment (varus, neutral, or valgus), history of knee injury or surgery, Kellgren/Lawrence grade in the contralateral knee, and body mass index (kg/m^2 [continuous]).Values are the beta coefficient (representing an increase of ≥1 point on the WOMAC pain subscale) and 95% confidence interval. Q1 = lowest quintile. Color figure can be viewed in the online issue, which is available at http://onlinelibrary.wiley.com/doi/10.1002/art.41222/abstract.

of the fat depots and OA incidence (Figure 1 and Supplementary Table 1, available on the *Arthritis & Rheumatology* web site at http://onlinelibrary.wiley.com/doi/10.1002/art.41222/abstract). Further, 11,738 of 35,864 cartilage subregions (32.7%) showed cartilage loss on MRI during follow-up, but we found no association of fat depot size with an increase in cartilage loss (Figure 1 and Supplementary Table 2, available on the *Arthritis & Rheumatology* web site at http://onlinelibrary.wiley.com/doi/10.1002/art.41222/abstract). Similarly, we found no relationship between fat depot size and worsening synovitis (Figure 1 and Supplementary Table 3, available on the *Arthritis & Rheumatology* web site at http://onlinelibrary.wiley.com/doi/10.1002/art.41222/abstract).

In contrast, we found a consistent association of total fat and the visceral fat depot with knee pain and with widespread pain outcomes, both before and after adjustment for BMI. For example, those subjects who were in the highest quintile for total body fat and visceral adiposity had greater worsening of their WOMAC pain

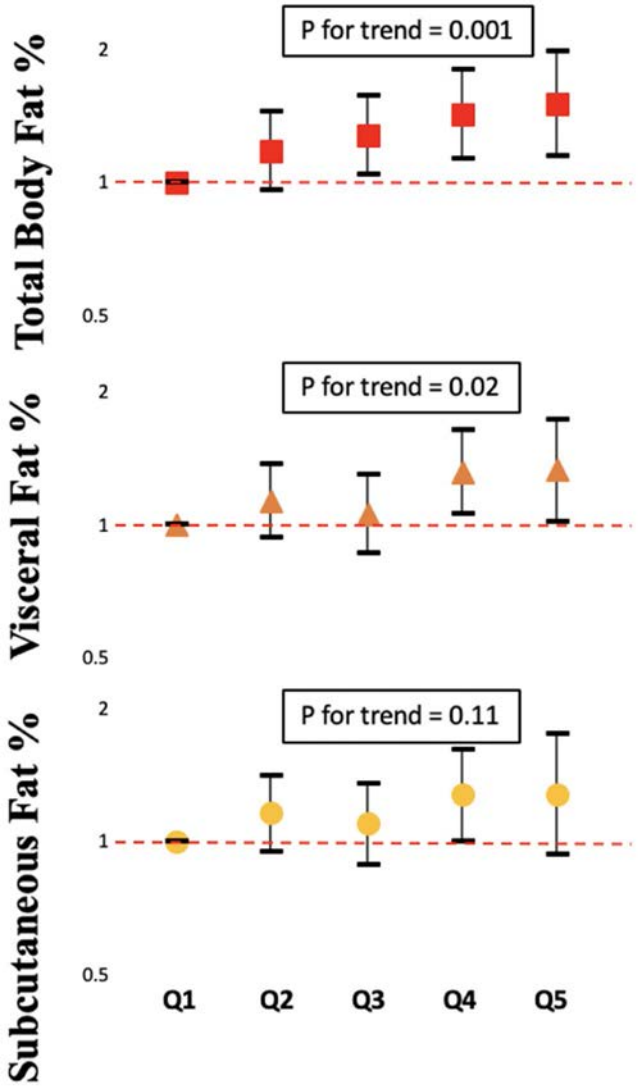

Figure 3. Association of total body fat, the visceral fat depot, and the subcutaneous fat depot with widespread pain in subjects in the Multicenter Osteoarthritis Study. Analyses were adjusted for age, sex, race (white versus nonwhite), education level (college or above [yes versus no]), smoking status (current, past, or never), physical activity (Physical Activity Scale for the Elderly score [continuous]), depressive symptoms, and body mass index kg/m^2 [continuous]). Values are the odds ratio and 95% confidence interval. Q1 = lowest quintile (reference group). Color figure can be viewed in the online issue, which is available at http://onlinelibrary.wiley.com/doi/10.1002/art.41222/abstract.

score than those in the lowest quintile (Figure 2 and Supplementary Table 4, available on the *Arthritis & Rheumatology* web site at http://onlinelibrary.wiley.com/doi/10.1002/art.41222/abstract). The result was consistent when we examined repeated widespread pain (Figure 3 and Supplementary Table 5, available on the *Arthritis & Rheumatology* web site at http://onlinelibrary.wiley.com/doi/10.1002/art.41222/abstract). There was a modest association between visceral fat and the number of painful joint sites (Figure 4 and Supplementary Table 6, available on the *Arthritis & Rheumatology* web site at http://onlinelibrary.wiley.com/doi/10.1002/art.41222/abstract), but number of painful joints was not significantly associated with total body fat. In contrast, after adjustment for BMI, subcutaneous fat depot size was unassociated with any pain outcomes.

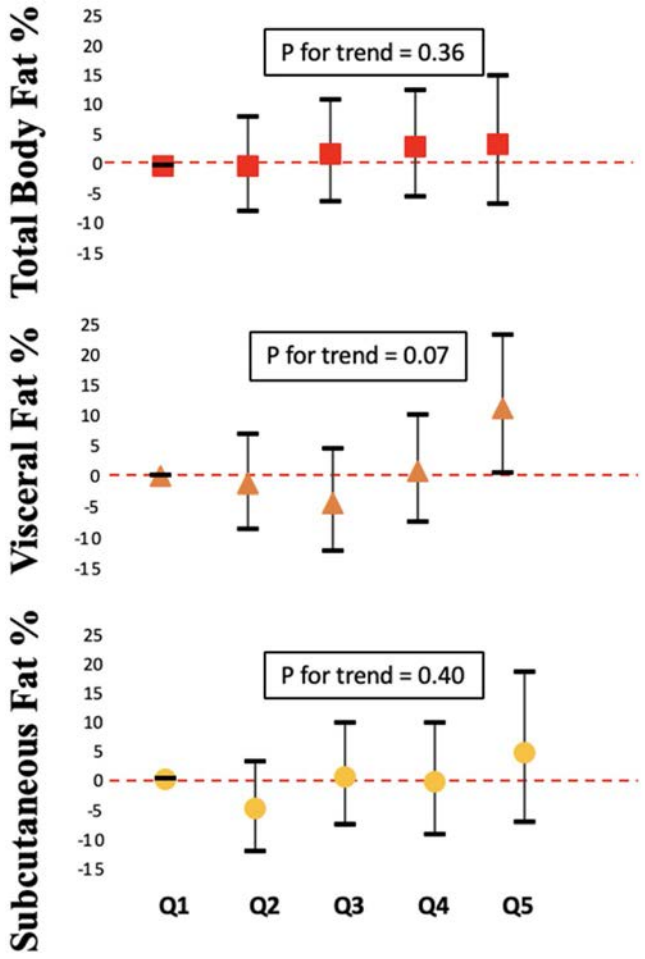

Figure 4. Association of total body fat, the visceral fat depot, and the subcutaneous fat depot with the number of painful joint sites in subjects in the Multicenter Osteoarthritis Study. Analyses were adjusted for age, sex, race (white versus nonwhite), education level (college or above [yes versus no]), smoking status (current, past, or never), physical activity (Physical Activity Scale for the Elderly score [continuous]), depressive symptoms, and body mass index (kg/m^2 [continuous]). Values are the mean percent change from baseline in the number of painful joints. Error bars show the 95% confidence interval. Q1 = lowest quintile. Color figure can be viewed in the online issue, which is available at http://onlinelibrary.wiley.com/doi/10.1002/art.41222/abstract.

DISCUSSION

We did not find evidence that visceral or total fat was associated with the occurrence of radiographic OA, cartilage loss, or synovitis. However, we found a consistent association of body fat, especially total and visceral fat, with worsening knee pain and with widespread pain, and this association was independent of BMI. Visceral fat was associated with an increase over time in the number of painful joints.

Ectopic fat deposition, including visceral fat, is characterized by an infiltration of macrophages and is a major source of proinflammatory cytokines including interleukin-6 and tumor necrosis factor (39,40). Further, it is a site for conversion of local macrophages to a proinflammatory M1 phenotype, which then enter the systemic circulation (41) and have been implicated in OA pathogenesis (42). Visceral fat accumulation has a range of other proinflammatory effects, including suppression of the transcription of adiponectin (43), an antiinflammatory cytokine found to have articular effects (44). The production of leptin, which has deleterious effects on chondrocyte metabolism (45), increases with visceral fat accumulation (46).

Given the range of consistently proinflammatory effects of visceral fat with consequences for the risk of type 2 diabetes mellitus, cardiovascular disease, and other cardiometabolic conditions, it is surprising that we were unable to detect an association of this accumulation with OA, an inflammatory disorder. A likely explanation is that while there is no blood–synovial barrier, the systemic concentrations of these proinflammatory effectors do not translate into injurious levels in the synovial fluid (22,47). The few studies examining the correlations between blood and synovial fluid concentrations of the salient molecules have not shown strong or consistent associations (48,49). Our findings have implications for efforts to modify the course of OA using systemic antiinflammatory treatment.

Other explanations for our null findings are that while inflammation affects OA risk, visceral adiposity may not be the inflammatory phenotype of greatest relevance. After all, we (and others) have also found no association of metabolic syndrome with OA occurrence (9). On the other hand, our findings suggest that the inflammatory environment created by the accumulation of visceral fat may aggravate pain independent of the loading effect of weight. These data suggest that pain needs to be added to the list of conditions affected by the accumulation of visceral fat. Musculoskeletal pain, including back pain, OA pain, and pain from other musculoskeletal disorders is the world's leading cause of disability (50). This study is important in providing new insights into potential treatable causes of this pain. Literature on body composition and pain is mainly cross-sectional and has focused on foot and lower back pain (51,52). A study of knee pain showed an association with systemic markers of inflammation (18). One study also suggested a dose-response relationship between painful joint burden and systemic inflammation among OA patients (53).

Widespread pain, a common condition, has not, to our knowledge, been evaluated.

Our study had a large sample size with long-term follow-up and detailed data on both structural pathology and pain symptoms in the knee. However, our study has limitations. Among them is the absence of data on products of visceral fat, including adipokines, that may mediate the relationship we identified. Further work is needed to identify the active product(s). Another limitation is that the majority of our study participants (84%) were white. Further studies of subjects of other races/ethnic groups are needed. The complex relationship between weight, visceral and total body fat, activity, and pain are worth examining further. While our sample was large, and findings regarding the association of visceral fat with structural OA outcomes were nonsignificant and hovered around the null value, the confidence bounds we report are compatible with modest associations of visceral fat with these outcomes. The high prevalence of widespread pain in our cohort suggests that the results may not be generalizable to other groups. Also, our finding of a lack of association of central fat depots with structural changes of OA may differ in less developed societies (54). The associations we report need to be replicated.

In conclusion, in this prospective cohort study of a community-dwelling population, we found no association independent of BMI between the size of the visceral fat depot and the occurrence of radiographic OA, cartilage loss, or synovitis. However, we found a positive and consistent independent association between visceral adiposity and pain outcomes, including knee pain severity, widespread pain, and the number of painful joints. These findings suggest that visceral adiposity may be an important source of biologic mediators for musculoskeletal pain.

ACKNOWLEDGMENTS

We appreciate the contributions of all participants in the MOST study and of study staff at the clinical sites and the coordinating center.

AUTHOR CONTRIBUTIONS

All authors were involved in drafting the article or revising it critically for important intellectual content, and all authors approved the final version to be published. Dr. Felson had full access to all of the data in the study and takes responsibility for the integrity of the data and the accuracy of the data analysis.

Study conception and design. Li, Neogi, Felson.

Acquisition of data. Nevitt, Lewis, Guermazi, Roemer, Segal.

Analysis and interpretation of data. Schwartz, LaValley, Wang, Desai, Sun.

REFERENCES

1. Longo M, Zatterale F, Naderi J, Parrillo L, Formisano P, Raciti GA, et al. Adipose tissue dysfunction as determinant of obesity-associated metabolic complications [review]. Int J Mol Sci 2019; 20:E2358.
2. Abraham TM, Pedley A, Massaro JM, Hoffmann U, Fox CS. Association between visceral and subcutaneous adipose depots and incident cardiovascular disease risk factors. Circulation 2015;132:1639–47.
3. Ouchi N, Parker JL, Lugus JJ, Walsh K. Adipokines in inflammation and metabolic disease [review]. Nat Rev Immunol 2011;11:85–97.
4. Yu JY, Choi WJ, Lee HS, Lee JW. Relationship between inflammatory markers and visceral obesity in obese and overweight Korean adults: an observational study. Medicine (Baltimore) 2019;98:e14740.
5. Berenbaum F. Osteoarthritis as an inflammatory disease (osteoarthritis is not osteoarthrosis!). Osteoarthritis Cartilage 2013;21:16–21.
6. Cross M, Smith E, Hoy D, Nolte S, Ackerman I, Fransen M, et al. The global burden of hip and knee osteoarthritis: estimates from the Global Burden of Disease 2010 study. Ann Rheum Dis 2014;73:1323–30.
7. Jin X, Beguerie JR, Zhang W, Blizzard L, Otahal P, Jones G, et al. Circulating C reactive protein in osteoarthritis: a systematic review and meta-analysis. Ann Rheum Dis 2015;74:703–10.
8. Kerkhof HJ, Bierma-Zeinstra SM, Castano-Betancourt MC, de Maat MP, Hofman A, Pols HA, et al. Serum C reactive protein levels and genetic variation in the CRP gene are not associated with the prevalence, incidence or progression of osteoarthritis independent of body mass index. Ann Rheum Dis 2010;69:1976–82.
9. Li S, Felson DT. What is the evidence to support the association between metabolic syndrome and osteoarthritis? A systematic review. Arthritis Care Res (Hoboken) 2019;71:875–84.
10. Vlad SC, Neogi T, Aliabadi P, Fontes JD, Felson DT. No association between markers of inflammation and osteoarthritis of the hands and knees. J Rheumatol 2011;38:1665–70.
11. Toussirot E, Michel F, Béreau M, Dehecq B, Gaugler B, Wendling D, et al. Serum adipokines, adipose tissue measurements and metabolic parameters in patients with advanced radiographic knee osteoarthritis. Clin Rheumatol 2017;36:2531–9.
12. Suh DH, Han KD, Hong JY, Park JH, Bae JH, Moon YW, et al. Body composition is more closely related to the development of knee osteoarthritis in women than men: a cross-sectional study using the Fifth Korea National Health and Nutrition Examination Survey (KNHANES V-1, 2). Osteoarthritis Cartilage 2016;24:605–11.
13. King LK, Henneicke H, Seibel MJ, March L, Anandacoomarasmy A. Association of adipokines and joint biomarkers with cartilage-modifying effects of weight loss in obese subjects. Osteoarthritis Cartilage 2015;23:397–404.
14. Richter M, Trzeciak T, Rybka JD, Suchorska W, Augustyniak E, Lach M, et al. Correlations between serum adipocytokine concentrations, disease stage, radiological status and total body fat content in the patients with primary knee osteoarthritis. Int Orthop 2017;41:983–9.
15. Eitner A, Pester J, Vogel F, Marintschev I, Lehmann T, Hofmann GO, et al. Pain sensation in human osteoarthritic knee joints is strongly enhanced by diabetes mellitus. Pain 2017;158:1743–53.
16. Eitner A, Hofmann GO, Schaible HG. Mechanisms of osteoarthritic pain: studies in humans and experimental models [review]. Front Mol Neurosci 2017;10:349.
17. Roux CH, Foltz V, Maheu E, Baron G, Gandjbakhch F, Lukas C, et al. MRI and serum biomarkers correlate with radiographic features in painful hand osteoarthritis. Clin Exp Rheumatol 2016;34:991–8.
18. Stannus OP, Jones G, Blizzard L, Cicuttini FM, Ding C. Associations between serum levels of inflammatory markers and change in knee pain over 5 years in older adults: a prospective cohort study. Ann Rheum Dis 2013;72:535–40.
19. Schaible HG. Mechanisms of chronic pain in osteoarthritis. Curr Rheumatol Rep 2012;14:549–56.
20. Fan YX, Qian C, Liu B, Wang C, Liu H, Pan X, et al. Induction of suppressor of cytokine signaling 3 via HSF-1-HSP70-TLR4 axis attenuates neuroinflammation and ameliorates postoperative pain. Brain Behav Immun 2018;68:111–22.

21. Choi JI, Svensson CI, Koehrn FJ, Bhuskute A, Sorkin LS. Peripheral inflammation induces tumor necrosis factor dependent AMPA receptor trafficking and Akt phosphorylation in spinal cord in addition to pain behavior. Pain 2010;149:243–53.
22. Rezuş E, Cardoneanu A, Burlui A, Luca A, Codreanu C, Tamba BI, et al. The link between inflammaging and degenerative joint diseases [review]. Int J Mol Sci 2019;20:614.
23. Generaal E, Vogelzangs N, Macfarlane GJ, Geenen R, Smit JH, Dekker J, et al. Basal inflammation and innate immune response in chronic multisite musculoskeletal pain. Pain 2014;155:1605–12.
24. Segal NA, Nevitt MC, Gross KD, Hietpas J, Glass NA, Lewis CE, et al. The Multicenter Osteoarthritis Study (MOST): opportunities for rehabilitation research. PM R 2013;5:647–54.
25. Sheehy L, Culham E, McLean L, Niu J, Lynch J, Segal NA, et al. Validity and sensitivity to change of three scales for the radiographic assessment of knee osteoarthritis using images from the Multicenter Osteoarthritis Study (MOST). Osteoarthritis Cartilage 2015;23:1491–8.
26. Kellgren JH, Lawrence JS. Radiological assessment of osteo-arthrosis. Ann Rheum Dis 1957;16:494–502.
27. Felson DT, Niu J, Neogi T, Goggins J, Nevitt MC, Roemer F, et al. Synovitis and the risk of knee osteoarthritis: the MOST Study. Osteoarthritis Cartilage 2016;24:458–64.
28. Peterfy CG, Guermazi A, Zaim S, Tirman PF, Miaux Y, White D, et al. Whole-Organ Magnetic Resonance Imaging Score (WORMS) of the knee in osteoarthritis. Osteoarthritis Cartilage 2004;12:177–90.
29. Lynch JA, Roemer FW, Nevitt MC, Felson DT, Niu J, Eaton CB, et al. Comparison of BLOKS and WORMS scoring systems. Part I. Cross sectional comparison of methods to assess cartilage morphology, meniscal damage and bone marrow lesions on knee MRI: data from the osteoarthritis initiative. Osteoarthritis Cartilage 2010;18:1393–401.
30. Bellamy N, Buchanan WW, Goldsmith CH, Campbell J, Stitt L. Validation study of WOMAC: a health status instrument for measuring clinically-important patient relevant outcomes following hip or knee arthroplasty in osteoarthritis. J Rheumatol 1988;15:1833–40.
31. Bredella MA, Gill CM, Keating LK, Torriani M, Anderson EJ, Punyanitya M, et al. Assessment of abdominal fat compartments using DXA in premenopausal women from anorexia nervosa to morbid obesity. Obesity (Silver Spring) 2013;21:2458–64.
32. Micklesfield LK, Goedecke JH, Punyanitya M, Wilson KE, Kelly TL. Dual-energy X-ray performs as well as clinical computed tomography for the measurement of visceral fat. Obesity (Silver Spring) 2012;21:1109–14.
33. Fourman LT, Kileel EM, Hubbard J, Holmes T, Anderson EJ, Looby SE, et al. Comparison of visceral fat measurement by dual-energy X-ray absorptiometry to computed tomography in HIV and non-HIV. Nutr Diabetes 2019;9:6.
34. Guermazi A, Eckstein F, Hayashi D, Roemer FW, Wirth W, Yang T, et al. Baseline radiographic osteoarthritis and semi-quantitatively assessed meniscal damage and extrusion and cartilage damage on MRI is related to quantitatively defined cartilage thickness loss in knee osteoarthritis: the Multicenter Osteoarthritis Study. Osteoarthritis Cartilage 2015;23:2191–8.
35. Bellamy N, Wells G, Campbell J. Relationship between severity and clinical importance of symptoms in osteoarthritis. Clinical Rheumatol 1991;10:138–43.
36. Felson DT, Niu J, Quinn EK, Neogi T, Lewis C, Lewis CE, et al. Multiple nonspecific sites of joint pain outside the knees develop in persons with knee pain. Arthritis Rheumatol 2017;69:335–42.
37. Washburn RA, Smith KW, Jette AM, Janney CA. The Physical Activity Scale for the Elderly (PASE): development and evaluation. J Clin Epidemiol 1993;46:153–62.
38. Radloff L. The CES-D Scale: a self-report depression scale for research in the general population. Appl Psychol Meas 1977;1:385–401.
39. Samaras K, Botelho NK, Chisholm DJ, Lord RV. Subcutaneous and visceral adipose tissue gene expression of serum adipokines that predict type 2 diabetes. Obesity (Silver Spring) 2010;18:884–9.
40. Villaret A, Galitzky J, Decaunes P, Estève D, Marques MA, Sengenès C, et al. Adipose tissue endothelial cells from obese human subjects: differences among depots in angiogenic, metabolic, and inflammatory gene expression and cellular senescence. Diabetes 2010;59:2755–63.
41. Ghigliotti G, Barisione C, Garibaldi S, Fabbi P, Brunelli C, Spallarossa P, et al. Adipose tissue immune response: novel triggers and consequences for chronic inflammatory conditions. Inflammation 2014;37:1337–53.
42. Kraus VB, McDaniel G, Huebner JL, Stabler TV, Pieper CF, Shipes SW, et al. Direct in vivo evidence of activated macrophages in human osteoarthritis. Osteoarthritis Cartilage 2016;24:1613–21.
43. Li S, Shin HJ, Ding EL, van Dam RM. Adiponectin levels and risk of type 2 diabetes: a systematic review and meta-analysis [review]. JAMA 2009;302:179–88.
44. Tang Q, Hu ZC, Shen LY, Shang P, Xu HZ, Liu HX. Association of osteoarthritis and circulating adiponectin levels: a systematic review and meta-analysis [review]. Lipids Health Dis 2018;17:189.
45. Su YP, Chen CN, Huang KC, Chang HI, Lee KC, Lo CM, et al. Leptin induces MMP1/13 and ADAMTS 4 expressions through bone morphogenetic protein-2 autocrine effect in human chondrocytes. J Cell Biochem 2018;119:3716–24.
46. Hajer GR, van Haeften TW, Visseren FL. Adipose tissue dysfunction in obesity, diabetes, and vascular diseases. Eur Heart J 2008;29:2959–71.
47. Vicenti G, Bizzoca D, Carrozzo M, Solarino G, Moretti B. Multi-omics analysis of synovial fluid: a promising approach in the study of osteoarthritis. J Biol Regul Homeost Agents 2018;32 Suppl 1:9–13.
48. Gandhi R, Takahashi M, Syed K, Davey JR, Mahomed NN. Relationship between body habitus and joint leptin levels in a knee osteoarthritis population. J Orthop Res 2010;28:329–33.
49. Zhang W, Likhodii S, Aref-Eshghi E, Zhang Y, Harper PE, Randell E, et al. Relationship between blood plasma and synovial fluid metabolite concentrations in patients with osteoarthritis. J Rheumatol 2015;42:859–65.
50. GBD 2017 Disease and Injury Incidence and Prevalence Collaborators. Global, regional, and national incidence, prevalence, and years lived with disability for 354 diseases and injuries for 195 countries and territories, 1990–2017: a systematic analysis for the Global Burden of Disease Study 2017. Lancet 2018;392:1789–858.
51. Walsh TP, Arnold JB, Gill TK, Evans AM, Yaxley A, Hill CL, et al. Foot pain severity is associated with the ratio of visceral to subcutaneous fat mass, fat-mass index and depression in women. Rheumatol Int 2017;37:1175–82.
52. Hussain SM, Urquhart DM, Wang Y, Shaw JE, Magliano DJ, Wluka AE, et al. Fat mass and fat distribution are associated with low back pain intensity and disability: results from a cohort study. Arthritis Res Ther 2017;19:26.
53. Perruccio AV, Chandran V, Power JD, Kapoor M, Mahomed NN, Gandhi R. Systemic inflammation and painful joint burden in osteoarthritis: a matter of sex? Osteoarthritis Cartilage 2017;25:53–9.
54. Wallace IJ, Felson DT, Worthington S, Duryea J, Clancy M, Aliabadi P, et al. Knee osteoarthritis risk in non-industrial societies undergoing an energy balance transition: evidence from the indigenous Tarahumara of Mexico. Ann Rheum Dis 2019;78:1693–8.

Arthritis & Rheumatology
Vol. 72, No. 7, July 2020, pp 1111–1122
DOI 10.1002/art.41210

American College of Rheumatology
Empowering Rheumatology Professionals

Identification of Cartilage Microbial DNA Signatures and Associations With Knee and Hip Osteoarthritis

Christopher M. Dunn,[1] Cassandra Velasco,[1] Alexander Rivas,[2] Madison Andrews,[1] Cassandra Garman,[1] Paul B. Jacob,[3] and Matlock A. Jeffries[1]

Objective. Alterations of the gut microbiota have been implicated in many forms of arthritis, but an examination of cartilage microbial patterns has not been performed. This study was undertaken to characterize the microbial DNA profile of articular cartilage and determine changes associated with osteoarthritis (OA).

Methods. We performed 16S ribosomal RNA gene deep sequencing on eroded and intact cartilage samples from knee OA patients (n = 21 eroded and 21 intact samples) and hip OA patients (n = 34 eroded and 33 intact samples) and cadaver controls (n = 10 knee samples and 10 hip samples). Microbial DNA diversity was assessed, groups were compared, and metagenomic profiles were reconstructed. Confirmation was performed in an independent cohort by clade-specific quantitative polymerase chain reaction. Findings in human cartilage were compared to those in cartilage from OA-susceptible C57BL/6 (B6) mice and OA-resistant MRL/MpJ (MRL) mice. Germ-free B6 mouse cartilage was analyzed as a methodologic control.

Results. Alpha diversity was reduced in human OA versus control samples ($P < 0.0001$), and in hip versus knee samples ($P < 0.0001$). Numerous clades were different in human OA versus control samples, and similar findings were noted in comparisons of murine B6 versus MRL mice. Hip samples were microbiologically distinct from knee samples. OA microbial DNA demonstrated increased gram-negative constituents ($P = 0.02$). Functional analysis demonstrated increases in lipopolysaccharide production ($P = 9.9 \times 10^{-3}$), phosphatidylinositol signaling ($P = 4.2 \times 10^{-4}$), and nitrogen metabolism ($P = 8 \times 10^{-3}$) and decreases in sphingolipid metabolism ($P = 7.7 \times 10^{-4}$) associated with OA.

Conclusion. Our study reveals a microbial DNA signature in human and mouse cartilage. Alterations in this signature, including increases in gram-negative constituents, occur during the development and progression of human OA. Furthermore, our findings indicate that strain-specific signatures exist within mouse cartilage that mirror human patterns. Further study of the establishment and potential pathogenic role of these DNA signatures is needed.

INTRODUCTION

Osteoarthritis (OA) is a chronic musculoskeletal disease characterized by progressive loss of joint function leading to pain, mobility loss, significant morbidity, and early mortality. It is the leading cause of chronic disability in the US, affecting roughly half of adults older than 65 years (1). Despite its impact, there are no disease-modifying drug therapies available, in no small part due to our incomplete understanding of OA pathogenesis. OA development involves the interplay of at least 3 major components: genetic predisposition, aging, and environmental factors. Genetic risk, particularly for knee OA, is relatively small, estimated in twin studies to be <50% (2). Thus, there has recently been significant interest in identifying nongenetic risk factors contributing to OA pathogenesis. Among these, innate immune activation, macrophage inflammatory responses, Toll-like receptor (TLR) activation, and complement activation (3–6) have recently been described.

The contents of this article are solely the responsibility of the authors and do not necessarily represent the official views of the National Institutes of Health.

Supported by NIH grants K08-AR-070891 and P20-GM-125528, a Physician Scientist Development award from the Presbyterian Health Foundation, and an Oklahoma Center for the Advancement of Science and Technology Oklahoma Health Research grant. Tissues used in this study were procured by the National Disease Research Interchange with support from the NIH (grant U42-OD-011158).

[1]Christopher M. Dunn, MS, Cassandra Velasco, BS, Madison Andrews, MD, Cassandra Garman, BS, Matlock A. Jeffries, MD: University of Oklahoma Health Sciences Center and Oklahoma Medical Research Foundation, Oklahoma City; [2]Alexander Rivas, BS: University of Arkansas for Medical Sciences, Little Rock; [3]Paul B. Jacob, DO: Oklahoma Joint Reconstruction Institute, Oklahoma City.

No potential conflicts of interest relevant to this article were reported.

Address correspondence to Matlock A. Jeffries, MD, University of Oklahoma Health Sciences Center, Oklahoma Medical Research Foundation, 825 NE 13th Street, Laboratory MC400, Oklahoma City, OK 73104. E-mail: matlock-jeffries@ouhsc.edu.

Submitted for publication November 7, 2019; accepted in revised form January 14, 2020.

One potential driver of chronic innate immune activation in OA is the microbiome. The gut microbiome in both humans and mice changes with aging and obesity, the two strongest nongenetic risk factors for OA (7,8). In mice, induction of obesity by feeding a high-fat diet leads to a proinflammatory shift in gut microbial contents and accelerates OA development following surgical destabilization of the medial meniscus (DMM). Intriguingly, supplementation of the mouse diet with the fiber oligofructose can reverse obesity-related gut microbial changes and protect mice against OA development (9). Furthermore, compared to mice housed conventionally, germ-free mice have reduced OA pathology following surgical DMM (10).

Microbial products are strongly immunogenic, and several have previously been linked with OA development. The innate immune receptors TLR-2 and TLR-4 are up-regulated in OA cartilage (11,12) and are stimulated by lipopolysaccharide (LPS), a constituent of the gram-negative bacterial cell wall. Serum LPS levels have been associated with osteophyte development in human OA, and synovial fluid LPS levels are associated with osteophytes, radiographic joint space narrowing, and pain/functional severity scores (13). Bacterial DNA is a potent stimulator of innate immunity (14,15), which has mainly been studied in the context of the gastrointestinal (16) and respiratory systems (17), although recent studies have suggested a role of both circulating and synovial fluid bacterial DNA in rheumatoid arthritis (RA) (18,19). The first examination of bacterial DNA using next-generation sequencing in synovial fluid and synovial biopsy specimens from the knees of OA and RA patients was published in 2018, and described a number of bacterial DNA clades that were characteristic of both disease states (20). However, to date there have been no evaluations of a cartilage microbial DNA signature in either humans or mice. In this study, we hypothesized that shifts in microbial diversity and/or composition would be associated with the development and progression of OA.

MATERIALS AND METHODS

Ethics statement. The institutional review boards of all involved institutions approved this study.

Human cartilage samples. Eroded and intact sections of hip and knee cartilage were obtained from patients undergoing arthroplasty for end-stage primary OA at the Oklahoma Joint Reconstruction Institute. Specimens were placed into sterile containers in the operating room and transferred to the laboratory. Control cartilage was obtained from the cadavers of patients without a history of OA (histologically confirmed) (Table 1), RA, systemic lupus erythematosus, or other autoimmune diseases by the National Disease Research Interchange (NDRI). NDRI personnel obtained sterile knee and hip articular cartilage within 24 hours of donor death. Cartilage was flash-frozen in liquid nitrogen and shipped on dry ice to our laboratory. Our final discovery cohort analysis included 34 eroded hip specimens, 33 intact hip specimens (1 specimen removed due to failed amplification), 21 eroded knee specimens, 21 intact knee specimens, 10 control hip specimens, and 10 control knee specimens.

Mouse cartilage samples. Eleven-week-old adult male C57BL/6 (B6) mice (n = 8) and 11-week-old adult male MRL/MpJ (MRL) mice (n = 8) were purchased from The Jackson Laboratory and housed at the Oklahoma Medical Research Foundation (OMRF). Husbandry adhered to the NIH Guide for the

Table 1. Demographic characteristics of the patients with OA and controls*

	Age	% female	BMI	Eroded cartilage OARSI score	Intact cartilage OARSI score
16S deep-sequencing cohort					
Hip					
OA (n = 34)	65 ± 2	58	29 ± 1†	13 ± 1	3.3 ± 0.6
Control (n = 10)	66 ± 3	40	27 ± 2	NA	1.5 ± 0.5
Knee					
OA (n = 21)	59 ± 2‡	57	34 ± 1	15 ± 1§	2.9 ± 0.6
Control (n = 10)	68 ± 4	40	30 ± 3	NA	0.0 ± 0.0
qPCR confirmation cohort					
Hip					
OA (n = 5)	67 ± 5	60	25 ± 1	9 ± 1	1.0 ± 0.3
Control (n = 5)	54 ± 4	20	33 ± 3	NA	0.0 ± 0.0
Knee					
OA (n = 5)	60 ± 4	20	35 ± 1	10 ± 2	2.0 ± 1.7
Control (n = 5)	59 ± 4	20	32 ± 1	NA	0.0 ± 0.0

* Except where indicated otherwise, values are the mean ± SEM. BMI = body mass index; OARSI = Osteoarthritis Research Society International; NA = not applicable.
† $P = 0.01$ versus patients with knee osteoarthritis (OA) in the 16S deep-sequencing cohort.
‡ $P = 0.03$ versus control knee samples in the 16S deep-sequencing cohort.
§ $P = 0.05$ versus patients with knee OA in the quantitative polymerase chain reaction (qPCR) confirmation cohort.

Care and Use of Laboratory Animals. At 12 weeks of age, mice were killed and mouse knee joints were dissected in a biosafety cabinet using sterilized instruments following skin and synovial capsule decontamination with chlorhexidine. Articular cartilage was removed from the tibia and femur and flash-frozen in liquid nitrogen. Germ-free, 12-week-old adult male C57BL/6 mice (n = 7) were obtained from the Gnotobiotic Mouse Core Facility at OMRF and dissected similarly.

Sample processing. Full-thickness cartilage sections were dissected from the femoral head (human hip samples) or tibial plateau (human and mouse knee samples). A representative section was saved in 4% paraformaldehyde for histopathologic scoring. Approximately 200 mg of cartilage tissue was cryogenically ground using a grinder mill (SPEX CertiPrep). Murine samples were cryogenically ground using a Precellys Cryolys (Bertin). DNA was isolated using a DNeasy kit (Qiagen). Plasticware and reagents were decontaminated by a 30-minute ultraviolet exposure as previously described (21,22). Polymerase chain reaction (PCR) Master Mixes were decontaminated with double-stranded DNAse treatment (PCR decontamination kit; ArcticZymes). Sterile water was processed using the same (murine) procedure and used as a negative control.

Histologic analysis. Following fixation in 4% paraformaldehyde, samples were embedded in paraffin, placed on slides, and stained with hematoxylin and eosin and Safranin O. OA samples (eroded and intact) and disease-free controls were scored using the Osteoarthritis Research Society International (OARSI) scale (23) to confirm gross categorization (Table 1).

16S ribosomal RNA (16S rRNA) gene sequencing. Microbial profiles were determined by sequencing an ~460-bp region including the V3 and V4 variable region of bacterial 16S rRNA genes. The gene fragment was amplified from ~30 ng of DNA in each sample using a high-fidelity polymerase (NEB Q5; New England Biolabs) (24) and confirmed by 1% agarose gel electrophoresis. (Primers are listed in Supplementary Table 1, available on the *Arthritis & Rheumatology* web site at http://onlinelibrary.wiley.com/doi/10.1002/art.41210/abstract.) Illumina Nextera XT indices were attached, pooled in equimolar amounts, and sequenced on an Illumina MiSeq sequencer using a 250-bp paired-end sequencing protocol by the Clinical Genomics Center at OMRF.

16S rRNA operational taxonomic unit (OTU) classification. Quality filtering, OTU classification, and microbial diversity analysis were performed using the Quantitative Insights into Microbial Ecology (QIIME) software package, version 1.9.1 (25). Sequences were assigned to OTUs using the UCLUST algorithm (26) using a 97% pairwise identity threshold, and taxonomy was assigned using the GreenGenes 13_8 database (27).

Diversity analyses. Alpha diversity was characterized using the observed OTUs method following rarefaction to the lowest number of OTUs present per group. Beta diversity was evaluated on a variance-adjusted, weighted UniFrac model. Principal components analysis was performed and an Adonis (permuted analysis of variance, a multifactor PERMANOVA) test with 999 permutations was used to calculate the statistical significance of group differences (28,29).

Group analyses. Group analyses were performed using the linear discriminant analysis effect size (LEfSe) pipeline (30). LEfSe performs a nonparametric Kruskal-Wallis rank sum test (31) to detect features with significant differential abundance between groups. P values ≤0.01 were considered significant. Next, it uses a linear discriminant analysis (LDA) (32) to estimate the effect size of each differentially abundant feature. An LDA threshold of ≥2 was considered significant (33). QIIME was used to calculate group Benjamini-Hochberg false discovery rate (FDR)–corrected q values; q ≤0.01 was chosen as the FDR-corrected significance threshold. For gram status comparisons, differences were evaluated by Student's *t*-tests, and P values ≤0.05 were considered significant.

Human confirmation cohort and clade-specific quantitative PCR (qPCR). An independent confirmation cohort including 10 eroded hip, 10 intact hip, 10 eroded knee, 10 intact knee, 5 cadaver control hip, and 5 cadaver control knee specimens was obtained as described above. Clade-specific qPCR analysis was performed to calculate the relative presence of Alphaproteobacteria (34,35), Firmicutes (36), Betaproteobacteria (36), Bacteroidetes (36), *Pseudomonas* (37), and Burkholderiales (38) in each sample compared to a universal bacterial primer set (Supplementary Table 1), using a Luna universal probe qPCR kit (New England Biolabs) on a Rotor-Gene Q instrument (Qiagen). The PCR cycling conditions were as follows: 95°C for 10 minutes, followed by 40 cycles of 95°C for 15 seconds and 60°C for 1 minute. Relative clade composition was calculated using the $\Delta\Delta C_t$ method (39). Group differences were calculated using Student's *t*-test. P values ≤0.05 were considered significant.

Prediction of metagenome content and imputed bacterial functional classification. The Phylogenetic Investigation of Communities by Reconstruction of Unobserved States (PICRUSt) software package (40) was used to impute bacterial metagenomes from our 16S deep sequencing microbial DNA data, and functional annotation was applied using the Kyoto Encyclopedia of Genes and Genomes (KEGG) catalog (41). Statistical analysis was performed using the Statistical Analysis of Metagenomic Profiles (STAMP) package (42). Statistical significance and effect sizes among 3 groups (human OA eroded, OA intact, and control) were calculated using analysis of variance. Statistical significance was defined as P ≤0.05 and Benjamini-Hochberg FDR–corrected q ≤0.1.

RESULTS

Reduced constituent microbial DNA diversity in human OA cartilage compared to control specimens. We performed 16S deep-sequencing analysis of human cartilage microbial DNA in 34 eroded hip specimens, 33 intact hip specimens (1 specimen removed due to failed amplification), 21 eroded knee specimens, 21 intact knee specimens, 10 control hip specimens, and 10 control knee specimens. There were no significant differences in the number of raw OTU counts in each of the groups (mean ± SEM 21,000 ± 4,000 in eroded specimens, 11,000 ± 2,000 in intact specimens, and 10,000 ± 2,000 in control specimens; $P = 0.24$ for eroded specimens versus controls, $P = 0.59$ for intact specimens versus controls, and $P = 0.06$ for eroded specimens versus intact specimens).

When hip and knee samples were compared, there was no difference in the raw count between cartilage specimen groups (mean ± SEM 16,000 ± 3,000 in knee samples versus 15,000 ± 3,000 in hip samples; $P = 0.8$), although there was a reduction in the raw count in hip control samples compared to knee control samples (mean ± SEM 17,000 ± 4,000 in knee samples versus 3,300 ± 600 in hip samples; $P = 0.002$).

Differences in bacterial alpha diversity were seen among groups following rarefaction, where disease-free control sections were more diverse than both eroded OA and intact OA sections (mean ± SEM OTU counts following rarefaction 124 ± 6 in controls versus 99 ± 4 in eroded OA samples [$P = 0.0005$] and 97 ± 3 in intact OA samples [$P < 0.0001$ versus controls]) (Figure 1a). No differences in alpha diversity were seen in eroded versus intact cartilage ($P = 0.57$). Hip samples demonstrated lower alpha diversity than knees, both in OA sections (mean ± SEM 89 ± 3 for hip versus 113 ± 4 for knee;

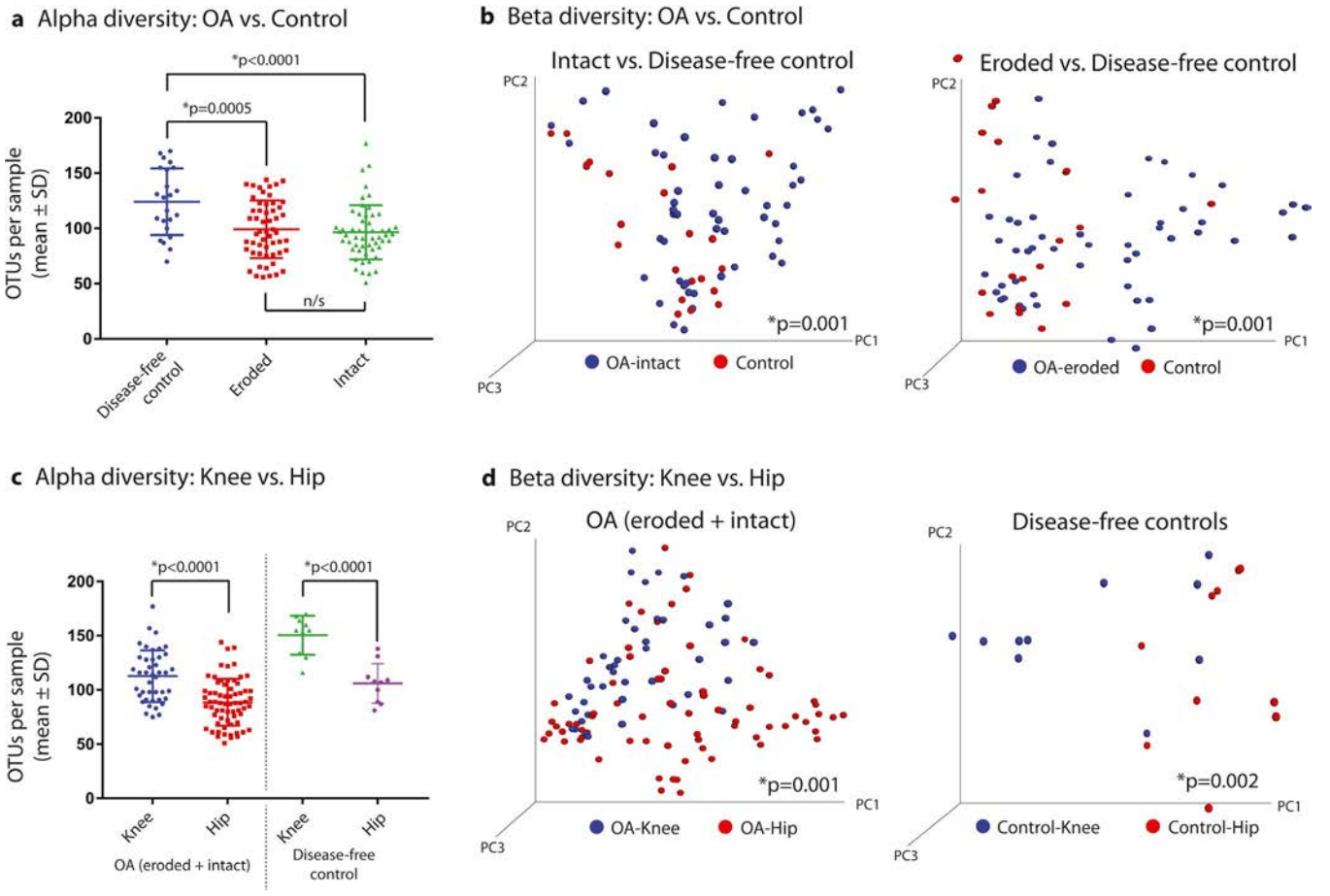

Figure 1. Differences in alpha and beta diversity of human cartilage microbial DNA clades in knee and hip tissue samples from disease-free controls and osteoarthritis (OA) patients. **a**, Alpha diversity in disease-free control samples, eroded OA samples, and intact OA samples. Symbols represent individual subjects; horizontal lines and error bars show the mean ± SD. **b**, Beta diversity in intact OA samples versus disease-free control samples and in eroded OA samples versus disease-free control samples. **c**, Alpha diversity in OA knee and hip samples and in disease-free control knee and hip samples. Symbols represent individual subjects; horizontal lines and error bars show the mean ± SD. **d**, Beta diversity in OA knee samples versus OA hip samples and in control knee samples versus control hip samples. Alpha diversity was compared using the observed operational taxonomic units (OTUs) method, and beta diversity is represented by a 3-dimensional principal components analysis. *P* values were determined by the Adonis method. NS = not significant; PC1 = first principal component.

$P < 0.0001$) and control sections (mean ± SEM 106 ± 6 for hip versus 151 ± 6 for knee; $P < 0.0001$) (Figure 1c). Differences were also seen in beta diversity when eroded tissue was compared to control tissue ($P = 0.001$) and when intact tissue was compared to control tissue ($P = 0.001$), but not when eroded tissue was compared to intact tissue ($P = 0.47$) (Figure 1b). Knee and hip samples demonstrated differences in beta diversity when OA knee and hip samples were compared ($P = 0.001$) and when control knee and hip samples were compared ($P = 0.002$) (Figure 1d).

Distinct microbial DNA signatures in human OA and control cartilage. We next examined clade differences among all OA samples (intact and eroded, from both knees and hips) and all control samples (knee and hip). LEfSe demonstrated 63 clades that were significantly different between the 2 groups (Figures 2a and b and Supplementary Table 2, available on the *Arthritis & Rheumatology* web site at http://onlinelibrary.wiley.com/doi/10.1002/art.41210/abstract). Among these, 35 passed FDR correction with q ≤0.01. Among OA specimens, members of the phylum Proteobacteria were enriched (LDA effect size 3.9; $P = 0.02$, q = 0.06); specifically, class Betaproteobacteria (LDA effect size 3.9; $P = 7 \times 10^{-6}$, q = 0.06). Enriched among control samples were members of the class Alphaproteobacteria (LDA effect size 3.6; $P = 0.004$, q = 0.01) class Clostridia (LDA effect size 3.5; $P = 0.03$, q = 0.06). When OA specimens were subdivided into eroded OA versus intact OA specimens and compared to controls, statistical power was reduced but a clear pattern emerged, with control specimens being characterized by members of the phylum Bacteroidetes and the class Alphaproteobacteria, and both eroded and intact specimens by members of the class Betaproteobacteria. LDA analysis demonstrated 42 clades as significantly different (Figure 2b and Supplementary Table 3, available on the *Arthritis & Rheumatology* web site at http://onlinelibrary.wiley.com/doi/10.1002/art.41210/abstract).

We then considered knee and hip samples separately. In hip samples, 3 clades were significantly different when eroded cartilage was compared to intact cartilage (Figure 2c and Supplementary Table 4, available on the *Arthritis & Rheumatology* web site at http://onlinelibrary.wiley.com/doi/10.1002/art.41210/abstract): order Vibrionales (LDA effect size 2.1; $P = 0.05$) in intact hip carti-

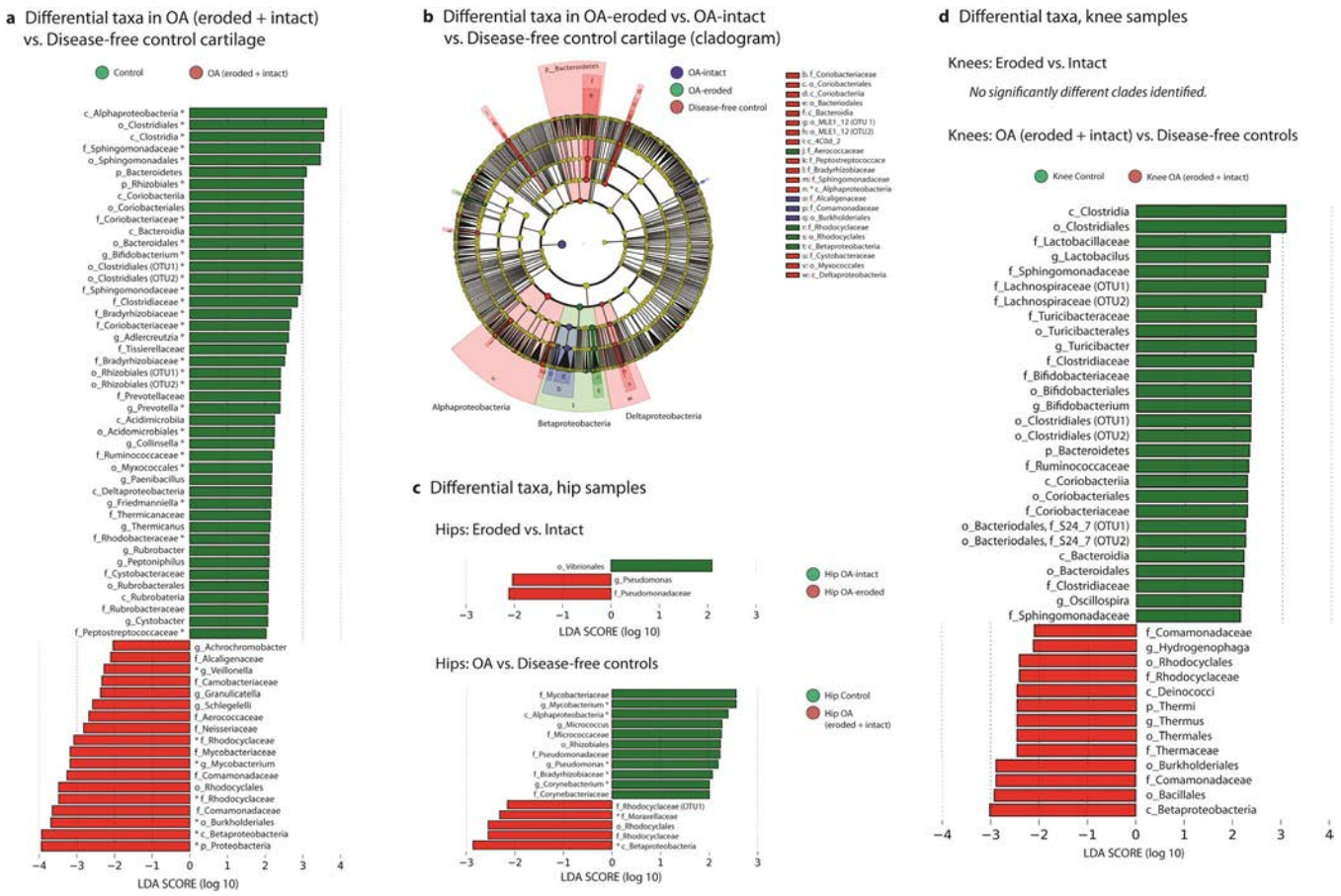

Figure 2. **a**, Significant differences in human microbial DNA clades in specimens from disease-free controls versus specimens from patients with osteoarthritis (OA). **b**, Cladogram comparing eroded OA specimens, intact OA specimens, and control specimens. **c**, Significant differences in clades in eroded OA hip versus intact OA hip specimens and in OA hip versus control hip specimens. **d**, Significant differences in clades in OA knee versus control knee specimens. Bars show linear discriminant analysis (LDA) effect size scores. **Asterisks** indicate clades that passed false discovery rate correction.

lage and family Pseudomonadaceae (LDA effect size 2.1; $P = 0.02$) and genus *Pseudomonas* (LDA effect size 2.04; $P = 0.03$) in eroded hip cartilage. When OA hip specimens were compared to control hip specimens, 16 clades were significantly different, with 7 meeting our FDR threshold (Figure 2c and Supplementary Table 5, available on the *Arthritis & Rheumatology* web site at http://onlinelibrary.wiley.com/doi/10.1002/art.41210/abstract). These included class Alphaproteobacteria (LDA effect size 2.4; $P = 0.03$, q = 0.05) and genus *Mycobacterium* (LDA effect size 2.6; $P = 0.002$, q = 0.05), which were increased in control samples, and class Betaproteobacteria (LDA effect size 2.9; $P = 0.007$, q = 0.05), which was increased in OA samples. In knee samples, no significant differences were seen between eroded and intact cartilage. When OA knee samples were compared to control knee samples, 41 clades were different (Figure 2d and Supplementary Table 6, available on the *Arthritis & Rheumatology* web site at http://onlinelibrary.wiley.com/doi/10.1002/art.41210/abstract). These included class Clostridia (LDA effect size 3.1, $P = 2 \times 10^{-4}$) and phylum Bacteroidetes (LDA effect size 2.3; $P = 0.003$), both increased in control cartilage, and class Betaproteobacteria (LDA effect size 3; $P = 2 \times 10^{-4}$) and order Burkholderiales (LDA effect size 3, $P = 6 \times 10^{-4}$), both increased in OA cartilage.

Human knee and hip samples have distinct microbial DNA signatures, which are shared among both OA and disease-free tissues. We next examined differences in cartilage microbiome composition based on joint location. First, we compared knee OA to hip OA specimens, where LEfSe identified 36 differential clades, 7 of which met our FDR threshold (Figures 3a and b and Supplementary Table 7, available on the *Arthritis & Rheumatology* web site at http://onlinelibrary.wiley.com/doi/10.1002/art.41210/abstract). Hip OA samples were characterized by members of the Proteobacteria phylum, including family Rhodocyclaceae (LDA effect size 2.1; $P = 0.0002$, q = 0.08), whereas knee samples included members of the phylum Actinobacteria, including family Micrococcaceae (LDA effect size 2.4; $P = 0.009$, q = 0.06), and multiple members of the phylum Firmicutes, including genus *Exiguobacterium* (LDA effect size 2.5; $P = 3 \times 10^{-11}$, $q = 8 \times 10^{-5}$).

Comparing disease-free control sections, we identified 46 differences, including many of the same clades found in the analysis of OA samples described above; one (genus *Lactobacillus*) met FDR criteria (Figure 3c and Supplementary Table 8, available on the *Arthritis & Rheumatology* web site at http://onlinelibrary.wiley.com/doi/10.1002/art.41210/abstract). Hips were characterized by members of the phylum Actinobacteria, including order Actinomycetales (LDA effect size 3.2; $P = 0.03$), and class *Betaproteobacteria*, including order Burkholderiales ($P = 0.02$) and family Comamonadaceae ($P = 0.01$). Knees were characterized by phylum Firmicutes, including genus *Lactobacillus* (LDA effect size 2.9; $P = 7 \times 10^{-5}$, q = 0.07), class *Clostridia* (LDA effect size 3.2; $P = 0.0004$), and order *Clostridiales* (LDA effect size 3.2; $P = 0.0004$).

Confirmation of 16S sequencing findings by clade-specific PCR in an independent cohort. We next confirmed our findings in a separate cohort of OA and disease-free control cartilage samples using clade-specific qPCR (Figure 4). All

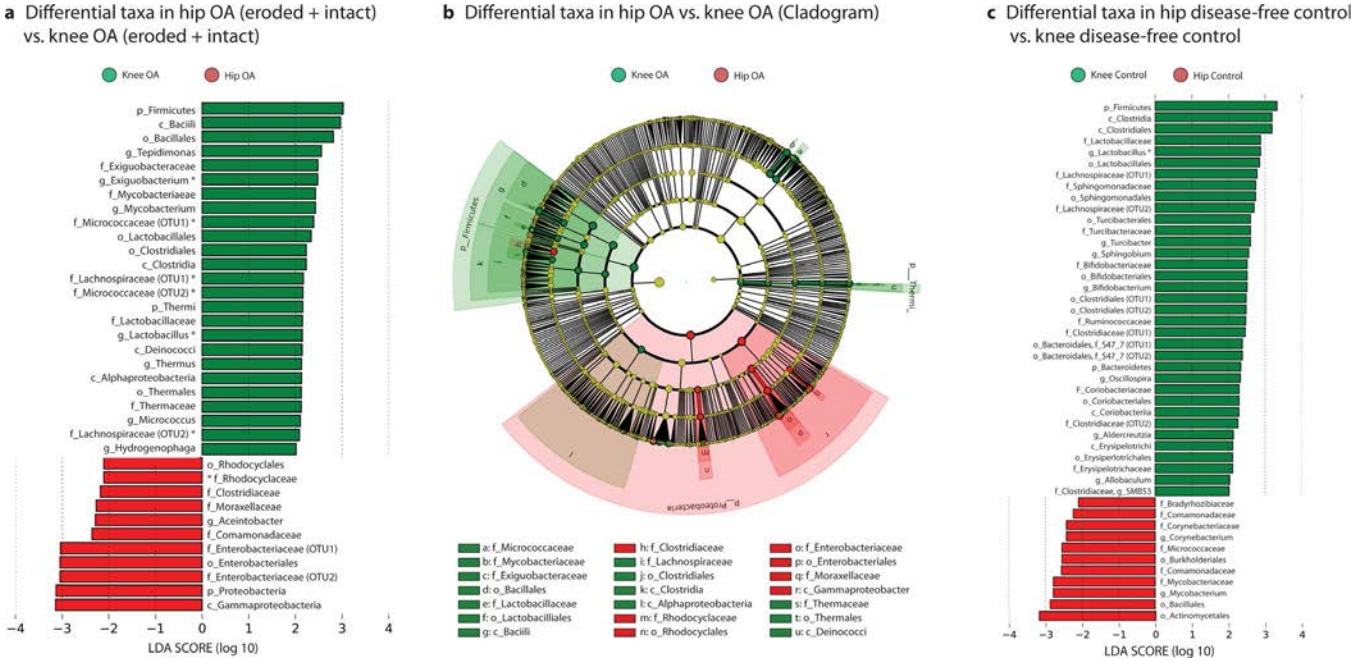

Figure 3. **a**, Significant differences in human microbial DNA clades in specimens from patients with knee osteoarthritis (OA) versus specimens from patients with hip OA. **b**, Cladogram comparing hip OA and knee OA specimens. **c**, Significant differences in clades in control hip versus control knee specimens. Bars represent linear discriminant analysis (LDA) effect size scores. **Asterisks** indicate clades that passed false discovery rate correction.

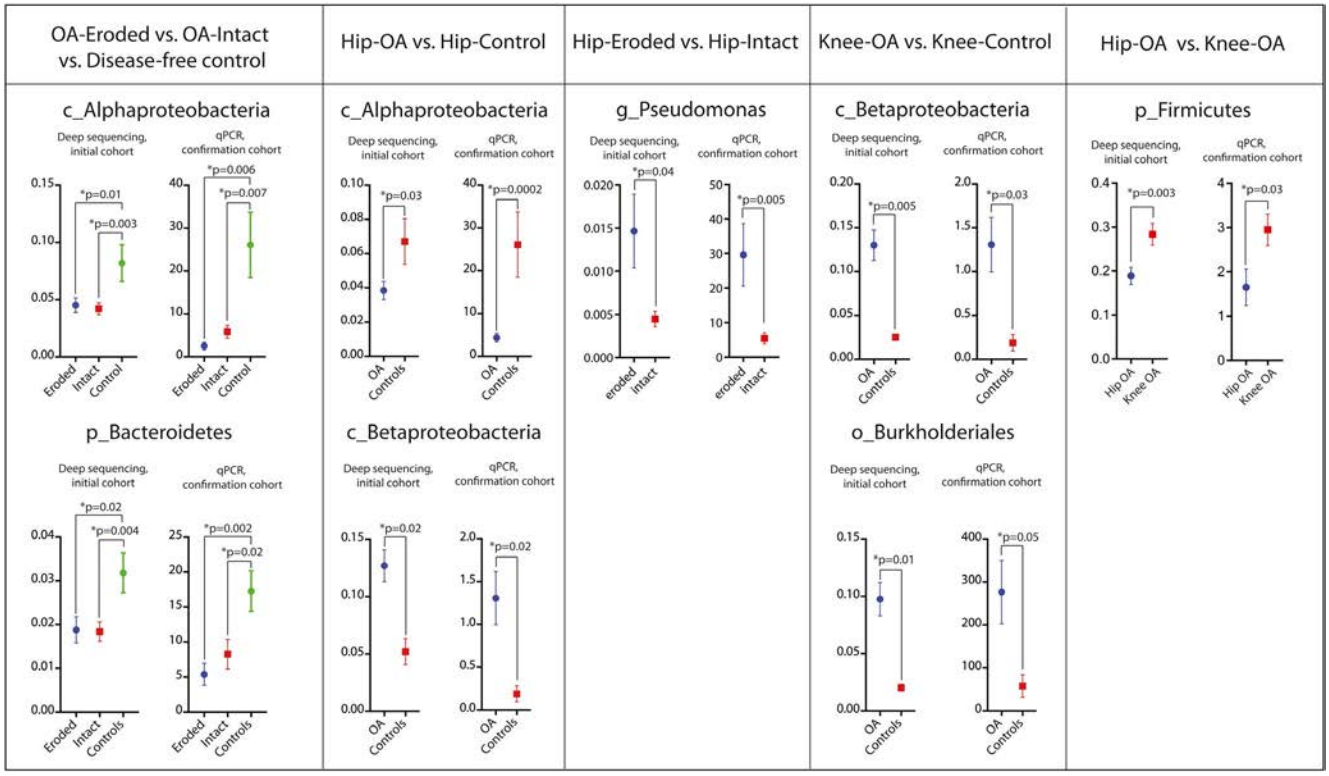

Figure 4. Confirmation of differential clades among knee and hip samples from patients with osteoarthritis (OA) and controls by clade-specific quantitative polymerase chain reaction (qPCR) in a separate confirmation cohort. For the deep-sequencing data in the initial cohort, the y-axis represents the fraction of total group clades. For the qPCR data in the confirmation cohort, the y-axis represents arbitrary units versus the universal bacterial primer set ($\Delta\Delta C_t$ method). Values are the mean ± SEM. Color figure can be viewed in the online issue, which is available at http://onlinelibrary.wiley.com/doi/10.1002/art.41210/abstract.

confirmation results were similar to those of our deep-sequencing analysis. Specifically, we confirmed the findings for both class Alphaproteobacteria ($P = 0.007$ for intact OA samples versus controls and $P = 0.006$ for eroded OA samples versus controls) and phylum Bacteroidetes ($P = 0.02$ for intact OA samples versus controls and $P = 0.002$ for eroded OA samples versus controls). For the comparison of OA hip samples to control hip samples, we confirmed the findings for class Alphaproteobacteria ($P = 0.0002$) and class Betaproteobacteria ($P = 0.02$). For the comparison of eroded hip samples to intact hip samples, we confirmed the findings for genus *Pseudomonas* ($P = 0.005$). For the comparison of OA knee samples to control knee samples, we confirmed the findings for class Betaproteobacteria ($P = 0.03$) and order Burkholderiales ($P = 0.05$). Finally, for the comparison of OA hip to OA knee samples, we confirmed the findings for phylum Firmicutes ($P = 0.03$).

Shift toward gram-negative constituents in human OA cartilage. Next, we identified substantial increases in the proportion of constituent microbial DNA from gram-negative organisms in OA patients compared to disease-free controls (mean ± SEM 37 ± 2% versus 27 ± 2%; $P = 0.02$). These differences persisted when eroded and intact sections were considered separately (37 ± 3% for intact OA sections versus 27 ± 2% for control sections [$P = 0.03$] and 38 ± 3% for eroded OA sections [$P = 0.02$ versus control sections]), whereas eroded OA and intact OA specimens were not significantly different ($P = 0.84$) (Supplementary Figure 1, available on the *Arthritis & Rheumatology* web site at http://onlinelibrary.wiley.com/doi/10.1002/art.41210/abstract).

Human cartilage imputed metagenomes suggest alterations in several canonical bacterial pathways. Given the significant changes in cartilage microbial DNA patterns we found in human cartilage samples, we next sought to determine alterations in imputed metagenome function using the PICRUSt package (40). Using PICRUSt, we found alterations in 37 KEGG pathways (Figure 5), including reductions in phenylpropanoid biosynthesis ($P = 9.9 \times 10^{-5}$, q = 0.03) and sphingolipid metabolism ($P = 7.7 \times 10^{-4}$, q = 0.05) in OA samples, increases in phosphatidylinositol signaling in OA ($P = 4.2 \times 10^{-4}$, q = 0.05), increases in nitrogen metabolism in OA ($P = 8.0 \times 10^{-3}$, q = 0.08), and increases in LPS biosynthesis in OA ($P = 9.9 \times 10^{-3}$, q = 0.1), among others (Supplementary Table 9, available on the *Arthritis & Rheumatology* web site at http://onlinelibrary.wiley.com/doi/10.1002/art.41210/abstract).

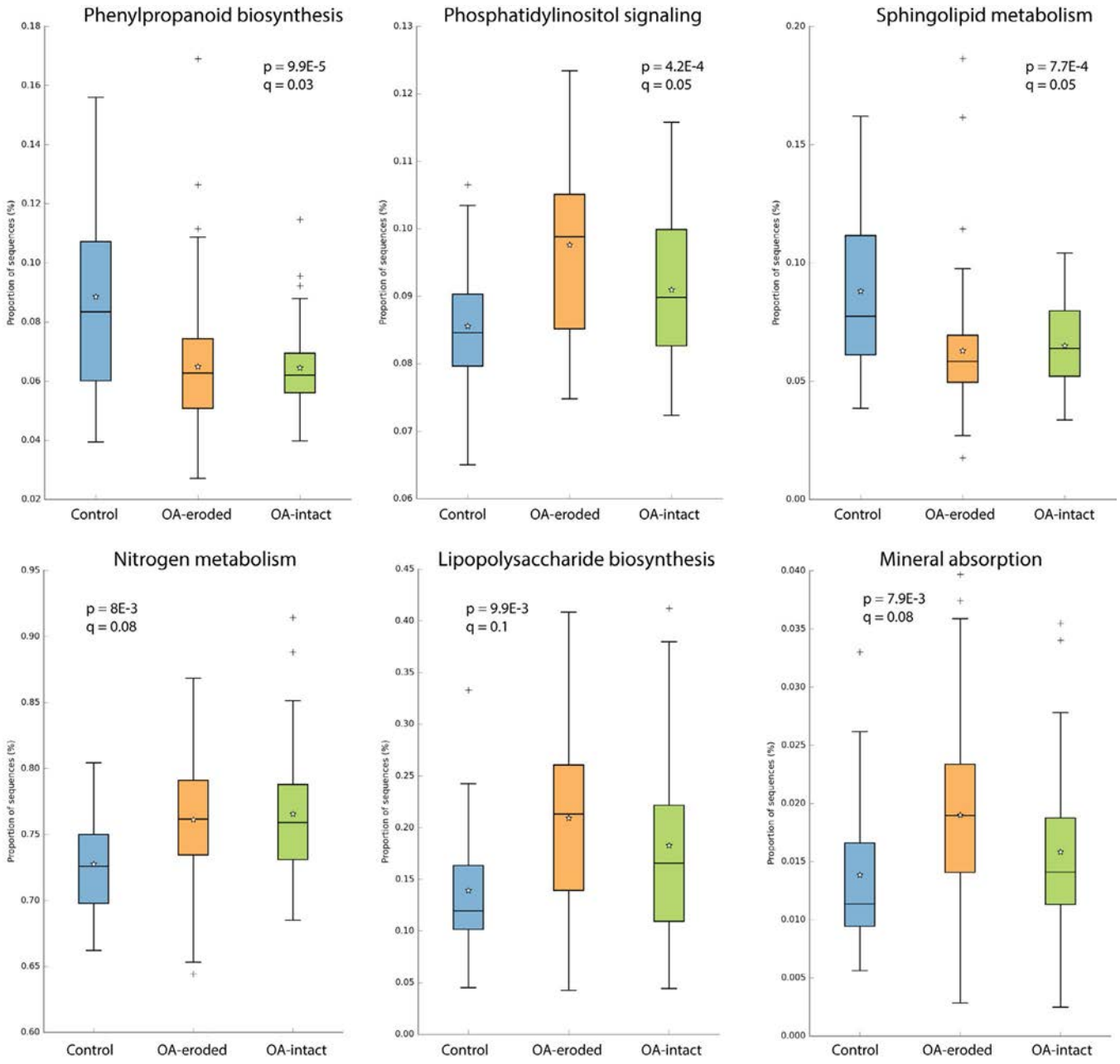

Figure 5. Differences in functional classification of bacterial species in human disease-free control, eroded osteoarthritis (OA), and intact OA cartilage identified through predictive metagenomic analysis using Phylogenetic Investigation of Communities by Reconstruction of Unobserved States (PICRUSt) software. Data are shown as box plots, where the boxes represent the interquartile range, the lines inside the boxes represent the median, and the lines outside the boxes represent the maximum and minimum values. Stars indicate the mean. Crosses indicate outliers. *P* values were determined by analysis of variance. Benjamini-Hochberg false discovery rate–corrected q values are shown. Color figure can be viewed in the online issue, which is available at http://onlinelibrary.wiley.com/doi/10.1002/art.41210/abstract.

Mouse knee cartilage sample microbial DNA signatures vary by strain and demonstrate changes similar to human knee cartilage samples, while germ-free mouse knee samples lack a cartilage microbial DNA signature. We next evaluated mouse knee cartilage samples from adult male OA-susceptible C57BL/6J mice (n = 8) and OA-resistant MRL/MpJ mice (n = 8). Raw OTU counts were lower than in human samples, likely owing to the smaller tissue mass in mice (mean ± SEM OTU counts 4,214 ± 913). There were no differences in alpha diversity between B6 mouse and MRL mouse samples (mean ± SEM 100 ± 27 for MRL mice versus 90 ± 27 for B6 mice; $P = 0.47$). The difference in beta diversity between the groups did not quite reach statistical significance ($P = 0.056$ by Adonis).

LEfSe identified 32 clade group differences between MRL mice and B6 mice (Supplementary Figure 2 and Supplementary Table 10, available on the *Arthritis & Rheumatology* web site at http://

onlinelibrary.wiley.com/doi/10.1002/art.41210/abstract). None met FDR criteria, likely due to small group sizes. MRL mouse cartilage had increases in members of the family Lactobacillaceae (LDA effect size 3.4; $P = 0.003$), family Turicibacteraceae (LDA effect size 2.98; $P = 0.01$), genus *Actinomyces* (LDA effect size 2.86; $P = 0.01$), and various members of the class Verrucomicrobiae (LDA effect size 3.27; $P = 0.03$). Characteristic of B6 mouse cartilage were nucleic acid signatures from family Comamonadaceae from within family Burkholderiales (LDA effect size 3.6; $P = 0.009$), class Betaproteobacteria (LDA effect size 3.7; $P = 0.01$), and family Tissierellaceae from order Clostridiales (LDA effect size 2.9; $P = 0.01$).

Eleven of the clades that differentiated human control knee cartilage from OA knee cartilage also differentiated OA-resistant MRL mouse cartilage from OA-susceptible B6 mouse cartilage. These included members of the order Lactobacillales, family Lachnospiraceae, genus *Lactobacillus*, order Turicibacterales, class Bacteroidia, and class Betaproteobacteria, among others. In every case, OTUs that overlapped shared a similar pattern: clades that were increased in human control cartilage were also increased in OA-resistant MRL mouse cartilage, whereas clades that were increased in human OA cartilage were also increased in OA-susceptible B6 mouse cartilage. Also mirroring our human data, we found an enrichment in gram-negative organism nucleic acid in B6 mouse cartilage compared to MRL mouse cartilage (mean ± SEM 50 ± 0.06% for B6 versus 35 ± 0.03% for MRL; $P = 0.028$) (Supplementary Figure 1, http://onlinelibrary.wiley.com/doi/10.1002/art.41210/abstract).

Finally, as methodologic controls, we examined cartilage samples sourced from germ-free C57BL/6 mice. We failed to identify a significant constituent microbial DNA signature in these mice; 16S PCR amplification bands were not seen on agarose gel electrophoresis, and deep sequencing demonstrated very low amplification (mean ± SEM raw OTU counts 196 ± 44; n = 7). Indeed, germ-free samples were indistinguishable from water controls (mean ± SEM raw OUT counts 270 ± 94; n=3) ($P = 0.44$).

DISCUSSION

In this study, we provide the first evidence of microbial nucleic acid signatures in human and mouse cartilage tissue. We identified shifts in this signature including reduced diversity following rarefaction and an increase in gram-negative constituents in OA cartilage compared to control cartilage. We identified a number of clades that were characteristic of human eroded OA, intact OA, and control cartilage. Furthermore, we demonstrated that knee and hip cartilage, both with and without OA, are distinct. We identified cartilage microbial DNA signatures in mouse knee tissues, which varied depending on mouse strain; OA-resistant MRL mice had bacterial DNA signatures similar to disease-free human control tissue, whereas OA-susceptible B6 mice had signatures similar to human OA tissue. We did not find a significant cartilage microbial DNA signature in germ-free mice.

Our data add to the growing body of literature that has uncovered constituent microbial DNA signatures in a variety of human tissues previously thought sterile, including the central nervous system (43). The reduction in microbial alpha diversity seen in OA mirrors findings in other rheumatic diseases, where reduced diversity has been associated with reactive arthritis (44), ankylosing spondylitis (45), and RA (46). Our findings are consistent with those of previous studies showing that members of the phylum Proteobacteria, specifically Betaproteobacteria, are markers of obesity in human patients and diet-induced obesity in mice (47), both of which are strongly associated with OA.

Few studies have examined gut microbiome perturbations in OA. Among these, a recent study by Boer et al investigated the gut microbiome composition of 867 adults within the Dutch Rotterdam (RSIII) and LifeLines-DEEP cohorts (48). Using 16S rRNA deep sequencing, they identified 4 bacterial clades associated with knee pain as measured by the Western Ontario and McMaster Universities Osteoarthritis Index score. These included class Bacilli, order Lactobacillales, family Streptococcaceae, and genus *Streptococcus.* We found Lactobacillales to be associated with control human and MRL mouse cartilage, although the families driving this association were not Streptococcaceae, but Aerococcaceae and Carnobacteriaceae. Interestingly, though, we did find that members of Lactobacillales were strongly associated with knee samples compared to hip samples.

In 2018, Schott et al demonstrated that prebiotic supplementation (oligofructose) protected against both cartilage degeneration and synovial hyperplasia in DMM-induced OA in mice fed a high-fat diet (9). Supplementation was associated with a shift in the gut microbiome toward an increase in Actinobacteria, several clades of which we identified as associated with disease-free control cartilage (i.e., Acidimicrobia, *Friedmanniella*, Coriobacteriia, and Rubrobacteria) (Figure 2 and Supplementary Table 2, available on the *Arthritis & Rheumatology* web site at http://onlinelibrary.wiley.com/doi/10.1002/art.41210/abstract). Indeed, the most-altered clade in oligofructose-supplemented mice was genus *Bifidobacterium*, which we found to be strongly associated with human control cartilage (FDR q value 0.003).

In 2018, Zhao and colleagues published the first deep sequencing–based evaluation of synovial fluid and synovial tissue from the knees of human OA and RA patients (20). Many of the bacterial DNA clades they found to be characteristic of knee OA synovial tissue we found to be associated with control cartilage, including family Lanchospiraceae, order Coriobacteriales, and family Clostridiaceae, although this discordance is likely related to study design. Considering knees and hips together, we found that Proteobacteria, specifically Betaproteobacteria, were associated with OA. Increases in Proteobacteria have been observed in mice fed a high-fat diet (49).

In our study, knee samples were characterized by nucleic acid sequences from multiple members of the phylum Firmicutes, one of the major constituents of the normal human gut microbiome (50). Among OA samples, geographic differences were

similar to what we encountered in controls, with knee microbial DNA again being characterized by Firmicutes, and hip microbial DNA by Proteobacteria, although why these joints seem to have conserved geographic speciation is not clear. Increases in the Firmicutes:Bacteroidetes ratio in the gut have been linked to obesity (51). Among our samples, patients with knee OA had a higher BMI than patients with hip OA (mean ± SEM 34 ± 1 versus 29 ± 1; $P = 0.01$), but we did not find a significant difference in the Firmicutes:Bacteroidetes DNA ratio in knee samples versus hip samples ($P = 0.22$). Knee OA samples were persistently characterized by Firmicutes, whereas hip OA samples were enriched in Proteobacteria, specifically, Beta- and Gammaproteobacteria. It should be noted that 8 of the 10 control knee and hip specimens were matched; that is, knee and hip cartilage specimens were from the same individual. This strengthens the argument that knee and hip microbial signature differences do indeed exist, and were not simply due to variations between individuals.

Intriguingly, we found significant overlap when comparing mouse and human cartilage microbial DNA patterns. For example, the family Comamonadaceae and the class Betaproteobacteria were found more frequently in OA-susceptible B6 mice and both were among the most highly significant clades increased in human knee OA. Conversely, genus *Lactobacillus*, order Burkholderiales, family Turcibateraceae, order Erysipelotrichales, and order Bacteroidales sequences were increased in OA-resistant MRL mice and were increased in disease-free human cartilage. In total, 11 clade overlaps were found between murine and human knee cartilage microbial DNA samples, representing one-third of the total number of significant clades in mice and including each of the top 6 most significant clades in murine cartilage. In every case, clades characteristic of human control cartilage were increased in MRL mouse samples, whereas clades characteristic of human OA cartilage were increased in B6 mouse samples. Although speculative, this raises the intriguing possibility that OA-associated cartilage microbial DNA patterns may precede OA development.

Recent studies have highlighted the role of chronic, low-level inflammation in OA, including innate immune activation (5), macrophage-predominant inflammatory responses (50), TLR activation (5), and complement activation (6). TLR-2 and TLR-4, which are up-regulated in OA cartilage (51), are stimulated by LPS, a constituent of the gram-negative bacterial cell wall. Serum LPS levels have been associated with osteophyte severity in human OA, and synovial fluid LPS has been associated with osteophyte severity, joint space narrowing, and total pain/functional severity scores (13). The source of LPS in OA patients is thought to be increased permeability from the gut, a feature of the diet-induced obesity model of OA (52); indeed, LPS elevation in obese patients has been suggested as a potential contributor to OA development (53). Consistent with the findings of those studies, in this study we showed that both human OA cartilage and OA-susceptible mouse cartilage contain an increased fraction of gram-negative constituent bacterial DNA compared to human controls and OA-resistant mice, respectively.

An interesting question is the timing and route of inoculation of the microbial DNA we describe, e.g., whether it is trafficked from the gastrointestinal tract via live bacterial organisms or carried into the articular space within immune cells. Another possibility is inoculation from subchondral bone via the osteochondral junction (54). We are also unable to comment on whether cartilage microbial DNA diversity decreases with age, as has been noted with the gut microbiome, although this may be an intriguing contributor to the increased OA risk seen with aging (55). Assuming that the cartilage bacterial DNA patterns we found in our study are indeed sourced from the systemic circulation, it is a curious finding that these patterns vary within the same joint (i.e., in eroded versus intact areas). There are several potential explanations for this finding. Perhaps eroded regions of cartilage are more exposed to products of systemic circulation, either via inflammatory cells or blood contact directly, and therefore experience more rapid deposition of and/or change in bacterial DNA compared to intact regions.

Our functional analysis, performed by reconstructing metagenomes using PICRUSt, identified several bacterial functional pathways predicted to be altered in association with OA. Several of these pathways are consistent with previous OA reports. For example, phenylpropanoids, which are reduced in OA-associated constituents, have reported antiinflammatory effects (56). Phosphatidylinositol signaling is intimately linked with oxidative stress in OA (57). Bone mineral resorption is a feature of late OA (58). There is a large volume of published data on the role of increased nitric oxide production in OA, which may be related to the increased nitrogen metabolism pathway seen in our functional analysis (59). Finally, we saw evidence of increased LPS production in our functional analysis, which is consistent with previous studies regarding LPS and OA, discussed in more detail above.

Our study does have several limitations. The first is the potential for contamination leading to false-positive results. We undertook several steps to identify and prevent potential contamination as outlined above, including processing samples in a sterile environment, running water controls, and decontaminating PCR reagents and plasticware. Critically, we did not find a microbial DNA signature when germ-free mouse cartilage was examined. Our analyses relied on detection and classification of microorganisms by nucleic acid analysis; therefore, we have not confirmed the presence of living bacteria within cartilage tissue. Given the inflammatory effects of bacterial DNA our findings nonetheless suggest a potential driver of local inflammation in OA. Our study may suffer from potential confounding, most likely in the form of comorbidities including obesity and aging (although neither of these risk factors differed significantly among groups). We did perform separate analyses to determine if any cartilage bacterial DNA clades were strongly correlated with either obesity or aging independent of disease state but did not find any significant associations. However, our study is likely underpowered to definitively state whether such correlations exist; future studies, particularly in mouse models, may be better equipped to answer these questions. Finally,

we are unable to draw conclusions regarding the direct role of any specific bacterial DNA in the development or progression of OA; this sort of hypothesis-driven research should be a focus of future investigations, particularly in mouse models of OA.

In summary, in this study we characterized a cartilage microbial DNA signature in human hip and knee cartilage and B6 and MRL mouse cartilage. Using a deep-sequencing approach, we identified a variety of microbial clades that are associated with disease-free control, intact OA, and eroded OA tissue, and identified reductions in alpha diversity in OA tissue compared to disease-free controls. In addition, we identified several clades that were differentially present in knee and hip cartilage. Further, we identified a shift in the composition of OA samples toward gram-negative constituents. Our human findings were reflected in a comparison of cartilage from OA-susceptible and OA-resistant mouse strains.

Confirmation of our findings will require further studies, and expansion to include examination of bacterial metabolites will allow better understanding of potential shifts in cartilage bacterial enzymes and their byproducts as a novel contributor to OA pathogenesis. An analysis of when and how the cartilage is inoculated with its microbiome should be undertaken in mouse models, as well as an evaluation of age-related shifts in the cartilage microbiome, which may offer a novel insight into age-related increases in OA susceptibility. Further studies examining the cartilage microbial DNA landscape in other, particularly inflammatory, arthropathies including RA are also in order. Finally, integrated longitudinal studies in animal models of OA, defining both cecal and cartilage microbiota may also enlighten the potential pathogenic role of certain bacterial species in the development of OA, and may provide an avenue for the development of novel therapeutics.

AUTHOR CONTRIBUTIONS

All authors were involved in drafting the article or revising it critically for important intellectual content, and all authors approved the final version to be published. Dr. Jeffries had full access to all of the data in the study and takes responsibility for the integrity of the data and the accuracy of the data analysis.

Study conception and design. Jeffries.

Acquisition of data. Dunn, Velasco, Rivas, Andrews, Garman, Jacob, Jeffries.

Analysis and interpretation of data. Jeffries.

REFERENCES

1. Centers for Disease Control and Prevention (CDC). Prevalence of doctor-diagnosed arthritis and arthritis-attributable activity limitation—United States, 2010–2012. MMWR Morb Mortal Wkly Rep 2013;62:869–73.
2. Magnusson K, Scurrah K, Ystrom E, Ørstavik RE, Nilsen T, Steingrímsdóttir ÓA, et al. Genetic factors contribute more to hip than knee surgery due to osteoarthritis—a population-based twin registry study of joint arthroplasty. Osteoarthritis Cartilage 2017;25:878–84.
3. Liu-Bryan R. Synovium and the innate inflammatory network in osteoarthritis progression. Curr Rheumatol Rep 2013;15:323.
4. Kraus VB, McDaniel G, Huebner JL, Stabler TV, Pieper CF, Shipes SW, et al. Direct in vivo evidence of activated macrophages in human osteoarthritis. Osteoarthritis Cartilage 2016;24:1613–21.
5. Scanzello CR, Plaas A, Crow MK. Innate immune system activation in osteoarthritis: is osteoarthritis a chronic wound? Curr Opin Rheumatol 2008;20:565–72.
6. Wang Q, Rozelle AL, Lepus CM, Scanzello CR, Song JJ, Larsen DM, et al. Identification of a central role for complement in osteoarthritis. Nat Med 2011;17:1674–9.
7. O'Toole PW, Jeffery IB. Gut microbiota and aging. Science 2015;350:1214–5.
8. John GK, Mullin GE. The gut microbiome and obesity. Curr Oncol Rep 2016;18:45.
9. Schott EM, Farnsworth CW, Grier A, Lillis JA, Soniwala S, Dadourian GH, et al. Targeting the gut microbiome to treat the osteoarthritis of obesity. JCI Insight 2018;3:95997.
10. Ulici V, Kelley KL, Azcarate-Peril MA, Cleveland RJ, Sartor RB, Schwartz TA, et al. Osteoarthritis induced by destabilization of the medial meniscus is reduced in germ-free mice. Osteoarthritis Cartilage 2018;26:1098–109.
11. Miller RE, Miller RJ, Ishihara S, Belmadani A, Golub SB, Fosang AJ, et al. A 32-mer fragment of aggrecan promotes knee hyperalgesia in the DMM model of osteoarthritis through direct nociceptor activation via TLR2 [abstract]. Osteoarthritis Cartilage 2016;24 Suppl 1:S452.
12. Midwood K, Sacre S, Piccinini AM, Inglis J, Trebaul A, Chan E, et al. Tenascin-C is an endogenous activator of Toll-like receptor 4 that is essential for maintaining inflammation in arthritic joint disease. Nat Med 2009;15:774–80.
13. Huang ZY, Stabler T, Pei FX, Kraus VB. Both systemic and local lipopolysaccharide (LPS) burden are associated with knee OA severity and inflammation. Osteoarthritis Cartilage 2016;24:1769–75.
14. Itagaki K, Adibnia Y, Sun S, Zhao C, Sursal T, Chen Y, et al. Bacterial DNA induces pulmonary damage via TLR-9 through cross-talk with neutrophils. Shock 2011;36:548–52.
15. Bauer S, Kirschning CJ, Häcker H, Redecke V, Hausmann S, Akira S, et al. Human TLR9 confers responsiveness to bacterial DNA via species-specific CpG motif recognition. Proc Natl Acad Sci U S A 2001;98:9237–42.
16. Gómez-Moreno R, Robledo IE, Baerga-Ortiz A. Direct detection and quantification of bacterial genes associated with inflammation in DNA isolated from stool. Adv Microbiol 2014;4:1065–75.
17. Schwartz DA, Quinn TJ, Thorne PS, Sayeed S, Yi AK, Krieg AM. CpG motifs in bacterial DNA cause inflammation in the lower respiratory tract. J Clin Invest 1997;100:68–73.
18. Martinez-Martinez RE, Abud-Mendoza C, Patiño-Marin N, Rizo-Rodríguez JC, Little JW, Loyola-Rodríguez JP. Detection of periodontal bacterial DNA in serum and synovial fluid in refractory rheumatoid arthritis patients. J Clin Periodontol 2009;36:1004–10.
19. Pretorius E, Akeredolu OO, Soma P, Kell DB. Major involvement of bacterial components in rheumatoid arthritis and its accompanying oxidative stress, systemic inflammation and hypercoagulability. Exp Biol Med (Maywood) 2017;242:355–73.
20. Zhao Y, Chen B, Li S, Yang L, Zhu D, Wang Y, et al. Detection and characterization of bacterial nucleic acids in culture-negative synovial tissue and fluid samples from rheumatoid arthritis or osteoarthritis patients. Sci Rep 2018;8:14305.
21. Stinson LF, Keelan JA, Payne MS. Identification and removal of contaminating microbial DNA from PCR reagents: impact on low-biomass microbiome analyses. Lett Appl Microbiol 2019;68:2–8.

22. Champlot S, Berthelot C, Pruvost M, Bennett EA, Grange T, Geigl EM. An efficient multistrategy DNA decontamination procedure of PCR reagents for hypersensitive PCR applications. PLoS One 2010;5:e13042.
23. Pritzker KP, Gay S, Jimenez SA, Ostergaard K, Pelletier JP, Revell PA, et al. Osteoarthritis cartilage histopathology: grading and staging. Osteoarthritis Cartilage 2006;14:13–29.
24. 16S metagenomic sequincing library preparation: preparing 16s ribosomal RNA gene amplicons for the illumina MiSeq system. URL: https://support.illumina.com/documents/documentation/chemistry_documentation/16s/16s-metagenomic-library-prep-guide-15044223-b.pdf.
25. Caporaso JG, Kuczynski J, Stombaugh J, Bittinger K, Bushman FD, Costello EK, et al. QIIME allows analysis of high-throughput community sequencing data. Nat Methods 2010;7:335–6.
26. Edgar RC. Search and clustering orders of magnitude faster than BLAST. Bioinformatics 2010;26:2460–1.
27. McDonald D, Price MN, Goodrich J, Nawrocki EP, DeSantis TZ, Probst A, et al. An improved Greengenes taxonomy with explicit ranks for ecological and evolutionary analyses of bacteria and archaea. ISME J 2012;6:610–8.
28. Chang Q, Luan Y, Sun F. Variance adjusted weighted UniFrac: a powerful beta diversity measure for comparing communities based on phylogeny. BMC Bioinformatics 2011;12:118.
29. Hamady M, Knight R. Microbial community profiling for human microbiome projects: tools, techniques, and challenges. Genome Res 2009;19:1141–52.
30. Segata N, Izard J, Waldron L, Gevers D, Miropolsky L, Garrett WS, et al. Metagenomic biomarker discovery and explanation. Genome Biol 2011;12:R60.
31. Kruskal WH, Wallis WA. Use of ranks in one-criterion variance analysis. J Am Stat Assoc 1952;47:583–621.
32. Fisher RA. The use of multiple measurements in taxonomic problems. Ann Eugen 1936;7:179–88.
33. Battaglia T. LefSe. In: An introduction to QIIME 1.9.1. URL: https://twbattaglia.gitbooks.io/introduction-to-qiime/content/lefse.html.
34. Blackwood CB, Oaks A, Buyer JS. Phylum- and class-specific PCR primers for general microbial community analysis. Appl Environ Microbiol 2005;71:6193–8.
35. Mühling M, Woolven-Allen J, Murrell JC, Joint I. Improved group-specific PCR primers for denaturing gradient gel electrophoresis analysis of the genetic diversity of complex microbial communities. ISME J 2008;2:379–92.
36. Yang YW, Chen MK, Yang BY, Huang XJ, Zhang XR, He LQ, et al. Use of 16S rRNA gene-targeted group-specific primers for real-time PCR analysis of predominant bacteria in mouse feces. Appl Environ Microbiol 2015;81:6749–56.
37. Khan IU, Yadav JS. Real-time PCR assays for genus-specific detection and quantification of culturable and non-culturable mycobacteria and pseudomonads in metalworking fluids. Mol Cell Probes 2004;18:67–73.
38. Miller TR, Franklin MP, Halden RU. Bacterial community analysis of shallow groundwater undergoing sequential anaerobic and aerobic chloroethene biotransformation. FEMS Microbiol Ecol 2007;60:299–311.
39. Livak KJ, Schmittgen TD. Analysis of relative gene expression data using real-time quantitative PCR and the 2(−ΔΔC(T)) method. Methods 2001;25:402–8.
40. Langille MG, Zaneveld J, Caporaso JG, McDonald D, Knights D, Reyes JA, et al. Predictive functional profiling of microbial communities using 16S rRNA marker gene sequences. Nat Biotechnol 2013;31:814–21.
41. Kanehisa M, Goto S. KEGG: kyoto encyclopedia of genes and genomes. Nucleic Acids Res 2000;28:27–30.
42. Parks DH, Tyson GW, Hugenholtz P, Beiko RG. STAMP: statistical analysis of taxonomic and functional profiles. Bioinformatics 2014;30:3123–4.
43. Emery DC, Shoemark DK, Batstone TE, Waterfall CM, Coghill JA, Cerajewska TL, et al. 16S rRNA next generation sequencing analysis shows bacteria in Alzheimer's post-mortem brain. Front Aging Neurosci 2017;9:195.
44. Manasson J, Shen N, Garcia Ferrer HR, Ubeda C, Iraheta I, Heguy A, et al. Gut microbiota perturbations in reactive arthritis and postinfectious spondyloarthritis. Arthritis Rheumatol 2018;70:242–54.
45. Xu YY, Tan X, He YT, Zhou YY, He XH, Huang RY. Role of gut microbiome in ankylosing spondylitis: an analysis of studies in literature. Discov Med 2016;22:361–70.
46. Scher JU, Joshua V, Artacho A, Abdollahi-Roodsaz S, Öckinger J, Kullberg S, et al. The lung microbiota in early rheumatoid arthritis and autoimmunity. Microbiome 2016;4:60.
47. Shin NR, Whon TW, Bae JW. Proteobacteria: microbial signature of dysbiosis in gut microbiota. Trends Biotechnol 2015;33:496–503.
48. Boer CG, Radjabzadeh D, Medina-Gomez C, Garmaeva S, Schiphof D, Arp P, et al. Intestinal microbiome composition and its relation to joint pain and inflammation. Nat Commun 2019;10:4881.
49. Hildebrandt MA, Hoffmann C, Sherrill-Mix SA, Keilbaugh SA, Hamady M, Chen YY, et al. High-fat diet determines the composition of the murine gut microbiome independently of obesity. Gastroenterology 2009;137:1716–24.
50. Bondeson J, Blom AB, Wainwright S, Hughes C, Caterson B, van den Berg WB. The role of synovial macrophages and macrophage-produced mediators in driving inflammatory and destructive responses in osteoarthritis [review]. Arthritis Rheum 2010;62:647–57.
51. Kim HA, Cho ML, Choi HY, Yoon CS, Jhun JY, Oh HJ, et al. The catabolic pathway mediated by Toll-like receptors in human osteoarthritic chondrocytes. Arthritis Rheum 2006;54:2152–63.
52. Wang J, Tang H, Zhang C, Zhao Y, Derrien M, Rocher E, et al. Modulation of gut microbiota during probiotic-mediated attenuation of metabolic syndrome in high fat diet-fed mice. ISME J 2015;9:1–15.
53. Metcalfe D, Harte AL, Aletrari MO, Al Daghri NM, Al Disi D, Tripathi G, et al. Does endotoxaemia contribute to osteoarthritis in obese patients? Clin Sci (Lond) 2012;123:627–34.
54. Berthelot JM, Sellam J, Maugars Y, Berenbaum F. Cartilage-gut-microbiome axis: a new paradigm for novel therapeutic opportunities in osteoarthritis [review]. RMD Open 2019;5:e001037.
55. Saraswati S, Sitaraman R. Aging and the human gut microbiota—from correlation to causality. Front Microbiol 2014;5:764.
56. Korkina LG, Mikhal'Chik E, Suprun MV, Pastore S, Dal Toso R. Molecular mechanisms underlying wound healing and anti-inflammatory properties of naturally occurring biotechnologically produced phenylpropanoid glycosides. Cell Mol Biol (Noisy-le-grand) 2007;53:84–91.
57. Yin W, Park JI, Loeser RF. Oxidative stress inhibits insulin-like growth factor-I induction of chondrocyte proteoglycan synthesis through differential regulation of phosphatidylinositol 3-kinase-Akt and MEK-ERK MAPK signaling pathways. J Biol Chem 2009;284:31972–81.
58. Findlay DM, Atkins GJ. Osteoblast-chondrocyte interactions in osteoarthritis. Curr Osteoporos Rep 2014;12:127–34.
59. Abramson SB. Osteoarthritis and nitric oxide. Osteoarthritis Cartilage 2008;16 Suppl 2:S15–20.

Arthritis & Rheumatology
Vol. 72, No. 7, July 2020, pp 1123–1133
DOI 10.1002/art.41230

American College of Rheumatology
Empowering Rheumatology Professionals

Positive Effects of a Young Systemic Environment and High Growth Differentiation Factor 11 Levels on Chondrocyte Proliferation and Cartilage Matrix Synthesis in Old Mice

Lu Li,[1] Xiaochun Wei,[1] Dongming Wang,[1] Zhi Lv,[1] Xiang Geng,[2] Pengcui Li,[1] Jiangong Lu,[1] Kaihang Wang,[3] Xiaohu Wang,[1] Jian Sun,[1] Xiaoming Cao,[1] and Lei Wei[4]

Objective. To investigate the effects of a young systemic environment and growth differentiation factor 11 (GDF-11) on aging cartilage.

Methods. A heterochronic parabiosis model (2-month-old mouse and 12-month-old mouse [Y/O]), an isochronic parabiosis model (12-month-old mouse and 12-month-old mouse [O/O]), and 12-month-old mice alone (O) were evaluated. Knee joints and chondrocytes from old mice were examined by radiography, histology, cell proliferation assays, immunohistochemistry, Western blotting, and quantitative reverse transcriptase–polymerase chain reaction 16 weeks after parabiosis surgery. GDF-11 was injected into 12-month-old mouse joints daily for 16 weeks. Cartilage degeneration, cell proliferation, and osteoarthritis-related gene expression were evaluated.

Results. Osteoarthritis Research Society International scores in old mice were significantly lower in the Y/O group than in the O/O and O groups (both $P < 0.05$). The percentage of 5-ethynyl-2′-deoxyuridine–positive chondrocytes in old mice was significantly higher in the Y/O group than in the other groups ($P < 0.05$). Type II collagen (CII) and SOX9 messenger RNA levels differed in cartilage from old mice in the Y/O group compared to the O/O and O groups (both $P < 0.05$). RUNX-2, CX, and matrix metalloproteinase 13 levels were significantly lower in cartilage from old mice in the Y/O group compared to the O/O and O groups (both $P < 0.05$). Similar results were obtained for protein expression levels and after GDF-11 treatment in vitro and in vivo. Phosphorylated Smad2/3 (pSmad2/3) levels were higher in the recombinant GDF-11–treated group than in the control group.

Conclusion. A young systemic environment promotes chondrocyte proliferation and cartilage matrix synthesis in old mice. GDF-11, a "young factor," contributes to these effects through the up-regulation of pSmad2/3.

INTRODUCTION

Osteoarthritis (OA) is one of the most common chronic diseases among the elderly and is related to age (1). Chondrocytes in the articular cartilage are specifically involved in the maintenance of cartilage hemostasis. Decreases in chondrocytes and in the cartilage proliferative capacity contribute to the degradation of the age-related OA cartilage matrix (2,3). As such, it is imperative to gain mechanistic insight into the factors that drive aging phenotypes in the cartilage in order to counteract vulnerability to cartilage dysfunction. Heterochronic parabiosis, the parabiotic pairing of 2 animals of different ages, can partially recover age-related regenerative faculties in old organs and tissues, such as the heart, olfactory nerve, and muscle (4–6). In heterochronic parabiosis, 2 animals of different ages develop vascular anastomoses and share a single circulatory system, providing an experimental system to evaluate systemic effects during cell and tissue aging and the development of age-related diseases (7). In this system, old tissue is exposed to the young systemic environment (8). However, it is not clear whether heterochronic parabiosis can improve articular cartilage in old mice.

Supported by the International Science and Technology Cooperation (project 2015DFA33050) and the National Natural Science Foundation of China (grant 81601949).

[1]Lu Li, MD, PhD, Xiaochun Wei, MD, PhD, Dongming Wang, MS, Zhi Lv, MD, PhD, Pengcui Li, MD, PhD, Jiangong Lu, MS, Xiaohu Wang, MD, PhD, Jian Sun, MD, PhD, Xiaoming Cao, MD, PhD: The Second Hospital of Shanxi Medical University, Taiyuan, China; [2]Xiang Geng, MS: Shanxi Health Vocational College, Jinzhong, China; [3]Kaihang Wang, BS: Subsidiary High School of Taiyuan Normal University, Taiyuan, China; [4]Lei Wei, MD, PhD: Warren Alpert Medical School of Brown University, Providence, Rhode Island.

No potential conflicts of interest relevant to this article were reported.

Address correspondence to Lei Wei, MD, PhD, Warren Alpert Medical School of Brown University, RIH PO Box G-A1, Providence, RI 02912 (e-mail: lei_wei@brown.edu); or to Xiaochun Wei, MD, PhD, The Second Hospital of Shanxi Medical University, Department of Orthopaedics, Shanxi Key Laboratory of Bone and Soft Tissue Injury Repair, 382 Wuyi Road, Taiyuan, Shanxi 030001, China (e-mail: sdeygksys@163.com).

Submitted for publication January 4, 2019; accepted in revised form February 6, 2020.

Heterochronic parabiosis can be used to identify factors that aggravate the age-dependent deterioration of the knee joint niche in mice, providing a basis for the development of treatments for age-related OA. For example, heterochronic parabiosis studies have shown that growth differentiation factor 11 (GDF-11), a "young factor" with higher levels in the blood of young mice than old mice, has positive effects on elderly tissue and organs. GDF-11 has broad roles in mammalian development and growth; it can regulate the development of organs, such as the pancreas, kidney, spleen, olfactory nerve, and retina (9–12). It can reverse rat heart muscle hypertrophy (4) and regenerate muscle tissues in old mice (13). GDF-11 can also activate the transforming growth factor β (TGFβ) signaling pathway, promote the proliferation of cerebral capillary endothelial cells by phosphorylating Smad2/3, and promote olfactory nerve regeneration (14). Considering that phosphorylated Smad2/3 in the TGFβ signaling pathway inhibit the hypertrophy of chondrocytes and promote the chondrocyte secretion of type II collagen (CII) (15,16), we hypothesized that a young systemic environment has a positive effect on chondrocyte proliferation and cartilage matrix synthesis. GDF-11 is a young factor that can promote CII production and cell proliferation in old mice via the phosphorylation of Smad2/3. To evaluate these hypotheses, we used a heterochronic parabiosis model and administered injections of recombinant GDF-11 (rGDF-11) to old mice.

MATERIALS AND METHODS

Animals. Aged (12-month-old) and young (2-month-old) male C57BL/6 mice were obtained from the Experimental Animal Center at Shanxi Medical University. Mice were housed under specific pathogen–free conditions and a 12-hour light/dark cycle. All animal handling and use was in accordance with the Guide for the Care and Use of Laboratory Animals and approved by the Institutional Review Board (IRB) of the Second Hospital of Shanxi Medical University (approval project identification code 2013025; January 2013–December 2018). For the parabiosis experiment, group 1 (also referred to as the young/old [Y/O] group; heterochronic parabiotic pairs, experimental group) included 2-month-old male C57BL/6 mice surgically joined to 12-month-old partners (n = 8

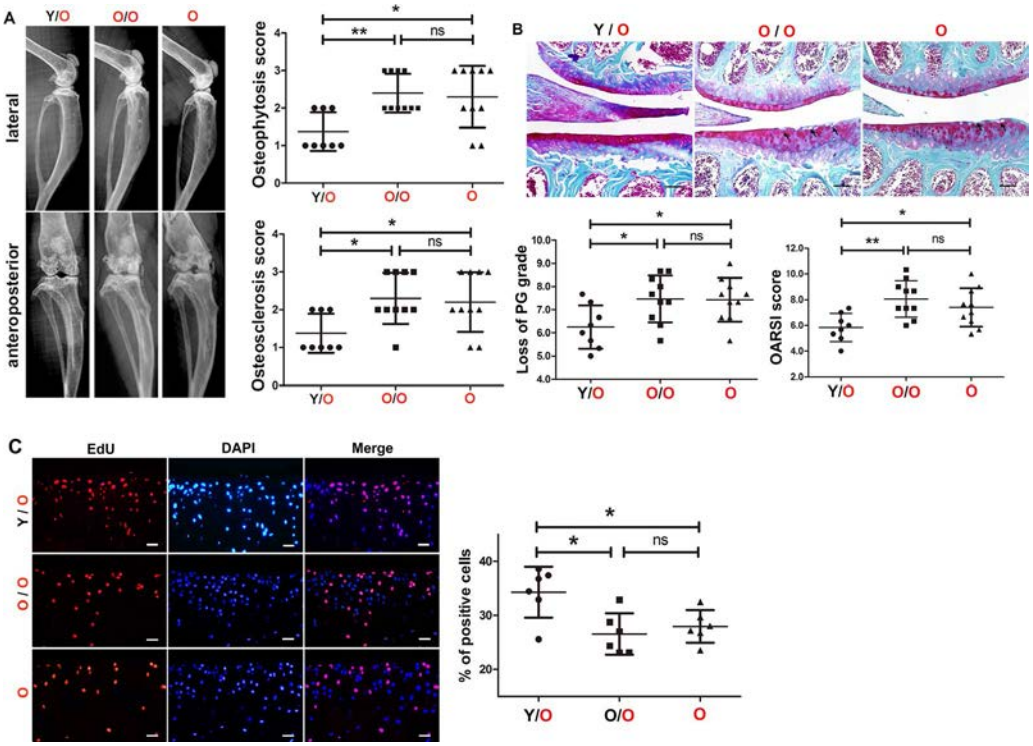

Figure 1. Positive effects of heterochronic parabiosis on chondrocyte proliferation in old mice. **A**, The presence and severity of osteophytosis and sclerosis were evaluated by microradiography. Osteophytosis, ligamentum ossification, and meniscus ossification were more severe around the knee joint in old mice in the old/old group (O/O; n = 10 mice) and old-alone group (O; n = 10 mice) than in the young/old group (Y/O; n = 8 mice). Osteophytosis and osteosclerosis scores in the Y/O group were lower compared to the other groups. **B**, Articular cartilage injury and proteoglycan (PG) grades decreased less in the cartilage from old mice in the Y/O group compared to the other groups. Representative images are shown. Bars = 500 μm. Histologic scores of the Y/O group were low. Cartilage loss (PG grade) and Osteoarthritis Research Society International (OARSI) scores in the Y/O group were significantly lower than those in the O/O and O groups. **C**, The Y/O group displayed a higher percentage of 5-ethynyl-2′-deoxyuridine (EdU)–positive chondrocytes (red). Original magnification × 400. Bars = 200 μm. Chondrocyte proliferation was elevated in the Y/O group (n = 6 per group) and was significantly higher compared to the other groups. Each symbol represents an individual mouse; bars show the mean ± SD. * = $P < 0.05$; ** = $P < 0.01$. NS = not significant.

pairs); group 2 (O/O; isochronic parabiotic pairs, surgery control group) included 12-month-old mice joined at identical ages (n = 5 pairs); and group 3 (O) included 12-month-old mice alone (n = 10 individual mice). For the in vivo GDF-11 experiment, 12-month-old mice were randomly divided into 2 groups: group 1 (experimental group) (rGDF-11 100 ng/kg, daily intraperitoneal injection for 16 weeks; no. 120-11, PeproTech) and group 2 (control group) (saline 100 ng/kg, daily intraperitoneal injection for 16 weeks).

Parabiosis surgery. Parabiosis surgery was performed according to previously described procedures (17). The specific procedure for parabiosis surgery is described in the Supplementary Methods (available on the *Arthritis & Rheumatology* web site at http://onlinelibrary.wiley.com/doi/10.1002/art.41230/abstract).

Human cartilage specimens. Articular cartilage samples were obtained at the time of knee replacement surgery (n = 6; 4 female and 2 male patients). The mean ± SD age in this group was 74.00 ± 1.13 years (range 70–78). Serum in the young group was collected from 10 patients (5 female and 5 male), with a mean ± SD age of 17.7 ± 0.68 years (range 14–20). Serum in the older group was collected from 10 patients (7 female and 3 male), with a mean ± SD age of 72.6 ± 1.10 years (range 66–78). Patients with rheumatoid arthritis and other autoimmune diseases, as well as chondrodysplasias and posttraumatic OA, were excluded from this study. The study was approved by the IRB of the Second Hospital of Shanxi Medical University, and informed consent was obtained from each tissue and serum donor.

Human serum collection and analysis. Human serum samples were aliquoted and frozen at −80°C until analysis. The level of GDF-11 in human serum was measured by Western blotting.

Chondrocyte isolation and primary culture. Human chondrocytes were isolated as previously described (18) and plated in 6-well culture plates at 1×10^6 cells/plate. At 90% confluence, the cells were cultured overnight under serum-free conditions and treated with human rGDF-11 (100 ng/ml) for 48 hours before collection and analysis.

Fluorescence molecular tomography (FMT). The heterochronic parabiosis model was built 2 weeks after surgery; an FMT4000 (PerkinElmer) was used to confirm common blood circulation. FMT is a noninvasive fluorescence-based technology with high molecular specificity and sensitivity for tissue imaging in live animals (19). ProSense 750 Fluorescent Agents (PerkinElmer) become fluorescent when activated by cathepsins (cathepsins B, L, S, and plasmin) but are optically silent in the inactivated state. The old mouse in the model was injected with ProSense 750FAST via the tail vein, and the young mouse was evaluated using an FMT4000 at 24 hours postinjection with a needle at the wound site.

Radiography. Knee joints were examined by microradiograph analyses (Faxitron) to identify morphologic changes in the entire knee before mice were euthanized. Radiographic grading was based on previously published numerical rating scales (20). The presence and severity of osteophytosis (0–3 scale), osteopenia (not evident during this study), and sclerosis (not evident during this study) were determined. Osteophytosis was graded subjectively on a 0–3 scale (0, normal; 1, mild; 2, moderate; 3, severe) based on severity at the margins of the knee joint.

Histology. Knee cartilage was collected from all 3 groups of 16-month-old mice at 16 weeks after parabiosis surgery. On the scheduled day of euthanasia, the mice were anesthetized by an intraperitoneal injection of pentobarbital sodium. The right knees were collected for histologic examination, 5-ethynyl-2′-deoxyuridine (EdU) staining, and immunohistochemical staining. The microscopic scoring of mouse cartilage degeneration followed previously described procedures (21). Blocks were trimmed to expose cartilage. Frontal serial sections (5 μm thick) across entire joints were obtained. Three 5-μm sections were placed on each slide to obtain 15 slides. Samples were harvested at ~80-μm intervals and stained with Safranin O–fast green for histologic scoring. Intervening sections were stored for EdU staining and immunohistochemical staining. Joint cartilage degeneration was assessed using the Osteoarthritis Research Society International (OARSI) scoring system (19), and proteoglycan (PG) depletion was measured subjectively based on Safranin O staining and a semiquantitative scoring system (21). Three independent and blinded observers (XW, JS, XC) scored each section, and the scores for all of the sections cut from the medial femoral condyle and medial tibial plateaus were summed within each joint. Three sections from each animal were used to obtain OARSI scores.

EdU incorporation. EdU staining was performed using a Cell-Light Apollo Stain Kit, according to the protocol provided by the manufacturer (RiboBio; no. C10371-1). The mice were intraperitoneally injected with 5 μg/gm/day EdU for 7 days before they were euthanized. After they were deparaffinated, sections were rinsed with glycine for 10 minutes, permeabilized with 0.5% Triton X-100 in phosphate buffered saline (PBS) for 10 minutes, rinsed 3 times for 10 minutes each, and incubated with Apollo reaction cocktail for 30 minutes at room temperature. Next, the slides were permeabilized with 0.5% Triton X-100 in PBS for 10 minutes and rinsed twice with methanol for 5 minutes each. Finally, nuclear counterstaining was performed using DAPI, and the samples were mounted with 50% glycerinum. Images were obtained by fluorescence microscopy. EdU-positive and DAPI-positive cells were counted using Image J, and the EdU labeling index (defined as the ratio of EdU-positive cells:DAPI-positive

cells) was calculated. The threshold fluorescence intensity was set based on the range that enables detection of these cells. Two fields per slide, 2 slides per knee, and 6 knees per group were analyzed.

Immunohistochemistry. Immunohistochemical staining was performed to detect CII, CX, matrix metalloproteinase 13 (MMP-13), SOX9, and RUNX-2 in the cartilage from old mice. To detect the expression of Smad2/3 and pSmad2/3 in cartilage, 6-μm sections were analyzed by immunofluorescence staining. These procedures are described in Supplementary Methods (http://onlinelibrary.wiley.com/doi/10.1002/art.41230/abstract).

Real-time polymerase chain reaction (PCR). The left knees in each group were collected for messenger RNA (mRNA) analyses, and cartilage samples were collected from the tibia. The cartilage samples were ground with a mortar and pestle under liquid nitrogen, and total RNA was isolated following previously described procedures (22) using an RNeasy Isolation Kit (no. 74704; Qiagen). Cartilage samples from 2 mouse tibial plateaus were dissected with a scalpel under a dissecting microscopy and pooled. Four pooled samples per group were used. A total of 1 μg of total RNA was reverse-transcribed to complementary DNA using the iScript cDNA Synthesis Kit (Bio-Rad). Complementary DNA (40 ng/μl) was used as a template to quantify relative mRNA levels using a QuantiTect SYBR Green PCR Kit (Qiagen), with a DNA

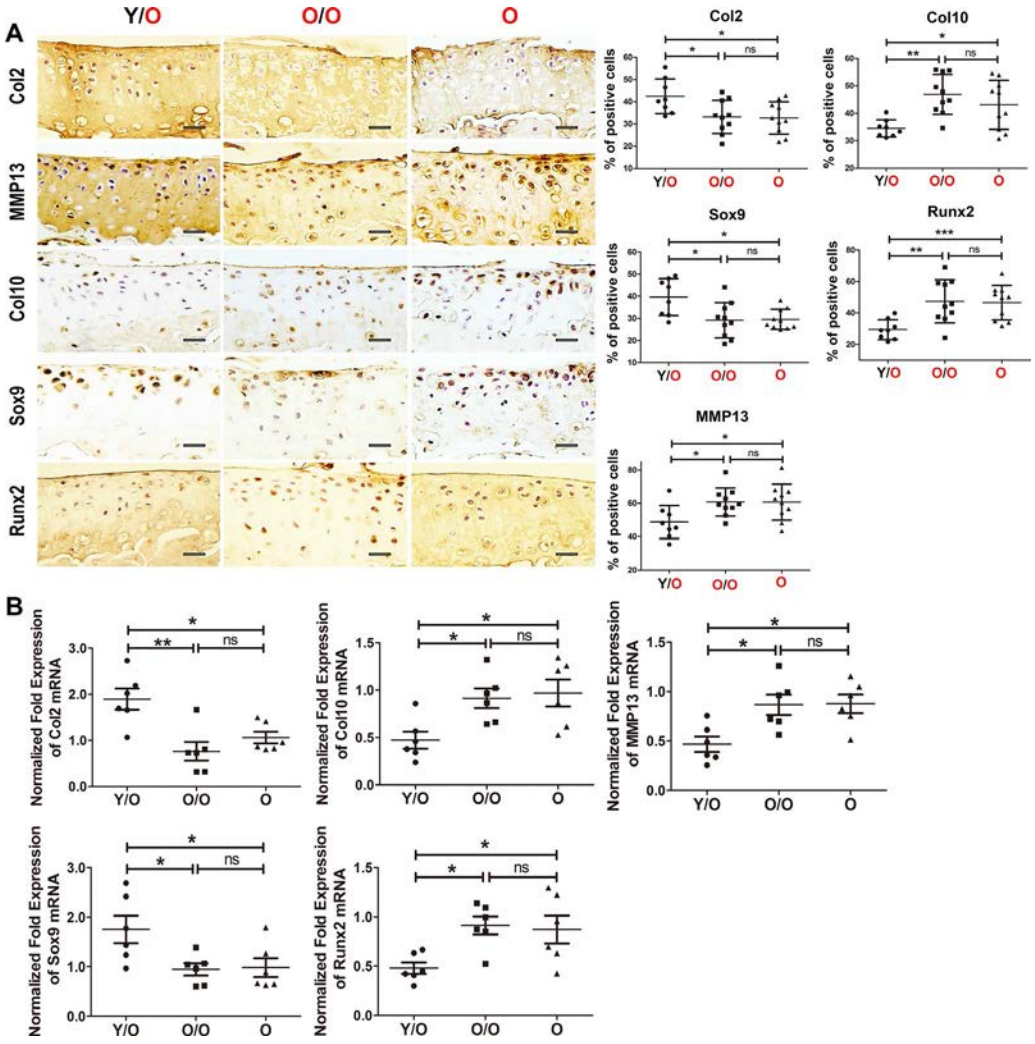

Figure 2. Protein and mRNA expression of type II collagen (CII; Col2), CX (Col10), matrix metalloproteinase 13 (MMP-13), SOX9, and RUNX-2 in cartilage from old mice. **A**, Protein expression levels of CII, CX, MMP-13, SOX9, and RUNX-2 in articular cartilage from old mice in the Y/O group (n = 8 mice), O/O group (n = 10 mice), and O group (n = 10 mice) were analyzed by immunohistochemistry. Positive chondrocytes are shown in brown. Bars = 200 μm. CII and SOX9 levels in cartilage from old mice were higher in the Y/O group compared to the O/O and O groups. However, protein levels of CX, MMP-13, and RUNX-2 were reduced in cartilage from old mice in the Y/O group compared to those in the O/O and O groups. **B**, Changes in CII, CX, MMP-13, SOX9, and RUNX-2 at the mRNA level mimicked the alterations observed at the protein level (n = 6 per group). Each symbol represents an individual mouse; bars show the mean ± SD. * = $P < 0.05$; ** = $P < 0.01$; *** = $P < 0.001$. See Figure 1 for other definitions.

Engine Opticon 2 Continuous Fluorescence Detection System (MJ Research). The primers are listed in Supplementary Tables 1 and 2 (http://onlinelibrary.wiley.com/doi/10.1002/art.41230/abstract).

Western blotting. Blood samples were collected from the abdominal vein, and Western blot analyses were performed as previously described (18). Specific procedures are described in Supplementary Methods (http://onlinelibrary.wiley.com/doi/10.1002/art.41230/abstract).

Statistical analysis. Data are expressed as the mean ± SD. Statistical analyses were performed using GraphPad Prism 5.0. The means for different groups in the analyses of parabiosis models were compared using one-way analysis of variance followed by Tukey's multiple comparisons test. Additionally, *t*-tests were used to compare protein and mRNA levels in cartilage or chondrocyte specimens in the GDF-11 and control groups. *P* values less than 0.05 were considered significant.

RESULTS

Increase in EdU-positive chondrocytes in cartilage from old mice exposed to a young systemic environment. The presence and severity of osteophytosis and osteosclerosis was detected by microradiography: osteophytosis, ligamentum ossification, and meniscus ossification were more severe around the knee joints in old mice in the O/O and O groups than in the Y/O group (Figure 1). Osteophytosis scores and osteosclerosis scores in old mice from the Y/O group were lower than those in the other 2 groups ($P < 0.05$) (Figure 1A). Safranin O staining was conducted to analyze changes in chondrocyte-derived PG levels. The loss of PG in cartilage from old mice was significantly lower in the Y/O group than in the O/O and O groups at 16 weeks post surgery, and the OARSI scores in cartilage from young mice in the Y/O group tended to be lower compared to the O/O and O groups (Figure 1B). Differences between the 3 groups were statistically significant ($P < 0.05$), indicating that a young systemic environment relieved cartilage damage and PG loss in cartilage from old mice.

The loss of PG in cartilage from young mice and the changes in SOX9 and RUNX-2 levels in young chondrocytes might be attributed, at least in part, to an age-related abatement in chondrocyte proliferation. Therefore, the contribution of an aged systemic environment to chondrocyte proliferation was investigated using EdU. EdU-positive chondrocytes were observed in the full layer of cartilage and mainly concentrated in the superficial layer, and EdU-positive cell clusters were not observed. Remarkably, the number of EdU-positive chondrocytes was higher in cartilage from old mice in the Y/O group than in the O/O and O groups (Figure 1C). These data suggest that a young systemic environment can positively affect PG synthesis and strengthen chondrocyte proliferation.

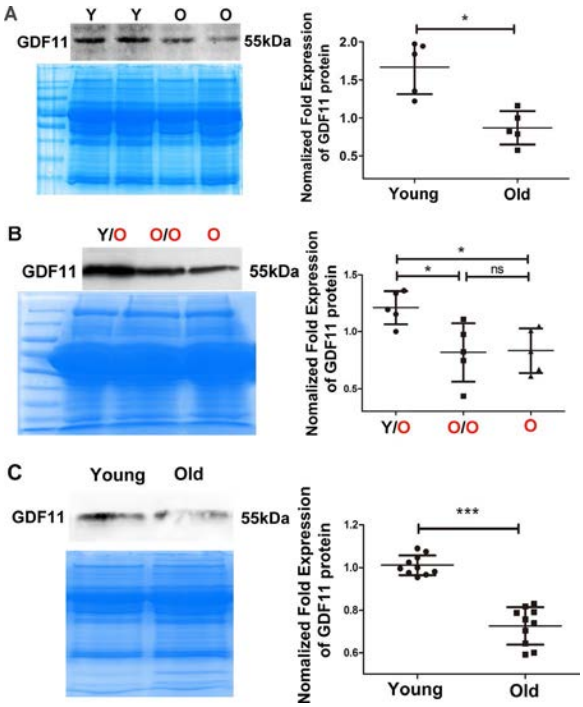

Figure 3. Circulating levels of growth differentiation factor 11 (GDF-11) are reduced in aged mice, and those in young mice are restored by heterochronic parabiosis. **A**, Western blot analysis showed lower serum levels of GDF-11 in old mice compared to young mice (n = 5 per group). GDF-11 protein levels were also lower in old mice compared to young mice. **B**, GDF-11 levels were lower in serum from old mice in the O/O and O groups than in the Y/O group (n = 5 per group). GDF-11 protein levels were higher in the Y/O group than in the O/O and O groups, and there was no significant difference between the O/O and O groups. **C**, GDF-11 level changes in human serum (n = 10 per group) were similar to the alterations observed in mouse serum. GDF-11 protein levels were lower in old mice compared to young mice. Each symbol represents an individual subject; bars show the mean ± SD. * = $P < 0.05$; *** = $P < 0.001$. See Figure 1 for other definitions.

Young systemic environment induces significant changes in protein and mRNA levels of CII, CX, MMP-13, SOX9, and RUNX-2. There were substantially more CII/SOX9-positive chondrocytes in cartilage from old mice in the Y/O group than in the O/O and O groups (Figure 2A). In contrast, there were fewer CX/MMP-13/RUNX-2–positive chondrocytes following exposure to an aged systemic environment (Figure 2A). Immunostaining was absent in the negative control sections (not shown). These results further confirmed that a young systemic environment positively affected old articular cartilage.

Restoration by heterochronic parabiosis of reduced GDF-11 in the circulation of aged mice. In order to determine the mechanisms underlying the age-dependent reduction of circulating GDF-11, we performed Western blotting to analyze its expression in serum samples collected from young and old mice. GDF-11 expression in old mice was significantly lower than that

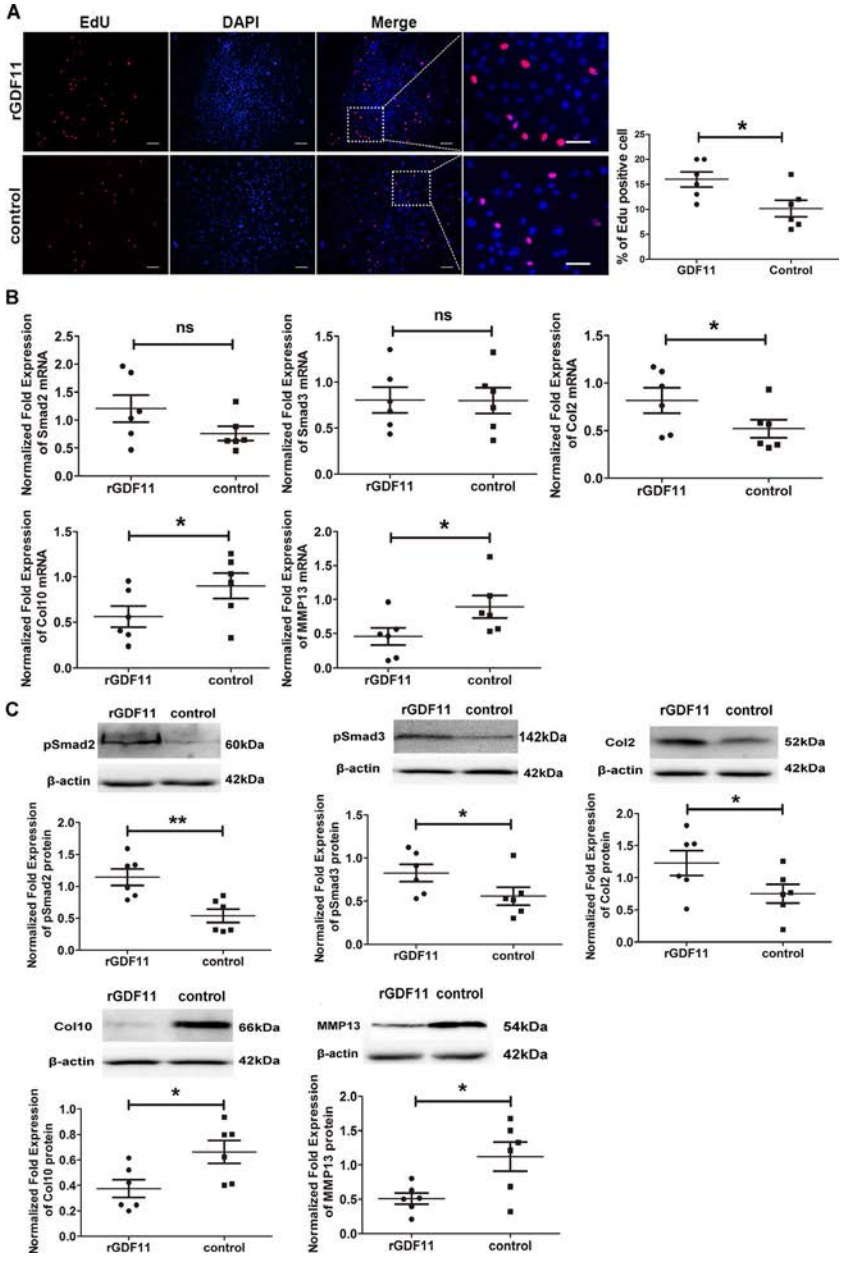

Figure 4. Growth differentiation factor 11 (GDF-11) increases chondrocyte proliferation, Smad2/3 phosphorylation, and type II collagen (CII; Col2) secretion in human subjects. **A**, EdU staining showed more positive chondrocytes (red) in the recombinant GDF-11 (rGDF-11) group compared to the control group. Bars = 200 μm. **B**, Expression levels of Smad2, Smad3, CII, CX (Col10), and matrix metalloproteinase 13 (MMP-13) in chondrocytes treated with rGDF-11 or saline are shown. Quantitative reverse transcriptase–polymerase chain reaction showed that CII mRNA levels were higher in the rGDF-11 group than in the control group, and the levels of CX and MMP-13 mRNA were lower in the rGDF-11 group than in the control group. There were no significant differences in Smad2 and Smad3 between the 2 groups. **C**, Results of Western blot analyses of chondrocytes stimulated for 48 hours with serum-free medium (control) or with the same medium containing rGDF-11 are presented. Levels of pSmad2, pSmad3, and CII were higher and levels of CX and MMP-13 were lower in the rGDF-11 group than in the control group. Each symbol represents an individual subject; bars show the mean ± SD. * = $P < 0.05$; ** = $P < 0.01$. See Figure 1 for other definitions.

in young mice ($P < 0.05$) (Figure 3A). To determine whether GDF-11 accounts for the regression in knee degeneration in old mice exposed to the young circulation, we also analyzed GDF-11 expression in serum samples from old mice subjected to heterochronic and isochronic parabiosis (16 weeks). GDF-11 expression in old mice was significantly greater in the Y/O group than in the O/O and O groups ($P < 0.05$) (Figure 3B). GDF-11 expression in humans was consistent with this (Figure 3C). Accordingly, GDF-11 was expressed at higher levels in young and heterochronic old serum than in old serum.

GDF-11 increases chondrocyte proliferation, Smad2/3 phosphorylation, and CII in vitro in human subjects. To explore whether GDF-11 could restore the age-related degeneration in articular cartilage and the role of the TGFβ signaling pathway, old chondrocytes collected from the tibial plateau after knee arthroplasty were treated with rGDF-11. More chondrocytes were detected in the rGDF-11 group than in the control group, and the migration ability of chondrocytes was greater in the rGDF-11 group (Supplementary Figures 2A and B, http://onlinelibrary.wiley.com/doi/10.1002/art.41230/abstract). Furthermore, there were significantly more EdU-positive chondrocytes in the rGDF-11 group than in the control group ($P < 0.05$) (Figure 4A). Based on quantitative reverse transcriptase–PCR (qRT-PCR), there were no statistically significant differences in relative levels of Smad2 or Smad3, but relative CII expression was higher in the rGDF-11 group than in the control group ($P < 0.05$) (Figure 4B), and CX and MMP-13 levels were lower in the rGDF-11 group (Figure 4B). Of note, protein expression levels of pSmad2, pSmad3, and CII, as determined by Western blotting, were higher in the rGDF-11 group than in the control group ($P < 0.05$) (Figure 4C). These data revealed that GDF-11 could increase the proliferation capacity of chondrocytes, Smad2/3 phosphorylation, and the secretion of CII.

GDF-11 attenuates age-related knee degeneration and increases EdU-positive chondrocytes in cartilage from old mice in vivo. To confirm the effect of GDF-11 on elderly articular cartilage in vivo, 12-month-old mice were treated with a daily intraperitoneal injection of either rGDF-11 (0.1 mg/kg mouse body weight, a dosing regimen that increases GDF-11 levels in old mice toward levels in young mice [13]; GDF-11 group) or normal saline (vehicle; control group), for 16 weeks. The presence and severity of osteophytosis and osteosclerosis in the 2 groups was evaluated by microradiography. Osteophytosis, ligamentum ossification, and meniscus ossification were more severe around the knee joint in old mice from the control group (Figure 5). Osteophytosis scores and osteosclerosis scores in old mice from the GDF-11 group were lower than those in the control group ($P < 0.05$) (Figure 5A).

Based on Safranin O staining, the loss of chondrocyte-derived PG from the cartilage in old mice in the GDF-11 group was significantly lower compared to the control group at 16 weeks after daily intraperitoneal injections, and the OARSI scores for cartilage from old mice in the GDF-11 group decreased more substantially compared to the control group ($P < 0.05$) (Figure 5B). We evaluated whether changes in Safranin O staining in cartilage from old mice in the GDF-11 group could be attributed, at least

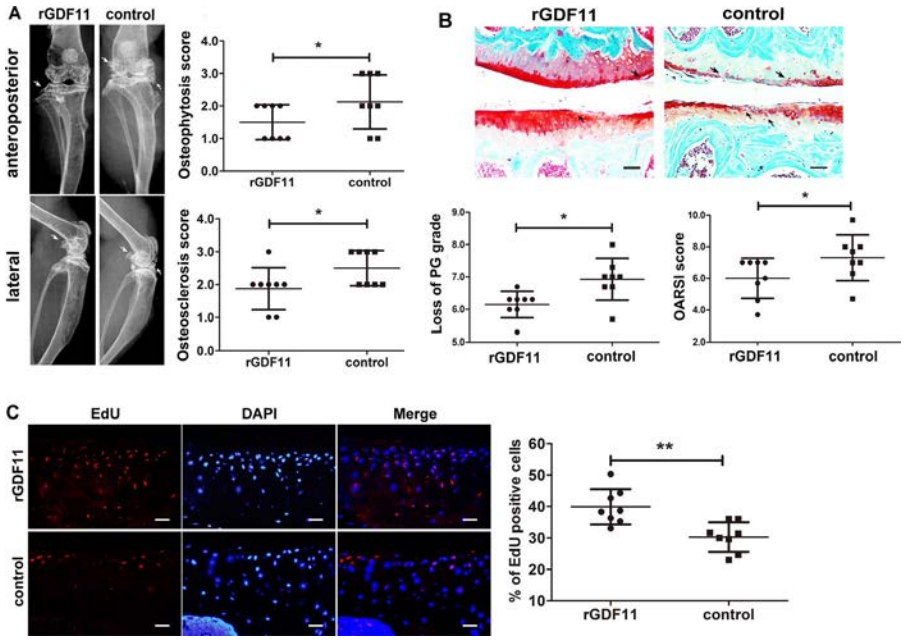

Figure 5. Age-related knee degeneration is attenuated, and EdU-positive chondrocytes are increased, by growth differentiation factor 11 (GDF-11) in cartilage from old mice. **A**, The presence and severity of osteopenia and sclerosis were assessed by microradiography. Osteophytosis, ligamentum ossification, and meniscus ossification (**arrows**) were more severe around the knee joints in old mice in the control group. Osteophytosis and osteosclerosis scores were lower in the recombinant GDF-11 (rGDF-11) group than in the control group. **B**, Articular cartilage injury (**arrows**) and PG grades in the cartilage from old mice were lower in the rGDF-11 group than in the control group. Representative images are shown (n = 8 per group). Bars = 200 μm. Cartilage loss (PG grade) and OARSI scores in the rGDF-11 group were significantly lower than in the control group. **C**, The rGDF-11 group displayed a higher percentage of EdU-positive chondrocytes (red). Original magnification × 400. Bars = 200 μm. Rates of chondrocyte proliferation were significantly higher in the rGDF-11 group compared to the control group (n = 8 per group). Each symbol represents an individual mouse; bars show the mean ± SD. * = $P < 0.05$; ** = $P < 0.01$. See Figure 1 for other definitions.

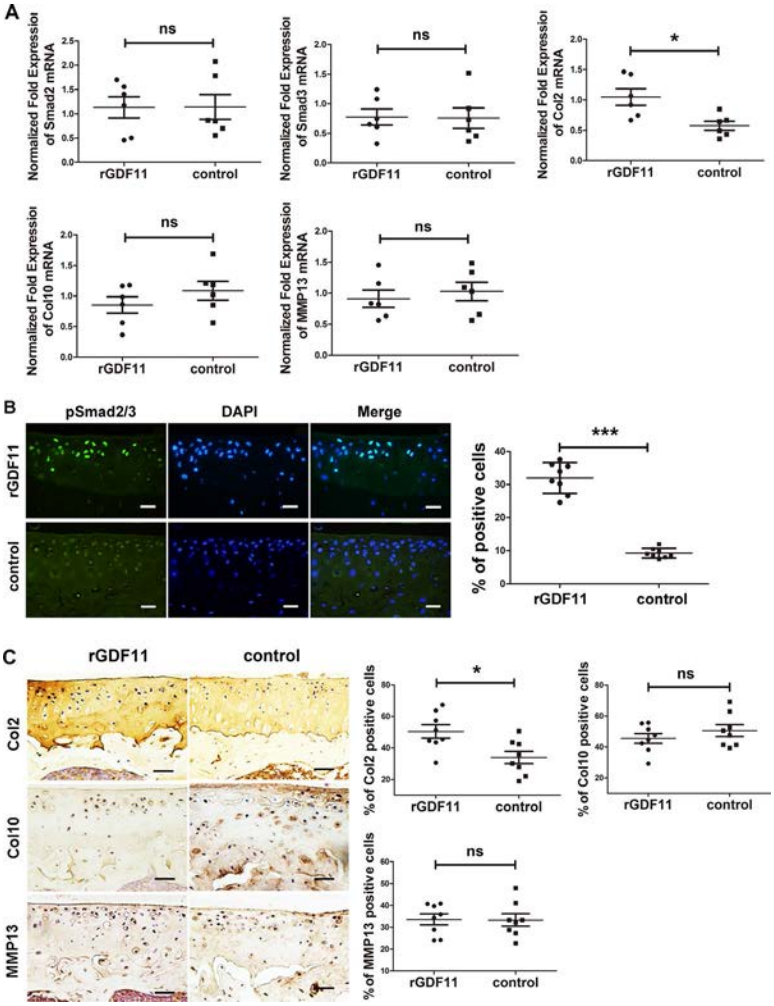

Figure 6. Secretion of CII in cartilage from old mice is promoted by GDF-11. **A**, Expression levels of Smad2, Smad3, CII, CX, and MMP-13 were determined by quantitative reverse transcriptase–polymerase chain reaction in the articular cartilage samples. No significant differences in the expression levels of Smad2, Smad3, CX, and MMP-13 were observed between the rGDF-11 group and the control group, but the expression of CII was significantly higher in the cartilage from old mice in rGDF-11 group compared to the control group. **B**, Cartilage samples from old mice in both groups were analyzed by immunofluorescence for pSmad2/3. Positive chondrocytes are shown in green. Bars = 200 μm. The level of pSmad2/3 was higher in cartilage from old mice in the GDF-11 group compared to the control group (n = 8 per group). **C**, Cartilage samples from old mice in the GDF-11 and control groups were analyzed by immunohistochemistry for CII, CX, and MMP-13. Bars = 200 μm. CX and MMP-13 levels in cartilage from young mice showed no significant differences between the GDF-11 and control groups. However, the CII level was higher in cartilage from old mice in the GDF-11 group compared to the control group (n = 8 per group). Each symbol represents an individual mouse; bars show the mean ± SD. * = $P < 0.05$; *** = $P < 0.001$. NS = not significant (see Figure 4 for other definitions).

in part, to an increase in chondrocyte proliferation using EdU. The number of EdU-positive chondrocytes was higher in cartilage from old mice in the GDF-11 group than in the control group ($P < 0.05$) (Figure 5C). These data suggest that GDF-11 positively affects PG synthesis and strengthens the proliferation of chondrocytes in vivo.

GDF-11 increases chondrocyte proliferation, Smad2/3 phosphorylation, and CII secretion by chondrocytes in vitro. To confirm that chondrocytes in cartilage from old mice were repaired by GDF-11 at levels in young subjects, OA-associated factors were detected by qRT-PCR and immunohistochemical staining. Although there were no statistically significant differences in the expression of mRNA for Smad2, Smad3, CX, or MMP-13 between the 2 groups ($P > 0.05$), CII mRNA expression was markedly higher in the cartilage from old mice in the GDF-11 group compared to the control group ($P < 0.05$) (Figure 6A). Next, alterations in protein levels were examined by immunofluorescence for pSmad2/3 and immunohistochemistry for CII, CX, and MMP-13. Significantly more pSmad2/3-positive and CII-positive cells were detected in cartilage from old mice in the GDF-11 group compared to the control group (Figures 6B and C). No significant differences between the 2 groups were detected in the numbers of CX-positive or MMP-13–positive cells ($P > 0.05$) (Figure 6C). There were also no statistically significant differences between the 2 groups in Smad2/3-positive cells in cartilage from old mice

($P > 0.05$) (Supplementary Figure 3, http://onlinelibrary.wiley.com/doi/10.1002/art.41230/abstract). These findings further confirmed that GDF-11 could phosphorylate Smad2/3 and promote the secretion of CII by chondrocytes in vivo.

DISCUSSION

This study provides the first evidence that a young systemic environment can delay the process of cartilage degeneration in the knee joints of elderly mice using a heterochronic parabiosis model. Although many experimental studies of heterotrophic parabiosis have confirmed that young blood can regenerate the organs and tissues from old subjects, the effects of heterochronic parabiosis on elderly knee joints had not previously been evaluated. At 2 weeks after parabiosis surgery, shared circulation was successfully established in the heterochronic parabiosis model (Supplementary Figure 1A, http://onlinelibrary.wiley.com/doi/10.1002/art.41230/abstract), which is consistent with the findings of previous studies (23–25). FMT imaging data confirmed cross-circulation in the parabiotic pairs (Supplementary Figure 1B).

Increased osteophytes and sclerosis around the knee are important manifestations of OA (26–28). A radiographic examination showed that the degrees of osteophyte and ossification were reduced in the Y/O group (Figure 1A), indicating that heterochronic parabiosis could effectively improve the surrounding microenvironment of cartilage and delay the degree of bone tissue degeneration around the knee joints in elderly mice. Decreases in OARSI and PG content scores in the cartilage from old mice in the Y/O group suggest that heterochronic parabiosis attenuated cartilage damage in the knees of old mice. Interestingly, we found that the percentage of EdU-positive chondrocytes in cartilage from old mice in the Y/O group was significantly higher compared to the O/O and O groups, indicating increased proliferation (Figure 1). The protein and mRNA expression levels of CII and SOX9 in the cartilage from old mice in the Y/O group were increased, and the levels of CX, MMP-13, and RUNX-2 were decreased (Figure 2). CII is important for the maintenance of the integrity of the extracellular matrix of cartilage, and MMP-13 is a key enzyme in the degradation of the cartilage matrix in OA (29,30). SOX9 is a key transcription factor for chondrogenesis; it promotes the formation of chondrogenic differentiation and the maintenance of cartilage morphology after birth (31–33). RUNX-2 can induce chondrocyte hypertrophy and promote the development of OA, and a decrease in RUNX-2 is often accompanied by an increase in SOX9 (34). Based on the expression of OA-related factors in cartilage from old mice, we further confirmed that heterochronic parabiosis can relieve cartilage damage and delay the degeneration of cartilage tissue in elderly mice.

Although our findings suggest a positive effect of the exposure of old murine cartilage to a young systemic environment on chondrocyte proliferation and matrix synthesis, the mechanism underlying this phenomenon requires further study. We hypothesize that these changes were caused by the effects of various components of the young humoral circulation. Some "young factors" in the blood have been shown to restore the regenerative capacity of tissues and organs in old mice, including GDF-11. The role of GDF-11 in the organ tissues of old subjects is highly controversial; some studies have shown that GDF-11 decreases with age and restores the regenerative function of tissues and organs (heart muscle, olfactory nerve, etc.) at an old age (4,13,14), while others have shown opposing results (35–38). Despite conflicting findings about the role of GDF-11 in old subjects, GDF-11 clearly phosphorylates Smad2 and Smad3 to activate intracellular pathways. Our results are consistent with these previous studies showing that the phosphorylation of Smad2 and Smad3 in the TGFβ signaling pathway by GDF-11 promotes the secretion of CII in chondrocytes.

To clarify the role of GDF-11 in aging cartilage, we first proved that the level of GDF-11 was reduced with age in the circulation in humans and mice, and its levels were restored by heterochronic parabiosis (Figure 2), which is consistent with previous results (4,6,13). Second, we showed that rGDF-11 increases chondrocyte proliferation (Figure 4A) and migration (Supplementary Figure 2, http://onlinelibrary.wiley.com/doi/10.1002/art.41230/abstract). Additionally, the expression levels of pSmad2 and pSmad3 increased, and the protein and mRNA levels of CII increased after rGDF-11 treatment in chondrocytes (Figure 4C), providing further evidence that GDF-11 phosphorylates Smad2/Smad3 and activates chondrocyte secretion of CII. However, there were no significant differences in the levels of Smad2 and Smad3 between groups at the protein (Supplementary Figure 3, http://onlinelibrary.wiley.com/doi/10.1002/art.41230/abstract) and mRNA levels, indicating that Smad2 and Smad3 act on downstream factors after they are phosphorylated. Furthermore, the protein and mRNA expression levels of CX and MMP-13, which are positively correlated with chondrocyte damage (39,40), were significantly lower in the experimental group than in the control group (Figure 4A), suggesting that the increase in GDF-11 was accompanied by decreases in CX and MMP-13. These findings indicate that GDF-11 might phosphorylate Smad2 and Smad3 and activate chondrocyte secretion of CII.

However, the internal environment of chondrocytes in vitro does not reflect the complex internal environment of the organism. Further in vivo experiments are needed to confirm the role of GDF-11. Recombinant GDF-11 was intraperitoneally injected into 12-month-old mice and evaluated after 16 weeks. The severity of osteophyte formation and the degree of sclerosis are positively correlated with the severity of OA (41,42). Our findings demonstrate that rGDF-11 could alleviate the degeneration of bone tissue around the knee joint (Figure 5A). The OARSI score and PG loss (Figure 5B) indicate that increases in the levels of GDF-11 in the circulation of aged mice to the levels in young mice could delay the degeneration of cartilage. Decreased secretion of PG is one of the main manifestations of decreased chondrocyte

proliferation in cartilage from old mice (43). Increases in rGDF-11 levels in the circulation of aged mice to the levels in young mice could improve the proliferation of chondrocytes in the cartilage.

The phosphorylation levels of Smad2 and Smad3 play an important role in maintaining environmental stability in cartilage (16). The occurrence of OA is closely related to decreases in Smad2/Smad3 phosphorylation (15). We observed that the relative expression level of CII mRNA and the proportions of pSmad2/3-positive and CII-positive cells were significantly higher in the experimental group than in the control group (Figure 6), suggesting that GDF-11 may promote the secretion of CII in chondrocytes by phosphorylating Smad2/3. However, there were no significant differences in the mRNA and protein expression levels of Smad2/Smad3 between the 2 groups, which only acted on downstream factors after being phosphorylated (Figure 6A and Supplementary Figure 4, http://onlinelibrary.wiley.com/doi/10.1002/art.41230/abstract). The relative CX and MMP-13 mRNA and protein expression levels in the cartilage from old mice in the experimental group did not differ from those in the control group (Figure 6).

It is possible that the improved chondrocyte proliferation capacity in response to rGDF-11 is not sufficient to completely counteract the cartilage damage caused by aging. It is also possible that some factors in the complex internal environment of the body block the effects of rGDF-11 on CX and MMP-13, requiring a larger dose of rGDF-11 or a longer treatment duration. In vivo experiments showed that rGDF-11 can improve the microenvironment around the knee joints in elderly mice, increase the chondrocyte proliferation capacity, promote the secretion of CII by phosphorylating Smad2/3, and delay the degeneration of cartilage in old mice.

In summary, a young systemic enviroment has a positive effect on chondrocyte proliferation and matrix synthesis in the knee cartilage of old mice. GDF-11, a young factor, promotes the secretion of CII and chondrocyte proliferation via the upregulation of Smad2/3. Thus, GDF-11 has a positive effect on chondrocyte proliferation and matrix synthesis in the knee cartilage of old mice. Future studies should evaluate other blood components that function as beneficial young factors. The limitations of this study include the use of mice that are not sufficiently old. Additionally, we only showed that the young environment and GDF-11 delayed the occurrence of OA, and it is necessary to further determine whether the young environment and young factors have therapeutic effects on old subjects with OA.

AUTHOR CONTRIBUTIONS

All authors were involved in drafting the article or revising it critically for important intellectual content, and all authors approved the final version to be published. Dr. L. Li had full access to all of the data in the study and takes responsibility for the integrity of the data and the accuracy of the data analysis.

Study conception and design. L. Li, X. Wei, D. Wang, Lv, Geng, P. Li, Lu, K. Wang, X. Wang, Sun, Cao, L. Wei.
Acquisition of data. L. Li, X. Wei, D. Wang, Lv, Geng, P. Li, Lu, K. Wang, X. Wang, Sun, Cao, L. Wei.
Analysis and interpretation of data. L. Li, X. Wei.

REFERENCES

1. Loeser RF. Aging and osteoarthritis. Curr Opin Rheumatol 2011;23:492–6.
2. Komori T. Cell death in chondrocytes, osteoblasts, and osteocytes [review]. Int J Mol Sci 2016;17:2045.
3. Rahmati M, Nalesso G, Mobasheri A, Mozafari M. Aging and osteoarthritis: central role of the extracellular matrix [review]. Ageing Res Rev 2017;40:20–30.
4. Loffredo FS, Steinhauser ML, Jay SM, Gannon J, Pancoast JR, Yalamanchi P, et al. Growth differentiation factor 11 is a circulating factor that reverses age-related cardiac hypertrophy. Cell 2013;153:828–39.
5. Conboy IM, Conboy MJ, Wagers AJ, Girma ER, Weissman EL, Rando RA. Rejuvenation of aged progenitor cells by exposure to a young systemic environment. Nature 2005;433:760–4.
6. Katsimpardi L, Litterman NK, Schein PA, Miller CM, Loffredo FS, Wojtkiewicz GR, et al. Vascular and neurogenic rejuvenation of the aging mouse brain by young systemic factors. Science 2014;344:630–4.
7. Eggel A, Wyss-Coray T. A revival of parabiosis in biomedical research [review]. Swiss Med Wkly 2014;144:w13914.
8. Conboy MJ, Conboy IM, Rando TA. Heterochronic parabiosis: historical perspective and methodological considerations for studies of aging and longevity [review]. Aging Cell 2013;12:525–30.
9. Wu HH, Ivkovic S, Murray RC, Jaramillo S, Lyons KM, Johnson JE, et al. Autoregulation of neurogenesis by GDF-11. Neuron 2003;37:197–207.
10. Kim J, Wu HH, Lander AD, Lyons KM, Matzuk MM, Calof AL. GDF-11 controls the timing of progenitor cell competence in developing retina. Science 2005;308:1927–30.
11. Esquela AF, Lee SJ. Regulation of metanephric kidney development by growth/differentiation factor 11. Dev Biol 2003;257:356–70.
12. Dichmann DS, Yassin H, Serup P. Analysis of pancreatic endocrine development in GDF-11-deficient mice. Dev Dyn 2006;235:3016–25.
13. Sinha M, Jang YC, Oh J, Khong D, Wu EY, Manohar R, et al. Restoring systemic GDF-11 levels reverses age-related dysfunction in mouse skeletal muscle. Science 2014;344:649–52.
14. Katsimpardi L, Litterman NK, Schein PA, Miller AM, Loffredo FS, Wojtkiewicz GR, et al. Vascular and neurogenic rejuvenation of the aging mouse brain by young systemic factors. Science 2014;344:630–4.
15. Finnson KW, Chi Y, Bou-Gharios G, Leask A, Philip A. TGFβ signaling in cartilage homeostasis and osteoarthritis. Front Biosci (Schol Ed) 2012;4:251–68.
16. Yang X, Chen L, Xu X, Li C, Huang C, Deng CX. TGFβ/Smad3 signals repress chondrocyte hypertrophic differentiation and are required for maintaining articular cartilage. J Cell Biol 2001;153:35–46.
17. Villeda SA, Plambeck KE, Middeldorp J, Castellano JM, Mosher KI, Luo J, et al. Young blood reverses age-related impairments in cognitive function and synaptic plasticity in mice. Nat Med 2014;20:659–63.
18. Wang SW, Wei XC, Zhou JM, Zhang J, Li K, Qian C, et al. Identification of α_2-macroglobulin as a master inhibitor of cartilage-degrading factors that attenuates the progression of posttraumatic osteoarthritis. Arthritis Rheumatol 2014;66:1843–53.
19. Glasson SS, Chambers MG, Van Den Berg WB, Little CB. The OARSI histopathology initiative: recommendations for histological

assessments of osteoarthritis in the mouse. Osteoarthritis Cartilage 2010;18 Suppl 3:S17–23.

20. Wei F, Zhou J, Wei X, Zhang J, Fleming BC, Terek R, et al. Activation of Indian hedgehog promotes chondrocyte hypertrophy and upregulation of MMP-13 in human osteoarthritic cartilage. Osteoarthritis Cartilage 2012;20:755–63.
21. Cao K, Wei L, Zhang Z, Guo L, Zhang C, Li Y, et al. Decreased histone deacetylase 4 is associated with human osteoarthritis cartilage degeneration by releasing histone deacetylase 4 inhibition of runt-related transcription factor-2 and increasing osteoarthritis-related genes: a novel mechanism of human osteoarthritis cartilage degeneration. Arthritis Res Ther 2014;16:491.
22. Wagers AJ, Sherwood RI, Christensen JL, Weissman IL. Little evidence for developmental plasticity of adult hematopoietic stem cells. Science 2002;297:2256–9.
23. Gibney BC, Chamoto K, Lee GS, Simpson DC, Miele LF, Tsuda A, et al. Cross-circulation and cell distribution kinetics in parabiotic mice. J Cell Physiol 2012;227:821–8.
24. Castellano JM, Palner M, Li SB, Freeman GM Jr, Nguyen A, Shen B, et al. In vivo assessment of behavioral recovery and circulatory exchange in the peritoneal parabiosis model. Sci Rep 2016;6:29015.
25. Burr DB, Gallant MA. Bone remodelling in osteoarthritis [review]. Nat Rev Rheumatol 2012;8:665–73.
26. Hudelmaier M, Wirth W. Differences in subchondral bone size after one year in osteoarthritic and healthy knees. Osteoarthritis Cartilage 2015;24:623–30.
27. Botter SM, van Osch GJ, Waarsing JH, van der Linden JC, Verhaar JA, Pols HA, et al. Cartilage damage pattern in relation to subchondral plate thickness in a collagenase-induced model of osteoarthritis. Osteoarthritis Cartilage 2008;16:506–14.
28. Sacitharan PK, Vincent TL. Cellular ageing mechanisms in osteoarthritis. Mamm Genome 2016;27:421–9.
29. Van der Kraan PM, van den Berg WB. Osteoarthritis in the context of ageing and evolution: loss of chondrocyte differentiation block during ageing [review]. Ageing Res Rev 2008;7:106–13.
30. Bi WM, Deng JM, Zhang ZP, Behringer R, de Crombrugghe B. SOX9 is required for cartilage formation [letter]. Nat Genet 1999;22:85–9.
31. Chavez RD, Coricor G, Perez J, Seo HS, Serra R. SOX9 protein is stabilized by TGF-β and regulates PAPSS2 mRNA expression in chondrocytes. Osteoarthritis Cartilage 2017;25:332–40.
32. Henry SP, Liang SD, Akdemir KC, de Crombugghe B. The postnatal role of SOX9 in cartilage. J Bone Miner Res 2012;27:2511–25.
33. Wang XB, Manner PA, Horner A, Shum L, Tuan RS, Nuckolls GH. Regulation of MMP-13 expression by RUNX2 and FGF2 in osteoarthritic cartilage. Osteoarthritis Cartilage 2004;12:963–73.
34. Orfanidou T, Iliopoulos D, Malizos KN, Tsezou A. Involvement of SOX-9 and FGF-23 in RUNX-2 regulation in osteoarthritic chondrocytes. J Cell Mol Med 2009;13:3186–94.
35. Liu W, Zhou L, Zhou C, Zhang S, Jing J, Xie L, et al. GDF-11 decreases bone mass by stimulating osteoclastogenesis and inhibiting osteoblast differentiation. Nat Commun 2016;7:12794.
36. Rodgers BD, Eldridge JA. Reduced circulating GDF11 is unlikely responsible for age-dependent changes in mouse heart, muscle, and brain. Endocrinology 2015;156:3885–8.
37. Poggioli T, Vujic A, Yang P, Macias-Trevino C, Uygur A, Loffredo FS, et al. Circulating growth differentiation factor 11/8 levels decline with age. Circ Res 2016;118:29–37.
38. Egerman MA, Cadena SM, Gilbert JA, Meyer A, Nelson HN, Swalley SE, et al. GDF-11 increases with age and inhibits skeletal muscle regeneration. Cell Metab 2015;22:164–74.
39. Van der Kraan PM, van den Berg WB. Chondrocyte hypertrophy and osteoarthritis: role in initiation and progression of cartilage degeneration? Osteoarthritis Cartilage 2012;20:223–32.
40. Loeser RF. Age-related changes in the musculoskeletal system and the development of osteoarthritis. Clin Geriatr Med 2010;26:371–86.
41. Martel-Pelletier J, Pelletier JP. Is osteoarthritis a disease involving only cartilage or other articular tissues? Eklem Hastalik Cerrahisi 2010;21:2–14.
42. Loeser RF. Aging and osteoarthritis: the role of chondrocyte senescence and aging changes in the cartilage matrix. Osteoarthritis Cartilage 2009;17:971–9.
43. Van der Kraan PM, Goumans MJ, Davidson EB, ten Dijke P. Age-dependent alteration of TGF-β signalling in osteoarthritis [review]. Cell Tissue Res 2011;347:257–65.

American College of Rheumatology
Empowering Rheumatology Professionals

Arthritis & Rheumatology
Vol. 72, No. 7, July 2020, pp 1134–1142
DOI 10.1002/art.41217

A Spatiotemporal Analysis of Organ-Specific Lupus Flares in Relation to Atmospheric Variables and Fine Particulate Matter Pollution

George Stojan, Anton Kvit, Frank C. Curriero, and Michelle Petri

Objective. To identify potential clusters of systemic lupus erythematosus (SLE) organ-specific flares and their relationship to fine particulate matter pollution (PM2.5), temperature, ozone concentration, resultant wind, relative humidity, and barometric pressure in the Hopkins Lupus Cohort, using spatiotemporal cluster analysis.

Methods. A total of 1,628 patients who fulfilled the Systemic Lupus International Collaborating Clinics classification criteria for SLE and who had a home address recorded were included in the analysis. Disease activity was assessed using the Lupus Activity Index. Assessment of rash, joint involvement, serositis, and neurologic, pulmonary, renal, and hematologic activity was quantified on a 0–3 visual analog scale (VAS). An organ-specific flare was defined as an increase in VAS of ≥1 point compared to the previous visit. Spatiotemporal clusters were detected using SaTScan software. Regression models were used for cluster adjustment and included individual, county-level, and environmental variables.

Results. Significant clusters unadjusted for environmental variables were identified for joint flares ($P < 0.05$; n = 3), rash flares ($P < 0.05$; n = 4), hematologic flares ($P < 0.05$; n = 3), neurologic flares ($P < 0.05$; n = 2), renal flares ($P < 0.001$; n = 4), serositis ($P < 0.001$; n = 2), and pulmonary flares ($P < 0.001$; n = 2). The majority of the clusters identified changed in significance, temporal extent, or spatial extent after adjustment for environmental variables.

Conclusion. We describe the first spatiotemporal clusters of lupus organ-specific flares. Seasonal, as well as multi-year, cluster patterns were identified, differing in extent and location for the various organ-specific flare types. Further studies focusing on each individual organ-specific flare are needed to better understand the driving forces behind these observed changes.

INTRODUCTION

Systemic lupus erythematosus (SLE) is a complex multisystem autoimmune disease with strong epidemiologic evidence of association with several environmental factors, including crystalline silica exposure (1), cigarette smoking (2), and exogenous estrogens (oral contraceptives and postmenopausal hormones) (3), as well as potential associations between other exogenous factors such as mercury (4), ultraviolet radiation, solvents, and pesticides (5).

With regard to atmospheric impact, significant seasonal variation in SLE disease activity has been described, with more arthritis activity in the spring and summer months, an increase in renal activity in the winter months, significantly higher anti–double-stranded DNA (anti-dsDNA) antibody titers in the fall, and a significant variation in global disease activity, as measured by the Safety of Estrogens in Lupus Erythematosus National Assessment version of the Systemic Lupus Erythematosus Disease Activity Index (SLEDAI), through the year (6). In a cohort of 2,802 SLE patients from China, the absolute number of patients with active SLE (SLEDAI >12) in a month was positively correlated with the amount of precipitation and wind speed (7). There was no significant correlation between average temperature, average humidity, or average percentage of sunshine hours and SLE activity.

Fine particulate matter pollution (PM2.5) averaged for up to 10 days prior to patient visit was associated with anti-dsDNA

Supported by the Office of the Assistant Secretary of Defense for Health Affairs and Lupus Research Program (award W81XWH19-1-0793), the National Center for Research Resources, NIH (grant UL1-RR-025005), and the NIH Roadmap for Medical Research. The Hopkins Lupus Cohort was supported by the NIH (grants AR-43727 and AR-69572). Dr. Stojan's work was supported by the Jerome L. Greene Foundation. Dr. Curriero's work was supported by the NIH (grant R01-AI-123931).

George Stojan, MD, Anton Kvit, MS, Frank C. Curriero, PhD, Michelle Petri, MD, MPH: Johns Hopkins University, Baltimore, Maryland.

Dr. Petri has received consulting fees, speaking fees, and/or honoraria from Amgen, EMD Serono, and Merck (less than $10,000 each) and research support from AstraZeneca, Exagen Diagnostics, and GlaxoSmithKline. No other disclosures relevant to this article were reported.

Address correspondence to George Stojan, MD, Johns Hopkins University, Division of Rheumatology, 1830 East Monument Street, Suite 7500, Baltimore, MD 21205. E-mail: gstojan1@jhmi.edu.

Submitted for publication July 29, 2019; accepted in revised form January 24, 2020.

antibodies and cellular casts, but not with global disease activity, in a Montreal lupus cohort (8). A population-based cohort study from Taiwan showed a positive association between a 10.2 μg/m^3 increase in fine particulate matter concentration and new diagnoses of SLE (9). Similarly, population-based studies from Alberta and Quebec showed that PM2.5 exposure may be associated with an increased risk of systemic autoimmune diseases, including SLE (10).

We pursued the development of spatiotemporal analytical models of lupus flares with the goal of identifying potential flare clusters and their relationship to PM2.5 and temperature changes. These spatiotemporal models serve as the foundation for a novel approach to the study of environmental factors in SLE.

PATIENTS AND METHODS

Patients and activity indices. As previously described (11), the Hopkins Lupus Cohort is a prospective cohort study of predictors of lupus flare, atherosclerosis, and health status in SLE. The study cohort includes all patients at the Hopkins Lupus Center who have a clinical diagnosis of SLE and meet classification criteria for SLE (12). All patients provided written informed consent to participate in the study. Patients enrolled in the cohort are followed up quarterly or more frequently if clinically necessary. Clinical features, laboratory findings, and damage accrual data are recorded at the time of entry into the cohort and are updated at subsequent visits. The Hopkins Lupus Cohort has been approved by the Johns Hopkins University School of Medicine Institutional Review Board and complies with the Health Insurance Portability and Accountability Act.

The Hopkins Lupus Cohort included 2,486 patients, with the vast majority of patients living in Maryland and the surrounding states. A 350-kilometer radial buffer around the Johns Hopkins Lupus Center was therefore considered as the study area, since it included a high and consistent density of patients necessary for cluster detection. This area included most of Maryland, Delaware, and Washington, DC, as well as parts of Pennsylvania, New Jersey, Virginia, and West Virginia (Figure 1).

Patients who had home addresses within the study area between 1999 and 2017 were included in the study. A 1999 cutoff was selected since consistent PM2.5 data were available beginning in that year. All address changes during study follow up were recorded and were considered. Disease activity was assessed by the Lupus Activity Index (13). Assessment of rash, joint involvement, serositis, and neurologic, pulmonary, renal, and hematologic activity was quantified on a 0–3 visual analog scale (VAS).

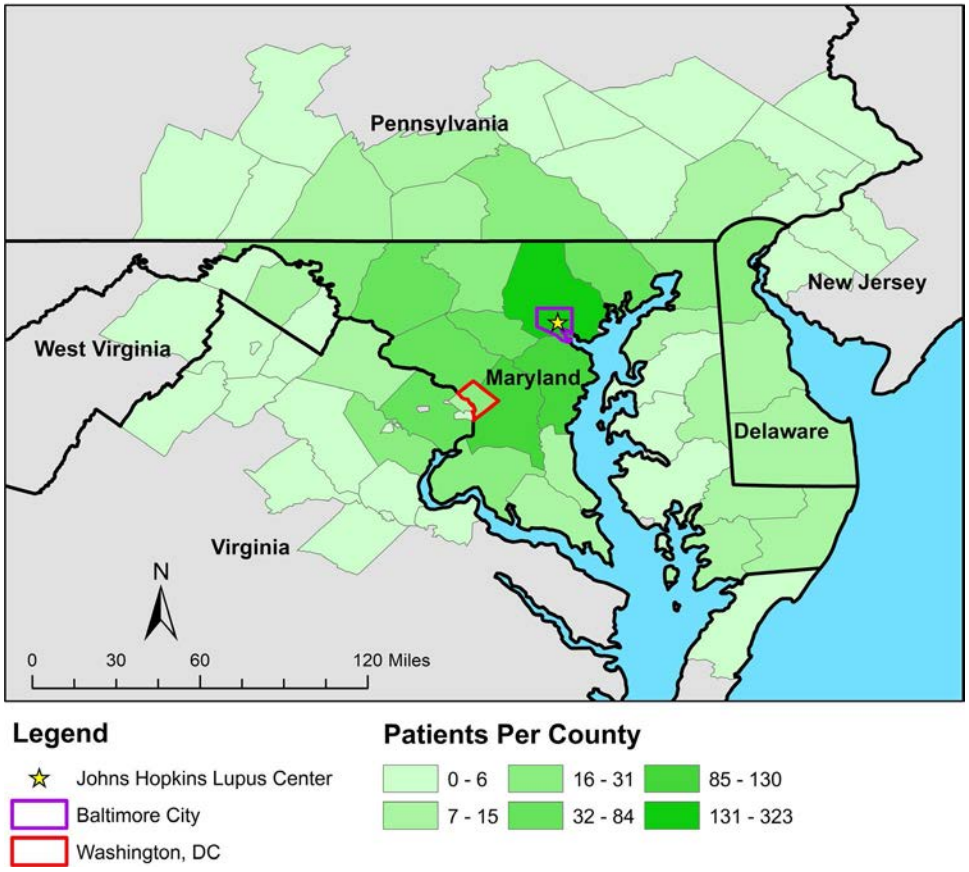

Figure 1. The Johns Hopkins Lupus Cohort study area. Patients with systemic lupus erythematosus in the Johns Hopkins Lupus Cohort who had home addresses within this study area during the period from 1999 to 2017 were included in the cluster analysis.

An organ-specific flare was defined as an increase in VAS of ≥1 point compared to the previous visit. For the increase to count as a flare, the previous visit must have been within 110 days of the current visit. Patients were generally asked to check in at least every 3 months; however, this time period varied, and 92 day, 100 day, and 110 day cutoffs were considered. A 110 day cutoff was considered the most appropriate, since it allowed retention of 70% of the records while still excluding patients who visited too rarely to determine whether a flare had occurred. After applying all of the criteria described above, 1,628 patients with a total of 29,677 visits were included in the study. Individual variables considered in the analysis included patient sex, age, race, smoking status, household income, years of education, and urban versus rural living environment. County-level variables included median income and the proportion of the population who were African American. Flare types included rash, joint, serositis, and neurologic, renal, pulmonary, and hematologic flares. Available data are further summarized in Table 1.

Daily PM2.5 data measured in micrograms per cubic meter, temperature measured in degrees Fahrenheit, ozone concentration measured in parts per million (ppm), resultant wind measured in miles per hour, relative humidity expressed as a percentage, and barometric pressure expressed as millimeters of mercury (mm Hg) were collected at various monitoring stations in the eastern US and obtained from the Environmental Protection Agency. Ordinary kriging was used via the "gstat" R package (14) to predict the 10-day average level of the environmental variables for each patient prior to each visit date. Ordinary kriging (15) is a widely used statistical interpolation method that allows the prediction of the value of a variable in any geographic location based on known variable measures at other locations, while taking into account the spatial dependence in the distribution of the measured variable. This method allowed us to predict environmental exposures for each patient based on appropriately weighted exposure measures at the surrounding monitoring stations.

Both univariate and multivariate generalized estimating equation (GEE) logistic regression models with an exchangeable correlation structure were built to study the association of individual variables (age, sex, race, smoking status, household income, years of education, and urban living status), county variables (county income and the proportion of the population who were African American), and environmental variables (PM2.5, temperature, ozone concentration, resultant wind, barometric pressure, and relative humidity) with the 7 different types of lupus disease activity listed above. GEE regression was used in order to account for the repeated measures each patient was subject to during their multiple clinic visits, thus violating the independence assumption necessary for ordinary regression.

Spatiotemporal cluster detection of flares was conducted using SaTScan software version 9.4.4. In order to detect such clusters, SaTScan utilizes a moving window of variable size, that centers at each data point location, and considers all possible time intervals, recording the number of observed and expected cases inside and outside the window. For each window location, size, and time, the observed and expected cases are compared, the likelihood function is maximized, identifying the window that is least likely to occur by chance, and this process is repeated 999 times through Monte Carlo hypothesis testing in order to obtain a *P* value, and identify the window as a statistically significant cluster. The method used to calculate expected cases depends

Table 1. Individual and county-level variables and lupus flare outcomes, by patient sex*

	Women (n = 1,504)	Men (n = 124)	Total (n = 1,628)
No. of clinic visits	27,376	2,301	29,677
Age, mean years	38.8	43.2	39.1
Race			
African American	618 (41.1)	41 (33.1)	659 (40.5)
White	761 (50.6)	74 (59.7)	835 (51.3)
Other	125 (8.3)	9 (7.3)	134 (8.2)
Years of education, mean	14.3	14.2	14.3
Annual household income, mean dollars	65,491.2	77,642.5	66,322.2
Ever smoker	157 (10.4)	9 (7.3)	166 (10.2)
Urban living environment	1,281 (85.2)	101 (81.5)	1,382 (84.9)
Annual county income, mean dollars	63,655.7	65,802.7	63,823.7
African American proportion of county population, mean %	29.9	27.0	29.7
Lupus flares†			
Rash flares	1,146 (4.2)	61 (2.7)	1,207 (4.1)
Joint flares	1,665 (6.1)	102 (4.4)	1,767 (6)
Serologic flares	470 (1.7)	25 (1.1)	495 (1.7)
Neurologic flares	292 (1.1)	22 (1.0)	314 (1.1)
Renal flares	1,696 (6.2)	188 (8.2)	1,884 (6.3)
Pulmonary flares	58 (0.2)	3 (0.1)	61 (0.2)
Hematologic flares	446 (1.6)	62 (2.7)	508 (1.7)

* Except where indicated otherwise, values are the number (%).
† Values are the number of flares (% of clinic visits).

Table 2. Associations between outcome variables and individual, county, and environmental covariates in univariate regression analysis*

Variable	Rash		Joints		Serositis		Neurologic		Renal		Pulmonary		Hematologic	
	OR	*P*	OR	*P*	OR	*P*	OR	*P*	OR	*P*	OR	*P*	OR	*P*
Age	0.989	0.021	1.000	>0.9	0.968	<0.001	0.997	>0.9	0.976	<0.001	0.993	>0.9	0.991	>0.9
Sex	0.620	0.5115	0.721	0.7095	0.683	>0.9	1.127	>0.9	1.341	0.3225	0.640	>0.9	1.822	0.3705
Race (other)	0.671	>0.9	0.571	0.0075	0.764	>0.9	0.448	0.6885	0.924	>0.9	1.450	>0.9	1.037	>0.9
Race (white)	0.668	<0.001	0.875	0.7965	0.658	0.0915	0.734	>0.9	0.536	<0.001	0.574	>0.9	0.986	>0.9
Ever smoker	1.862	<0.001	1.201	0.8745	0.499	0.8475	0.990	>0.9	0.957	>0.9	1.166	>0.9	1.023	>0.9
Household income†	0.993	>0.9	0.989	0.153	0.995	>0.9	0.998	>0.9	0.998	>0.9	1.009	>0.9	1.004	>0.9
Years of education	0.943	0.012	0.972	0.4605	0.943	0.498	1.007	>0.9	0.943	<0.001	0.980	>0.9	1.007	>0.9
Urban living environment	0.975	>0.9	0.929	>0.9	0.954	>0.9	0.812	>0.9	0.840	0.9225	0.936	>0.9	0.968	>0.9
African American proportion of county population (%)‡	1.044	0.438	1.006	>0.9	0.959	>0.9	1.005	>0.9	1.034	0.6795	0.989	>0.9	1.025	>0.9
Median county income†	0.980	>0.9	0.969	0.0015	0.994	>0.9	0.949	0.144	0.964	0.0015	0.908	0.153	0.985	>0.9
PM2.5	1.029	<0.001	1.026	<0.001	1.028	0.0525	1.026	0.399	1.004	>0.9	1.043	0.8625	1.025	0.138
Temperature (degrees F)‡	1.065	0.033	1.047	0.0285	1.061	0.6135	1.068	>0.9	0.960	0.072	1.108	>0.9	1.095	0.027
Ozone concentration (ppm)	1.013	<0.001	1.004	>0.9	1.011	0.3255	1.002	>0.9	0.992	0.0105	1.010	>0.9	1.005	>0.9
Resultant wind (miles/hour)‡	1.009	>0.9	1.039	<0.001	1.007	>0.9	1.099	<0.001	1.028	0.0165	1.135	0.0045	1.046	0.147
Barometric pressure (mm Hg)‡	0.993	0.5655	1.004	>0.9	1.006	>0.9	0.989	>0.9	0.998	>0.9	1.053	0.6585	1.007	>0.9
Relative humidity (%)‡	0.991	>0.9	1.163	<0.001	1.125	>0.9	1.297	0.0765	1.045	>0.9	1.293	>0.9	1.159	0.1365

* *P* values less than 0.05 were considered significant; *P* values less than 0.1 were considered marginally significant. All *P* values were Bonferroni adjusted. PM2.5 = fine particulate matter pollution; ppm = parts per million.
† Odds ratio (OR) per $5,000.
‡ OR per 10 units.

on the selected statistical model. Patient data were aggregated to 66 counties that spanned the study area and were considered the spatial units for the analysis. A discrete Poisson SaTScan model was utilized, where the total number of each type of lupus flares per day, in each county, is considered to be the case, and the total number of patient visits per day, in each county, is considered to be the population, if the cluster is unadjusted.

In order to determine whether individual, county, or environmental covariates help explain the identified clusters, the expected number of flares determined from the GEE logistic regressions described above can be used in place of the population within the SaTScan Poisson model. In this study, 2 adjusted spatiotemporal cluster analyses were conducted. In the first, only adjustments for individual and county level socioeconomic factors were made. In the second, in addition to the individual and county variables, adjustments based on environmental variables were included. One-month–long minimum time intervals were considered for this analysis, and spatially overlapping clusters were allowed as long as the overlapping cluster did not contain the centroid of the cluster that was already there.

Data availability

The data that support the findings of this study are available upon request from the corresponding author. The data are not publicly available since they contain information that could compromise research participant privacy.

RESULTS

In a univariate regression analysis, rash flares (odds ratio [OR] 1.029) and joint flares (OR 1.026) were found to be positively associated with PM2.5 exposure ($P < 0.05$), while serositis (OR 1.028) was found to be marginally associated ($P = 0.053$). Rash flares (OR 1.065), joint flares (OR 1.047), and hematologic flares (OR 1.095) were found to be significantly positively associated with temperature, while renal flares (OR 0.960) were found to be marginally negatively associated with temperature ($P = 0.072$). Ozone concentration was associated with rash (OR 1.01, $P < 0.05$) and negatively associated with renal flares (OR 0.992). Resultant wind was positively associated ($P < 0.05$) with joint flares (OR 1.039), neurologic flares (OR 1.099), renal flares (OR 1.028), and pulmonary flares (OR 1.135). Relative humidity was associated with joint flares (OR 1.163, $P < 0.05$) and marginally associated with neurologic flares (OR 1.297, $P = 0.077$). No significant associations were found for barometric pressure. Furthermore, rash, serositis, and renal flares were found to be negatively associated with age ($P < 0.05$). Rash and serositis symptoms were found to be more likely in African American than white populations (marginally for serositis [$P = 0.092$]), and odds of joint flare were higher for African American patients than for patients of other nonwhite races. Rash flares were found to be more likely in smokers (OR 1.862) and to be negatively associated ($P < 0.05$) with years of education (OR 0.943). Renal flares were also negatively associated with years of education (OR 0.943). Finally, joint flares (OR 0.969) and renal flares (OR 0.964) were found to be negatively associated with median county income ($P < 0.05$). These findings are summarized in Table 2.

For most outcomes, the clusters identified changed spatially or temporally when environmental variables were considered in addition to county and individual ones. The general interpretation of cluster behavior after adjustment for environmental covariates can be classified into the following 3 categories:

1. Clusters that remain unchanged temporally or spatially after adjustment for environmental covariates indicate areas where no association between environmental covariates and flare occurrence was identified.
2. Clusters that disappear or decrease spatially or temporally after adjustment for environmental covariates indicate areas where there were high levels of covariates along with a general positive association of the covariates with the number of flares, or low levels of covariates with a general negative association.
3. Clusters that emerge or increase spatially or temporally after adjustment for environmental covariates indicate areas where there were low levels of covariates along with a general positive association of the covariates with the number of flares, or high levels of covariates with a general negative association.

Three statistically significant ($P < 0.05$) environmentally unadjusted clusters were identified for joint flares. One encompassed most of Maryland's Eastern Shore and Delaware and ranged from July 2001 to July 2005. A second cluster was located to the southwest, including Washington, DC and parts of Virginia and Maryland, and ranged from April 2001 to July 2009. The third cluster centered around the city of Baltimore and Baltimore County and ranged from January 2002 to September 2005. After adjustment for environmental variables, cluster 1 located on the Eastern Shore decreased temporally, cluster 2 in the west remained unchanged, and cluster 3 decreased spatially and shifted temporally. A new cluster (cluster 4) appeared in the northeast after adjustment (Figure 2).

After adjustment for individual and county variables, 4 significant ($P < 0.05$) rash flare clusters were identified in eastern Maryland, southeastern Pennsylvania, and Delaware. Clusters 1 and 2 located on the Eastern Shore and north of the city of Baltimore, respectively, decreased spatially after adjustment, while clusters 3 and 4, located in the southwest and northeast, respectively, increased spatially after adjustment (Figure 3).

Three significant environmentally unadjusted ($P < 0.05$) hematologic clusters were identified. Two were around New Jersey (from September 2000 to February 2002 and from February 2001 to February 2002), and one was located in western Maryland and Virginia (from December 2002 to December 2005). None

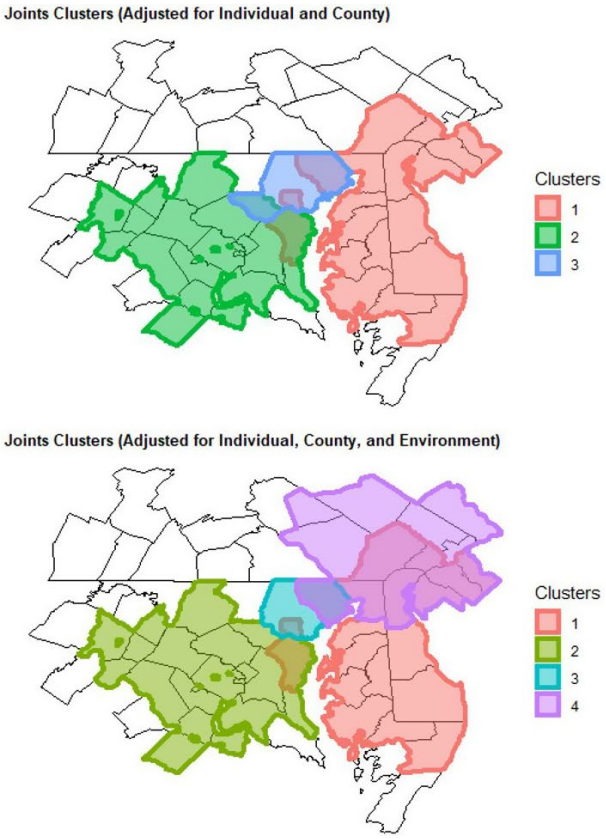

Cluster	Start Date	End Date	P-Value	Observed	Expected	Area
1	2001/7/28	2005/7/27	< 0.001	314	207	21403
2	2001/4/28	2009/7/27	< 0.001	423	315	18270
3	2002/1/28	2005/9/27	< 0.001	273	190	3726

Cluster	Start Date	End Date	P-Value	Observed	Expected	Area
1	2004/2/28	2005/6/27	< 0.001	126	64.0	21403
2	2001/4/28	2009/7/27	0.003	423	329.8	18270
3	2003/1/28	2007/4/27	0.004	262	187.2	3071
4	2004/4/28	2005/6/27	0.028	38	14.7	17141

Figure 2. Top, Clusters of joint flares in patients with systemic lupus erythematosus (SLE) after adjustment for individual variables (age, sex, race, smoking status, household income, years of education, and urban living status) and county variables (county income and the proportion of the population who were African American). Bottom, Clusters of joint flares in SLE patients after adjustment for individual variables, county variables, and environmental variables (fine particulate matter pollution, temperature, ozone concentration, resultant wind, barometric pressure, and relative humidity). After adjustment for environmental variables, cluster 1 decreased temporally, cluster 2 remained unchanged, and cluster 3 decreased spatially and shifted temporally. A new cluster (cluster 4) in the northeast was identified after adjustment. The beginning and end dates, *P* value, observed and expected values, and area in square kilometers are shown for each cluster.

of these clusters remained significant after adjustment for atmospheric variables and PM2.5 (Figure 4).

Two large significant neurologic flare clusters were identified, in the eastern and western halves of the study area ($P < 0.05$) (Supplementary Figure 1, available on the *Arthritis & Rheumatology* web site at http://onlinelibrary.wiley.com/doi/10.1002/art.41217/abstract). After adjustment for atmospheric variables and PM2.5, spatially and temporally smaller clusters during time periods different from the original clusters appeared. Two significant environmentally unadjusted serositis clusters were identified, and both remained temporally and spatially unchanged after adjustment for environmental variables ($P < 0.001$) (Supplementary Figure 2, available on the *Arthritis & Rheumatology* web site at http://onlinelibrary.wiley.com/doi/10.1002/art.41217/abstract).

Four highly significant renal clusters were identified ($P < 0.001$) (Supplementary Figure 3, available on the *Arthritis & Rheumatology* web site at http://onlinelibrary.wiley.com/doi/10.1002/art.41217/abstract), spanning from 2001, 2002, and 2004 to 2006, taking up much of the map except for some counties in the west and south. These clusters remained largely unchanged spatially after adjustment for atmospheric variables and PM2.5, while clusters 2 and 3 became slightly smaller temporally after adjustment.

Two significant pulmonary flare clusters were identified in the northwest, spanning from January to July of 1999 ($P < 0.001$) (Supplementary Figure 4, available on the *Arthritis & Rheumatology* web site at http://onlinelibrary.wiley.com/doi/10.1002/art.41217/abstract). Both clusters became spatially smaller after adjustment for atmospheric variables and PM2.5, and a third cluster appeared in the northeast after adjustment.

DISCUSSION

Cluster detection, the identification of spatial units adjacent in space that are associated with distinctive patterns of data of interest relative to background variation, is an important tool in disciplines such as spatial epidemiology and disease surveillance (16). Clusters have distinctive risks of an event of interest, typically elevated, but possibly reduced, relative to background variation (16).

We performed a spatiotemporal cluster analysis of the Hopkins Lupus Cohort and detected the first spatiotemporal lupus flare

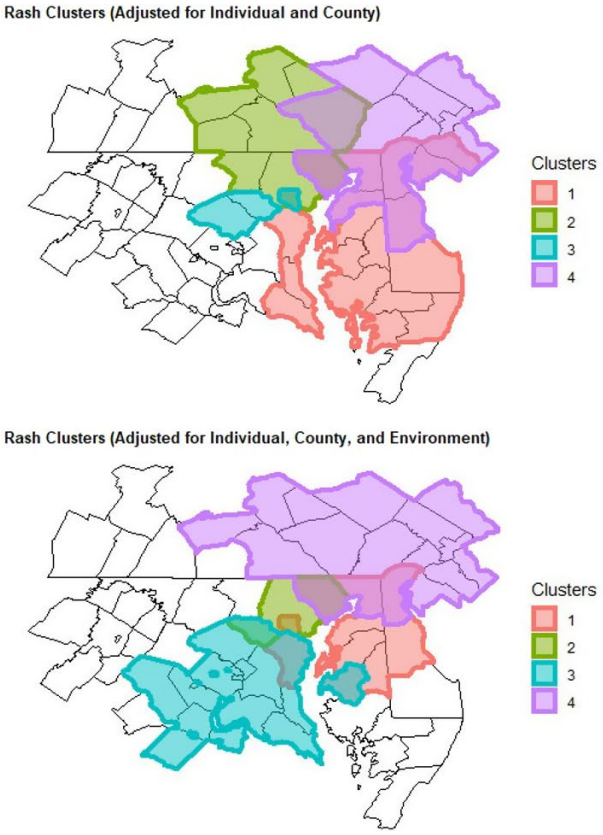

Cluster	Start Date	End Date	P-Value	Observed	Expected	Area
1	2003/6/28	2009/8/27	< 0.001	315	202	21009
2	2003/12/28	2007/9/27	< 0.001	194	117	14313
3	2003/1/28	2007/9/27	< 0.001	174	102	2207
4	2003/4/28	2007/5/27	0.012	67	32	18537

Cluster	Start Date	End Date	P-Value	Observed	Expected	Area
1	2002/11/28	2009/11/27	< 0.001	331	219.1	9816
2	2003/1/28	2009/7/27	< 0.001	312	219.7	3726
3	2003/3/28	2007/6/27	< 0.001	171	105.1	14467
4	2002/9/28	2007/9/27	0.001	89	44.8	22371

Figure 3. Top, Clusters of rash flares in patients with systemic lupus erythematosus (SLE) after adjustment for individual variables (age, sex, race, smoking status, household income, years of education, and urban living status) and county variables (county income and the proportion of the population who were African American). Bottom, Clusters of rash flares in SLE patients after adjustment for individual variables, county variables, and environmental variables (fine particulate matter pollution, temperature, ozone concentration, resultant wind, barometric pressure, and relative humidity). After adjustment for environmental variables, clusters 1 and 2 decreased spatially, while clusters 3 and 4 increased spatially. The beginning and end dates, *P* value, observed and expected values, and area in square kilometers are shown for each cluster.

clusters. Seasonal, as well as multi-year, cluster patterns were identified, differing in extent and location for the various organ-specific flare types. The large-scale, multi-year clusters we defined did not conform to any known pattern of infectious disease or environmental exposure.

After adjustment for individual or environmental covariates, there were at least slight changes in the temporal or spatial extent, or significance, of nearly all of the identified clusters, with serositis clusters being the only ones that remained almost entirely

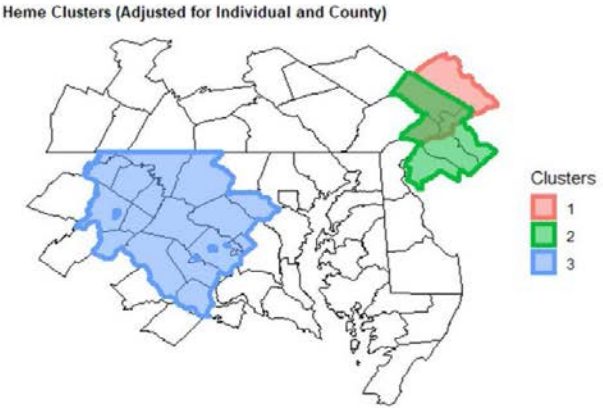

Cluster	Start Date	End Date	P-Value	Observed	Expected	Area
1	2001/2/28	2002/2/27	0.038	6	0.292	3738
2	2000/9/28	2002/2/27	0.04	7	0.481	4491
3	2002/12/28	2005/12/27	0.043	45	20.064	14994

Figure 4. Clusters of hematologic (heme) flares in patients with systemic lupus erythematosus (SLE) after adjustment for individual variables (age, sex, race, smoking status, household income, years of education, and urban living status) and county variables (county income and the proportion of the population who were African American). No significant clusters ($P < 0.05$) were identified after adjustment for individual variables, county variables, and environmental variables (fine particulate matter pollution, temperature, ozone concentration, resultant wind, barometric pressure, and relative humidity). The beginning and end dates, *P* value, observed and expected values, and area in square kilometers are shown for each cluster.

unchanged. Generally, a decrease in temporal extent, as seen for some of the joint flare clusters (Figure 2) or renal flare clusters (Supplementary Figure 3), or spatial extent, as seen for the neurologic flare clusters and pulmonary flare clusters (Supplementary Figures 1 and 4), after adjustment for covariates indicates that the adjusted covariates were partially driving the occurrence of that cluster at that time and location. After adjustment for environmental variables, some clusters increased in spatial extent, such as rash flare cluster 3, or temporal extent, such as rash flare cluster 1 (Figure 3). An increase in cluster size, temporal extent, or significance after adjustment for covariates might suggest an area where flare activity is high, despite the presence of individual and environmental covariates that are associated with lower flare activity, and thus this is an area of particular interest for further research.

GEE-based regression analysis was used to quantify the effects of individual, county, and environmental variables on the odds of flare outcomes. While these results were needed to properly adjust the cluster detection analysis, a more in-depth analysis was outside the scope of this study. An inference-based approach that not only identifies and quantifies these effects but also allows further investigation into effect modification, separating residual variability at the individual and county level (multilevel modeling) and deriving the most parsimonious models for each flare outcome, is of interest and will be the primary focus of our future work.

The potential mechanisms underlying the effect of environmental factors on lupus flares is an interesting subject to speculate on. Elevated temperature has profound effects on the immune system, particularly by increasing T cell proliferation rates, interleukin-1 (IL-1)–driven secretion of IL-2, and primary antibody responses to T-dependent antigens (17,18), but whether changes in environmental temperature affect the immune response is unknown. Rodó et al described a causal relationship between large-scale wind currents originating in northeastern China and the major epidemics of Kawasaki disease in Japan, Hawaii, and San Diego (19). *Candida* were the dominant fungal species (54% of all fungal DNA clones) isolated in the aerosol samples from these wind currents (20), underlining the potential of aerosols transported by wind currents over long distances to trigger human disease. PM2.5 has been shown to alter innate immunity by affecting Toll-like receptor signaling, inflammasome activation, and oxidative stress (21–23). One could speculate that similar mechanisms underlie the effect of these environmental factors on lupus flares.

The shortcoming of cluster analysis as an epidemiologic method is the low likelihood of establishing a definitive cause-and-effect relationship between the health event and an exposure. Clusters are useful for generating hypotheses but may not be as useful for testing hypotheses. The issues raised by a cluster cannot be definitively answered by the investigation per se, since they require an alternative epidemiologic approach. This is also true regarding the interpretation of the cluster changes after adjustment. While a change in clusters after adjustment for individual or environmental covariates suggests that these covariates in part drive the formation, location, or temporal extent of these clusters, the exact interpretation of every change can be difficult and requires further study.

The difficulty in interpretation is partially driven by SaTScan software itself, which produces a ranked list of clusters based on significance. To make reporting and interpretability easier, by default SaTScan reports only clusters that do not spatially overlap, meaning that there can be multiple significant overlapping clusters identified in an area, but only the most significant of those would be reported. A slight change in the significance of the clusters could lead to a change in ranking order, and ultimately change what clusters are mapped and reported, even if the change in significance is minimal. By loosening the default restrictions and allowing SaTScan to report spatially overlaying clusters as long as they do not contain the centroids of more significant clusters, we allowed more significant clusters to be reported, without making the plots overwhelming.

We describe the first spatiotemporal clusters of lupus organ-specific disease activity. Seasonal, as well as multi-year, cluster patterns were identified, differing in extent and location for the various organ-specific flare types. Many of the clusters identified changed in significance, temporal extent, or spatial extent after adjusting for environmental or individual covariates. Further study focusing on each individual lupus organ-specific flare is needed to better understand the driving forces behind these observed changes.

AUTHOR CONTRIBUTIONS

All authors were involved in drafting the article or revising it critically for important intellectual content, and all authors approved the final version to be published. Dr. Stojan had full access to all of the data in the study and takes responsibility for the integrity of the data and the accuracy of the data analysis.

Study conception and design. Stojan.
Acquisition of data. Stojan, Petri.
Analysis and interpretation of data. Stojan, Kvit, Curriero, Petri.

REFERENCES

1. Parks CG, Cooper GS, Nylander-French LA, Sanderson WT, Dement JM, Cohen PL, et al. Occupational exposure to crystalline silica and risk of systemic lupus erythematosus: a population-based, case–control study in the Southeastern United States. Arthritis Rheum 2002;46:1840–50.
2. Costenbader KH, Kim DJ, Peerzada J, Lockman S, Nobles-Knight D, Petri M, et al. Cigarette smoking and the risk of systemic lupus erythematosus: a meta-analysis. Arthritis Rheum 2004;50:849–57.
3. Costenbader KH, Feskanich D, Stampfer MJ, Karlson EW. Reproductive and menopausal factors and risk of systemic lupus erythematosus in women. Arthritis Rheum 2007;56:1251–62.
4. Mok CC, Leung B, Fong B, Wong CK. THU0300 serum mercury level and disease activity of systemic lupus erythematosus (SLE): a case-control study [abstract]. Ann Rheum Dis 2013;72 Suppl 3:A267.
5. Parks CG, de Souza Espindola Santos A, Barbhaiya M, Costenbader KH. Understanding the role of environmental factors in the development of systemic lupus erythematosus. Best Pract Res Clin Rheumatol 2017;31:306–20.

6. Duarte-García A, Fang H, To CH, Magder LS, Petri M. Seasonal variation in the activity of systemic lupus erythematosus. J Rheumatol 2012;39:1392–8.
7. Yang J, Lu YW, Pan HF, Tao JH, Zou YF, Bao W, et al. Seasonal distribution of systemic lupus erythematosus activity and its correlation with climate factors. Rheumatol Int 2012;32:2393–9.
8. Bernatsky S, Fournier M, Pineau CA, Clarke AE, Vinet E, Smargiassi A. Associations between ambient fine particulate levels and disease activity in patients with systemic lupus erythematosus (SLE). Environ Health Perspect 2011;119:45–9.
9. Jung CR, Chung WT, Chen WT, Lee RY, Hwang BF. Long-term exposure to traffic-related air pollution and systemic lupus erythematosus in Taiwan: a cohort study. Sci Total Environ 2019;668:342–9.
10. Bernatsky S, Smargiassi A, Barnabe C, Svenson LW, Brand A, Martin RV, et al. Fine particulate air pollution and systemic autoimmune rheumatic disease in two Canadian provinces. Environ Res 2016;146:85–91.
11. Petri M. Hopkins Lupus Cohort: 1999 update. Rheum Dis Clin North Am 2000;26:199–213.
12. Petri M, Orbai AM, Alarcon GS, Gordon C, Merrill JT, Fortin PR, et al. Derivation and validation of the Systemic Lupus International Collaborating Clinics classification criteria for systemic lupus erythematosus. Arthritis Rheum 2012;64:2677–86.
13. Petri M, Genovese M, Engle E, Hochberg M. Definition, incidence, and clinical description of flare in systemic lupus erythematosus: a prospective cohort study. Arthritis Rheum 1991;34:937–44.
14. Pebesma EJ. Multivariable geostatistics in S: the gstat package. Comput Geosci 2004;30:683–91.
15. Cressie N. Spatial prediction and ordinary kriging. Math Geol 1988; 20:405–21.
16. Lee J, Gangnon RE, Zhu J. Cluster detection of spatial regression coefficients. Stat Med 2017;36:1118–33.
17. Lederman HM, Brill CR, Murphy PA. Interleukin 1-driven secretion of interleukin 2 is highly temperature-dependent. J Immunol 1987;138:3808–11.
18. Gern JE, Jayman JR, Goldberg LI, Murphy PA, Lederman HM. Temperature is a powerful promoter of interleukin 2 transcription. Cytokine 1991;3:389–97.
19. Rodó X, Ballester J, Cayan D, Melish ME, Nakamura Y, Uehara R, et al. Association of Kawasaki disease with tropospheric wind patterns. Sci Rep 2011;1:152.
20. Rodó X, Curcoll R, Robinson M, Ballester J, Burns JC, Cayan DR, et al. Tropospheric winds from northeastern China carry the etiologic agent of Kawasaki disease from its source to Japan. Proc Natl Acad Sci U S A 2014;111:7952–7.
21. Davis BK, Wen H, Ting JP. The inflammasome NLRs in immunity, inflammation, and associated diseases. Annu Rev Immunol 2011;29:707–35.
22. Bauer RN, Diaz-Sanchez D, Jaspers I. Effects of air pollutants on innate immunity: the role of Toll-like receptors and nucleotide-binding oligomerization domain–like receptors. J Allergy Clin Immunol 2012;129:14–24.
23. Miller RL, Peden DB. Environmental effects on immune responses in patients with atopy and asthma. J Allergy Clin Immunol 2014;134: 1001–8.

Arthritis & Rheumatology
Vol. 72, No. 7, July 2020, pp 1143–1153
DOI 10.1002/art.41208

American College of Rheumatology
Empowering Rheumatology Professionals

Methionine Commits Cells to Differentiate Into Plasmablasts Through Epigenetic Regulation of BTB and CNC Homolog 2 by the Methyltransferase EZH2

Mingzeng Zhang,[1] Shigeru Iwata,[2] Maiko Hajime,[2] Naoaki Ohkubo,[2] Yasuyuki Todoroki,[2] Hiroko Miyata,[2] Masanobu Ueno,[2] He Hao,[1] Tong Zhang,[2] Jie Fan,[2] Shingo Nakayamada,[2] Kaoru Yamagata,[2] and Yoshiya Tanaka[2]

Objective. Plasmablasts play important roles in autoimmune diseases, including systemic lupus erythematosus (SLE). Activation of mechanistic target of rapamycin complex 1 (mTORC1) is regulated by amino acid levels. In patients with SLE, mTORC1 is activated in B cells and modulates plasmablast differentiation. However, the detailed mechanisms of amino acid metabolism in plasmablast differentiation remain elusive. We undertook this study to evaluate the effects of methionine in human B cells.

Methods. Purified CD19+ cells from healthy donors (n = 21) or patients with SLE (n = 35) were cultured with Toll-like receptor 7/9 ligand, interferon-α (IFNα), and B cell receptor crosslinking, and we determined the types of amino acids that were important for plasmablast differentiation and amino acid metabolism. We also identified the transcriptional regulatory mechanisms induced by amino acid metabolism, and we assessed B cell metabolism and its relevance to SLE.

Results. The essential amino acid methionine strongly committed cells to plasmablast differentiation. In the presence of methionine, Syk and mTORC1 activation synergistically induced methyltransferase EZH2 expression. EZH2 induced H3K27me3 at BTB and CNC homolog 2 (Bach2) loci and suppressed Bach2 expression, leading to induction of B lymphocyte–induced maturation protein 1 and X-box binding protein 1 expression and plasmablast differentiation. CD19+ cells from patients with SLE overexpressed EZH2, which was correlated with disease activity and autoantibody production.

Conclusion. Our findings show that methionine activated signaling by controlling immunologic metabolism in B cells and played an important role in the differentiation of B cells into plasmablasts through epigenome modification of Bach2 by the methyltransferase EZH2.

INTRODUCTION

B cells play critical roles in autoimmune diseases through antibody and cytokine production and antigen presentation. We and others have reported that abnormalities in B cell differentiation, particularly plasmablast differentiation, are closely correlated with the pathogenesis of autoimmune diseases, such as systemic lupus erythematosus (SLE) (1–5). B cells are activated and differentiated mainly by B cell receptor (BCR) crosslinking, followed by exposure to costimulatory molecules, such as CD40/CD40L, Toll-like receptors (TLRs), and various cytokines (e.g., interleukin-21 [IL-21] and interferon-α [IFNα]) (6,7). Their activation in turn leads to the activation of various downstream signaling pathways, including the following: spleen tyrosine kinase (Syk), Bruton's tyrosine kinase, and phospholipase Cγ (PLCγ) (BCR signal); myeloid differentiation factor 88, tumor necrosis factor receptor–associated factor 6 (TRAF6), and NF-κB (TLR signal); JAK/signal transducer and activator of transcription (cytokine

Supported in part by a Kakenhi Grant-in-Aid for Scientific Research (JP16K09928) from the Japan Society for the Promotion of Science and the University of Occupational and Environmental Health (UOEH), Japan (UOEH Grants for Advanced Research H29-903 and H30-905).

[1]Mingzeng Zhang, MD, He Hao, MD: University of Occupational and Environmental Health Japan, Kitakyushu, Japan, and Fourth Hospital of Hebei Medical University, Shijiazhuang, China; [2]Shigeru Iwata, MD, PhD, Maiko Hajime, MD, Naoaki Ohkubo, MD, Yasuyuki Todoroki, MD, Hiroko Miyata, MD, Masanobu Ueno, MD, Tong Zhang, MD, Jie Fan, MD, Shingo Nakayamada, MD, PhD, Kaoru Yamagata, PhD, Yoshiya Tanaka, MD, PhD: University of Occupational and Environmental Health Japan, Kitakyushu, Japan.

Dr. Nakayamada has received speaking fees from Bristol Myers Squibb, Sanofi, AbbVie, Eisai, Eli Lilly, Chugai, Pfizer, and Takeda (less than $10,000 each) and research support from Mitsubishi Tanabe, Novartis, and MSD. Dr. Tanaka has received research support from Mitsubishi Tanabe, Takeda, Daiichi Sankyo, Chugai, Bristol Myers Squibb, MSD, Astellas, AbbVie, and Eisai. No other disclosures relevant to this article were reported.

Address correspondence to Yoshiya Tanaka, MD, PhD, University of Occupational and Environmental Health Japan School of Medicine, The First Department of Internal Medicine, 1-1 Iseigaoka, Yahata-nishi, Kitakyushu, Fukuoka 807-8555, Japan. E-mail: tanaka@med.uoeh-u.ac.jp.

Submitted for publication July 30, 2019; accepted in revised form January 14, 2020.

signal); and induction of transcription factors, such as BTB and CNC homolog 2 (Bach2), B cell chronic lymphocytic leukemia/lymphoma 6, IFN regulatory factor 4 (IRF-4), positive regulatory domain zinc-finger protein 1 (PRDM-1), and X-box binding protein 1 (XBP-1), which are critical for plasmablast differentiation (8–12).

Recent studies have focused on the significance of cellular metabolism in the activation and differentiation of immunocompetent cells (13). Activation and differentiation of immunocompetent cells require the biosynthesis of cell structure components and various biomolecules, such as nucleic acids and lipids. This process uses enormous amounts of energy, such as that provided by adenosine triphosphate (ATP) (14).

Recent studies in rodents have demonstrated that a metabolic shift to anabolism, including aerobic glycolysis, is also necessary for the activation of various types of immune cells (15,16). To date, 6 key metabolic pathways, including glycolysis, oxidative phosphorylation, the pentose phosphate pathway, fatty acid β-oxidation, fatty acid synthesis, and amino acid pathways/glutaminolysis, are known to play important roles in the generation of key products to promote cell survival/growth. Each pathway has a unique purpose in the cell and is regulated by metabolic control factors, such as mechanistic target of rapamycin complex 1 (mTORC1), AMP-activated protein kinase (AMPK), hypoxia-inducible factor 1α (HIF-1α), and c-Myc (17–22). In mouse strains, B cell activation is induced by enhancement of phosphatidylinositol 3-kinase/Akt/mTORC1 signaling, glycolysis, and oxidative phosphorylation, with glucose intake fueling de novo lipogenesis to modulate B cell proliferation and growth (23–27). However, whether amino acids play a role in human B cell differentiation remains unclear.

With regard to abnormalities in cellular metabolism in SLE B cells, transgenic mice that overexpress B cell–activating factor have been shown to produce lupus-like autoantibodies, and B cells from these mice are more glycolytic than B cells from nontransgenic littermates (26). Interestingly, mTORC1 is activated in B cells of lupus-prone mice in several disease models and in patients with SLE (24,28,29). The activation of mTORC1 is regulated at the amino acid level, and mTORC1 plays important roles in the process of plasmablast differentiation. However, the relevance and detailed mechanisms of amino acid metabolism in human B cell differentiation and the role of amino acid metabolism in the pathogenesis of SLE have not been fully elucidated.

Accordingly, the aim of this in vitro and in vivo study was to determine the relevance of amino acid metabolism in human B cell differentiation and its role in the pathogenesis of SLE.

PATIENTS AND METHODS

Cell isolation. Peripheral blood mononuclear cells (PBMCs) were isolated from healthy adults using lymphocyte separation medium (Cedarlane) and treated with magnetic beads (Dynabeads CD19 and DetachaBead; ThermoFisher Scientific). The purity of CD19+ cells was >99%. Human IgD+CD27– naive B cells, IgD+CD27+ unswitched memory B cells, and IgD–CD27+ class-switched memory B cells were separated using a FACS Aria II system (BD Biosciences) as previously described (24).

Cell stimulation. Purified CD19+ cells were cultured with or without 1,000 units/ml IFNα, 0.5 μ*M* CpG-containing oligonucleotide, 1 μg/ml anti-BCR, and/or other reagents. Additionally, 10 ng/ml IL-2 was added under all conditions in our in vitro experiments involving CD19+ cells. Goat anti-human IgG and IgM (heavy and light chain) BCR was used in experiments involving CD19+ cells. Anti-human IgM BCR was used for plasmablast differentiation from naive and unswitched memory B cells. Anti-human IgG BCR was used for plasmablast differentiation from class-switched memory B cells. Each subset of B cells was cultured with or without the aforementioned treatments. Cells were cultured in RPMI 1640 supplemented with 10% fetal calf serum. Normal RPMI 1640, RPMI 1640 without glutamine and leucine, and RPMI 1640 without glutamine, methionine, and cystine/cysteine were purchased from MP Biomedicals. Leucine-free RPMI 1640 was prepared by adding L-glutamine to RPMI 1640 without glutamine and leucine. The cystine/cysteine-free medium (L-cysteine is oxidized to L-cystine in vitro; therefore, we designated this cystine-free medium) or methionine-free medium was prepared by adding L-glutamine and L-methionine or L-glutamine and L-cystine/L-cysteine to RPMI 1640 without glutamine, methionine, and cystine/cysteine, respectively.

Patients. Thirty-five patients with SLE according to the American College of Rheumatology revised criteria for SLE (30) and 21 age- and sex-matched healthy donors were enrolled in this study. The clinical features of the patients are listed in Supplementary Table 1, on the *Arthritis & Rheumatology* web site at http://onlinelibrary.wiley.com/doi/10.1002/art.41208/abstract. The collection of peripheral blood samples from patients and healthy donors was approved by the Human Ethics Review Committee of the University of Occupational and Environmental Health, Japan, and each subject provided a signed consent form (H29-045). PBMCs were obtained from peripheral blood from each patient and then stained with anti-CD19, anti-CD29, anti-CD98, anti–L-type amino acid transporter (anti-LAT1), anti-pS6K, and anti-EZH2 antibodies or dihexyloxacarbocyanine iodide ($DiOC_6$) for intracellular staining (Supplementary Table 2, http://onlinelibrary.wiley.com/doi/10.1002/art.41208/abstract).

Flow cytometry. Cells were stained for 30 minutes at 4°C with antibodies listed in Supplementary Table 2. For intracellular staining, cells were first fixed and permeabilized with a Transcription Factor Buffer Set (BD Biosciences) and washed with fluorescence-assisted cell sorting solution (24). For exclusive

analysis of live populations, cells were also stained with Fixable Viability Dye (eBioscience) and analyzed with FACSVerse (BD Biosciences) and FlowJo, version 10.

Proliferation assay. Purified B cells were stimulated in 96-well plates, cultured for 3 days, and pulsed with 0.5 mCi (18.5 kBq)/well of tritiated thymidine during the last 12 hours of culture. Cells were then harvested with a semiautomatic cell harvester (Abe Kagaku), and the uptake of tritiated thymidine was determined with a scintillation counter (PerkinElmer TopCount NXT).

Uptake experiment. CD19+ cells were stimulated for 3 days. After washing, the cells were recultured with leucine-free, methionine-free, or glutamine-free culture medium containing ^{3}H-L-leucine, ^{3}H-L-methionine, or ^{14}C-L-glutamine (PerkinElmer) at 4°C or 37°C for 1 hour. Cells were filtered, lysed with 0.1*N* NaOH and 0.5 ml 20% trichloroacetic acid solution, and washed 3 times with 5% trichloroacetic acid solution. Radioactivity was measured using a Tri-Carb 2900TR (PerkinElmer).

Real-time quantitative reverse transcription polymerase chain reaction (qPCR). Cells were stimulated for 5 days. Total RNA was extracted using an RNeasy Mini Kit, and synthesized complementary DNA was used in real-time qPCR with a Step One Plus instrument (Applied Biosystems). TaqMan assays for carnitine palmitoyltransferase IA (*CPT1A*), carnitine palmitoyltransferase II (*CPT2*), fatty acid synthase (*FASN*), sterol regulatory element binding transcription factor 1 (*SREBF1*), *BACH2*, *IRF4*, *PRDM1*, *XBP1*, *EZH2*, and B lymphoma Moloney murine leukemia virus insertion region 1 homolog (*BMI1*) were purchased from Applied Biosystems (all assay IDs are listed in Supplementary Table 3, http://onlinelibrary.wiley.com/doi/10.1002/art.41208/abstract). The expression level of each messenger RNA was normalized to the level of the endogenous control 18S ribosomal RNA.

Intracellular reactive oxygen species (ROS) levels. After 5-day culture, CD19+ cells were gently washed twice with 37°C phosphate buffered saline. ROS levels were then measured using an OxiSelect Intracellular ROS Assay Kit according to the protocol described by the manufacturer (Green Fluorescence).

Lactate assay. B cells were cultured for 5 days in 96-well plates. The medium and supernatant lactate contents were measured spectrophotometrically using a Lactate Assay Kit II according to instructions from the manufacturer (BioVision).

Extracellular flux analysis. CD19+ cells were stimulated with BCR crosslinking, CpG, and IFNα in the presence or absence of amino acids for 3 days. An XF96 Extracellular Flux analyzer (Seahorse Bioscience) and XF Real-Time ATP Rate Assay Kit (Agilent Technologies) were used to quantify the oxygen consumption rate (OCR) and extracellular acidification rate (ECAR).

Electron microscopy. Cells were collected on day 3, immersed in 2% glutaraldehyde and 2% paraformaldehyde, and stained with 1% osmium tetroxide. Cells were then dehydrated using a series of graded alcohol solutions. After freeze-drying in *t*-butyl alcohol, samples were visualized using an electron microscope (JEM-1200EX; JEOL).

Chromatin immunoprecipitation (ChIP) PCR. B cells were cultured for 5 days. CD19+ cells were crosslinked with formaldehyde, and chromatin was fragmented to 200–300 bp by sonication for 20 minutes. DNA was extracted from the cells and purified using an EZ ChIP Kit (Millipore). DNA was immunoprecipitated with antibodies, and PCR was performed with the designed primers (Supplementary Table 3, http://onlinelibrary.wiley.com/doi/10.1002/art.41208/abstract).

Gas chromatography mass spectrometry (GC-MS). CD19+ cells were stimulated for 3 days. The cell metabolome under different conditions was extracted with 50% acetonitrile/water. Dried powder was dissolved in 20 mg/ml pyridine in methoxylamine HCl and then *N*-methyl-*N*-(trimethylsilyl)trifluoroacetamide reagent. The metabolome was identified using GC-MS instruments (JMS-Q1500 and 7890GC; JEOL) equipped with a direct capillary column DB-5MS (film thickness 30m × 0.25 mm × 0.25 μm). The column temperature was set at 80°C for 2 minutes, gradually increased by 15°C/minute until reaching 320°C, and then held for 12 minutes. The temperature of the injector was adjusted to 230°C, and the MS transfer line was adjusted to 250°C. Helium gas was used as the carrier gas and was injected at a constant flow rate of 1.5 ml/minute. One microliter of the sample was injected with a solvent delay at 2 minutes. An autosampler (7650A) was coupled with the GC and set in split mode for automatic injection of the samples and solvents. The effluent of the GC column was directly transferred to the source of the MS through the transfer line. Electron ionization mass spectrometry fragments were initiated at 70 eV within the range of 30–500 m/z in full-scan mode. The temperature of the ion source was adjusted to 200°C. The National Institute of Standards and Technology mass spectral libraries were used to identify the obtained mass spectra of the active molecules in the extract.

Statistical analysis. Differences between groups were examined for statistical significance using paired *t*-tests. Pearson correlation coefficients were used to test the relationships between 2 variables of interest. *P* values less than 0.05 were considered significant. All data are expressed as the mean ± SD. Statistical analyses were conducted using Prism software, except

in experiments to isolate important amino acid–related molecules associated with EZH2 expression, for which univariate and multivariate analyses were applied using JMP9 software (SAS Institute Japan).

RESULTS

Crucial role of methionine, an essential amino acid, in plasmablast differentiation. We first assessed the optimal conditions for plasmablast differentiation. Under CpG/loxoribine (Lox) stimulation, IFNα stimulation, and BCR crosslinking to CD19+ B cells induced the strongest $CD27^{high}CD38^{high}$ plasmablast differentiation. CpG tended to result in more potent levels of differentiation than Lox (Figure 1A), suggesting the significance of TLR-9–related stimulation.

Consistent with the tendency toward plasmablast differentiation, stimulation of B cells with CpG/IFNα and BCR crosslinking resulted in the largest increase in the uptake of essential amino acids, i.e., leucine and methionine (Figure 1B). TLR-7–induced plasmablast differentiation (Lox, IFNα, and BCR) was significantly decreased only in the absence of methionine, but not leucine or cystine. Furthermore, plasmablast differentiation induced by TLR-9 stimulation (CpG, IFNα, and BCR) was significantly decreased in the absence of methionine and to a lesser extent in the absence of leucine, but not in the absence of cystine (Figure 1C). The weak plasmablast differentiation in the absence of L- and D-methionine was strengthened by L-methionine in a dose-dependent manner, but not by D-methionine (Figure 1D). Considered together, these results indicate that methionine, and to a lesser extent leucine, are important for plasmablast differentiation.

Next, we assessed the effects of amino acid deficiency on the apoptosis and survival of B cells. Treatment of B cells with BCR crosslinking, CpG, and IFNα resulted in the most profound decrease in the percentage of annexin V+/propidium iodide (PI)+ apoptotic cells, which recovered partially in the absence of cystine, leucine, or methionine with reduced levels of apoptosis inhibition (Figure 1E). Furthermore, the high survival rate and IL-6 production induced by CpG, IFNα, and BCR did not change in the absence of cystine, leucine, or methionine (Figures 1F and G).

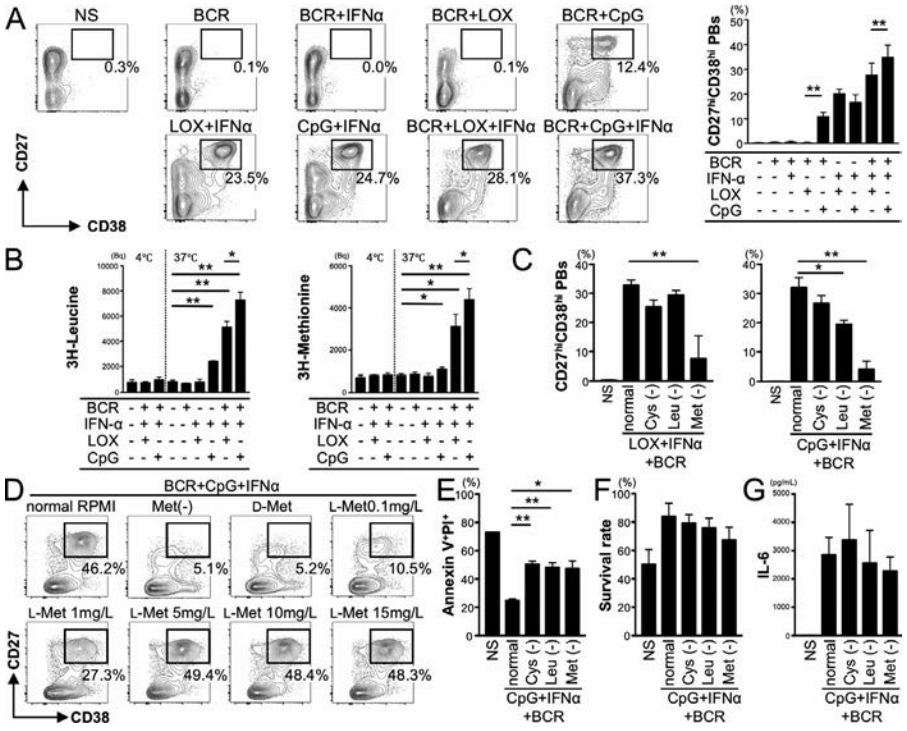

Figure 1. Importance of methionine and leucine in plasmablast differentiation. **A**, Percentage of $CD27^{high}CD38^{high}$ plasmablasts on day 5 after culture of CD19+ B cells and stimulation with B cell receptor (BCR), interferon-α (IFNα), Toll-like receptor 7 (TLR-7; loxoribine [Lox]), and/or TLR-9 (CpG). **B**, Uptake of ^{3}H-leucine and ^{3}H-methionine assessed at 4°C and 37°C on day 3. **C**, Percentage of $CD27^{high}CD38^{high}$ plasmablasts in the presence or absence of amino acids (cystine [Cys], leucine [Leu], and methionine [Met]) on day 5. **D**, Percentage of $CD27^{high}CD38^{high}$ plasmablasts in the presence or absence of D-methionine (D-Met) or different concentrations of L-methionine (L-Met) on day 5. **E**, Percentage of annexin V+/propidium iodide (PI)+ apoptotic cells on day 5. **F**, Percentage of surviving cells as determined by Fixable Viability Dye staining on day 5. **G**, Interleukin-6 (IL-6) production on day 5. In **A**–**C** and **E**–**G**, bars show the mean ± SD from 3 independent experiments using CD19+ cells from healthy donors. * = $P < 0.05$; ** = $P < 0.01$. NS = no stimulation; PBs = plasmablasts.

Importance of methionine in plasmablast differentiation from memory B cells. Next, we examined the separate effects of methionine and leucine on plasmablast differentiation using naive B cells (purity >99%), unswitched memory B cells (purity >90%), and class-switched memory B cells (purity >99%) (Supplementary Figure 1, http://onlinelibrary.wiley.com/doi/10.1002/art.41208/abstract). Treatment with CpG/IFNα/BCR markedly induced plasmablast differentiation in both class-switched and unswitched memory B cells (Figures 2A and B). CpG/IFNα/BCR-induced differentiation of class-switched memory B cells was significantly reduced in the absence of methionine (Figure 2A) and partially but significantly reduced in the absence of leucine (Figure 2B). Under similar stimulation, the absence of methionine (Figure 2A), but not leucine (Figure 2B), reduced the differentiation of unswitched memory B cells. These results suggest that methionine controlls BCR-dependent and BCR-independent plasmablast differentiation induction signals in B cells and that methionine and leucine regulate signaling and immune metabolic pathways by different mechanisms.

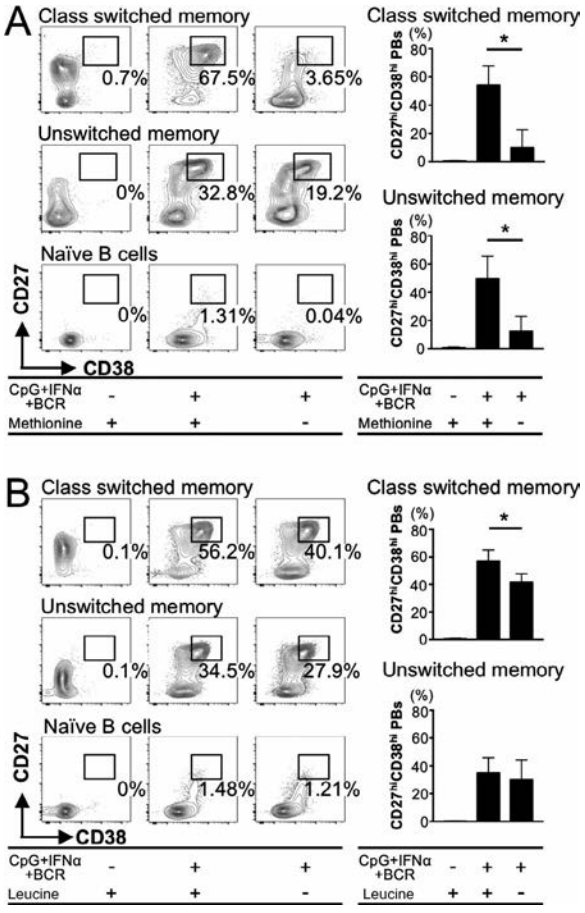

Figure 2. Importance of methionine in BCR-dependent and BCR-independent plasmablast differentiation from both class-switched and unswitched memory B cells. CD19+ cells were sorted into IgD+CD27– naive B cells, IgD+CD27+ unswitched memory B cells, and IgD–CD27+ class-switched memory B cells. The cells were cultured for 5 days under stimulation with CpG, IFNα, and BCR. **A**, Percentage of $CD27^{high}CD38^{high}$ plasmablasts in the presence or absence of methionine on day 5. **B**, Percentage of $CD27^{high}CD38^{high}$ plasmablasts in the presence or absence of leucine on day 5. Bars show the mean ± SD from 3 independent experiments using cells from healthy donors. * = $P < 0.05$. See Figure 1 for definitions.

BCR and mTORC1 signals are regulated differently by methionine and leucine, with distinct changes in glycolysis, mitochondrial function, and lipid synthesis. Next, we examined the mechanisms by which essential amino acids affect the signaling and energy metabolic pathways during plasmablast differentiation. Stimulation with BCR crosslinking/CpG/IFNα induced Syk and PLCγ phosphorylation, TRAF6 signaling, Akt and S6K phosphorylation, and c-Myc and HIF-1α expression (Figures 3A–D and Supplementary Figures 2A–D, http://onlinelibrary.wiley.com/doi/10.1002/art.41208/abstract). Lack of methionine, but not leucine, reduced Syk and PLCγ phosphorylation and TRAF6 expression (Figures 3A and B). Lack of either methionine or leucine reduced Akt and S6K phosphorylation but had no effect on c-Myc or HIF-1α expression (Figures 3C and D). The same stimulation increased lactate production and ECAR, reflecting aerobic glycolysis, which was decreased in the absence of leucine or methionine (Figure 3E).

We then evaluated the effects of amino acids on lipid metabolism in B cells. Stimulation with BCR crosslinking/CpG/IFNα did not change β-oxidation via *CPT1A* and *CPT2*, but it increased fatty acid synthesis via *FASN* and *SREBF1*, and the lack of leucine or methionine reduced both effects (Figure 3E). The absence of leucine or methionine had no effect on the levels of various lipids, such as palmitic acid and stearic acid (Figure 3E). Stimulation with BCR crosslinking/CpG/IFNα decreased citric acid levels, reflecting changes in aerobic glycolysis and lipid synthesis. The levels of citric acid were significantly decreased in the absence of methionine (Figure 3E). The same stimulation increased the uptake of glutamine, but this effect was decreased in the absence of leucine or methionine (Figure 3E). Stimulation with BCR crosslinking/CpG/IFNα increased the OCR, ROS production, and the size and number of mitochondria, which all decreased in the absence of leucine and methionine (Figures 3F–H). These results suggest that methionine and leucine regulate BCR and mTORC1 signals in a different manner, leading to distinct changes in aerobic glycolysis; the size, number, and function of mitochondria; and lipid synthesis.

Bach2-mediated plasmablast differentiation in the presence of methionine. To determine the mechanism by which methionine and leucine regulate plasmablast differentiation via BCR and mTORC1 signals, we first assessed the effects of the amino acids on the expression of transcription factors critical for plasmablast differentiation in healthy donors. Stimulation with BCR crosslinking/CpG/IFNα down-regulated

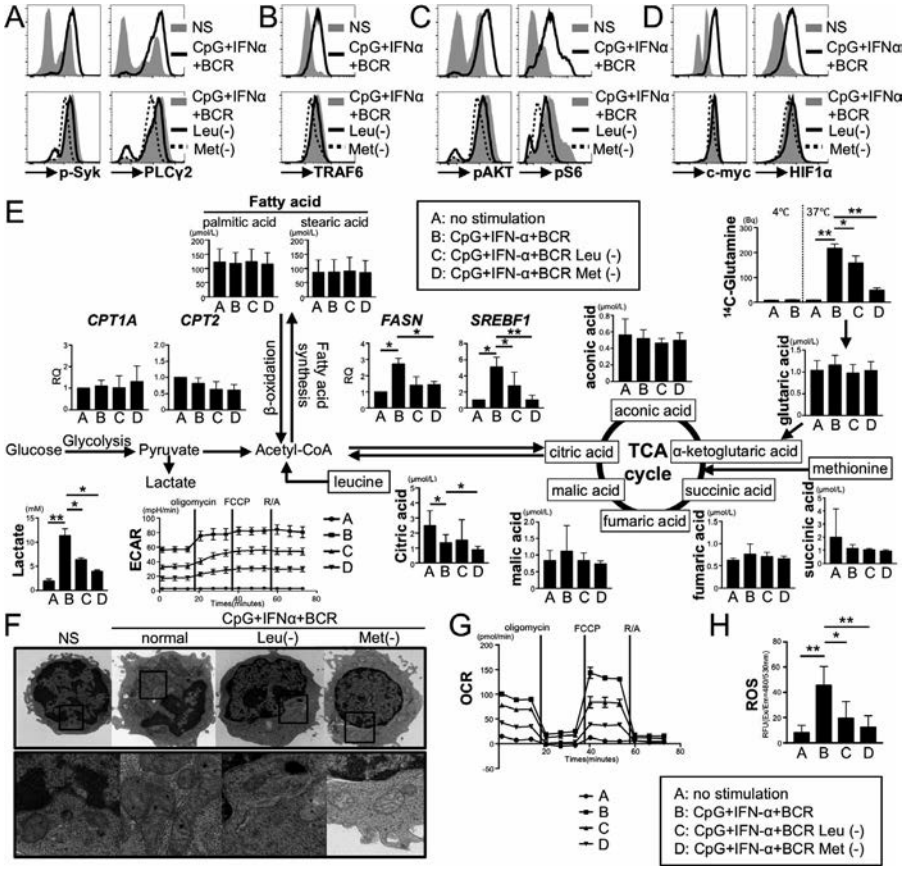

Figure 3. Differences in regulation of BCR and mechanistic target of rapamycin complex 1 signals by methionine and leucine, leading to distinct changes in glycolysis, mitochondrial function, and lipid synthesis. CD19+ B cells were cultured and stimulated with CpG, BCR, and IFNα in the presence or absence of leucine or methionine. **A**–**D**, Expression of p-Syk and phospholipase Cγ (PLCγ) (**A**), tumor necrosis factor receptor–associated factor 6 (TRAF6) (**B**), p-Akt and pS6K (**C**), and c-Myc and hypoxia-inducible factor 1α (HIF-1α) (**D**) on day 3. **E**, Schematic diagrams of the metabolic pathways of aerobic glycolysis, oxidative phosphorylation, fatty acid oxidation, and fatty acid synthesis in the presence or absence of amino acids. The concentrations of palmitic acid, stearic acid, citric acid, and other amino acids were assessed by gas chromatography mass spectrometry (GC-MS) on day 3. For GC-MS data, bars show the mean ± SD from 5 independent experiments using cells from healthy donors. **F**, The shape of mitochondria as assessed by electron microscopy on day 3. **G**, Oxygen consumption rate (OCR) on day 3. **H**, Reactive oxygen species (ROS) production on day 5. For ROS data, bars show the mean ± SD from 4 independent experiments using cells from healthy donors. For other data in **E**–**G**, bars show the mean ± SD from 3 independent experiments using cells from healthy donors. * = $P < 0.05$; ** = $P < 0.01$. Acetyl CoA = acetyl coenzyme A; ECAR = extracellular acidification rate; TCA = trichloroacetic acid; R/A = rotenone/antimycin A (see Figure 1 for other definitions).

BACH2 and up-regulated *IRF4*, *PRDM1*, and *XBP1* (Figure 4A). Deficiency of either methionine or leucine down-regulated *PRDM1* and *XBP1*, but not *IRF4*, whereas deficiency of methionine, but not leucine, enhanced *BACH2* expression (Figure 4B).

Next, we examined the expression of *BACH2*, *PRDM1*, and *XBP1* using SLE B cells. Interestingly, *PRDM1* and *XBP1* expression was not different compared to that of healthy donors under unstimulated conditions, whereas *BACH2* expression was selectively reduced (Figure 4C). After SLE B cells were stimulated with BCR crosslinking/CpG/IFNα, *BACH2* expression was further decreased, whereas *PRDM1* and *XBP1* expression and plasmablast differentiation were enhanced. *BACH2* expression was increased, whereas *PRDM1* and *XBP1* expression and plasmablast differentiation were decreased, in the context of methionine deficiency (Figures 4D and E).

Syk and mTORC1 signals synergistically induce EZH2 expression, leading to epigenetic modification of BACH2 loci. Next, we examined the effects of BCR and mTORC1 stimulation signals on *BACH2* expression in the presence of methionine. Methionine is the precursor of S-adenosylmethionine, the methyl donor utilized by all methyltransferases, including the polycomb repressor complex 2 (PRC2)–specific EZH2 (31). Less is known about how metabolic signals, such as mTORC1, regulate the expression of transcription factors via epigenetic enzymes involved in methyltransferase reactions. We found that stimulation of B cells with BCR crosslinking/CpG/IFNα maximized

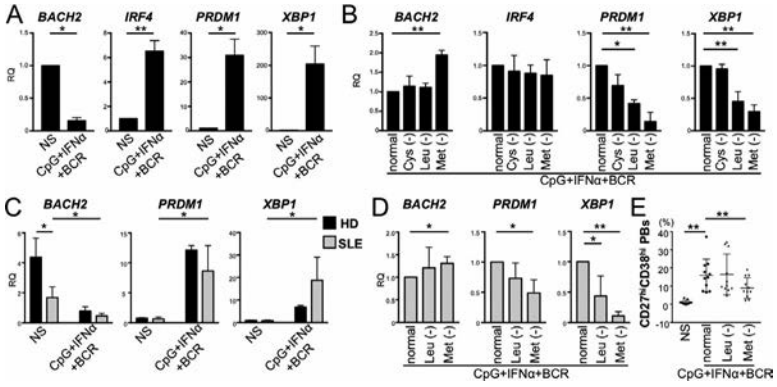

Figure 4. Transcription factor Bach2 mediates plasmablast differentiation in the presence of methionine. CD19+ cells from healthy donors (HD) or systemic lupus erythematosus (SLE) patients were cultured and stimulated with TLR-9 (CpG), BCR, and IFNα in the presence or absence of leucine or methionine. **A** and **B**, Gene expression of *BACH2*, *IRF4*, *PRDM1*, and *XBP1* in normal B cells determined by real-time polymerase chain reaction (PCR) on day 5. Bars show the mean ± SD from 3 independent experiments using cells from different healthy donors. **C** and **D**, Gene expression of *BACH2*, *PRDM1*, and *XBP1* in normal B cells or SLE B cells determined by real-time PCR on day 5. Bars show the mean ± SD from 4 independent experiments using cells from different healthy donors or SLE patients. **E**, Percentage of $CD27^{high}CD38^{high}$ plasmablasts in SLE B cells on day 5. Each symbol represents an individual donor from independent experiments (n = 11). Bars show the mean ± SD from 11 independent experiments using cells from different SLE patients. * = $P < 0.05$; ** = $P < 0.01$. RQ = relative quantity. See Figure 1 for other definitions.

EZH2 expression levels. EZH2 expression induced by CpG, IFNα, and BCR was completely inhibited in the absence of methionine and partially inhibited by the lack of leucine. No changes in the expression BMI1 polycomb group protein were observed (Figure 5A and Supplementary Figures 3A–C, http://onlinelibrary.wiley.com/doi/10.1002/art.41208/abstract). After stimulation with BCR crosslinking/CpG/IFNα, EZH2 expression was enhanced in SLE B cells; in contrast, EZH2 expression was significantly suppressed under conditions of methionine deficiency (Figure 5B). Rapamycin (an mTORC1 inhibitor), but not dorsomorphin (an AMPK inhibitor) or Pim1/AKK1-IN-1 (an LKB1 inhibitor), suppressed the expression of EZH2 (Supplementary Figure 3D). EZH2 expression levels were also down-regulated by BAY61-3606 (a Syk inhibitor) in a dose-dependent manner, but not by Src inhibitors such as Lyn peptide inhibitors, PP1, and PP2. Furthermore, the addition of rapamycin and BAY61-3606 synergistically reduced EZH2 expression levels (Figure 5C).

Bach2 is a critical transcriptional factor for B cell differentiation (32). *BACH2* suppresses *PRDM1* (33), which is upstream of *XBP1* (34). In the next step, we used EZH2 to examine epigenetic regulation of the *BACH2* gene locus. EZH2, SUZ12, and YY-1 were recruited to the *BACH2* promoter, and H3K27me3 was induced in B cells by stimulation with BCR crosslinking/CpG/IFNα (Figure 5D). Treatment with the EZH2 inhibitor GSK343 recovered the expression of *BACH2*, further suppressed *PRDM1* and *XBP1*, and inhibited plasmablast differentiation (Figures 5E and F).

Methionine is an amino acid involved in most methylation reactions, and EZH2 is known to induce DNA methylation in addition to bringing about H3K27me3 modification (35). Therefore, we further investigated the involvement of DNA methylation in the regulation of *BACH2* expression. Our results confirmed that the decrease in *BACH2* expression following stimulation with BCR crosslinking/CpG/IFNα was restored by 5-azacytidine, an inhibitor of DNA methyltransferase (Figure 5G). Thus, EZH2 expression induced by methionine could stimulate not only H3K27me3 but also DNA methylation and could negatively regulate *BACH2* expression.

In CD4+ and CD8+ T cells, microRNA-26a (miR-26a) and miR-101 negatively regulate EZH2 expression, and CD4+ T cells in patients with SLE exhibit decreased miR-26a and miR-101 expression and increased EZH2 expression (35,36). In this study, we investigated the effects of miR-26a and miR-101 on EZH2 expression and plasmablast differentiation using B cells from healthy individuals and patients with lupus. There were no changes in miR-101 expression in B cells from patients with lupus, and only miR-26a expression was decreased (Supplementary Figure 4A, http://onlinelibrary.wiley.com/doi/10.1002/art.41208/abstract). In studies using peripheral blood B cells from healthy donors, miR-26a expression was reduced by stimulation with BCR crosslinking/CpG/IFNα and recovered by treatment with the glycolysis inhibitor 2-deoxyglucose or in the absence of methionine (Supplementary Figures 4B and C). However, miR-26a mimic (overexpression) had no effect on EZH2 or plasmablast differentiation (Supplementary Figures 4D and E). Thus, miR-26a expression was decreased in B cells from patients with SLE but was not involved in EZH2 expression or plasmablast differentiation. These findings indicate that Syk and mTORC1 signals synergistically induce EZH2 expression, suppressing *BACH2* expression via epigenome modification, leading to the induction of plasmablast differentiation in the presence of methionine.

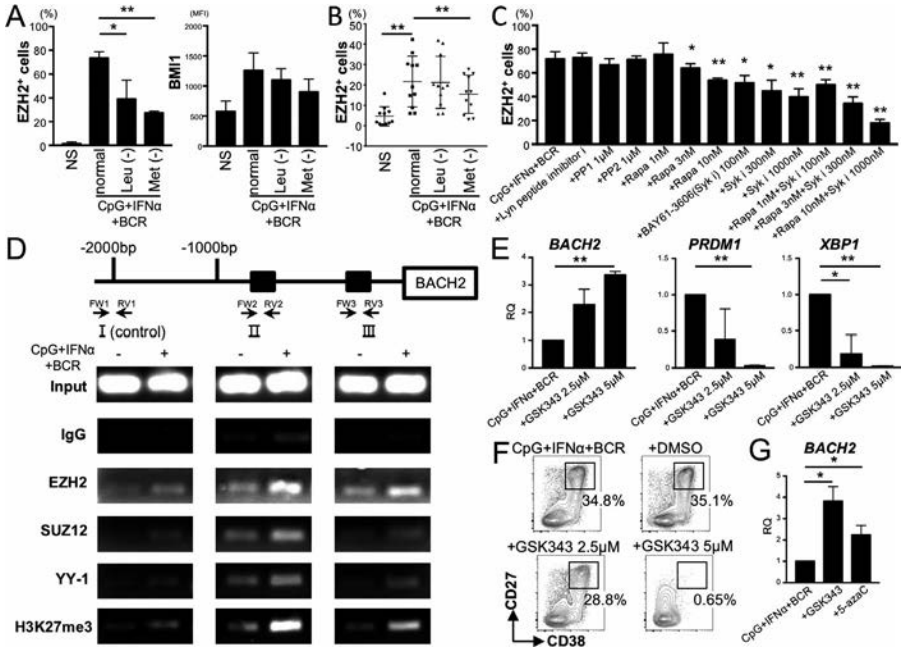

Figure 5. Synergistic induction of EZH2 expression and epigenetic regulation of Bach2. CD19+ cells from healthy donors or systemic lupus erythematosus (SLE) patients were cultured and stimulated with different agonists or inhibitors and assessed on day 5. **A**, Expression of EZH2 and B lymphoma Moloney murine leukemia virus insertion region 1 homolog (BMI1). **B**, Expression of EZH2 in SLE B cells. **C**, Effects of Src family kinase inhibitors (Lyn peptide inhibitor, PP1, PP2, Syk inhibitor BAY61-3606, and mechanistic target of rapamycin complex 1 inhibitor Rapa) on EZH2 expression. **D**, DNA–protein interactions detected by chromatin immunoprecipitation (ChIP) polymerase chain reaction. ChIP for *BACH2* is shown at the indicated loci. Data are representative of 3 independent experiments in healthy donors. **E** and **F**, Effects of the EZH2 inhibitor GSK343 on *BACH2*, *PRDM1*, and *XBP1* expression and plasmablast differentiation. **G**, Effects of DNA methyltransferase (10 μ*M* 5-azacytidine [5-azaC]) on *BACH2* expression. In **A**, **C**, **E**, and **G**, bars show the mean ± SD from 3 independent experiments using cells from healthy donors. In **B**, bars show the mean ± SD from 11 independent experiments using cells from different SLE patients. Each symbol represents an individual donor from independent experiments (n = 11). * = $P < 0.05$; ** = $P < 0.01$. See Figure 1 for other definitions.

Correlation of EZH2 expression levels in B cells from SLE patients with disease activity and autoantibody production. Finally, we examined the expression of EZH2 in B cells in SLE. The clinical backgrounds of SLE patients are listed in Supplementary Table 1 (http://onlinelibrary.wiley.com/doi/10.1002/art.41208/abstract). EZH2 expression levels were significantly higher in CD19+ cells from SLE patients than in those from healthy donors (Figure 6A). EZH2 expression levels in CD19+ cells were significantly correlated with erythrocyte sedimentation rate and disease activity scores, such as the SLE Disease Activity Index (37) and British Isles Lupus Assessment Group (BILAG) score (38). In addition, EZH2 levels were higher in anti–double-stranded DNA (anti-dsDNA) antibody–positive or BILAG A1/B2–positive patients with SLE than in their SLE counterparts without these features (Figure 6B).

$DiOC_6$ reflects mitochondrial membrane potential and its activity. LAT1 (solute carrier family 7 member 5 [SLC7A5]) forms a covalent complex with its obligate chaperone SLC3A2 (CD98) on the cell surface (39), and CD98 has 2 distinct functions: facilitation of amino acid transport and mediation of β1 integrin (CD29) signals (40,41). In the final step, we examined the correlation between the expression level of EZH2 and that of $DiOC_6$, pS6K, LAT1, CD98, and CD29 in CD19+ cells from healthy donors and patients with SLE. The expression levels of $DiOC_6$, pS6K, and CD98 were significantly higher in patients with SLE than in healthy donors (Figure 6C). Furthermore, the expression levels of pS6K, CD98, and CD29 in CD19+ cells were significantly correlated with EZH2 expression in patients with SLE (Figure 6D). Multivariate analysis identified pS6K and CD98 as the major determinants of EZH2 expression (Supplementary Table 4, http://onlinelibrary.wiley.com/doi/10.1002/art.41208/abstract). These results suggest the involvement of amino acid transporters and EZH2 overexpression in B cells from patients with SLE during plasmablast differentiation.

DISCUSSION

In this study, we examined the importance of amino acid metabolism in human B cell function. Our findings highlight the importance of methionine, an essential amino acid, in plasmablast differentiation.

With regard to the involvement of amino acids in T cell function, previous studies have demonstrated the importance of amino acids, such as leucine, and their transporter LAT1 in T cell differentiation

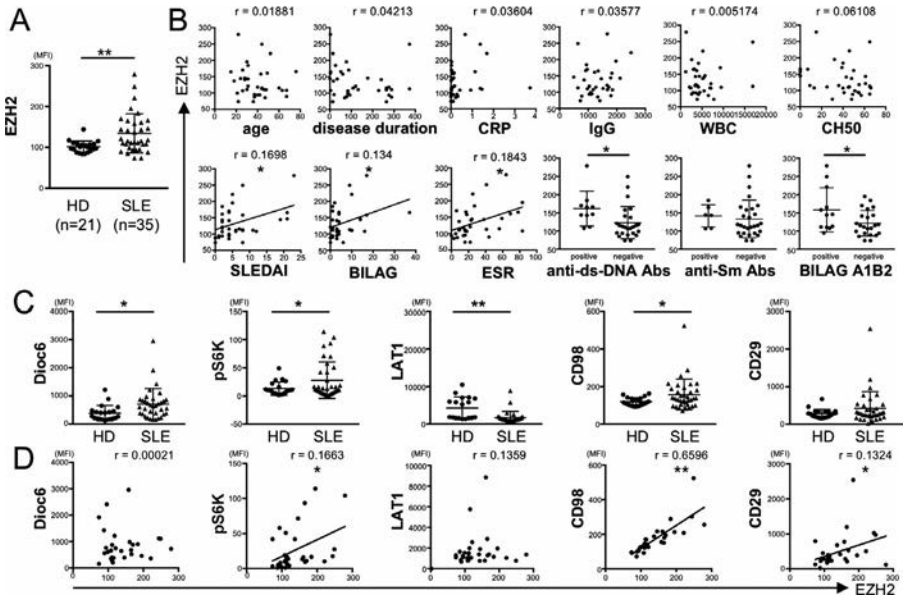

Figure 6. Overexpression of EZH2 in CD19+ cells and correlation with disease activity and autoantibody production in systemic lupus erythematosus (SLE). Peripheral blood mononuclear cells were isolated from the peripheral blood of healthy donors (HD) and SLE patients and assessed by flow cytometry. **A**, Mean fluorescence intensity (MFI) of EZH2 in CD19+ cells from the 2 groups. **B**, Correlation between EZH2 expression levels in SLE patients and age, disease duration, C-reactive protein (CRP) level, IgG level, white blood cell (WBC) count, CH50 level, SLE Disease Activity Index (SLEDAI) score, British Isle Lupus Assessment Group (BILAG) score, and erythrocyte sedimentation rate (ESR), and comparisons of EZH2 levels between SLE patients classified as positive or negative for anti–double-stranded DNA (anti-dsDNA) antibodies (Abs), anti-Sm antibodies, and BILAG A1/B2 domain scores. **C**, Comparisons of levels of dihexyloxacarbocyanine iodide ($DiOC_6$), pS6K, L-type amino acid transporter (LAT1), CD98, and CD29 in CD19+ cells among healthy donors and SLE patients. **D**, Correlation between EZH2 expression and $DiOC_6$, pS6K, LAT1, CD98, and CD29 levels, as analyzed by Pearson correlation coefficient. Each symbol represents an individual donor. In **A**–**C**, bars show the mean ± SD. * = $P < 0.05$; ** = $P < 0.01$.

(21,42). However, the roles of amino acids in B cell function are not as clear. One study showed the importance of glucose-independent glutamine in B cell proliferation and survival (43). Moreover, in the present study, we provided evidence for the critical role of methionine, an essential amino acid, in plasmablast differentiation.

BCR ligation by antigens leads to activation of protein kinases, including the Src family kinase Lyn and Syk (44). Syk activation is a key event for further propagation of downstream signaling molecules in B cells (45). Syk also regulates mTORC1 signals in B cells (46,47). In the present study, we found that methionine and leucine regulated BCR and mTORC1 signals differently; that is, the BCR signal was susceptible to methionine but not leucine, whereas the mTORC1 pathway was susceptible to both methionine and leucine. In the presence of amino acids, Syk and mTORC1 signals synergistically induced EZH2 expression.

PRC2 is a protein complex that contains the histone methyltransferase EZH2, which catalyzes the H3K27. H3K27me3 is found in promoters and along the transcribed regions of repressed genes as well as in the promoters of genes that are poised for activation (48). During normal B cell differentiation, EZH2 expression is induced when naive B cells enter the germinal center for affinity maturation and antibody class switching (49).

Rohraff et al showed that EZH2 expression was increased in neutrophils, monocytes, CD4+ T cells, and B cells in the peripheral blood of SLE patients. Additionally, EZH2 inhibition was observed in MLR/*lpr* mice (50). Schrezenmeier et al demonstrated that EZH2 expression was increased in the peripheral blood of SLE patients, particularly in plasmablasts (51). In addition, EZH2 and H3K27me3 levels were increased in CD4+ T cells in the peripheral blood of SLE patients, and miR-26a and miR-101, which negatively regulate EZH2 expression, were identified (35).

In this study, we found that Syk and mTORC1 signals synergistically up-regulate EZH2, subsequently leading to *BACH2*-mediated plasmablast differentiation in the presence of methionine. These results underscore the importance of methionine in human plasmablast differentiation through EZH2 induction. Furthermore, EZH2 expression in B cells was significantly higher in SLE patients than in healthy donors and was related to disease activity and production of autoantibodies, such as anti-dsDNA antibodies. Taken together, these findings suggest that EZH2 inhibitors may be an effective treatment for SLE.

Bach2 is known to repress the expression of *PRDM1*, which encodes the transcription factor B lymphocyte–induced maturation protein 1, thereby promoting the differentiation of plasma cells (52). These findings indicate that Bach2 is important for B cell differentiation in mice. In the present study, we found that methionine regulated EZH2 expression, leading to reduced *BACH2* expression and the promotion of plasmablast differentiation from human

B cells. Furthermore, selective reduction of *BACH2* and increased expression of EZH2 in SLE B cells were observed among transcription factors important for differentiation, confirming the important roles of these targets in methionine-dependent plasmablast differentiation.

In summary, we found that methionine plays a pivotal role in the following sequences during B cell differentiation into plasmablasts: activation of Syk and mTORC1 signals, expression of methyltransferase EZH2, histone modification of *BACH2* and its suppression, induction of *PRDM1* and *XBP1* expression, and plasmablast differentiation. Such signaling pathways were found to be relevant to the differentiation of CD19+ B cells into autoantibody-producing plasmablasts in patients with SLE, in whom the levels of EZH2 were highly associated with SLE disease activity. Taken together, our findings show that amino acid metabolism and the methionine–EZH2 interaction are important for plasmablast differentiation and may be an attractive option for improving therapeutic effectiveness in patients with SLE.

ACKNOWLEDGMENTS

We thank the patients and volunteers for their participation and cooperation. We also thank Ms N. Sakaguchi (The First Department of Internal Medicine, UOEH), T. Umata (RI Center, UOEH), and K. Hara (Shared-Use Research Center, UOEH).

AUTHOR CONTRIBUTIONS

All authors were involved in drafting the article or revising it critically for important intellectual content, and all authors approved the final version to be published. Dr. M. Zhang had full access to all of the data in the study and takes responsibility for the integrity of the data and the accuracy of the data analysis.

Study conception and design. M. Zhang, Iwata, Tanaka.
Acquisition of data. M. Zhang, Iwata, Hajime, Ohkubo, Todoroki, Miyata, Ueno, Hao, T. Zhang, Fan, Nakayamada, Yamagata.
Analysis and interpretation of data. M. Zhang, Iwata.

REFERENCES

1. Jacobi AM, Mei H, Hoyer BF, Mumtaz IM, Thiele K, Radbruch A, et al. HLA-DRhigh/CD27high plasmablasts indicate active disease in patients with systemic lupus erythematosus. Ann Rheum Dis 2010;69:305–8.
2. Iwata S, Saito K, Tokunaga M, Yamaoka K, Nawata M, Yukawa S, et al. Phenotypic changes of lymphocytes in patients with systemic lupus erythematosus who are in longterm remission after B cell depletion therapy with rituximab. J Rheumatol 2011;38:633–41.
3. Tipton CM, Fucile CF, Darce J, Chida A, Ichikawa T, Gregoretti I, et al. Diversity, cellular origin and autoreactivity of antibody-secreting cell population expansions in acute systemic lupus erythematosus. Nat Immunol 2015;16:755–65.
4. Jenks SA, Cashman KS, Zumaquero E, Marigorta UM, Patel AV, Wang X, et al. Distinct effector B cells induced by unregulated Toll-like receptor 7 contribute to pathogenic responses in systemic lupus erythematosus. Immunity 2018;49:725–39.
5. Tanaka Y, Kubo S, Iwata S, Yoshikawa M, Nakayamada S. B cell phenotypes, signaling and their roles in secretion of antibodies in systemic lupus erythematosus. Clin Immunol 2018;186:21–5.
6. Ruprecht CR, Lanzavecchia A. Toll-like receptor stimulation as a third signal required for activation of human naive B cells. Eur J Immunol 2006;36:810–6.
7. Wang S, Wang J, Kumar V, Karnell JL, Naiman B, Gross PS, et al. IL-21 drives expansion and plasma cell differentiation of autoreactive CD11c^{hi}T-bet^{+} B cells in SLE. Nat Commun 2018;9:1758.
8. Igarashi K, Ochiai K, Itoh-Nakadai A, Muto A. Orchestration of plasma cell differentiation by Bach2 and its gene regulatory network [review]. Immunol Rev 2014;261:116–25.
9. Iwata S, Yamaoka K, Niiro H, Nakano K, Wang SP, Akashi K, et al. Amplification of Toll-like receptor-mediated signaling through spleen tyrosine kinase in human B-cell activation. J Allergy Clin Immunol 2012;129:1594–601.
10. Kobayashi T, Kim TS, Jacob A, Walsh MC, Kadono Y, Fuentes-Pananá E, et al. TRAF6 is required for generation of the B-1a B cell compartment as well as T cell-dependent and -independent humoral immune responses. PLoS One 2009;4:e4736.
11. Kurosaki T, Shinohara H, Baba Y. B cell signaling and fate decision [review]. Annu Rev Immunol 2010;28:21–55.
12. Niiro H, Clark EA. Regulation of B-cell fate by antigen-receptor signals [review]. Nat Rev Immunol 2002;2:945–56.
13. Choi WS, Yang JI, Kim W, Kim HE, Kim SK, Won Y, et al. Critical role for arginase II in osteoarthritis pathogenesis. Ann Rheum Dis 2019;78:421–8.
14. Andrejeva G, Rathmell JC. Similarities and distinctions of cancer and immune metabolism in inflammation and tumors. Cell Metab 2017;26:49–70.
15. O'Sullivan D, Pearce EL. Expanding the role of metabolism in T cells. Science 2015;348:976–7.
16. Buck MD, Sowell RT, Kaech SM, Pearce EL. Metabolic instruction of immunity. Cell 2017;169:570–86.
17. Powell JD, Pollizzi KN, Heikamp EB, Horton MR. Regulation of immune responses by mTOR [review]. Annu Rev Immunol 2012;30:39–68.
18. Corcoran SE, O'Neill LA. HIF1α and metabolic reprogramming in inflammation. J Clin Invest 2016;126:3699–707.
19. Blagih J, Coulombe F, Vincent EE, Dupuy F, Galicia-Vázquez G, Yurchenko E, et al. The energy sensor AMPK regulates T cell metabolic adaptation and effector responses in vivo. Immunity 2015;42:41–54.
20. Wang R, Dillon CP, Shi LZ, Milasta S, Carter R, Finkelstein D, et al. The transcription factor Myc controls metabolic reprogramming upon T lymphocyte activation. Immunity 2011;35:871–82.
21. Sinclair LV, Rolf J, Emslie E, Shi YB, Taylor PM, Cantrell DA. Control of amino-acid transport by antigen receptors coordinates the metabolic reprogramming essential for T cell differentiation. Nat Immunol 2013;14:500–8.
22. O'Neill LA, Kishton RJ, Rathmell J. A guide to immunometabolism for immunologists [review]. Nat Rev Immunol 2016;16:553–65.
23. Jellusova J, Rickert RC. The PI3K pathway in B cell metabolism. Crit Rev Biochem Mol Biol 2016;51:359–78.
24. Torigoe M, Iwata S, Nakayamada S, Sakata K, Zhang M, Hajime M, et al. Metabolic reprogramming commits differentiation of human CD27^{+}IgD^{+} B cells to plasmablasts or CD27^{-}IgD^{-} cells. J Immunol 2017;199:425–34.
25. Doughty CA, Bleiman BF, Wagner DJ, Dufort FJ, Mataraza JM, Roberts MF, et al. Antigen receptor-mediated changes in glucose metabolism in B lymphocytes: role of phosphatidylinositol 3-kinase signaling in the glycolytic control of growth. Blood 2006;107:4458–65.
26. Caro-Maldonado A, Wang R, Nichols AG, Kuraoka M, Milasta S, Sun LD, et al. Metabolic reprogramming is required for antibody production that is suppressed in anergic but exaggerated in chronically BAFF-exposed B cells. J Immunol 2014;192:3626–36.

27. Jellusova J, Cato MH, Apgar JR, Ramezani-Rad P, Leung CR, Chen C, et al. Gsk3 is a metabolic checkpoint regulator in B cells. Nat Immunol 2017;18:303–12.
28. Wu T, Qin X, Kurepa Z, Kumar KR, Liu K, Kanta H, et al. Shared signaling networks active in B cells isolated from genetically distinct mouse models of lupus. J Clin Invest 2007;117:2186–96.
29. Wu C, Fu Q, Guo Q, Chen S, Goswami S, Sun S, et al. Lupus-associated atypical memory B cells are mTORC1-hyperactivated and functionally dysregulated. Ann Rheum Dis 2019;78:1090–100.
30. Tan EM, Cohen AS, Fries JF, Masi AT, McShane DJ, Rothfield NF, et al. The 1982 revised criteria for the classification of systemic lupus erythematosus. Arthritis Rheum 1982;25:1271–7.
31. Dann SG, Ryskin M, Barsotti AM, Golas J, Shi C, Miranda M, et al. Reciprocal regulation of amino acid import and epigenetic state through Lat1 and EZH2. EMBO J 2015;34:1773–85.
32. Igarashi K, Kurosaki T, Roychoudhuri R. BACH transcription factors in innate and adaptive immunity [review]. Nat Rev Immunol 2017;17:437–50.
33. Ochiai K, Katoh Y, Ikura T, Hoshikawa Y, Noda T, Karasuyama H, et al. Plasmacytic transcription factor Blimp-1 is repressed by Bach2 in B cells. J Biol Chem 2006;281:38226–34.
34. Shaffer AL, Shapiro-Shelef M, Iwakoshi NN, Lee AH, Qian SB, Zhao H, et al. XBP1, downstream of Blimp-1, expands the secretory apparatus and other organelles, and increases protein synthesis in plasma cell differentiation. Immunity 2004;21:81–93.
35. Tsou PS, Coit P, Kilian NC, Sawalha AH. EZH2 modulates the DNA methylome and controls T cell adhesion through junctional adhesion molecule A in lupus patients. Arthritis Rheumatol 2018;70:98–108.
36. Zhao E, Maj T, Kryczek I, Li W, Wu K, Zhao L, et al. Cancer mediates effector T cell dysfunction by targeting microRNAs and EZH2 via glycolysis restriction. Nat Immunol 2016;17:95–103.
37. Bombardier C, Gladman DD, Urowitz MB, Caron D, Chang DH, and the Committee on Prognosis Studies in SLE. Derivation of the SLEDAI: a disease activity index for lupus patients. Arthritis Rheum 1992;35:630–40.
38. Hay EM, Bacon PA, Gordon C, Isenberg DA, Maddison P, Snaith ML, et al. The BILAG index: a reliable and valid instrument for measuring clinical disease activity in systemic lupus erythematosus. Q J Med 1993;86:447–58.
39. Scalise M, Galluccio M, Console L, Pochini L, Indiveri C. The human SLC7A5 (LAT1): the intriguing histidine/large neutral amino acid transporter and its relevance to human health [review]. Front Chem 2018;6:243.
40. Fenczik CA, Sethi T, Ramos JW, Hughes PE, Ginsberg MH. Complementation of dominant suppression implicates CD98 in integrin activation. Nature 1997;390:81–5.
41. Cho JY, Fox DA, Horejsi V, Sagawa K, Skubitz KM, Katz DR, et al. The functional interactions between CD98, β1-integrins, and CD147 in the induction of U937 homotypic aggregation. Blood 2001;98:374–82.
42. Ren W, Liu G, Yin J, Tan B, Wu G, Bazer FW, et al. Amino-acid transporters in T-cell activation and differentiation [review]. Cell Death Dis 2017;8:e2655.
43. Le A, Lane AN, Hamaker M, Bose S, Gouw A, Barbi J, et al. Glucose-independent glutamine metabolism via TCA cycling for proliferation and survival in B cells. Cell Metab 2012;15:110–21.
44. Taniguchi T, Kobayashi T, Kondon J, Takahashi K, Nakamura H, Suzuki J, et al. Molecular cloning of a porcine gene syk that encodes a 72-kDa protein-tyrosine kinase showing high susceptibility to proteolysis. J Biol Chem 1991;266:15790–6.
45. Kulathu Y, Grothe G, Reth M. Autoinhibition and adapter function of Syk [review]. Immunol Rev 2009;232:286–99.
46. Leseux L, Hamdi SM, Al Saati T, Capilla F, Recher C, Laurent G, et al. Syk-dependent mTOR activation in follicular lymphoma cells. Blood 2006;108:4156–62.
47. Holroyd AK, Michie AM. The role of mTOR-mediated signaling in the regulation of cellular migration. Immunol Lett 2018;196:74–9.
48. Voigt P, Tee WW, Reinberg D. A double take on bivalent promoters. Genes Dev 2013;27:1318–38.
49. Béguelin W, Popovic R, Teater M, Jiang Y, Bunting KL, Rosen M, et al. EZH2 is required for germinal center formation and somatic EZH2 mutations promote lymphoid transformation. Cancer Cell 2013;23:677–92.
50. Rohraff DM, He Y, Farkash EA, Schonfeld M, Tsou PS, Sawalha AH. Inhibition of EZH2 ameliorates lupus-like disease in MRL/lpr mice. Arthritis Rheumatol 2019;71:1681–90.
51. Schrezenmeier E, Lino AC, Alexander T, Dörner T. EZH2 inhibition in B cell subsets: comment on the article by Rohraff et al [letter]. Arthritis Rheumatol 2020;72:371-3.
52. Tanaka H, Muto A, Shima H, Katoh Y, Sax N, Tajima S, et al. Epigenetic regulation of the Blimp-1 gene (Prdm1) in B cells involves Bach2 and histone deacetylase 3. J Biol Chem 2016;291:6316–30.

American College of Rheumatology
Empowering Rheumatology Professionals

Arthritis & Rheumatology
Vol. 72, No. 7, July 2020, pp 1154–1159
DOI 10.1002/art.41233

BRIEF REPORT

Comparison of Aortitis Versus Noninflammatory Aortic Aneurysms Among Patients Who Undergo Open Aortic Aneurysm Repair

Laarni Quimson,[1] Adam Mayer,[2] Sarah Capponi,[2] Bryan Rea,[3] and Rennie L. Rhee[1]

Objective. Distinguishing aortitis-induced aneurysms from noninflammatory aortic aneurysms is difficult and often incidentally diagnosed on histologic examination after surgical repair. This study was undertaken to examine surgically diagnosed aortitis and identify patient characteristics and imaging findings associated with the disease.

Methods. In this case–control study, cases had newly diagnosed, biopsy-proven noninfectious aortitis after open thoracic aortic aneurysm surgical repair. Five controls were matched with cases for year of surgery and lacked significant inflammation on surgical pathology analysis. Data on comorbidities, demographic characteristics, and laboratory and imaging abnormalities prior to surgery were collected. Associations between exposures and outcomes were evaluated using conditional logistic regression. Backward stepwise logistic regression was used to determine factors independently associated with aortitis. Odds ratios (ORs) with 95% confidence intervals (95% CIs) were calculated.

Results. The study included 262 patients (43 patients with aortitis and 219 controls). Patients with aortitis were older at the time of surgery, predominantly female, and less likely to have a history of coronary artery disease (CAD). Multivariable analysis revealed that aortitis was independently associated with an older age at the time of surgery (OR 1.08 [95% CI 1.03–1.13], $P < 0.01$), female sex (OR 2.36 [95% CI 1.01–5.51], $P = 0.04$), absence of CAD (OR 6.92 [95% CI 2.14–22.34], $P = 0.04$), a larger aneurysm diameter (OR 1.74 [95% CI 1.02–2.98], $P = 0.04$), and arterial wall thickening on imaging (OR 56.93 [95% CI 4.31–752.33], $P < 0.01$).

Conclusion. Among patients who undergo open surgical repair of an aortic aneurysm, elderly women with no history of CAD who have evidence of other aortic or arterial wall thickening on imaging are more likely to have histologic evidence of aortitis. Patients with these characteristics may benefit from further rheumatologic evaluation.

INTRODUCTION

Aortitis comprises a group of disorders characterized by aortic wall inflammation from infectious or noninfectious causes (1). Aortitis can lead to the development of aortic aneurysms, aortic dissections, and aortic wall rupture, which can have a significant impact on morbidity and mortality (2). Noninfectious aortitis is mainly caused by giant cell arteritis (GCA) and Takayasu arteritis (TAK). Other diseases associated with noninfectious aortitis include IgG4-related disease, relapsing polychondritis, Cogan's syndrome, granulomatosis with polyangiitis, and sarcoidosis (1,3,4). Aortitis without evidence of systemic disease or infection is referred to as isolated aortitis (5,6). Cases of isolated aortitis can be incidentally identified on surgical pathology or by imaging studies such as computed tomography (CT) or magnetic resonance imaging (MRI) (5,7).

Previous studies of isolated aortitis have shown that it more commonly occurs in women age >50 years and predominantly involves the ascending aorta. Furthermore, noninfectious, isolated aortitis is detected on review of aortic surgical pathology in 2–12% of cases (2,5,8–12). Although isolated aortitis can be identified radiologically using MRI or CT, imaging is neither sensitive nor specific in diagnosing noninfectious etiologies (1). Current data are lack-

[1]Laarni Quimson, DO, Rennie L. Rhee, MD, MSCE: Hospital of the University of Pennsylvania, Philadelphia; [2]Adam Mayer, MD, Sarah Capponi, MD: University of Pennsylvania Perelman School of Medicine, Philadelphia; [3]Bryan Rea, MD: University of Pittsburgh School of Medicine, Pittsburgh, Pennsylvania.

No potential conflicts of interest relevant to this article were reported.

Address correspondence to Rennie Rhee, MD, MSCE, University of Pennsylvania, Division of Rheumatology, White Building 5th Floor, 3400 Spruce Street, Philadelphia, PA 19104. E-mail: rennie.rhee@uphs.upenn.edu.

Submitted for publication June 11, 2019; accepted in revised form February 13, 2020.

ing regarding the epidemiology of and predictive factors for aortitis confirmed by pathologic examination. Better risk-stratifying for aortitis-induced aneurysms can lead to additional diagnostic evaluation, including referral to a rheumatologist and prompter therapeutic intervention to improve peri- and postoperative outcomes.

The objective of this study was to identify factors associated with aortitis-related aneurysms compared to noninflammatory aortic aneurysms confirmed by histopathologic examination after open aortic aneurysm repair.

PATIENTS AND METHODS

Study design and data source. We conducted a matched case–control study of patients who underwent open surgical repair of a thoracic aortic aneurysm within the University of Pennsylvania Health System between 2007 and 2017. Patients were identified using surgical pathology and included if they had available radiologic data. The study was approved by the University of Pennsylvania Institutional Review Board.

Case definition. All patients who underwent open thoracic aortic aneurysm repair were eligible for this study. Cases with noninfectious aortitis were identified by pathology report and had significant inflammation, such as granulomatous inflammation, giant cells, or adventitial inflammation in the absence of any infectious etiology (9,13). Patients with an existing diagnosis of a systemic autoimmune disease associated with aortitis (e.g., GCA), and those who underwent surgical revisions were excluded.

Control selection. For each case, 5 controls without pathologic evidence of aortitis at the index date were selected and matched for year of surgical open thoracic aortic aneurysm repair (within 1 year of the date of surgery for the matched case).

Covariates and statistical analysis. Data on demographic characteristics, comorbid conditions, and medications received were collected. Clinical data, including symptoms of chest pain, dyspnea, abdominal pain, weight loss, fevers, medications received, vital signs, and laboratory values were extracted from preoperative outpatient visits or notes from hospital admissions prior to surgical intervention if the preoperative visit was not available. Available radiology data prior to surgical intervention were recorded, including CT, MRI, CT angiography, or magnetic resonance angiography findings. For the radiology data, the type of imaging, characteristics and size of the repaired aneurysm, presence of other arterial or unrepaired aortic abnormalities (such as wall thickening, stenosis, occlusions, or thrombus), and presence of calcifications or atheroma were extracted from the radiology report.

For univariate analyses comparing characteristics between groups, we used conditional logistic regression or, when sample sizes were small, Fisher's exact tests. Backward stepwise conditional logistic regression was used to determine factors independently associated with aortitis. *P* values less than 0.05 were considered significant for all tests. All analyses were performed using Stata 14.1.

RESULTS

Study population and clinical features. The pathology database identified a total of 1,373 patients with available tissue pathology findings from open aortic aneurysm repairs between 2007 and 2017. Among these, 55 patients (4%) were identified as having isolated aortitis on pathologic examination (Figure 1). To analyze the risk factors associated with aortitis, 262 patients were included in the study (43 patients with aortitis and 219 matched controls). Compared to matched controls, patients with aortitis were older at the time of surgery

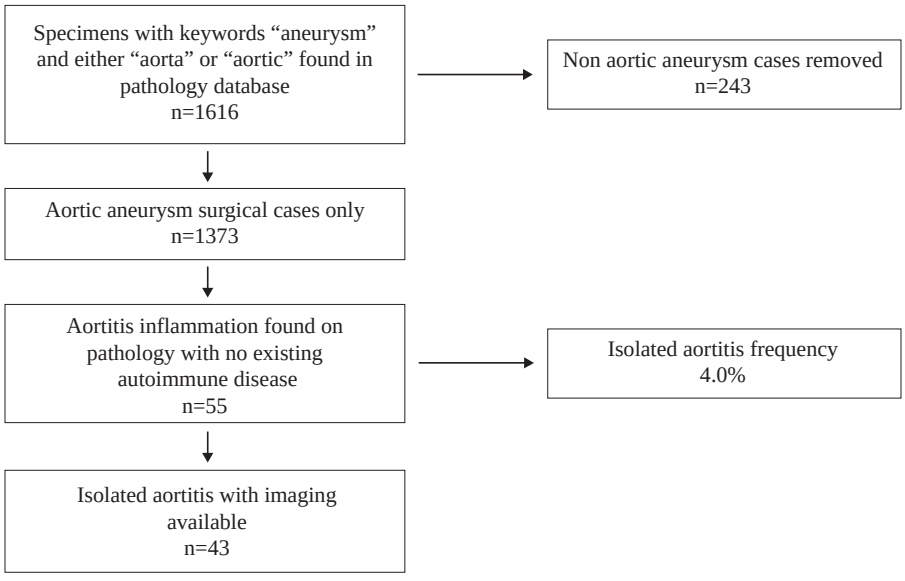

Figure 1. Flow chart showing the selection of aortitis specimens for inclusion in the study.

with a mean age of 70 years versus 63 years ($P < 0.01$), and they were more likely to be female (65% versus 31%; $P < 0.01$). On review of medical comorbidities, the aortitis group was less likely to have a history of coronary artery disease (CAD) (21% versus 44%; $P = 0.01$). Furthermore, though both groups had a high prevalence of hypertension, the aortitis group had a higher percentage of patients with hypertension than the control group (88% versus 71%; $P = 0.02$). There was no significant difference between the 2 groups regarding a history of hyperlipidemia, type 2 diabetes mellitus, brain ischemia, smoking history, or body mass index.

Vital signs examined at the preoperative outpatient visit or from the preoperative inpatient hospital visit revealed that the aortitis group had a higher systolic blood pressure (BP), with a mean systolic BP of 142 mm Hg compared to a mean systolic BP of 134 mm Hg in the control group ($P = 0.01$). Other vital signs including heart rate, temperature, weight, and height were not significantly different between the 2 groups. White blood cell count and platelet count were similar between the groups. The mean hemoglobin concentration in the aortitis group was 13 gm/dl, compared to 14 gm/dl in the control group ($P = 0.01$). We were unable to examine the erythrocyte sedimentation rate or C-reactive protein level, since only a small minority of patients were tested around the time of surgery.

Radiologic features. Of repaired aneurysms, 95% were located in the ascending aorta in both groups (Table 1). Wall thickening within the repaired aneurysm was exclusively present in patients with aortitis (7% versus 0%; $P < 0.01$). There was no significant difference in the presence of stenosis, occlusion, calcifications, atheromas, or thrombi located in the repaired aneurysm between the 2 groups. Patients with aortitis had a greater aneurysm diameter prior to surgical repair (60 mm versus 50 mm; $P = 0.04$). The aortitis group also had a higher rate of increase in aneurysm diameter per year prior to surgical repair compared to the controls (2.9 mm/year versus −1.6 mm/year; $P = 0.22$), although the difference was not statistically significant, possibly due to the small number of patients who underwent serial imaging (Table 1). Of note, the total number of serial images obtained and the time from the initial imaging study to surgery were similar between the 2 groups.

Imaging abnormalities in the vasculature aside from the surgically repaired aneurysm (including aorta and its main branches) were also evaluated. The aortitis group had more wall thickening in other vasculature outside of the repaired aneurysm (12% versus 0.5%; $P < 0.01$). A higher rate of noncontiguous aortic aneurysms was identified in the aortitis group (35% versus 15%; $P = 0.04$) (Table 1). There was no significant difference regarding the presence of stenosis, occlusion, calcifications, atheromas, or thrombi located in other vasculature between the 2 groups.

Table 1. Characteristics of repaired aortic aneurysm and preoperative imaging abnormalities in patients with aortitis and matched controls*

	Aortitis group (n = 43)	Control group (n = 219)	*P*
Location of repaired aneurysm			
Ascending aorta	41 (95)	207 (95)	0.83
Aortic arch	0 (0)	7 (3)	0.60
Descending thoracic aorta	2 (5)	5 (2)	0.32
Pathologic findings†			
Granulomatous inflammation	15 (35)	0 (0)	–
Giant cells	37 (86)	0 (0)	–
Adventitial inflammation	30 (70)	20 (9)	–
Calcific atherosclerosis	22 (51)	93 (43)	–
Imaging abnormalities in repaired aneurysm			
Wall thickening	3 (7)	0 (0)	<0.01
Stenosis or occlusion	1 (2)	1 (1)	0.30
Calcification or atheroma	16 (38)	62 (29)	0.22
Thrombus	2 (5)	6 (3)	0.62
Largest diameter of aneurysm, mean ± SD mm	60.0 ± 10	50.0 ± 10	0.04
Rate of change in diameter of aneurysm, mean ± SD mm/year‡	2.9 ± 5.2	−1.6 ± 13.2	0.22
Imaging abnormalities in any unrepaired vasculature (aorta or main branches)			
Other noncontiguous aortic aneurysms	15 (35)	33 (15)	0.04
Wall thickening	5 (12)	1 (0.5)	<0.01
Stenosis or occlusion	11 (26)	29 (13)	0.04
Calcification or atheroma	22 (51)	92 (42)	0.24

* Except where indicated otherwise, values are the number (%).
† Statistical tests were not performed since no hypothesis was tested (i.e., differences between groups are by design).
‡ Data were available for 17 patients in the aortitis group and 90 patients in the control group.

Table 2. Characteristics associated with aortitis in multivariate analysis*

	Unadjusted OR (95% CI)	*P*	Adjusted OR (95% CI)†	*P*
Age at time of surgery	1.06 (1.03–1.10)	<0.01	1.08 (1.03–1.13)	<0.01
Female sex	4.11 (2.08–8.12)	<0.01	2.36 (1.01–5.51)	0.04
Absence of CAD	2.92 (1.32–6.45)	<0.01	6.92 (2.14–22.34)	0.04
Hypertension	3.13 (1.17–8.35)	0.02	2.98 (0.94–9.48)	0.06
Diameter of aneurysm, per mm	1.60 (1.03–2.48)	0.03	1.74 (1.02–2.98)	0.04
Any aortic or arterial wall thickening on imaging	24.94 (2.91–213.94)	<0.01	56.93 (4.31–752.33)	<0.01

* OR = odds ratio; 95% CI = 95% confidence interval; CAD = coronary artery disease.
†Adjusted for all other variables.

Histopathologic features. Among patients with aortitis, 35% had granulomatous inflammation and 86% had giant cells (Table 1). A greater percentage of patients in the aortitis group had adventitial inflammation, but adventitial inflammation was also identified in some patients in the control group (70% versus 9%). Calcific atherosclerosis was present on pathologic examination in 51% of the patients in the aortitis group and 43% of the patients in the control group.

Multivariable analysis, adjusted for all variables, revealed that aortitis was independently associated with an older age at the time of surgery, female sex, absence of CAD, larger diameter of aneurysm, and presence of arterial wall thickening on imaging with statistical significance (Table 2).

DISCUSSION

Aortitis can be difficult to distinguish from noninflammatory aortic aneurysms and is often incidentally discovered during histopathologic review of resected aneurysms (5,9). This study identified novel risk factors associated with a diagnosis of noninfectious aortitis after open thoracic aortic aneurysm repair.

A major finding was the significantly lower prevalence of CAD among patients with isolated aortitis. To our knowledge, this study is the first to evaluate the relationship between CAD and isolated aortitis. This relationship is further supported by a prior study of vascular calcification in patients with vasculitis which showed a lower prevalence of coronary artery calcification in patients with vasculitis compared to those with atherosclerosis or hyperlipidemia (14). This difference likely reflects the underlying pathophysiologic process leading to aneurysm formation. In patients with noninflammatory aneurysms, the leading cause of the aneurysm is atherosclerosis, which predominantly affects the coronary arteries (14). On the other hand, the coronary arteries are relatively spared in vascular causes of inflammation including aortitis. The absence of CAD in a patient with a thoracic aortic aneurysm can alert a clinician to consider an evaluation for vasculitis, including analysis of markers of inflammation and further inquiry into rheumatologic symptoms.

Radiologic imaging including CT and MRI may aid in the identification of vasculitis, especially if the images have characteristic findings of aortitis. Imaging may typically show irregular thickening of the aortic wall and periaortic inflammation, a tapering luminal narrowing, and involvement of the ascending aorta and aortic arch, but milder forms of inflammation or wall edema may not be evident (1,10,15). A major strength of this study was the availability of detailed radiologic data, including for a subgroup of patients who underwent serial imaging. This study identified aneurysms mostly located in the ascending aorta, which is similar to the findings of previous studies (5,9). The diameter of the aneurysm in the aortitis group was significantly larger than that in the control group, suggesting either that the aneurysms of patients with aortitis were being diagnosed later than those of patients in the control group or that aortitis-induced aneurysms have a faster rate of growth. To investigate this further, serial imaging was evaluated prior to surgical intervention and a numerically faster rate of aneurysm growth in patients with aortitis (although not statistically significant likely due to small sample size) was identified, despite similarities in frequency of imaging and time from first imaging to surgery. This suggests that a large and fast-growing aneurysm in the ascending aorta could raise suspicion for an underlying vasculitis.

This study also demonstrated a significantly higher rate of reported wall thickening in other vasculature outside of the repaired aneurysm and a higher rate of noncontiguous aortic aneurysms in patients with aortitis versus controls (35% versus 15%; $P = 0.04$). After histopathologic identification of aortitis, the use of imaging to detect other vascular abnormalities and close postoperative surveillance should be considered. Of note, although the presence of wall thickening was exclusively found in the aortitis group, the prevalence was surprisingly low (7%).

The prevalence of incidentally diagnosed aortitis in this cohort was 4% among aortic surgical specimens. This result is similar to previous case series of aortic surgical pathology that have shown a range of noninfectious isolated aortitis (2–12%) (5). Compared to the control group, patients with aortitis in this study were mostly women with a mean age of 70 years, which is also similar to other North American studies. However, a study by Wang et al identified a cohort of isolated aortitis among Asians with a younger population (mean age 46 years) and a higher percentage of males compared to the North American studies (50%) (11). These differences likely reflect geographic variation in the prevalence of GCA (seen

at a higher rate in northern Europeans and older women) and in the prevalence of TAK (more common in younger Asians).

The presence of granulomatous inflammation and giant cells on pathologic examination were diagnostic features of aortitis and therefore seen solely in the aortitis group. Adventitial inflammation is a characteristic of aortitis, although it is not specific for the diagnosis, and it has been seen in vascular injury including cardiovascular disease (14). This is likely the reason for the overlap of adventitial inflammation seen between the aortitis group and control group (70% versus 9%, respectively).

This study has several strengths. By identifying patients through a pathology database, we were able to accurately capture the population of interest. Access to granular data, including progress notes, radiology reports, and laboratory findings, allowed for an in-depth investigation. Furthermore, to our knowledge, this is the first study to track serial radiographic imaging prior to surgical intervention and identify progressive aneurysm changes.

There are a few limitations to consider. Due to the retrospective nature of data collection, the images and radiology interpretations were not standardized. The images were read at a variety of radiology centers and by radiologists at different institutions, and the exact measurements of wall thickening were not standardized or routinely mentioned in the interpretations. Type and frequency of imaging was not standardized among patients, which could lead to ascertainment bias. However, we expect such misclassification bias to be nondifferential and therefore more likely to bias to the null. Therefore, the differences identified in this study may underestimate the true effect size.

Findings from this study may not be generalizable to other populations, since the University of Pennsylvania Health System receives a large number of referrals for thoracic aortic aneurysm repairs. Furthermore, due to the increase in endovascular aneurysm repairs, for which tissue pathology findings are not obtained, abdominal aortic aneurysms were not included in this study, which may have biased our findings.

There are several potential implications of these findings. First, the patients were not evaluated by a rheumatologist prior to surgery and may have unreported manifestations of an undiagnosed condition associated with aortitis (e.g., GCA). Identifying patients who are at a higher risk of aortitis may lead to earlier referral to a rheumatologist who can evaluate the patient for a systemic rheumatic disease. Additionally, perioperative use of glucocorticoids has been found to improve outcomes of vascular surgery in patients with active vasculitis (3). In patients with high risk factors for aortitis, a multidisciplinary approach integrating rheumatology may optimize peri- and postoperative treatment. Future studies are needed to determine the natural history of patients with isolated aortitis and the incidence of new aneurysms or other arterial abnormalities. As such, the appropriate postoperative management of isolated aortitis remains unclear.

In summary, this study revealed that among patients who undergo open surgical repair of an ascending thoracic aortic aneurysm, elderly women with no prior history of CAD and evidence of other radiographic abnormalities, including wall thickening and other identified aneurysms, are more likely to have histologic evidence of aortitis. Patients with a combination of these risk factors may benefit from further rheumatologic evaluation and assistance with perioperative management.

AUTHOR CONTRIBUTIONS

All authors were involved in drafting the article or revising it critically for important intellectual content, and all authors approved the final version to be published. Dr. Quimson had full access to all of the data in the study and takes responsibility for the integrity of the data and the accuracy of the data analysis.

Study conception and design. Quimson, Rhee.
Acquisition of data. Quimson, Mayer, Capponi, Rea.
Analysis and interpretation of data. Quimson, Rhee.

REFERENCES

1. Gornik HL, Creager MA. Aortitis. Circulation 2008;117:3039–51.
2. Hiratzka LF, Bakris GL, Beckman JA, Bersin RM, Carr VF, Casey DE Jr, et al. 2010 ACCF/AHA/AATS/ACR/ASA/SCA/SCAI/SIR/STS/SVM guidelines for the diagnosis and management of patients with thoracic aortic disease: executive summary—a report of the American College of Cardiology Foundation/American Heart Association Task Force on Practice Guidelines, American Association for Thoracic Surgery, American College of Radiology, American Stroke Association, Society of Cardiovascular Anesthesiologists, Society for Cardiovascular Angiography and Interventions, Society of Interventional Radiology, Society of Thoracic Surgeons, and Society for Vascular Medicine. Catheter Cardiovasc Interv 2010;76:E43–86.
3. Fields CE, Bower TC, Cooper LT, Hoskin T, Noel AA, Panneton JM, et al. Takayasu's arteritis: operative results and influence of disease activity. J Vasc Surg 2006;43:64–71.
4. Ladich E, Yahagi K, Romero ME, Virmani R. Vascular diseases: aortitis, aortic aneurysms, and vascular calcification. Cardiovasc Pathol 2016;25:432–41.
5. Rojo-Leyva F, Ratliff NB, Cosgrove DM III, Hoffman GS. Study of 52 patients with idiopathic aortitis from a cohort of 1,204 surgical cases. Arthritis Rheum 2000;43:901–7.
6. Homme JL, Aubry MC, Edwards WD, Bagniewski SM, Shane Pankratz V, Kral CA, et al. Surgical pathology of the ascending aorta: a clinicopathologic study of 513 cases. Am J Surg Pathol 2006;30:1159–68.
7. Schmidt WA. Imaging in vasculitis. Best Pract Res Clin Rheumatol 2013;27:107–18.
8. Svensson LG, Arafat A, Roselli EE, Idrees J, Clifford A, Tan C, et al. Inflammatory disease of the aorta: patterns and classification of giant cell aortitis, Takayasu arteritis, and nonsyndromic aortitis. J Thorac Cardiovasc Surg 2015;149 Suppl:S170–5.
9. Miller DV, Isotalo PA, Weyand CM, Edwards WD, Aubry MC, Tazelaar HD. Surgical pathology of noninfectious ascending aortitis: a study of 45 cases with emphasis on an isolated variant. Am J Surg Pathol 2006;30:1150–8.
10. Liang KP, Chowdhary VR, Michet CJ, Miller DV, Sundt TM, Connolly HM, et al. Noninfectious ascending aortitis: a case series of 64 patients. J Rheumatol 2009;36:2290–7.
11. Wang H, Li L, Wang L, Chang Q, Pu J. Comparison of clinical and pathological characteristics of isolated aortitis and Takayasu arteritis with ascending aorta involvement. J Clin Pathol 2012;65:362–6.
12. Pacini D, Leone O, Turci S, Camurri N, Giunchi F, Martinelli GN, et al. Incidence, etiology, histologic findings, and course of

thoracic inflammatory aortopathies. Ann Thorac Surg 2008;86: 1518–23.
13. Stone JR, Bruneval P, Angelini A, Bartoloni G, Basso C, Batoroeva L, et al. Consensus statement on surgical pathology of the aorta from the Society for Cardiovascular Pathology and the Association for European Cardiovascular Pathology: I. Inflammatory diseases [review]. Cardiovasc Pathol 2015;24:267–78.
14. Banerjee S, Bagheri M, Sandfort V, Ahlman MA, Malayeri AA, Bluemke DA, et al. Vascular calcification in patients with large-vessel vasculitis compared to patients with hyperlipidemia. Semin Arthritis Rheum 2019;48:1068–73.
15. Katabathina VS, Restrepo CS. Infectious and noninfectious aortitis: cross-sectional imaging findings. Semin Ultrasound CT MR 2012;33:207–21.

DOI 10.1002/art.41279

Clinical Images: Acute bilateral pseudogout of the temporomandibular joint

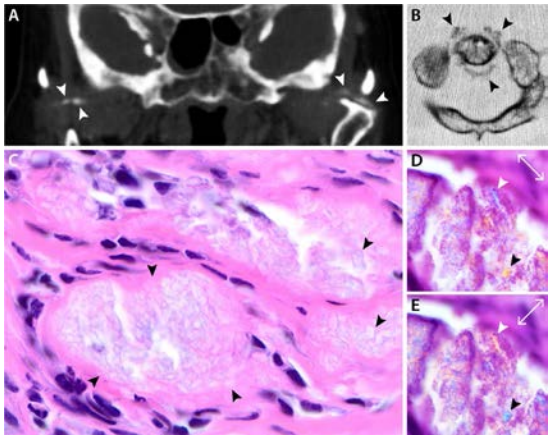

The patient, an 84-year-old woman, was transferred to a tertiary care center with a 3-day history of fever, trismus, acute bilateral temporomandibular joint (TMJ) pain, and neck pain following a dental procedure. She had been treated empirically with broad-spectrum antibiotics, and hypotension had developed, requiring vasopressors. The C-reactive protein level and erythrocyte sedimentation rate were elevated (>300 mg/liter and 111 mm/hour, respectively). Given fever and "temporal pain out of proportion" to her exam, surgical incision of the TMJs and temporal artery biopsy had been performed prior to transfer to exclude septic arthritis and giant cell arteritis (GCA), respectively. Purulent fluid and creamy, "curd-like" material were drained from the right and left TMJs, respectively. Gram, fungal, acid-fast stains, and cultures were negative. Computed tomography (coronal view) showed radiodense material in both TMJs consistent with calcium deposition (**arrowheads** in **A**) and crown-shaped radiodense deposits surrounding the odontoid process (**arrowheads** in **B**). Hematoxylin and eosin staining of bilateral TMJ soft tissue and TMJ synovial biopsy samples showed marked acute inflammation and foreign body reaction to positively birefringent rhomboid crystals (**arrowheads** in **C)**. The temporal arteries were normal. Positively birefringent rhomboid-shaped crystals were also seen by polarized microscopy (**arrowheads** in **D** and **E**; **arrows** in **D** and **E** indicate axis of slow vibration using a first-order red compensator). Acute calcium pyrophosphate dihydrate deposition disease (CPPD) was diagnosed. The disease course was complicated by deep vein thrombosis, right ventricular dysfunction, and shock due to presumed massive pulmonary embolism, requiring rescue thrombolysis. Acute CPPD, "pseudogout," and "calcium gout" all refer to the same form of acute crystal-induced arthritis, commonly presenting with fever and marked systemic inflammation (1). Depending on the site of involvement, pseudogout can mimic a plethora of autoimmune rheumatic, infectious, and neoplastic diseases. Symmetric TMJ arthritis is a rare complication of CPPD (2,3). In this patient, fulminant bilateral TMJ arthritis coinciding with acute atlantoaxial arthritis (crowned dens syndrome) was the first presentation of CPPD. Pseudogout should be considered in the differential diagnosis for diseases as diverse as GCA, septic arthritis, and meningitis. Familiarity with this rare manifestation of CPPD facilitates early diagnosis, initiation of appropriate therapy, and avoidance of unnecessary invasive procedures.

Supported by the NIH (National Institute of Arthritis and Musculoskeletal and Skin Diseases award T32-AR-04-8522).

1. Kohn NN, Hughes RE, McCarty DJ Jr, Faires JS. The significance of calcium phosphate crystals in the synovial fluid of arthritic patients: the "pseudogout syndrome". II. Identification of crystals. Ann Intern Med 1962;56:738–45.
2. Chuong R, Piper MA. Bilateral pseudogout of the temporomandibular joint: report of case and review of literature. J Oral Maxillofac Surg 1995;53:691–4.
3. Greaves S, Fordyce A. Bilateral temporomandibular joint pseudogout. Br Dent J 2002;192:25–7.

Maximilian F. Konig, MD
Massachusetts General Hospital
Boston, MA
Garrey T. Faller, MD
Good Samaritan Medical Center
Brockton, MA

American College of Rheumatology
Empowering Rheumatology Professionals

Arthritis & Rheumatology
Vol. 72, No. 7, July 2020, pp 1160–1169
DOI 10.1002/art.41243

Profibrotic Activation of Human Macrophages in Systemic Sclerosis

Rajan Bhandari,[1] Michael S. Ball,[1] Viktor Martyanov,[2] Dillon Popovich,[2] Evelien Schaafsma,[1] Saemi Han,[1] Mohamed ElTanbouly,[1] Nicole M. Orzechowski,[3] Mary Carns,[4] Esperanza Arroyo,[4] Kathleen Aren,[4] Monique Hinchcliff,[4] Michael L. Whitfield,[5] and Patricia A. Pioli[1]

Objective. Genome-wide gene expression studies implicate macrophages as mediators of fibrosis in systemic sclerosis (SSc), but little is known about how these cells contribute to fibrotic activation in SSc. We undertook this study to characterize the activation profile of SSc monocyte-derived macrophages and assessed their interaction with SSc fibroblasts.

Methods. Plasma and peripheral blood mononuclear cells (PBMCs) were obtained from whole blood from SSc patients (n = 24) and age- and sex-matched healthy controls (n = 12). Monocytes were cultured with autologous or allogeneic plasma to differentiate cells into macrophages. For reciprocal activation studies, macrophages were cocultured with fibroblasts using Transwell plates.

Results. The gene expression signature associated with blood-derived human SSc macrophages was enriched in SSc skin in an independent cohort and correlated with skin fibrosis. SSc macrophages expressed surface markers associated with activation and released CCL2, interleukin-6, and transforming growth factor β under basal conditions (n = 8) ($P < 0.05$). Differentiation of healthy donor monocytes in plasma from SSc patients conferred the immunophenotype of SSc macrophages (n = 13) ($P < 0.05$). Transwell experiments demonstrated that coculture of SSc macrophages with SSc fibroblasts induced fibroblast activation (n = 3) ($P < 0.05$).

Conclusion. These data demonstrate that the activation profile of SSc macrophages is profibrotic. SSc macrophages are activated under basal conditions and release mediators and express surface markers associated with both alternative and inflammatory macrophage activation. These findings also suggest that activation of SSc macrophages arises from soluble factors in local microenvironments. These studies implicate macrophages as likely drivers of fibrosis in SSc and suggest that therapeutic targeting of these cells may be beneficial in ameliorating disease in SSc patients.

INTRODUCTION

Mounting evidence implicates a role for macrophages in the pathogenesis and progression of systemic sclerosis (SSc), an autoimmune disease of unknown etiology that is characterized by vascular injury, fibrosis, and inflammation. Activated macrophages have been implicated as regulators of fibrosis in patients with SSc (1,2), and cytokine and gene expression analyses suggest that activated and differentiating monocytes modulate inflammation in patients with limited SSc and pulmonary arterial hypertension (3). We have previously shown that several genes associated with monocyte/macrophage recruitment and differentiation are

Mr. Bhandari and Dr. Ball's work was supported by the John Osborn Polak Endowment. Drs. Hinchcliff, Whitfield, and Pioli's work was supported by the NIH (Small Business Innovative Research grants). Dr. Whitfield's work was supported by the Congressionally Directed Medical Research Program (grant W81XWH-14-1-0224), the Scleroderma Research Foundation, and the Dr. Ralph and Marian Falk Medical Research Trust. Dr. Pioli's work was supported by the NIH (grants R56-AR-0639835 and R03-AR-068097 from the National Institute of Arthritis and Musculoskeletal and Skin Diseases) and by funding from the Scleroderma Foundation.

[1]Rajan Bhandari, BA, Michael S. Ball, PhD, Evelien Schaafsma, MS, Saemi Han, BS, Mohamed ElTanbouly, BS, Patricia A. Pioli, PhD: Geisel School of Medicine at Dartmouth, Lebanon, New Hampshire; [2]Viktor Martyanov, PhD, Dillon Popovich, BS: Geisel School of Medicine at Dartmouth, Hanover, New Hampshire; [3]Nicole M. Orzechowski, DO: Dartmouth-Hitchcock Medical Center, Lebanon, New Hampshire; [4]Mary Carns, MS, Esperanza Arroyo, BS, Kathleen Aren, MPH, Monique Hinchcliff, MD: Northwestern University Feinberg School of Medicine, Chicago, Illinois; [5]Michael L. Whitfield, PhD: Geisel School of Medicine at Dartmouth, Hanover and Geisel School of Medicine at Dartmouth, Lebanon, New Hampshire.

Mr. Bhandari and Dr. Ball contributed equally to this work.

Dr. Whitfield has received consulting fees, speaking fees, and/or honoraria from Celdara Medical, LLC (less than $10,000). No other disclosures relevant to this article were reported.

Address correspondence to Patricia A. Pioli, PhD, Dartmouth-Hitchcock Medical Center, One Medical Center Drive, 644 East Borwell, Lebanon, NH 03756. E-mail: Pioli@Dartmouth.edu.

Submitted for publication December 18, 2018; accepted in revised form February 25, 2020.

overexpressed in SSc compared with healthy controls (4), and gene expression profiling indicates that macrophages constitute the dominant inflammatory signature in SSc skin (5). Integrative analysis of 10 independent gene expression data sets containing samples from patients with SSc and related comorbidities has identified a common immune–fibrotic axis, consisting of activated macrophages and fibroblasts, across SSc tissues (6). Thus, activated macrophages may play a significant role in mediating fibrosis and in maintaining an inflammatory environment in SSc.

In support of this, recent findings demonstrate that macrophages regulate renal and pulmonary fibrosis through modulation of fibroblast activation. Depletion of alternatively activated macrophages significantly attenuates fibrosis and is associated with decreased production of interleukin-6 (IL-6), transforming growth factor β (TGFβ), and type IV collagen in a murine model of chronic kidney disease (7). Additionally, elimination of circulating monocytes through clodronate depletion or the use of *CCR*$^{-/-}$ mice reduces the severity of fibrosis, which is consistent with a role for monocytic cells as mediators of fibrosis (8–10). More recently, genetic deletion of monocyte-derived macrophages in a mouse model of bleomycin-induced lung injury was shown to significantly attenuate fibrosis (11), further implicating these cells as potential regulators of disease pathogenesis.

Because macrophages are activated by local microenvironmental factors, in vivo macrophage polarization spans a broad spectrum of states (12). In vitro cytokine-mediated differentiation of monocytes has led to the identification of 2 extreme ends of the macrophage activation spectrum, M1 and M2. M1-activated cells produce proinflammatory cytokines and mediate resistance to pathogens, while M2 macrophages secrete antiinflammatory mediators and modulate tissue remodeling. However, activating stimuli are diverse and include cytokines and chemokines such as IL-4, IL-13, tumor necrosis factor (TNF), IL-6, TGFβ, and CCL2, which are elevated in SSc plasma and have been implicated as potential mediators of disease in SSc (3,13–16). Therefore, SSc macrophage activation may be shaped by the interplay of many factors, resulting in an immunophenotype that supports disease development and progression.

In the present study, we characterize the activation profile of human SSc macrophages as profibrotic. We demonstrate that the gene expression signature of blood-derived, plasma-differentiated SSc macrophages is significantly enriched in SSc skin in an independent cohort. For the first time, we report that SSc macrophages express higher levels of TGFβ, CCL2, and IL-6, and have elevated surface marker expression of CD163, CD206, and HLA–DR compared with age- and sex-matched controls under basal conditions. Gene expression profiling demonstrates increased expression of fibrotic signaling pathways (extracellular matrix, matrisome, collagen) in SSc macrophages compared with controls. Significantly, healthy control macrophages differentiated in plasma from SSc patients recapitulate the immunophenotype of SSc macrophages, suggesting that soluble mediators in SSc plasma regulate macrophage activation. Finally, we show that coculture of SSc plasma–differentiated macrophages with SSc fibroblasts induces their activation and expression of fibrotic mediators, including α-smooth muscle actin (α-SMA), from SSc fibroblasts. Collectively, these studies implicate macrophages as drivers of fibrosis in SSc and suggest that therapeutic targeting of these cells may be beneficial in ameliorating disease in SSc patients.

MATERIALS AND METHODS

Patients and cells. Plasma and peripheral blood mononuclear cells (PBMCs) were obtained from whole blood from 24 SSc patients or 12 age- and sex-matched healthy controls, following written informed consent. Ethics approval was provided for this study by the Northwestern University Institutional Review Board and the Geisel School of Medicine Committee for the Protection of Human Subjects (protocol nos. STU00080328 and 24902, respectively). Dermal fibroblasts were kindly provided by Dr. Maria Trojanowska. Skin biopsy samples were taken from affected areas of the dorsal forearms of treatment-naive patients with diffuse cutaneous SSc (dcSSc). Control samples were taken from the forearms of healthy donors matched with SSc patients for age, sex, and race. Fibroblast lines were used at passages 3–7.

Patients with SSc fulfilled the American College of Rheumatology/European League Against Rheumatism revised classification criteria (17). All patients were female and were diagnosed as having dcSSc or limited cutaneous SSc (lcSSc). Patient and healthy control characteristics and patient clinical data are delineated in Table 1.

Table 1. Demographic and clinical characteristics of the healthy controls and SSc patients*

	Healthy controls (n = 12)	SSc patients (n = 24)
Age, mean ± SD years	52 ± 9	53 ± 11
Women	11 (92)	24 (100)
White race	12 (100)	24 (100)
SSc disease duration, mean ± SD months	–	35 ± 25
dcSSc	–	12 (50)
lcSSc	–	12 (50)
MRSS, mean ± SD	–	7 ± 5
Autoantibodies	–	20 (83)
Anticentromere	–	5 (21)
Anti–RNA polymerase III	–	7 (29)
Anti–topoisomerase I (anti–Scl-70)	–	8 (33)
Current therapies		
None	–	12 (50)
Mycophenolate mofetil	–	9 (38)
Hydroxychloroquine	–	3 (13)

* Except where indicated otherwise, values are the number (%) of subjects. SSc = systemic sclerosis; dcSSc = diffuse cutaneous SSc; lcSSc = limited cutaneous SSc; MRSS = modified Rodnan skin thickness score.

Isolation of human peripheral blood monocytes and cell culture. Mononuclear cells were separated on Ficoll-Paque Premium (density 1.077; GE Healthcare) and enriched for CD14+ monocytes by magnetic bead selection (Miltenyi Biotec). Monocyte purity was assessed to be ≥95% using cytospin, Wright-Giemsa staining, and flow cytometric analysis of CD14 expression. To generate patient- or healthy donor–derived macrophages, CD14+ monocytes were cultured in complete HEPES-buffered RPMI 1640 (2.05 m*M* L-glutamine) supplemented with 10% autologous or allogeneic plasma (as indicated), 10 ng/ml macrophage colony-stimulating factor (M-CSF), 0.25*M* HEPES, and 12 μg/ml gentamicin for 7 days. For activation studies, cells were stimulated with or without 10 ng/ml lipopolysaccharide (LPS) (lot 33-505-LPS; Invitrogen) for 24 hours following 6 days of plasma differentiation. Fibroblasts were cultured in HEPES-buffered Dulbecco's modified Eagle's medium (DMEM)/high glucose media supplemented with 10% healthy or SSc plasma.

RNA extraction, complementary DNA synthesis, and quantitative real-time polymerase chain reaction. Total RNA was obtained using a miRNeasy Mini Kit or AllPrep RNA/Protein kit according to instructions from the manufacturer (Qiagen). Complementary DNA (cDNA) was synthesized from 100 ng total RNA and random hexamers using a SuperScript III First-Strand Synthesis System (Life Technologies). Quantitative real-time polymerase chain reaction (PCR) was performed using TaqMan Probe single tube assays (Life Technologies) for *TGFB1*, *TGFBRI*, *TGFBRII*, *IL6*, *IL10*, *CCL2*, *CCL18*, *TNF*, *IRF4*, *IRF5*, and *VEGF* genes. A StepOnePlus Real-Time PCR System (Applied Biosystems) was used for amplification and detection. Threshold cycle number was determined using Opticon software. Messenger RNA (mRNA) levels were normalized to β-actin, using the equation $2^{-(Et-Rt)}$, where Rt is the mean cycle threshold for the control gene and Et is the mean threshold for the experimental gene. Thermal cycling conditions consisted of an initial incubation at 50°C for 2 minutes and 95°C for 10 minutes, followed by 40 cycles of 95°C for 15 seconds and 60°C for 1 minute. Product accumulation was measured during the extension phase, and all samples were run in triplicate.

Multiplex cytokine assay and enzyme-linked immunosorbent assay. Macrophages were plated at 1.5×10^6 cells/well in 12-well tissue culture dishes in complete RPMI supplemented with autologous plasma for 7 days. As noted, cells were washed with fresh media in the absence of plasma overnight, prior to the collection of supernatants. In some experiments, macrophages were stimulated with or without 10 ng/ml LPS for 24 hours prior to supernatant collection and RNA isolation. Cell-free culture supernatants were aliquoted and stored at –80°C until further use. A Milliplex suspension array system using fluorescent-dyed Luminex microspheres (beads) was used (EMD Millipore) to measure cytokine secretion. Standards were prepared in the same fresh medium used to culture experimental samples and were assayed in triplicate. Assays were performed in 96-well filtration plates at room temperature according to the manufacturer's protocol. The fluorescence intensity for each bead was measured using a Bio-Plex array reader. Bio-Plex manager software with 5-parameter curve fitting was used for data analysis. The level of detection of each analyte was 7.8 pg/ml. Macrophage cell supernatants were also analyzed by enzyme-linked immunosorbent assay (ELISA) (R&D Systems) for secretion of IL-6 and CCL-2. A Legend Max Free Active TGFβ1 ELISA kit (BioLegend) was used to quantify TGFβ levels. Cells were lysed and total and phosphorylated STAT3 were quantified using PathScan Total and Phospho STAT3 sandwich ELISA kits (Cell Signaling Technologies).

Flow cytometry. All fluorophore-conjugated antibodies were obtained from BioLegend (18). Cell staining was performed for 1 hour at 4°C, with 2 mg/ml Globulins Cohn fraction II, III (Sigma) to reduce antibody binding to Fc receptors. In all conditions, only adherent cells were stained following cell culture, and doublets were excluded by forward scatter A (FSC-A) versus FSC-H gating. Cells were analyzed using an 8-color MACSQuant 10 (Miltenyi Biotec) with 3 laser sources (405 nm, 488 nm, 635 nm) and FlowLogic 501.2A software (Inivai Technologies).

Differential gene expression and pathway enrichment. DNA microarrays were performed and processed as previously described (19). The expression data sets had missing values imputed on Gene Pattern (PMID 16642009); the probe sets were collapsed to gene sets using an Agilent 4 × 44K chipset and were median-centered by gene. Differentially expressed genes (DEGs) were identified using Significance Analysis of Microarrays (PMID 11309499), and DEGs with a false discovery rate (FDR) of <10% were treated as significant. Pathway enrichment analysis was performed using a GenePattern implementation of Gene Set Enrichment Analysis (GSEA) (PMID 12808457 and 16199517), canonical pathways from Molecular Signatures Database (PMID 21546393), and Hallmark Pathway Database (PMID: 26771021). Pathways with an FDR of <5% were treated as significant.

Coculture experiments. Healthy or SSc dermal fibroblasts (2.5×10^5 cells/well) alone, healthy monocytes (1.2×10^6 cells/well) alone, or cocultures were seeded in 6-well plates for 5 days. For Transwell experiments, healthy control monocytes were plated in the lower chambers of 6-well plates in the presence of RPMI/control or SSc plasma supplemented with 10 ng/ml M-CSF. Healthy or SSc dermal fibroblasts were plated in the upper chambers of Transwell plates in DMEM/control or SSc plasma. Cocultures were maintained for 5 days. Fibroblasts were plated at a lower initial concentration to account for cell division; fibroblasts were confluent at conclusion of the experiment and cell counts averaged 2.5×10^6 cells/well. Cell supernatants were collected,

and RNA was isolated from macrophages and fibroblasts for analysis by microarray.

Statistical analysis. Figures are representative of ≥3 independent experiments. At least 3 technical replicates were included in each assay, unless otherwise noted. Results are shown as the mean ± SEM and were analyzed by one-way analysis of variance. *P* values less than 0.05 were considered significant.

RESULTS

Gene expression signature for blood-derived SSc macrophages is significantly enriched in SSc skin. Recent studies demonstrate that a significant macrophage population in human skin is derived from monocyte precursors (20,21). Because macrophage activation is regulated by the interplay of cytokines, chemokines, growth factors, and other mediators in the local microenvironment, we reasoned that in vitro culture of SSc peripheral blood–derived monocytes with autologous plasma would result in development of a macrophage activation profile that mimics that found in vivo in skin. To test this hypothesis, monocytes from 4 SSc patients (2 lcSSc and 2 dcSSc) or 4 age- and sex-matched healthy control donors were differentiated in autologous plasma for 7 days, followed by isolation of RNA and analysis by DNA microarray. We identified 491 DEGs when comparing SSc and control macrophages. Of these, 371 DEGs had increased expression and 120 DEGs had decreased expression in SSc macrophages relative to control samples (Figure 1A). SSc macrophages demonstrated enrichment in pathways related to extracellular matrix deposition and tissue structure (e.g., extracellular matrix organization, core matrisome, and collagen formation), immune activation (allograft rejection, graft-versus-host disease, and antigen processing and presentation), and chemokine signaling (peptide ligand binding receptors and chemokine receptors). A full list of the pathways enriched in SSc and healthy control macrophages can be found in Supplementary Table 1 (available on the *Arthritis & Rheumatology* web site at http://onlinelibrary.wiley.com/doi/10.1002/art.41243/abstract).

We obtained a library of gene expression in SSc and control skin biopsies (22), which included 359 skin biopsy specimens. From these, we selected 157 baseline skin biopsy samples, which included 88 dcSSc, 30 lcSSc and 39 healthy control samples. Of the 371 genes with increased expression in SSc macrophages, 277 genes were present in the skin biopsy data set. We performed GSEA between SSc patients and healthy controls using the 277 genes with increased expression in SSc blood–derived macrophages and found that this gene signature was significantly enriched in SSc skin biopsy samples compared with healthy control skin biopsy samples (GSEA FDR 6.5%, significant at FDR <25% cutoff for phenotype permutation). Fifty-five of the 277 genes formed the core enrichment set in the SSc samples (i.e., they were the top contributors to the significant

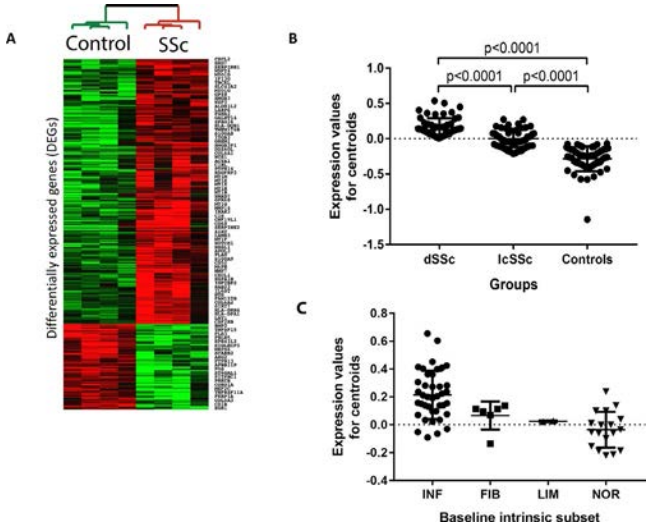

Figure 1. Significantly enriched gene expression signature of blood-derived systemic sclerosis (SSc) macrophages in SSc skin. Monocytes were isolated from peripheral blood from SSc patients or age- and sex-matched healthy controls and were differentiated in autologous plasma for 7 days. **A**, RNA was extracted and analyzed by DNA microarray to generate the gene expression signature enriched in SSc macrophages (371 genes; false discovery rate <10%) that was used to interrogate an independent cohort. **B** and **C**, The gene expression signature of SSc blood–derived macrophages was found to be significantly enriched in the skin of patients with diffuse cutaneous SSc (dSSc) and limited cutaneous SSc (lcSSc) compared with healthy controls (**B**), and in the skin of patients whose disease was in the inflammatory molecular subset (INF) compared with the skin of patients with fibroproliferative (FIB), limited (LIM), or normal-like (NOR) SSc (**C**). Each symbol represents an individual subject; bars show the mean ± SEM.

enrichment of SSc blood macrophage signature in SSc skin), and they included *CD68*, *COL6A1*, *CXCL1*, *CXCL2*, *HLA–DRB4*, *IL6ST*, *PLAU*, *S100A8*, *SERPINE2*, *SERPINH1*, and *WDFY4*. We determined the average expression for these genes in dcSSc, lcSSc, and healthy samples from a previous study by our group (22) and found that the SSc blood–derived macrophage signature core enrichment gene set was expressed most highly in dcSSc skin biopsy samples, at intermediate levels in lcSSc skin biopsy samples, and lowest in healthy control skin biopsy samples (Figure 1B). This demonstrates significant enrichment of the SSc blood–derived macrophage signature in SSc skin from patients with dcSSc and lcSSc compared with healthy control skin. Across all SSc skin samples, baseline modified Rodnan skin thickness score (MRSS) (23), a measure of skin fibrosis, displayed a significant positive correlation with the expression of the SSc blood macrophage gene signature (Pearson's r = 0.2932, *P* = 0.0169).

Although SSc is clinically heterogeneous, prior work has shown that SSc patients can be classified into 4 distinct molecular subsets based on gene expression signatures: inflammatory, fibroproliferative, limited, and normal-like (24). To determine the

enrichment of the blood-derived macrophage activation signature among the molecular sets, we identified the subset assignments of the patients (Figure 1B). As demonstrated in Figure 1C, the blood-derived macrophage activation signature was most highly enriched in patients in the inflammatory subset, which is consistent with a previously reported role for strong immune activation in this subset (4,22).

Immunophenotypic characterization of human SSc macrophages. After validating the gene expression signature of blood-derived, plasma-differentiated macrophages in SSc skin, studies were undertaken to analyze the immunophenotypic characteristics of plasma-differentiated macrophages. As demonstrated in Figure 2A, levels of mRNA for TGFβ, IL-6, and CCL2 were elevated under basal conditions in SSc macrophages compared with healthy controls. Intriguingly, LPS failed to induce expression of these cytokines in SSc cells, in contrast to observations in healthy controls. One potential explanation for this is endotoxin tolerance—i.e., prior exposure of SSc cells to microbial products resulted in hyporesponsiveness to subsequent challenge with endotoxin (25). However, although SSc macrophages secreted low levels of TNF under basal conditions, TNF production was LPS-inducible to levels commensurate with those released by healthy control cells. Moreover, LPS levels assayed in SSc and healthy plasma were <0.01 ng/ml (data not shown). These findings demonstrate that TGFβ, IL-6, and CCL2 are elevated in SSc macrophages and cannot be further induced by LPS under basal conditions.

To determine if increased levels of mRNA for TGFβ, IL-6, and CCL2 reflected increased protein expression, cell supernatants were collected from cultures (Figure 2A) and assayed by multiplex and ELISA. As shown in Figure 2B, SSc macrophages secreted increased levels of IL-6 and CCL2 in the absence of exogenous stimulation, in accordance with mRNA. However, secretion of TGFβ1 by SSc macrophages was not significantly altered compared with control cultures. Because macrophage production of TGFβ in models of pulmonary fibrosis requires spatial proximity to fibroblasts (26), supernatants from cocultures of SSc macrophages and fibroblasts were analyzed by ELISA for release of bioactive TGFβ.

As seen in Figure 2C, bioactive secreted TGFβ protein levels in SSc macrophage/fibroblast cocultures were elevated compared

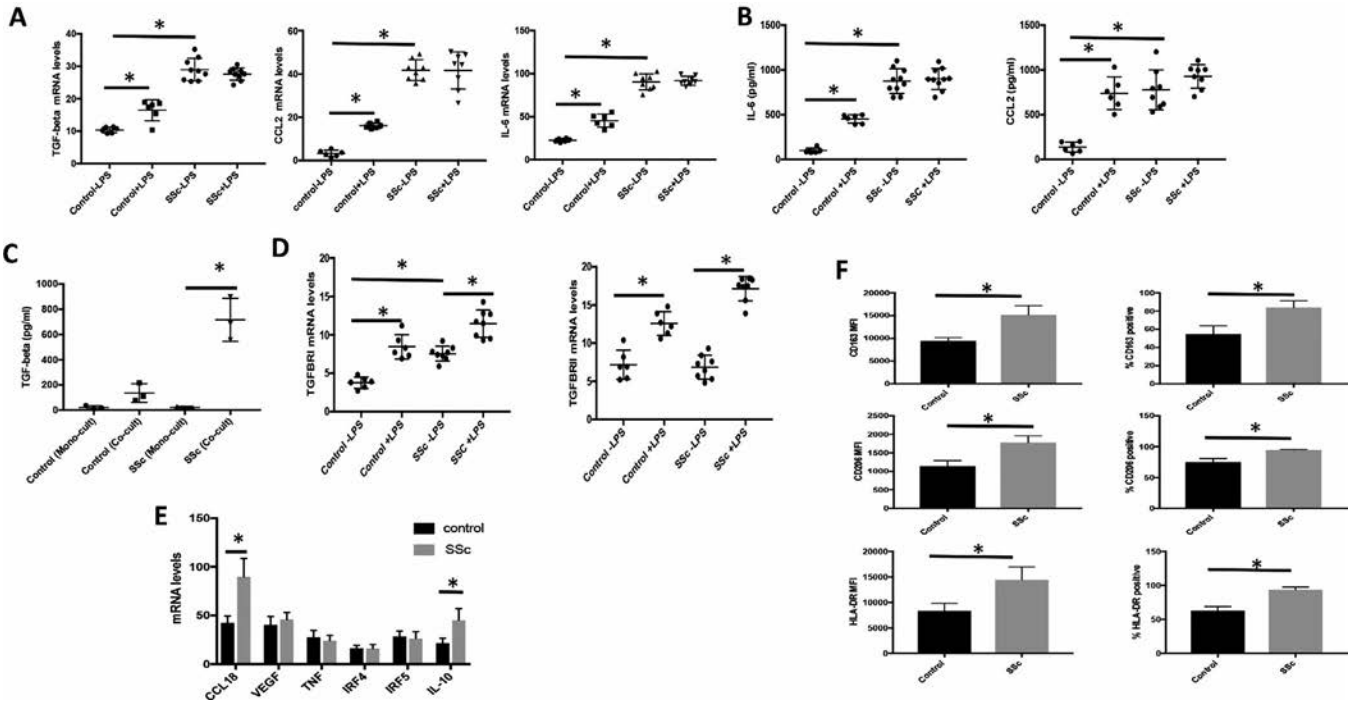

Figure 2. Immunophenotypic characterization of systemic sclerosis (SSc) macrophages. Monocytes from healthy controls or SSc patients were differentiated in autologous plasma for 7 days and left unstimulated or stimulated with 10 ng/ml lipopolysaccharide (LPS) for 24 hours. **A**, RNA was extracted and analyzed by quantitative real-time polymerase chain reaction (PCR) for cytokine mRNA levels. **B**, Supernatants were collected and analyzed by enzyme-linked immunosorbent assay (ELISA) for secreted protein production. **C**, Supernatants were collected from healthy or SSc macrophage/fibroblast cocultures (co-cult) or monocultures (mono-cult), as indicated, and secreted transforming growth factor β1 (TGFβ1) levels were measured by ELISA. **D** and **E**, Messenger RNA levels of TGFβ receptors (TGFβRI and TGFβRII) (**D**) or macrophage activation markers (**E**) were quantified by real-time PCR. **F**, Surface marker expression was quantified using flow cytometry and is presented as the mean fluorescence intensity (MFI). Gating of positively stained cells was determined by fluorescence minus one controls (healthy controls, n = 7; SSc patients, n = 8. In **A**–**D**, each symbol represents an individual subject; bars show the mean ± SEM. In **E** and **F**, values are the mean ± SEM. * = $P < 0.05$. IL-6 = interleukin-6; VEGF = vascular endothelial cell growth factor; IRF4 = interferon regulatory factor.

with control cultures, suggesting that a similar requirement is necessary in SSc skin disease. However, because this is a coculture system, it is not possible to discriminate between the potential contributions of SSc fibroblasts or macrophages to the total secreted TGFβ protein levels. To determine how TGFβ mRNA levels differ between SSc fibroblasts and macrophages, RNA was extracted from cocultured cells and analyzed by quantitative real-time PCR. Intriguingly, both SSc fibroblasts and macrophages expressed elevated TGFβ mRNA levels compared with control cells (Supplementary Figure 1, http://onlinelibrary.wiley.com/doi/10.1002/art.41243/abstract). Although TGFβ mRNA levels do not necessarily directly correlate with bioactive TGFβ protein expression, these results suggest that macrophages and fibroblasts may synergistically contribute to increases in secreted TGFβ protein in SSc.

Because TGFβ has been identified as a key regulator of fibroblast activation in SSc and due to its role in mediating macrophage polarization, TGFβ receptor (TGFBR) expression was assayed by quantitative real-time PCR. As demonstrated in Figure 2D, expression of mRNA for TGFBRI but not TGFBRII under basal conditions was elevated in SSc macrophages compared with controls. However, stimulation of SSc macrophages with LPS resulted in the induction of expression of both receptors in SSc and control macrophages (Figure 2D).

To interrogate the range of mediators expressed by SSc macrophages, mRNA levels of cytokines and transcription factors characteristic of macrophage activation were assayed by quantitative real-time PCR (Figure 2E). Consistent with previous findings (2), elevated levels of mRNA for CCL18, which has been associated with alternative activation of macrophages, were detected in SSc macrophages compared with healthy control cells. While no statistically significant differences in expression of vascular endothelial growth factor (VEGF), TNF, interferon regulatory factor 4 (IRF-4), or IRF-5 were noted between SSc and control cells, expression of mRNA for IL-10, which has been reported to be increased in SSc sera (27), was higher in patients compared with controls. However, we failed to detect increased secretion of IL-10 protein in SSc cell supernatants (data not shown).

Macrophage activation can also be assessed by analysis of characteristic surface marker and cytokine expression. Previous studies ascribed an M2 activation state to SSc macrophages based on elevated expression of *CD163*. To more completely characterize surface marker expression on SSc macrophages, flow cytometry was performed. Consistent with prior results (28), *CD163* expression was increased on human SSc macrophages compared with control cells. Additionally, surface levels of *CD206*, the macrophage mannose receptor, and HLA–DR were elevated on SSc macrophages (Figure 2F), while no statistically significant differences in expression of *CD14*, *CD80*, or *CD1A* were detected between healthy control and SSc macrophages. Significantly, *CD206*-expressing macrophages have been implicated as mediators of fibrotic activation through enhanced secretion of TGFβ (29), and HLA class II effects on SSc susceptibility have been reported (30).

STAT3 is phosphorylated in SSc macrophages under basal conditions. IL-6 levels are elevated in the skin and sera of SSc patients compared with healthy controls, and IL-6 has been implicated in disease pathogenesis in SSc (31). IL-6 signals are transduced in *cis* through binding of IL-6 to membrane-bound IL-6R and/or in *trans* through engagement of soluble IL-6 receptor (sIL-6R), resulting in STAT3 activation. Because our data indicated that SSc macrophages synthesize and release IL-6 under basal conditions and because these cells express IL-6R, we investigated STAT3 phosphorylation in SSc macrophages. To test this, macrophages were differentiated in control or SSc plasma for five days, washed, and then cultured with fresh media without plasma for an additional day in the presence or absence of control or anti–IL-6 blocking antibody. As shown in Figure 3, STAT3 is phosphorylated in macrophages from SSc patients, unlike cells from healthy donors. Total STAT3 levels did not differ between healthy control and SSc macrophages (data not shown). Additionally, IL-6 blockade attenuated STAT3 phosphorylation, suggesting that increased expression of IL-6 by SSc macrophages accounts, at least in part, for increased signaling. This inhibition is specific, as inclusion of IgG control antibody did not significantly reduce STAT3 activation (Figure 3).

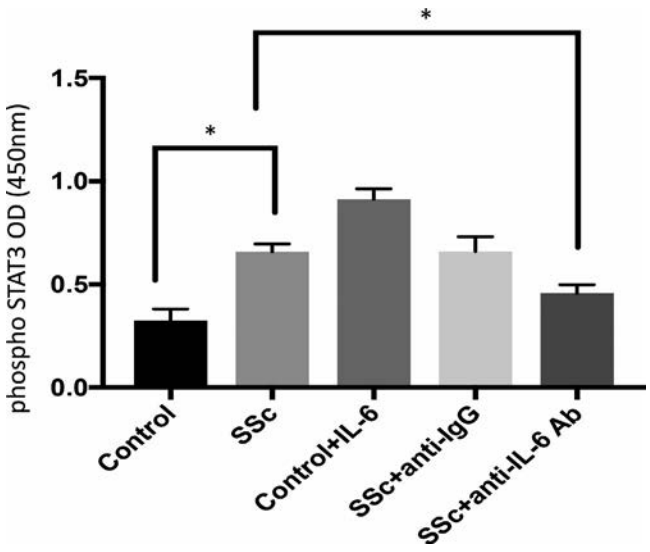

Figure 3. Phosphorylation of STAT3 in diffuse cutaneous systemic sclerosis (dcSSc) macrophages under basal conditions. Monocytes from dcSSc patients (n = 4) or healthy controls (n = 4) were differentiated with autologous plasma for 5 days, washed, and cultured in fresh media without plasma for an additional day in the presence of blocking anti–interleukin-6 (anti–IL-6) or isotype control antibody (Ab). Whole-cell lysates were prepared and analyzed using a phospho-STAT3 enzyme-linked immunosorbent assay. Total STAT3 levels were not significantly different between healthy and dcSSc macrophages (not shown). Data are plotted as absorbance units at 450 nm. Bars show the mean ± SEM. * = $P < 0.05$.

Notably, constitutive STAT3 phosphorylation was detected only in cells derived from a subset of dcSSc patients. This finding supports genome-wide expression data that demonstrate immune activation in SSc patients (2,4–6,32).

Healthy control monocytes differentiated in SSc plasma recapitulate SSc macrophage phenotype. Because macrophage activation is regulated by microenvironmental factors, we hypothesized that the phenotypic and functional activation profiles of SSc macrophages might derive from soluble mediators in SSc plasma. To test this, healthy control macrophages were differentiated in allogeneic plasma from SSc donors, and surface marker and mRNA levels and protein secretion of these cells were compared with control macrophages differentiated in autologous (control) plasma. As demonstrated in Figure 4A, surface levels of HLA–DR, CD206, and CD163 in healthy cells differentiated in SSc plasma increased to levels comparable with those observed on macrophages derived from SSc patients. Moreover, when monocytes from SSc patients were differentiated in healthy donor plasma, expression of these surface markers decreased. Consistent with these results, differentiation of healthy control monocytes in SSc plasma resulted in increased IL-6, CCL2, and TGFβ mRNA and protein levels in these cells (Figures 4B and C), with a loss of expression of the mediators in SSc patient–derived macrophages cultured in healthy plasma. These results implicate a role for plasma-associated factors in the induction of SSc macrophage activation.

SSc plasma–differentiated macrophages induce SSc fibroblast activation. Macrophages have been shown to regulate activation of cardiac, renal, and liver fibroblasts through the secretion of inflammatory mediators. As our studies have demonstrated, SSc macrophages produce high basal levels of CCL2, TGFβ, and IL-6, and we hypothesized that coculture of SSc plasma–differentiated macrophages with SSc dermal fibroblasts would induce fibroblast activation. To test this, healthy control macrophages were differentiated in SSc or healthy control plasma and cocultured with healthy control or SSc dermal fibroblasts in control or SSc plasma for 5 days (Figure 5A). To confirm fibrotic activation of these cells, quantitative real-time PCR was performed to assess levels of mRNA for α-SMA, which is highly expressed by activated myofibroblasts (33). As seen in Figure 5B, elevated expression of this fibrotic regulator was detected in SSc fibroblasts cocultured with SSc plasma–differentiated macrophages. Both monocultured and cocultured healthy control fibroblasts or SSc fibroblasts were incubated with healthy control plasma or SSc plasma.

To assess genome-wide effects on macrophage and fibroblast activation, RNA was extracted from each cell type and analyzed by DNA microarray. As depicted in Figure 5C, macrophage gene expression was primarily defined by the presence or absence of SSc plasma. Notably, pathways associated with oxidative phosphorylation and fatty acid metabolism were significantly up-regulated in SSc macrophages, regardless of culture with SSc fibroblasts. TNF/NF-κB signaling was induced in macrophages differentiated with SSc plasma and cocultured

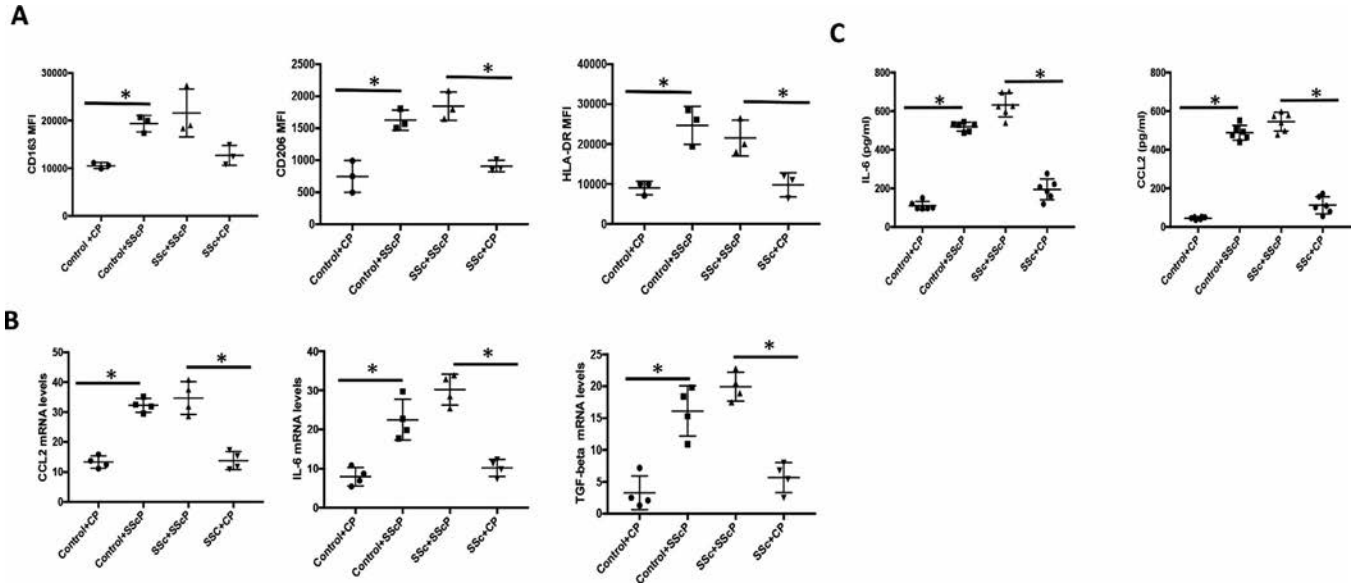

Figure 4. Differentiation of healthy cells in SSc plasma confers SSc macrophage activation. Healthy donor (control) monocytes were differentiated in autologous control plasma (CP) or SSc patient plasma (SScP) for 7 days, and SSc patient monocytes were differentiated in autologous SSc or healthy donor plasma, as indicated. Macrophages were immunophenotyped using flow cytometry (n = 3 control and 3 SSc patients) (**A**), quantitative real-time PCR (n = 4 control and 4 SSc patients) (**B**), and ELISA (n = 6 control and 6 SSc patients) (**C**). Each symbol represents an individual subject; bars show the mean ± SEM. * = $P < 0.05$. See Figure 2 for other definitions.

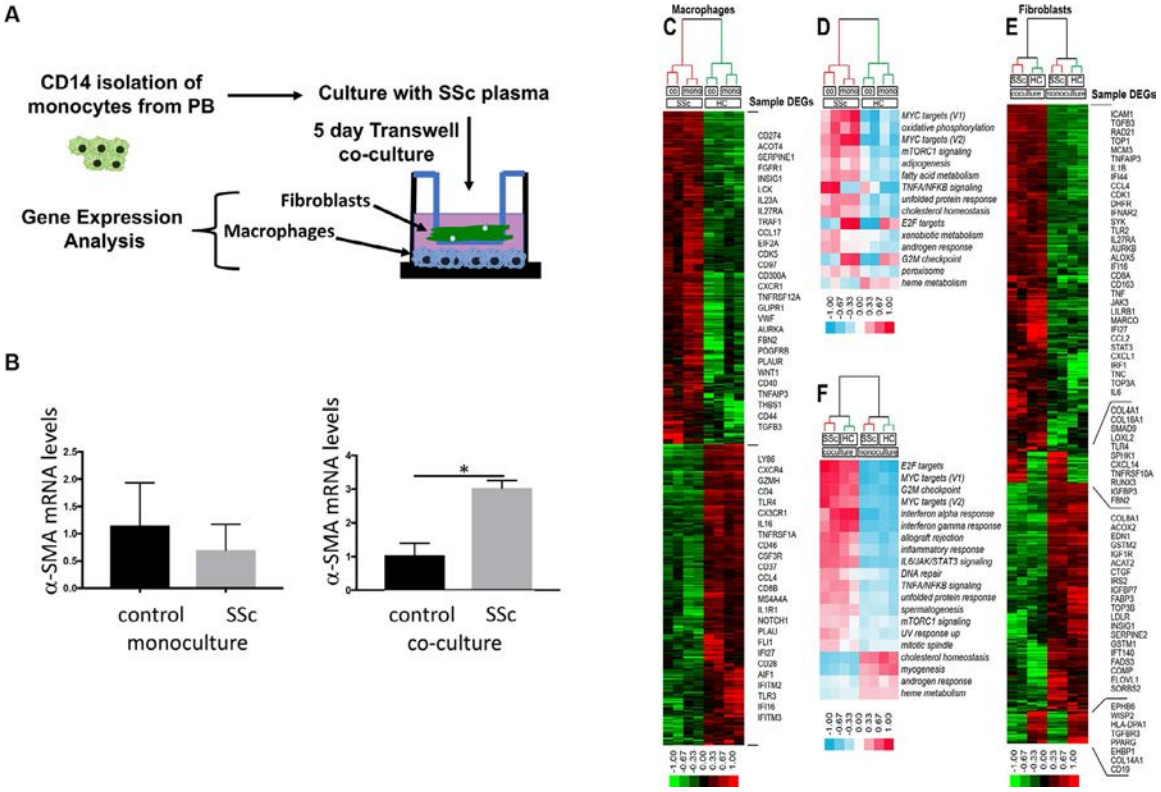

Figure 5. Systemic sclerosis (SSc) plasma–differentiated macrophages activate SSc fibroblasts. **A**, Healthy donor monocytes were differentiated in control or SSc plasma and cocultured with SSc or control dermal fibroblasts using Transwell plates for 5 days. **B**, RNA was extracted from fibroblasts cultured alone (monoculture) or with SSc plasma–differentiated macrophages (coculture) and assayed for α-smooth muscle actin (α-SMA) expression by quantitative real-time polymerase chain reaction. Bars show the mean ± SEM. * = $P < 0.05$. **C**–**F**, RNA from monocultured or cocultured macrophages (**C** and **D**) and fibroblasts (**E** and **F**) was analyzed by microarray for changes in gene expression and pathway enrichment. Data are representative of 3 independent experiments using cells derived from 3 healthy controls (HC) and 3 SSc patients. PB = peripheral blood; DEGs = differentially expressed genes; mTORC1 = mechanistic target of rapamycin complex 1.

with SSc fibroblasts (Figure 5D), which is consistent with a role for these cells in the induction of immune activation. In contrast, the presence or absence of SSc plasma did not appear to significantly alter gene expression in fibroblasts (Figure 5F). Rather, gene expression in fibroblasts was determined primarily by coculture with macrophages. Pathways associated with interferon responses and inflammation were up-regulated in fibroblasts cocultured with macrophages compared with control plasma (Figure 5E), in accordance with previous results (34,35). These data indicate that macrophages provide signals to fibroblasts that induce interferon responses and fibrotic activation.

DISCUSSION

The link between inflammation and fibrosis is widely recognized, and macrophages mediate both immune activation and tissue repair. At early stages of tissue injury, macrophages release matrix metalloproteinases and cytokines that initiate inflammatory processes, while later stages are focused on fibrotic activation and wound healing. While this process is essential for the resolution of tissue damage, prolonged macrophage–fibroblast activation can result in pathology. In this study, we demonstrated that coculture of SSc fibroblasts and SSc plasma–differentiated macrophages results in the activation of signaling pathways involved in the regulation of inflammation and fibrosis, suggesting that these cells engage in active communication. Thus, we hypothesize that macrophages and fibroblasts engage in sustained interaction and activation in SSc, resulting in enhanced inflammation and collagen deposition characteristic of this disease.

While operationally useful, M1/M2 designations of activation are an oversimplification of in vivo macrophage heterogeneity. As demonstrated by our results, SSc macrophages bear hallmarks of M1 activation (increased HLA–DR surface expression, IL-6 production) and M2 activation (enhanced surface expression of *CD163* and *CD206* and increased production of TGFβ and CCL2). Therefore, it is difficult to impose M1/M2 descriptors on these cells. Because SSc macrophages release elevated levels of fibrotic inducers that include CCL2, IL-6, and TGFβ under basal conditions compared with healthy control cells and because SSc plasma–differentiated macrophages induce fibroblast activation, we propose classifying these cells as profibrotic.

The discovery that the differentiation of healthy cells with SSc plasma confers an SSc macrophage phenotype implicates a role for soluble plasma-derived mediators in the regulation of SSc macrophage polarization. Identification of these regulators could provide additional therapeutic targets for SSc, which is an area of active investigation in our laboratories. One candidate is IL-6, which is up-regulated in SSc plasma and is synthesized by many cells, including fibroblasts and macrophages. IL-6 has been shown to regulate macrophage activation in obesity through induction of IL-4Rα (36), and our data demonstrate similar effects in SSc macrophages (Bhandari R, Pioli PA: unpublished observations), suggesting that IL-6 potentiates IL-4 signaling in these cells. It is notable that treatment of SSc patients with the humanized anti–IL-6R antibody tocilizumab has shown clinical benefit in a randomized phase II trial (37). In addition to direct effects on IL-6 signaling blockade, tocilizumab may provide further benefit by impeding profibrotic SSc macrophage activation.

Consistent with studies that demonstrate that STAT3 is constitutively activated in SSc fibroblasts and skin (38), we have also shown that STAT3 is phosphorylated in a subset of dcSSc patient–derived macrophages. STAT3 signaling, which is induced by IL-6, is a key mediator of macrophage activation in a variety of pathologic conditions (39,40), and is a regulator of macrophage migration (41). Intriguingly, drug-mediated inhibition of CCL2 has been shown to correlate with reduced macrophage recruitment to the skin of SSc patients, stabilization or reduction in MRSS, and reduced inflammatory skin gene expression signature (22). These results suggest that therapeutic inhibition of STAT3 in SSc patients may be beneficial by inhibiting activation of both fibroblasts and macrophages and by curtailing macrophage recruitment to end-target organs.

Although macrophages are implicated in SSc pathogenesis, little is known about their role in inflammation and fibroblast activation in this disease. Functional studies with primary human SSc macrophages have been limited by the ability to recover sufficient cells from SSc tissue. To circumvent this obstacle, we differentiated SSc blood–derived monocytes in autologous plasma to preserve the local cytokine/mediator milieu to which these cells are exposed in vivo. We have now also shown enrichment of the SSc plasma–differentiated macrophage signature in SSc skin, suggesting that these cells are represented in SSc skin. For the first time, we have demonstrated that SSc macrophages secrete elevated levels of inflammatory and profibrotic mediators under basal conditions compared with healthy control cells. Our results indicate that SSc macrophage activation derives from factors in SSc plasma, as differentiation of healthy cells in SSc plasma results in an SSc immunophenotype. Immunophenotypic analysis demonstrated that SSc macrophages have a profibrotic phenotype, and gene expression studies showed that SSc macrophages induce fibroblast activation.

Our study has several limitations. We included patients with lcSSc and dcSSc together in our analyses. All patients had a disease duration of <5 years (mean ± SD 35 ± 25 months) (Table 1). Another limitation is that we were unable to study a completely treatment-naive population. Twelve of the SSc patients (50%) were not receiving concurrent immunosuppressive therapy, 9 (38%) were receiving mycophenolate mofetil, and 3 (13%) were receiving hydroxychloroquine. The study was underpowered to further subdivide the analyses by disease duration or treatment status.

Taken together, the present findings implicate macrophages as mediators of inflammation and fibrosis in SSc. They also suggest that immunotherapeutic targeting of these cells may provide significant patient benefit.

AUTHOR CONTRIBUTIONS

All authors were involved in drafting the article or revising it critically for important intellectual content, and all authors approved the final version to be published. Dr. Pioli had full access to all of the data in the study and takes responsibility for the integrity of the data and the accuracy of the data analysis.

Study conception and design. Hinchcliff, Whitfield, Pioli.

Acquisition of data. Bhandari, Ball, Schaafs, Han, ElTanbouly, Orzechowski, Carns, Arroyo, Aren, Hinchcliff.

Analysis and interpretation of data. Bhandari, Ball, Martyanov, Popovich, Hinchcliff, Whitfield, Pioli.

REFERENCES

1. Christmann RB, Hayes E, Pendergrass S, Padilla C, Farina G, Affandi AJ, et al. Interferon and alternative activation of monocyte/macrophages in systemic sclerosis–associated pulmonary arterial hypertension. Arthritis Rheum 2011;63:1718–28.
2. Christmann RB, Sampaio-Barros P, Stifano G, Borges C, de Carvalho CR, Kairalla R, et al. Association of Interferon- and transforming growth factor β–regulated genes and macrophage activation with systemic sclerosis–related progressive lung fibrosis. Arthritis Rheumatol 2014;66:714–25.
3. Pendergrass SA, Hayes E, Farina G, Lemaire R, Farber HW, Whitfield ML, et al. Limited systemic sclerosis patients with pulmonary arterial hypertension show biomarkers of inflammation and vascular injury. PLoS One 2010;5:e12106.
4. Mahoney JM, Taroni J, Martyanov V, Wood TA, Green CS, Pioli PA, et al. Systems level analysis of systemic sclerosis shows a network of immune and profibrotic pathways connected with genetic polymorphisms. PLoS Comput Biol 2015;11:e1004005.
5. Assassi S, Swindell WR, Wu M, Tan FD, Khanna D, Furst DE, et al. Dissecting the heterogeneity of skin gene expression patterns in systemic sclerosis. Arthritis Rheumatol 2015;67:3016–26.
6. Taroni JN, Green CS, Martyanov V, Wood TA, Christmann RB, Farber HW, et al. A novel multi-network approach reveals tissue-specific cellular modulators of fibrosis in systemic sclerosis. Genome Med 2017;9:27.
7. Kim MG, Kim SC, Ko YS, Lee HY, Jo SK, Cho W. The role of M2 macrophages in the progression of chronic kidney disease following acute kidney injury. PLoS One 2015;10:e0143961.
8. Gautier EL, Shay T, Miller J, Greter M, Jakubzick C, Ivanov S, et al. Gene-expression profiles and transcriptional regulatory pathways that underlie the identity and diversity of mouse tissue macrophages. Nat Immunol 2012;13:1118–28.

9. Gibbings SL, Goyal R, Desch AN, Leach SM, Prabagar M, Atif SM, et al. Transcriptome analysis highlights the conserved difference between embryonic and postnatal-derived alveolar macrophages. Blood 2015;126:357–66.
10. Lavin Y, Winter D, Blecher-Gonen R, David E, Keren-Shaul H, Merad M, et al. Tissue-resident macrophage enhancer landscapes are shaped by the local microenvironment. Cell 2014;159: 1312–26.
11. Misharin AV, Morales-Nebreda L, Reyfman PA, Cuda CM, Walter JM, McQuattie-Pimentel AC, et al. Monocyte-derived alveolar macrophages drive lung fibrosis and persist in the lung over the life span. J Exp Med 2017;214:2387–404.
12. Murray PJ, Allen JE, Biswas SK, Fisher EA, Gilroy DW, Goerdt S, et al. Macrophage activation and polarization: nomenclature and experimental guidelines. Immunity 2014;41:14–20.
13. Greenblatt MB, Sargen JL, Farina G, Tsang K, Lafyatis R, Glimcher LH, et al. Interspecies comparison of human and murine scleroderma reveals IL-13 and CCL2 as disease subset-specific targets. Am J Pathol 2012;180:1080–94.
14. Hasegawa M, Sato S, Takehara K. Augmented production of chemokines (monocyte chemotactic protein-1 (MCP-1), macrophage inflammatory protein-1α (MIP-1α) and MIP-1β) in patients with systemic sclerosis: MCP-1 and MIP-1α may be involved in the development of pulmonary fibrosis. Clin Exp Immunol 1999;117: 159–65.
15. Ihn H, Yamane K, Kubo M, Tamaki K. Blockade of endogenous transforming growth factor β signaling prevents up-regulated collagen synthesis in scleroderma fibroblasts: association with increased expression of transforming growth factor β receptors. Arthritis Rheum 2001;44:474–80.
16. Kawakami T, Ihn H, Xu W, Smith E, LeRoy C, Trojanowska M. Increased expression of TGF-β receptors by scleroderma fibroblasts: evidence for contribution of autocrine TGF-β signaling to scleroderma phenotype. J Invest Dermatol 1998;110:47–51.
17. Van den Hoogen F, Khanna D, Fransen J, Johnson SR, Baron M, Tyndall A, et al. 2013 classification criteria for systemic sclerosis: an American College of Rheumatology/European League Against Rheumatism collaborative initiative. Arthritis Rheum 2013;65: 2737–47.
18. Ball MS, Shipman EP, Kim H, Liby KT, Pioli PA. CDDO-Me redirects activation of breast tumor associated macrophages. PLoS One 2016;11:e0149600.
19. Hinchcliff M, Huang CC, Wood TA, Mahoney JM, Martyanov V, Bhattacharyya S, et al. Molecular signatures in skin associated with clinical improvement during mycophenolate treatment in systemic sclerosis. J Invest Dermatol 2013;133:1979–89.
20. Jakubzick C, Gautier EL, Gibbings SL, Sojka DK, Schlitzer A, Johnson TE, et al. Minimal differentiation of classical monocytes as they survey steady-state tissues and transport antigen to lymph nodes. Immunity 2013;39:599–610.
21. Tamoutounour S, Guilliams M, Montanana Sanchis F, Liu H, Terhorst D, Malosse C, et al. Origins and functional specialization of macrophages and of conventional and monocyte-derived dendritic cells in mouse skin. Immunity 2013;39:925–38.
22. Hinchcliff M, Toledo DM, Taroni JN, Wood TA, Franks JM, Ball MS, et al. Mycophenolate mofetil treatment of systemic sclerosis reduces myeloid cell numbers and attenuates the inflammatory gene signature in skin. J Invest Dermatol 2018;138:1301–10.
23. Clements P, Lachenbruch P, Seibold J, White B, Weiner S, Martin R, et al. Inter and intraobserver variability of total skin thickness score (modified Rodnan TSS) in systemic sclerosis. J Rheumatol 1995;22:1281–5.
24. Milano A, Pendergrass SA, Sargen JL, George LK, McCalmont TH, Connolly MK, et al. Molecular subsets in the gene expression signatures of scleroderma skin. PLoS One 2008;3:e2696.
25. Biswas SK, Lopez-Collazo E. Endotoxin tolerance: new mechanisms, molecules and clinical significance. Trends Immunol 2009;30: 475–87.
26. Khalil N, Bereznay O, Sporn M, Greenberg AH. Macrophage production of transforming growth factor β and fibroblast collagen synthesis in chronic pulmonary inflammation. J Exp Med 1989;170:727–37.
27. Hasegawa M, Fujimoto M, Kikuchi K, Takehara K. Elevated serum levels of interleukin 4 (IL-4), IL-10, and IL-13 in patients with systemic sclerosis. J Rheumatol 1997;24:328–32.
28. Higashi-Kuwata N, Makino T, Inoue Y, Takeya M, Ihn H. Alternatively activated macrophages (M2 macrophages) in the skin of patient with localized scleroderma. Exp Dermatol 2009;18:727–9.
29. Bellón T, Martínez V, Lucendo B, del Peso G, Castro MJ, Aroeira LS, et al. Alternative activation of macrophages in human peritoneum: implications for peritoneal fibrosis. Nephrol Dial Transplant 2011;26:2995–3005.
30. Arnett FC, Gourh P, Shete S, Ahn CS, Honey RE, Agarwal SK, et al. Major histocompatibility complex (MHC) class II alleles, haplotypes and epitopes which confer susceptibility or protection in systemic sclerosis: analyses in 1300 Caucasian, African-American and Hispanic cases and 1000 controls. Ann Rheum Dis 2010;69:822–7.
31. O'Reilly S, Cant R, Ciechomska M, van Laar JM. Interleukin-6: a new therapeutic target in systemic sclerosis? Clin Transl Immunology 2013;2:e4.
32. Luo Y, Zhou H, Krueger J, Kaplan C, Lee SH, Dolman C, et al. Targeting tumor-associated macrophages as a novel strategy against breast cancer. J Clin Invest 2006;116:2132–41.
33. Hinz B. Myofibroblasts. Exp Eye Res 2016;142:56–70.
34. Fang F, Ooka K, Sun X, Shah R, Ghattacharyya S, Wei J, et al. A synthetic TLR3 ligand mitigates profibrotic fibroblast responses by inducing autocrine IFN signaling. J Immunol 2013;191:2956–66.
35. Artlett CM, Sassi-Gaha S, Hope JL, Feghali-Bostwick CA, Katsikis PD. Mir-155 is overexpressed in systemic sclerosis fibroblasts and is required for NLRP3 inflammasome-mediated collagen synthesis during fibrosis. Arthritis Res Ther 2017;19:144.
36. Mauer J, Chaurasia B, Goldau J, Vogt MC, Ruud J, Nguyen KD, et al. Signaling by IL-6 promotes alternative activation of macrophages to limit endotoxemia and obesity-associated resistance to insulin. Nat Immunol 2014;15:423–30.
37. Khanna D, Denton CP, Jahreis A, van Laar JM, Frech TM, Anderson ME, et al. Safety and efficacy of subcutaneous tocilizumab in adults with systemic sclerosis (faSScinate): a phase 2, randomised, controlled trial. Lancet 2016;387:2630–40.
38. Chakraborty D, Šumová B, Mallano T, Chen CW, Distler A, Bergmann C, et al. Activation of STAT3 integrates common profibrotic pathways to promote fibroblast activation and tissue fibrosis. Nat Commun 2017;8:1130.
39. Nakamura R, Sene A, Santeford A, Gdoura A, Kubota S, Zapata N, et al. IL10-driven STAT3 signalling in senescent macrophages promotes pathological eye angiogenesis. Nat Commun 2015; 6:7847.
40. Fu XL, Duan W, Su CY, Mao FY, Lv YP, Teng YS, et al. Interleukin 6 induces M2 macrophage differentiation by STAT3 activation that correlates with gastric cancer progression. Cancer Immunol Immunother 2017;66:1597–608.
41. Zhang C, Li Y, Wu Y, Wang L, Wang X, Du J. Interleukin-6/signal transducer and activator of transcription 3 (STAT3) pathway is essential for macrophage infiltration and myoblast proliferation during muscle regeneration. J Biol Chem 2013;288:1489–99.

Arthritis & Rheumatology
Vol. 72, No. 7, July 2020, pp 1170–1183
DOI 10.1002/art.41215

American College of Rheumatology
Empowering Rheumatology Professionals

Muscle Weakness in Myositis: MicroRNA-Mediated Dystrophin Reduction in a Myositis Mouse Model and Human Muscle Biopsies

Travis B. Kinder,[1] Christopher R. Heier,[1] Christopher B. Tully,[2] Jack H. Van der Muelen,[2] Eric P. Hoffman,[3] Kanneboyina Nagaraju,[3] and Alyson A. Fiorillo[1]

Objective. Muscle inflammation is a feature in myositis and Duchenne muscular dystrophy (DMD). Autoimmune mechanisms are thought to contribute to muscle weakness in patients with myositis. However, a lack of correlation between the extent of inflammatory cell infiltration and muscle weakness indicates that nonimmune pathologic mechanisms may play a role. The present study focused on 2 microRNA (miRNA) sets previously identified as being elevated in the muscle of patients with DMD—an "inflammatory" miRNA set that is dampened with glucocorticoids, and a "dystrophin-targeting" miRNA set that inhibits dystrophin translation—to test the hypothesis that these miRNAs are similarly dysregulated in the muscle of patients with myositis, and could contribute to muscle weakness and disease severity.

Methods. A major histocompatibility complex class I–transgenic mouse model of myositis was utilized to study gene and miRNA expression and histologic features in the muscle tissue, with the findings validated in human muscle biopsy tissue from 6 patients with myositis. Mice were classified as having mild or severe myositis based on transgene expression, body weight, histologic disease severity, and muscle strength/weakness.

Results. In mice with severe myositis, muscle tissue showed mononuclear cell infiltration along with elevated expression of type I interferon and NF-κB–regulated genes, including *Tlr7* (3.8-fold increase, $P < 0.05$). Furthermore, mice with severe myositis showed elevated expression of inflammatory miRNAs (miR-146a, miR-142-3p, miR-142-5p, miR-455-3p, and miR-455-5p; ~3–40-fold increase, $P < 0.05$) and dystrophin-targeting miRNAs (miR-146a, miR-146b, miR-31, and miR-223; ~3–38-fold increase, $P < 0.05$). Bioinformatics analyses of chromatin immunoprecipitation sequencing (ChIP-seq) data identified at least one NF-κB consensus element within the promoter/enhancer regions of these miRNAs. Western blotting and immunofluorescence analyses of the muscle tissue from mice with severe myositis demonstrated reduced levels of dystrophin. In addition, elevated levels of NF-κB–regulated genes, *TLR7*, and miRNAs along with reduced dystrophin levels were observed in muscle biopsy tissue from patients with histologically severe myositis.

Conclusion. These data demonstrate that an acquired dystrophin deficiency may occur through NF-κB–regulated miRNAs in myositis, thereby suggesting a unifying theme in which muscle injury, inflammation, and weakness are perpetuated both in myositis and in DMD.

Supported by the Foundation to Eradicate Duchenne, the Clark Charitable Foundation, the Department of Defense, and the NIH. Dr. Kinder's work was supported by the National Institute of Arthritis and Musculoskeletal and Skin Diseases, NIH (grant F31-AR-065362). Dr. Heier's work was supported by the NIH (grants K99-HL-130035, R00-HL-130035, L40-AR-068727, and T32-AR-056993). Dr. Nagaraju's work is supported by grants from the National Institute of Allergy and Infectious Diseases, NIH (1R21AI128248-01), the National Institute of Neurological Disorders and Stroke, NIH (1R56NS097229-01), and the Myositis Foundation. Dr. Fiorillo's work was supported by the Department of Defense (grant W81XWH-17-1-047), the NIH (grants L40-AR-070539 and T32-AR-056993), the Foundation to Eradicate Duchenne, and the Clark Charitable Foundation. The microscopic analysis for this study, conducted at the Children's Research Institute Light Microscopy and Image Analysis Core, is supported by the Children's Research Institute and Eunice Kennedy Shriver National Institute of Child Health and Human Development, NIH (Intellectual and Developmental Disabilities Research Center award U54-HD-090257).

[1]Travis B. Kinder, PhD (current address: National Center for Advancing Translation Sciences, NIH, Bethesda, Maryland), Christopher R. Heier, PhD, Alyson A. Fiorillo, PhD: George Washington University and Children's National Hospital, Washington, DC; [2]Christopher B. Tully, BS, Jack H. Van der Muelen, PhD: Children's National Hospital, Washington, DC; [3]Eric P. Hoffman, PhD, Kanneboyina Nagaraju, PhD, DVM: Binghamton University, Binghamton, New York, and ReveraGen BioPharma, Rockville, Maryland.

Dr. Hoffman owns stock or stock options in ReveraGen BioPharma and Agada Biosciences. Dr. Nagaraju owns stock or stock options in ReveraGen

INTRODUCTION

The idiopathic inflammatory myopathies are a heterogeneous group of systemic connective tissue diseases characterized by chronic muscle inflammation and weakness. This group of diseases, which includes dermatomyositis (DM), polymyositis, and inclusion body myositis (IBM) (collectively referred to as myositis), affects both adults and children. Although rare, there is evidence that disease incidence is increasing (1). Histologic features of myositis include the following: 1) endomysial, perimysial, or perivascular infiltration by inflammatory cells, consisting predominantly of macrophages and T cells (2,3); 2) myofiber-specific expression of major histocompatibility complex (MHC) class I molecules; and 3) bouts of muscle degeneration/regeneration, fibrosis, and fat deposition (4). Of these, the most striking feature is the overexpression of MHC class I in the muscle of patients with myositis (5,6).

The role of the innate and adaptive immune systems in myositis is well known, but results recently reported suggest that nonimmune mechanisms also contribute to the disease (for review, see refs 7 and 8), as there is not a strong correlation between the extent of inflammatory cell infiltration and muscle weakness in patients with myositis (9). Interestingly, myositis muscle seems primed for inflammatory signaling events, since it inappropriately expresses Toll-like receptors (TLRs) (10,11) and MHC class I (5,6), which act as receptors that are normally confined to immune cells. Stimulation of TLR-7 and MHC class I activates the proinflammatory transcription factor NF-κB. In addition, TLR-7 is a potent inducer of type I interferon (IFN) genes (12); this gene expression signature correlates with disease severity both in patients with DM (13–16) and in those with juvenile DM (15,17).

NF-κB is a key regulator of inflammation in immune cells; however, it is also active in skeletal muscle under inflammatory conditions. Not surprisingly, in the muscle of patients with myositis, NF-κB is highly activated and its activation corresponds to disease severity (18). Classic NF-κB activation is triggered via inflammatory cytokines such as tumor necrosis factor (TNF), which is found at high levels in the muscle of patients with myositis (19). Nonclassic NF-κB activation occurs through endoplasmic reticulum stress and autophagy; both of these processes/pathways are increased in myositis (20,21). It has been previously shown that muscle-specific MHC class I expression activates the NF-κB pathway and turns on classic NF-κB target genes such as *TNF* and *TLR7*, exacerbating inflammatory signaling (22). As further confirmation of its importance in disease pathogenesis, downstream gene targets of NF-κB are highly up-regulated in myositis muscle (19,23).

At the molecular and histologic levels, there is significant overlap between inflammatory myopathies and other muscle disorders, in particular, Duchenne muscular dystrophy (DMD), Becker muscular dystrophy (BMD), and manifesting DMD female carriers (24,25). Similar to myositis, muscles of patients with DMD show increased TLR-7 expression (26), elevated NF-κB activation (18,27), and overexpression of muscle-specific MHC class I (28). Previously, we described 2 distinct sets of microRNAs (miRNAs) that are elevated in DMD muscle. The first is an "inflammatory set" of miRNAs whose expression is increased in *mdx* mice and is reduced by administration of 2 different antiinflammatory drugs (29). The second set of miRNAs is a "dystrophin-targeting" set (termed dystrophin-targeting miRNAs [DTMs]). DTMs are elevated both in DMD and in BMD, and are prohibitory to dystrophin protein production in BMD and to exon-skipping–mediated dystrophin rescue in a mouse model of DMD (30). Some of these miRNAs show increased expression in inflammatory connective tissue disorders that overlap with myositis, including scleroderma, rheumatoid arthritis, and Sjögren's syndrome, suggesting that inflammatory miRNAs and DTMs play a broader role in regulating chronic inflammation.

In mice, skeletal muscle–specific conditional overexpression of MHC class I induces myositis (3). Following MHC class I upregulation, female mice develop early histologic and functional changes mirroring human myositis, while male mice develop a more mild disease (3). In the present study, we tested the hypothesis that inflammatory miRNAs and DTMs contribute to the pathologic processes of myositis by reducing dystrophin in muscle fibers.

MATERIALS AND METHODS

Mice. All mouse studies were performed with adherence to the NIH Guide for the Care and Use of Laboratory Animals. All experiments were conducted according to protocols within the guidelines of and with the approval of the Institutional Animal Care and Use Committee of Children's National Medical Center. Animals were housed at room temperature in a 12-hour/12-hour light/dark cycle. Genotyping was carried out in all mice at age 3–4 weeks, as previously described (21). The mouse model of myositis used in this study is known as the HT mouse model of myositis, using (TRE)-H-2Kb (H) and mCK-tTA (T) mice, as has been described previously (3). For this study, transgene expression was induced by withdrawal of doxycycline from the drinking water of the mice at age 5 weeks, followed by analyses at ages 9–13 weeks. Female mice were used for all studies, as the disease manifestations are more severe in female mice.

BioPharma and Agada Biosciences. Dr. Fiorillo holds a patent for methods and agents to increase therapeutic dystrophin expression in muscle. No other disclosures relevant to this article were reported.

Address correspondence to Kanneboyina Nagaraju, PhD, DVM, Binghamton University, School of Pharmacy and Pharmaceutical Sciences, 4400 Vestal Parkway East, Binghamton, NY 13902 (e-mail: nagaraju@binghamton.edu); or to Alyson A. Fiorillo, PhD, Center for Genetic Medicine Research, Children's National Medical Center, 111 Michigan Avenue NW, Washington, DC 20010 (e-mail: afiorillo@childrensnational.org).

Submitted for publication March 1, 2019; accepted in revised form January 24, 2020.

Human muscle biopsy tissue. Muscle biopsy tissue samples from human subjects were obtained from a member of the Telethon Network of Genetic Biobanks (project no. GTB12001). The samples obtained included skeletal muscle, peripheral nerve samples, DNA samples, and cell lines. Further details can be found in the Supplementary Materials and Methods (available on the *Arthritis & Rheumatology* web site at http://onlinelibrary.wiley.com/doi/10.1002/art.41215/abstract).

Quantitative reverse transcription–polymerase chain reaction (qRT-PCR) analyses of miRNAs and messenger RNAs (mRNAs). Analyses of miRNA and mRNA expression by qRT-PCR were performed in muscle tissue samples in a manner as previously reported (29,30). Details can be found in the Supplementary Materials and Methods (http://onlinelibrary.wiley.com/doi/10.1002/art.41215/abstract).

Western blot analysis. Proteins from muscle were collected using a lysis buffer containing 75 m*M* Tris HCl (pH 6.8), 10% sodium dodecyl sulfate, 10 m*M* EDTA, and 5% 2-mercaptoethanol. Protein samples (25 μg) were separated using a 3–8% Tris–acetate gel (Bio-Rad) and then transferred onto a nitrocellulose membrane (20V at 4°C) overnight, followed by a 1-hour pulse (80V at 4°C). Antibodies used included the DYS-1 mouse monoclonal antibody against dystrophin (1:100; Novacastra), and a rabbit polyclonal antibody against vinculin (1:1,000, clone N3C1; GenTex). Horseradish peroxidase–conjugated anti-mouse immunoglobulin or anti-rabbit goat immunoglobulin (1:5,000; Millipore) were used as secondary antibodies. Enzyme chemiluminescence (Pierce) was used for detection of the proteins. The blots were scanned digitally with a ChemiDoc Touch Imager.

Hematoxylin and eosin (H&E) staining and histologic grading of the muscle tissue sections. Sections of muscle tissue (8 μ*M*) were cut from frozen mouse quadriceps muscles or from frozen human muscle biopsy tissue. Sections were air-dried for 1 hour on SuperFrost Plus slides and then stained with H&E. Stained slides were imaged on a VS120 Virtual Slide microscope (Olympus) at 20× magnification. Details on the grading of histopathologic features of the muscle can be found in the Supplementary Materials and Methods (http://onlinelibrary.wiley.com/doi/10.1002/art.41215/abstract).

Immunofluorescence. Frozen muscle sections (8 μ*M*) were dried for 1 hour on SuperFrost Plus slides and then stored at –80°C. For staining, slides were thawed for 1 hour at room temperature and then fixed in either ice-cold acetone (4°C) for 10 minutes or 4% paraformaldehyde for 10 minutes at room temperature. Further details on the primary and secondary antibody dilutions and incubation times can be found in the Supplementary Materials and Methods (http://onlinelibrary.wiley.com/doi/10.1002/art.41215/abstract).

Evaluation of force contractions on isolated skeletal muscle. Extensor digitorum longus (EDL) muscle was isolated from live anesthetized mice prior to their euthanization, and contractile properties of the skeletal muscle were then measured ex vivo. Details can be found in the Supplementary Materials and Methods (http://onlinelibrary.wiley.com/doi/10.1002/art.41215/abstract).

Bioinformatics analysis. We examined each miRNA gene promoter by bioinformatics analysis, to gain insight into the mechanisms of response to treatment, as has been previously reported (29). Details on the identification of NF-κB/RelA binding sites can be found in the Supplementary Materials and Methods (http://onlinelibrary.wiley.com/doi/10.1002/art.41215/abstract).

RESULTS

Variable disease severity in mice with myositis. In the present study, we utilized female mice that overexpress MHC class I, and we performed our studies after withdrawal of doxycycline from the drinking water of the mice at age 5 weeks. At 4–8 weeks after doxycycline withdrawal, we observed variable disease severity among the mice, allowing us to investigate the molecular factors driving disease progression.

We initially observed that mice with a lower body weight at the time of euthanization appeared to have a more aggressive disease. To determine whether the body weight of mice is related to transgene expression, we plotted the weight of the mice at the time of euthanization against the extent of transgenic MHC class I expression in the most severely affected muscle (quadriceps). As shown in Figure 1A, body weight and transgene expression showed a strong inverse correlation (Spearman's rho = –0.9146), thus corroborating our observations that mice with a lower body weight develop a more severe disease, which can likely be attributed to increased MHC class I expression.

The scatter plot of the correlation between body weight and transgene expression revealed 2 distinct mouse phenotypes: HT mice with mild myositis (HT-M) and HT mice with severe myositis (HT-S). Mice classified in the HT-S myositis group weighed 12–16 grams at the time of euthanization, and their expression of muscle-specific MHC class I was at a level of >300-fold relative to wild-type (WT) mice. Mice classified in the HT-M myositis group weighed 17–20 grams and showed MHC class I transgene expression at a level of ≤300-fold relative to WT mice.

To determine whether differences in transgene expression were reflected in the muscle pathology, we used a grading system on H&E-stained muscle tissue from the HT-M and HT-S groups of mice. The muscle of mice with severe myositis showed 1) higher endomysial inflammation with invasion into the myofibers, 2) more highly variable muscle fiber size, and 3) increased necrosis and degeneration, with a mean histologic grade of 2.3 (on a scale of 0–3) ($P < 0.0001$ versus WT). In contrast, the muscle of mice with mild myositis showed 1) less endomysial

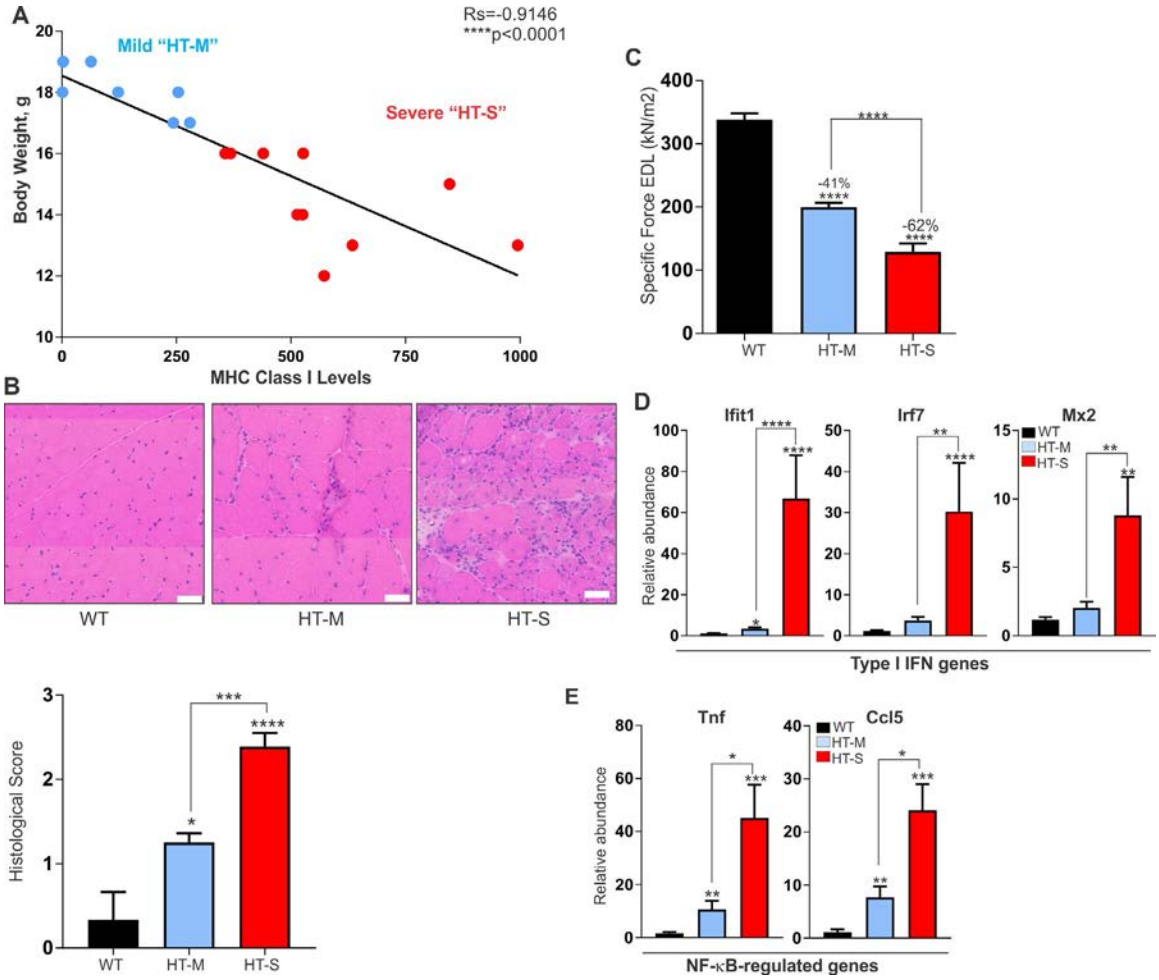

Figure 1. Variable disease severity in the HT mouse model of myositis. **A**, Classification system used for grouping HT mice according to the severity of myositis, based on body weight plotted against the extent of major histocompatibility complex (MHC) class I transgene expression. HT-M = mice with mild myositis, body weight of >16 grams, and MHC class I expression of ≤300-fold relative to wild-type (WT) mice. HT-S = mice with severe myositis, body weight of ≤16 grams, and MHC class I expression of >300-fold relative to WT mice. Correlations were determined using Spearman's correlation coefficients. **B**, Representative images of histologic staining with hematoxylin and eosin (top) and histologic scores of staining (bottom) of the quadriceps muscle from WT mice and mice in the mild or severe myositis groups (n = 5 WT, n = 7 HT-M, and n = 10 HT-S). Bars = 50 μ*M*. **C**, Isolated measurements of specific force contractions of the extensor digitorum longus (EDL) muscle in each group of mice (n ≥ 10 per group). **D** and **E**, Type I interferon (IFN) gene expression levels (genes for IFN-induced protein with tetratricopeptide repeats 1 [*Ifit*], IFN regulatory factor 7 [*Irf7*], and MX dynamin like GTPase 2 [*Mx2*]) (**D**) and NF-κB–induced gene expression (genes for tumor necrosis factor [*Tnf*] and C–C motif chemokine ligand 5 gene [*Ccl5*]) (**E**) in the quadriceps muscle of WT, HT-M, and HT-S mice (n = 5 WT, n = 7 HT-M, and n = 10 HT-S). Data were normalized to the values for 18S ribosomal RNA. Results in **B**–**E** are the mean ± SEM. * = $P < 0.05$; ** = $P < 0.01$; *** = $P < 0.001$; **** = $P < 0.0001$ for the indicated comparisons or versus WT mice, by analysis of variance.

inflammation with no invasion into fibers, 2) less fiber size variation, and 3) little-to-no necrosis and degeneration, with a mean histologic grade of 1.3 ($P < 0.001$ versus HT-S) (Figure 1B).

To determine whether the differences in molecular and histologic features between the HT-S and HT-M groups of mice resulted in functional differences, we assessed the muscle strength of isolated EDL muscles ex vivo. Specific force in the EDL muscle was reduced by 62% in mice with severe myositis and was reduced by 41% in mice with mild myositis (each $P < 0.0001$ versus WT mice) (Figure 1C). Collectively, these data show that mice classified as HT-S indeed display a more severe disease as compared to mice classified as classified as HT-M.

Type I IFN signature and NF-κB activation in mice with severe myositis. Results of recent studies have suggested that molecules induced by type I IFNs play a mechanistic role in the pathogenesis of myositis (13–16); this is most commonly observed in adult and juvenile patients with DM (15,17). To determine whether type I IFN gene expression was related to disease severity in our study, we performed qRT-PCR on 3 type I IFN signature genes, the genes for IFN-induced protein with tetratricopeptide repeats 1 (*Ifit*), IFN regulatory factor 7 (*Irf7*), and MX dynamin like GTPase 2 (*Mx2*). Muscle tissue from mice with severe myositis showed significant increases (~10–80-fold) in the relative expression of all 3 genes as compared to WT mice ($P < 0.0001$ for *Ifit*

and *Irf7*, and $P < 0.01$ for *Mx2*) (Figure 1D). In comparison, muscle tissue from mice with mild myositis showed modest increases in *Ifit1*, *Irf7,* and *Mx2*, with only the levels of *Ifit1* reaching a statistically significant difference compared to WT mice ($P < 0.05$) (Figure 1D).

We have previously shown that NF-κB is highly activated in human inflammatory myopathies and mouse models of myositis (22). To determine whether NF-κB activation is associated with disease severity, we assessed the NF-κB–activated genes *Tnf* and C–C motif chemokine ligand 5 gene (*Ccl5*). Both *Tnf* and *Ccl5* followed a similar pattern as that of type I IFN signature genes. In the muscle of mice in the HT-S group, the levels of both *Tnf* and *Ccl5* were highly increased over the levels in WT mice ($P < 0.001$) (Figure 1E). In the HT-M group of mice, NF-κB–induced gene expression in the muscle also showed significant elevations compared to WT mice ($P < 0.01$), but to a lesser extent.

In response to their cognate ligands, TLRs induce both type I IFN and inflammatory (NF-κB) gene expression (31). Investigators have recently observed myofiber-specific expression of TLR-7 in several muscle disorders (10,26,32). Because we observed elevated expression of both types of gene expression signatures in mice with severe myositis, we next assessed TLR-7 expression in both the HT-M and HT-S myositis groups of mice. Using immunofluorescence, we observed an almost complete absence of TLR-7 from WT mouse muscle (Figure 2A). In contrast, the muscle of mice with mild myositis showed modest TLR-7 staining, while the muscle of mice with severe myositis showed strong TLR-7 staining (Figure 2A).

Using confocal microscopy, we observed colocalization of TLR-7 and lysosome-associated membrane protein 1 (LAMP-1), a marker of late endosomes/early lysosomes, in the mouse muscle (Figure 2B; positive controls are shown in Supplementary Figure 1, available on the *Arthritis & Rheumatology* web site at http://onlinelibrary.wiley.com/doi/10.1002/art.41215/abstract), indicating

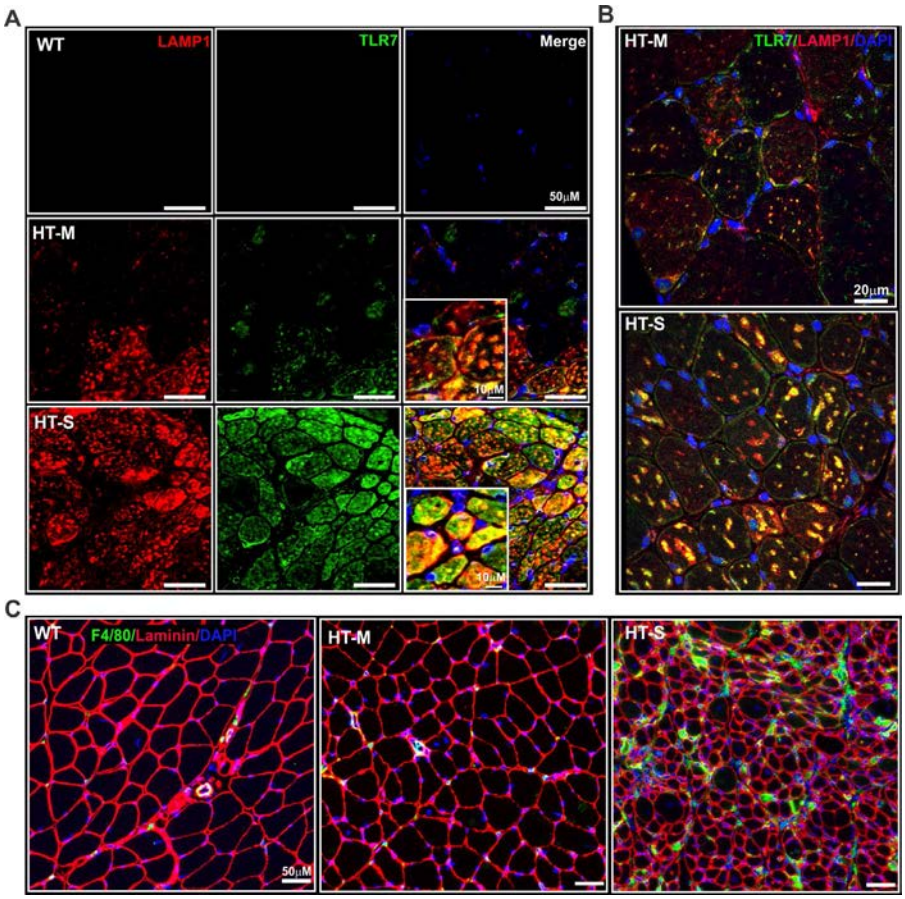

Figure 2. Increased Toll-like receptor 7 (TLR-7) staining and macrophage infiltration in the muscle of mice with severe myositis. **A** and **B**, Representative images of the quadriceps muscle of a WT mouse, mouse with mild myositits, and mouse with severe myositis, immunolabeled with an antibody against TLR-7 (green) and lysosome-associated membrane protein 1 (LAMP-1) (red). DAPI counterstaining was used to visualize nuclei (blue). Images in **A** were obtained with a VS-120 scanning microscope at 20× magnification, and images in **B** are from a second set of immunostained muscle tissue sections visualized using confocal microscopy. In both **A** and **B**, colocalization of TLR-7 and LAMP-1, a marker of late endosomes/early lysosomes, is an indication that TLR-7 is localized to the endosomes and is in an activated state. **C**, Muscle tissue from HT-M and HT-S mouse quadriceps stained with an antibody against F4/80, which recognizes a glycoprotein expressed by murine macrophages (green), and with an antibody against laminin (red), which confirms the integrity of the muscle tissue, with DAPI counterstaining of the nuclei (blue). See Figure 1 for other definitions.

that TLR-7 was in an activated state (33). Analyses by qRT-PCR corroborated the immunofluorescence data, showing elevated levels of *Tlr7* in the muscle of mice with severe myositis (see Supplementary Figure 2A, available on the *Arthritis & Rheumatology* web site at http://onlinelibrary.wiley.com/doi/10.1002/art.41215/abstract). In addition, qRT-PCR analyses indicated that *Lamp1* gene expression was increased in the muscle of mice with severe myositis; however, the difference compared to WT mice did not reach significance (see Supplementary Figure 2B [http://onlinelibrary.wiley.com/doi/10.1002/art.41215/abstract]).

Signaling through TLR-7 promotes macrophage recruitment and invasion into muscle fibers. Immunofluorescence analyses of mouse macrophage marker F4/80 showed increased macrophage infiltration in the muscle of mice with severe myositis as compared to WT mice or mice with mild myositis (Figure 2C). This observation was confirmed by qRT-PCR analyses of a macrophage-specific marker, endothelial growth factor–like module-containing mucin-like hormone receptor–like 1 (*Emr1*). Analyses by qRT-PCR showed that the muscle of mice with severe myositis expressed elevated levels of *Emr1* ($P < 0.05$) (see Supplementary Figure 2C [http://onlinelibrary.wiley.com/doi/10.1002/art.41215/abstract]). Taken together, these data suggest that progression of myositis involves distinct changes in the molecular signature of myofibers, which begin to take on an innate immune–like state via expression of type I IFN signature genes, NF-κB–regulated genes, and myofiber-specific expression of TLR-7, all of which may result in increased macrophage recruitment.

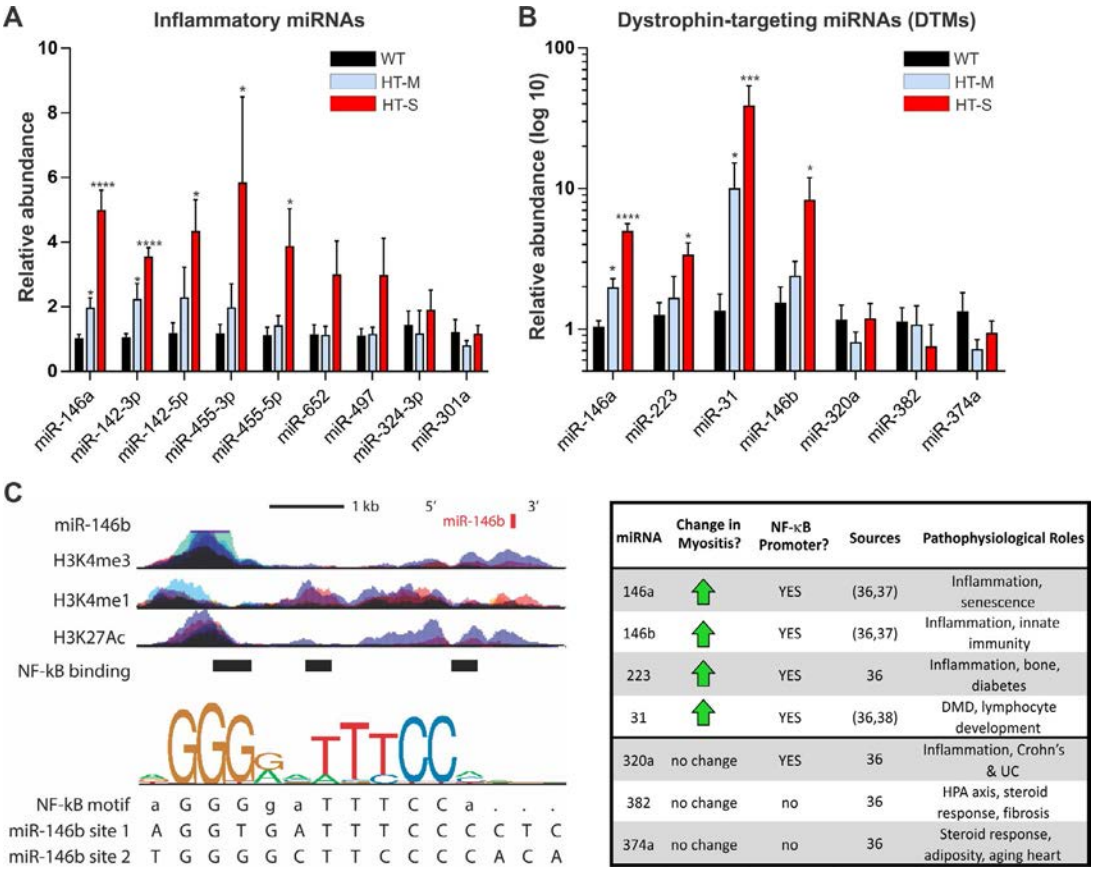

miRNA	Change in Myositis?	NF-κB Promoter?	Sources	Pathophysiological Roles
146a	↑	YES	(36,37)	Inflammation, senescence
146b	↑	YES	(36,37)	Inflammation, innate immunity
223	↑	YES	36	Inflammation, bone, diabetes
31	↑	YES	(36,38)	DMD, lymphocyte development
320a	no change	YES	36	Inflammation, Crohn's & UC
382	no change	no	36	HPA axis, steroid response, fibrosis
374a	no change	no	36	Steroid response, adiposity, aging heart

Figure 3. Expression of inflammatory microRNAs (miRNAs) and dystrophin-targeting miRNAs (DTMs) in the quadriceps muscle of mice classified as having severe or mild myositis disease. **A** and **B**, The relative abundance of inflammatory miRNAs (**A**) and DTMs (**B**) was analyzed by quantitative reverse transcription–polymerase chain reaction in the quadriceps muscle from each group of mice. Data were normalized to the values for *sno202*. Results are the mean ± SEM (n = 5 WT, n = 6 HT-M, and n = 8 HT-S). * = $P < 0.05$; *** = $P < 0.001$; **** = $P < 0.0001$ versus WT mice, by analysis of variance. **C**, Transcription factor (NF-κB) binding sites and histone (H3) modifications that mark regulatory regions were examined using chromatin immunoprecipitation sequencing data from ENCODE. Binding motifs for each transcription factor were identified through the Factorbook repository. Left Top, Schematic diagram of the gene locus for miR-146b, illustrating the binding sites of 3 neighboring DNA loci bound directly by NF-κB. Epigenetic modification maps show the location of histone modifications associated with active promoters (H3K4me3) and poised/active enhancers (H3K4me1/H3K27Ac). Left Bottom, Sequence logo pictogram of the base frequency at NF-κB binding sites with the consensus NF-κB motif. Two representative NF-κB binding site sequences near miR-146b are also shown. Right, Summary of promoter analysis and literature data for all DTMs, indicating each miRNA and known factors associated with its transcriptional regulation. DMD = Duchenne muscular dystrophy; UC = ulcerative colitis; HPA = hypothalamic–pituitary–adrenal axis (see Figure 1 for other definitions).

Association between muscle levels of inflammatory and dystrophin-targeting miRNAs with the severity of myositis. To further characterize the molecular changes that drive myositis disease progression, we analyzed 2 defined sets of miRNAs in the mouse quadriceps muscle. The first set encompassed 9 miRNAs (termed inflammatory miRNAs) that we previously found to be elevated in dystrophic mice. This set of miRNAs are regulated by NF-κB and their expression decreases in response to antiinflammatory treatment (29). Of these, the levels of 5 miRNAs (miR-146a, miR-142-3p, miR-142-5p, miR-455-3p, and miR-455-5p) were significantly elevated in the muscle of mice with severe myositis compared to WT mice (~4–6-fold increase, $P < 0.05$) (Figure 3A). In the muscle of mice with mild myositis, the levels of miR-142-3p

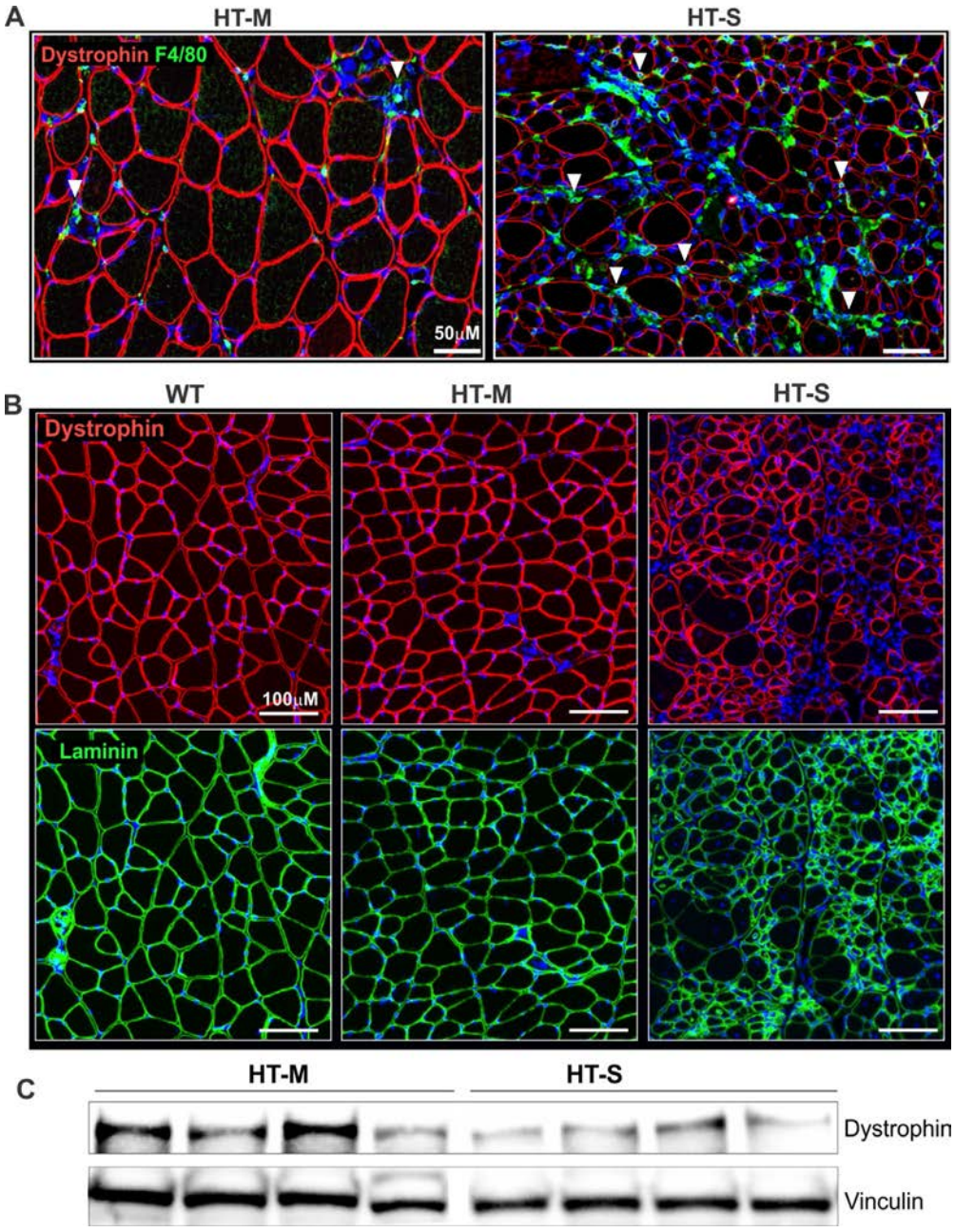

Figure 4. Reduced dystrophin levels in mice with severe myositis. **A**, Representative images of the quadriceps muscle of mice in the mild or severe myositis groups, immunolabeled with an antibody against dystrophin (red) and macrophage staining (F4/80; green). **Arrowheads** indicate regions with high macrophage infiltration (F4/80; green) where neighboring myofibers are observed to show diminished dystrophin levels (red). **B**, Representative images of the quadriceps muscle of mice in the mild or severe myositis groups compared to WT mice, using immunolabeling with an antibody against dystrophin (red). An anti-laminin antibody (green) was used as a control to show sarcolemnal integrity of the muscle tissue. DAPI counterstaining was used to visualize nuclei (blue). **C,** Western blotting for dystrophin, using protein extracts from the tibialis anterior muscle of mice in the mild or severe myositis groups (n = 4 per group). Vinculin was used as a loading control and was run on the same Western blot. See Figure 1 for definitions.

and miR-146a were also significantly elevated compared to WT mice, but to a lesser extent.

We next assayed a second defined set of miRNAs (termed DTMs), which we previously reported to be up-regulated both in patients with DMD and in those with BMD. These miRNAs bind to the dystrophin 3′-untranslated region (3′-UTR) to inhibit its translation. Analyses by qRT-PCR showed that the expression levels of 4 of 7 DTMs (miR-146a, miR-223, miR-31, and miR-146b) were highly elevated (~3–40-fold increase, $P < 0.05$) in the quadriceps muscle of mice with severe myositis compared to WT mice (Figure 3B). We also observed significantly elevated levels of miR-146a and miR-31 in the muscle of mice with mild myositis compared to WT mice, but to a lesser extent.

Because we observed elevated TLR-7 expression in myositis muscles, we also assessed expression of 3 miRNAs known to activate TLR-7: miR-21 (34), miR-29a (34), and let-7 (35). In our analyses, miR-21 was undetectable in all samples assessed, while the expression of miR-29a and let-7 showed no significant differences between WT, HT-M, and HT-S mouse muscles (see Supplementary Figure 3, available on the *Arthritis & Rheumatology* web site at http://onlinelibrary.wiley.com/doi/10.1002/art.41215/abstract).

DTMs (miR-146a and miR-223) are induced by TNF in dystrophic myotubes, suggesting that they are regulated by NF-κB (30). To gain insight into DTM regulation in myositis, we performed bioinformatics analyses on chromatin immunoprecipitation sequencing (ChIP-seq) data at the sites of each miRNA promoter/enhancer region. Bioinformatics analyses showed that all 4 elevated DTMs possessed sites that are directly bound by NF-κB at consensus elements within their promoter/enhancer regions (Figure 3C) (36). These elements overlapped with corresponding ChIP-seq data indicating the presence of histone modifications, all of which corresponded to active regions of transcriptional regulation (H3K4me3, H3K27Ac, and H3K4me1). These findings are supported by previous studies in which miR-146a (37), miR-146b (37), miR-223 (38), and miR-31 (39) were found to be regulated by NF-κB. Taken together, these data suggest that both defined sets of miRNAs play a key role in the progression of myositis, and that NF-κB regulates their expression.

Reduction in dystrophin expression linked to the severity of myositis. Our laboratory has demonstrated that DTMs inhibit the translation of dystrophin, and that DTM levels inversely correlate with the levels of dystrophin in the muscle of patients with BMD and in the exon-skipping–treated muscle of *mdx* mice in the model of DMD (30). To determine whether elevated levels of DTMs reduce dystrophin in myositis muscle, we performed dystrophin immunostaining in the quadriceps muscle of WT mice and mice in the HT-M and HT-S groups. Dystrophin expression was markedly reduced in the muscle of mice with severe myositis as compared to mice with mild myositis, most notably in areas of inflammation as shown by macrophage (F4/80) staining (Figure 4A; arrowheads indicating macrophage staining alongside myofibers showing reduced dystrophin).

We next performed immunostaining for both dystrophin and laminin to better visualize the muscle fibers lacking dystrophin. In the HT-S group of mice, muscle fibers that lacked dystrophin stained positively for laminin, indicating the presence of intact muscle fibers (Figure 4B). To corroborate the immunofluorescence findings, we also performed Western blotting on muscle tissue extracts from the HT-M and HT-S groups of mice. The results similarly showed that dystrophin levels were reduced in muscle from mice with severe myositis (Figure 4C).

To determine the relevance of these findings to human disease, we obtained human muscle biopsy tissue from patients with DM and those with IBM as well as muscle biopsy tissue from healthy control subjects. Analysis by H&E staining revealed different levels of histologic severity in the muscle tissue based on the extent of inflammation and muscle fiber size variability. According to the histologic findings, we partitioned the patients into "histologically mild" or "histologically severe" cohorts. Two biopsy samples from patients with DM and 1 from a patient with IBM were grouped as "histologically mild," and the remaining 3 biopsy samples (from patients with IBM) were grouped as "histologically severe." Representative images are shown in Figure 5A.

We next assessed MHC class I (HLA–B) gene expression in human muscle biopsy tissue. Those in the histologically severe group showed a ~6-fold elevation in MHC class I expression ($P < 0.05$), whereas muscle tissue from the histologically mild group showed no significant elevation in MHC class I expression above the levels in healthy controls. Muscle with histologically severe disease showed elevated levels of NF-κB–driven gene expression, with evidence of increased expression of *TNF* and *CCL5* (each $P < 0.05$ versus healthy controls), whereas muscle with histologically mild disease showed no appreciable up-regulation in gene expression (Figure 5B). We also observed elevated expression of *TLR7* in histologically severe muscle ($P < 0.05$ versus healthy controls) (Figure 5B), consistent with our observations in the muscle of mice with severe myositis.

We assessed type I IFN gene expression and found no significant differences between the healthy control and histologically mild or histologically severe groups of human muscle biopsy tissue. We did, however, observe elevated expression of type I IFN genes in 1 of 2 muscle biopsy samples from patients with DM (data not shown), consistent with previous studies in which it was shown that this gene expression signature is a hallmark of DM, particularly in muscles that have perifascicular atrophy (15,17).

We next assessed levels of NF-κB–regulated DTMs, which were found to be elevated in the human muscle tissue with histologically severe disease. We observed that the expression of both miR-146a ($P < 0.10$) and miR-146b ($P < 0.001$) was increased in histologically severe muscle biopsy tissue compared to healthy controls, while that from the histologically mild group

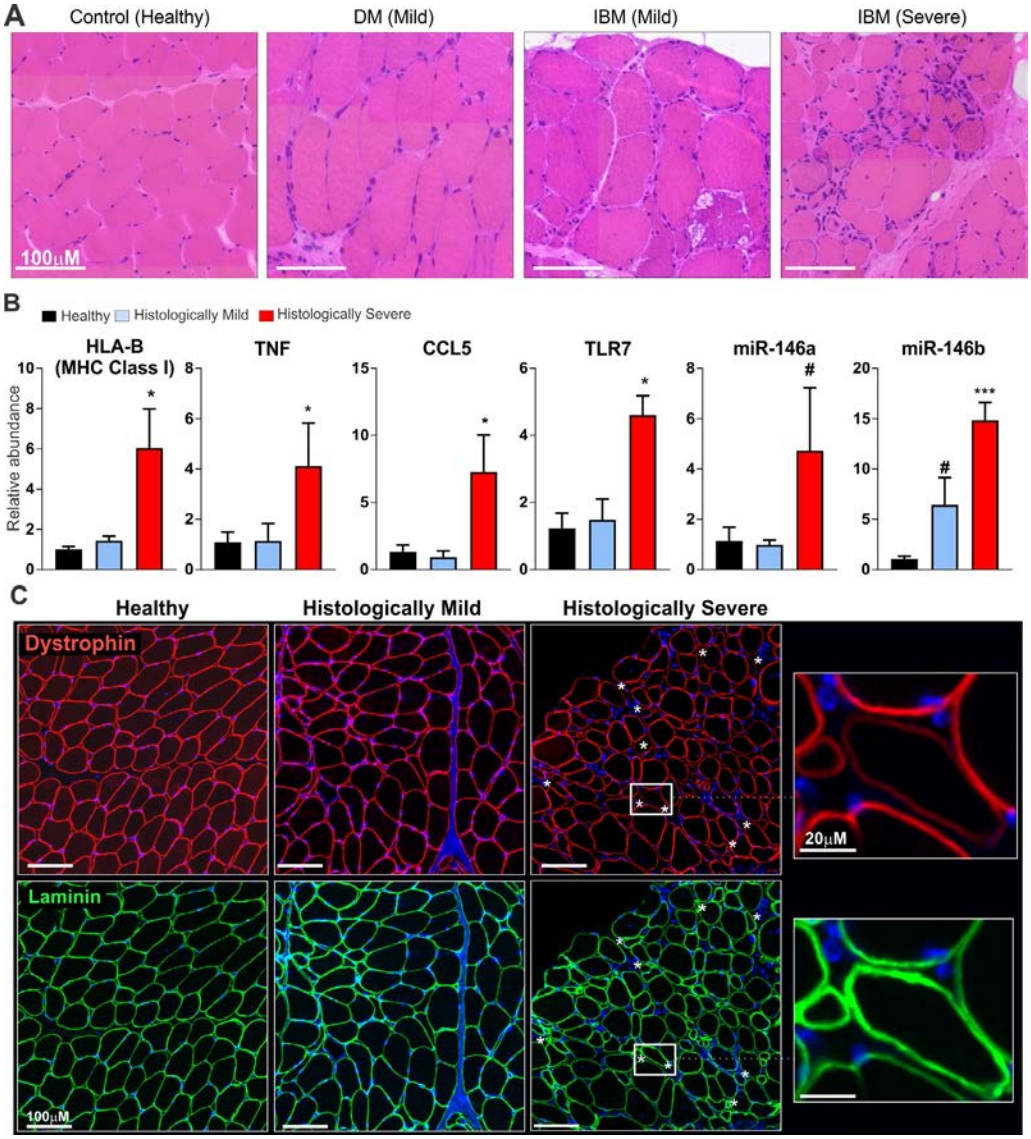

Figure 5. Elevations in major histocompatibility complex (MHC) class I expression, NF-κB–driven gene expression, and dystrophin-targeting microRNAs (miRNAs) and reduction in dystrophin levels in histologically severe human muscle biopsy tissue. **A**, Representative images of hematoxylin and eosin–stained human muscle biopsy tissue obtained from a healthy control, a patient with dermatomyositis (DM) classified as having histologically mild muscle disease, and 2 patients with inclusion body myositis (IBM), of whom 1 was classified as having histologically mild muscle disease and 1 as having histologically severe muscle disease. **B**, Gene and miRNA expression levels in human muscle biopsy tissue from each group (n = 3 per group). Data for mRNAs were normalized to the values for *Hprt*, and data for miRNAs were normalized to the values for *RNU48*. # = $P < 0.10$; * = $P < 0.05$; *** = $P < 0.001$ versus healthy controls, by Student's *t*-test. **C**, Representative images of human muscle biopsy tissue from a healthy control, a patient with histologically mild muscle disease, and a patient with histologically severe muscle disease, using immunolabeling with an antibody against dystrophin (red). An anti-laminin antibody (green) was used as a control to show sarcolemnal integrity of the muscle tissue. **Asterisks** in the histologically severe muscle highlight muscle fibers in which laminin staining is uniform, but dystrophin staining is either reduced, discontinuous, or absent. DAPI counterstaining was used to visualize nuclei (blue). TNF = human gene for tumor necrosis factor; TLR7 = human gene for Toll-like receptor 7.

showed no differences in miR-146a expression, but did show slightly higher miR-146b levels in comparison to healthy muscles ($P < 0.10$) (Figure 5B).

We then performed immunofluorescence analysis of dystrophin expression in the human muscle biopsy samples, using sarcolemmal-localized laminin as a control for the integrity of the muscle fibers. Whereas staining for dystrophin in the healthy control and histologically mild muscle tissue was uniform, we found areas of reduced and discontinuous dystrophin staining in histologically severe muscle tissue (Figure 5C).

Collectively, our data suggest a mechanism whereby increased TLR-7 signaling activates inflammation and NF-κB–driven miRNAs to promote muscle weakness through reduced

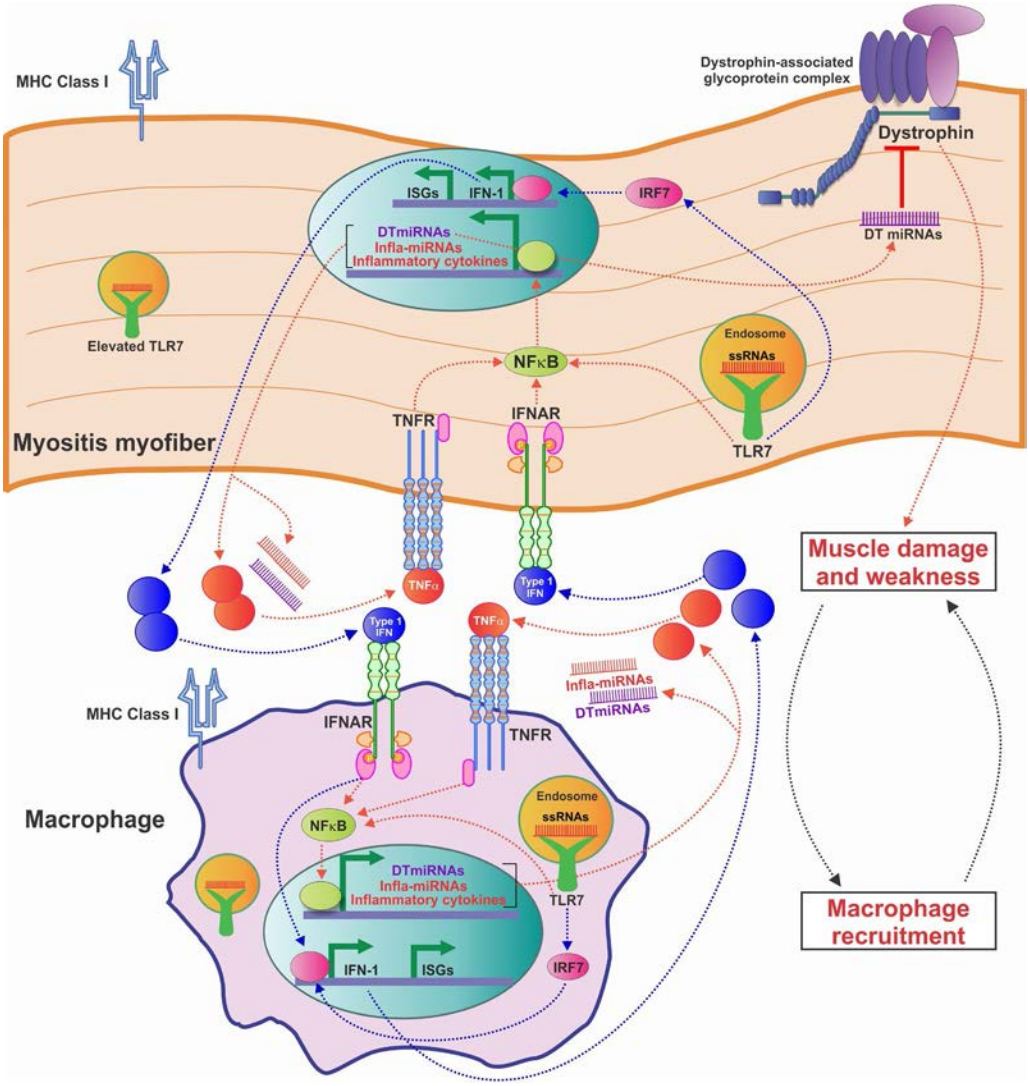

Figure 6. Model of the hypothesized self-amplifying feedback loop between macrophages and myofibers in myositis. Progression of myositis is driven by myofibers that adopt a more immune-like state, as evidenced by inappropriate expression of Toll-like receptor 7 (TLR-7) and major histocompatibility complex (MHC) class I. TLR-7 activates NF-κB–driven gene expression, eliciting the release of inflammatory cytokines and promoting macrophage recruitment. Activation of NF-κB–driven genes such as tumor necrosis factor (TNF) and interferon-α/β (IFN) genes leads to a feed–forward loop in which these cytokines activate their receptors (TNFR and IFNAR, respectively), thereby enhancing NF-κB activation. TLR-7 additionally activates the IFN regulatory factor 7 gene (*IRF7*), driving production of IFN-1, which in turn activates IFNAR and expression of type I IFN–stimulated genes (ISGs), which includes *IRF7*. NF-κB also triggers expression of inflammatory and dystrophin-targeting microRNAs (miRNAs) (infla-miRNA and DT-miRNA, respectively), leading to reduction in the levels of dystrophin and muscle weakness, which in turn causes increased release of proinflammatory signals. All of these components contribute to a positive, self-amplifying inflammatory feedback loop. ssRNAs = single-stranded RNAs.

expression of dystrophin (refer to model in Figure 6). Furthermore, elevated levels of DTMs may be responsible for the reduced and discontinuous dystrophin expression observed in myositis muscle, both in the HT mouse model and in patients with idiopathic inflammatory myopathies.

DISCUSSION

Herein, we utilized a mouse model of myositis using HT mice with variable disease severity to better understand the molecular and cellular pathways that contribute to myositis. Previous reports have described the common occurrence of a chronic disease progression in these mice, in which reduced locomotor activity is seen as early as 1 month after doxycycline withdrawal, and clinical and histopathologic signs are observable at ~2 months, which thereafter become profound and severe by 4–6 months (3). Due to the sensitivity of our assay, the analyses performed herein in mice at 1–2 months after being taken off doxycycline enabled us to identify early molecular aberrations and additionally to measure weakness in isolated EDL mouse muscles ex vivo.

The cohort of HT mice in our study possessed variable rates of disease progression. Thus, because of the progressive nature of the model, we predict that the disease in HT mice with mild myositis will become more severe through time.

We classified mice into 2 distinct cohorts: HT-M mice with low transgenic expression of muscle-specific MHC class I, and HT-S mice with high MHC class I transgene expression. Comparing these 2 groups and age-matched WT littermates, we found that mice in the HT-S group developed a more severe disease, as shown by a lower body weight, histologic severity of the disease in the muscle tissue, and reduced muscle strength/weakness, as well as elevated levels of type I IFN and NF-κB gene signatures. Furthermore, mice in the HT-S group showed inappropriate expression of endolysosomal-localized TLR-7 within myofibers and increased macrophage infiltration as visualized by F4/80 staining. Correspondingly, the muscle of mice in the HT-S group displayed markedly increased levels of miRNAs from 2 defined sets: an inflammatory set previously described in a DMD mouse model (29), and a dystrophin-targeting set previously described both in patients with BMD and in exon-skipping–treated muscle of *mdx* mice that model DMD (30). All of the miRNAs that showed elevated expression in severe myositis muscle from these sets possessed at least one NF-κB regulatory element within their promoter or enhancer regions.

Using both immunofluorescence and Western blot analyses, we demonstrated that dystrophin was reduced in the muscle of mice with severe myositis. To corroborate our data in the HT mouse model, we additionally analyzed human muscle biopsy samples from patients with myositis, and found that histologically severe muscles had elevated levels of MHC class I, elevated NF-κB–driven gene expression, and high levels of miR-146a and miR-146b. Human muscle with histologically severe myositis also showed patchy/reduced levels of dystrophin immunostaining. Importantly, the muscle biopsy samples classified as severe were from patients with IBM, whereas the muscle biopsy samples from patients with DM were classified as mild. This is consistent with previous studies in which MHC expression was shown to be more prominent in the muscle of patients with IBM (40). Collectively, our data suggest a model whereby progression of myositis is driven by myofibers adopting a more immune-like state, as evidenced by the inappropriate expression of TLR-7 and MHC class I. TLR-7 activates NF-κB–driven gene expression, eliciting release of inflammatory cytokines and leading to macrophage recruitment. NF-κB–driven gene expression also triggers an NF-κB feed-forward loop, in which production of inflammatory cytokines, including TNF, further turns on NF-κB. TLR-7 activation also leads to production of type I IFN, which, in turn, triggers expression of NF-κB and type I IFN–stimulated genes. NF-κB additionally activates dystrophin-targeting miRNAs, which down-regulate dystrophin protein levels. Taken together, these findings indicate that this combination of events appears to contribute to a self-amplifying inflammatory feedback loop of muscle damage and inflammation. As dystrophin is required for maintenance of mechanical stability in the muscle, our observations suggest that reduced dystrophin levels in myositis muscle may contribute to muscle weakness (Figure 6).

Many signaling pathways described herein are similarly overexpressed or overactive in DMD. For instance, in muscles from patients with DMD there is strong activation of multiple components of the innate immune system before the onset of clinical symptoms, including elevated signaling from TLRs (TLR-4 and TLR-7), NF-κB activation, and expression of MHC class I molecules. It is recognized that there is substantial overlap between the histopathologic presentation of myositis and muscular dystrophies, specifically DMD, BMD, and manifesting DMD female carriers. Transcriptional profiling also shows shared pathways between these diseases (41). In a few case studies, DMD female carriers were found to be initially misdiagnosed as having myositis, further illustrating the multitude of confounding factors that blur the boundaries between the 2 diseases (25,42). In the present study, we describe miRNAs whose levels were elevated in both diseases. These similarities give rationale for the development of therapeutic strategies that could target shared pathways in DMD and myositis.

Recent studies have demonstrated inappropriate expression of TLR-7 in myofibers from myositis patients (10,11), and have shown that this increase in expression exacerbates disease (43). Similarly, TLR-7 levels are elevated in the myofibers of patients with DMD at an early age (<1 year of age) (27). Because of the high TLR-7 levels observed in DMD muscle, it is postulated that myofiber-derived RNA molecules may be the most potent of all of the contributing damage-associated molecular patterns (DAMPs), as they serve as the natural ligand for TLR-7 (44). In support of this, we have previously found that a more common feature of DMD and BMD muscle is miRNA up-regulation as opposed to miRNA down-regulation (30). Further, recent studies have suggested that the overabundance of specific miRNAs may trigger activation of TLR-7 (34,35). Collectively, high levels of miRNAs in muscle disease and the misexpression of TLR-7 in myofibers seem to be alluding to a mechanism whereby diseased muscle itself is primed to activate a strong inflammatory response.

TLR-7 is trafficked to the endolysosomal compartment when activated (45). In the present study we observed elevated levels of endosomally localized TLR-7 in muscle affected with severe myositis. We also observed elevated LAMP-1 expression, which may be indicative of impaired autophagy (21,46). It has been reported that autophagy is required for the activation of NF-κB (47), and that TLR-7 and its ligands regulate autophagy (48,49). Thus, these seemingly intertwined pathways make attractive targets for myositis and perhaps for other inflammation-associated muscle disorders.

MicroRNAs are responsible for fine-tuning gene expression in all cell and tissue types, including muscle and immune cells. When the balance of miRNAs is shifted in a specific tissue type,

gene expression programs are altered, driving tissue from a healthy state to a diseased state. In HT mice with severe myositis, we found significant up-regulation of 5 of the 9 miRNAs from a predefined "inflammatory" set (miR-146a, miR-142-3p, miR-142-5p, miR-455-3p, and miR-455-5p) and 4 of the 7 miRNAs from a predefined "dystrophin-targeting" set (miR-146a, miR-223, miR-31, and miR-146b). We additionally found elevated levels of miR-146a and miR-146b in human muscle biopsy tissue with a classification of histologically severe disease. All of these miRNAs are regulated by the inflammatory transcription factor NF-κB (36), and some, in turn, regulate key components of the NF-κB signaling pathway. This highlights the importance of NF-κB signaling in the pathogenesis of myositis. We will discuss the significance of these miRNAs below.

Levels of miR-146a are highly up-regulated in mice with severe myositis. Moreover, miR-146a is induced by NF-κB in immune cells (37) and is expressed directly in muscle (30). In diseases in which chronic inflammation is present, miR-146a levels are highly elevated both in the serum and in the tissue affected by disease (50–57). Similarly, miR-146b is overexpressed in severe myositis, is induced by TNF/NF-κB (37,58), and is elevated in the serum of patients with inflammatory disorders such as inflammatory bowel disease (57). Both miR-146a and miR-146b are defined as DTMs, and we have shown that they down-regulate dystrophin by binding to its 3′-UTR (30). The miR-142 family is highly expressed in monocytes (59) and lymphocytes (60). We and others have reported increased miR-142 levels in DMD as well as in other genetic muscular dystrophies (29,61). The miR-142 locus possesses 13 NF-κB binding sites within its promoter/enhancer region, illustrating the interdependence of its expression and inflammatory signaling. Increased expression of miR-31 has been reported in DMD patients, BMD patients, and *mdx* mice (30,62–64). In addition, miR-31 regulates dystrophin expression by targeting its 3′-UTR (30,65), and its expression is induced by NF-κB (39). Collectively, the miRNAs described herein seem to be uniquely primed to shift the balance toward a proinflammatory phenotype as they become increasingly expressed in diseased muscle.

A few early studies noted reduced and discontinuous dystrophin staining in human muscle biopsy tissue from patients with myositis (66,67). Herein, we investigated dystrophin levels in a mouse model of myositis and in human muscle biopsy tissue after we observed elevated levels of DTMs in HT mice with severe myositis. Immunofluorescence analysis revealed that the quadriceps muscle of mice affected with severe myositis possessed a reduced and mosaic pattern of dystrophin staining that partly resembled the pattern that has been previously observed in the muscles of patients with BMD or the muscles from DMD female carriers. Reduced dystrophin expression was associated, in part, with the extent of inflammation, as shown by macrophage (F4/80) staining. Given that DTMs are regulated by inflammation, it is plausible that DTMs within the muscle microenvironment could dictate the local expression of dystrophin. As disease progresses, both inflammation and dystrophin reduction could "spread" through the muscle, as patches of damaged muscle communicate through DAMPs to healthy areas, in turn activating inflammatory signaling, further reducing dystrophin levels, and causing muscle weakness. Interestingly, reduced levels of dystrophin have been reported in other muscle disorders in which dysregulated NF-κB signaling and chronic inflammation are present (67–69). Loss of dystrophin could provide a possible mechanism for muscle weakness in myositis which, to date, is not fully understood. It will be particularly important to study dystrophin deficiency in other muscle disorders, especially those characterized by high inflammation, to determine whether a secondary dystrophin deficiency could contribute to disease.

In this study, we have provided novel insights into the mechanisms driving muscle weakness and disease progression in myositis, using a murine model and human muscle biopsy tissue. Future work will be aimed at determining 1) whether the microRNAs described herein also play a role in other muscle/inflammatory disorders, and 2) whether these miRNAs could serve as therapeutic targets in muscle disease.

AUTHOR CONTRIBUTIONS

All authors were involved in drafting the article or revising it critically for important intellectual content, and all authors approved the final version to be published. Drs. Nagaraju and Fiorillo had full access to all of the data in the study and take responsibility for the integrity of the data and the accuracy of the data analysis.

Study conception and design. Kinder, Heier, Tully, Fiorillo.

Acquisition of data. Kinder, Heier, Tully, Van der Muelen, Fiorillo.

Analysis and interpretation of data. Kinder, Heier, Tully, Hoffman, Nagaraju, Fiorillo.

ADDITIONAL DISCLOSURE

Author Hoffman is the Treasurer, Secretary, and Vice President of Research of ReveraGen BioPharma as well as the President and CEO of AGADA Biosciences. Author Nagaraju is the President and CEO of ReveraGen BioPharma as well as the Founder and Vice President of AGADA Biosciences.

REFERENCES

1. Meyer A, Meyer N, Schaeffer M, Gottenberg JE, Geny B, Sibilia J. Incidence and prevalence of inflammatory myopathies: a systematic review. Rheumatology (Oxford) 2015;54:50–63.
2. Li CK, Knopp P, Moncrieffe H, Singh B, Shah S, Nagaraju K, et al. Overexpression of MHC class I heavy chain protein in young skeletal muscle leads to severe myositis: implications for juvenile myositis. Am J Pathol 2009;175:1030–40.
3. Nagaraju K, Casciola-Rosen L, Rosen A, Thompson C, Loeffler L, Parker T, et al. The inhibition of apoptosis in myositis and in normal muscle cells. J Immunol 2000;164:5459–65.
4. Dalakas MC. Inflammatory muscle diseases. N Engl J Med 2015; 373:393–4.
5. Karpati G, Pouliot Y, Carpenter S. Expression of immunoreactive major histocompatibility complex products in human skeletal muscles. Ann Neurol 1988;23:64–72.
6. Li CK, Varsani H, Holton JL, Gao B, Woo P, Wedderburn LR. MHC class I overexpression on muscles in early juvenile dermatomyositis. J Rheumatol 2004;31:605–9.

7. Coley W, Rayavarapu S, Nagaraju K. Role of non-immune mechanisms of muscle damage in idiopathic inflammatory myopathies [review]. Arthritis Res Ther 2012;14:209.
8. Rayavarapu S, Coley W, Kinder TB, Nagaraju K. Idiopathic inflammatory myopathies: pathogenic mechanisms of muscle weakness [review]. Skelet Muscle 2013;3:13.
9. Nyberg P, Wikman AL, Nennesmo I, Lundberg I. Increased expression of interleukin 1α and MHC class I in muscle tissue of patients with chronic, inactive polymyositis and dermatomyositis. J Rheumatol 2000;27:940–8.
10. Tournadre A, Lenief V, Miossec P. Expression of Toll-like receptor 3 and Toll-like receptor 7 in muscle is characteristic of inflammatory myopathy and is differentially regulated by Th1 and Th17 cytokines. Arthritis Rheum 2010;62:2144–51.
11. Cappelletti C, Baggi F, Zolezzi F, Biancolini D, Beretta O, Severa M, et al. Type I interferon and Toll-like receptor expression characterizes inflammatory myopathies. Neurology 2011;76:2079–88.
12. Kawai T, Akira S. The role of pattern-recognition receptors in innate immunity: update on Toll-like receptors. Nat Immunol 2010;11: 373–84.
13. Greenberg SA. Type 1 interferons and myositis [review]. Arthritis Res Ther 2010;12 Suppl 1:S4.
14. Wenzel J, Scheler M, Bieber T, Tüting T. Evidence for a role of type I interferons in the pathogenesis of dermatomyositis. Br J Dermatol 2005;153:462–3.
15. Greenberg SA, Pinkus JL, Pinkus GS, Burleson T, Sanoudou D, Tawil R, et al. Interferon-α/β-mediated innate immune mechanisms in dermatomyositis. Ann Neurol 2005;57:664–78.
16. De Paepe B. Interferons as components of the complex web of reactions sustaining inflammation in idiopathic inflammatory myopathies. Cytokine 2015;74:81–7.
17. Salajegheh M, Kong SW, Pinkus JL, Walsh RJ, Liao A, Nazareno R, et al. Interferon-stimulated gene 15 (ISG15) conjugates proteins in dermatomyositis muscle with perifascicular atrophy. Ann Neurol 2010;67:53–63.
18. Monici MC, Aguennouz M, Mazzeo A, Messina C, Vita G. Activation of nuclear factor-κB in inflammatory myopathies and Duchenne muscular dystrophy. Neurology 2003;60:993–7.
19. Lundberg I, Ulfgren AK, Nyberg P, Andersson U, Klareskog L. Cytokine production in muscle tissue of patients with idiopathic inflammatory myopathies. Arthritis Rheum 1997;40:865–74.
20. Vattemi G, Engel WK, McFerrin J, Askanas V. Endoplasmic reticulum stress and unfolded protein response in inclusion body myositis muscle. Am J Pathol 2004;164:1–7.
21. Alger HM, Raben N, Pistilli E, Francia DL, Rawat R, Getnet D, et al. The role of TRAIL in mediating autophagy in myositis skeletal muscle: a potential nonimmune mechanism of muscle damage. Arthritis Rheum 2011;63:3448–57.
22. Nagaraju K, Casciola-Rosen L, Lundberg I, Rawat R, Cutting S, Thapliyal R, et al. Activation of the endoplasmic reticulum stress response in autoimmune myositis: potential role in muscle fiber damage and dysfunction. Arthritis Rheum 2005;52:1824–35.
23. Lundberg I, Brengman JM, Engel AG. Analysis of cytokine expression in muscle in inflammatory myopathies, Duchenne dystrophy, and non-weak controls. J Neuroimmunol 1995;63:9–16.
24. Nirmalananthan N, Holton JL, Hanna MG. Is it really myositis? A consideration of the differential diagnosis. Curr Opin Rheumatol 2004;16:684–91.
25. Ng KP, Smith CR, Isenberg DA. Muscular dystrophy mimicking refractory idiopathic inflammatory myositis: a trio of cases [letter]. Rheumatology (Oxford) 2007;46:1618–9.
26. Henriques-Pons A, Yu Q, Rayavarapu S, Cohen TV, Ampong B, Cha HJ, et al. Role of Toll-like receptors in the pathogenesis of dystrophin-deficient skeletal and heart muscle. Hum Mol Genet 2014;23:2604–17.
27. Chen YW, Nagaraju K, Bakay M, McIntyre O, Rawat R, Shi R, et al. Early onset of inflammation and later involvement of TGFβ in Duchenne muscular dystrophy. Neurology 2005;65:826–34.
28. Appleyard ST, Dunn MJ, Dubowitz V, Rose ML. Increased expression of HLA ABC class I antigens by muscle fibres in Duchenne muscular dystrophy, inflammatory myopathy, and other neuromuscular disorders. Lancet 1985;1:361–3.
29. Fiorillo AA, Tully CB, Damsker JM, Nagaraju K, Hoffman EP, Heier CR. Muscle miRNAome shows suppression of chronic inflammatory miRNAs with both prednisone and vamorolone. Physiol Genomics 2018;50:735–45.
30. Fiorillo AA, Heier CR, Novak JS, Tully CB, Brown KJ, Uaesoontrachoon K, et al. TNF-α-induced microRNAs control dystrophin expression in Becker muscular dystrophy. Cell Rep 2015;12:1678–90.
31. Kawai T, Akira S. Signaling to NF-κB by Toll-like receptors. Trends Mol Med 2007;13:460–9.
32. Cappelletti C, Salerno F, Canioni E, Mora M, Mantegazza R, Bernasconi P, et al. Up-regulation of Toll-like receptors 7 and 9 and its potential implications in the pathogenic mechanisms of LMNA-related myopathies. Nucleus 2018;9:398–409.
33. Petes C, Odoardi N, Gee K. The toll for trafficking: Toll-like receptor 7 delivery to the endosome [review]. Front Immunol 2017;8: 1075.
34. Fabbri M, Paone A, Calore F, Galli R, Gaudio E, Santhanam R, et al. MicroRNAs bind to Toll-like receptors to induce prometastatic inflammatory response. Proc Natl Acad Sci U S A 2012;109: E2110–6.
35. Lehmann SM, Krüger C, Park B, Derkow K, Rosenberger K, Baumgart J, et al. An unconventional role for miRNA: let-7 activates Toll-like receptor 7 and causes neurodegeneration. Nat Neurosci 2012;15:827–35.
36. Wang J, Zhuang J, Iyer S, Lin X, Whitfield TW, Greven MC, et al. Sequence features and chromatin structure around the genomic regions bound by 119 human transcription factors. Genome Res 2012;22:1798–812.
37. Taganov KD, Boldin MP, Chang KJ, Baltimore D. NF-κB-dependent induction of microRNA miR-146, an inhibitor targeted to signaling proteins of innate immune responses. Proc Natl Acad Sci U S A 2006;103:12481–6.
38. Kumar V, Palermo R, Talora C, Campese AF, Checquolo S, Bellavia D, et al. Notch and NF-kB signaling pathways regulate miR-223/FBXW7 axis in T-cell acute lymphoblastic leukemia. Leukemia 2014;28:2324–35.
39. Yan S, Xu Z, Lou F, Zhang L, Ke F, Bai J, et al. NF-κB-induced microRNA-31 promotes epidermal hyperplasia by repressing protein phosphatase 6 in psoriasis. Nat Commun 2015;6:7652.
40. Emslie-Smith AM, Arahata K, Engel AG. Major histocompatibility complex class I antigen expression, immunolocalization of interferon subtypes, and T cell-mediated cytotoxicity in myopathies. Hum Pathol 1989;20:224–31.
41. Hoffman EP, Rao D, Pachman LM. Clarifying the boundaries between the inflammatory and dystrophic myopathies: insights from molecular diagnostics and microarrays. Rheum Dis Clin North Am 2002;28:743–57.
42. Yoon J, Kim SH, Ki CS, Kwon MJ, Lim MJ, Kwon SR, et al. Carrier woman of Duchenne muscular dystrophy mimicking inflammatory myositis. J Korean Med Sci 2011;26:587–91.
43. Sciorati C, Monno A, Doglio MG, Rigamonti E, Ascherman DP, Manfredi AA, et al. Exacerbation of murine experimental autoimmune myositis by Toll-like receptor 7/8. Arthritis Rheumatol 2018;70: 1276–87.

44. Rosenberg AS, Puig M, Nagaraju K, Hoffman EP, Villalta SA, Rao VA, et al. Immune-mediated pathology in Duchenne muscular dystrophy [review]. Sci Transl Med 2015;7:299rv4.
45. Sasai M, Linehan MM, Iwasaki A. Bifurcation of Toll-like receptor 9 signaling by adaptor protein 3. Science 2010;329:1530–4.
46. Nogalska A, D'Agostino C, Terracciano C, Engel WK, Askanas V. Impaired autophagy in sporadic inclusion-body myositis and in endoplasmic reticulum stress-provoked cultured human muscle fibers. Am J Pathol 2010;177:1377–87.
47. Criollo A, Chereau F, Malik SA, Niso-Santano M, Mariño G, Galluzzi L, et al. Autophagy is required for the activation of NFκB. Cell Cycle 2012;11:194–9.
48. Delgado MA, Deretic V. Toll-like receptors in control of immunological autophagy. Cell Death Differ 2009;16:976–83.
49. Delgado MA, Elmaoued RA, Davis AS, Kyei G, Deretic V. Toll-like receptors control autophagy. EMBO J 2008;27:1110–21.
50. Eisenberg I, Eran A, Nishino I, Moggio M, Lamperti C, Amato AA, et al. Distinctive patterns of microRNA expression in primary muscular disorders. Proc Natl Acad Sci U S A 2007;104: 17016–21.
51. Panguluri SK, Bhatnagar S, Kumar A, McCarthy JJ, Srivastava AK, Cooper NG, et al. Genomic profiling of messenger RNAs and microRNAs reveals potential mechanisms of TWEAK-induced skeletal muscle wasting in mice. PloS One 2010;5:e8760.
52. Olivieri F, Lazzarini R, Recchioni R, Marcheselli F, Rippo MR, Di Nuzzo S, et al. MiR-146a as marker of senescence-associated pro-inflammatory status in cells involved in vascular remodelling. Age (Dordr) 2013;35:1157–72.
53. Lu J, Yan M, Wang Y, Zhang J, Yang H, Tian FF, et al. Altered expression of miR-146a in myasthenia gravis. Neurosci Lett 2013;555: 85–90.
54. Vasa-Nicotera M, Chen H, Tucci P, Yang AL, Saintigny G, Menghini R, et al. MiR-146a is modulated in human endothelial cell with aging. Atherosclerosis 2011;217:326–30.
55. Lukiw WJ. Micro-RNA speciation in fetal, adult and Alzheimer's disease hippocampus. Neuroreport 2007;18:297–300.
56. Ma X, Zhou J, Zhong Y, Jiang L, Mu P, Li Y, et al. Expression, regulation and function of microRNAs in multiple sclerosis. Int J Med Sci 2014;11:810–8.
57. Heier CR, Fiorillo AA, Chaisson E, Gordish-Dressman H, Hathout Y, Damsker JM, et al. Identification of pathway-specific serum biomarkers of response to glucocorticoid and infliximab treatment in children with inflammatory bowel disease. Clin Transl Gastroenterol 2016;7:e192.
58. Shi C, Zhu L, Chen X, Gu N, Chen L, Zhu L, et al. IL-6 and TNF-α induced obesity-related inflammatory response through transcriptional regulation of miR-146b. J Interferon Cytokine Res 2014;34:342–8.
59. Fordham JB, Naqvi AR, Nares S. Regulation of miR-24, miR-30b, and miR-142-3p during macrophage and dendritic cell differentiation potentiates innate immunity. J Leukoc Biol 2015;98:195–207.
60. Kramer NJ, Wang WL, Reyes EY, Kumar B, Chen CC, Ramakrishna C, et al. Altered lymphopoiesis and immunodeficiency in miR-142 null mice. Blood 2015;125:3720–30.
61. Israeli D, Poupiot J, Amor F, Charton K, Lostal W, Jeanson-Leh L, et al. Circulating miRNAs are generic and versatile therapeutic monitoring biomarkers in muscular dystrophies. Sci Rep 2016;6:28097.
62. Greco S, De Simone M, Colussi C, Zaccagnini G, Fasanaro P, Pescatori M, et al. Common micro-RNA signature in skeletal muscle damage and regeneration induced by Duchenne muscular dystrophy and acute ischemia. FASEB J 2009;23:3335–46.
63. Roberts TC, Blomberg KE, McClorey G, El Andaloussi S, Godfrey C, Betts C, et al. Expression analysis in multiple muscle groups and serum reveals complexity in the microRNA transcriptome of the mdx mouse with implications for therapy. Mol Ther Nucleic Acids 2012;1:e39.
64. Roberts TC, Coenen-Stass AM, Wood MJ. Assessment of RT-qPCR normalization strategies for accurate quantification of extracellular microRNAs in murine serum. PloS One 2014;9:e89237.
65. Cacchiarelli D, Incitti T, Martone J, Cesana M, Cazzella V, Santini T, et al. MiR-31 modulates dystrophin expression: new implications for Duchenne muscular dystrophy therapy. EMBO Rep 2011;12:136–41.
66. Sewry CA, Clerk A, Heckmatt JZ, Vyse T, Dubowitz V, Strong PN. Dystrophin abnormalities in polymyositis and dermatomyositis. Neuromuscul Disord 1991;1:333–9.
67. Voit T, Stuettgen P, Cremer M, Goebel HH. Dystrophin as a diagnostic marker in Duchenne and Becker muscular dystrophy: correlation of immunofluorescence and western blot. Neuropediatrics 1991;22:152–62.
68. Acharyya S, Butchbach ME, Sahenk Z, Wang H, Saji M, Carathers M, et al. Dystrophin glycoprotein complex dysfunction: a regulatory link between muscular dystrophy and cancer cachexia. Cancer Cell 2005;8:421–32.
69. Vainzof M, Passos-Bueno MR, Canovas M, Moreira ES, Pavanello RC, Marie SK, et al. The sarcoglycan complex in the six autosomal recessive limb-girdle muscular dystrophies. Hum Mol Genet 1996;5:1963–9.

American College of Rheumatology
Empowering Rheumatology Professionals

Arthritis & Rheumatology
Vol. 72, No. 7, July 2020, pp 1184–1191
DOI 10.1002/art.41219

Do Serum Urate–Associated Genetic Variants Differentially Contribute to Gout Risk According to Body Mass Index? Analysis of the UK Biobank

Vicky Tai,[1] Ravi K. Narang,[1] Greg Gamble,[1] Murray Cadzow,[2] Lisa K. Stamp,[3] Tony R. Merriman,[2] and Nicola Dalbeth[1]

Objective. To examine whether urate-associated genetic variants differ in their influence on gout risk according to body mass index (BMI).

Methods. This research was conducted using the UK Biobank Resource (n = 358,728). Participants were divided into 3 groups: BMI <25 kg/m^2 (low/normal), BMI ≥25 kg/m^2–<30 kg/m^2 (overweight), and BMI ≥30 kg/m^2 (obese). Gene–BMI interactions for gout association were tested by logistic regression using a urate genetic risk score (GRS).

Results. Compared to participants with a GRS less than the mean, the prevalence of gout was higher in those with a GRS greater than or equal to the mean in the low/normal BMI group (0.27% versus 0.77%), in the overweight BMI group (1.02% versus 3.02%), and in the obese BMI group (2.49% versus 6.23%). A GRS greater than or equal to the mean was positively associated with gout compared to a GRS less than the mean in the low/normal BMI group (odds ratio [OR] 2.89 [95% confidence interval (95% CI) 2.42–3.47]), in the overweight BMI group (OR 3.09 [95% CI 2.84–3.36]), and in the obese BMI group (OR 2.65 [95% CI 2.46–2.86]). There was a mildly attenuated effect of the GRS on gout risk in the obese BMI group compared to the overweight BMI group, but no difference in the effect of the GRS between the low/normal BMI and overweight BMI groups, nor between the low/normal BMI and obese BMI groups.

Conclusion. The association of a urate GRS with gout is mildly attenuated in obese individuals compared to overweight individuals. However, genetic variants have a strong effect on gout risk in those with overweight and obese BMIs, with an effect similar to that observed in low/normal BMI.

INTRODUCTION

Several large prospective studies, including the Health Professionals Follow-Up Study, the Framingham Heart Study, and the Atherosclerosis Risk in Communities Study, have demonstrated an association between body mass index (BMI) and risk of incident gout. This has been observed in both men and women and in studies conducted across Europe, Asia, and the US (1–10). The association between high BMI and gout may be mediated through multiple factors. High BMI is associated with other established risk factors for gout, such as metabolic syndrome, purine-rich diets, sugar-sweetened beverages, alcohol consumption, renal disease, and the use of diuretics and antihypertensive drugs (11–14). Obesity is also associated with hyperuricemia, a key step in the pathogenesis of gout (15–17). High BMI may contribute to the presentation of gout by promoting an inflammatory response to deposited monosodium urate crystals (18), potentially through the effects of adipokines such as leptin (19).

The importance of genetic factors in the development of hyperuricemia and gout has been uncovered in the past decade. Genome-wide association studies (GWAS) have identified many single-nucleotide polymorphisms (SNPs) associated with serum urate levels, some of which are also associated with gout. Many of the identified loci include genes encoding renal and gut urate

Supported by the Health Research Council of New Zealand (grant 14-527).

[1]Vicky Tai, MBChB, Ravi K. Narang, MBChB, Greg Gamble, MSc, Nicola Dalbeth, MD, FRACP: University of Auckland, Auckland, New Zealand; [2]Murray Cadzow, PhD, Tony R. Merriman, PhD: University of Otago, Dunedin, New Zealand; [3]Lisa K. Stamp, PhD: University of Otago, Christchurch, New Zealand.

Dr. Merriman has received consulting fees from Ardea Biosciences and AstraZeneca (less than $10,000 each) and research support from those companies. Dr. Dalbeth has received consulting fees, speaking fees, and/or honoraria from Hengrui, Selecta, Arthrosi, AstraZeneca, Horizon, Dyve Biosciences, AbbVie, and Janssen (less than $10,000 each) and research support from those companies. No other disclosures relevant to this article were reported.

Address correspondence to Nicola Dalbeth, MD, FRACP, Department of Medicine, Faculty of Medical and Health Sciences, University of Auckland, 85 Park Road, Grafton, Auckland 1023, New Zealand. E-mail: n.dalbeth@auckland.ac.nz.

Submitted for publication August 18, 2019; accepted in revised form January 28, 2020.

transporters. Among these, *SLC2A9* and *ABCG2* have the strongest effect on serum urate (20) and gout risk (21).

Although some studies have investigated interactions between BMI and genetic variants on serum urate concentrations and gout (22–25), it is currently unclear whether serum urate–associated genetic variants differentially contribute to gout risk according to BMI. The aim of the present study was to systematically examine whether serum urate–associated genetic variants differ in their influence on gout risk according to BMI.

SUBJECTS AND METHODS

Study population and BMI category classification. This research was conducted using the UK Biobank Resource (approval no. 12611). Participants of European ancestry ages 40–69 years, with genome-wide genotypes, were included in this study. Exclusion criteria included mismatch between self-reported sex and genetic sex, genotyping quality control failure, and subjects who are related. Gout was identified using a validated definition of the following: self-report of gout or urate-lowering therapy use (includes allopurinol, febuxostat, sulphinpyrazone), and with no hospital diagnosis of leukemia or lymphoma based on the International Classification of Diseases, Tenth Revision codes C81–C96 (26). For participants who did not fulfill the gout definition, exclusion criteria included prescriptions for glucocorticoids, nonsteroidal antiinflammatory drugs (NSAIDs), or probenecid, as previously defined (26). Medication use, comorbidities, alcohol intake, and smoking status data were collected via self-report. BMI was analyzed according to 3 categories, as recommended by the US Centers for Disease Control and Prevention: <25 kg/m^2 (low/normal), ≥25 kg/m^2–<30 kg/m^2 (overweight), and ≥30 kg/m^2 (obese) (27).

Genotyping analysis. UK Biobank samples were genotyped using an Axiom array (820,967 markers; Affymetrix) and imputed to ~73.3 million SNPs using SHAPEIT3 and IMPUTE2 with a combined UK10K and 1000 Genomes Project reference panel. We analyzed the 30 serum urate–associated SNPs that were reported by Kottgen et al (20) in the large (>140,000 European participants) Global Urate Genetics Consortium GWAS.

Genetic risk score. A weighted urate genetic risk score (GRS) from this UK Biobank data set was calculated to model the cumulative effects of a subject's risk for gout for the 30 variants. For each of the 30 serum urate–associated SNPs, allelic odds ratios (ORs) were calculated to determine the risk of gout, adjusting for age and sex. For GRS modeling, we used the associated urate-raising allele so that the OR for gout was >1 for all serum urate–associated SNPs. ORs were converted into a logarithmic value and for each subject, these logarithmic values were multiplied by the number of urate-raising alleles and summed to yield a weighted GRS. Higher scores indicate a greater genetic predisposition for gout.

Study power. Power calculations were performed using Quanto version 1.2.4 (University of Southern California) and PASS 16 Power Analysis and Sample Size Software (NCSS). The power to detect an association with gout in the overweight BMI and obese BMI groups (compared to the low/normal BMI group) at $P < 0.05$ was calculated based on previously reported association data between BMI and gout (5). The power was >99.9% for both BMI groups. Similarly, the power to detect an association between GRS and gout for each BMI group was >99.9% in all 3 BMI groups.

The power to detect an association between individual serum urate–associated SNPs and gout was calculated at $P < 0.0017$ with Bonferroni correction for multiple testing, based on previously reported association data between serum urate–associated SNPs and gout (28). The power was >80% for 4 SNPs in the low/normal BMI group and 18 SNPs each in the overweight and obese BMI groups (Supplementary Table 1, on the *Arthritis & Rheumatology* web site at http://onlinelibrary.wiley.com/doi/10.1002/art.41219/abstract). In all BMI groups, the power was >99.0% for *ABCG2* (rs2231142), *SLC2A9* (rs12498742), and *GCKR* (rs1260326).

Power calculations for the categorical GRS–BMI interaction analysis were determined at $P < 0.05$ for a range of presumed interaction effects (ORs 2.00–10.00). These were calculated post hoc, using association data generated from this analysis of GRS with gout and of BMI with gout. The power was >99.9% for all presumed interaction effects.

Statistical analysis. Data were analyzed using IBM SPSS Statistics 25 software. Baseline characteristics according to BMI group were summarized using standard descriptive statistics including the mean ± SD for continuous variables as well as number and percent for categorical variables, and were compared using one-way analysis of variance or Pearson's chi-square test, as appropriate. Logistic regression of BMI group and GRS group with gout as the dependent variable were performed in an unadjusted model, a partially adjusted model (adjusting for age, sex, diuretic use, and renal failure), and a fully adjusted model (adjusting for age, sex, diuretic use, renal failure, diabetes mellitus, hypertension, hypercholesterolemia, alcohol intake, and smoking status). Gene–BMI interactions for gout association were performed in order to examine whether the effect of genetic factors on gout differed according to BMI group. These were assessed using logistic regression models that included a GRS by BMI interaction term.

In the main analysis, the interaction model was calculated with the GRS categorized into 2 groups (less than the GRS mean or greater than or equal to the GRS mean), consistent with previous urate-related gene–environment interaction analyses, such as those performed by McAdams-DeMarco et al (29) and Bao et al (30). In addition, the interaction model was repeated with the GRS categorized into tertiles (upper, middle, and lower) and as a continuous variable. Huffman et al (24) have previously reported an attenuated effect of *ABCG2* on serum urate levels in obese men compared to lean men. Thus, a sensitivity analysis for the GRS–BMI interac-

Table 1. Participant characteristics according to BMI category*

	BMI <25 kg/m^2 (n = 122,493)		BMI ≥25–<30 kg/m^2 (n = 153,563)		BMI ≥30 kg/m^2 (n = 82,672)	
	Control (n = 121,859; 99.5%)†	Gout (n = 634; 0.5%)	Control (n = 150,463; 98.0%)†	Gout (n = 3,100; 2.0%)	Control (n = 79,095; 95.7%)†	Gout (n = 3,577; 4.3%)
Age, mean ± SD years	56.1 ± 8.1	60.5 ± 6.8	57.4 ± 7.9	60.2 ± 7.0	57.2 ± 7.7	59.7 ± 6.8
Male sex	43,475 (35.7)	563 (88.8)	81,863 (54.4)	2,940 (94.8)	39,025 (49.3)	3,237 (90.5)
Diuretic use‡	4,706 (3.9)	68 (10.7)	11,668 (7.8)	354 (11.4)	12,190 (15.4)	776 (21.7)
Comorbidities‡						
Hypercholesterolemia	8,606 (10.7)	145 (23.1)	19,899 (18.0)	793 (25.8)	14,268 (21.9)	1,112 (31.2)
Hypertension	17,580 (21.9)	263 (41.9)	38,901 (35.3)	1,513 (49.2)	32,731 (50.1)	2,363 (66.4)
PVD	301 (0.4)	4 (0.6)	199 (0.2)	4 (0.1)	111 (0.2)	2 (0.1)
Angina	1,827 (2.3)	44 (7.0)	4,973 (4.5)	218 (7.1)	4,405 (6.7)	397 (11.1)
Myocardial infarction	1,406 (1.7)	49 (7.8)	3,746 (3.4)	163 (5.3)	3,058 (4.7)	305 (8.6)
Heart failure	41 (0.1)	2 (0.3)	76 (0.1)	15 (0.5)	75 (0.1)	27 (0.8)
Arrhythmia	625 (0.8)	5 (0.8)	817 (0.7)	27 (0.9)	503 (0.8)	39 (1.1)
Stroke	1,052 (1.3)	21 (3.3)	2,014 (1.8)	75 (2.4)	1,595 (2.4)	154 (4.3)
TIA	354 (0.4)	6 (1.0)	584 (0.5)	25 (0.8)	399 (0.6)	28 (0.8)
Renal failure	123 (0.2)	19 (3.0)	181 (0.2)	43 (1.4)	130 (0.2)	46 (1.3)
Diabetes mellitus	1,536 (1.9)	27 (4.3)	4,689 (4.3)	229 (7.4)	7,293 (11.2)	602 (16.9)
Smoking status‡						
Most days	10,375 (8.5)	64 (10.1)	10,692 (7.1)	198 (6.4)	5,403 (6.8)	168 (4.7)
Occasionally	2,893 (2.4)	24 (3.8)	4,166 (2.8)	110 (3.6)	2,058 (2.6)	91 (2.5)
Never	108,523 (89.1)	545 (86.1)	135,524 (90.1)	2,788 (90.1)	71,598 (90.6)	3,318 (92.8)
Alcohol frequency‡						
Daily/almost daily	28,325 (23.3)	265 (41.8)	33,176 (22.1)	1,188 (38.4)	12,621 (16.0)	1,017 (28.5)
3 or 4 times/week	31,027 (25.5)	169 (26.7)	38,225 (25.4)	911 (29.4)	15,766 (19.9)	939 (26.3)
1 or 2 times/week	31,234 (25.6)	101 (15.9)	40,332 (26.8)	673 (21.7)	21,328 (27.0)	883 (24.7)
Infrequent§	23,593 (19.4)	67 (10.6)	29,836 (19.8)	231 (7.5)	22,445 (28.4)	534 (14.9)
Never	7,596 (6.2)	32 (5.0)	8,806 (5.9)	92 (3.0)	6,877 (8.7)	201 (5.6)

* Except where indicated otherwise, values are the number (%) of participants. BMI = body mass index; PVD = peripheral vascular disease; TIA = transient ischemic attack.
† Participants taking probenecid (n = 2), nonsteroidal antiinflammatory drugs (n = 72,288), and prednisone (n = 5,693) were excluded from the control group.
‡ Data on medication use, comorbidity data, smoking status, and alcohol frequency were collected via self-report.
§ Defined as 1–3 times per month or special occasions only.

tion for gout was performed excluding *ABCG2* from the weighted GRS. Association analyses of the serum urate–associated SNPs with gout were calculated based on the presence or absence of the serum urate effect allele. Age, sex, diuretic use, renal failure, diabetes mellitus, hypertension, hypercholesterolemia, alcohol intake, and smoking status were included as variables in all interaction analyses. Where multiple testing was used in the individual SNP analysis, data were reported using experiment-wide significance ($P < 0.0017$).

RESULTS

Clinical features of participants. Data including genome-wide genotypes were available for 358,728 participants. There were 122,493 participants (34.1%) in the low/normal BMI group (1,932 of whom had a BMI <18.5 kg/m^2), 153,563 participants (42.8%) in the overweight BMI group, and 82,672 participants (23.0%) in the obese BMI group. Overall, there were 7,311 participants (2.0%) with gout. Gout was present in 634 subjects (0.5%) in the low/normal BMI group, 3,100 (2.0%) in the overweight BMI group, and 3,577 (4.3%) in the obese BMI group.

Clinical characteristics of subjects according to BMI group are shown in Table 1. In patients with gout, those with a higher BMI had a higher prevalence of diuretic use (10.7% in the low/normal BMI group, 11.4% in the overweight BMI group, and 21.7% in the obese BMI group; $P = 4.87 \times 10^{-32}$). They also had a higher prevalence of comorbidities including diabetes mellitus (4.3% in the low/normal BMI group, 7.4% in the overweight BMI group, and 16.9% in the obese BMI group; $P = 1.19 \times 10^{-39}$), hypertension (41.9%, 49.2%, and 66.4%, respectively; $P = 7.69 \times 10^{-58}$), and hypercholesterolemia (21.3%, 25.8%, and 31.2%, respectively; $P = 6.07 \times 10^{-8}$). Participants receiving NSAIDs (n = 72,288) were excluded from the control group. The baseline characteristics for participants without gout receiving NSAIDs and those not receiving NSAIDs were similar.

Association between BMI and gout. Supplementary Table 2 (http://onlinelibrary.wiley.com/doi/10.1002/art.41219/abstract) shows unadjusted and adjusted ORs for prevalent gout according to BMI group. Compared to the low/normal BMI group, the unadjusted OR for gout was 3.96 (95% confidence interval [95% CI] 3.63–4.31) in the overweight BMI group, and 8.69 (95% CI 7.98–9.46) in the obese BMI group. In the partially and fully adjusted models, the association with gout was attenuated but still significant in the overweight BMI group (partially adjusted model: OR 2.46 [95% CI 2.26–2.69]; fully adjusted model: OR 2.33 [95% CI 2.14–2.55]) and in the obese BMI group (partially adjusted model: OR 5.25 [95% CI 4.82–5.73]; fully adjusted model: OR 4.91 [95% CI 4.50–5.37]) (Supplementary Table 2).

Association between GRS and gout. The distribution of the GRS in the entire study population followed a normal distribution, and this was observed in each BMI group (Supplementary Figure 1, http://onlinelibrary.wiley.com/doi/10.1002/art.41219/abstract). The mean ± SD GRS for all participants was 1.65 ± 0.27. In the entire data set, 177,352 participants (49.4%) had a GRS greater than or equal to the mean. Compared to participants without gout, the mean GRS was significantly higher in participants with gout (mean ± SD 1.65 ± 0.27 versus mean ± SD 1.81 ± 0.27); $P < 1 \times 10^{-300}$).

Table 2. Mean GRS for gout according to BMI category*

	GRS		
	Control	Gout	*P*
Low/normal BMI (<25 kg/m^2)	1.65 ± 0.27	1.82 ± 0.29	2.45×10^{-60}
Overweight BMI (≥25–<30 kg/m^2)	1.65 ± 0.27	1.83 ± 0.27	$<1 \times 10^{-300}$
Obese BMI (≥30 kg/m^2)	1.64 ± 0.27	1.80 ± 0.27	6.43×10^{-261}

* Values are the mean ± SD. GRS = genetic risk score; BMI = body mass index.

Unadjusted and adjusted ORs for prevalent gout according to GRS category are shown in Supplementary Table 3 (http://onlinelibrary.wiley.com/doi/10.1002/art.41219/abstract). Compared to participants with a GRS less than the mean, the unadjusted OR for gout was 2.74 (95% CI 2.60–2.89) in participants with a GRS greater than or equal to the mean. A significant association persisted in the partially adjusted model (OR 2.78 [95% CI 2.64–2.93]) and the fully adjusted model (OR 2.80 [95% CI 2.66–2.96]) (Supplementary Table 3).

Association between GRS and gout, according to BMI group. When participants were analyzed according to BMI group, the mean GRS was significantly higher in those with gout compared to those without gout in all BMI groups (Table 2). Data on the prevalence of gout according to GRS category and BMI group are shown

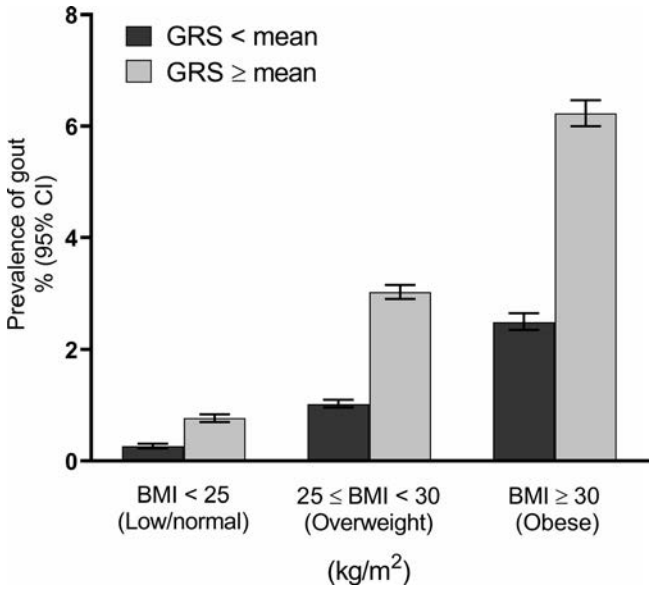

Figure 1. Prevalence of gout according to genetic risk score (GRS) and body mass index (BMI) categories. 95% CI = 95% confidence interval.

Table 3. Association and interaction between GRS category and BMI category for gout*

	OR for gout if GRS < mean†	OR (95% CI) for gout if GRS ≥ mean†	*P*
Low/normal BMI (<25 kg/m^2)‡	1 (referent)	2.89 (2.42–3.47)	7.48×10^{-31}
Overweight BMI (≥25–<30 kg/m^2)‡	1 (referent)	3.09 (2.84–3.36)	1.35×10^{-156}
Obese BMI (≥30 kg/m^2)‡	1 (referent)	2.65 (2.46–2.86)	5.77×10^{-142}

* Pairwise interaction comparisons as follows: low/normal BMI versus overweight BMI, *P* = 0.47; low/normal BMI versus obese BMI, *P* = 0.48; overweight BMI versus obese BMI, *P* = 0.01. OR = odds ratio; 95% CI = 95% confidence interval (see Table 2 for other definitions).
† GRS categorized according to the mean GRS for the entire study population (1.65). Data were adjusted for age, sex, diuretic use, renal failure, diabetes mellitus, hypertension, hypercholesterolemia, alcohol intake, and smoking status.
‡ *P* for interaction among the 3 BMI categories = 0.046, calculated using a GRS by BMI interaction term.

in Figure 1. Compared to participants with a GRS less than the mean, the prevalence of gout was higher in those with a GRS greater than or equal to the mean in the low/normal BMI group (0.27% [95% CI 0.23–0.31%] versus 0.77% [95% CI 0.70–0.84%]), in the overweight BMI group (1.02% [95% CI 0.96–1.10%] versus 3.02% [95% CI 2.90–3.15%]), and in the obese BMI group (2.49% [95% CI 2.35–2.65%] versus 6.23% [95% CI 6.00–6.47%]) (Figure 1).

The association between GRS category and gout according to BMI group is shown in Table 3. A GRS greater than or equal to the mean was positively associated with gout, compared to a GRS less than the mean in the low/normal BMI group (OR 2.89 [95% CI 2.42–3.47]; $P = 7.48 \times 10^{-31}$), in the overweight BMI group (OR 3.09 [95% CI 2.84–3.36]; $P = 1.35 \times 10^{-156}$), and in the obese BMI group (OR 2.65 [95% CI 2.46–2.86]; $P = 5.77 \times 10^{-142}$).

A non-additive GRS–BMI interaction was observed when the GRS was categorized according to the mean. To further investigate the interaction, we compared groups using pairwise comparisons. This demonstrated that there was a mildly attenuated effect of GRS greater than or equal to the mean on gout risk in the obese BMI group compared to the overweight BMI group (*P* for interaction = 0.01), but no GRS–BMI interactions were observed for comparisons between the low/normal and overweight BMI groups (*P* for interaction = 0.47), nor between the low/normal and obese BMI groups (*P* for interaction = 0.48) (Table 3).

When the analysis was repeated using GRS tertiles, a GRS in the middle and upper tertiles was positively associated with gout compared to a GRS in the lower tertile in the low/normal, overweight, and obese BMI groups (Supplementary Table 4, http://onlinelibrary.wiley.com/doi/10.1002/art.41219/abstract). No significant GRS–BMI interaction was observed when the GRS was categorized according to tertiles (*P* for interaction = 0.20), nor when performing pairwise interaction comparisons (Supplementary Table 4).

When the GRS was analyzed as a continuous variable, a non-additive GRS–BMI interaction was observed (*P* = 0.04) (Figure 2). When performing pairwise interaction comparisons, a significant interaction was observed between the overweight BMI group and the obese BMI group (*P* for interaction = 0.01); however, no significant GRS–BMI interaction was observed for comparisons between the low/normal and overweight BMI groups (*P* for interaction = 0.26), nor between the low/normal and obese BMI groups (*P* for interaction = 0.73). In the sensitivity analysis, after excluding *ABCG2* from GRS modeling, no significant GRS–BMI interaction was observed with GRS categorized according to the mean (*P* for interaction = 0.20) (Supplementary Table 5, http://onlinelibrary.wiley.com/doi/10.1002/art.41219/abstract), suggesting that *ABCG2* drove the statistical interaction.

Association between serum urate–associated SNPs and gout, according to BMI group. Genotype distribution of the serum urate–associated SNPs according to BMI group is shown in Supplementary Table 6 (http://onlinelibrary.wiley.com/doi/10.1002/art.41219/abstract). Experiment-wide association of gout was observed for *ABCG2* (rs2231142), *SLC2A9* (rs12498742), *GCKR* (rs1260326), and *INHBE* (rs3741414) in all BMI groups (Table 4). In total, experiment-wide significance was achieved for 4 SNPs in the low/normal BMI group, 18 SNPs in the overweight BMI group, and 11 SNPs in the obese BMI group. The *ABCG2* and *SLC2A9* effect alleles exerted the highest ORs for gout in participants in all BMI groups, with similar ORs and overlapping confidence intervals. No non-additive SNP–BMI interactions were observed (Table 4).

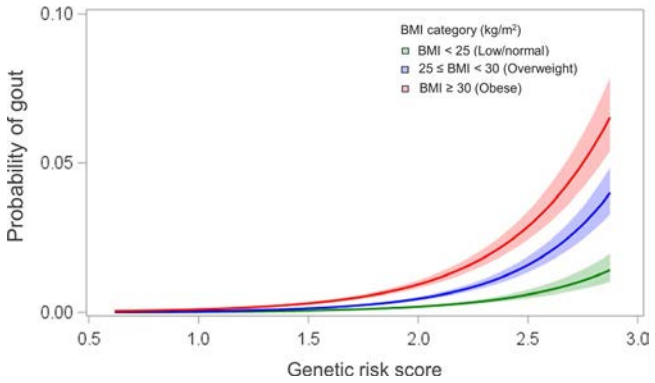

Figure 2. Probability of gout according to GRS and BMI category. GRS is shown as a continuous variable. Data are adjusted for age, sex, diuretic use, renal failure, diabetes mellitus, hypertension, hypercholesterolemia, alcohol intake, and smoking status. *P* = 0.04 for GRS–BMI interaction. See Figure 1 for definitions.

Table 4. Association and interaction of serum urate–associated SNPs with gout according to BMI category*

Locus, SNP (effect allele)	Odds ratio for gout (95% confidence interval)					
	Low/normal BMI (<25 kg/m^2) (n = 122,493)	*P*	Overweight BMI (≥25–<30 kg/m^2) (n = 153,563)	*P*	Obese BMI (≥30 kg/m^2) (n = 82,672)	*P*
ABCG2, rs2231142 (T)	2.28 (1.93–2.69)	7.21×10^{-23}	2.42 (2.24–2.61)	1.56×10^{-115}	2.22 (2.06–2.39)	8.93×10^{-99}
SLC2A9, rs12498742 (A)	3.52 (1.88–6.60)	8.54×10^{-5}	3.13 (2.40–4.07)	1.94×10^{-17}	2.95 (2.33–3.75)	5.28×10^{-19}
GCKR, rs1260326 (T)	1.37 (1.15–1.63)	4.76×10^{-4}	1.43 (1.32–1.55)	1.47×10^{-18}	1.35 (1.26–1.46)	2.15×10^{-15}
SLC17A3, rs1165151 (T)	0.81 (0.68–0.96)	0.01	0.84 (0.78–0.91)	1.70×10^{-5}	0.78 (0.72–0.84)	1.11×10^{-11}
SLC22A12, rs478607 (A)	0.67 (0.44–1.04)	0.08	0.73 (0.59–0.91)	0.01	0.81 (0.65–1.01)	0.06
PDZK1, rs1471633 (A)	1.32 (1.09–1.59)	3.74×10^{-3}	1.28 (1.18–1.39)	1.25×10^{-8}	1.21 (1.12–1.31)	1.98×10^{-6}
INHBE, rs3741414 (T)	0.76 (0.64–0.90)	1.12×10^{-3}	0.81 (0.75–0.88)	6.98×10^{-8}	0.84 (0.78–0.90)	8.91×10^{-7}
SLC16A9, rs1171614 (T)	0.86 (0.73–1.01)	0.06	0.77 (0.71–0.83)	3.07×10^{-11}	0.87 (0.81–0.94)	2.43×10^{-4}
SLC22A11, rs2078267 (T)	0.95 (0.78–1.15)	0.60	0.71 (0.65–0.77)	4.56×10^{-16}	0.81 (0.75–0.88)	3.48×10^{-7}
RREB1, rs675209 (T)	1.09 (0.93–1.27)	0.30	1.13 (1.05–1.21)	1.13×10^{-3}	1.08 (1.01–1.16)	0.03
PKLR, rs11264341 (T)	0.85 (0.72–1.00)	0.05	0.86 (0.80–0.93)	8.17×10^{-5}	0.85 (0.79–0.91)	5.11×10^{-6}
INHBB, rs17050272 (A)	0.99 (0.84–1.17)	0.94	1.06 (0.98–1.14)	0.16	1.00 (0.93–1.08)	0.98
ACVR2A, rs2307394 (T)	0.95 (0.72–1.24)	0.70	0.85 (0.76–0.96)	0.01	0.96 (0.86–1.08)	0.53
MUSTN1, rs6770152 (T)	0.89 (0.73–1.09)	0.27	0.81 (0.74–0.89)	4.36×10^{-6}	0.86 (0.79–0.94)	6.76×10^{-4}
TMEM171, rs17632159 (C)	0.86 (0.73–1.01)	0.07	0.83 (0.78–0.90)	1.29×10^{-6}	0.90 (0.84–0.96)	2.41×10^{-3}
VEGFA, rs729761 (T)	1.02 (0.87–1.21)	0.77	0.92 (0.85–0.99)	0.03	0.95 (0.89–1.02)	0.20
MLXIPL, rs1178977 (A)	1.43 (0.86–2.35)	0.17	1.19 (0.97–1.46)	0.09	1.33 (1.09–1.62)	0.01
PRKAG2, rs10480300 (T)	1.00 (0.85–1.17)	0.99	1.13 (1.05–1.22)	7.46×10^{-4}	1.06 (0.98–1.13)	0.13
STC1, rs17786744 (A)	0.96 (0.77–1.18)	0.69	1.08 (0.97–1.19)	0.16	1.00 (0.92–1.10)	0.92
HNF4G, rs2941484 (T)	1.00 (0.84–1.20)	0.96	1.08 (1.00–1.17)	0.06	1.05 (0.97–1.14)	0.19
ASAH2, rs10821905 (A)	1.24 (1.05–1.46)	0.01	1.09 (1.01–1.18)	0.03	1.13 (1.05–1.21)	1.58×10^{-3}
LTBP3, rs642803 (T)	1.00 (0.84–1.19)	0.99	0.87 (0.80–0.94)	5.48×10^{-4}	0.91 (0.85–0.99)	0.02
PTPN11, rs653178 (T)	0.87 (0.72–1.04)	0.11	0.83 (0.77–0.90)	1.27×10^{-5}	0.95 (0.88–1.03)	0.24
NRG4, rs1394125 (A)	1.07 (0.91–1.26)	0.44	1.08 (1.01–1.17)	0.03	1.08 (1.00–1.16)	0.04
IGF1R, rs6598541 (A)	1.10 (0.94–1.30)	0.23	1.13 (1.05–1.22)	1.33×10^{-3}	1.08 (1.00–1.15)	0.05
NFAT5, rs7193778 (T)	0.64 (0.40–1.02)	0.06	0.68 (0.55–0.85)	4.90×10^{-4}	0.94 (0.75–1.17)	0.56
MAF, rs7188445 (A)	0.88 (0.75–1.03)	0.11	0.92 (0.86–0.99)	0.03	0.98 (0.91–1.05)	0.52
HLF, rs7224610 (A)	0.78 (0.63–0.96)	0.02	0.85 (0.77–0.94)	1.10×10^{-3}	0.94 (0.86–1.04)	0.23
C17ORF82, rs2079742 (T)	0.66 (0.40–1.10)	0.11	1.23 (0.91–1.68)	0.18	1.24 (0.93–1.64)	0.14
PRPSAP1, rs164009 (A)	1.16 (0.92–1.47)	0.21	1.07 (0.96–1.18)	0.23	0.97 (0.88–1.07)	0.58

* Odds ratios for gout were calculated with absence of effect allele as the referent group. Data were adjusted for age, sex, diuretic use, renal failure, diabetes mellitus, hypertension, hypercholesterolemia, alcohol intake, and smoking status. Experiment-wide significance is $P < 0.0017$. There were no significant *P* values for single-nucleotide polymorphism (SNP)–body mass index (BMI) interactions.

DISCUSSION

In this large cohort of subjects of European ancestry, we have shown that a higher urate GRS is associated with increased odds of gout in individuals across all BMI groups. This effect is slightly attenuated in obese people compared to overweight people. However, genetic variants have a strong effect on gout risk in those with overweight and obese BMIs, with an effect similar to that observed in low/normal BMIs.

The major finding of our study is that genetic susceptibility significantly contributes to gout risk across all BMI categories. As expected, in the GRS analysis, participants with gout had a higher GRS compared to those without gout. This association was observed across all BMI groups. In addition, a GRS greater than or equal to the mean was significantly associated with gout across all BMI groups, with similar ORs and overlapping 95% CIs. The individual serum urate–associated SNP analysis also demonstrated a similar strength of association of gout across the 3 BMI groups, and experiment-wide significance of gout association was observed for *ABCG2*, *SLC2A9*, *GCKR*, and *INHBE* in all BMI groups. Compared to the overweight and obese BMI groups, fewer SNPs reached experiment-wide significance in the low/normal BMI group; this may be due to less power to detect an association or due to the lower prevalence of gout in the low/normal BMI group. Consistent with previous studies, *ABCG2* and *SLC2A9* demonstrated the highest ORs for gout (20,21,31), and these were of similar magnitude in all BMI groups.

A significant GRS–BMI interaction for gout was observed when the GRS was analyzed according to the mean (greater than or equal to versus less than the mean) and as a continuous variable. The interaction was due to a slight attenuation in the effect of a GRS greater than or equal to the mean or a higher GRS in the obese BMI group compared to the overweight BMI group. However, it should be noted that the difference in the ORs for gout between the overweight and obese BMI groups for a GRS greater than or equal to the mean was small (OR 3.09 versus OR 2.65) and may not be of clinical significance. Also, no significant differences were observed between the low/normal and overweight BMI groups, or between the low/normal and obese BMI groups. Furthermore, an OR of 2.65 for gout in those with an

obese BMI and a GRS greater than or equal to the mean is likely to be clinically important. Overall, our data suggest that genetic susceptibility does play an important role in gout risk in people with an obese BMI, with an effect similar to those with a low/normal BMI. It should also be noted that the large sample size of the UK Biobank data set (>350,000 subjects) likely contributed to the detection of statistically significant associations that may not be clinically meaningful.

Previous analyses examining interactions of serum urate–associated genetic variants and BMI with serum urate levels and incident gout have demonstrated conflicting results. Brandstätter et al (22) reported that the effects of 4 SNPs within *SLC2A9* (rs6855911, rs7442295, rs6449213, and rs12510549) on serum urate were significantly modified by BMI, with a greater effect in women with higher BMIs compared to men. Another study of a predominantly female population, however, suggested a stronger effect of *SLC2A9* on serum urate in normal-weight women compared to obese women (23). Recently, Huffman et al (24) conducted a genome-wide association meta-analysis to investigate the extent to which genetic variants affecting serum urate are modulated by BMI. When stratified by BMI, *ABCG2* demonstrated a statistically significant difference in effect between obese men (BMI >30) and lean men (BMI <25), with the magnitude of effect of *ABCG2* rs2231142 on urate more than halved in the obese group compared to the lean group. Weak statistical evidence for modulation of *SLC2A9*, *GCKR*, and *PDZK1* variant effects by BMI were also observed in that study (24). In their analysis of the original and offspring cohorts in the Framingham Heart Study, Reynolds et al (25) demonstrated that BMI and urate SNPs were both highly associated with gout risk. However, they did not find any significant interactions of BMI with SNP or of BMI with serum urate GRS for 8 serum urate loci (*SLC17A1* rs1165196, *R3HDM2* rs1106766, rs1967017, *GCKR* rs780093, *SLC2A9* rs13129697, *ABCG2* rs2199936, *RREB1* rs675209, and *SLC22A11* rs2078267) (25). Our study did not demonstrate non-additive SNP–BMI interactions for gout, which is consistent with the findings of Reynolds et al (25).

In the present study, a higher BMI was associated with higher odds of gout. Previous observational studies have shown a higher risk of incident gout with increasing BMI (32). A systematic review and meta-analysis of 10 prospective studies of BMI and gout risk found that the relative risks were 1.78, 2.67, 3.62, and 4.64 for subjects with a BMI of 25, 30, 35, and 40, respectively, compared to those with a BMI of 20 (32). Mendelian randomization studies have also demonstrated that a genetically higher BMI is positively associated with serum urate and risk of gout, although the effect size for serum urate is weak (0.10–0.64 μmoles/liter per genetically determined increase in BMI) (17,33). The association between higher BMI and gout might be explained by the effect of obesity on increasing serum urate levels, mediated through obesity-induced hyperinsulinemia, which enhances renal proximal reabsorption of urate (34,35). The association between obesity and gout may also be mediated via higher circulating leptin in people with obesity; a recent study showed that levels of leptin and leptin receptor are also elevated in patients with gout flares (19).

We acknowledge the limitations of this study. First, our analysis was restricted to participants of European ancestry, and our results may not be generalizable to populations with non-European ancestry. The age range for recruitment into the UK Biobank means that younger people with early-onset gout and older participants >70 years of age were not included in the analysis. A large number of UK Biobank participants who did not fulfill the definition of gout reported taking NSAIDs (n = 72,288) and were excluded from the analysis. This may have introduced bias into the analysis; however, the baseline characteristics of participants without gout who were receiving NSAIDs and those not receiving NSAIDs were similar (Supplementary Table 7, http://onlinelibrary.wiley.com/doi/10.1002/art.41219/abstract). NSAIDs are widely prescribed for gout without concurrent prescription of urate-lowering therapy (36). Thus, inclusion of participants taking NSAIDs in the control group may result in misclassification of gout cases as controls. In addition, this exclusion criterion was applied when defining control participants when we initially validated the definition of gout for research using the UK Biobank (26).

Despite the large size of the UK Biobank, the power to detect an association for some serum urate–associated SNPs with gout was low. This is likely due to a very high or very low minor allele frequency for some SNPs. Comorbidity and medication use data collected via the UK Biobank resource was performed by self-report. This method of data collection may not accurately represent the true prevalence of comorbidities such as renal failure and medication use. However, this imprecision is likely to have applied systemically to all groups in the analysis. Finally, as this is a cross-sectional study, it is not possible to differentiate between causation and reverse causation for BMI and gout risk. Strengths of this study include the large sample size with consistent methods of data collection and comprehensive assessment including patient interviews, hospitalization record, and medical information.

In conclusion, in individuals of European ancestry, genetic susceptibility significantly contributes to gout risk across all BMI categories. The association of genetic factors with gout risk is mildly attenuated in subjects with obesity compared to those with overweight. However, genetic variants have a strong effect on gout risk in those with overweight and obese BMIs, with a similar effect to that observed with low/normal BMI.

ACKNOWLEDGMENT

This research has been conducted using the UK Biobank Resource under Application Number 12611.

AUTHOR CONTRIBUTIONS

All authors were involved in drafting the article or revising it critically for important intellectual content, and all authors approved the final version to be published. Dr. Tai had full access to all of the data in the study and

takes responsibility for the integrity of the data and the accuracy of the data analysis.

Study conception and design. Tai, Narang, Merriman, Dalbeth.

Acquisition of data. Tai, Narang, Cadzow, Merriman, Dalbeth.

Analysis and interpretation of data. Tai, Narang, Gamble, Stamp, Merriman, Dalbeth.

REFERENCES

1. Campion EW, Glynn RJ, DeLabry LO. Asymptomatic hyperuricemia: risks and consequences in the Normative Aging Study. Am J Med 1987;82:421–6.
2. Roubenoff R, Klag MJ, Mead LA, Liang KY, Seidler AJ, Hochberg MC. Incidence and risk factors for gout in white men. JAMA 1991;266:3004–7.
3. Choi HK, Atkinson K, Karlson EW, Curhan G. Obesity, weight change, hypertension, diuretic use, and risk of gout in men: the Health Professionals Follow-up Study. Arch Intern Med 2005; 165:742–8.
4. Williams PT. Effects of diet, physical activity and performance, and body weight on incident gout in ostensibly healthy, vigorously active men. Am J Clin Nutr 2008;87:1480–7.
5. Bhole V, de Vera M, Rahman MM, Krishnan E, Choi H. Epidemiology of gout in women: fifty-two–year follow-up of a prospective cohort. Arthritis Rheum 2010;62:1069–76.
6. Cea Soriano L, Rothenbacher D, Choi HK, García Rodríguez LA. Contemporary epidemiology of gout in the UK general population. Arthritis Res Ther 2011;13:R39.
7. Maynard JW, McAdams DeMarco MA, Baer AN, Köttgen A, Folsom AR, Coresh J, et al. Incident gout in women and association with obesity in the Atherosclerosis Risk in Communities (ARIC) Study. Am J Med 2012;125:717.
8. McAdams-DeMarco MA, Maynard JW, Baer AN, Coresh J. Hypertension and the risk of incident gout in a population-based study: the Atherosclerosis Risk in Communities cohort. J Clin Hypertens (Greenwich) 2012;14:675–9.
9. Chen JH, Pan WH, Hsu CC, Yeh WT, Chuang SY, Chen PY, et al. Impact of obesity and hypertriglyceridemia on gout development with or without hyperuricemia: a prospective study. Arthritis Care Res (Hoboken) 2013;65:133–40.
10. Lin KC, Lin HY, Chou P. Community based epidemiological study on hyperuricemia and gout in Kin-Hu, Kinmen. J Rheumatol 2000; 27:1045–50.
11. Dalbeth N, Merriman TR, Stamp LK. Gout. Lancet 2016;388:2039–52.
12. Roddy E, Choi HK. Epidemiology of gout. Rheum Dis Clin North Am 2014;40:155–75.
13. Kuo CF, Grainge MJ, Zhang W, Doherty M. Global epidemiology of gout: prevalence, incidence and risk factors. Nat Rev Rheumatol 2015;11:649–62.
14. Rai SK, Fung TT, Lu N, Keller SF, Curhan GC, Choi HK. The Dietary Approaches to Stop Hypertension (DASH) diet, Western diet, and risk of gout in men: prospective cohort study. BMJ 2017;357:j1794.
15. Matsuura F, Yamashita S, Nakamura T, Nishida M, Nozaki S, Funahashi T, et al. Effect of visceral fat accumulation on uric acid metabolism in male obese subjects: visceral fat obesity is linked more closely to overproduction of uric acid than subcutaneous fat obesity. Metabolism 1998;47:929–33.
16. Gao B, Zhou J, Ge J, Zhang Y, Chen F, Lau WB, et al. Association of maximum weight with hyperuricemia risk: a retrospective study of 21,414 Chinese people. PLoS One 2012;7:e51186.
17. Lyngdoh T, Vuistiner P, Marques-Vidal P, Rousson V, Waeber G, Vollenweider P, et al. Serum uric acid and adiposity: deciphering causality using a bidirectional Mendelian randomization approach. PLoS One 2012;7:e39321.
18. Dalbeth N, Pool B, Yip S, Cornish J, Murphy R. Effect of bariatric surgery on the inflammatory response to monosodium urate crystals: a prospective study [letter]. Ann Rheum Dis 2013;72:1583–4.
19. Yu Y, Yang J, Fu S, Xue Y, Liang M, Xuan D, et al. Leptin promotes monosodium urate crystal-induced inflammation in human and murine models of gout. J Immunol 2019;202:2728–36.
20. Köttgen A, Albrecht E, Teumer A, Vitart V, Krumsiek J, Hundertmark C, et al. Genome-wide association analyses identify 18 new loci associated with serum urate concentrations. Nat Genet 2013;45:145–54.
21. Phipps-Green AJ, Merriman ME, Topless R, Altaf S, Montgomery GW, Franklin C, et al. Twenty-eight loci that influence serum urate levels: analysis of association with gout. Ann Rheum Dis 2016;75: 124–30.
22. Brandstätter A, Kiechl S, Kollerits B, Hunt SC, Heid IM, Coassin S, et al. Sex-specific association of the putative fructose transporter SLC2A9 variants with uric acid levels is modified by BMI. Diabetes Care 2008;31:1662–7.
23. Li WD, Jiao H, Wang K, Zhang CK, Glessner JT, Grant SF, et al. A genome wide association study of plasma uric acid levels in obese cases and never-overweight controls. Obesity (Silver Spring) 2013;21:E490–4.
24. Huffman JE, Albrecht E, Teumer A, Mangino M, Kapur K, Johnson T, et al. Modulation of genetic associations with serum urate levels by body-mass-index in humans. PLoS One 2015;10:e0119752.
25. Reynolds RJ, Vazquez AI, Srinivasasainagendra V, Klimentidis YC, Bridges SL Jr, Allison DB, et al. Serum urate gene associations with incident gout, measured in the Framingham Heart Study, are modified by renal disease and not by body mass index. Rheumatol Int 2016;36:263–70.
26. Cadzow M, Merriman TR, Dalbeth N. Performance of gout definitions for genetic epidemiological studies: analysis of UK Biobank. Arthritis Res Ther 2017;19:181.
27. Centers for Disease Control and Prevention. Defining adult overweight and obesity. URL: https://www.cdc.gov/obesity/adult/defining.html.
28. Narang RK, Topless R, Cadzow M, Gamble G, Stamp LK, Merriman TR, et al. Interactions between serum urate-associated genetic variants and sex on gout risk: analysis of the UK Biobank. Arthritis Res Ther 2019;21:13.
29. McAdams-DeMarco MA, Maynard JW, Baer AN, Kao LW, Kottgen A, Coresh J. A urate gene-by-diuretic interaction and gout risk in participants with hypertension: results from the ARIC study. Ann Rheum Dis 2013;72:701–6.
30. Bao Y, Curhan G, Merriman T, Plenge R, Kraft P, Choi HK. Lack of gene-diuretic interactions on the risk of incident gout: the Nurses' Health Study and Health Professionals Follow-up Study. Ann Rheum Dis 2015;74:1394–8.
31. Dehghan A, Köttgen A, Yang Q, Hwang SJ, Kao WL, Rivadeneira F, et al. Association of three genetic loci with uric acid concentration and risk of gout: a genome-wide association study. Lancet 2008; 372:1953–61.
32. Aune D, Norat T, Vatten LJ. Body mass index and the risk of gout: a systematic review and dose–response meta-analysis of prospective studies [review]. Eur J Nutr 2014;53:1591–601.
33. Larsson SC, Burgess S, Michaëlsson K. Genetic association between adiposity and gout: a Mendelian randomization study. Rheumatology (Oxford) 2018;57:2145–8.
34. Facchini F, Chen YD, Hollenbeck CB, Reaven GM. Relationship between resistance to insulin-mediated glucose uptake, urinary uric acid clearance, and plasma uric acid concentration. JAMA 1991;266:3008–11.
35. Quiñones Galvan A, Natali A, Baldi S, Frascerra S, Sanna G, Ciociaro D, et al. Effect of insulin on uric acid excretion in humans. Am J Physiol 1995;268:E1–5.
36. Doherty M, Jenkins W, Richardson H, Sarmanova A, Abhishek A, Ashton D, et al. Efficacy and cost-effectiveness of nurse-led care involving education and engagement of patients and a treat-to-target urate-lowering strategy versus usual care for gout: a randomised controlled trial. Lancet 2018;392:1403–12.

American College of Rheumatology
Empowering Rheumatology Professionals

Arthritis & Rheumatology
Vol. 72, No. 7, July 2020, pp 1192–1202
DOI 10.1002/art.41245

Direct Binding to NLRP3 Pyrin Domain as a Novel Strategy to Prevent NLRP3-Driven Inflammation and Gouty Arthritis

Gabsik Yang,[1] Hye E. Lee,[1] Su-Jin Moon,[2] Kyung M. Ko,[3] Jung H. Koh,[3] Jin K. Seok,[1] Jun-Ki Min,[3] Tae-Hwe Heo,[1] Han C. Kang,[1] Yong-Yeon Cho,[1] Hye S. Lee,[1] Katherine A. Fitzgerald,[4] and Joo Y. Lee[1]

Objective. The NLRP3 inflammasome is closely linked to the pathophysiology of a wide range of inflammatory diseases. This study was undertaken to identify small molecules that directly bind to NLRP3 in order to develop pharmacologic interventions for NLRP3-related diseases.

Methods. A structure-based virtual screening analysis was performed with ~62,800 compounds to select efficient NLRP3 inhibitors. The production of caspase 1-p10 and interleukin-1β (IL-1β) was measured by immunoblotting and enzyme-linked immunosorbent assay to examine NLRP3 inflammasome activation. Two gouty arthritis models and an air pouch inflammation model induced by monosodium urate monohydrate (MSU) crystal injection were used for in vivo experiments. Primary synovial fluid cells from gout patients were used to determine the relevance of NLRP3 inflammasome inhibition in human gout.

Results. Beta-carotene (provitamin A) suppressed the NLRP3 inflammasome activation induced by various activators, including MSU crystals, in mouse bone marrow–derived primary macrophages ($P < 0.05$). Surface plasmon resonance analysis demonstrated the direct binding of β-carotene to the pyrin domain (PYD) of NLRP3 ($K_D = 3.41 \times 10^{-6}$). Molecular modeling and mutation assays revealed the interaction mode between β-carotene and the NLRP3 PYD. Inflammatory symptoms induced by MSU crystals were attenuated by oral administration of β-carotene in gouty arthritis mouse models ($P < 0.05$), correlating with its suppressive effects on the NLRP3 inflammasome in inflamed tissues. Furthermore, β-carotene reduced IL-1β secretion from human synovial fluid cells isolated from gout patients ($P < 0.05$), showing its inhibitory efficacy in human gout.

Conclusion. Our results present β-carotene as a selective and direct inhibitor of NLRP3, and the binding of β-carotene to NLRP3 PYD as a novel pharmacologic strategy to combat NLRP3 inflammasome–driven diseases, including gouty arthritis.

INTRODUCTION

Inflammasomes are multimolecular assemblies composed of a sensor protein, a caspase, and an adaptor protein, such as an ASC. The NLRP3 inflammasome is the best characterized inflammasome and is well known as playing an essential role in the regulation of immune and inflammatory responses. The NLRP3 inflammasome is activated by a diverse array of pathogen- and danger-associated signals, triggering the formation of a cytoplasmic complex consisting of NLRP3, ASC, and procaspase 1 for caspase 1 activation, culminating in proteolytic maturation of the proinflammatory cytokines, interleukin-1β (IL-1β) and IL-18, and in pyroptotic cell death (1).

The NLRP3 inflammasome is closely linked to the initiation and progression of a wide range of inflammatory diseases, thereby highlighting the NLRP3 inflammasome as an efficient therapeutic target (2). NLRP3 inflammasome inhibition can be achieved both indirectly and directly, with indirect inhibition occurring by regulating upstream or downstream signaling events and direct inhibition occurring by targeting NLRP3 inflammasome components. Efforts

Supported by the National Research Foundation of Korea grants NRF-2017R1A2B2006281, NRF-2019R1A2C2085739, NRF-2017R1A4A1015036, and NRF-2020R1A4A2002894 from the Republic of Korea's Ministry of Science, ICT, and Future Planning.

[1]Gabsik Yang, PhD, Hye E. Lee, PhD, Jin K. Seok, PhD, Tae-Hwe Heo, PhD, Han C. Kang, PhD, Yong-Yeon Cho, PhD, Hye S. Lee, PhD, Joo Y. Lee, PhD: College of Pharmacy, The Catholic University of Korea, Bucheon, Republic of Korea; [2]Su-Jin Moon, MD, PhD: St. Mary's Hospital, Uijeongbu, Republic of Korea, and The Catholic University of Korea, Seoul, Republic of Korea; [3]Kyung M. Ko, MD, PhD, Jung H. Koh, MD, PhD, Jun-Ki Min, MD, PhD: St. Mary's Hospital, Bucheon, Republic of Korea, and The Catholic University of Korea, Seoul, Republic of Korea; [4]Katherine A. Fitzgerald, PhD: University of Massachusetts Medical School, Worcester.

Drs. Yang and H. E. Lee contributed equally to this work.

No potential conflicts of interest relevant to this article were reported.

Address correspondence to Joo Y. Lee, PhD, Jibong-ro 43, Bucheon, Gyeonggi-do 14662, Republic of Korea. E-mail: joolee@catholic.ac.kr.

Submitted for publication July 29, 2019; accepted in revised form February 27, 2020.

to develop pharmacologic inhibitors of the NLRP3 inflammasome have been reported with sulforaphane, β-hydroxybutyrate, CY-09, and MCC950 (3–6). We first reported directly targeting ASC with a small molecule to inhibit the activation of the NLRP3 inflammasome (7). While searching for inhibitors that directly target the NLRP3 inflammasome, we intended to find small molecules that directly bind to NLRP3.

Upon activation, NLRP3 with a pyrin domain (PYD), a nucleotide-binding and oligomerization (NACHT) domain, and a leucine-rich repeat (LRR) domain, self-oligomerizes and recruits ASC containing a PYD and a caspase recruitment domain (CARD) through PYD–PYD interactions (8) (Supplementary Figure 1A, available on the *Arthritis & Rheumatology* web site at http://onlinelibrary.wiley.com/doi/10.1002/art.41245/abstract), inducing a helical assembly of the ASC PYD filaments (9). ASC fibrils form into large ASC speck structures, which recruit procaspase 1 through CARD–CARD interactions, leading to autoproteolytic activation (9–11). We hypothesized that the PYD of NLRP3 would be an efficient target since its inhibition would block the initiation phase of NLRP3 inflammasome activation (Supplementary Figure 1A). To identify novel candidate inhibitors that directly bind to the NLRP3 PYD, we performed a structure-based virtual screening with molecular docking calculations using the NLRP3 PYD structure 3QF2 in the Protein Data Bank (12). The scores of ~62,800 compounds were analyzed with affinity- and efficiency-based metrics, such as binding energy (ΔG) and Glide score (Supplementary Figure 1B). Among the 11 compounds that were chosen for their high in silico binding affinity scores and commercial availability, β-carotene was selected for further study in the development of an NLRP3 inhibitor.

MATERIALS AND METHODS

Study design. Our study was designed to examine the efficacy of the NLRP3 inhibitor, β-carotene, in cell systems and animal disease models. Cell studies with mouse primary bone marrow–derived macrophages (BMMs) were performed with at least 3 replicates per experiment, in addition to preliminary optimization studies for dose and time determination. Animal disease models include foot gout, gouty arthritis, and air pouch inflammation relevant to acute gout inflammation. Age-matched mice were randomly grouped for β-carotene or vehicle treatment. Animal numbers for each group or experiment were empirically determined based on pilot studies or previous experiments.

Human synovial fluid samples. Synovial fluid was obtained from the knee joints of gout patients with serum uric acid levels of >400 μmoles/liter and joint effusion. Experiments were approved by the Institutional Review Board (IRB) of human subjects at Bucheon St. Mary's Hospital (no. HC18TESI0098) at The Catholic University of Korea, and were carried out in accordance with IRB guidelines and regulations and the Declaration of Helsinki. Written informed consent was obtained from all patients.

Animals and cell culture. Mice (C57BL/6; Orient Bio) were maintained under specific pathogen–free conditions in an animal facility with relative humidity of 40–60% and controlled temperature of 23°C (±3°C). Animal care and the experimental procedures were conducted under the approval of the Institutional Animal Care and Use Committee (IACUC) of The Catholic University of Korea (permission no. 2014-015). BMMs and 293T cells (human embryonic kidney cells) were prepared and cultured as described previously (13).

Virtual screening analysis and molecular docking modeling. For virtual screening, we used the commercially available ZINC natural compounds database (http://zinc.docking.org/), which contains more than 6 million compounds in ready-to-dock, 3-dimensional formats. Chemical structures for docking analysis were generated using the LigPrep module in Schrodinger. A crystal structure of the human NLRP3 PYD in the RCSB Protein Data Bank (PDB code: 3QF2) was employed in the docking calculations with the Glide module in the Schrodinger molecular simulation package. After the cocrystal ligand was removed, the resulting structure was used as the receptor model. The structure was subjected to restrained minimization to remove steric clashes by the application of an optimized potential for liquid simulations force field using the Protein Preparation Wizard. The minimization was terminated when the root mean square deviation came to a maximum value of 0.3 Å. The computational docking of all the compounds was performed with the Glide program.

Immunoblot analysis of inflammasome activation. BMMs cultured in 6-well plates (2×10^6 cells/ml) were primed with purified lipopolysaccharide (LPS) from *Escherichia coli* (100 ng/ml; List Biological Laboratory) for 4 hours. LPS was washed out with phosphate buffered saline (PBS), and β-carotene (Sigma-Aldrich) was added. After 1 hour, cells were stimulated with the inflammasome activators as follows: 500 μg/ml of monosodium urate (MSU) crystals for 4.5 hours, 5 m*M* of ATP for 1 hour, 10 μ*M* of nigericin for 1.5 hours, 1 μg/ml of poly(dA-dT) for 5.5 hours, and 10 μg/ml of flagellin for 5.5 hours in serum-free medium. Cell lysates were processed for immunoblot assays as previously described (7).

Enzyme-linked immunosorbent assays (ELISAs). Cell supernatants were analyzed for IL-1β and IL-18 using specific ELISA kits (R&D Systems), and for IL-1α, IL-18, IL-6, and keratinocyte chemoattractant (KC), and monocyte chemotactic protein 1 (MCP-1) using a Milliplex MAP Mouse Cytokine/Chemokine Kit (Millipore) (14).

Surface plasmon resonance (SPR) analysis. Recombinant PYD protein of NLRP3 was prepared as previously described (12). The PYD protein of NLRP3 was covalently immobilized to a CM5 sensor chip (catalog no. BR-1005-30; GE Healthcare). Beta-carotene cultured in PBS with 0.005% Tween 20 and 5% DMSO was run in the flow cell with a 5 μl/minute flow rate at 25°C. The association/dissociation phases were monitored using a Biacore T200 system (GE Healthcare), and the affinity constants were calculated with T200 evaluation software (version 2.0), as described previously (7).

Transient transfection and luciferase assay. A pcDNA3.1 nV5-hNLPR3 plasmid was kindly provided by Dr. You-Me Kim (Pohang University of Science and Technology, Pohang, South Korea). ASC- and caspase 1–expression plasmids were generously provided by Dr. Giulio Superti-Furga (Austrian Academy of Sciences, Vienna, Austria) and an iGLuc plasmid was generously provided by Dr. Veit Hornung (University of Bonn, Bonn, Germany). A pCMV-proIL-1β plasmid was obtained from Addgene. Transfection procedure and luciferase assays were performed as previously described (13).

Immunoprecipitation (IP) and immunoblot assays. Cell lysates were incubated with an anti-NLRP3 antibody (Adipogen), followed by incubation with Protein A–Sepharose beads (GE Healthcare). Coimmunoprecipitated proteins were processed for immunoblot assays.

Confocal microscopy analysis. For confocal microscopy, 293T cells were incubated with an anti-NLRP3 antibody (Adipogen) or an anti-ASC antibody (Santa Cruz Biotechnology), followed by incubation with a secondary antibody, such as an Alexa Fluor 488–conjugated anti-mouse IgG antibody and a fluorescein isothiocyanate–conjugated anti-rabbit IgG antibody. Cells were observed using an LSM 710 confocal microscope (Carl Zeiss AG) (15).

Air pouch inflammation model. An air pouch was formed in the back of each 7- to 8- week-old C57BL/6 mouse by subcutaneous injection of sterile air, as previously described (6). On day 4, 0.2 ml of sterilized water containing vehicle (0.02% DMSO) or 30 mg/kg of β-carotene was administered via oral gavage. After 1 hour, 3 mg of MSU crystals suspended in 1 ml of sterile, endotoxin-free PBS was injected into the pouch. Six hours later, the air pouch lavages were collected and processed for ELISAs, immunoblot assays, and histologic analysis (6).

In vitro caspase 1 activity assay. Caspase 1 activity was measured with a fluorometric caspase 1 assay kit (Abcam) with recombinant human caspase 1 (BioVision). Fluorescence was measured at 400 nm after 505 nm excitation.

Myeloperoxidase (MPO) activity assay. MPO activity was measured with an MPO Colorimetric Activity Assay Kit (BioVision).

A foot gout model in mice. For induction of foot gout, 30 mg/kg of β-carotene in 0.2 ml of sterilized water was orally administered to 7- to 8- week-old C57BL/6 mice. As a control, 0.02% DMSO vehicle was used. After 1 hour, either MSU crystals in 2 mg/0.1 ml of sterile, endotoxin-free PBS or PBS alone was administered via subcutaneous injection on the right paw plantar surface (16). Changes in paw thickness were measured for 24 hours. The foot tissues were homogenized in radioimmunoprecipitation assay (RIPA) buffer (50 m*M* Tris HCl, pH 7.4; 1% NP-40; 0.25% sodium deoxycholate; 150 m*M* NaCl; 1 m*M* EGTA; 1 m*M* PMSF; 1 m*M* Na_3VO_4; 10 μg/ml of aprotinin; 10 μg/ml of leupeptin), and centrifuged at 12,000 revolutions per minute for 10 minutes. Supernatants were used for MPO assays, ELISAs, immunoblot assays, and histologic analysis (16).

A gouty arthritis model in mice. A knee joint gouty arthritis model in mice was performed as previously described (17). For induction of gout, 30 mg/kg of β-carotene in 0.2 ml of sterilized water was orally administered to 7- to 8-week-old C57BL/6 mice. As a control, 0.02% DMSO vehicle was used. After 1 hour, either MSU crystals in 100 μg/20 μl of PBS or PBS alone was injected into the right knee joint of each mouse. After 24 hours, joint tissue was homogenized in RIPA buffer and centrifuged at 12,000 rpm for 30 minutes. Supernatant was collected for MPO assays and cytokine ELISAs.

Statistical analysis. Data are presented as the mean ± SEM. Statistically significant differences were analyzed by one-way analysis of variance followed by Duncan's test for multiple comparisons using GraphPad Prism 7.0 (GraphPad). *P* values less than 0.05 were considered significant.

RESULTS

Suppression of the NLRP3 inflammasome by β-carotene in BMMs. We first confirmed the inhibitory effect of β-carotene on the NLRP3 inflammasome in a cell-based system stimulated with representative NLRP3 activators. Beta-carotene suppressed ATP-induced cleavage of procaspase 1 and proIL-1β to caspase 1-p10 and mature IL-1β, respectively, in mouse BMMs, as shown by immunoblotting (Figure 1A). Similarly, β-carotene prevented the production of caspase 1-p10 and IL-1β induced by nigericin or MSU crystals in BMMs (Figure 1A). Consistent with this, secretion of mature IL-1β induced by ATP, nigericin, or MSU crystals was suppressed by β-carotene, as measured by an ELISA of cell culture supernatants (Figure 1B). The results demonstrate that β-carotene suppresses activation of the NLRP3 inflammasome induced by various activators. In contrast, β-carotene

did not inhibit the production of caspase 1 and IL-1β induced by poly(dA-dT) or flagellin in BMMs (Figures 1C and D), showing that β-carotene did not inhibit the activation of AIM2 and NLRC4.

Direct binding of β-carotene to the PYD of NLRP3. ATP, nigericin, and MSU crystals have different activation pathways upstream of NLRP3. The common inhibitory effects of β-carotene on different activators suggest that the target of β-carotene is not signaling molecules or events upstream of NLRP3. Thus, we investigated whether β-carotene directly inhibited the NLRP3 inflammasome complex independently of the activators. NLRP3 inflammasome activation was induced by overexpression of the NLRP3 inflammasome components in 293T cells along with the iGLuc luciferase reporter gene, which responds to inflammasome activation (18). Beta-carotene suppressed the expression of the iGLuc luciferase reporter when 293T cells were transfected with NLRP3, ASC, and caspase 1 (Supplementary Figure 2A, available on the *Arthritis & Rheumatology* web site at http://onlinelibrary.wiley.com/doi/10.1002/art.41245/abstract). The results suggest that β-carotene directly inhibits the NLRP3 inflammasome complex independently of activators. Interestingly, β-carotene was not able to inhibit the expression of the iGLuc luciferase reporter induced by ASC+ caspase 1 or caspase 1 alone in 293T cells (Supplementary Figures 2B and C), suggesting that the inhibitory effect of β-carotene requires the presence of NLRP3.

To investigate whether β-carotene could directly bind to NLRP3, an SPR assay was performed with recombinant human NLRP3 PYD. Beta-carotene directly bound to the PYD of NLRP3, but not to ASC, in a dose-dependent manner (Figure 2A).

Molecular modeling analysis of the crystal structure of dimeric human NLRP3 PYD suggests a docking model between β-carotene and the PYD domain of NLRP3. A single molecule of β-carotene bound to NLRP3 PYD, and the final model contained amino acid residues 5–94 (Figures 2B and C). The electron density of β-carotene was evident in the solved NLRP3 PYD structure, which featured β-carotene on the surface formed by H5 and H6 of NLRP3 PYD (Figures 2B and C). Beta-carotene bound to the hydrophobic groove that was composed of hydrophobic residues, including Ala[69], Val[72], Trp[73], Tyr[84], and Glu[91], in H5 and H6 (Figures 2B and C and Supplementary Figure 3A, available

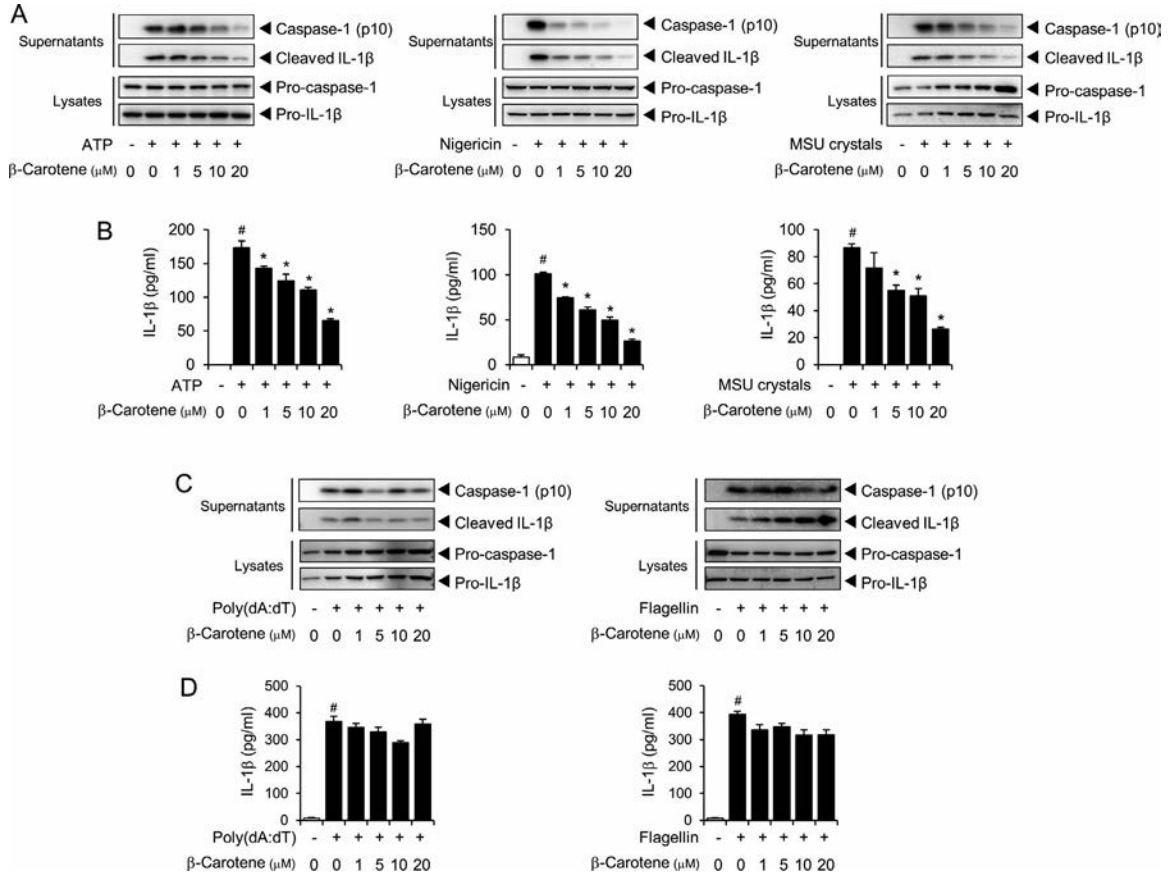

Figure 1. Beta-carotene suppression of NLRP3 inflammasome activation. Mouse primary bone marrow–derived macrophages were primed with lipopolysaccharide for 4 hours. Cells were treated with β-carotene for 1 hour and then stimulated with the indicated agonist. **A** and **C**, Cell culture supernatants and cell lysates were immunoblotted for caspase 1-p10, interleukin-1β (IL-1β), procaspase 1, and proIL-1β. **B** and **D**, Cell culture supernatants were analyzed for secreted IL-1β by enzyme-linked immunosorbent assay. Values are the mean ± SEM (n = 3 mice per group). Results are representative of at least 2 independent experiments. # = $P < 0.05$ versus vehicle alone. * = $P < 0.05$ versus ATP, nigericin, or monosodium urate (MSU) crystals alone.

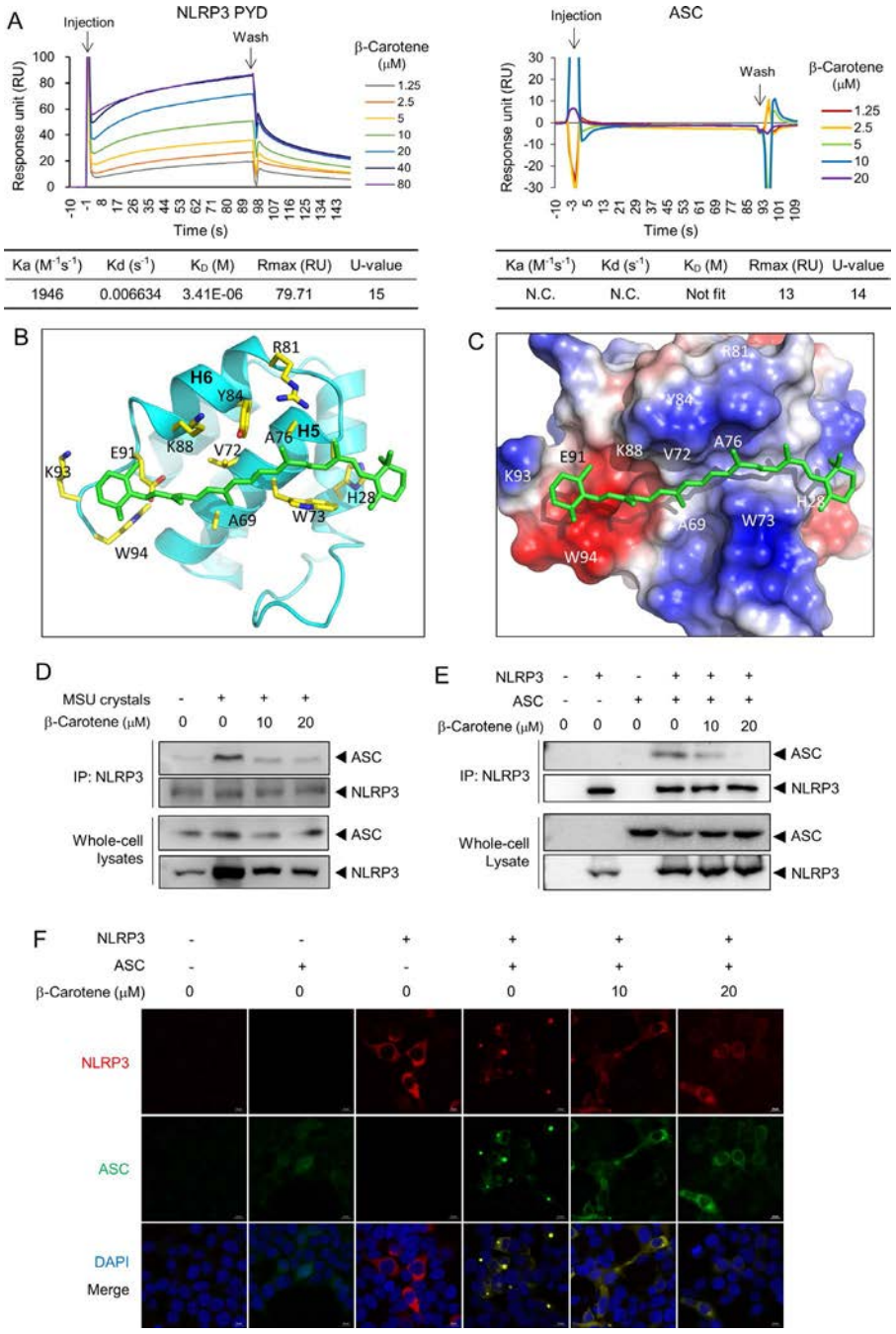

Figure 2. Beta-carotene directly binds to the pyrin domain (PYD) of NLRP3. **A**, Sensorgrams of β-carotene binding to the recombinant protein of human NLRP3 PYD or human ASC obtained from surface plasmon resonance (SPR) analysis. Tables show kinetic parameters of the binding between β-carotene and the recombinant proteins. Maximal expected binding level (Rmax) was calculated with Biacore T200 evaluation software. N.C. = not calculated. **B**, Proposed molecular docking model for β-carotene binding to NLRP3 PYD. **C**, Electrostatic surface binding model for β-carotene (green) and NLRP3 PYD, with negative charge (red) and positive charge (blue). **D**, Mouse primary bone marrow–derived macrophages were primed with lipopolysaccharide. Cells were treated with β-carotene for 1 hour and then stimulated with 500 μg/ml of monosodium urate (MSU) crystals for 6 hours. Cell lysates were analyzed by immunoprecipitation (IP) with an anti–NLRP3 antibody, followed by immunoblotting as indicated, to demonstrate the association of endogenous NLRP3 and endogenous ASC and the impact of β-carotene on that association. **E**, NLRP3 or ASC expression plasmids were used to transfect 293T cells, and 293T cells were treated with β-carotene for 16 hours. Cell lysates were immunoprecipitated with an anti–NLRP3 antibody, followed by immunoblotting as indicated, to demonstrate the interaction between NLRP3 and ASC induced upon exogenous expression in 293T cells. **F**, NLRP3 or ASC expression plasmids were used to transfect 293T cells, and 293T cells were treated with β-carotene. Cells were stained for NLRP3 (red) and ASC (green). Nuclei were stained with DAPI (blue). Results are representative of at least 2 independent experiments.

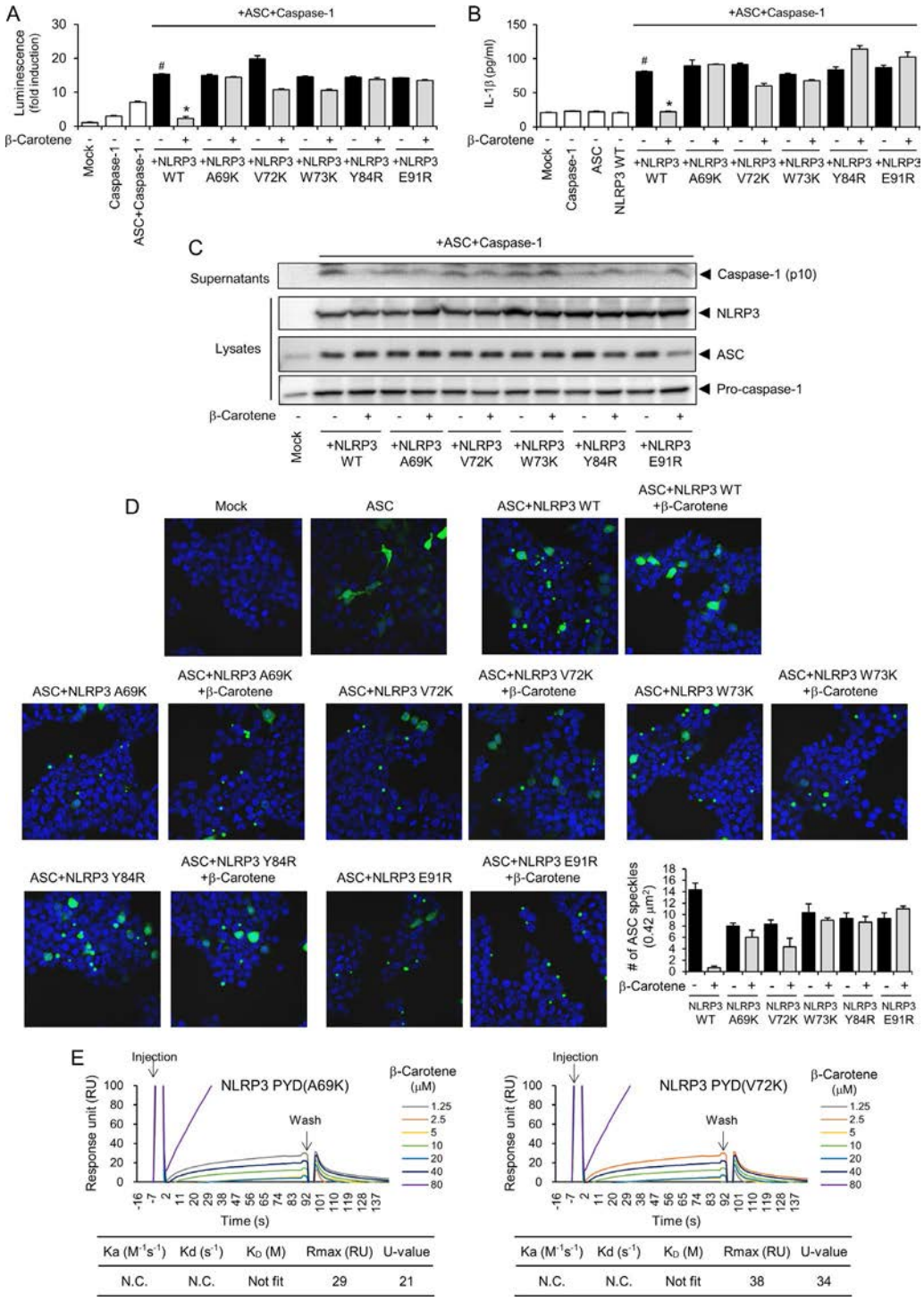

Figure 3. Identification of essential amino acids for the interaction between β-carotene and NLRP3 PYD. **A**–**D**, 293T cells were transiently transfected with expression plasmids of wild-type (WT) NLRP3, NLRP3 mutants, ASC, and caspase 1. The iGLuc luciferase reporter plasmid (**A**) and pro–interleukin-1β (proIL-1β) expression plasmid (**B**) were also transfected. After 8 hours, cells were treated with 20 μ*M* of β-carotene for 16 hours. **A**, Cell lysates were analyzed for luciferase activity derived from iGLuc activation. Activity was normalized to the β-galactosidase activity transfected as an internal control in each sample. **B**, Cell culture supernatants were analyzed for secreted IL-1β by enzyme-linked immunosorbent assay. **C**, Cell culture supernatants and cell lysates were immunoblotted for detection of the indicated molecules. **D**, Cells were stained for ASC (green). Nuclei were stained with DAPI (blue). The bar graph presents the number of ASC specks formed (n = 3). **E**, Sensorgrams of β-carotene binding to the recombinant protein of the human NLRP3 PYD mutant with A69K or V72K were obtained from SPR analysis as described in Figure 2. In **A**, **B**, and **D**, values are the mean ± SEM (n = 3 mice per group). # = $P < 0.05$ versus mock alone. * = $P < 0.05$ versus NLRP3 WT + ASC + caspase 1 without β-carotene. Results are representative of at least 2 independent experiments. See Figure 2 for other definitions. Color figure can be viewed in the online issue, which is available at http://onlinelibrary.wiley.com/doi/10.1002/art.41245/abstract.

on the *Arthritis & Rheumatology* web site at http://onlinelibrary.wiley.com/doi/10.1002/art.41245/abstract). NLRP3 associates with ASC through PYD–PYD interactions (19). Molecular modeling suggested that the direct binding of β-carotene to NLRP3 PYD interferes with the interaction between NLRP3 PYD and ASC PYD (Supplementary Figure 3B, http://onlinelibrary.wiley.com/doi/10.1002/art.41245/abstract).

Consequently, we next investigated whether β-carotene blocked the association between NLRP3 and ASC using an IP assay with an anti-NLRP3 antibody, followed by immunoblotting with an anti-ASC antibody. MSU crystal stimulation of BMMs resulted in the association of endogenous NLRP3 and endogenous ASC (Figure 2D), while β-carotene prevented the MSU crystal–induced association of NLRP3 and ASC (Figure 2D). Furthermore, β-carotene disrupted the interaction between NLRP3 and ASC induced upon exogenous expression in 293T cells (Figure 2E). These results demonstrate that the binding of β-carotene to the PYD of NLRP3 blocks the assembly of the NLRP3 inflammasome complex.

Since ASC undergoes oligomerization upon association with NLRP3 (20), we further investigated whether the binding of β-carotene to the PYD of NLRP3 affected ASC oligomerization. Confocal microscopy showed that exogenous expression of NLRP3 together with ASC in 293T cells led to speck formation of NLRP3 and ASC as a result of NLRP3 and ASC oligomerization (Figure 2F). In contrast, β-carotene blocked speck formation by NLRP3 and ASC (Figure 2F), demonstrating that β-carotene disrupts the interaction between NLRP3 and ASC.

To confirm the significance of the interaction motif in NLRP3 PYD revealed by molecular docking modeling, we investigated whether mutating the interacting amino acid residues of NLRP3 PYD affected the inhibitory activity of β-carotene. The 5 amino acid residues in NLRP3 that formed the β-carotene binding pocket were mutated to lysine or arginine. Exogenous expression of wild-type (WT) NLRP3 along with ASC, caspase 1, and the iGLuc luciferase reporter in 293T cells resulted in increased luciferase expression, while β-carotene suppressed the luciferase expression induced by the NLRP3 inflammasome (Figure 3A). Exogenous expression of NLRP3 mutants harboring A69K, V72K, W73K, Y84R, or E91R induced luciferase expression to a similar degree as WT NLRP3 (Figure 3A). However, β-carotene failed to suppress the luciferase expression induced by the NLRP3 mutants (Figure 3A).

Reconstitution of WT NLRP3 with ASC and caspase 1 induced an increase in the secretion of IL-1β in 293T cells (Figure 3B). Beta-carotene reduced the IL-1β secretion induced by the WT NLRP3 inflammasome (Figure 3B). While reconstitution of NLRP3 mutants with ASC and caspase 1 increased IL-1β secretion to a similar degree as WT NLRP3, β-carotene was not able to block the IL-1β secretion induced by the NLRP3 mutants (Figure 3B). Additionally, exogenous expression of WT NLRP3, ASC, and caspase 1 in 293T cells resulted in the production of cleaved caspase 1 in 293T cells, while β-carotene inhibited the production of cleaved caspase 1 (Figure 3C). The inhibition of the production of cleaved caspase 1 by β-carotene was not prominent with NLRP3 mutants (Figure 3C).

Furthermore, β-carotene suppressed ASC speck formation in 293T cells transfected with WT NLRP3 and ASC, while ASC speck formation by NLRP3 mutants was not blocked by β-carotene (Figure 3D). Finally, SPR analysis showed that β-carotene did not bind to recombinant human NLRP3 PYD with the A69K or V72K mutation (Figure 3E). The results indicate that the amino acids in NLRP3 PYD are essential for the interaction between β-carotene and NLRP3, confirming the interactive motif suggested by the molecular docking model.

Prevention of acute gouty arthritis by oral administration of β-carotene by blocking NLRP3 inflammasome activation. We assessed the in vivo suppressive effects of β-carotene on the NLRP3 inflammasome using a mouse air pouch inflammation model. Oral administration of β-carotene abolished the production of caspase 1-p10 and mature IL-1β induced by MSU crystals in air pouch exudates (Supplementary Figure 4A, available on the *Arthritis & Rheumatology* web site at http://onlinelibrary.wiley.com/doi/10.1002/art.41245/abstract). Beta-carotene reduced caspase 1 activity increased by MSU crystals in air pouch exudates (Supplementary Figure 4B). Oral administration of β-carotene also prevented the MSU crystal–induced release of IL-1β and IL-18 into the air pouch exudates, as measured by ELISA (Supplementary Figure 4C). These results confirm the in vivo suppressive effects of β-carotene on the activation of the NLRP3 inflammasome. Histologic examination and MPO activity showed that neutrophil infiltration in the air pouch tissues and exudates was reduced by β-carotene (Supplementary Figures 4D and E). These results demonstrate the in vivo suppression of NLRP3 inflammasome activation by β-carotene, leading to attenuated in vivo inflammatory responses.

We then investigated whether β-carotene exerted in vivo suppressive activity against NLRP3 inflammasome–related diseases using acute gout mouse models. After mice were orally administered β-carotene, MSU crystals was injected into the hind feet of the mice (Figure 4A). MSU crystal injection led to an increase in paw thickness and neutrophil infiltration in foot tissues, as shown by histologic examination and MPO activity, while β-carotene decreased paw thickness to almost normal levels and blocked MSU crystal–induced recruitment of neutrophils to foot tissues (Figures 4B–E). The results demonstrate that oral administration of β-carotene alleviates the inflammatory symptoms of acute gout in mice. In this experiment, β-carotene prevented MSU crystal–induced production of caspase 1-p10 and IL-1β in mouse foot tissues (Figure 4F). Furthermore, β-carotene reduced caspase 1 activity increased by MSU crystals in foot tissue homogenates (Figure 4G). MSU crystal–induced IL-1β and IL-18 production in foot tissues was decreased by β-carotene (Figure 4H).

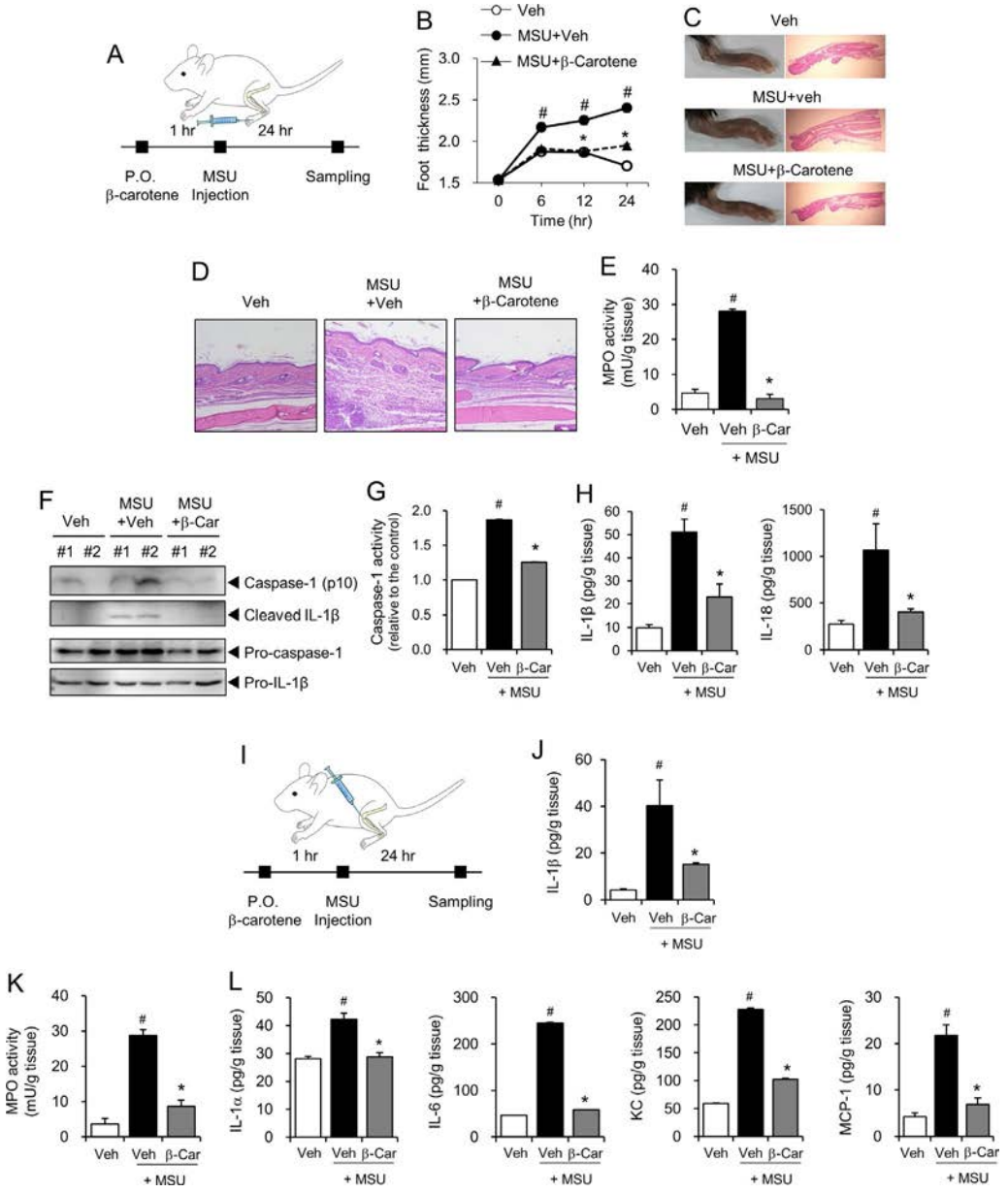

Figure 4. Oral administration of β-carotene attenuates in vivo activation of the NLRP3 inflammasome and inflammatory symptoms in acute gout models in mice. **A**–**H**, Either 30 mg/kg of β-carotene (β-Car) or 0.02% DMSO vehicle (Veh) in water was orally administered (P.O.) in mice. After 1 hour, either monosodium urate (MSU) crystals in 2 mg/0.1 ml of phosphate buffered saline (PBS) or PBS alone was subcutaneously injected into the right hind footpad. After 24 hours, footpad tissues were collected for further analysis. **A**, Experimental scheme. **B**, Time course of paw thickness. **C**, Hematoxylin and eosin (H&E) staining of hind feet. **D**, H&E staining of infiltrated neutrophils. Original magnification × 400. **E**, Myeloperoxidase (MPO) activity. **F**, Immunoblotting for the indicated molecules in footpad tissue. **G**, Caspase 1 enzyme activity in footpad tissue. **H**, Levels of interleukin-1β (IL-1β) and IL-18, as measured by enzyme-linked immunosorbent assay (ELISA). **I**–**L**, Either 30 mg/kg of β-carotene or 0.02% DMSO vehicle in water was orally administered in mice. After 1 hour, either 100 μg of MSU crystals in 10 μl of PBS or PBS alone was injected into the right knee joint of each mouse. After 24 hours, joint tissue homogenates were prepared for further analysis. **I**, Experimental scheme. **J**, IL-1β levels in the joint tissues of mice, as measured by ELISA. **K**, MPO activity in the joint tissues. **L**, IL-1α, IL-6, keratinocyte chemoattractant (KC), and monocyte chemotactic protein 1 (MCP-1) in the joint tissues, as measured by ELISA. Values are the mean ± SEM (n = 6 mice per group). # = $P < 0.05$ versus vehicle. * = $P < 0.05$ versus MSU crystals alone. Results are representative of at least 2 independent experiments. Color figure can be viewed in the online issue, which is available at http://onlinelibrary.wiley.com/doi/10.1002/art.41245/abstract.

To further investigate whether β-carotene would be effective in the treatment of gouty arthritis, MSU crystals was injected into the knee joints of mice after oral administration of β-carotene (Figure 4I). Beta-carotene prevented the increase of IL-1β induced by MSU crystals in the joint tissues, demonstrating the suppressive effects of β-carotene on the NLRP3

inflammasome in the joint tissues (Figure 4J). Oral administration of β-carotene in mice led to a decrease in MPO activity and inflammatory cytokines and chemokines, such as IL-1α, IL-6, KC, and MCP-1, in joint tissues injected with MSU crystals (Figures 4K and L). These results show that β-carotene suppresses MSU crystal–induced activation of the NLRP3 inflammasome and subsequent inflammatory symptoms in knee joint tissues. The results demonstrate the in vivo suppressive effects of β-carotene on NLRP3-dependent inflammatory responses, correlating well with its inhibition of NLRP3 inflammasome activation in gouty tissues.

Inhibition of the NLRP3 inflammasome by β-carotene in synovial fluid cells obtained from gout patients. To examine the efficacy of β-carotene in human cells, synovial fluid cells freshly isolated from the knee joints of gout patients were treated with β-carotene (Figure 5 and Supplementary Figure 5, available on the *Arthritis & Rheumatology* web site at http://onlinelibrary.wiley.com/doi/10.1002/art.41245/abstract). Production of caspase 1-p10 and mature IL-1β was detected in the culture supernatants of synovial fluid cells obtained from gout patients, while β-carotene treatment reduced the production of caspase 1-p10 and IL-1β (Figure 5A and Supplementary 5A). Consistent with this, IL-1β secretion from synovial fluid cells obtained from gout patients was decreased by β-carotene treatment in a dose-dependent manner (Figure 5B and Supplementary Figure 5B). The results show that β-carotene effectively suppressed the activation of the NLRP3 inflammasome and the secretion of mature IL-1β in the synovial fluid cells of gout patients, suggesting its efficacy in inhibiting NLRP3 inflammasome–mediated inflammation in human subjects.

DISCUSSION

To the best of our knowledge, this is the first study to present a direct binding antagonist for the PYD of NLRP3. Our results show that β-carotene directly binds to the PYD of NLRP3, thereby blocking the association between NLRP3 with ASC, and ultimately suppressing NLRP3 inflammasome activation. We provide the interaction motif for the binding of β-carotene to NLRP3 PYD, suggesting a new inhibitory platform for future antagonist development. Our study suggests that the PYD of NLRP3 could be an efficient target in the screening of drug candidates for the treatment of NLRP3-related diseases. Our findings further demonstrate a novel strategy to regulate the activity of the NLRP3 inflammasome and the pathology of related chronic diseases.

The NLRP3 inflammasome is composed of 3 domains: an LRR domain, a NACHT domain, and a PYD. The LRR domain is located at the carboxy terminal and recognizes microbial ligands and endogenous danger molecules. The NACHT domain comprises Walker A and Walker B motifs to exert ATPase activity and participates in the oligomerization of the NLRP3 inflammasome. The PYD domain at the amino-terminal is critical to associate with ASC via ASC via PYD–PYD interactions (21). There are some recent studies regarding inhibitors binding to NLRP3. CY-09 was reported to act as a direct inhibitor of NLRP3, thus enabling NLRP3 to bind to the Walker A motif of the NACHT domain, and thereby interfering with ATP binding to NLRP3 (5). Oridonin covalently binds to the cysteine 279 of NACHT domain, interrupting NLRP3 to interact with NEK7 (22). MCC950 was shown to directly bind to the Walker B motif to block ATPase activity (23). Tranilast directly binds to the NACHT domain to inhibit NLRP3–NLRP3 interaction via an ATPase-independent manner (24). Additionally, OLT1177 inhibits ATPase activity of the NLRP3, suggesting its

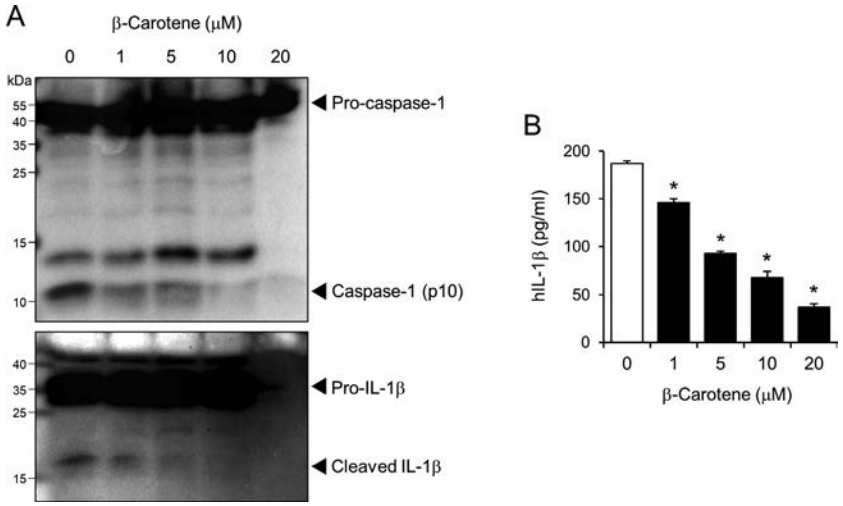

Figure 5. Efficacy of β-carotene in the suppression of the NLRP3 inflammasome in primary synovial fluid cells from a gout patient. Primary synovial fluid cells were isolated from a gout patient and treated with various doses of β-carotene for 16 hours. **A**, Levels of procaspase 1, caspase 1-p10, pro–interleukin-1β (proIL-1β), and IL-1β were analyzed by immunoblotting. **B**, Human IL-1β (hIL-1β) was assessed in cell supernatants using enzyme-linked immunosorbent assay. Values are the mean ± SEM of 5 separate assays run on the sample from 1 gout patient, at each dose of β-carotene. * = $P < 0.05$ versus group that received vehicle alone.

binding to NLRP3 (25). Mostly, these inhibitors target the NACHT domain of the NLRP3, resulting in the suppression of ATPase activity, while inhibitors targeting the PYD domain have been rarely studied. Therefore, our study provides a novel inhibitory method to suppress the NLRP3 inflammasome by directly binding to its PYD domain.

Beta-carotene is also called plant-derived provitamin A, yielding 2 molecules of vitamin A (retinol) by β-carotene 15, 15′-monoxygenase in the intestinal mucosa (26). Although the antioxidant activity of β-carotene is widely reported, our study is the first to reveal a novel mechanism by which β-carotene exerts antiinflammatory activity and regulates immune responses. The results of our study demonstrate that β-carotene effectively prevents NLRP3 inflammasome activation, linking to in vivo inhibitory efficacy for NLRP3-driven diseases such as gout. Our findings corroborate with results from an epidemiologic study of a population in the US (27), which demonstrated that there is an inverse association between serum uric acid level and serum β-carotene level and that the intake of β-carotene may be beneficial in protecting against hyperglycemia and gout. Our findings suggest that pharmacologic application of β-carotene could improve inflammatory symptoms related to the NLRP3 inflammasome, such as gout. In future studies, the application of β-carotene could be expanded to other diseases related to NLRP3 inflammasome–mediated autoinflammation (e.g., adult-onset Still's disease, juvenile idiopathic arthritis, and Behçet's disease) (28).

In healthy subjects, basal serum β-carotene levels are <1 μmoles/liter. However, several intervention studies have shown the eminent elevation of serum β-carotene levels after supplementation of β-carotene. Micozzi et al reported that continuous intake of 30 mg of β-carotene each day for 6 weeks increased plasma β-carotene levels in healthy men from 0.303 ± 0.130 μmoles/liter at baseline to 7.901 ± 1.381 μmoles/liter (29). The Carotene and Retinol Efficacy Trial showed that the intake of 30 mg of β-carotene each day for 10 months resulted in a marked increase in serum β-carotene levels from a mean 0.13 μmoles/liter to 3.75 μmoles/liter (30). In the Carotene Prevention Trial, with the supplementation of 50 mg of β-carotene each day, plasma β-carotene concentrations increased by 9–10-fold throughout the 60 month study period with a median of 0.225 μmoles/liter (interquartile range [IQR] 0.125–0.355) at baseline to 2.255 μmoles/liter (IQR 1.170–4.395) at 3 months, 3.015 μmoles/liter (IQR 1.535–5.830) at 48 months, and 2.775 μmoles/liter (IQR 1.945–6.320) at 60 months (31). In the Skin Cancer Prevention Study, median plasma β-carotene levels increased from 0.335 μmoles/liter at entry to 3.163 μmoles/liter in subjects who received a 1-year supplementation of 50 mg of β-carotene per day. Plasma β-carotene concentrations even ranged up to 16.090 μmoles/liter (32). These findings suggest that consistent supplementation with β-carotene may lead to the elevation of serum β-carotene levels to inhibitory doses in the 10–20 μmoles range.

In summary, the crucial role of the NLRP3 inflammasome in the pathology of acute gout has been confirmed in human studies (33–35). Therefore, our experimental results may further support the clinical relevance of the NLRP3 inflammasome in gout by demonstrating that β-carotene supplementation hampers NLRP3 inflammasome activity and resolves the progression of acute gout. Although further investigation in human subjects is needed to validate the therapeutic significance of our work, we present pivotal evidence that β-carotene acts as an antiinflammatory vitamin that inhibits the NLRP3 inflammasome.

AUTHOR CONTRIBUTIONS

All authors were involved in drafting the article or revising it critically for important intellectual content, and all authors approved the final version to be published. Dr. Lee had full access to all of the data in the study and takes responsibility for the integrity of the data and the accuracy of the data analysis.

Study conception and design. Yang, H. E. Lee, Kang, H. S. Lee, J. Y. Lee.

Acquisition of data. Yang, H. E. Lee, Moon, Ko, Koh, Seok, Min, J.Y. Lee.

Analysis and interpretation of data. Yang, H. E. Lee, Heo, Cho, Fitzgerald, J. Y. Lee.

REFERENCES

1. Franchi L, Munoz-Planillo R, Nunez G. Sensing and reacting to microbes through the inflammasomes. Nat Immunol 2012;13:325–32.
2. Mangan MS, Olhava EJ, Roush WR, Seidel HM, Glick GD, Latz E. Targeting the NLRP3 inflammasome in inflammatory diseases [review]. Nat Rev Drug Discov 2018;17:588–606.
3. Coll RC, Robertson AA, Chae JJ, Higgins SC, Munoz-Planillo R, Inserra MC, et al. A small-molecule inhibitor of the NLRP3 inflammasome for the treatment of inflammatory diseases. Nat Med 2015;21:248–55.
4. Youm YH, Nguyen KY, Grant RW, Goldberg EL, Bodogai M, Kim D, et al. The ketone metabolite β-hydroxybutyrate blocks NLRP3 inflammasome-mediated inflammatory disease. Nat Med 2015;21:263–9.
5. Jiang H, He H, Chen Y, Huang W, Cheng J, Ye J, et al. Identification of a selective and direct NLRP3 inhibitor to treat inflammatory disorders. J Exp Med 2017;214:3219–38.
6. Yang G, Yeon SH, Lee HE, Kang HC, Cho YY, Lee HS, et al. Suppression of NLRP3 inflammasome by oral treatment with sulforaphane alleviates acute gouty inflammation. Rheumatology (Oxford) 2018;57:727–36.
7. Lee HE, Yang G, Kim ND, Jeong S, Jung Y, Choi JY, et al. Targeting ASC in NLRP3 inflammasome by caffeic acid phenethyl ester: a novel strategy to treat acute gout. Sci Rep 2016;6:38622.
8. Masumoto J, Taniguchi S, Sagara J. Pyrin N-terminal homology domain- and caspase recruitment domain-dependent oligomerization of ASC. Biochem Biophys Res Commun 2001;280:652–5.
9. Lu A, Magupalli VG, Ruan J, Yin Q, Atianand MK, Vos MR, et al. Unified polymerization mechanism for the assembly of ASC-dependent inflammasomes. Cell 2014;156:1193–206.
10. Franklin BS, Bossaller L, de Nardo D, Ratter JM, Stutz A, Engels G, et al. The adaptor ASC has extracellular and 'prionoid' activities that propagate inflammation. Nat Immunol 2014;15:727–37.
11. Schmidt FI, Lu A, Chen JW, Ruan J, Tang C, Wu H, et al. A single domain antibody fragment that recognizes the adaptor ASC defines

the role of ASC domains in inflammasome assembly. J Exp Med 2016;213:771–90.
12. Bae JY, Park HH. Crystal structure of NALP3 protein pyrin domain (PYD) and its implications in inflammasome assembly. J Biol Chem 2011;286:39528–36.
13. Joung SM, Park ZY, Rani S, Takeuchi O, Akira S, Lee JY. Akt contributes to activation of the TRIF-dependent signaling pathways of TLRs by interacting with TANK-binding kinase 1. J Immunol 2011;186:499–507.
14. Yang G, Lee HE, Shin SW, Um SH, Lee JD, Kim KB, et al. Efficient transdermal delivery of DNA nanostructures alleviates atopic dermatitis symptoms in NC/Nga mice. Adv Funct Mater 2018;28:1801918.
15. Yang G, Lee HE, Yeon SH, Kang HC, Cho YY, Lee HS, et al. Licochalcone A attenuates acne symptoms mediated by suppression of NLRP3 inflammasome. Phytother Res 2018;32:2551–9.
16. Lee HE, Yang G, Park YB, Kang HC, Cho YY, Lee HS, et al. Epigallocatechin-3-gallate prevents acute gout by suppressing NLRP3 inflammasome activation and mitochondrial DNA synthesis. Molecules 2019;24:E2138.
17. Amaral FA, Costa VV, Tavares LD, Sachs D, Coelho FM, Fagundes CT, et al. NLRP3 inflammasome-mediated neutrophil recruitment and hypernociception depend on leukotriene B(4) in a murine model of gout. Arthritis Rheum 2012;64:474–84.
18. Bartok E, Bauernfeind F, Khaminets MG, Jakobs C, Monks B, Fitzgerald KA, et al. iGLuc: a luciferase-based inflammasome and protease activity reporter. Nat Methods 2013;10:147–54.
19. Vajjhala PR, Mirams RE, Hill JM. Multiple binding sites on the pyrin domain of ASC protein allow self-association and interaction with NLRP3 protein. J Biol Chem 2012;287:41732–43.
20. Fernandes-Alnemri T, Wu J, Yu JW, Datta P, Miller B, Jankowski W, et al. The pyroptosome: a supramolecular assembly of ASC dimers mediating inflammatory cell death via caspase-1 activation. Cell Death Differ 2007;14:1590–604.
21. Latz E, Xiao TS, Stutz A. Activation and regulation of the inflammasomes [review]. Nat Rev Immunol 2013;13:397–411.
22. He H, Jiang H, Chen Y, Ye J, Wang A, Wang C, et al. Oridonin is a covalent NLRP3 inhibitor with strong anti-inflammasome activity. Nat Commun 2018;9:2550.
23. Coll RC, Hill JR, Day CJ, Zamoshnikova A, Boucher D, Massey NL, et al. MCC950 directly targets the NLRP3 ATP-hydrolysis motif for inflammasome inhibition. Nat Chem Biol 2019;15:556–9.
24. Huang Y, Jiang H, Chen Y, Wang X, Yang Y, Tao J, et al. Tranilast directly targets NLRP3 to treat inflammasome-driven diseases. EMBO Mol Med 2018;10:e8689.
25. Marchetti C, Swartzwelter B, Gamboni F, Neff CP, Richter K, Azam T, et al. OLT1177, a β-sulfonyl nitrile compound, safe in humans, inhibits the NLRP3 inflammasome and reverses the metabolic cost of inflammation. Proc Natl Acad Sci U S A 2018;115:E1530–9.
26. Stutz H, Bresgen N, Eckl PM. Analytical tools for the analysis of β-carotene and its degradation products. Free Radic Res 2015;49:650–80.
27. Ford ES, Choi HK. Associations between concentrations of uric acid with concentrations of vitamin A and β-carotene among adults in the United States. Nutr Res 2013;33:995–1002.
28. Jesus AA, Goldbach-Mansky R. IL-1 blockade in autoinflammatory syndromes. Annu Rev Med 2014;65:223–44.
29. Micozzi MS, Brown ED, Edwards BK, Bieri JG, Taylor PR, Khachik F, et al. Plasma carotenoid response to chronic intake of selected foods and β-carotene supplements in men. Am J Clin Nutr 1992;55:1120–5.
30. Redlich CA, Chung JS, Cullen MR, Blaner WS, van Bennekum AM, Berglund L. Effect of long-term β-carotene and vitamin A on serum cholesterol and triglyceride levels among participants in the Carotene and Retinol Efficacy Trial (CARET). Atherosclerosis 1999;143:427–34.
31. Mayne ST, Cartmel B, Silva F, Kim CS, Fallon BG, Briskin K, et al. Effect of supplemental β-carotene on plasma concentrations of carotenoids, retinol, and α-tocopherol in humans. Am J Clin Nutr 1998;68:642–7.
32. Nierenberg DW, Stukel TA, Baron JA, Dain BJ, Greenberg ER, for the Skin Cancer Prevention Study Group. Determinants of increase in plasma concentration of β-carotene after chronic oral supplementation. Am J Clin Nutr 1991;53:1443–9.
33. Wang LF, Ding YJ, Zhao Q, Zhang XL. Investigation on the association between NLRP3 gene polymorphisms and susceptibility to primary gout. Genet Mol Res 2015;14:16410–4.
34. Deng J, Lin W, Chen Y, Wang X, Yin Z, Yao C, et al. rs3806268 of NLRP3 gene polymorphism is associated with the development of primary gout. Int J Clin Exp Pathol 2015;8:13747–52.
35. Meng DM, Zhou YJ, Wang L, Ren W, Cui LL, Han L, et al. Polymorphisms in the NLRP3 gene and risk of primary gouty arthritis. Mol Med Rep 2013;7:1761–6.

Arthritis & Rheumatology
Vol. 72, No. 7, July 2020, pp 1203–1213
DOI 10.1002/art.41220

American College of Rheumatology
Empowering Rheumatology Professionals

Aberrant Salience? Brain Hyperactivation in Response to Pain Onset and Offset in Fibromyalgia

Catherine S. Hubbard,[1] Asimina Lazaridou,[2] Christine M. Cahalan,[2] Jieun Kim,[3] Robert R. Edwards,[4] Vitaly Napadow,[5] and Marco L. Loggia[5]

Objective. While much brain research on fibromyalgia (FM) focuses on the study of hyperresponsiveness to painful stimuli, some studies suggest that the increased pain-related brain activity often reported in FM studies may be partially explained by stronger responses to salient aspects of the stimulation rather than, or in addition to, the stimulation's painfulness. Therefore, this study was undertaken to test our hypothesis that FM patients would demonstrate elevated brain responses to both pain onset and offset—2 salient sensory events of opposing valences.

Methods. Thirty-eight FM patients (mean ± SD age 46.1 ± 13.4 years; 33 women) and 15 healthy controls (mean ± SD age 45.5 ± 12.4; 10 women) received a moderately painful pressure stimulus to the leg during blood oxygen level–dependent (BOLD) functional magnetic resonance imaging. Stimulus onset and offset transients were analyzed using a general linear model as stick functions.

Results. During pain onset, higher BOLD signal response was observed in FM patients compared to healthy controls in dorsolateral and ventrolateral prefrontal cortices (DLPFC and VLPFC, respectively), orbitofrontal cortex (OFC), frontal pole, and precentral gyrus (PrCG). During pain offset, higher and more widespread BOLD signal response was demonstrated in FM patients compared to controls in frontal regions significantly hyperactivated in response to onset. In FM patients, some of these responses were positively correlated with pain unpleasantness ratings (VLPFC, onset; r = 0.35, $P = 0.03$), pain catastrophizing scores (DLPFC, offset; r = 0.33, $P = 0.04$), or negatively correlated with stimulus intensity (OFC, offset; r = –0.35, $P = 0.03$) (PrCG, offset; r = –0.39, $P = 0.02$).

Conclusion. Our results suggest that the increased sensitivity exhibited by FM patients in response to the onset and offset of painful stimuli may reflect a more generalized hypersensitivity to salient sensory events, and that brain hyperactivation may be a mechanism potentially involved in the generalized hypervigilance to salient stimuli in FM.

INTRODUCTION

Fibromyalgia (FM) is a poorly understood condition characterized by a constellation of symptoms including chronic widespread musculoskeletal pain and tenderness, extreme fatigue, and disturbances in mood, cognition, sleep, and memory (1–3). While the pathogenesis of FM is not well understood, the current consensus is that this condition is principally a disorder of central origin, arising from sensitized afferent nociceptive circuits and/or disrupted descending pain modulatory signaling, which in turn leads to widespread amplification of pain (1,4–6) (although some studies have provided evidence of peripheral changes in a subgroup of FM patients [7,8]). This persistent state of heightened central nervous system (CNS) reactivity or central pain amplification often manifests clinically with increased sensitivity to painful stimuli (hyperalgesia) and the tendency to perceive nonpainful stimuli as painful (allodynia).

Psychophysical studies utilizing quantitative sensory testing (QST) have shown that FM patients, when subjected to levels of stimulus intensity equivalent to those in healthy controls, report

Supported by the NIH (National Center for Research Resources grants P41-RR-14075, S10-RR-021110, and S10-RR-023043). Dr. Napadow's work was supported by the NIH (National Center for Complementary and Integrative Health grant P01-AT-006663 and National Institute of Arthritis and Musculoskeletal and Skin Diseases grant R01-AR-064367). Dr. Loggia's work was supported by the NIH (National Institute of Neurological Disorders and Stroke grant R01-NS-094306-01A1), the International Association for the Study of Pain (Early Career Research grant), and the US Department of Defense (grant W81XWH-14-1-0543).

[1]Catherine S. Hubbard, PhD: Harvard Medical School and Massachusetts General Hospital, Boston, Massachusetts; [2]Asimina Lazaridou, PhD, Christine M. Cahalan, BS: Brigham and Women's Hospital, Boston, Massachusetts; [3]Jieun Kim, PhD: Massachusetts General Hospital, Charlestown; [4]Robert R. Edwards, PhD: Brigham and Women's Hospital and Harvard Medical School, Boston, Massachusetts; [5]Vitaly Napadow, PhD, Marco L. Loggia, PhD: Harvard Medical School, Massachusetts General Hospital, and Brigham and Women's Hospital, Boston, Massachusetts.

No potential conflicts of interest relevant to this article were reported.

Address correspondence to Marco L. Loggia, PhD, Massachusetts General Hospital, A. A. Martinos Center for Biomedical Imaging, 149 Thirteenth Street, Room 2301, Charlestown, MA 02129. E-mail: marco.loggia@mgh.harvard.edu.

Submitted for publication October 11, 2019; accepted in revised form January 28, 2020.

greater perceived pain to a variety of sensory stimuli, including mechanical (deep blunt pressure), thermal (heat and cold), and electrical stimuli (9,10). Moreover, compared to controls, FM patients exhibit markedly reduced pain thresholds, potentiated temporal summation, and attenuated descending pain modulatory responses (11,12). Neuroimaging studies complement and extend these findings by providing a glimpse into the putative neural substrates underlying the pathophysiology of FM. For example, FM patients relative to controls display altered structural, neurochemical, neuroinflammatory, and brain network connectivity patterns as well as augmented brain responses to painful and nonpainful somatosensory stimuli in sensory-discriminative (e.g., primary and secondary somatosensory cortex), affective-motivational (e.g., cingulate and insular-opercular regions), and cognitive-attentional (e.g., dorsolateral prefrontal cortex) pain processing areas, as well as regions involved in the processing of punishing and rewarding events (ventral tegmental area) (13–20).

In addition to heightened pain perception and augmented pain-related brain responses to tactile stimuli, evidence of generalized hypersensitivity to visual, auditory, and olfactory stimuli has also been observed in FM patients (10,21–24). Given that FM patients appear to be hypersensitive to different types of sensory stimuli, we hypothesized that this increased sensitivity in response to noxious stimuli may partly reflect a more generalized hypersensitivity to salient sensory events. Thus, we implemented an analysis approach to evaluate the distinct brain responses to evoked pain onset and offset, which are 2 salient sensory events with opposing hedonic value. We reasoned that heightened responses to both pain onset and pain offset would support the view of a generalized hypersensitivity to salient stimuli in FM. Moreover, given that FM patients tend to report higher levels of negative affect, particularly pain catastrophizing, compared to controls, we hypothesized that exaggerated brain responses to pain onset/offset in FM would be positively associated with pain catastrophizing.

PATIENTS AND METHODS

Subject characteristics. A total of 53 FM patients (mean ± SD age 46.3 ± 11.4 years) and 17 control subjects (mean ± SD age 44.1 ± 14.8 years) initially entered the study. Each subject provided written informed consent prior to commencement of the study, and all study procedures were approved by the local institutional review board. Inclusion criteria included an age of ≥18 years and a diagnosis of FM by a rheumatologist for ≥1 year according to the American College of Rheumatology 2010 classification criteria for FM (2). Exclusion criteria included a history of psychiatric, neurologic, or autoimmune disorders; cardiac events and/or head injury; claustrophobia or magnetic resonance imaging (MRI) contraindication; current recreational drug use, including opioids; and pregnancy or plans to become pregnant. Patients were instructed to continue their medication regimens throughout the course of the study, which included antidepressants, gabapentin, nonsteroidal antiinflammatory drugs, and/or acetaminophen. Healthy control subjects were frequency-matched with the FM patients for age and sex.

It should be mentioned that while the number of control subjects in the present investigation is typical for group comparisons in functional MRI (fMRI) studies, we have elected to include a significantly larger number of FM patients. This unbalanced design was adopted to maximize statistical power and dynamic range for regression analyses evaluating the association between brain activations and behavioral variables within the patient group (see below), thereby enhancing our ability to understand the clinical significance of the functional changes observed across groups, as demonstrated in previous studies (19,25).

Experimental design and procedures. In our previous study (25), we examined brain responses to the prolonged painful cuff stimulation period, as well as the 15-second post-stimulus offset period to model painful after-sensations in the same sample of FM patients and controls. In contrast, in the present study, we investigated brain response to cuff stimulus onset and offset, both rapid transitory events, in order to examine the degree to which FM patients are hypersensitive to salient sensory stimuli represented by pain onset (cuff inflation) and pain offset (cuff deflation).

Subjects participated in a behavioral visit performed at Brigham and Women's Hospital and an MRI visit held at Athinoula A. Martinos Center for Biomedical Imaging. At the behavioral visit, subjects were asked to rate the severity and extent of their pain using a numerical rating scale (NRS) followed by administration of the Brief Pain Inventory (26), Neuropathic Pain Questionnaire (27), Widespread Pain Inventory, Symptom Severity Index (2), Pain Catastrophizing Scale (PCS) (28), Beck Depression Inventory (29), and a verbal anxiety NRS. Given the significant association between PCS scores and perceptual differences in painful after-sensations in FM patients that was previously reported by our group (25), we focused on the PCS to further evaluate the role between catastrophizing and brain processing of salient aspects of the painful stimulation (i.e., pain onset/offset).

Upon completion of self-report measures, subjects underwent QST, which included a cuff pain threshold assessment. Each subject's cuff pain threshold was individually determined using cuff pain algometry with an E20 Rapid Cuff Inflation System (Hokanson), which was adapted to inflate (i.e., reach the target pressures) and deflate (i.e., return to baseline) in ~2 seconds, in order to minimize the risk of startling the participants. For cuff pain threshold assessment, a 13 × 85 centimeter wide vascular pressure cuff was placed around the subject's left calf and secured with a Velcro strap. The cuff was connected to the E20 device and inflated to a pressure (mm Hg) individually calibrated to elicit a target pain intensity rating of ~40 on a 100-point scale

ranging from a score of 0 (indicating no pain) to100 (indicating worst pain imaginable). The pressure at which the subject rated a pain intensity of 40 on a 100-point scale was then used during the MRI cuff pain paradigm.

MRI acquisition, preprocessing, and statistical analyses. Functional MRI data were acquired using a 3T Siemens Tim Trio scanner equipped with a 32-channel head coil (Siemens Healthcare). A high-resolution structural scan was collected using a multiecho magnetization-prepared rapid gradient-echo pulse sequence (repetition time [TR] 2.53 seconds, echo time [TE] of TE1 1.64 msec, TE2 3.5 msec, TE3 5.36 msec, and TE4 7.22 msec, flip angle 7°, voxel size 1 × 1 × 1 mm). A T2*-weighted echo-planar image pulse sequence was also used to obtain high-resolution functional images during the cuff pain paradigm (TR 2 seconds, TE 30 msec, 37 slices, voxel size 3.1 × 3.1 × 3.6 mm). A total of 4 blood oxygen level–dependent (BOLD) runs were acquired (25). For each run, 2 block cuff pressure pain stimuli were delivered at the pressure previously determined during the threshold assessment procedure. The cuff pressure stimuli were delivered with a variable duration (75–105 seconds with a mean ± SD duration of 90 ± 10 seconds) to limit predictability. Following the end of each run, subjects were asked to rate the average pain intensity and unpleasantness of the stimulus using the NRS.

Functional MRI data preprocessing and analyses was performed with fMRI Expert Analysis Tool (FEAT; version 6), part of the Functional Magnetic Resonance Imaging of the Brain (FMRIB) Software Library (www.fmrib.ox.ac.uk/fsl). Our imaging pipeline included slice timing (slicetimer) followed by motion correction using FMRIB's Linear Image Registration Tool (MCFLIRT) (30), skull stripping using FMRIB Software Library's brain extraction tool (BET) (31), realignment of mean fMRI volume with FLIRT (30,32), grand mean intensity normalization by a single multiplicative factor, high-pass temporal filtering (Gaussian-weighted least-squares straight-line fitting [σ = 136–164 seconds depending on the run, estimated using cutoffcalc]), and spatial smoothing with a full-width half-maximum of 5 mm. Time-series statistical analysis was conducted using FMRIB's Improved Linear Model (FILM) with local autocorrelation correction (33). Cortical surface reconstruction was performed using FreeSurfer software (bbregister tool) for improved structural/functional coregistration purposes (34).

A within-subject analysis using a general linear model was performed by modeling the stimulus onset and offset transients as stick functions (35–37), each lasting a single TR in duration, corresponding to the approximate time of the cuff inflation and deflation (i.e., 2 seconds). In addition, the sustained tonic response between the onset and the offset periods was modeled as a boxcar function and designated as a regressor of no interest in the design matrix, lasting 75–105 seconds in duration. The model also included the 15-second post-stimulus period after stimulus offset, which we previously used to evaluate brain activity associated with painful after-sensations (25). All regressors were convolved with a canonical double-gamma hemodynamic response function (HRF). To minimize the effect of motion in our estimates of brain responses to pain onsets and pain offsets, the 6 head motion parameters (6 translations and 6 rotations), as well as a regressor of no interest for each volume determined to be an outlier in terms of motion (computed using fsl_motions_outliers), were entered into the design matrix. Time points within each run were flagged as outliers if they were deemed to have been significantly affected by motion based on the root mean square frame displacement (38), as performed in our previous study (25).

The relatively conservative approach of scrubbing motion outliers was used given our specific focus on stimulus onset and offset, transition phases that might be particularly vulnerable to stimulus-correlated motion. However, group comparisons revealed no significant differences in head motion (25). The resulting first-level parameter estimates and variance maps were registered to the Montreal Neurological Institute (MNI) 152 standard space using FMRIB's Non-linear Image Registration Tool (FNIRT) (39). Group maps were generated for the cuff pain onset and offset periods using a series of whole-brain voxelwise general linear models with FMRIB's Local Analysis of Mixed Effects (FLAME) 1+2 (40) and enabled automatic outlier detection enabled. The use of FLAME 1+2 is well suited for unbalanced designs such as this one because of its ability to model different variances using Metropolis–Hastings Markov chain Monte Carlo sampling (41,42) (https://fsl.fmrib.ox.ac.uk/fsl/fslwiki/FEAT/UserGuide). Statistical maps were cluster-corrected for multiple comparisons using FMRIB Software Library's default cluster-forming voxelwise threshold ($Z > 2.3$) and a corrected cluster significance threshold ($P < 0.05$).

Given that comparisons of pain onset and pain offset yielded significant differences in FM patients compared to controls (with significantly higher pain onset/offset effects in overlapping regions of the brain in FM patients), we generated an intersection mask of both contrast maps and parcellated it using anatomic labels derived from the Harvard Oxford Atlas in the FMRIB Software Library. Using an arbitrary threshold of 30, this parcellation method resulted in 5 subregions, which included the dorsolateral prefrontal cortex (DLPFC), ventrolateral prefrontal cortex (VLPFC), orbitofrontal cortex (OFC), precentral gyrus (PrCG), and frontal pole (FP). These subregions were used as masks to extract and display percent signal change and time courses for illustrative purposes. To calculate percent signal change, the contrasts for parameter estimates from the onset and offset phases for each subject, along with the peak-peak height of the regressor and the mean of the functional time series data, were extracted from each voxel within our masks for each subject and averaged within groups. To visualize differences in percent signal change between groups for each mask, bar graphs were created to display the mean ± SEM for cuff pain onset and offset.

Table 1. Demographic, clinical, and psychosocial characteristics of the study cohort*

Variable	Healthy controls (n = 15)	Fibromyalgia patients (n = 38)	*P*
Age, years	45.53 ± 12.40	46.13 ± 13.44	0.882
PCS score, 0–52 scale	5.93 ± 5.97	23.16 ± 13.08	<0.001
CPA threshold	190.67 ± 85.81	101.18 ± 57.20	<0.001
NRS score, 0–100 scale	42.54 ± 3.82	44.84 ± 7.70	0.309

* Values are the mean ± SD. PCS = Pain Catastrophizing Scale; CPA = cuff pressure algometry; NRS = numerical rating scale.

Additionally, Pearson's 2-tailed bivariate correlational analyses were performed in patients between percent signal change values obtained from each of the aforementioned 5 masks (i.e., DLPFC, VLPFC, OFC, PrCG, and the FP) for onset, offset, and PCS scores. Lastly, given that salience can be determined both by the intensity of a stimulation as well as its painfulness, we performed an additional series of within-group exploratory correlational analyses via Pearson's 2-tailed correlation coefficient test between percent signal change values extracted from each of the 5 masked subregions during both onset and offset, cuff pressure levels (mm Hg), and pain ratings. Since these were not planned comparisons, but instead post hoc adjunctive correlational analyses, correction for multiple comparisons was not performed.

RESULTS

A total of 43 FM patients and 15 controls participated in the fMRI visit. Five subjects were excluded from analyses due to either technical difficulties encountered during scanning,

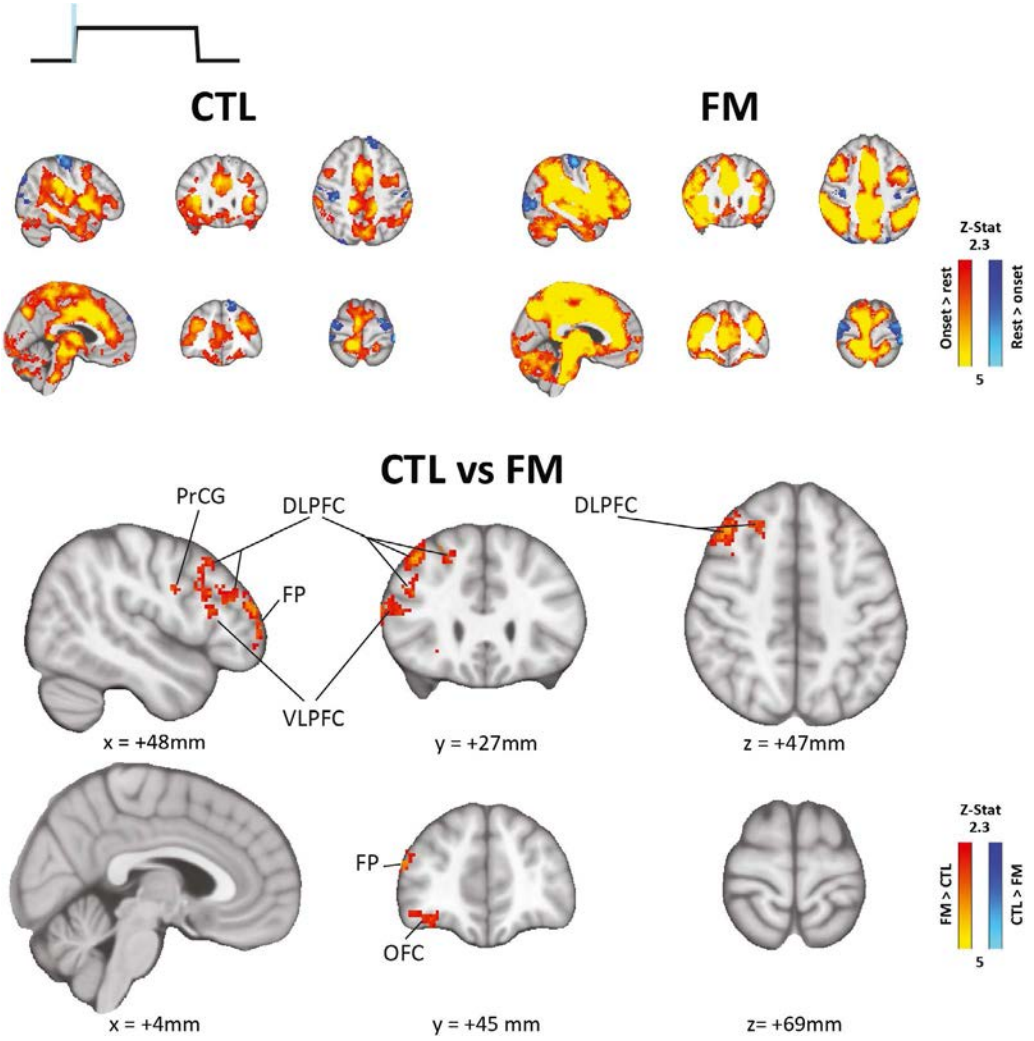

Figure 1. Statistical maps showing within-group brain responses to cuff pain onset for healthy controls (CTL) and fibromyalgia (FM) patients (top), with the group difference map indicating enhanced activation in several brain regions in FM patients compared to healthy controls (bottom). Increased brain activity in response to pain onset in the frontal cortical areas was observed in FM patients compared to controls, including in the dorsolateral prefrontal cortex (DLPFC), ventrolateral PFC (VLPFC), orbitofrontal cortex (OFC), precentral gyrus (PrCG), and frontal pole (FP).

incorrect scan parameters used, incomplete scan sessions, and in one case, due to a subject falling asleep during scanning. Therefore, the final sample for all subsequent analyses consisted of 38 FM patients (mean ± SD age 46.1 ± 13.4 years; 33 women) and 15 healthy controls (mean ± SD age 45.5 ± 12.4 years; 10 women). Demographic and behavioral data from the final sample of FM patients and controls are shown in Table 1. As expected and previously reported (25), the pressure required to elicit comparable pain ratings was significantly lower in FM patients compared to controls.

Functional MRI response to pain onset and offset. During cuff pain onset, both groups showed widespread increases in BOLD signaling, including in the primary somatosensory/motor (S1/M1; leg area), secondary somatosensory (S2), anterior and posterior insular, posterior parietal, pregenual anterior, middle and posterior cingulate, and lateral and medial prefrontal cortices, as well as in the cerebellum, basal ganglia, thalamus, and brainstem. Both groups also showed deactivation in S1/M1 (outside of the leg area) and higher-order visual cortices (e.g., lateral occipital cortex) (Figure 1).

Results from the whole-brain voxelwise group comparison analyses demonstrated that in response to cuff pain onset, FM patients (relative to controls) showed significantly greater activation in the frontal cortex, including the VLPFC (i.e., the inferior frontal gyrus), DLPFC (i.e., middle and superior frontal gyri), OFC, PrCG, and FP (see Table 2 for cluster information).

During pain offset, activations were demonstrated in both groups in the S2 anterior and posterior insulae and anterior middle cingulate cortices and in the basal ganglia, thalamus, and brainstem, with deactivations observed in the S1/M1 area (outside of the leg representation) and in the occipital, medial prefrontal, and dorsolateral prefrontal cortices (Figure 2). For FM patients, in response to stimulus offset, elevated BOLD signaling was demonstrated in the frontal cortex, including the DLPFC, VLPFC, OFC, PrCG, and FP, compared to healthy controls. Relative to controls, greater BOLD signal increases were seen in FM patients in regions not statistically significant in the onset contrast, including the dorsomedial prefrontal cortex, supplementary motor area, paracentral lobule, posterior cingulate gyrus, precuneus, posterior parietal cortex, fusiform and lingual gyri, middle temporal gyrus, bilateral thalamus, caudate nuclei, and cerebellum (see Table 2 for cluster information).

While the contrast maps for both pain onset and offset demonstrated that activation of several brain regions—including the DLPFC, VLPFC, OFC, PrCG, and FP—were each significantly enhanced in FM patients compared to healthy controls (Figures 3A and B), we found that such group differences were driven by variations in the activity patterns in the 2 phases. In response to the stimulus onset, both groups generally responded with activations in these regions, which were larger in FM patients (Figure 3C). During stimulus offset, however, activations were demonstrated in regions in FM patients in which deactivations were demonstrated in healthy controls

Table 2. Group differences in brain responses to pain onset and offset*

	Cluster size, no. of voxels	*P*	Z statistic	Peak		
				X	Y	Z
Pain onset						
FM patients > healthy controls						
R MFG	1,397	0.000404	4.41	42	14	36
R SFG			4.32	24	28	50
R MFG			4.17	40	26	46
R IFG			3.64	60	18	18
R FP			3.57	48	48	14
R PrCG			3.58	48	0	28
R OFG			3.29	28	32	−8
Pain offset						
FM patients > healthy controls						
R precuneus	17,067	1.79×10^{-23}	4.97	8	−76	48
R SFG			4.87	24	10	48
L PrCG			4.84	−2	−16	58
R FP			4.72	50	44	16
R OFG			3.71	32	40	−8
R MTG	8,567	1.63×10^{-14}	4.72	56	−48	−10
L fusiform gyrus			4.7	−20	−90	−20
L lingual/parahippocampal gyrus			3.25	−30	−46	−6
L thalamus	1,711	0.000212	4.45	−14	−6	14
R PCG			4.22	4	−50	10

* No significant group differences in brain responses to pain offset or onset were observed in healthy controls. FM = fibromyalgia; MFG = middle frontal gyrus; SFG = superior frontal gyrus; IFG = inferior frontal gyrus; FP = frontal pole; PrCG = precentral gyrus; OFG = orbital frontal gyrus; MTG = middle temporal gyrus; PCG = posterior cingulate gyrus.

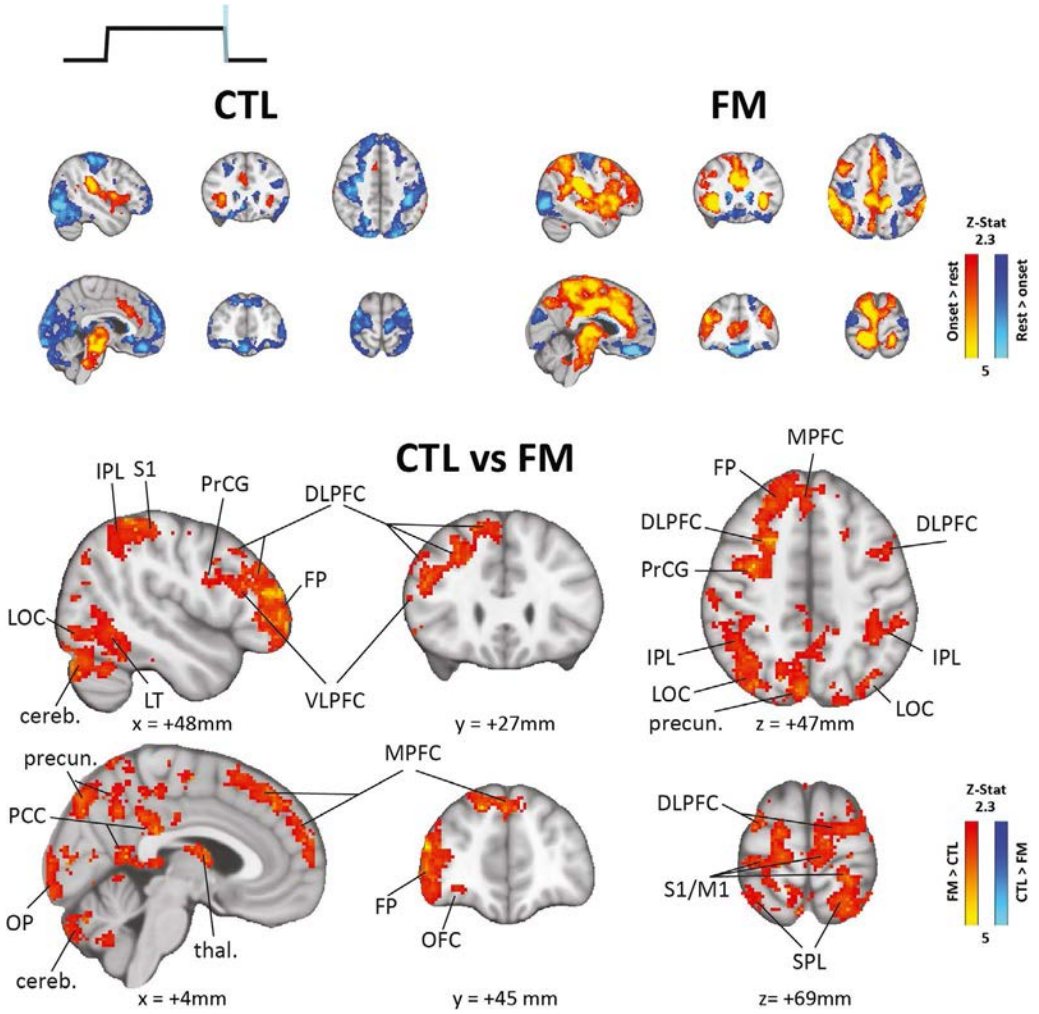

Figure 2. Statistical maps illustrating within-group brain responses to cuff pain offset for healthy controls and FM patients (top), with the group difference map displaying the contrast of enhanced activation in the brain regions of FM patients compared to healthy controls (bottom). Increased brain activity in response to pain offset in the lateral prefrontal cortical areas was observed in FM patients compared to controls, including in the DLPFC, VLPFC, OFC, PrCG, and FP. cereb. = cerebellum; LOC = lateral occipital cortex; IPL = inferior parietal lobule; S1 = primary somatosensory cortex; LT = lateral temporal cortex; precun. = precuneus; MPFC = medial prefrontal cortex; OP = occipital pole; PCC = posterior cingulate cortex; thal. = thalamus; M1 = primary motor cortex; SPL = superior parietal lobule (see Figure 1 for other definitions). Color figure can be viewed in the online issue, which is available at http://onlinelibrary.wiley.com/doi/10.1002/art.41220/abstract.

(Figure 3D). Examination of the time courses extracted from these regions revealed marked differences in neural response patterns between groups (Figure 3E). The most striking effect among the regions evaluated was the observed increases in BOLD signaling at the termination of cuff pain in the DLPFC, VLPFC, PrCG, and FP in FM patients compared to controls.

Correlational analyses. Results from the correlational analysis revealed a significant positive association between PCS scores and DLPFC signal changes during pain offset in FM patients (r = 0.33, $P = 0.04$) (Figure 4A). There was a trend toward a significant positive association between PCS scores and FP signal changes during pain offset as well (r = 0.30, $P = 0.07$). No other correlations with PCS reached statistical significance ($P > 0.07$).

Correlational analyses revealed no significant associations between brain response to cuff onset and cuff pressure in FM patients or controls. During cuff offset, however, we observed significant negative correlations between cuff pressure and activation in the OFC (r = –0.35, $P = 0.03$) and PrCG (r = –0.39, $P = 0.02$) in FM patients only (Figures 4B and C). No significant relationship between pain intensity ratings and brain response to cuff onset or offset in either group emerged, although there was a trend toward an association between pain intensity and PrCG activation at cuff onset (r = 0.31, $P = 0.06$). There was a significant positive correlation between pain unpleasantness ratings and VLPFC activity in patients during cuff onset (r = 0.35, $P = 0.03$) (Figure 4D) whereas in controls, there was a positive correlation between pain unpleasantness and VLPFC activation during cuff offset (r = 0.6, $P = 0.02$).

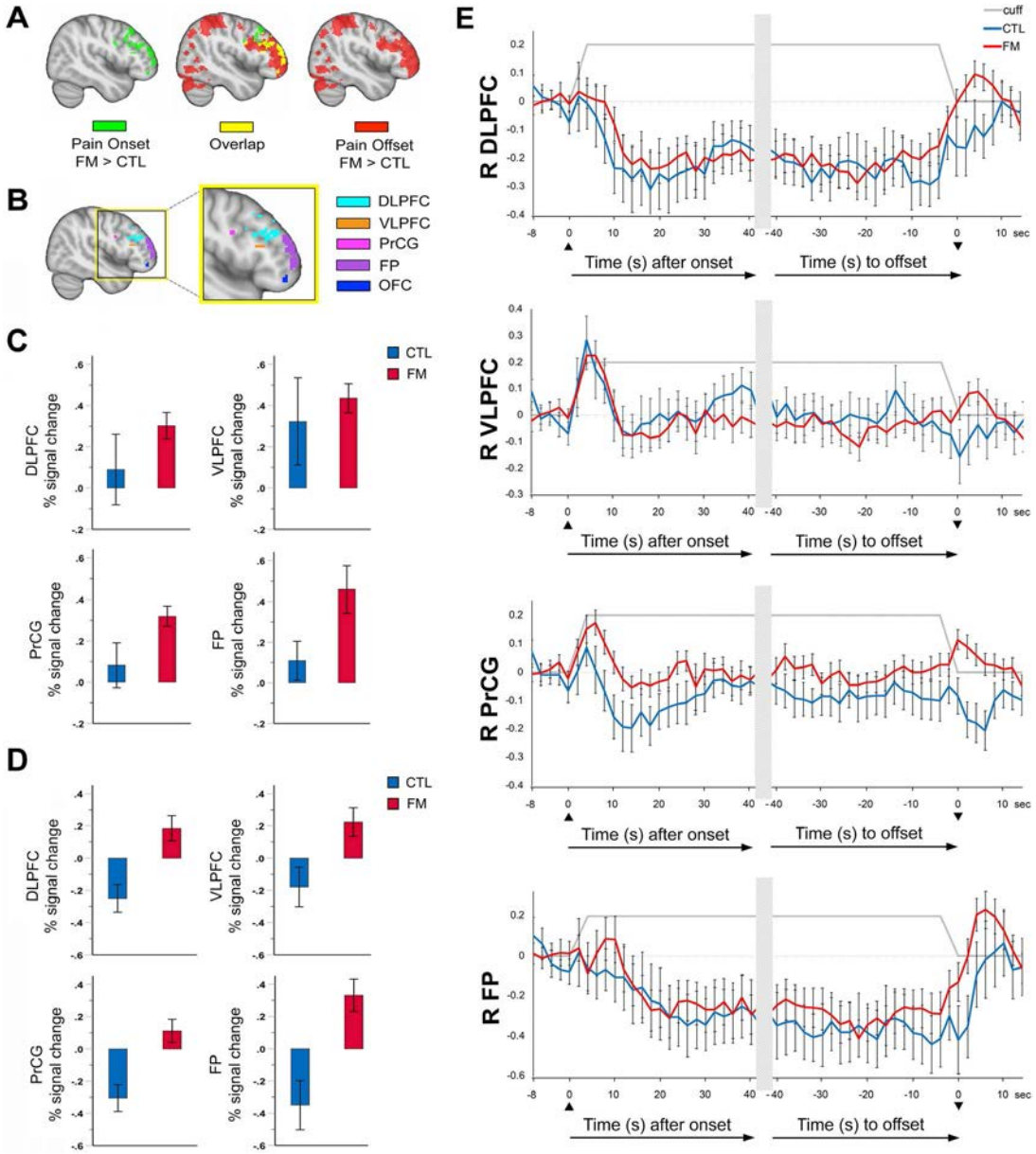

Figure 3. Group contrasts of pain onset and offset in various brain regions in FM patients compared to healthy controls showing shared regions of heightened response in the lateral PFC (LPFC) and in derived region of interest (ROI) masks. **A**, Statistical maps showing group differences in brain responses for FM patients compared to healthy controls during pain onset and pain offset, with overlapping regions common to both groups indicated. **B**, ROI masks included the DLPFC, VLPFC, PrCG, FP, and OFC. **C**, Mean percent signal changes extracted for anatomically parcellated ROIs created from the intersection mask for pain onset, including the DLPFC, VLPFC, PrCG, and FP. **D**, Mean percent signal changes extracted for anatomically parcellated ROIs (DLPFC, VLPFC, PrCG, and FP) created from the intersection mask for pain offset. **E**, Time courses for extracted blood-oxygenation level–dependent signal responses from anatomically parcellated subregions derived from the LPFC intersection mask for pain onset and offset. Values are the mean ± SEM. See Figure 1 for other definitions. Color figure can be viewed in the online issue, which is available at http://onlinelibrary.wiley.com/doi/10.1002/art.41220/abstract.

DISCUSSION

Our findings demonstrated that patients with FM, compared to controls, show extensive brain hyperactivity in response to both cuff pain onset and offset. While an increased response to pain onset was expected, particularly given the extensive literature demonstrating overall stronger brain responses to pain stimuli in FM, the large group differences observed at pain offset were striking. Such differences were noted in frontal regions that were also differentiated between FM patients and controls for pain onset (i.e., DLPFC, VLPFC, OFC, PrCG, and FP) as well as additional parietal, temporal, and occipital areas. Not only were group differences at offset more widespread than at onset, they reflected different activation/deactivation patterns—during offset, significant activations

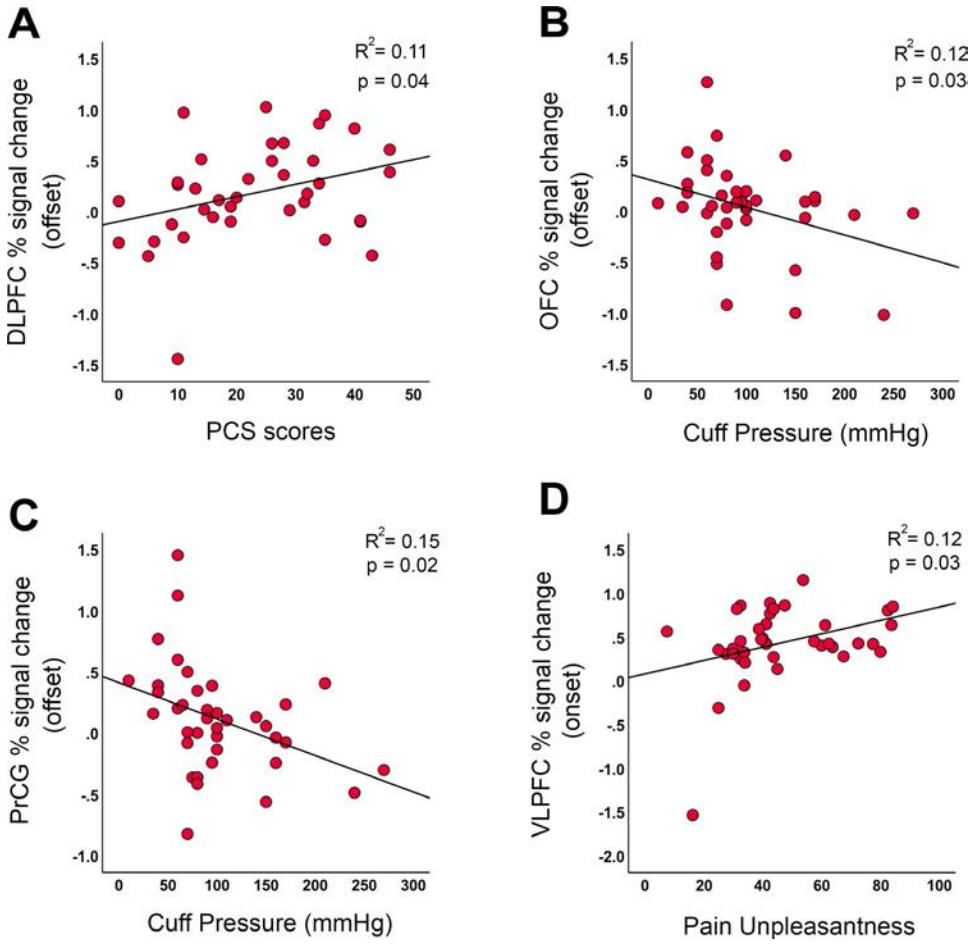

Figure 4. Scatterplots depicting correlations between brain activations extracted from anatomically parcellated regions of interest (ROIs) created from the intersection mask for pain onset and offset and pain catastrophizing scale (PCS) scores, cuff pressure (mm Hg), and pain unpleasantness ratings in FM patients only. **A**–**C**, DLPFC percent signal change in response to pain offset was positively correlated with PCS scores (**A**), and OFC (**B**) and PrCG (**C**) percent signal change in response to pain offset were negatively correlated with cuff pressure. **D**, VLPFC percent signal change in response to pain onset was demonstrated to be positively correlated with ratings of pain unpleasantness. See Figure 1 for other definitions. Color figure can be viewed in the online issue, which is available at http://onlinelibrary.wiley.com/doi/10.1002/art.41220/abstract.

in many regions were demonstrated in FM patients whereas deactivations were exhibited in healthy controls. Moreover, the magnitude of such hyperresponsiveness in FM patients was rather remarkable, particularly considering that intensity of stimuli presented to this group was 37.5% less than that for controls (mean ± SD 100 ± 43 mm Hg in FM patients and 160 ± 74 mm Hg in controls [25]), due to individualized calibration of the stimulus to achieve a pain intensity rating of ~40 on a 100-point scale.

Because increased brain responses to both onset (i.e., the event signaling the beginning of pain) and offset (i.e., its termination) were demonstrated in FM patients, our results are compatible with the notion that FM patients might generally be more sensitive to salient events (although this interpretation awaits proper corroboration with behavioral data). Several studies have reported a generalized increased sensitivity to non-noxious and non-somatic sensations, including auditory, gustatory, and olfactory stimuli (21–24). For instance, when presented with intense auditory stimuli of varying intensities, shorter auditory evoked potential (N1 and P2) latencies were demonstrated in FM patients compared to controls (24). Other studies using self-report questionnaires have demonstrated that FM patients tend to report greater sensitivity to everyday sounds and smells than their non-FM counterparts (22,23). Altogether, results from these studies, as well as our own demonstration of brain hyperresponsiveness to both cuff pain onset and offset, suggest that increased pain-related brain activity often reported in FM studies might perhaps reflect a more generalized hypersensitivity to salient aspects of the pain stimuli, rather than (or in addition to) their painful quality per se.

In addition, the positive association between pain unpleasantness ratings and VLPFC activation during cuff onset in FM patients may hint at dysregulated modulatory processing in regard to perceived controllability over pain in FM patients, given that a few studies have demonstrated greater VLPFC-related activity during self-controlled, painful stimulation (43) and less perceived pain during uncontrollable pain conditions, compared to controllable pain conditions, in healthy subjects (44).

Clinically, these results would support the use of cognitive and behavioral interventions focused on training salience detection/stimulus–driven orienting of attention, such as mindfulness meditation (45).

A notable finding gleaned from the present study is that FM patients showed frontal hyperresponsiveness to both cuff pain onset and offset compared to controls, particularly in the lateral PFC. The lateral PFC comprises multiple brain regions that work together to integrate cognitive inhibitory control functions and regulatory processes associated with threat detection (46,47). There is growing evidence that augmented activity in the lateral PFC, and the DLPFC in particular, may be associated with increased sensitivity to painful and non-painful somatic stimuli, perhaps indicative of impaired somatosensory gating in these patients (10,48).

While our data may be compatible with the hypothesis of dysregulation of salience detection, it should be noted that we did not observe group differences in canonical salience network nodes, such as the dorsal ACC or anterior insula, but rather, both groups showed similar levels of activations in these regions. Our findings warrant further investigation to determine the mechanism underlying PFC hyperactivation in FM, and whether this is driven by an overactivity in salience-related circuitry and/or an inability to sufficiently regulate/dampen these responses. Alternate explanations for greater prefrontal activation in response to stimulus onset/offset may correspond to a slower hemodynamic response recovery at offset (i.e., aberrant neurovascular coupling) and/or disruption in top-down control mechanisms, including greater catastrophizing or altered stimulus appraisal.

Another key finding was the significant positive association between pain catastrophizing and BOLD signal response in the DLPFC during cuff pain offset in FM patients. It is well understood that catastrophizing is an important contributing factor to the experience and expression of pain as well as its progression into persistent pain (49,50). Indeed, patients who tend to catastrophize about their pain report overall greater pain severity, rating higher in pain intensity and unpleasantness, than those patients who tend to not catastrophize (23). Moreover, the degree of catastrophizing has been shown to be predictive of whether or not an acute pain event actually develops into a chronic pain state (51). However, much less is known about the neurobiologic mechanism that drives this phenomenon. Our recent studies have shown that in patients with chronic pain, engaging in catastrophizing thoughts about clinical pain activates medial prefrontal and posterior cingulate cortices (52), though different circuits may support how catastrophizing influences perception of evoked pain in these patients. One theory posited is that catastrophizers are unable to disengage attention away from their pain and direct more attentional resources toward non-painful or salient stimuli encountered in their environment. This attentional bias, over time, may sensitize the system, overwhelming it to the point to which it can no longer compensate via descending inhibitory pathways. This, in turn, could lead to a host of pathologic downstream effects, including but not limited to pain amplification (hyperalgesia), the development of allodynic responses to previously innocuous signals, and/or a generalized hypersensitivity manifest across multiple sensory modalities. Our previous study showed that greater PCS scores were associated with greater connectivity between somatosensory (i.e., S1) and salience (i.e., anterior insula) processing regions during sustained evoked pain, which was compared to a resting state elevated S1–insula connectivity (53,54).

A confluence of evidence also points to the DLPFC as a possible candidate region responsible for driving this interaction, given its involvement in cognitive inhibitory control functions and attentional processes related to pain perception, as well as the detection and mediation of adaptive behavioral responses to aversive threats exhibited in this region (55). Our data provide support for this theory by demonstrating a significant association between DLPFC activity and catastrophizing during cuff pain offset in FM patients, suggesting that the tendency to catastrophize may be linked to an inability to appropriately disengage attention away from the salient sensory event—in this case, the termination of the cuff pain stimulus—despite the fact that the stimulus has ended and is therefore no longer noxious or threatening.

Other neuroimaging studies have reported findings that are consistent with our results. For example, Gracely and colleagues found that FM patients with high catastrophizing showed greater DLPFC activity during pain perception, a finding that persisted even when statistically controlling for depressive symptoms (56). Ellingson et al reported a significant positive correlation between catastrophizing, pain ratings, and DLPFC signal responses in FM patients, but not performance, during a cognitive attention/distraction task (Stroop task) (57). Specifically, the ability of FM patients to modulate their pain was impaired and varied depending on the degree of catastrophizing reported, and the magnitude of this relationship was linked to DLPFC signal responding—greater DLPFC activity was demonstrated in patients with higher catastrophizing. One interpretation suggested by Ellingson et al was that catastrophizing likely interferes with the pain modulatory system via descending pathways arising from the DLPFC, by weakening engagement of attentional resources to inhibit incoming nociceptive signals. Our result, in the context of their findings, provides further support for this theory, although more research is needed.

Several limitations should be considered when interpreting the present findings. First, given that our study utilized a cross-sectional design, drawing predictive conclusions (with regard to the relationship between brain response to cuff pain offset and the degree of pain catastrophizing) is not possible. Future studies employing a longitudinal design to investigate the causal nature of these relationships are needed. Second, medication usage was not controlled. Some patients were undergoing antidepressant therapy or receiving analgesics (gabapentin, nonsteroidal antiinflammatory drugs, and/or acetaminophen). As such, it is unclear to what extent medication might have affected

our results. Moreover, it remains to be determined whether the patterns of hyperactivation observed in FM patients can also be observed in other groups, including pain-free participants with similarly elevated levels of catastrophizing. Unfortunately, we were unable to evaluate the effects of PCS on BOLD signaling in our control participants as the dynamic range in their PCS scores was too narrow. Lastly, due to the secondary nature of this study, we did not collect behavioral data directly measuring salience, and our interpretation about differences in salience detection is only speculative at this point and will need to be confirmed in future investigations.

AUTHOR CONTRIBUTIONS

All authors were involved in drafting the article or revising it critically for important intellectual content, and all authors approved the final version to be published. Dr. Loggia had full access to all of the data in the study and takes responsibility for the integrity of the data and the accuracy of the data analysis.

Study conception and design. Kim, Edwards, Napadow, Loggia.
Acquisition of data. Cahalan, Kim, Loggia.
Analysis and interpretation of data. Hubbard, Lazaridou, Cahalan, Kim, Edwards, Napadow, Loggia.

REFERENCES

1. Clauw DJ. Fibromyalgia: a clinical review. JAMA 2014;311:1547–55.
2. Wolfe F, Clauw DJ, Fitzcharles MA, Goldenberg DL, Katz RS, Mease P, et al. The American College of Rheumatology preliminary diagnostic criteria for fibromyalgia and measurement of symptom severity. Arthritis Care Res (Hoboken) 2010;62:600–10.
3. Wolfe F, Ross K, Anderson J, Russell IJ, Hebert L. The prevalence and characteristics of fibromyalgia in the general population. Arthritis Rheum 1995;38:19–28.
4. Harris RE, Clauw DJ. How do we know that the pain in fibromyalgia is "real"? Curr Pain Headache Rep 2006;10:403–7.
5. Meeus M, Nijs J. Central sensitization: a biopsychosocial explanation for chronic widespread pain in patients with fibromyalgia and chronic fatigue syndrome. Clin Rheumatol 2007;26:465–73.
6. Tracey I, Mantyh PW. The cerebral signature for pain perception and its modulation. Neuron 2007;55:377–91.
7. Oaklander AL, Herzog ZD, Downs HM, Klein MM. Objective evidence that small-fiber polyneuropathy underlies some illnesses currently labeled as fibromyalgia. Pain 2013;154:2310–6.
8. Üçeyler N, Zeller D, Kahn AK, Kewenig S, Kittel-Schneider S, Schmid A, et al. Small fibre pathology in patients with fibromyalgia syndrome. Brain 2013;136:1857–67.
9. López-Solà M, Woo CW, Pujol J, Deus J, Harrison BJ, Monfort J, et al. Towards a neurophysiological signature for fibromyalgia. Pain 2017;158:34–47.
10. Ceko M, Bushnell MC, Gracely RH. Neurobiology underlying fibromyalgia symptoms. Pain Res Treat 2012;2012:585419.
11. Julien N, Goffaux P, Arsenault P, Marchand S. Widespread pain in fibromyalgia is related to a deficit of endogenous pain inhibition. Pain 2005;114:295–302.
12. Kosek E, Hansson P. Modulatory influence on somatosensory perception from vibration and heterotopic noxious conditioning stimulation (HNCS) in fibromyalgia patients and healthy subjects. Pain 1997;70:41–51.
13. Gracely RH, Petzke F, Wolf JM, Clauw DJ. Functional magnetic resonance imaging evidence of augmented pain processing in fibromyalgia. Arthritis Rheum 2002;46:1333–43.
14. Cook DB, Lange G, Ciccone DS, Liu WC, Steffener J, Natelson BH. Functional imaging of pain in patients with primary fibromyalgia. J Rheumatol 2004;31:364–78.
15. Pujol J, López-Solà M, Ortiz H, Vilanova JC, Harrison BJ, Yücel M, et al. Mapping brain response to pain in fibromyalgia patients using temporal analysis of FMRI. PloS One 2009;4:e5224.
16. Williams DA, Gracely RH. Biology and therapy of fibromyalgia: functional magnetic resonance imaging findings in fibromyalgia [review]. Arthritis Res Ther 2006;8:224.
17. Bradley LA, McKendree-Smith NL, Alberts KR, Alarcón GS, Mountz JM, Deutsch G. Use of neuroimaging to understand abnormal pain sensitivity in fibromyalgia. Curr Rheumatol Rep 2000;2:141–8.
18. Cagnie B, Coppieters I, Denecker S, Six J, Danneels L, Meeus M. Central sensitization in fibromyalgia? A systematic review on structural and functional brain MRI. Semin Arthritis Rheum 2014;44:68–75.
19. Loggia ML, Berna C, Kim J, Cahalan CM, Gollub RL, Wasan AD, et al. Disrupted brain circuitry for pain-related reward/punishment in fibromyalgia. Arthritis Rheumatol 2014;66:203–12.
20. Albrecht DS, Forsberg A, Sandström A, Bergan C, Kadetoff D, Protsenko E, et al. Brain glial activation in fibromyalgia—a multi-site positron emission tomography investigation. Brain Behav Immun 2019;75:72–83.
21. Wilbarger JL, Cook DB. Multisensory hypersensitivity in women with fibromyalgia: implications for well being and intervention. Arch Phys Med Rehabil 2011;92:653–6.
22. Hollins M, Harper D, Gallagher S, Owings EW, Lim PF, Miller V, et al. Perceived intensity and unpleasantness of cutaneous and auditory stimuli: an evaluation of the generalized hypervigilance hypothesis. Pain 2009;141:215–21.
23. Geisser ME, Glass JM, Rajcevska LD, Clauw DJ, Williams DA, Kileny PR, et al. A psychophysical study of auditory and pressure sensitivity in patients with fibromyalgia and healthy controls. J Pain 2008;9:417–22.
24. Carrillo-de-la-Peña MT, Vallet M, Pérez MI, Gómez-Perretta C. Intensity dependence of auditory-evoked cortical potentials in fibromyalgia patients: a test of the generalized hypervigilance hypothesis. J Pain 2006;7:480–7.
25. Schreiber KL, Loggia ML, Kim J, Cahalan CM, Napadow V, Edwards RR. Painful after-sensations in fibromyalgia are linked to catastrophizing and differences in brain response in the medial temporal lobe. J Pain 2017;18:855–67.
26. Tan G, Jensen MP, Thornby JI, Shanti BF. Validation of the Brief Pain Inventory for chronic nonmalignant pain. J Pain 2004;5:133–7.
27. Bouhassira D, Attal N, Alchaar H, Boureau F, Brochet B, Bruxelle J, et al. Comparison of pain syndromes associated with nervous or somatic lesions and development of a new neuropathic pain diagnostic questionnaire (DN4). Pain 2005;114:29–36.
28. Sullivan MJ, Bishop SR, Pivik J. The Pain Catastrophizing Scale: development and validation. Psychol Assess 1995;7:524–32.
29. Beck AT, Steer RA, Carbin MG. Psychometric properties of the Beck Depression Inventory: twenty-five years of evaluation. Clin Psychol Rev 1988;8:77–100.
30. Jenkinson M, Bannister P, Brady JM, Smith SM. Improved optimisation for the robust and accurate linear registration and motion correction of brain images. Neuroimage 2002;2:825–41.
31. Popescu V, Battaglini M, Hoogstrate WS, Verfaillie SC, Sluimer IC, van Schijndel RA, et al, on behalf of the MAGNIMS Study Group. Optimizing parameter choice for FSL-Brain Extraction Tool (BET) on 3D T1 images in multiple sclerosis. Neuroimage 2012;61:1484–94.
32. Jenkinson M, Smith SM. A global optimisation method for robust affine registration of brain images. Med Image Anal 2001;5:143–56.

33. Woolrich MW, Ripley BD, Brady M, Smith SM. Temporal autocorrelation in univariate linear modeling of FMRI data. Neuroimage 2001;14:1370–86.
34. Greve DN, Fischl B. Accurate and robust brain image alignment using boundary-based registration. Neuroimage 2009;48:63–72.
35. Uludağ K. Transient and sustained BOLD responses to sustained visual stimulation. Magn Reson Imaging 2008;26:863–9.
36. Becerra L, Navratilova E, Porreca F, Borsook D. Analogous responses in the nucleus accumbens and cingulate cortex to pain onset (aversion) and offset (relief) in rats and humans. J Neurophysiol 2013;110:1221–6.
37. Konishi S, Donaldson DI, Buckner RL. Transient activation during block transition. Neuroimage 2001;13:364–74.
38. Jenkinson M. Measuring transformation error by RMS deviation: FMRIB technical report TR99MJ1. URL: https://www.fmrib.ox.ac.uk/datasets/techrep/tr99mj1/tr99mj1.pdf.
39. Andersson JL, Jenkinson M, Smith S. Non-linear registration aka spatial normalisation: FMRIB technical report TR07JA2. 2007. URL: https://www.fmrib.ox.ac.uk/datasets/techrep/tr07ja2/tr07ja2.pdf.
40. Beckmann CF, Jenkinson M, Smith SM. General multi-level linear modelling for group analysis in FMRI: FMRIB technical report TR01CB1. URL: https://www.fmrib.ox.ac.uk/datasets/techrep/tr01cb1/tr01cb1.pdf.
41. Woolrich MW, Behrens TE, Beckmann CF, Jenkinson M, Smith SM. Multilevel linear modelling for FMRI group analysis using Bayesian inference. Neuroimage 2004;21:1732–47.
42. Mumford JA. A comprehensive review of group level model performance in the presence of heteroscedasticity: can a single model control Type I errors in the presence of outliers? Neuroimage 2017;147:658–68.
43. Wiech K, Kalisch R, Weiskopf N, Pleger B, Stephan KE, Dolan RJ. Anterolateral prefrontal cortex mediates the analgesic effect of expected and perceived control over pain. J Neurosci 2006;26:11501–9.
44. Salomons TV, Johnstone T, Backonja MM, Shackman AJ, Davidson RJ. Individual differences in the effects of perceived controllability on pain perception: critical role of the prefrontal cortex. J Cogn Neurosci 2007;19:993–1003.
45. Lazaridou A, Kim J, Cahalan CM, Loggia ML, Franceschelli O, Berna C, et al. Effects of cognitive-behavioral therapy (CBT) on brain connectivity supporting catastrophizing in fibromyalgia. Clin J Pain 2017;33:215–21.
46. Gray JR, Braver TS, Raichle ME. Integration of emotion and cognition in the lateral prefrontal cortex. Proc Nat Acad Sci U S A 2002;99:4115–20.
47. Peers PV, Simons JS, Lawrence AD. Prefrontal control of attention to threat. Front Hum Neurosci 2013;7:24.
48. Loggia ML, Berna C, Kim J, Cahalan CM, Martel MO, Gollub RL, et al. The lateral prefrontal cortex mediates the hyperalgesic effects of negative cognitions in chronic pain patients. J Pain 2015;16:692–9.
49. Keefe FJ, Brown GK, Wallston KA, Caldwell DS. Coping with rheumatoid arthritis pain: catastrophizing as a maladaptive strategy. Pain 1989;37:51–6.
50. Sullivan MJ, Stanish W, Waite H, Sullivan M, Tripp DA. Catastrophizing, pain, and disability in patients with soft-tissue injuries. Pain 1998;77:253–60.
51. Burton AK, Tillotson KM, Main CJ, Hollis S. Psychosocial predictors of outcome in acute and subchronic low back trouble. Spine (Phila Pa 1976) 1995;20:722–8.
52. Lee J, Protsenko E, Lazaridou A, Franceschelli O, Ellingsen DM, Mawla I, et al. Encoding of self-referential pain catastrophizing in the posterior cingulate cortex in fibromyalgia. Arthritis Rheumatol 2018;70:1308–18.
53. Kim J, Loggia ML, Cahalan CM, Harris RE, Beissner F, Garcia RG, et al. The somatosensory link in fibromyalgia: functional connectivity of the primary somatosensory cortex is altered by sustained pain and is associated with clinical/autonomic dysfunction. Arthritis Rheumatol 2015;67:1395–405.
54. Kim J, Loggia ML, Edwards RR, Wasan AD, Gollub RL, Napadow V. Sustained deep-tissue pain alters functional brain connectivity. Pain 2013;154:1343–51.
55. Seminowicz DA, Moayedi M. The dorsolateral prefrontal cortex in acute and chronic pain. J Pain 2017;18:1027–35.
56. Gracely RH, Geisser ME, Giesecke T, Grant MA, Petzke F, Williams DA, et al. Pain catastrophizing and neural responses to pain among persons with fibromyalgia. Brain 2004;127:835–43.
57. Ellingson LD, Stegner AJ, Schwabacher IJ, Lindheimer JB, Cook DB. Catastrophizing interferes with cognitive modulation of pain in women with fibromyalgia. Pain Med 2018;19:2408–22.

Arthritis & Rheumatology
Vol. 72, No. 7, July 2020, pp 1214–1226
DOI 10.1002/art.41236

American College of Rheumatology
Empowering Rheumatology Professionals

Endothelial and Inflammation Biomarker Profiles at Diagnosis Reflecting Clinical Heterogeneity and Serving as a Prognostic Tool for Treatment Response in Two Independent Cohorts of Patients With Juvenile Dermatomyositis

Judith Wienke,[1] Lauren M. Pachman,[2] Gabrielle A. Morgan,[2] Joo Guan Yeo,[3] Maria C. Amoruso,[2] Victoria Hans,[2] Sylvia S. M. Kamphuis,[4] Esther P. A. H. Hoppenreijs,[5] Wineke Armbrust,[6] J. Merlijn van den Berg,[7] Petra C. E. Hissink Muller,[8] Kyra A. Gelderman,[9] Thaschawee Arkachaisri,[3] Femke van Wijk,[1] and Annet van Royen-Kerkhof[1]

Objective. Juvenile dermatomyositis (DM) is a heterogeneous systemic immune-mediated vasculopathy. This study was undertaken to 1) identify inflammation/endothelial dysfunction–related biomarker profiles reflecting disease severity at diagnosis, and 2) establish whether such biomarker profiles could be used for predicting the response to treatment in patients with juvenile DM.

Methods. In total, 39 biomarkers related to activation of endothelial cells, endothelial dysfunction, and inflammation were measured using multiplex technology in serum samples from treatment-naive patients with juvenile DM from 2 independent cohorts (n = 30 and n = 29). Data were analyzed by unsupervised hierarchical clustering, nonparametric tests with correction for multiple comparisons, and Kaplan-Meier tests with Cox proportional hazards models for analysis of treatment duration. Myositis-specific antibodies (MSAs) were measured in the patients' serum using line blot assays.

Results. Severe vasculopathy in patients with juvenile DM was associated with low serum levels of intercellular adhesion molecule 1 (Spearman's rho [r_s] = 0.465, P = 0.0111) and high serum levels of endoglin (r_s = –0.67, $P < 0.0001$). In the discovery cohort, unsupervised hierarchical clustering analysis of the biomarker profiles yielded 2 distinct patient clusters, of which the smaller cluster (cluster 1; n = 8) exhibited high serum levels of CXCL13, CCL19, galectin-9, CXCL10, tumor necrosis factor receptor type II (TNFRII), and galectin-1 (false discovery rate <0.0001), and this cluster had greater severity of muscle disease and global disease activity (each $P < 0.05$ versus cluster 2). In the validation cohort, correlations between the serum levels of galectin-9, CXCL10, TNFRII, and galectin-1 and the severity of global disease activity were confirmed (r_s = 0.40–0.52, $P < 0.05$). Stratification of patients according to the 4 confirmed biomarkers identified a cluster of patients with severe symptoms (comprising 64.7% of patients) who were considered at high risk of requiring more intensive treatment in the first 3 months after diagnosis (P = 0.0437 versus other cluster). Moreover, high serum levels of galectin-9, CXCL10, and TNFRII were predictive of a longer total treatment duration ($P < 0.05$). The biomarker-based clusters were not evidently correlated with patients' MSA serotypes.

Conclusion. Results of this study confirm the heterogeneity of new-onset juvenile DM based on serum biomarker profiles. Patients with high serum levels of galectin-9, CXCL10, TNFRII, and galectin-1 may respond suboptimally to conventional treatment, and may therefore benefit from more intensive monitoring and/or treatment.

The Chicago Juvenile Dermatomyositis (DM) Registry/Biorepository was supported by the Cure JM Foundation and the National Institute of Nursing Research, NIH (grant NR-012692). The Dutch juvenile DM cohort was supported by the Princess Beatrix Fund, the BAS Foundation, Innovatiefonds Zorgverzekeraars, and the Cure JM Foundation. The Singaporean juvenile DM cohort was supported by the Singapore Ministry of Health's National Medical Research Council (grants NMRC-CG-M003-2017, NMRC-STaR-020-2013, MOHIAFCAT2-2-08, and NMRC-TA-0059-2017). Dr. Pachman's work was supported by the NIH (grant 1R43-AR-073547-01).

[1]Judith Wienke, MD, PhD, Femke van Wijk, PhD, Annet van Royen-Kerkhof, MD, PhD: University Medical Center Utrecht and Utrecht University, Utrecht, The Netherlands; [2]Lauren M. Pachman, MD, Gabrielle A. Morgan, MA, CCRP, Maria C. Amoruso, MPH, CCRP, Victoria Hans, BS: Ann & Robert H. Lurie Children's Hospital of Chicago, Northwestern

INTRODUCTION

Juvenile dermatomyositis (DM) is a rare systemic immune-mediated disease with an incidence of 2–4 cases per million per year (1). The clinical presentation is heterogeneous, as patients can develop a spectrum of symptoms, ranging from the typical symptoms of proximal skeletal muscle weakness and pathognomonic skin rash, to involvement of vital organs such as the lungs, heart, brain, and intestines (2). The clinical heterogeneity of juvenile DM has been linked to myositis-specific autoantibodies (MSAs), the levels of which may distinguish distinct clinical phenotypes and could be prognostic for the disease course and the need for second-line therapy (3). Despite this disease heterogeneity, current treatment guidelines are not yet adapted to subgroup-specific needs (4). Stratification of patients, e.g., into high-risk or low-risk groups, may facilitate the development of personalized monitoring and treatment strategies.

In addition to inflammation of the muscles and skin, vasculopathy is an important hallmark of juvenile DM (5,6). The disease is characterized by a loss of capillaries, morphologic changes to the endothelium, endothelial cell activation, and small vessel angiopathy (5–8). Complement and immune complexes are involved in its pathogenesis, but a disturbed balance between angiostatic and angiogenic factors also plays a role (9–11). The degree of vasculopathy is correlated with the expression of interferon (IFN)–inducible angiostatic chemokines (11), indicating that vascular injury may be related to the IFN signature (5). This IFN signature has been identified in the serum and many cell types, including endothelial cells, from patients with juvenile DM (11–17).

The degree of vasculopathy is clinically relevant: pathologic changes in nailfold capillaries are associated with clinical disease activity (18), and prominent vascular injury evident in muscle biopsy tissue was found to be associated with severe clinical presentation and outcomes (19,20). Recently, Gitiaux et al identified a subgroup of juvenile DM patients with severe disease, based on trajectories of clinical parameters during follow-up (19). Juvenile DM in these patients was characterized by severe muscle weakness, frequent limb edema, gastrointestinal involvement, higher myopathologic scores (e.g., capillary dropout), and low remission rates (19). Most of these manifestations could be related to vasculopathy (19).

Herein we used a minimally invasive biomarker-based approach to identify juvenile DM patients, both from a discovery cohort and from an independent validation cohort, who had a severe disease course already present at diagnosis. The biomarker panel analyzed included previously described and novel markers related to endothelial cell activation, endothelial dysfunction, and IFN-driven inflammation (5,17). Specifically, we investigated whether biomarker profiles were linked to vasculopathy, disease severity, and frequency of MSA subtypes, and whether the levels of these biomarkers might be predictive of the response to induction therapy and the time required to attain drug-free remission (DFR).

PATIENTS AND METHODS

Participants. For this study, 59 patients meeting the Bohan and Peter criteria for definite or probable juvenile DM (21,22), from Chicago, Illinois for the discovery cohort (n = 30) and from Utrecht, The Netherlands and Singapore for the validation cohort (n = 25 and n = 4), were included before the start of treatment, between March 2004 and June 2018. Scores on the Childhood Myositis Assessment Scale (CMAS) (scale 0–52, or scale 0–49 for ages 4–5 years) (23) were recorded in both cohorts as a measure of muscle disease activity. Disease Activity Scores (DAS) for the muscle (DAS-M) (scale 0–11) and skin (DAS-S) (scale 0–9), and global DAS for total disease activity (DAS-T) (scale 0–20) were recorded in the discovery cohort (24), while in the validation cohort, the physician's global assessment of disease activity (PhGA) (scale 0–10) (25) and the cutaneous assessment tool (CAT) for juvenile DM (scale 0–116) (26) were used.

Intensification of treatment was defined as the addition of new immunosuppressive medication or an increase in the dose of a previous medication. Time to attainment of DFR was defined as the time (in months) between the date at the start of immunosuppressive treatment and the date at the time of withdrawal of all immunosuppressive drugs. In the discovery cohort, treatment regimens were individualized, while in the validation cohort, treatment regimens were based on the SHARE (Single Hub and Access point for pediatric Rheumatology in Europe) recommendations (4).

End row loops (ERLs), as a proxy for the severity of vasculopathy (27), were assessed by nailfold capillaroscopy. Standardized digital nailfold images from 8 fingers, excluding the thumbs, were obtained, and findings were analyzed by counting the

University Feinberg School of Medicine, and the Cure JM Center of Excellence, Chicago, Illinois; [3]Joo Guan Yeo, MBBS, PhD, Thaschawee Arkachaisri, MD: KK Women's and Children's Hospital, and Duke-NUS Medical School, Singapore, Singapore; [4]Sylvia S. M. Kamphuis, MD, PhD: Sophia Children's Hospital and Erasmus University Medical Centre, Rotterdam, The Netherlands; [5]Esther P. A. H. Hoppenreijs, MD: Amalia Children's Hospital and Radboud University Medical Centre, Nijmegen, The Netherlands; [6]Wineke Armbrust, MD, PhD: Beatrix Children's Hospital and University Medical Centre Groningen, Groningen, The Netherlands; [7]J. Merlijn van den Berg, MD, PhD: Emma Children's Hospital and Amsterdam University Medical Center, Amsterdam, The Netherlands; [8]Petra C. E. Hissink Muller, MD: Sophia Children's Hospital and Erasmus University Medical Centre, Rotterdam, The Netherlands, and Leiden University Medical Centre, Leiden, The Netherlands; [9]Kyra A. Gelderman, PhD: Sanquin Diagnostic Services, Amsterdam, The Netherlands.

Drs. van Wijk and van Royen-Kerkhof contributed equally to this work.

Dr. Pachman has received research support from ReveraGen Biopharma. No other disclosures relevant to this article were reported.

All data and protocols from the biomarker cohort study are available to the scientific community upon reasonable request.

Address correspondence to Femke van Wijk, PhD, Lundlaan 6, PO Box 85090, 3508 AB Utrecht, The Netherlands. E-mail: f.vanwijk@umcutrecht.nl.

Submitted for publication April 30, 2019; accepted in revised form February 6, 2020.

ERLs in a 3-mm segment, yielding the average count of ERLs/mm. The lower limit of normal for this value is 7 ERLs/mm (interquartile range 7.61–8.94), as previously reported (27). To define severe vasculopathy, a cutoff ERL score of <4 was used, based on the median value for all abnormal ERL scores in the cohort (abnormal ERL defined as a score of <7; n = 27). ERLs were only assessed in the discovery cohort.

In addition, serum samples from all patients were assessed for the frequency of MSAs. Serum MSAs were measured by line blot assay (Euroimmun DL 1530-1601-4 G/5001-4 G/6401-4 G).

This study was approved by the institutional ethics committees of the involved centers: the UMC Utrecht (METC approval no. 15-191), the SingHealth centralized Institutional Review Board (IRB) (CIRB approval no. 2014/083/E), and the

Table 1. Baseline characteristics of the juvenile dermatomyositis patients from the discovery and validation cohorts*

	Discovery cohort (Chicago, IL) (n = 30)	Validation cohort (Netherlands and Singapore) (n = 25 and n = 4)	*P*
Age at sampling, median (IQR) years	5.1 (3.7–8.6)	7 (3.9–12.1)	0.192
Sex, no. (%) female	26 (86.7)	18 (62.1)	0.039
Ethnicity, % white/Hispanic/African American/Asian	77/20/3/0	76/0/10/14	0.012
Duration of untreated disease, median (IQR) months	5.9 (3.6–14.8)	3.2 (1.4–9.1)	0.020
Intensification of treatment in first 3 months, no. (%)	17 (56.7)	8 (28.6)	0.038
Disease activity at diagnosis			
CMAS (scale 0–52 or 0–49 for ages 4–5 years), median (IQR)	33 (23.5–44)†	33 (15–40.5)‡	0.334
PhGA, median (IQR) (scale 0–10)	–	5.8 (4.0–7.7)‡	NA
DAS total, median (IQR) (scale 0–20)	12 (9.4–13.3)	–	NA
DAS muscle, median (IQR) (scale 0–11)	6 (3.8–8)	–	NA
DAS skin, median (IQR) (scale 0–9)	5 (5–6.3)	–	NA
CAT score, median (IQR) (scale 0–116)	–	5 (3.5–11)	NA
Muscle enzyme levels at diagnosis, median (IQR) IU/liter			
CK	131 (88–680)	510 (138–4,357)	0.053
LDH	364 (270–460)†	497 (358–837)‡	0.010
AST	46 (35–80)	65 (41–307)§	0.118
ALT	26 (17–43)†	45 (23–112)	0.158
Myositis-specific antibodies, no. (%)			
Negative	14 (46.7)	16 (55.2)	0.800
MDA-5	2 (6.7)	2 (6.9)	1.000
Mi-2	3 (10)	0 (0)	0.237
NXP-2			
Total	2 (6.7)	5 (17.2)	0.254
Strongly positive	1 (3.3)	3 (10.3)	
Weakly positive	1 (3.3)	2 (6.9)	
SAE-1	0 (0)	2 (6.9)	0.237
TIF-1γ			
Total	9 (30.0)	4 (13.8)	0.209
TIF-1γ only	8 (26.7)	3 (10.3)	
TIF-1γ + PL-7	0 (0)	1 (3.4)	
TIF-1γ + PL-12	1 (3.3)	0 (0)	
Initial therapy after diagnosis, no. (%)			
Oral Pred.	1 (3.3)	0 (0.0)	1.000
MTX + oral Pred.	2 (6.7)	0 (0.0)	0.492
IVMP + oral Pred.	1 (3.3)	1 (3.4)	1.000
IVMP + oral Pred. + MTX	19 (63.3)	20 (69.0)	0.7847
IVMP + oral Pred. + IVIG	0 (0.0)	1 (3.4)	0.492
IVMP + oral Pred. + MTX + IVIG	1 (3.3)	0 (0.0)	1.000
IVMP + oral Pred. + MTX + HCQ	6 (20.0)	7 (24.1)	0.761

* *P* values were calculated by Mann-Whitney U test for continuous variables, and by Fisher's exact test for categorical variables (comparisons of 2 categories) or chi-square test (comparisons of >2 categories). Myositis-specific antibodies were measured by line blot assay. Normalization of muscle enzyme levels to the age- and center-specific upper limits of normal did not change the results. IQR = interquartile range; CMAS = Childhood Myositis Assessment Scale; PhGA = physician's global assessment of disease activity; NA = not applicable; DAS = Disease Activity Score; CAT = cutaneous assessment tool (for juvenile dermatomyositis); CK = creatine kinase; LDH = lactate dehydrogenase; AST = aspartate aminotransferase; ALT = alanine aminotransferase; MDA-5 = melanoma differentiation–associated protein; NXP-2 = nuclear matrix protein 2; SAE-1 = small ubiquitin-like modifier-1 activating enzyme; TIF-1γ = transcription intermediary factor 1γ; Pred. = prednisone; MTX = methotrexate; IVMP = intravenous methylprednisolone; IVIG = intravenous immunoglobulin; HCQ = hydroxychloroquine.
† Data not reported for 1 patient.
‡ Data not reported for 4 patients.
§ Data not reported for 2 patients.

Ann & Robert H. Lurie Children's Hospital of Chicago (IRB approval nos. 2001-11715 and 2010-14117). The study was conducted in patients in accordance with the Declaration of Helsinki. Age-appropriate written informed consent was obtained prior to inclusion of each patient in the study.

Analysis of a biomarker panel in patients' serum. Serum was spun down and stored at –80°C within 4 hours after collection. In total, 39 biomarkers related to endothelial cell activation, endothelial dysfunction, and inflammation were simultaneously measured using multiplex technology (xMAP; Luminex) in 50 μl of serum, as described previously (28). The markers were selected based on previously noted associations with endothelial cell activation, endothelial dysfunction, or inflammation and/or juvenile DM pathogenesis.

Statistical analysis. Statistical analyses were performed using GraphPad Prism version 7.0, SPSS version 21 (IBM), or R version 3.5.1 (CRAN). Values below the detection limit were imputed as being 0.5 times the lowest measured value. For Spearman's rank correlation (r_s) analysis, imputed values were excluded. Cutoff values for receiver operating characteristic (ROC) curves were based on the Youden's index. For comparisons between 2 groups, the Mann-Whitney U test was used for continuous variables and the Fisher's exact test was used for categorical variables, with correction for multiple comparisons based on the false discovery rate (FDR), where applicable. *P* values less than 0.05 or an FDR less than 0.05 were considered statistically significant.

For unsupervised clustering by principal component analysis (PCA) and heatmap analysis with hierarchical clustering (Euclidian/Ward), data were mean-centered and scaled per marker. Five markers (plasminogen activator inhibitor 1, fibronectin, oncostatin M, E-selectin, and thrombomodulin) had >30% of values below the limit of detection and were therefore excluded from the clustering analyses. For time until reaching DFR, a Kaplan-Meier estimator (dichotomized at the median value) and Cox proportional hazards model with log-transformed data were used, along with the log-rank test.

RESULTS

Patient characteristics. The median age of the patients in the discovery and validation cohorts was 5.1 years and 7.0 years, respectively (Table 1). The majority of patients in both cohorts were female, with a significantly higher frequency of female patients in the discovery cohort compared to the validation cohort (86.7% versus 62.1%; $P = 0.039$) and slightly higher frequency of white patients (77% versus 76%). Moreover, the majority of patients in each cohort were white (77% in the discovery cohort versus 76% in the validation cohort). The duration of untreated disease was higher in the discovery cohort (median 5.9 months versus 3.2 months in the validation cohort; $P = 0.02$), and treatment intensification was needed in 57% of the discovery cohort, compared to 29% of the validation cohort ($P = 0.038$). Muscle disease activity was similar in both cohorts (median CMAS 33 in each). Muscle enzyme levels were higher in the validation cohort.

In both cohorts, MSAs were detected in ~50% of patients. Although none of the MSAs differed significantly in their frequency, anti–transcription intermediary factor 1γ (anti–TIF-1γ) and anti–Mi-2 antibodies were more frequent in the discovery cohort compared to the validation cohort (for anti–TIF-1γ, 30% versus 14%; for anti–Mi-2, 10% versus 0%), whereas anti–nuclear matrix protein 2 (anti–NXP-2) and anti–small ubiquitin-like modifier-1 activating enzyme (anti–SAE-1) antibodies were more frequent in the validation cohort compared to the discovery cohort (for anti–NXP-2, 17% versus 7%; for anti–SAE-1, 7% versus 0%). The frequency of anti–melanoma differentiation–associated protein 5 (anti–MDA-5) antibodies was equal in both cohorts (each 7%), despite a higher frequency of children with an Asian background in the validation cohort. The initial treatment that was started after diagnosis was similar between the cohorts (Table 1).

Association between biomarker profiles and muscle disease activity. To investigate the heterogeneity of biomarker profiles in treatment-naive juvenile DM patients, we performed unsupervised hierarchical clustering in the discovery cohort, which led to splitting the patients into 2 distinct clusters, comprising 8 patients (cluster 1) and 22 patients (cluster 2). Compared to the larger cluster (cluster 2), the smaller cluster (cluster 1) stood out because of the patients' significantly higher serum levels of CXCL13, CCL19, galectin-9 (Gal-9), tumor necrosis factor receptor type II (TNFRII), Gal-1, CXCL10, CXCL9, interleukin-18 (IL-18), chitinase-3–like protein 1 (YKL-40), CCL2, CCL4, vascular endothelial growth factor (VEGF), E-selectin, intercellular adhesion molecule 1 (ICAM-1), and CCL18 and the patients' significantly lower serum levels of fetuin (FDR <0.05) (Figures 1A and B).

To assess whether distinct biomarker profiles corresponded to specific clinical profiles, we compared disease characteristics between the clusters (Figure 1C). Total disease activity (median DAS-T score) was significantly higher in cluster 1 than in cluster 2 ($P = 0.0265$), which was attributable to significantly higher muscle disease activity in cluster 1 (median DAS-M score, $P = 0.0486$; median CMAS score, $P = 0.011$) (Figure 1C). Skin disease activity scores and creatine kinase levels in the muscle were comparable, but patients in cluster 1 had higher lactate dehydrogenase (LDH) levels in the muscle ($P = 0.0285$).

Multidimensional PCA identified muscle disease activity as an important factor explaining the variance in biomarker profiles, and confirmed that patients with the highest DAS-M score spatially overlapped with cluster 1 (Figure 1D). ERL scores were similar between the clusters. Levels of 12 of the 16 biomarkers that

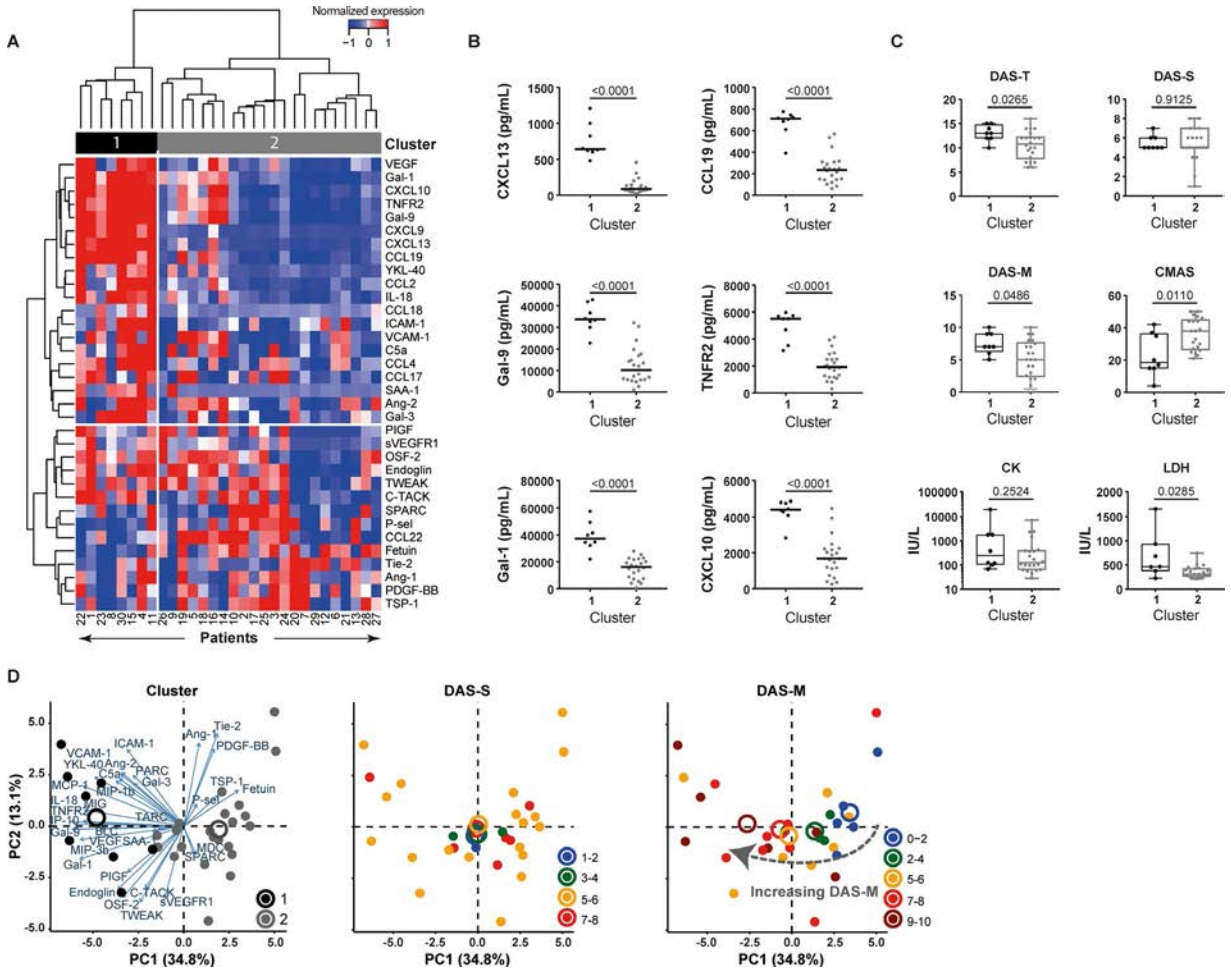

Figure 1. Association of heterogeneous biomarker profiles with differences in clinical disease activity in patients with juvenile dermatomyositis (DM). A panel of biomarkers for endothelial dysfunction and inflammation was measured by multiplex assay in the serum of 30 treatment-naive juvenile DM patients (discovery cohort). **A**, Unsupervised hierarchical clustering (by Euclidian distance and Ward's method) of 30 patients in the discovery cohort based on serum levels of 34 biomarkers (mean-centered and scaled values) yielded 2 distinct patient clusters (clusters 1 and 2). Values at the bottom represent unique patient identifiers (not ranked). **B**, Serum levels of the 6 markers most significantly different between cluster 1 (n = 8) and cluster 2 (n = 22) were compared by Mann-Whitney U test, with correction for multiple comparisons based on the false discovery rate. Symbols represent individual patients; horizontal lines show the median. **C**, Clinical scores for global Disease Activity Score (DAS-T), skin Disease Activity Score (DAS-S), muscle Disease Activity Score (DAS-M), Childhood Myositis Assessment Scale (CMAS) score, and muscle enzyme levels (creatine kinase [CK] and lactate dehydrogenase [LDH]) were compared between the 2 clusters. *P* values were determined by Mann-Whitney U test. Results are shown as box plots, where the boxes represent the 25th to 75th percentiles, the lines within the boxes represent the median, and the lines outside the boxes represent the 10th and 90th percentiles. **D**, Principal components (PC1 and PC2) analysis based on the 34 mean-centered markers shows patients stratified by cluster, DAS-S scores, and DAS-M scores. Circles with different colors represent clusters 1 and 2 or ranges of DAS-S and DAS-M scores. Closed circles represent individual patients, while open circles represent cluster centers. VEGF = vascular endothelial growth factor; Gal-1 = galectin-1; TNFRII = tumor necrosis factor receptor type II; YKL-40 = chitinase-3–like protein 1; IL-18 = interleukin-18; ICAM-1 = intercellular adhesion molecule 1; VCAM-1 = vascular cell adhesion molecule 1; SAA1 = serum amyloid A 1; Ang-2 = angiopoietin-2; PIGF = placental growth factor; sVEGFR1 = soluble VEGF receptor 1; OSF-2 = periostin; TWEAK = TNF-related weak inducer of apoptosis; C-TACK = cutaneous T cell–attracting chemokine; SPARC = secreted protein acidic and rich in cysteine; P-sel = P-selectin; Tie-2 = angiopoeitin-1 receptor; PDGF-BB = platelet-derived growth factor BB; TSP-1 = thrombospondin-1.

were differentially expressed between the clusters correlated with the DAS-T, DAS-M, or CMAS scores. These included CXCL13, CCL19, Gal-9, TNFRII, Gal-1, CXCL10, CXCL9, IL-18, YKL-40, CCL2, CCL4, and ICAM-1 ($|r_s|$ = 0.35–0.67, $P < 0.05$) (Table 2). High serum levels of these markers may therefore identify a subgroup of patients with more severe disease.

Association of biomarker profiles with vasculopathy. We next assessed which of the 39 markers showed a direct correlation with ERL scores (discovery cohort, n = 29). ERL scores correlated negatively with the serum levels of endoglin (r_s = –0.67, $P < 0.0001$) as well as thrombospondin-1 (TSP-1) and VEGF (each r_s = –0.415, P = 0.0252), and

Table 2. Spearman's rank correlations of serum biomarker levels with clinical disease activity scores in juvenile dermatomyositis patients in the discovery and validation cohorts*

	Discovery cohort			Validation cohort	
	DAS-T (n = 30)	DAS-M (n = 30)	CMAS (n = 29)	PhGA (n = 25)	CMAS (n = 25)
CXCL13	0.538†	0.539†	−0.476†	NS	NS
CCL19	0.541†	0.553†	−0.497†	NS	NS
Gal-9	0.519†	0.496†	−0.428‡	0.403‡	NS
TNFRII	0.518†	0.489†	−0.377‡	0.439‡	NS
Gal-1	0.471†	0.495†	NS	0.486‡	NS
CXCL10	0.505†	0.458‡	−0.397‡	0.445‡	NS
CXCL9	0.432‡	NS	NS	NS	NS
IL-18	0.503†	0.415‡	−0.490†	NS	NS
YKL-40	0.465†	0.524†	−0.667§	NS	NS
CCL2	0.557†	0.566†	−0.532†	NS	NS
CCL4	0.388‡	NS	−0.396‡	NS	NS
VEGF	NS	NS	NS	NS	NS
E-selectin	NS	NS	NS	NS	NS
ICAM-1	NS	NS	−0.515†	NS	NS
Fetuin	NS	NS	NS	NS	NS
CCL18	NS	NS	NS	NS	NS
sVEGFR-1¶	0.422‡	0.427‡	NS	NS	−0.454‡

* Spearman's rank correlation coefficients are shown for those biomarkers whose serum levels were significantly different between cluster 1 and cluster 2. For biomarkers with out-of-range values (i.e., below the detection limit), the values were imputed (for CXCL9 and E-selectin), and imputed values were excluded from the analysis to prevent skewing of the data. DAS-T = Disease Activity Score for total disease activity; DAS-M = Disease Activity Score for the muscle; CMAS = Childhood Myositis Assessment Scale; PhGA = physician's global assessment of disease activity; NS = not significant; Gal-9 = galectin-9; TNFRII = tumor necrosis factor receptor type II; IL-18 = interleukin-18; YKL-40 = chitinase 3–like protein 1; VEGF = vascular endothelial growth factor; ICAM-1 = intercellular adhesion molecule 1.
† $P < 0.01$.
‡ $P < 0.05$.
§ $P < 0.0001$.
¶ This marker, soluble VEGF receptor 1 (sVEGFR-1), only identifies patients in cluster 1 in the validation cohort, but not in the discovery cohort.

correlated positively with the serum levels of ICAM-1 ($r_s = 0.465$, $P = 0.0111$) (Figure 2A). Patients with an ERL score of <4, indicating severe vasculopathy, had significantly higher serum endoglin levels and lower serum ICAM-1 levels compared to patients with an ERL score of ≥4 ($P = 0.012$ and $P = 0.0079$, respectively) (Figure 2B).

With regard to serum levels of endoglin, the area under the ROC curve (AUC) for identifying patients with low ERL scores (indicative of severe vasculopathy) relative to high ERL scores was 0.771 ($P = 0.0129$). An optimal cutoff value of 2,286 pg/ml for the endoglin level yielded a sensitivity of 85.7% and specificity of 73.3% for identifying patients with a low ERL score. With regard to serum levels of ICAM-1, the AUC for identifying patients with a low ERL score was 0.786 ($P = 0.0088$), and a cutoff value of 386,425 pg/ml yielded a sensitivity of 85.7% and specificity of 80%. The combination of the 2 markers in a prediction model improved the AUC to 0.833 ($P = 0.0023$), but did not yield a higher sensitivity (79%) or specificity (80%) than that with ICAM-1 alone. The presence of low serum levels of ICAM-1 (and/or high serum levels of endoglin) may thus be suitable to identify patients with severe vasculopathy.

Validation of biomarker and clinical profiles in an independent cohort. To validate the association between biomarker profiles and clinical disease, the same biomarker panel was measured in an independent validation cohort of patients with juvenile DM (n = 29). The 16 markers that identified patients with severe (muscle) disease activity in the discovery cohort were again assessed for correlations with clinical disease activity in the validation cohort. Four markers correlated significantly with clinical disease activity in both the discovery and validation cohorts: Gal-9, TNFRII, Gal-1, and CXCL10 ($r_s = 0.40$–0.52 for correlations with the DAS-T and PhGA scores) (Table 2 and Figures 3A–D). Reciprocal analysis of the 2 cohorts using the same criteria, i.e., 1) clustering of the validation cohort by all markers, 2) selection of markers identifying the more severely affected cluster, and 3) subsequent assessment of correlations with clinical disease parameters, yielded the same 4 markers (Gal-9, TNFRII, Gal-1, and CXCL10), as well as soluble VEGF receptor 1 (sVEGFR-1) (Table 2). Since sVEGFR-1 was not one of the markers identifying cluster 1 in the discovery cohort, it was not included as an additional marker in subsequent analyses.

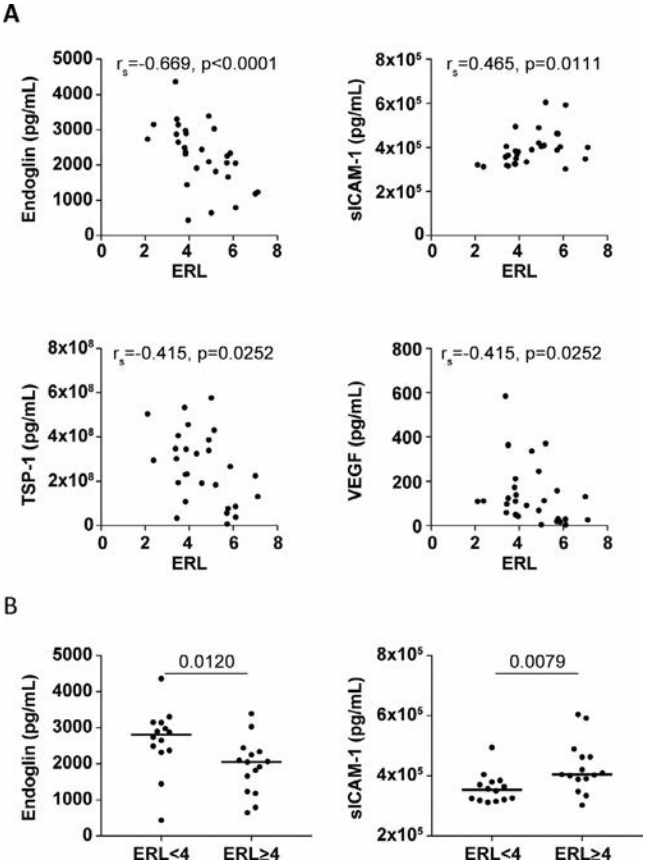

Figure 2. Correlation of biomarker levels with end row loop (ERL) scores. A panel of biomarkers for endothelial dysfunction and inflammation was measured by multiplex assay in the serum of 30 treatment-naive juvenile dermatomyositis (DM) patients (discovery cohort). ERL scores (a count of ERLs/mm in the fingers, as a measure of the severity of vasculopathy) were assessed by nailfold capillaroscopy. **A**, Spearman's rank correlations (r_s) were determined to assess the correlation between serum biomarker levels and ERL scores in 29 juvenile DM patients. **B**, Serum levels of endoglin and soluble intercellular adhesion molecule 1 (sICAM-1) were assessed in juvenile DM patients stratified according to low ERL scores (defined as <4) and high ERL scores (defined as ≥4). Symbols represent individual patients; horizontal lines show the median. Values above the graphs are *P* values, determined by Mann-Whitney U test. TSP-1 = thrombospondin-1; VEGF = vascular endothelial growth factor.

We next examined whether these 4 markers would be able and sufficient to identify severely affected patients. Hierarchical clustering of the 2 cohorts based on these 4 markers yielded 2 distinct patient clusters in each cohort (clusters of 9 patients and 21 patients in the discovery cohort, and clusters of 6 patients and 23 patients in the validation cohort) (Figures 3E and F). Indeed, in both cohorts, the smaller subgroup of patients with high levels of Gal-9, TNFRII, Gal-1, and CXCL10 (cluster 1D and cluster 1V from the discovery and validation cohorts, respectively) had significantly higher total disease activity and muscle disease activity scores compared to patients in cluster 2. Patients in cluster 1D had higher DAS-T scores (*P* = 0.0078), higher DAS-M scores (*P* = 0.0181), and lower CMAS scores (*P* = 0.0148) compared to patients in cluster 2D, and patients in cluster 1V had higher PhGA scores (*P* = 0.0013) and lower CMAS scores (*P* = 0.0053) compared to patients in cluster 2V (Figures 3G and H). Skin disease activity did not differ between the clusters in the discovery cohort, but in the validation cohort, skin disease activity (CAT score) was significantly higher in cluster 1V than in cluster 2V (*P* = 0.0131). In both cohorts, LDH levels were higher in cluster 1 than in cluster 2 (*P* < 0.05 in each cohort). Thus, the combination of high serum levels of Gal-9, TNFRII, Gal-1, and CXCL10 may be sufficient to identify a subgroup of patients with severe global and muscle disease.

To assess the potency of each individual marker for identifying severely affected patients, patients were stratified into severe disease (those in the >75th percentile of PhGA, DAS-T, and DAS-M scores or those in the <25th percentile of CMAS scores) and nonsevere (muscle or global) disease, and the AUCs of the ROC curves were determined for each marker. TNFRII had the highest AUC for identifying patients with severe muscle disease (AUC 0.80) and severe global disease (AUC 0.73), with a sensitivity of 80% and 69% and specificity of 82% and 76%, respectively, at a cutoff level of 3,010 pg/ml for levels of TNFRII. Due to the high correlations between the markers (r_s = 0.76–0.95), a combined model with these markers was not constructed. Therefore, it can be concluded that high serum levels of Gal-9, TNFRII, Gal-1, and CXCL10 can identify severely affected patients at the time of diagnosis, with TNFRII being the best indicator of severe disease.

Association of biomarker profiles with MSAs. Since MSA serotypes were previously linked to disease phenotypes, including (muscle) disease severity (7,8), we compared the frequencies of MSAs (according to MSA category) between the biomarker-based clusters. The cohorts were combined into a single cohort to yield a sufficient number of patients per MSA category. Clustering by Gal-9, CXCL10, TNFRII, and Gal-1 expression produced 2 clusters of patients (combined cohort clusters 1C and 2C) (Figure 4A).

Although none of the MSAs differed significantly in frequency between these 2 clusters, MSA-negative patients were relatively more frequent in cluster 2C than in cluster 1C (57% versus 35%) (Figures 4A and B). Frequencies of patients with anti–TIF-1γ antibodies were similar between the clusters (21% in cluster 1C and 23% in cluster 2C). The numbers of patients with anti–SAE-1, anti–Mi-2, anti–NXP-2, and anti–MDA-5 antibodies were too small to statistically compare their frequencies between clusters, but it was notable that all 4 patients with anti–MDA-5 autoantibodies were in cluster 2C. Moreover, all patients with strong expression of anti–NXP-2 antibodies were in cluster 1C, whereas patients with weak anti–NXP-2 expression were present only in cluster 2C. Since weak antibody positivity may sometimes indicate a false-positive measurement, this might imply a difference in

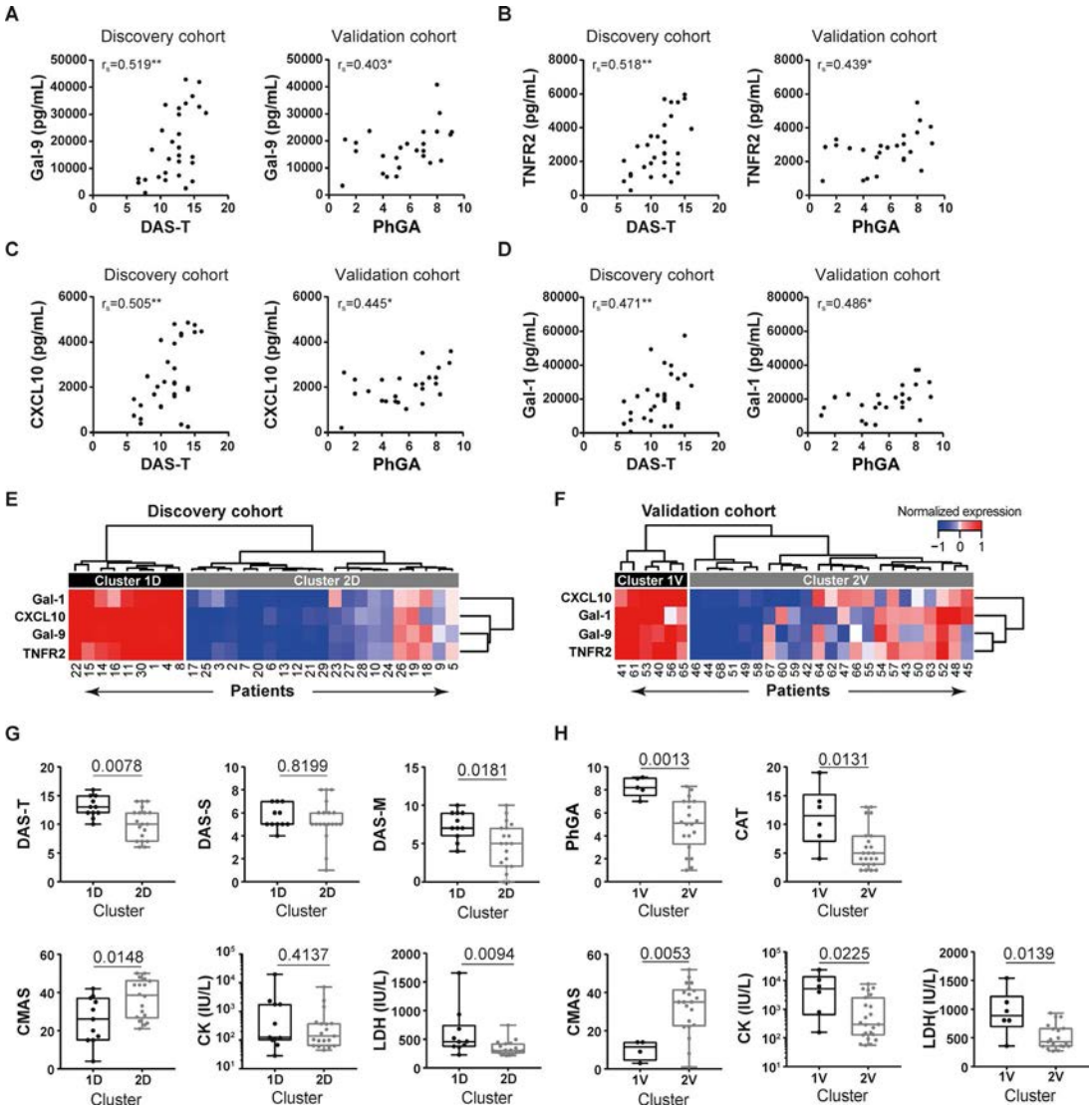

Figure 3. Identification of galectin-9 (Gal-9), tumor necrosis factor receptor type II (TNFRII), CXCL10, and Gal-1 as biomarkers for stratification of patients with severe juvenile dermatomyositis (DM). A panel of biomarkers for endothelial dysfunction and inflammation was measured by multiplex assay in the serum of 59 treatment-naive juvenile DM patients. **A–D**, Spearman's rank correlations (r_s) were determined to assess the correlations of serum levels of Gal-9 (**A**), TNFRII (**B**), CXCL10 (**C**), and Gal-1 (**D**) with global disease activity as measured by the global Disease Activity Score (DAS-T) in the discovery (D) cohort and the physician's global assessment of disease activity (PhGA) in the validation (V) cohort. * = $P < 0.05$; ** = $P < 0.01$. **E** and **F**, Unsupervised hierarchical clustering of juvenile DM patients in the discovery cohort (**E**) and validation cohort (**F**) was performed according to the normalized serum expression values for Gal-9, TNFRII, CXCL10, and Gal-1. Values at the bottom represent unique patient identifiers (not ranked). **G** and **H**, Clinical measures of disease activity were compared between cluster 1 and cluster 2 (the same clusters as identified in **E** and **F**) in the discovery cohort (**G**) and validation cohort (**H**). Results are shown as box plots, where the boxes represent the 25th to 75th percentiles, the lines within the boxes represent the median, and the lines outside the boxes represent the 10th and 90th percentiles. Values above the graphs are *P* values, determined by Mann-Whitney U test. DAS-S = Disease Activity Score for the skin; DAS-M = Disease Activity Score for the muscle; CMAS = Childhood Myositis Assessment Scale (score); CK = creatine kinase; LDH = lactate dehydrogenase; CAT = cutaneous assessment tool for juvenile DM. Color figure can be viewed in the online issue, which is available at: http://onlinelibrary.wiley.com/doi/10.1002/art.41236/abstract.

anti–NXP-2 frequencies between cluster 1C and cluster 2C. The findings thus suggest that MSA serotypes were not directly linked to the biomarker-based patient clusters, but that patients with strong anti–NXP-2 positivity may be more likely to be in the severe disease cluster, characterized by high biomarker levels, whereas the opposite may be true for patients with anti–MDA-5 antibodies.

Prognostic value of biomarkers for suboptimal response to initial treatment. We next assessed whether high serum levels of Gal-9, CXCL10, TNFRII, and/or Gal-1 could be prognostic for a suboptimal response to initial treatment. The frequency at which intensification of treatment was required within the first 3 months after diagnosis was significantly higher in

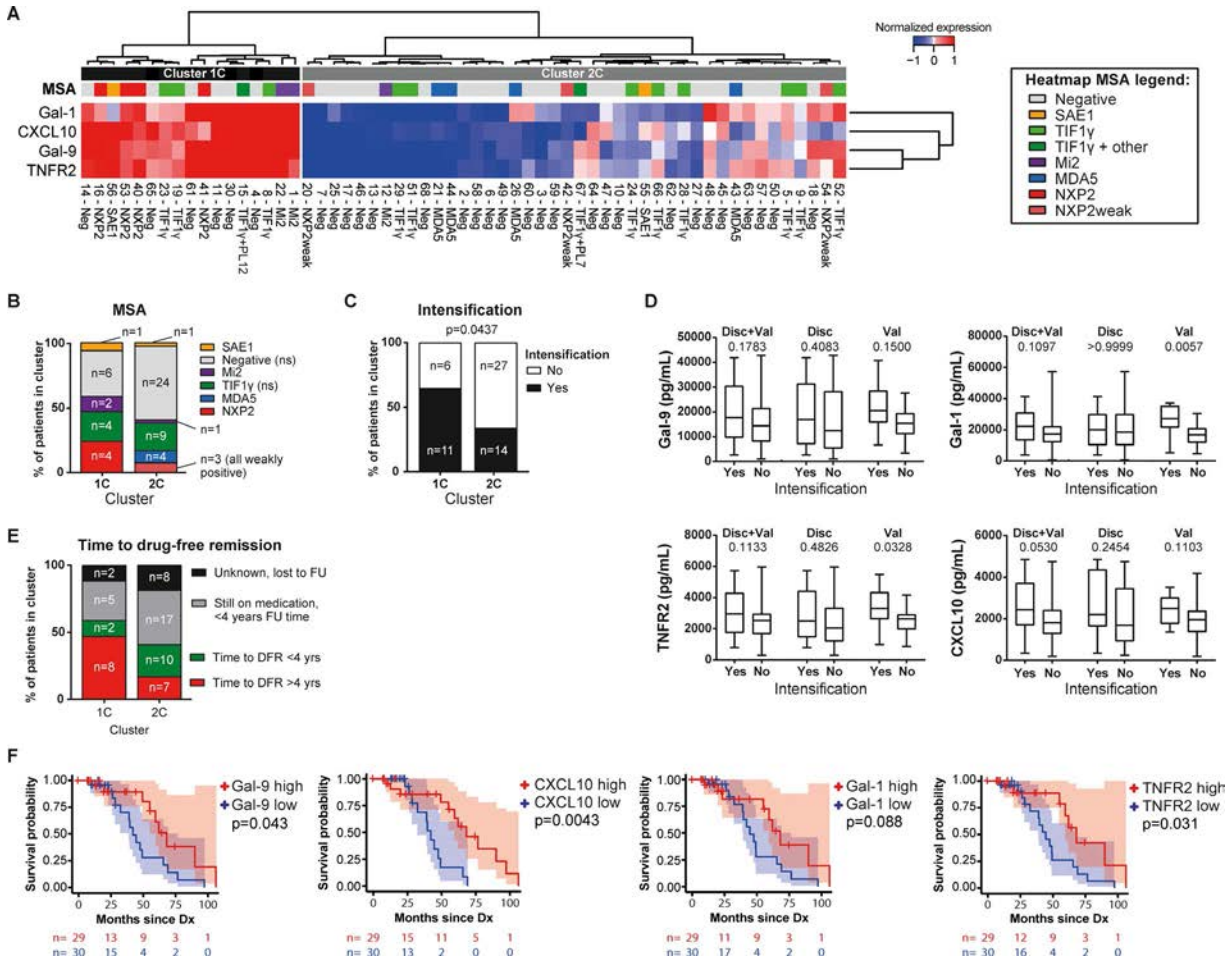

Figure 4. Identification of galectin-1 (Gal-1), CXCL10, Gal-9, and tumor necrosis factor receptor type II (TNFRII) as biomarkers for patient stratification and for prognosis of response to therapy. A panel of biomarkers for endothelial dysfunction and inflammation was measured by multiplex assay in the serum of 59 treatment-naive juvenile dermatomyositis (DM) patients. **A**, Unsupervised hierarchical clustering of 59 juvenile DM patients in the discovery and validation cohorts combined (C) was performed according to the normalized serum expression values for Gal-9, CXCL10, TNFRII, and Gal-1 and status of each myositis-specific antibody (MSA) serotype. The heatmap legend indicates the different MSA serotypes according to different colors. Values at the bottom represent unique patient identifiers (not ranked). **B**, Cumulative frequencies of MSA serotypes were compared between clusters 1C and 2C. *P* values for cluster 1C versus cluster 2C, as determined by chi-square test, were not significant (NS) for the MSA-negative and anti–transcription intermediary factor 1γ (anti–TIF1γ)–positive patients. **C**, Cumulative frequencies of patients needing intensification of treatment within the first 3 months after diagnosis were compared between cluster 1C and cluster 2C. Due to missing data on intensification of treatment for 1 patient in cluster 2C, the analysis was performed after exclusion of this patient. *P* values were determined by Fisher's exact test. **D**, The capacity of serum levels of Gal-9, CXCL10, TNFRII, and Gal-1 to differentiate patients requiring intensification of treatment was assessed in the combined cohort and in the discovery (Disc) and validation (Val) cohorts separately. Results are shown as box plots, where the boxes represent the 25th to 75th percentiles, the lines within the boxes represent the median, and the lines outside the boxes represent the 10th and 90th percentiles. Values above the graphs are *P* values, determined by Mann-Whitney U test. **E**, Cumulative frequencies of patients 1) with time to attainment of drug-free remission (DFR) of >4 years, 2) with time to attainment of DFR of <4 years, 3) who were still receiving medication at <4 years of follow-up (FU), or 4) whose medication use was unknown and who were lost to follow-up were compared between cluster 1C and cluster 2C. **F**, Kaplan-Meier curves show the months from diagnosis (Dx) until achievement of remission while not receiving immunosuppressive treatment among patients stratified according to the median serum levels of Gal-9, CXCL10, Gal-1, and TNFRII (high levels [n = 29] versus low levels [n = 30]). Shaded areas show the confidence intervals. Values below the plots are the number of patients at risk in the high-level (red) and low-level (blue) groups at each time point. *P* values were determined by log-rank test. Neg = negative; NXP-2 = nuclear matrix protein 2; SAE-1 = small ubiquitin-like modifier-1 activating enzyme; MDA-5 = melanoma differentiation–associated protein 5. Color figure can be viewed in the online issue, which is available athttp://onlinelibrary.wiley.com/doi/10.1002/art.41236/abstract.

cluster 1C than in cluster 2C (64.7% versus 34.1%; *P* = 0.0437) (Figure 4C), suggesting that, indeed, high biomarker levels may identify an "at risk" group of patients who might require intensification of their initial treatment.

Although this combination of biomarkers could identify "at risk" patients, the individual biomarkers showed only a trend toward being higher in patients needing intensification of treatment in the combined cohort (for CXCL10, *P* = 0.053; for

Gal-1, $P = 0.1097$; for Gal-9, $P = 0.1783$; for TNFRII, $P = 0.1133$) (Figure 4D). In the validation cohort, higher serum levels of Gal-1 and TNFRII potently identified patients needing intensification of treatment (for Gal-1, $P = 0.0057$; for TNFRII, $P = 0.0328$) (Figure 4D). The results of the corresponding ROC curves are available from the corresponding author upon request. Again, due to the high correlation between the biomarkers, a combined model of these markers was not constructed. Thus, the combination of the 4 markers—Gal-9, CXCL10, TNFRII, and Gal-1—may identify patients who would be considered at risk for a suboptimal response to induction therapy.

Prognostic value of biomarkers for predicting time to attainment of DFR. Finally, we examined whether patients with high serum levels of Gal-9, CXCL10, TNFRII, and/or Gal-1 at diagnosis would need a longer time to attain DFR. At the time of analysis, 24 (41%) of 59 patients had attained DFR (median follow-up time 4.0 years). Of the 10 patients in cluster 1C with a known time until DFR or with more than 4 years of follow-up, 8 (80%) were still receiving medication after 4 years, whereas this was the case for only 7 (41%) of 17 patients in cluster 2C ($P < 0.05$) (Figure 4E).

Kaplan-Meier survival analysis with dichotomization of the single biomarkers into "high" and "low" serum levels according to the median values showed that patients with high serum levels of CXCL10, Gal-9, or TNFRII at diagnosis needed a significantly longer time to attain DFR than patients with low biomarker levels ($P < 0.05$) (Figure 4F), although some cross-over of the Kaplan-Meier curves was evident, indicating that confounding factors may play a role, and the confidence intervals overlapped.

In Cox proportional hazards models, high biomarker levels showed a trend toward conferring a higher risk of "not getting off treatment" as compared to low biomarker levels (for Gal-9, hazard ratio [HR] 0.32, $P = 0.06$; for TNFRII, HR 0.24, $P = 0.08$; for CXCL10, HR 0.39, $P = 0.1$; for Gal-1, HR 0.41, $P = 0.1$). Patients with an ERL score of <4, indicating severe vasculopathy, also showed a trend toward needing longer time to attain DFR (Kaplan-Meier log-rank $P = 0.069$). Taken together, these results indicate that patients with high serum levels of Gal-9, CXCL10, or TNFRII at diagnosis may be at risk for a longer disease course.

DISCUSSION

Herein we have shown that juvenile DM is a heterogeneous disease, not only in the clinical presentation, but also in the biomarker profiles at diagnosis. In 2 independent cohorts of patients with juvenile DM, we were able to identify a subgroup of patients, constituting approximately one-third of the study population, who exhibited high serum levels of Gal-9, CXCL10, TNFRII, and Gal-1 and higher muscle and global disease activity, who were considered at risk of requiring intensification of initial treatment, and who experienced a longer time to reach DFR. These biomarkers could thus be used to identify a severely affected subgroup at diagnosis, and may be prognostic for the disease course. The biomarker-based clusters were not evidently correlated with MSA serotypes, but patients with strong anti–NXP-2 positivity were more likely to be in the subgroup with high serum levels of Gal-9, CXCL10, TNFRII, and Gal-1 at diagnosis.

Our results are consistent with the findings from a study by Gitiaux et al, in which approximately one-third of patients were identified as being severely affected (19). In our study, the severely affected subgroup of patients were not identified as having more severe vasculopathy based on their ERL scores. Moreover, the vasculopathy-associated biomarkers endoglin, ICAM-1, TSP-1, and VEGF did not aid in the identification of this subgroup. However, the observed correlations of VEGF and endoglin serum levels with severe vasculopathy are consistent with the findings of a recent study in which both proteins were shown to be upregulated in lesions with active capillary injury in the muscle of patients with juvenile DM (7). Endoglin and VEGF were also found to be expressed in the muscle of patients with DM in other studies (29,30). Soluble endoglin has more widely been described as an antiangiogenic molecule and marker for vasculopathy (31). TSP-1 was previously suggested to be an antiangiogenic regulator (32) with a vasculopathic role in patients with juvenile DM (in particular, patients with the TNF-308A allele) (33). We found a positive association between the serum ICAM-1 levels and ERL scores in the present study. Since endothelial activation is one of the hallmarks of juvenile DM–associated vasculopathy (34), and soluble ICAM-1 levels are correlated with endothelial surface ICAM-1 expression (35), this finding is difficult to explain in the context of the disease. Future studies may provide insights into the underlying biologic processes.

Two of the 4 identified severity markers, Gal-9 and CXCL10, are known IFN-related proteins (36,37). The correlation between severe muscle disease activity and high levels of IFN-related markers or the IFN signature (in blood and biopsy samples) has been previously demonstrated in juvenile DM patients at the time of disease onset (13,38,39) and during follow-up (16). A higher IFN signature was also associated with a longer time to reach clinically inactive disease (39). The serum levels of Gal-9, CXCL10, and TNFRII were shown to specifically correlate with muscle disease activity during follow-up in our cohorts of patients with juvenile DM, and Gal-9 and CXCL10 serum levels were recently validated as biomarkers for disease activity in patients with juvenile DM (17,40). Moreover, patients experiencing a disease flare within the first year after the start of treatment had higher levels of Gal-9 and CXCL10 at diagnosis (40). TNFRII levels were found to be high in adult DM patients with a high type I IFN score, and neutralization of the IFN signature by an anti-IFNα monoclonal antibody resulted in decreased levels of TNFRII, suggesting that TNFRII may also be related to IFN-driven inflammation (41).

The increased expression of circulating IFN-inducible proteins in severely affected patients further supports the pathogenic role of IFNs in juvenile DM immunopathology. Gal-1 has not been pre-

viously linked to DM, but degeneration of injured muscles induces high expression of Gal-1, and its expression may increase muscle regeneration in experimental models (42,43). In addition, Gal-1 is an antiviral effector molecule expressed by endothelial cells and a negative regulator of both T cell recruitment to the endothelium and transendothelial migration (44–46).

Consistent with our results indicating that muscle disease activity was more pronounced in the severely affected patient cluster, the anti–NXP-2 antibody serotype was previously associated with more severe muscle disease, whereas anti–MDA-5–positive patients were less likely to have muscle weakness (3). In contrast with the findings from previous studies, we did not observe high levels of IFN-related markers in patients with anti–MDA-5 antibodies (47).

As opposed to muscle disease activity, skin disease activity was not related to any of the markers or marker profiles in the 2 cohorts. Possible explanations for this finding could be that skin disease activity showed relatively low variance across patients (mainly in the discovery cohort), or that muscle disease had a dominant effect on the biomarker profiles (as also suggested by the PCA plots in Figure 1D), which could overrule any moderate correlations with skin disease.

Whereas in the validation cohort, Gal-1 and TNFRII serum levels were higher in patients requiring intensification of treatment, this was not the case in the discovery cohort. This difference could not be explained by differences in the initial treatment approach, as the approaches were similar between the cohorts. We could speculate that the standardized treatment regimen in the validation cohort (as opposed to the more individualized strategy employed in the discovery cohort) led to a homogeneous/well-defined group of patients receiving intensification of treatment—with certain specific characteristics conforming to the applied protocol. This homogeneity could be reflected in their biomarker profiles. In addition, the difference may be related to the longer duration of untreated disease in the discovery cohort compared to the validation cohort.

Juvenile DM is a very rare disease, which hampers the collection of large sample numbers for study purposes. A unique strength of our study is that we were able to perform biomarker profiling in 2 large (given the rarity of the disease), independent cohorts of treatment-naive patients. We were thereby able to analyze the unmodified disease signatures in different patients without possible treatment effects on biomarker profiles. Although the cohorts showed some differences in baseline characteristics (e.g., duration of untreated disease, MSA frequencies, requirement of treatment intensification, ethnicity), which could have conferred bias in their biomarker profiles, we were able to validate our findings, showing that Gal-9, TNFRII, Gal-1, and CXCL10 are robust markers for the identification of a subgroup of patients with severe disease, even in cohorts with different patient characteristics. A limitation of this study is the difference in the methods used to record disease activity between the 2 cohorts, which was attributable to historical and regional differences in the data collection methods. However, the PhGA and DAS-T scores, as well as the CAT and DAS-S scores, have been shown to correlate strongly (48).

Further validation of these data in a large prospective cohort will allow for the construction of prediction models that could be used to predict those patients who will require intensification of treatment or to predict the length of time to attainment of DFR, possibly combining one or more of the biomarkers with clinical parameters (such as age at onset and clinical disease activity). We speculate that patients in the "at risk" group could benefit from more intensive monitoring during induction treatment in order to detect suboptimal response to therapy in an early phase. This early detection would promote a swift intensification of treatment. Future studies will have to point out whether more aggressive or targeted initial treatment (e.g., with JAK inhibition or anti-IFN antibodies) could also be a treatment option in these patients (49,50). Considering the longer time to remission, it may be useful to discuss with patients and parents the expectations of treatment length and the possible effect on cumulative medication dose, as these may have implications for the long-term outcomes.

In conclusion, the results of this study underline the clinical and serologic heterogeneity of juvenile DM. Moreover, the identification of high serum levels of the biomarkers Gal-9, TNFRII, CXCL10, and Gal-1 in patients with juvenile DM would suggest that these markers may be useful tools for identifying severely affected patients who could be at risk of a suboptimal response to standard immunosuppressive treatment.

ACKNOWLEDGMENTS

We thank the pediatric rheumatology research group at Lurie Children's Hospital, Chicago, which is supported by the CureJM Foundation, and KK Women's and Children's Hospital, Singapore, for kindly providing the samples and the extensive clinical expertise with which to perform this study. We thank the Dutch juvenile DM network, and especially Annette van Dijk-Hummelman and Ellen Schatorjé, for their help and support in the collection and inclusion of patients and samples. We also thank the Luminex core facility for performing all biomarker measurements. A special thanks goes to the board members of the patient group Myositis of the VSN (Vereniging Spierziekten Nederland), the Stichting KAISZ (Kinderen met Auto-ImmuunSysteemZiekten), and the Bas Stichting (Dutch juvenile DM patient organization) for their explicit and continuous support for our biomarker research in juvenile DM, as well as the CureJM Foundation, which has enabled the Chicago Center to amass the biobank data for this study.

AUTHOR CONTRIBUTIONS

All authors were involved in drafting the article or revising it critically for important intellectual content, and all authors approved the final version to be published. Drs. van Wijk and van Royen-Kerkhof had full access to

all of the data in the study and take responsibility for the integrity of the data and the accuracy of the data analysis.

Study conception and design. Wienke, Pachman, van Wijk, van Royen-Kerkhof.

Acquisition of data. Wienke, Pachman, Morgan, Yeo, Amoruso, Hans, Kamphuis, Hoppenreijs, Armbrust, van den Berg, Hissink Muller, Gelderman, Arkachaisri, van Wijk, van Royen-Kerkhof.

Analysis and interpretation of data. Wienke, Pachman, van Wijk, van Royen-Kerkhof.

ADDITIONAL DISCLOSURES

Author Gelderman is an employee of Sanquin Diagnostic Services.

REFERENCES

1. Meyer A, Meyer N, Schaeffer M, Gottenberg J-E, Geny B, Sibilia J. Incidence and prevalence of inflammatory myopathies: a systematic review. Rheumatology (Oxford) 2015;54:50–63.
2. Shah M, Mamyrova G, Targoff IN, Huber AM, Malley JD, Rice MM, et al. The clinical phenotypes of the juvenile idiopathic inflammatory myopathies. Medicine (Baltimore) 2013;92:25–41.
3. Tansley SL, Simou S, Shaddick G, Betteridge ZE, Almeida B, Gunawardena H, et al. Autoantibodies in juvenile-onset myositis: their diagnostic value and associated clinical phenotype in a large UK cohort. J Autoimmun 2017;84:55–64.
4. Enders FB, Bader-Meunier B, Baildam E, Constantin T, Dolezalova P, Feldman BM, et al. Consensus-based recommendations for the management of juvenile dermatomyositis. Ann Rheum Dis 2017;76:329–40.
5. Wienke J, Deakin CT, Wedderburn LR, van Wijk F, van Royen-Kerkhof A. Systemic and tissue inflammation in juvenile dermatomyositis: from pathogenesis to the quest for monitoring tools [review]. Front Immunol 2018;9:2951.
6. Papadopoulou C, McCann LJ. The vasculopathy of juvenile dermatomyositis. Front Pediatr 2018;6:284.
7. Baumann M, Gumpold C, Mueller-Felber W, Schoser B, Haberler C, Loescher WN, et al. Pattern of myogenesis and vascular repair in early and advanced lesions of juvenile dermatomyositis. Neuromuscul Disord 2018;28:973–85.
8. Kim E, Cook-Mills J, Morgan G, Sredni ST, Pachman LM. Increased expression of vascular cell adhesion molecule 1 in muscle biopsy samples from juvenile dermatomyositis patients with short duration of untreated disease is regulated by miR-126. Arthritis Rheum 2012;64:3809–17.
9. Goncalves FG, Chimelli L, Sallum AM, Marie SK, Kiss MH, Ferriani VP. Immunohistological analysis of CD59 and membrane attack complex of complement in muscle in juvenile dermatomyositis. J Rheumatol 2002;29:1301–7.
10. Kissel JT, Mendell JR, Rammohan KW. Microvascular deposition of complement membrane attack complex in dermatomyositis. N Engl J Med 1986;314:329–34.
11. Fall N, Bove KE, Stringer K, Lovell DJ, Brunner HI, Weiss J, et al. Association between lack of angiogenic response in muscle tissue and high expression of angiostatic ELR-negative CXC chemokines in patients with juvenile dermatomyositis: possible link to vasculopathy. Arthritis Rheum 2005;52:3175–80.
12. Gitiaux C, Latroche C, Weiss-Gayet M, Rodero MP, Duffy D, Bader-Meunier B, et al. Myogenic progenitor cells exhibit type I interferon–driven proangiogenic properties and molecular signature during juvenile dermatomyositis. Arthritis Rheumatol 2018;70:134–45.
13. O'Connor KA, Abbott KA, Sabin B, Kuroda M, Pachman LM. MxA gene expression in juvenile dermatomyositis peripheral blood mononuclear cells: association with muscle involvement. Clin Immunol 2006;120:319–25.
14. Rice GI, Melki I, Fremond M-L, Briggs TA, Rodero MP, Kitabayashi N, et al. Assessment of type I interferon signaling in pediatric inflammatory disease. J Clin Immunol 2017;37:123–32.
15. Rodero MP, Decalf J, Bondet V, Hunt D, Rice GI, Werneke S, et al. Detection of interferon alpha protein reveals differential levels and cellular sources in disease. J Exp Med 2017;214:1547–55.
16. Reed AM, Peterson E, Bilgic H, Ytterberg SR, Amin S, Hein MS, et al. Changes in novel biomarkers of disease activity in juvenile and adult dermatomyositis are sensitive biomarkers of disease course. Arthritis Rheum 2012;64:4078–86.
17. Bellutti Enders F, van Wijk F, Scholman R, Hofer M, Prakken BJ, van Royen-Kerkhof A, et al. Correlation of CXCL10, tumor necrosis factor receptor type II, and galectin 9 with disease activity in juvenile dermatomyositis. Arthritis Rheumatol 2014;66:2281–9.
18. Schmeling H, Stephens S, Goia C, Manlhiot C, Schneider R, Luthra S, et al. Nailfold capillary density is importantly associated over time with muscle and skin disease activity in juvenile dermatomyositis. Rheumatology (Oxford) 2011;50:885–93.
19. Gitiaux C, de Antonio M, Aouizerate J, Gherardi RK, Guilbert T, Barnerias C, et al. Vasculopathy-related clinical and pathological features are associated with severe juvenile dermatomyositis. Rheumatology (Oxford) 2016;55:470–9.
20. Wargula JC, Lovell DJ, Passo MH, Bove KE, Santangelo JD, Levinson JE. What more can we learn from muscle histopathology in children with dermatomyositis/polymyositis? Clin Exp Rheumatol 2006;24:333–43.
21. Bohan A, Peter JB. Polymyositis and dermatomyositis: part 1. N Engl J Med 1975;292:344–7.
22. Bohan A, Peter JB. Polymyositis and dermatomyositis: part 2. N Engl J Med 1975;292:403–7.
23. Quiñones R, Morgan GA, Amoruso M, Field R, Huang C-C, Pachman LM. Lack of achievement of a full score on the childhood myositis assessment scale by healthy four-year-olds and those recovering from juvenile dermatomyositis. Arthritis Care Res (Hoboken) 2013;65:1697–701.
24. Bode RK, Klein-Gitelman MS, Miller ML, Lechman TS, Pachman LM. Disease activity score for children with juvenile dermatomyositis: reliability and validity evidence. Arthritis Rheum 2003;49:7–15.
25. Rider LG, Feldman BM, Perez MD, Rennebohm RM, Lindsley CB, Zemel LS, et al, in coopoeration with the Juvenile Dermatomyositis Disease Activity Collaborative Study Group. Development of validated disease activity and damage indices for the juvenile idiopathic inflammatory myopathies: I. Physician, parent, and patient global assessments. Arthritis Rheum 1997;40:1976–83.
26. Huber AM, Dugan EM, Lachenbruch PA, Feldman BM, Perez MD, Zemel LS, et al. Preliminary validation and clinical meaning of the cutaneous assessment tool in juvenile dermatomyositis. Arthritis Rheum 2008;59:214–21.
27. Christen-Zaech S, Seshadri R, Sundberg J, Paller AS, Pachman LM. Persistent association of nailfold capillaroscopy changes and skin involvement over thirty-six months with duration of untreated disease in patients with juvenile dermatomyositis. Arthritis Rheum 2008;58:571–6.
28. De Jager W, Prakken BJ, Bijlsma JW, Kuis W, Rijkers GT. Improved multiplex immunoassay performance in human plasma and synovial fluid following removal of interfering heterophilic antibodies. J Immunol Methods 2005;300:124–35.
29. Grundtman C, Tham E, Ulfgren A-K, Lundberg IE. Vascular endothelial growth factor is highly expressed in muscle tissue of patients with polymyositis and patients with dermatomyositis. Arthritis Rheum 2008;58:3224–38.

30. Konttinen YT, Mackiewicz Z, Povilenaite D, Sukura A, Hukkanen M, Virtanen I. Disease-associated increased HIF-1, αvβ3 integrin, and Flt-1 do not suffice to compensate the damage-inducing loss of blood vessels in inflammatory myopathies. Rheumatol Int 2004;24:333–9.
31. Venkatesha S, Toporsian M, Lam C, Hanai J, Mammoto T, Kim YM, et al. Soluble endoglin contributes to the pathogenesis of preeclampsia. Nat Med 2006;12:642–9.
32. Jiménez B, Volpert OV, Crawford SE, Febbraio M, Silverstein RL, Bouck N. Signals leading to apoptosis-dependent inhibition of neovascularization by thrombospondin-1. Nat Med 2000;6:41–8.
33. Lutz J, Huwiler KG, Fedczyna T, Lechman TS, Crawford S, Kinsella TR, et al. Increased plasma thrombospondin-1 (TSP-1) levels are associated with the TNF α-308A allele in children with juvenile dermatomyositis. Clin Immunol 2002;103:260–3.
34. Nagaraju K, Rider LG, Fan C, Chen Y-W, Mitsak M, Rawat R, et al. Endothelial cell activation and neovascularization are prominent in dermatomyositis. J Autoimmune Dis 2006;3:2.
35. Kjærgaard AG, Dige A, Krog J, Tønnesen E, Wogensen L. Soluble adhesion molecules correlate with surface expression in an in vitro model of endothelial activation. Basic Clin Pharmacol Toxicol 2013; 113:273–9.
36. Van den Hoogen LL, van Roon JA, Mertens JS, Wienke J, Lopes AP, de Jager W, et al. Galectin-9 is an easy to measure biomarker for the interferon signature in systemic lupus erythematosus and antiphospholipid syndrome. Ann Rheum Dis 2018;77:1810–4.
37. Antonelli A, Ferrari SM, Giuggioli D, Ferrannini E, Ferri C, Fallahi P. Chemokine (C–X–C motif) ligand (CXCL)10 in autoimmune diseases [review]. Autoimmun Rev 2014;13:272–80.
38. Soponkanaporn S, Deakin CT, Schutz PW, Marshall LR, Yasin SA, Johnson CM, et al. Expression of myxovirus-resistance protein A: a possible marker of muscle disease activity and autoantibody specificities in juvenile dermatomyositis. Neuropathol Appl Neurobiol 2018;45:410–20.
39. Moneta GM, Marafon DP, Marasco E, Rosina S, Verardo M, Fiorillo C, et al. Muscle expression of type I and type II interferons is increased in juvenile dermatomyositis and related to clinical and histological features. Arthritis Rheumatol 2019;71:1011–21.
40. Wienke J, Enders FB, Lim J, Mertens JS, van den Hoogen LL, Wijngaarde CA, et al. Galectin-9 and CXCL10 as biomarkers for disease activity in juvenile dermatomyositis: a longitudinal cohort study and multicohort validation. Arthritis Rheumatol 2019;71:1377–90.
41. Guo X, Higgs BW, Rebelatto M, Zhu W, Greth W, Yao Y, et al. Suppression of soluble T cell-associated proteins by an anti-interferon-alpha monoclonal antibody in adult patients with dermatomyositis or polymyositis. Rheumatology (Oxford) 2014;53:686–95.
42. Cerri DG, Rodrigues LC, Stowell SR, Araujo DD, Coelho MC, Oliveira SR, et al. Degeneration of dystrophic or injured skeletal muscles induces high expression of galectin-1. Glycobiology 2008;18:842–50.
43. Chan J, O'Donoghue K, Gavina M, Torrente Y, Kennea N, Mehmet H, et al. Galectin-1 induces skeletal muscle differentiation in human fetal mesenchymal stem cells and increases muscle regeneration. Stem Cells 2006;24:1879–91.
44. Garner OB, Yun T, Pernet O, Aguilar HC, Park A, Bowden TA, et al. Timing of galectin-1 exposure differentially modulates Nipah virus entry and syncytium formation in endothelial cells. J Virol 2015;89:2520–9.
45. Norling LV, Sampaio AL, Cooper D, Perretti M. Inhibitory control of endothelial galectin-1 on in vitro and in vivo lymphocyte trafficking. FASEB J 2008;22:682–90.
46. He J, Baum LG. Endothelial cell expression of galectin-1 induced by prostate cancer cells inhibits T-cell transendothelial migration. Lab Invest 2006;86:578–90.
47. Ono N, Kai K, Maruyama A, Sakai M, Sadanaga Y, Koarada S, et al. The relationship between type 1 IFN and vasculopathy in anti-MDA5 antibody-positive dermatomyositis patients. Rheumatology (Oxford) 2019;58:786–91.
48. Campanilho-Marques R, Almeida B, Deakin C, Arnold K, Gallot N, de Iorio M, et al. Comparison of the utility and validity of three scoring tools to measure skin involvement in patients with juvenile dermatomyositis. Arthritis Care Res (Hoboken) 2016;68:1514–21.
49. Ladislau L, Suárez-Calvet X, Toquet S, Landon-Cardinal O, Amelin D, Depp M, et al. JAK inhibitor improves type I interferon induced damage: proof of concept in dermatomyositis. Brain 2018;141:1609–21.
50. Higgs BW, Zhu W, Morehouse C, White WI, Brohawn P, Guo X, et al. A phase 1b clinical trial evaluating sifalimumab, an anti-IFN-α monoclonal antibody, shows target neutralisation of a type I IFN signature in blood of dermatomyositis and polymyositis patients. Ann Rheum Dis 2014;73:256–62.

Arthritis & Rheumatology
Vol. 72, No. 7, July 2020, pp 1227–1236
DOI 10.1002/art.41274

American College of Rheumatology
Empowering Rheumatology Professionals

LETTERS

DOI 10.1002/art.41274

Is methotrexate as efficacious as etanercept in psoriatic arthritis patients? Comment on the article by Mease et al

To the Editor:

We read with great interest the article by Dr. Mease et al comparing the efficacy of etanercept (ETN) or ETN plus methotrexate (MTX) with MTX monotherapy in the Study of ETN and MTX in Subjects with Psoriatic Arthritis (SEAM-PsA) trial (1). The authors reported significantly higher response rates in both biologic arms versus MTX monotherapy for the primary end point, the American College of Rheumatology (ACR) 20% improvement response (2), and several secondary end points. Interestingly, Mease et al expressed their surprise about the high efficacy of MTX monotherapy. We commend them for presenting this very balanced view. While the evidence supporting MTX treatment for PsA is controversial, recommendations by both the European League Against Rheumatism (EULAR) and ACR support its use, with EULAR recommending it more strongly (3,4). However, currently MTX is not recommended for the treatment of enthesitis.

Looking at the results of the SEAM-PsA trial data, we noticed that the response of the Enthesitis Index (5) to MTX was essentially the same as the response to ETN or ETN plus MTX (Table 1). This unexpected result is of particular interest, since it suggests that enthesitis may respond at least as well to MTX as to ETN as monotherapy or combination therapy. A good response of enthesitis to MTX was also reported previously in the Tight Control of PsA trial (6). Furthermore, we were surprised that even the improvement in psoriasis-affected body surface area was similar for MTX and ETN; patients in the combination treatment arm had a slightly better response but also the lowest mean baseline value, with the MTX group having the highest baseline value (Table 1). Across the 3 study arms, the Leeds Dactylitis Index (7) and Nail Psoriasis Severity Index (8) also showed levels of improvement with MTX alone that were similar to those seen with ETN plus MTX or ETN alone (Table 1). Finally, and probably most important for patients, physical function measured by the Health Assessment Questionnaire disability index (HAQ DI) (9) improved to a very similar degree across arms, with the MTX group having the worst functional impairment at baseline, in parallel with the highest mean tender and swollen joint counts. Indeed, when exploratory unpaired 2-tailed *t*-tests were performed to assess the differences between groups, the MTX group was found to have significantly worse baseline scores for the HAQ DI and 36-item Short Form health survey (10) versus the other treatment groups, and significantly worse baseline scores for swollen joint count versus the combination treatment group at baseline (Table 1). This imbalance despite randomization is noteworthy, since higher baseline disease activity may be associated with worse outcomes in this PsA population, in which most patients had polyarticular disease (11,12).

We could not find respective data on changes in joint counts in the main body of Mease and colleagues' article nor in the supplementary material. However, we found these data in the sponsor's report provided to ClinicalTrials.gov (13). As we anticipated from looking at the HAQ DI results, the changes in the swollen joint count and tender joint count were also very similar across treatment arms (Table 1). The very small (though significant) difference in progression of joint damage, which was essentially halted in all groups, is likely due to the stronger effect of tumor necrosis factor inhibitors on the mechanisms leading to joint damage rather than on inflammatory response (14,15).

In summary, we fully support Mease and colleagues' findings that MTX provided excellent efficacy, which was the case in terms of improvement of joint counts, physical function, enthesitis, dactylitis, nail involvement, and even skin involvement. This suggests that clinically there is little difference between MTX and ETN monotherapy or between MTX and ETN plus MTX. Indeed, if Mease et al had used an optimized target MTX dosage of 25 mg rather than 20 mg per week (6,16), the efficacy of MTX might have been even better. While the study had no placebo group as a control arm, the data provided in this trial clearly support the use of MTX in PsA.

Thus, based on their results, we wonder if Mease et al would recommend MTX as first-line therapy for PsA patients even if they have enthesitis. Furthermore, we would like to advocate that reports on clinical trials in PsA include pertinent information on all variables in the article, or at least in supplementary material, as suggested in the EULAR/ACR guidance document for rheumatoid arthritis clinical trials published several years ago (17). Easier availability of this more comprehensive information on clinical trial results would be useful in clinical practice and research.

Andreas Kerschbaumer, MD
Josef S. Smolen, MD
Daniel Aletaha, MD
Medical University of Vienna
Vienna, Austria

Table 1. Selected variables with baseline levels and changes*

Treatment arm	n at baseline	Mean ± SD [or mean ± SEM] at baseline	*P*†	n at primary end point (week 24)	Mean change from baseline
Tender joint count (of 68 joints)					
MTX	284	20.9 ± 15.0	Referent	253	−10.8
ETN	283	18.8 ± 14.5	0.091	257	−10.9
ETN + MTX	282	20.0 ± 15.3	0.480	257	−11.0
Swollen joint count (of 66 joints)					
MTX	284	12.9 ± 9.9	Referent	253	−7.0
ETN	283	11.5 ± 9.6	0.088	257	−7.6
ETN + MTX	282	11.2 ± 9.1	0.034	257	−7.7
Physician global assessment, 100-mm VAS					
MTX	284	58.6 ± 19.4	Referent	250	−29.6
ETN	284	58.3 ± 18.2	0.849	257	−35.7
ETN + MTX	282	58.0 ± 17.8	0.702	257	−35.8
Patient global assessment, 100-mm VAS					
MTX	283	60.7 ± 22.5	Referent	252	−23.0
ETN	284	62.9 ± 22.1	0.241	258	−32.3
ETN + MTX	282	61.0 ± 20.8	0.869	257	−29.6
Patient's assessment of pain, 100-mm VAS					
MTX	283	56.1 ± 21.7	Referent	252	−20.6
ETN	284	56.5 ± 22.3	0.829	258	−26.4
ETN + MTX	282	55.7 ± 21.6	0.826	257	−26.9
HAQ DI					
MTX	283	1.27 ± 0.6 [1.27 ± 0.04]	Referent	252	−0.41
ETN	284	1.15 ± 0.6 [1.15 ± 0.04]	0.018	258	−0.44
ETN + MTX	282	1.15 ± 0.6 [1.15 ± 0.04]	0.018	257	−0.47
SF-36 PCS score					
MTX	282	[35.6 ± 0.5]	Referent	253	6.0
ETN	284	[37.8 ± 0.5]	0.002	256	7.8
ETN + MTX	282	[37.4 ± 0.6]	0.022	257	8.0
CRP, mg/liter					
MTX	284	10.52 ± 16.29	Referent	246	−2.60
ETN	282	10.72 ± 15.59	0.881	249	−6.91
ETN + MTX	283	8.7 ± 11.65	0.127	247	−5.82
mNAPSI					
MTX	183	[3.4 ± 0.2]	Referent	121	−1.1
ETN	205	[3.5 ± 0.2]	0.725	115	−1.5
ETN + MTX	195	[3.6 ± 0.2]	0.480	123	−1.7
LDI					
MTX	98	[164.9 ± 26.9]	Referent	89	−128.8
ETN	96	[147.6 ± 20.8]	0.613	89	−119.1
ETN + MTX	90	[138.2 ± 23.9]	0.462	87	−110.2
SPARCC Enthesitis Index					
MTX	191	[5.7 ± 0.3]	Referent	167	−3.1
ETN	189	[5.5 ± 0.3]	0.638	173	−3.0
ETN + MTX	196	[5.9 ± 0.3]	0.638	179	−2.9
% affected body surface area‡					
MTX	284	12.68 ± 18.78	Referent	179	−66.1
ETN	284	10.76 ± 14.66	0.175	166	−69.8
ETN + MTX	283	10.74 ± 15.58	0.181	163	−75.5
SHS					
MTX	269	[2.76 ± 0.12]	Referent	216	0.08
ETN	273	[2.97 ± 0.13]	0.236	225	−0.04
ETN + MTX	274	[2.70 ± 0.12]	0.724	226	−0.01

* *P* values for baseline comparisons were obtained by unpaired 2-tailed *t*-test (α = 0.05). VAS = visual analog scale; HAQ DI = Health Assessment Questionnaire disability index; SF-36 = 36-item Short Form health survey; PCS = physical component summary; CRP = C-reactive protein; mNAPSI = modified Nail Psoriasis Severity Index; LDI = Leeds Dactylitis Index; SPARCC = Spondyloarthritis Research Consortium of Canada; SHS = modified Sharp/van der Heijde score.

† Data on methotrexate (MTX) was obtained from references 1 and 13.

‡ For mean change from baseline, data shown are for patients with ≥3% affected body surface area at baseline; other data shown are for all patients. For patients with ≥3% affected body surface area at baseline, the mean ± SD affected body surface area at baseline was 18.1 ± 1.5% in the MTX group (n = 192), 16.4 ± 1.2% in the etanercept (ETN) group (n = 179), and 16.4 ± 1.3% in the ETN + MTX group (n = 177) (*P* < 0.001, MTX group versus the ETN group and versus the ETN + MTX group).

1. Mease PJ, Gladman DD, Collier DH, Ritchlin CT, Helliwell PS, Liu L, et al. Etanercept and methotrexate as monotherapy or in combination for psoriatic arthritis: primary results from a randomized, controlled phase III trial. Arthritis Rheumatol 2019;71:1112–24.
2. Felson DT, Anderson JJ, Boers M, Bombardier C, Furst D, Goldsmith C, et al. American College of Rheumatology preliminary definition of improvement in rheumatoid arthritis. Arthritis Rheum 1995;38:727–35.
3. Gossec L, Smolen JS, Ramiro S, de Wit M, Cutolo M, Dougados M, et al. European League Against Rheumatism (EULAR) recommendations for the management of psoriatic arthritis with pharmacological therapies: 2015 update. Ann Rheum Dis 2016;75:499–510.
4. Singh JA, Guyatt G, Ogdie A, Gladman DD, Deal C, Deodhar A, et al. 2018 American College of Rheumatology/National Psoriasis Foundation guideline for the treatment of psoriatic arthritis. Arthritis Rheumatol 2019;71:5–32.
5. Maksymowych WP, Mallon C, Morrow S, Shojania K, Olszynski WP, Wong RL, et al. Development and validation of the Spondyloarthritis Research Consortium of Canada (SPARCC) Enthesitis Index. Ann Rheum Dis 2009;68:948–53.
6. Coates LC, Moverley AR, McParland L, Brown S, Navarro-Coy N, O'Dwyer JL, et al. Effect of tight control of inflammation in early psoriatic arthritis (TICOPA): a UK multicentre, open-label, randomised controlled trial. Lancet 2015;386:2489–98.
7. Helliwell PS, Firth J, Ibrahim GH, Melsom RD, Shah I, Turner DE. Development of an assessment tool for dactylitis in patients with psoriatic arthritis. J Rheumatol 2005;32:1745–50.
8. Cassell SE, Bieber JD, Rich P, Tutuncu ZN, Lee SJ, Kalunian KC, et al. The modified Nail Psoriasis Severity Index: validation of an instrument to assess psoriatic nail involvement in patients with psoriatic arthritis. J Rheumatol 2007;34:123–9.
9. Fries JF, Spitz P, Kraines RG, Holman HR. Measurement of patient outcome in arthritis. Arthritis Rheum 1980;23:137–45.
10. Ware JE Jr, Sherbourne CD. The MOS 36-item Short-Form health survey (SF-36). I. Conceptual framework and item selection. Med Care 1992;30:473–83.
11. Aletaha D, Funovits J, Ward MM, Smolen JS, Kvien TK. Perception of improvement in patients with rheumatoid arthritis varies with disease activity levels at baseline. Arthritis Rheum 2009;61:313–20.
12. Aletaha D, Funovits J, Keystone EC, Smolen JS. Disease activity early in the course of teatment predicts response to therapy after one year in rheumatoid arthritis patients. Arthritis Rheum 2007;56:3226–35.
13. Amgen, sponsor. Etanercept and methotrexate in combination or as monotherapy in psoriatic arthritis. ClinicalTrials.gov identifier: NCT02376790; 2015.
14. Smolen JS, Han C, van der Heijde DM, Emery P, Bathon JM, Keystone E, et al, for the Active-Controlled Study of Patients Receiving Infliximab for the Treatment of Rheumatoid Arthritis of Early Onset (ASPIRE) Study Group. Radiographic changes in rheumatoid arthritis patients attaining different disease activity states with methotrexate monotherapy and infliximab plus methotrexate: the impacts of remission and tumour necrosis factor blockade. Ann Rheum Dis 2009;68:823–7.
15. Binder NB, Puchner A, Niederreiter B, Hayer S, Leiss H, Blüml S, et al. Tumor necrosis factor–inhibiting therapy preferentially targets bone destruction but not synovial inflammation in a tumor necrosis factor–driven model of rheumatoid arthritis. Arthritis Rheum 2013;65:608–17.
16. Mease P. Methotrexate in psoriatic arthritis. Bull Hosp Jt Dis (2013) 2013;71 Suppl 1:S41–5.
17. Aletaha D, Landewe R, Karonitsch T, Bathon J, Boers M, Bombardier C, et al. Reporting disease activity in clinical trials of patients with rheumatoid arthritis: EULAR/ACR collaborative recommendations. Arthritis Rheum 2008;59:1371–7.

DOI 10.1002/art.41273

Reply

To the Editor:

We appreciate the comments by Dr. Kerschbaumer et al highlighting the MTX monotherapy results in our article on the primary results from the SEAM-PsA trial. Since MTX is a drug that has long been used in PsA without much data from rigorous and well-controlled clinical trials, we sought to provide reliable data about MTX through the SEAM-PsA trial. The primary aim of the study was to compare MTX monotherapy with ETN monotherapy and assess the value of combining MTX and ETN in the treatment of PsA. As such, the MTX data should be interpreted relative to ETN. The ACR 20% improvement response (1) was selected as the primary end point for the SEAM-PsA study as it continues to be the primary end point required by regulatory agencies for PsA trials. Given the heterogeneous nature of PsA and the variability of the component measures of clinical domains, such as enthesitis and skin disease, minimal disease activity was chosen as the key secondary end point as it is a validated and well-accepted composite end point. These prespecified and appropriately adjusted measures demonstrated statistical superiority of both ETN-containing arms over MTX monotherapy.

Evaluation of other secondary and exploratory end points, which should be considered descriptive with nominal *P* values, showed similar changes from baseline between the treatment arms for several measures. But a closer examination considering the variability of these measures still supports the conclusion that MTX is less effective than ETN in PsA. For example, though the mean change in the Spondyloarthritis Research Consortium of Canada Enthesitis Index (2) was similar in the 3 treatment arms, the proportion of patients with enthesitis resolution was numerically greater in the ETN arms. The observations that patients in the ETN arms also showed a numerically greater response for resolution or near resolution (as seen with the Leeds Dactylitis Index [3] and the modified Nail Psoriasis Severity Index [4]) and overall greater response in those with greater disease

1. Mease PJ, Gladman DD, Collier DH, Ritchlin CT, Helliwell PS, Liu L, et al. Etanercept and methotrexate as monotherapy or in combination for psoriatic arthritis: primary results from a randomized, controlled phase III trial. Arthritis Rheumatol 2019;71:1112–24.
2. Felson DT, Anderson JJ, Boers M, Bombardier C, Furst D, Goldsmith C, et al. American College of Rheumatology preliminary definition of improvement in rheumatoid arthritis. Arthritis Rheum 1995;38:727–35.
3. Gossec L, Smolen JS, Ramiro S, de Wit M, Cutolo M, Dougados M, et al. European League Against Rheumatism (EULAR) recommendations for the management of psoriatic arthritis with pharmacological therapies: 2015 update. Ann Rheum Dis 2016;75:499–510.
4. Singh JA, Guyatt G, Ogdie A, Gladman DD, Deal C, Deodhar A, et al. 2018 American College of Rheumatology/National Psoriasis Foundation guideline for the treatment of psoriatic arthritis. Arthritis Rheumatol 2019;71:5–32.
5. Maksymowych WP, Mallon C, Morrow S, Shojania K, Olszynski WP, Wong RL, et al. Development and validation of the Spondyloarthritis Research Consortium of Canada (SPARCC) Enthesitis Index. Ann Rheum Dis 2009;68:948–53.
6. Coates LC, Moverley AR, McParland L, Brown S, Navarro-Coy N, O'Dwyer JL, et al. Effect of tight control of inflammation in early psoriatic arthritis (TICOPA): a UK multicentre, open-label, randomised controlled trial. Lancet 2015;386:2489–98.
7. Helliwell PS, Firth J, Ibrahim GH, Melsom RD, Shah I, Turner DE. Development of an assessment tool for dactylitis in patients with psoriatic arthritis. J Rheumatol 2005;32:1745–50.
8. Cassell SE, Bieber JD, Rich P, Tutuncu ZN, Lee SJ, Kalunian KC, et al. The modified Nail Psoriasis Severity Index: validation of an instrument to assess psoriatic nail involvement in patients with psoriatic arthritis. J Rheumatol 2007;34:123–9.
9. Fries JF, Spitz P, Kraines RG, Holman HR. Measurement of patient outcome in arthritis. Arthritis Rheum 1980;23:137–45.
10. Ware JE Jr, Sherbourne CD. The MOS 36-item Short-Form health survey (SF-36). I. Conceptual framework and item selection. Med Care 1992;30:473–83.
11. Aletaha D, Funovits J, Ward MM, Smolen JS, Kvien TK. Perception of improvement in patients with rheumatoid arthritis varies with disease activity levels at baseline. Arthritis Rheum 2009;61:313–20.
12. Aletaha D, Funovits J, Keystone EC, Smolen JS. Disease activity early in the course of teatment predicts response to therapy after one year in rheumatoid arthritis patients. Arthritis Rheum 2007;56:3226–35.
13. Amgen, sponsor. Etanercept and methotrexate in combination or as monotherapy in psoriatic arthritis. ClinicalTrials.gov identifier: NCT02376790; 2015.
14. Smolen JS, Han C, van der Heijde DM, Emery P, Bathon JM, Keystone E, et al, for the Active-Controlled Study of Patients Receiving Infliximab for the Treatment of Rheumatoid Arthritis of Early Onset (ASPIRE) Study Group. Radiographic changes in rheumatoid arthritis patients attaining different disease activity states with methotrexate monotherapy and infliximab plus methotrexate: the impacts of remission and tumour necrosis factor blockade. Ann Rheum Dis 2009;68:823–7.
15. Binder NB, Puchner A, Niederreiter B, Hayer S, Leiss H, Blüml S, et al. Tumor necrosis factor–inhibiting therapy preferentially targets bone destruction but not synovial inflammation in a tumor necrosis factor–driven model of rheumatoid arthritis. Arthritis Rheum 2013;65:608–17.
16. Mease P. Methotrexate in psoriatic arthritis. Bull Hosp Jt Dis (2013) 2013;71 Suppl 1:S41–5.
17. Aletaha D, Landewe R, Karonitsch T, Bathon J, Boers M, Bombardier C, et al. Reporting disease activity in clinical trials of patients with rheumatoid arthritis: EULAR/ACR collaborative recommendations. Arthritis Rheum 2008;59:1371–7.

DOI 10.1002/art.41273

Reply

To the Editor:

We appreciate the comments by Dr. Kerschbaumer et al highlighting the MTX monotherapy results in our article on the primary results from the SEAM-PsA trial. Since MTX is a drug that has long been used in PsA without much data from rigorous and well-controlled clinical trials, we sought to provide reliable data about MTX through the SEAM-PsA trial. The primary aim of the study was to compare MTX monotherapy with ETN monotherapy and assess the value of combining MTX and ETN in the treatment of PsA. As such, the MTX data should be interpreted relative to ETN. The ACR 20% improvement response (1) was selected as the primary end point for the SEAM-PsA study as it continues to be the primary end point required by regulatory agencies for PsA trials. Given the heterogeneous nature of PsA and the variability of the component measures of clinical domains, such as enthesitis and skin disease, minimal disease activity was chosen as the key secondary end point as it is a validated and well-accepted composite end point. These prespecified and appropriately adjusted measures demonstrated statistical superiority of both ETN-containing arms over MTX monotherapy.

Evaluation of other secondary and exploratory end points, which should be considered descriptive with nominal *P* values, showed similar changes from baseline between the treatment arms for several measures. But a closer examination considering the variability of these measures still supports the conclusion that MTX is less effective than ETN in PsA. For example, though the mean change in the Spondyloarthritis Research Consortium of Canada Enthesitis Index (2) was similar in the 3 treatment arms, the proportion of patients with enthesitis resolution was numerically greater in the ETN arms. The observations that patients in the ETN arms also showed a numerically greater response for resolution or near resolution (as seen with the Leeds Dactylitis Index [3] and the modified Nail Psoriasis Severity Index [4]) and overall greater response in those with greater disease

burden (as seen in patients with ≥10% affected body surface area at baseline) are evidence of an overall better response with ETN when the end points are sufficiently rigorous to highlight differences. Regarding the HAQ, we do not agree with the view that a worse baseline level necessarily presents a greater challenge in demonstrating improvement. On the contrary, greater changes are sometimes evident due to lack of floor effects as well as to the tendency of reversion to the mean. Finally, since the SEAM-PsA trial enrolled a population of patients with early PsA who were not preselected for radiographic progression, the demonstration of a difference in the radiographic end point, though small in magnitude, is meaningful.

As pointed out by Kerschbaumer et al, changes in the joint counts were not included in the main body of the article or in the supplementary material. However, in addition to providing the joint count information on ClinicalTrials.gov, we have subsequently presented a detailed analysis of the contribution of individual component end points, including joint counts, to the performance of the various composite measures used in the SEAM-PsA study (5).

Considering the points above, we believe that there is a significant and clinically meaningful difference between MTX and ETN efficacy in PsA. As to whether using a target MTX dosage of 25 mg rather than 20 mg would have resulted in a better outcome with MTX, it is possible that it would have led to a worse result. The potential for greater efficacy with 25 mg is not certain, and the higher dosage could lead to a greater incidence of adverse events. In addition, institution of the higher target MTX dosage could have led to a greater number of discontinuations in the MTX arm, which would have resulted in a lower response in the prespecified nonresponder analysis of the primary and key secondary end points. In the SEAM-PsA trial, the patients in the treatment arms that included MTX achieved and maintained a mean MTX dose of >18.8 mg (median 20 mg), thus addressing a key limitation of the Methotrexate in Psoriatic Arthritis trial (6). We agree with Kerschbaumer et al that data from our trial support the efficacy of MTX in PsA, for which data have been scant historically. However, overall, we believe that the results of the SEAM-PsA trial support the ACR/National Psoriasis Foundation guidelines for sequencing treatments in PsA: to initiate therapy with a tumor necrosis factor inhibitor prior to MTX (7).

Philip J. Mease, MD
Swedish Medical Center/Providence St. Joseph Health and the University of Washington
Seattle, WA
David H. Collier, MD
Gregory Kricorian, MD
James B. Chung, MD, PhD
Amgen Inc.
Thousand Oaks, CA

1. Felson DT, Anderson JJ, Boers M, Bombardier C, Furst D, Goldsmith C, et al. American College of Rheumatology preliminary definition of improvement in rheumatoid arthritis. Arthritis Rheum 1995;38:727–35.
2. Maksymowych WP, Mallon C, Morrow S, Shojania K, Olszynski WP, Wong RL, et al. Development and validation of the Spondyloarthritis Research Consortium of Canada (SPARCC) Enthesitis Index. Ann Rheum Dis 2009;68:948–53.
3. Helliwell PS, Firth J, Ibrahim GH, Melsom RD, Shah I, Turner DE. Development of an assessment tool for dactylitis in patients with psoriatic arthritis. J Rheumatol 2005;32:1745–50.
4. Cassell SE, Bieber JD, Rich P, Tutuncu ZN, Lee SJ, Kalunian KC, et al. The modified Nail Psoriasis Severity Index: validation of an instrument to assess psoriatic nail involvement in patients with psoriatic arthritis. J Rheumatol 2007;34:123–9.
5. Coates LC, Merola JF, Mease P, Ogdie A, Gladman D, Strand V, et al. The performance characteristics of composite measures used in a randomized trial examining etanercept and methotrexate as monotherapy or in combination in patients with psoriatic arthritis [abstract]. Arthritis Rheumatol 2019;71 Suppl 10. URL: https://acrabstracts.org/abstract/the-performance-characteristics-of-composite-measures-used-in-a-randomized-trial-examining-etanercept-and-methotrexate-as-monotherapy-or-in-combination-in-patients-with-psoriatic-arthritis/.
6. Kingsley GH, Kowalczyk A, Taylor H, Ibrahim F, Packham JC, McHugh NJ, et al. A randomized placebo-controlled trial of methotrexate in psoriatic arthritis. Rheumatology (Oxford) 2012;51:1368–77.
7. Singh JA, Guyatt G, Ogdie A, Gladman DD, Deal C, Deodhar A, et al. 2018 American College of Rheumatology/National Psoriasis Foundation guideline for the treatment of psoriatic arthritis. Arthritis Rheumatol 2019;71:5–32.

DOI 10.1002/art.41242

Increased awareness of hypogammaglobulinemia after B cell–targeted therapy: comment on the article by Md Yusof et al

To the Editor:

I would like to congratulate Dr. Md Yusof et al (1) on an excellent large-scale study that focuses attention on an important but underestimated clinical problem: secondary hypogammaglobulinemia can present significant issues in autoimmune rheumatic disease patients treated with B cell–targeted therapy. The clinicians' commitment to following recommendations for B cell–targeted therapy monitoring is admirable, as a result of which immunoglobulin measurements were obtained in very high rates in routine clinical settings. Immunoglobulin data for rituximab (RTX) cycle 1 were available in 666 of 700 patients (95%).

There are national and international guidelines advocating for testing immunoglobulin levels at baseline and at various time points following initiation of B cell–targeted therapy (2). Despite

this, awareness remains low. Barmettler et al reported that in 3,824 of 4,479 RTX-treated patients (85%) (both with autoimmune rheumatic diseases and hematologic disorders) (3), immunoglobulin levels were not tested prior to initiation of B cell–targeted therapy. Of the minority who had been tested at baseline, 48% had hypogammaglobulinemia. Winthrop et al, using data from the Study Of Rituxan in Patients With Rheumatoid Arthritis After an Inadequate Response to Previous Anti–Tumor Necrosis Factor Therapy registry, reported on the 5-year safety of RTX, including serious infection events (SIEs) (4). No immunoglobulin data were collected, which the authors acknowledged as a limitation of the study. Immunoglobulin data on patients treated with B cell–targeted therapy were also not collected in the British Society for Rheumatology Biologics Register (2). Immunoglobulin measurements should be considered a valuable parameter for addressing the infectious complications of B cell–targeted therapy, and there is a possibility that symptomatic hypogammaglobulinemia is an underlying explanation for these complications.

Interestingly, immunoglobulin replacement (IGR) therapy use reported by Md Yusof et al was only 1%—much lower than in other large studies in the field. The rate of IGR therapy was 0.6% in rheumatoid arthritis (RA) patients, 2.1% in systemic lupus erythematosus (SLE) patients, and 2.0% in antineutrophil cytoplasmic antibody–associated vasculitis (AAV) patients (1). Barmettler et al reported that 201 of 4,479 patients (4.5%) received IGR therapy, though this study also included patients without an autoimmune rheumatic disease (3). Roberts et al noted that 12 of 288 autoimmune rheumatic disease patients (4.2%) treated with B cell–targeted therapy received subsequent IGR therapy (5). The most likely explanation for the low rate of IGR therapy reported by Md Yusof et al is the close monitoring of immunoglobulin levels and frequent clinical assessment of the patients. Another contributing factor could be the distribution of autoimmune rheumatic disease patients, with a higher proportion of patients with RA (507 [72.4%]) compared to SLE (94 [13.4%]) and AAV (49 [7.0%]). In the study by Roberts et al, the main diagnoses were AAV (160 of 243 [65.8%]) and SLE (44 of 243 [18.1%]) (5). Higher rates of IGR therapy (14–21%) have also been reported in smaller studies of AAV (5).

It would be dangerous to become complacent as a result of Md Yusof and colleagues' data. As 99% of patients did not require IGR therapy, it could be argued that frequent immunoglobulin monitoring should be restricted to patients with SIEs. Alternatively, the testing protocol could differ between RA patients and patients with SLE or AAV. However, this approach would not allow for early assessment or diagnosis and intervention in patients with significant hypogammaglobulinemia, and contradicts the major guidelines. Of note, IgG levels normalized in only 4 of 11 patients (36.4%) after switching to another biologic, and only 1 of 7 patients (14.3%) who were treated with IGR therapy was able to discontinue treatment. This illustrates the importance of early recognition, to allow for introduction of alternative immunosuppressive therapy if appropriate.

In contrast to assiduous testing of immunoglobulin levels, measurement of specific antimicrobial antibodies (pneumococcus and *Haemophilus influenzae*) was less frequent, tested only in 29 patients with hypogammaglobulinemia or an SIE. As noted by Md Yusof and colleagues, testing for specific antibody responses was "as decided by physicians." These measurements are recommended as standard practice by major guidelines for the assessment of hypogammaglobulinemia, but have not been put into widespread practice beyond the field of immunology. The majority of those tested for specific antimicrobial antibodies had low baseline and postvaccine responses, which demonstrates the value of this approach for stratifying patients. Specific antibody deficiencies should also be considered in autoimmune rheumatic disease patients with recurrent or severe SIEs and normal immunoglobulin levels (6).

Dr. Karim's work was supported by Roche Pharmaceuticals (UK) (grant number GDRC-FEB-001-2017).

Mohammed Yousuf Karim, MA, MSc, MBBChir, FRCP, FRCPath
Sidra Medicine
Doha, Qatar

1. Md Yusof MY, Vital EM, McElvenny DM, Hensor EM, Das S, Dass S, et al. Predicting severe infection and effects of hypogammaglobulinemia during therapy with rituximab in rheumatic and musculoskeletal diseases. Arthritis Rheumatol 2019;71:1812–23.
2. Wijetilleka S, Jayne D, Mukhtyar C, Karim MY. Iatrogenic antibody deficiency from B-cell targeted therapies in autoimmune rheumatic diseases. Lupus Sci Med 2019;30:e000337.
3. Barmettler S, Ong MS, Farmer JR, Choi H, Walter J. Association of immunoglobulin levels, infectious risk, and mortality with rituximab and hypogammaglobulinemia. JAMA Netw Open 2018;1:e184169.
4. Winthrop KL, Saag K, Cascino MD, Pei J, John A, Jahreis A, et al. Long-term safety of rituximab in patients with rheumatoid arthritis: results of a five-year observational study. Arthritis Care Res (Hoboken) 2019;71:993–1003.
5. Roberts DM, Jones RB, Smith RM, Alberici F, Kumaratne DS, Burns S, et al. Immunoglobulin G replacement for the treatment of infective complications of rituximab-associated hypogammaglobulinemia in autoimmune disease: a case series. J Autoimmun 2015;57:24–9.
6. Wijetilleka S, Chander S, Karim MY. A 74-year-old female with recurrent infections receiving methotrexate for rheumatoid arthritis. Rheumatology (Oxford) 2019;58:1309–10.

DOI 10.1002/art.41244

Reply

To the Editor:

We thank Dr Karim for his comments on our article, in which we reported a low percentage of patients in our cohort study (7 of 700 [1%]) requiring IGR therapy for recurrent infections despite

treatment with prophylactic antibiotics or hypogammaglobulinemia during RTX therapy. This was the lowest rate compared to other published cohort studies, which predominantly included patients with AAV (4–21% of patients in each cohort) (1–3). The low rate of IGR therapy in our cohort was attributed to the variability in the diagnoses of rheumatic and musculoskeletal diseases (RMDs) studied. Of 7 patients who required IGR therapy in our cohort, rates were higher among those with SLE and AAV (2 of 94 [2.1%] and 1 of 49 [2.0%], respectively) compared to RA (3 of 507 [0.6%]). We believe these higher rates of low IgG levels (<6 gm/liter) at RTX initiation and subsequent requirement of IGR therapy during RTX treatment in SLE and AAV compared to RA could be attributed to the intensity of treatment with previous remission induction agents including cyclophosphamide, depicted in Figure 1 of our article.

In comparison to cohort studies reported on by Roberts et al (1,4), Besada et al (2), and Venhoff et al (3) in which rates of IGR therapy among patients with AAV were 8 of 288 (2.8%), 5 of 35 (14.3%), and 7 of 33 (21.2%), respectively, the low rate of required IGR therapy in our cohort was likely due to the difference in RTX re-treatment strategy. We used a re-treatment–on–clinical relapse strategy (with relapse defined as an increase in the Birmingham Vasculitis Activity Score (5) of ≥1) compared to the fixed re-treatment strategy intervals of every 6–12 months in the cohorts mentioned above. One concern in using this re-treatment strategy was that allowing relapse might result in organ-threatening flares or necessitate exposure to further high doses of glucocorticoids. However, we previously reported that the re-treatment–on–clinical relapse strategy was effective: no patients had discontinued RTX therapy at 7 years due to loss of efficacy, disease activity at each subsequent relapse was less severe than that at RTX initiation, the mean daily oral prednisolone dose was significantly reduced with more than one-third of patients having discontinued glucocorticoid treatment at the last follow-up, and none of the patients had developed severe organ damage (defined as a Vasculitis Damage Index score (6) of ≥5) (7). Additionally, results from the MAINRITSAN2 randomized controlled trial demonstrated that AAV relapse rates did not differ significantly between individually tailored and fixed-schedule RTX regimens at 28 months, with fewer RTX cycles administered using the former strategy (8).

Although the rate of IGR therapy was lowest among patients with RA, we agree that this is not a reason to become complacent, since patients with RA need more frequent cycles for life-long therapy, with a median duration of response to RTX in RA, SLE, and AAV of 10 months (9), 12 months (10), and 18 months (7), respectively. In our cohort study, there were 10 infection-associated deaths among 110 patients who had low IgG levels either at baseline or after 4 months of RTX therapy (9.1%). Moreover, as noted by Dr. Karim, IgG levels had normalized in only 4 of 11 RA patients (36.4%) at ≥2 years after switching to a different biologic disease-modifying antirheumatic drug, thus posing a treatment dilemma in the management of difficult-to-treat RA from the perspective of infection once RTX is discontinued. Therefore, our data provide strong evidence that regardless of RMD diagnosis, immunoglobulin levels should be monitored at baseline and before each RTX cycle, particularly in patients with comorbidities and low baseline immunoglobulin levels, in order to identify patients at risk of SIEs.

Finally, we agree with Dr. Karim that specific antibody responses to tetanus, *Haemophilus*, and pneumococcus should be measured more frequently in clinical practice in patients with low IgG levels or an SIE in the previous RTX cycle in order to facilitate effective pre-RTX vaccination and to identify patients who have an inadequate response to an appropriate vaccination challenge and may require treatment with IGR.

The views expressed are those of the authors and not necessarily those of the NHS, the NIHR, or the Department of Health. Supported by Octapharma, the NIHR, and NIHR Leeds Biomedical Research Centre Leeds Teaching Hospitals National Health Service Trust (grant DRF-2014-07-155). Dr. Vital has received honoraria from Roche, GlaxoSmithKline, and AstraZeneca (less than $10,000 each) and research support from those companies. Dr. Emery has received consulting fees from Bristol-Myers Squibb, Abbott, Pfizer, MSD, Novartis, Roche, and UCB (less than $10,000 each) and research support from Abbott, Bristol-Myers Squibb, Pfizer, MSD, and Roche (paid to the University of Leeds). Dr Savic has received honoraria from Novartis, Sobi, and SIRE (less than $10,000 each) and research support from Novartis, Sobi, Octapharma, and CSL Behring. No other disclosures relevant to this article were reported.

Md Yuzaiful Md Yusof, PhD, MRCP
Edward M. Vital, PhD, MRCP
Paul Emery, MA, MD, FMedSci
Sinisa Savic, PhD, FRCPath
University of Leeds
and NIHR Leeds Biomedical Research Centre
Leeds Teaching Hospitals NHS Trust
Leeds, UK

1. Roberts DM, Jones RB, Smith RM, Alberici F, Kumaratne DS, Burns S, et al. Rituximab-associated hypogammaglobulinemia: incidence, predictors and outcomes in patients with multi-system autoimmune disease. J Autoimmun 2015;57:60–5.
2. Besada E, Koldingsnes W, Nossent JC. Long-term efficacy and safety of pre-emptive maintenance therapy with rituximab in granulomatosis with polyangiitis: results from a single centre. Rheumatology (Oxford) 2013;52:2041–7.
3. Venhoff N, Effelsberg NM, Salzer U, Warnatz K, Peter HH, Lebrecht D, et al. Impact of rituximab on immunoglobulin concentrations and B cell numbers after cyclophosphamide treatment in patients with ANCA-associated vasculitides. PLoS One 2012;7:e37626.

4. Roberts DM, Jones RB, Smith RM, Alberici F, Kumaratne DS, Burns S, et al. Immunoglobulin G replacement for the treatment of infective complications of rituximab-associated hypogammaglobulinemia in autoimmune disease: a case series. J Autoimmun 2015;57:24–9.
5. Luqmani RA, Bacon PA, Moots RJ, Janssen BA, Pall A, Emery P, et al. Birmingham Vasculitis Activity Score (BVAS) in systemic necrotizing vasculitis. Q J Med 1994;87:671–8.
6. Exley AR, Bacon PA, Luqmani RA, Kitas GD, Gordon C, Savage CO, et al. Development and initial validation of the Vasculitis Damage Index for the standardized clinical assessment of damage in the systemic vasculitides. Arthritis Rheum 1997;40:371–80.
7. Md Yusof MY, Vital EM, Das S, Dass S, Arumugakani G, Savic S, et al. Repeat cycles of rituximab on clinical relapse in ANCA-associated vasculitis: identifying B cell biomarkers for relapse to guide retreatment decisions. Ann Rheum Dis 2015;74:1734–8.
8. Charles P, Terrier B, Perrodeau É, Cohen P, Faguer S, Huart A, et al. Comparison of individually tailored versus fixed-schedule rituximab regimen to maintain ANCA-associated vasculitis remission: results of a multicentre, randomised controlled, phase III trial (MAINRITSAN2). Ann Rheum Dis 2018;77:1143–9.
9. Cañamares I, Merino L, López J, Llorente I, García-Vadillo A, Ramirez E, et al. Experience with the use of rituximab for the treatment of rheumatoid arthritis in a tertiary hospital in Spain: RITAR study. J Clin Rheumatol 2019;25:258–63.
10. Md Yusof MY, Shaw D, El-Sherbiny YM, Dunn E, Rawstron AC, Emery P, et al. Predicting and managing primary and secondary non-response to rituximab using B-cell biomarkers in systemic lupus erythematosus. Ann Rheum Dis 2017;76:1829–36.

DOI 10.1002/art.41235

Anti–apolipoprotein A-I in systemic lupus erythematosus: comment on the article by Kim et al

To the Editor:

I read with great interest the review by Dr. Kim and colleagues exploring the role of high-density lipoproteins (HDLs) as potential disease biomarkers and therapeutic targets in systemic lupus erythematosus (SLE) (1). I believe the discussion of anti–apolipoproteinA-I (anti–Apo A-I) autoantibodies warrants some comments.

First, the frequency of elevated levels of anti–Apo A-I is not specific to SLE as suggested by Kim et al, referring to a publication from 2004 (2). Recently published reports of studies performed in the general population, HIV patients, and SLE patients, for example, show anti–Apo A-I seropositivity prevalences of 20%, 48%, and 43%, respectively (3–5), indicating that high levels of these antibodies can be encountered frequently, even in non-autoimmune settings. Such autoantibodies are therefore not specific to SLE.

Second, though these autoantibodies have been shown to be independent predictors of poor cardiovascular and overall outcomes in different clinical settings (e.g., general population, acute coronary syndromes, ischemic stroke, carotid stenosis, rheumatoid arthritis, and renal transplant) (3,6), such prognostic value has not been replicated in SLE patients to date. Indeed, 2 recent studies showed that though anti–Apo A-I antibodies were significantly and independently associated with disease severity scores (Systemic Lupus Erythematosus Disease Activity Index and British Isles Lupus Assessment Group [7,8]), they were not associated with cardiovascular events in SLE (5,9). These results do not make a strong case for considering anti–Apo A-I as a biomarker of cardiovascular risk in SLE. Further investigation of the possible reasons for the association of these antibodies with SLE disease activity but not with cardiovascular events would be of interest.

Last, the hypothesis proposed by Kim et al suggesting that increased levels of anti–Apo A-I occur in response "to oxidized free Apo A-I" and "oxidized Apo A-I protein is likely more immunogenic" obviously contrasts with existing data. The sole extensive anti–Apo A-I assay validation published to date (using liquid chromatography mass spectrometry coupled with peptide engineering) showed that the assay specifically detects antibodies against lipid-free Apo A-I in native configuration, devoid of any posttranslational modifications such as oxidation or glycation (10,11). Furthermore, immunoreactivity of patient sera was not enhanced when glycated and oxidized Apo A-I were used as coating antigens in the assay (10). Along the same lines, the concept of misfolded immunogenic Apo A-I to generating an anti–Apo A-I response is not supported by current evidence, as maintaining Apo A-I in a given tertiary conformation has been shown to be of utmost importance for both the detection and the neutralization of these antibodies (11). To be exhaustive, Kim et al should have mentioned that a specific genetic locus in the FCRL3 gene (associated with numerous autoimmune diseases and the production of various autoantibodies) has been shown to act as an expression quantitative trait locus for anti–Apo A-I levels, according to the results of a genome-wide association study performed in the general population (12). Finally, the authors should have referred to the EXPLORE study, a phase II randomized controlled trial that highlighted the fact that some HDL cholesterol–increasing agents (including extended-release niacin) could induce an anti–Apo A-I response, neutralizing the antioxidant properties of HDL molecules (13). Addressing these concepts, grounded in existing contemporary literature that encompasses the accepted contributions of both genetic and environmental factors as triggers for autoantibody devel-

opment, would have been welcome to complete this excellent review.

Dr. Vuilleumier has received research support from Roche.

Nicolas Vuilleumier, MD
Geneva University Hospital and Geneva University Geneva, Switzerland

1. Kim SY, Yu M, Morin EE, Kang J, Kaplan MJ, Schwendeman A. High-density lipoprotein in lupus: disease biomarkers and potential therapeutic strategy [review]. Arthritis Rheumatol 2020;72:20–30.
2. Vuilleumier N, Reber G, James R, Burger D, de Moerloose P, Dayer JM, et al. Presence of autoantibodies to apolipoprotein A-1 in patients with acute coronary syndrome further links autoimmunity to cardiovascular disease. J Autoimmun 2004;23:353–60.
3. Satta N, Frias MA, Vuilleumier N, Pagano S. Humoral immunity against HDL particle: a new perspective in cardiovascular diseases? Curr Pharm Des 2019;25:3128–46.
4. Satta N, Pagano S, Montecucco F, Gencer B, Swiss HIV Cohort Study, Mach F, et al. Anti-apolipoprotein A-1 autoantibodies are associated with immunodeficiency and systemic inflammation in HIV patients. J Infect 2018;76:186–95.
5. Nigolian H, Ribi C, Courvoisier DS, Pagano S, Alvarez M, Trendelenburg M, et al. Anti-apolipoprotein A-1 autoantibodies correlate with disease activity in systemic lupus erythematosus. Rheumatology (Oxford) 2020;59:534–44.
6. Anderson JL, Pagano S, Virzi J, Dullaart RP, Annema W, Kuipers F, et al. Autoantibodies to apolipoprotein A-1 as independent predictors of cardiovascular mortality in renal transplant recipients. J Clin Med 2019;8:E948.
7. Bombardier C, Gladman DD, Urowitz MB, Caron D, Chang DH, and the Committee on Prognosis Studies in SLE. Derivation of the SLEDAI: a disease activity index for lupus patients. Arthritis Rheum 1992;35:630–40.
8. Symmons DP, Coppock JS, Bacon PA, Bresnihan B, Isenberg DA, Maddison P, et al, and Members of the British Isles Lupus Assessment Group (BILAG). Development and assessment of a computerized index of clinical disease activity in systemic lupus erythematosus. Q J Med 1988;69:927–37.
9. Croca S, Bassett P, Chambers S, Davari M, Alber KF, Leach O, et al. IgG anti-apolipoprotein A-1 antibodies in patients with systemic lupus erythematosus are associated with disease activity and corticosteroid therapy: an observational study. Arthritis Res Ther 2015;17:26.
10. Antiochos P, Marques-Vidal P, Virzi J, Pagano S, Satta N, Hartley O, et al. Impact of CD14 polymorphisms on anti-apolipoprotein A-1 IgG-related coronary artery disease prediction in the general population. Arterioscler Thromb Vasc Biol 2017;37:2342–9.
11. Pagano S, Gaertner H, Cerini F, Mannic T, Satta N, Teixeira PC, et al. The human autoantibody response to apolipoprotein A-I is focused on the C-terminal helix: a new rationale for diagnosis and treatment of cardiovascular disease? PLoS One 2015;10:e0132780.
12. Antiochos P, Marques-Vidal P, Virzi J, Pagano S, Satta N, Hartley O, et al. Anti-apolipoprotein A-1 IgG predict all-cause mortality and are associated with Fc receptor-like 3 polymorphisms. Front Immunol 2017;8:437.
13. Batuca JR, Amaral MC, Favas C, Paula FS, Ames PR, Papoila AL, et al. Extended-release niacin increases anti-apolipoprotein A-I antibodies that block the antioxidant effect of high-density lipoprotein-cholesterol: the EXPLORE clinical trial. Br J Clin Pharmacol 2017;83:1002–10.

DOI 10.1002/art.41237

Reply

To the Editor:

We thank Dr. Vuilleumier for his interest in our review of HDLs in SLE and his comments on anti–Apo A-I autoantibodies. Dr. Vuilleumier raises an important point, with which we fully agree, that the prevalence of increased levels of anti–Apo A-I is not specific to SLE. The frequency of positivity for these antibodies in different diseases is summarized in Table 1. Inconsistent results could be attributed to between-assay differences introduced by the use of different enzyme-linked immunosorbent assays (ELISAs) and different cutoff values used to assess positivity (1).

Questions were also raised concerning whether anti–Apo A-I is an independent predictor of cardiovascular events in SLE patients. Indeed, it has not been found to be independently associated with cardiovascular events in SLE (2,3) though, as pointed out by Dr. Vuilleumier, an association between anti–Apo A-I and cardiovascular events has been demonstrated in a broad array of other clinical settings (4). This inconsistency certainly warrants further investigation.

Dr. Vuilleumier also raised questions about our hypothesis that oxidized Apo A-I may play a role in inducing anti–Apo A-I autoantibodies. We acknowledge that the formation of anti–Apo A-I autoantibodies could be attributed to various genetic and environmental factors, as he notes. At the same time, our hypothesis is based on our experience in the biopharmaceutical field, where oxidation and misfolding are recognized immunogenic factors for therapeutic proteins and peptides (5,6). In the case of Apo A-I, oxidation at Met-112 and Met-148 has been suggested to cause conformational change of Apo A-I by disrupting the α-helix structure (7,8). Methionine oxidation on Apo A-I has also been shown to induce the formation of amyloid fibril, which could be immunogenic (9). Studies by Henson and Venditto showed that Apo A-I peptide with oxidized Met-148 could bind with goat polyclonal antibodies against human Apo A-1 (10), and oxidized Apo A-I appeared to be more immunogenic in mouse models (11). In addition to methionine oxidation, Apo A-I could undergo other oxidative modifications, such as with 3-chlorotyrosine and 3-nitrotyrosine in autoimmune settings (12,13). Particularly, 3-nitrotyrosine modification has been proven to be immunogenic for other proteins and was suggested to be responsible for impaired immunologic tolerance (14). Thus, further studies on 3-chlorotyrosine– and 3-nitrotyrosine–modified Apo A-I would be helpful to inves-

Table 1. Prevalence of anti–Apo A-I autoantibodies in different populations*

Author, year (ref.)	Population	Prevalence, %	Positivity cutoff
Antiochos et al, 2017 (15)	5,220 participants from the general population (mean age 52.6 years)	19.9	97.5% of the reference distribution from 140 healthy blood donors
Satta et al, 2018 (16)	237 HIV patients with no current lipid-lowering therapy	58	97.5% of the reference distribution from 140 healthy blood donors
Pruijm et al, 2012 (17)	71 patients receiving maintenance hemodialysis	20	97.5% of the reference distribution from healthy blood donors
Vuilleumier et al, 2010 (18)	69 RA patients, 46 matched controls	17 in RA patients; 2 in healthy controls	97.5% of the reference distribution from healthy blood donors
Nigolian et al, 2020 (3)	76 patients meeting EULAR/ACR criteria for SLE (19)	43	97.5% of the reference distribution from 48 healthy donors
Butuca et al, 2007 (20)	55 SLE patients, 150 age- and sex-matched healthy controls	36 in SLE patients; 0.7 in healthy controls	>5 SD above the mean in healthy controls
O'Neill et al, 2010 (21)	39 SLE patients with high disease activity, 42 SLE patients with low disease activity, 34 healthy controls	35.9 in SLE patients with high activity; 12 in SLE patients with low activity	>3 SD above the mean in healthy controls
El-Lebedy et al, 2016 (22)	102 patients with type 2 DM, 112 patients with type 2 DM and CVD, 88 healthy controls	8.8 in patients with type 2 DM; 35.7 in patients with both type 2 DM and CVD; 6.1 in healthy controls	Absorbance ≥2.1 OD using human anti–apolipoprotein AI antibody ELISA kit (#MBS7034; MyBioSource)

* Anti–Apo A-I = anti–aolipoprotein A-I; RA = rheumatoid arthritis; EULAR = European League Against Rheumatism; ACR = American College of Rheumatology; SLE = systemic lupus erythematosus; DM = diabetes mellitus; CVD = cardiovascular disease; ELISA = enzyme-linked immunosorbent assay.

tigate the underlying mechanisms of anti–Apo A-I autoantibodies in autoimmune settings.

Supported by the American Heart Association (grant 19PRE344 00017).

Minzhi Yu, MS
Sang Y. Kim, PhD
Emily E. Morin, PhD
Anna Schwendeman, PhD
University of Michigan
Ann Arbor, MI

1. Frias MA, Virzi J, Batuca J, Pagano S, Satta N, Delgado Alves J, et al. ELISA methods comparison for the detection of auto-antibodies against apolipoprotein A1. J Immunol Methods 2019;469:33–41.
2. Croca S, Bassett P, Chambers S, Davari M, Alber KF, Leach O, et al. IgG anti-apolipoprotein A-1 antibodies in patients with systemic lupus erythematosus are associated with disease activity and corticosteroid therapy: an observational study. Arthritis Res Ther 2015;17:26.
3. Nigolian H, Ribi C, Courvoisier DS, Pagano S, Alvarez M, Trendelenburg M, et al. Anti-apolipoprotein A-1 autoantibodies correlate with disease activity in systemic lupus erythematosus. Rheumatology (Oxford) 2020;59:534–44.
4. Satta N, Frias MA, Vuilleumier N, Pagano S. Humoral immunity against HDL particle: a new perspective in cardiovascular diseases? Curr Pharm Design 2019;25:3128–46.
5. Torosantucci R, Schöneich C, Jiskoot W. Oxidation of therapeutic proteins and peptides: structural and biological consequences. Pharm Res 2014;31:541–53.
6. Maas C, Hermeling S, Bouma B, Jiskoot W, Gebbink MF. A role for protein misfolding in immunogenicity of biopharmaceuticals. J Biol Chem 2007;282:2229–36.
7. Shao B, Cavigiolio G, Brot N, Oda MN, Heinecke JW. Methionine oxidation impairs reverse cholesterol transport by apolipoprotein A-I. Proc Natl Acad Sci U S A 2008;105:12224–9.
8. Jayaraman S, Gantz DL, Gursky O. Effects of protein oxidation on the structure and stability of model discoidal high-density lipoproteins. Biochemistry 2008;47:3875–82.
9. Wong YQ, Binger KJ, Howlett GJ, Griffin MD. Methionine oxidation induces amyloid fibril formation by full-length apolipoprotein A-I. Proc Natl Acad Sci U S A 2010;107:1977–82.
10. Henson D, Venditto V. Evaluation of antibody responses toward post-translationally modified and unmodified peptide epitopes of apolipoprotein A-I in cardiovascular disease [abstract]. Arterioscler Thromb Vasc Biol 2016;36:A416.
11. Kline RH, Henson D, Venditto VJ. Evaluation of antibody responses in mice toward apolipoprotein A-I. Arterioscler Thromb Vasc Biol 2017;37:A395.
12. Vivekanandan-Giri A, Slocum JL, Byun J, Tang C, Sands RL, Gillespie BW, et al. High density lipoprotein is targeted for oxidation by myeloperoxidase in rheumatoid arthritis. Ann Rheum Dis 2013;72:1725–31.
13. Arungovind G, Kamalanathan AS, Padmanabhan V, Manoharan A, Chandrashekara S, Venkataraman K. Modifications of human plasma apolipoprotein A1 in systemic autoimmune diseases and myocardial infarction: a comparative study. J Proteins Proteom 2019;10:235–43.
14. Ohmori H, Kanayama N. Immunogenicity of an inflammation-associated product, tyrosine nitrated self-proteins. Autoimmun Rev 2005;4:224–9.
15. Antiochos P, Marques-Vidal P, Virzi J, Pagano S, Satta N, Hartley O, et al. Anti-apolipoprotein A-1 IgG predict all-cause mortality and are associated with Fc receptor-like 3 polymorphisms. Front Immunol 2017;8:437.
16. Satta N, Pagano S, Montecucco F, Gencer B, Swiss HIV Cohort Study, Mach F, et al. Anti-apolipoprotein A-1 autoantibodies are associated with immunodeficiency and systemic inflammation in HIV patients. J Infect 2018;76:186–95.
17. Pruijm M, Schmidtko J, Aho A, Pagano S, Roux-Lombard P, Teta D, et al. High prevalence of anti-apolipoprotein/A-1 autoantibodies in maintenance hemodialysis and association with dialysis vintage. Ther Apher Dial 2012;16:588–94.
18. Vuilleumier N, Bratt J, Alizadeh R, Jogestrand T, Hafström I, Frostegård J. Anti-apoA-1 IgG and oxidized LDL are raised in

rheumatoid arthritis (RA): potential associations with cardiovascular disease and RA disease activity. Scand J Rheumatol 2010;39:447–53.
19. Aringer M, Costenbader K, Daikh D, Brinks R, Mosca M, Ramsey-Goldman R, et al. 2019 European League Against Rheumatism/American College of Rheumatology classification criteria for systemic lupus erythematosus. Arthritis Rheumatol 2019;71:1400–12.
20. Batuca JR, Ames PR, Isenberg DA, Alves JD. Antibodies toward high-density lipoprotein components inhibit paraoxonase activity in patients with systemic lupus erythematosus. Ann N Y Acad Sci 2007;1108:137–46.
21. O'Neill SG, Giles I, Lambrianides A, Manson J, D'Cruz D, Schrieber L, et al. Antibodies to apolipoprotein A-I, high-density lipoprotein, and C-reactive protein are associated with disease activity in patients with systemic lupus erythematosus. Arthritis Rheum 2010;62:845–54.
22. El-Lebedy D, Rasheed E, Kafoury M, Abd-El Haleem D, Awadallah E, Ashmawy I. Anti-apolipoprotein A-1 autoantibodies as risk biomarker for cardiovascular diseases in type 2 diabetes mellitus. J Diabetes Complications 2016;30:580–5.

DOI 10.1002/art.41262

Clinical Images: Giant calcinosis in dermatomyositis and scleroderma overlap

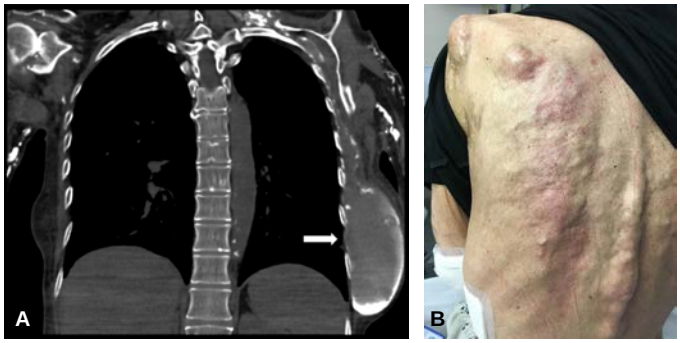

The patient, a 56-year-old woman with a history of dermatomyositis and scleroderma overlap with positive PM/Scl-75, was admitted with a severe myopathy flare. The disease had been characterized by Raynaud's phenomenon, extensive calcinosis cutis, mild interstitial lung disease, elevated creatine kinase level, and proximal muscle weakness. Previous treatment with methotrexate had been discontinued 6 months prior, due to a severely infected area of calcinosis with a subsequent septic arm. Monthly intravenous immunoglobulin (IVIG) and low-dose prednisone were continued. Three months after finishing antibiotic treatment, the patient presented with severe dysphagia, dyspnea, Gottron's papules, and weakness. Interestingly, a new lump in the posterior aspect of the left flank had been growing progressively. Computed tomography of the chest showed a lobulated, heterogeneous fluid collection (9.8 × 5.6 × 16.5 cm) (**arrow** in **A**) within the subcutaneous soft tissue of the left lateral chest wall and extensive calcinoses covering the margins and in isolated pouches. Needle aspiration yielded 1 ml of white, dense matter suggestive of calcinosis. A drainage tub was surgically inserted for a week, emptying the collection. Cultures were negative. After 2 weeks, a stable, minimal amount of fluid (2 × 2 × 4 cm) reappeared (**B**). Previous calcinoses had been drained in the flexures, and an attempt at injecting intralesional sodium thiosulfate had been unsuccessful. Calcinosis is a common, impairing manifestation of dermatomyositis and scleroderma that can appear unrelated to disease flares. No proven treatments are available. The myositis flare in this patient was treated with methylprednisolone boluses, IVIG, and intravenous cyclosporine and gradually improved.

Dr. Fernández-Codina's work was supported by the Scleroderma Society of Ontario and St. Joseph's Hospital Foundation in London, Ontario (Kay Eldson donor). Dr. Fernández-Codina has received consulting fees from Actelion (less than $10,000). Dr. Pope has received consulting fees from AbbVie, Actelion, Amgen, Bristol-Myers Squibb, GlaxoSmithKline, Eli Lilly, Merck, Novartis, Roche, Sandoz, Sanofi, and UCB (less than $10,000 each) and from Pfizer (more than $10,000) and research support from Bristol-Myers Squibb, Merck, Roche, and UCB. No other disclosures relevant to this article were reported.

Andreu Fernández-Codina, MD, MSc, PhD
University of Western Ontario
London, Ontario, Canada
Windsor Regional Hospital
Windsor, Ontario, Canada
and Vall d'Hebron University Hospital
Barcelona, Spain
Maria Camprodon-Gómez, MD
Vall d'Hebron University Hospital
Barcelona, Spain
Janet E. Pope, MD, MPH
University of Western Ontario
London, Ontario, Canada